DIAGNOSTIC CRITERIA OF ELECTROCHEMICAL REACTION MECHANISMS USING CYCLIC SQUARE WAVE VOLTAMMETRY

A Dissertation
Presented to
The Academic Faculty

by

Megan Arlena Mann

In Partial Fulfillment
of the Requirements for the Degree
Doctor of Philosophy in the
School of Chemistry and Biochemistry

Georgia Institute of Technology

May 2016

DIAGNOSTIC CRITERIA OF ELECTROCHEMICAL REACTION MECHANISMS USING CYCLIC SQUARE WAVE VOLTAMMETRY

Approved by:

Dr. Lawrence A. Bottomley, Advisor
School of Chemistry & Biochemistry
Georgia Institute of Technology

Dr. Jiri (Art) Janata
School of Chemistry & Biochemistry
Georgia Institute of Technology

Dr. Miroslawa (Mira) Josowicz
School of Chemistry & Biochemistry
Georgia Institute of Technology

Dr. Charles Liotta
School of Chemistry & Biochemistry
Georgia Institute of Technology

Dr. Paul Kohl
School of Chemical & Biomolecular Engineering
Georgia Institute of Technology

Date Approved: March 30, 2016

DEDICATION

In honor of Lena May Fields, Arline Marie Damm, and Sheila Grace Haney…

ACKNOWLEDGEMENTS

I would like to thank my advisor, Dr. Lawrence A. Bottomley, for his guidance, support, and passion for electrochemistry over the last few years. His genuine desire to help me grow as an analytical chemist is deeply appreciated. Thanks to him, I have learned much about research, scientific writing, teaching, and mechanistic electrochemistry. Being the last Bottomley grad student has truly been an experience that I will never forget, and for that, I'm grateful. Live long and prosper.

I would like to thank my committee, Dr. Art Janata, Dr. Mira Josowicz, Dr. Charles Liotta, and Dr. Paul Kohl, for their expertise and suggestions throughout my grad school journey. Their advice has been invaluable. I would like to thank the numerous undergrads who have done research in the Bottomley lab. Their efforts to help with experiments in lab are greatly appreciated. Thank you to Dr. Leigh Bottomley, Dr. Carrie Shepler, and Dr. Christy O'Mahony for being fantastic role models. I'm thankful to Dr. Robert Braga for teaching me so much about the instruments in the analytical lab. Thank you to my classmates and friends Amy Jablonski, Denise Okafor, Rachel Stryffeler, and Johanna Smeekens for your comradery and many laughs.

I would also like to thank my family and friends. Thank you to my parents, John and Jill Damm and Sharon and Pat McMillen, for supporting my goals and dreams. Thank you for letting me practice presentations, sending words of encouragement via texts and phone calls, and sending WV care packages. Thank you to my siblings, Kieran and Taryn Damm and Matt McMillen, for being the best siblings that I could ask for. Thank

you to Erica Harvey, Ashley Grose, Stephanie Jordan, Deborah Westbrook, and Kimberly Simms for your friendship and all that you do for my heart and soul before grad school, during grad school, and always.

Lastly, I would like to thank my husband, Gary (Andy) Mann Jr., and our dogs, Apollo, Orion, Kate, and Abby, for their never-ending love and support. Andy, thank you for standing by me, encouraging me, understanding me, and forgiving me when I'm stressed. I'm forever grateful for all that you do and for every day that I'm blessed to call you my husband and best friend. You are amazing, and I love you with all that I am.

TABLE OF CONTENTS

LIST OF TABLES

LIST OF FIGURES

LIST OF ABBREVIATIONS AND SYMBOLS

ABBREVIATIONS

A = area of the electrode in cm^2

C^*_{Ox} = concentration of the Ox at the beginning of the experiment

C_{Ox} (x, t) = concentration of Ox at the electrode surface and any time t

C_{Red} (x, t) = concentration of Red at the electrode surface and any time t

C^T(x, t) = total initial concentration of Ox and Y

D_{Ox} = Diffusion coefficient for the Ox in cm^2/s

D_{Red} = Diffusion coefficient for the Red in cm^2/s

$E_{applied}$ = applied potential

E_p = peak potential

$E_{p,f}$ = peak potential for the forward sweep

$E_{p,r}$ = peak potential for the reverse sweep

ΔE_p = peak separation between $E_{p,r}$ and $E_{p,f}$ in mV

E_{SW} = amplitude in mV

δE = increment in mV

F = Faraday's constant

I_p = peak current

$I_{p,f}$ = peak current for the forward sweep

$I_{p,r}$ = peak current for the reverse sweep

ΔI_p = difference peak current

$\Delta I_{p,f}$ = difference peak current for the forward sweep

$\Delta I_{p,r}$ = difference peak current for the reverse sweep

K = equilibrium constant = k_f/k_b

k^0 = heterogeneous electron transfer rate in cm/s or 1/s

k_f = forward rate constant for a chemical reaction in 1/s

k_b = reverse rate constant for a chemical reaction in 1/s

n = number of electrons transferred

Ox = oxidized species

R = gas law constant

Red = reduced species

T = temperature in Kelvin

Y = electroninactive species in a chemical reaction preceding an electron transfer

Z = electroninactive species in a chemical reaction following an electron transfer

SYMBOLS

α = electron transfer coefficient describing the symmetry of the potential wells

λ = switching potential in mV vs. E^0

τ = period (ms)

Ψ = dimensionless current

Ψ_{odd} = dimensionless current resulting from odd numbered

Ψ_{even} = dimensionless current resulting from even numbered

$\Delta\Psi_p$ = dimensionless difference peak current

$\Delta\Psi^+$ = dimensionless difference current for diffusion-controlled processes corrected for its relationship to time

$\Delta\Psi^+_{p,f}$ = corrected dimensionless forward peak current for diffusion-controlled processes

$\Delta\Psi^+_{p,r}$ = corrected dimensionless reverse peak current for diffusion-controlled processes

$\Delta\Psi^s$ = dimensionless difference current for surface-confined processes corrected for its relationship to time

$\Delta\Psi^s_{p,f}$ = corrected dimensionless forward peak current for surface-confined processes

$\Delta\Psi^s_{p,r}$ = corrected dimensionless reverse peak current for surface-confined processes

SUMMARY

An electrode reaction is an electron transfer that occurs at the surface of the working electrode in a typical three electrode cell. The electron transfer may be reversible or it may be complicated by sluggish electron transfer kinetics, preceding chemical reactions, and/or following chemical reactions. Furthermore, the species within the reaction may be adsorbed to the electrode surface.

This thesis investigates reversible electron transfers that are coupled to chemical reactions, kinetically controlled electron transfers (both diffusional and adsorbed on the electrode surface), and kinetically controlled electron transfers that are coupled to chemical reactions. Each chapter explores a specific mechanism to determine its diagnostic criteria using cyclic square wave voltammetry. The reactions for each mechanism are written containing both the electroactive and electroinactive species. From these reactions and appropriate diffusion equations and boundary conditions, the expressions of concentrations of each species can be formulated. Using these expressions, an equation that evaluates current as a function of time and potential is derived and subsequently coded in MATLAB. Systematic variation of empirical parameters is performed, and the impact on peak parameters is analyzed. Diagnostic trends in peak parameters can be used for qualitative mechanism assignment then quantitatively determine reaction kinetics. Subsets of mechanisms are compared to one another so that the experimentalist can discern between mechanisms. All results are summarized in a table for each mechanism so that the information is rapidly available to the experimentalist. By following a set of recommended experiments and subsequently

generating plots, experimenters will be able to compare their results to those presented for each mechanism investigated.

The significant results within this thesis prove that both kinetically controlled and chemically coupled mechanisms can be identified and that rates can be determined using cyclic square wave voltammetry. Furthermore, this thesis exemplifies that the cyclic square wave waveform has added benefits over other electrochemical techniques. This work broadly impacts both the electrochemistry and non-electrochemistry communities as it intended for both the expert and non-expert to rapidly, easily, and most importantly, correctly interpret data.

CHAPTER 1

HISTORICAL BACKGROUND OF MECHANISTIC ELECTROCHEMISTRY

1.1 Voltammetric Techniques

1.1.1 Linear Sweep Voltammetry

Mechanistic electrochemistry is the use of an electrochemical technique to determine the reaction pathway of an electrode reaction mechanism. The history of mechanistic electrochemistry began decades ago with chronopotentiometry.[1-9] Advances in instrumentation led to the development of linear sweep voltammetry or LSV.[10] With LSV, an electroactive species, which is the analyte of interest, is dissolved in solution with an electrolyte in a three-electrode cell. In this configuration, one electrode serves as a working electrode where the electron transfer reaction takes place, one serves as a counter or auxiliary electrode to complete the circuit, and one serves as a reference electrode with a known potential. A linear potential ramp is applied to the working electrode versus the reference electrode; the current is measured and plotted as a function of applied potential. Potentials either begin negatively and are swept towards positive values or begin positively and are swept towards negative values (see Figure 1.1a). Regardless of direction, potentials change in a linear fashion with the potential sweep rate equal to potential over time. The measurable quantities from the voltammogram are peak current, I_p, and peak potential, E_p, as well as the half wave potential, $E_{p/2}$ (see Figure 1.1b). Instrumentation at that time was analog. The theory developed to predict trends in peak current and peak potentials as a function of sweep rate for a given mechanism fit the

analog instrumentation. The only variables available to an experimenter to gain information about the electrode reaction mechanism are concentration of the analyte and the potential sweep rate.

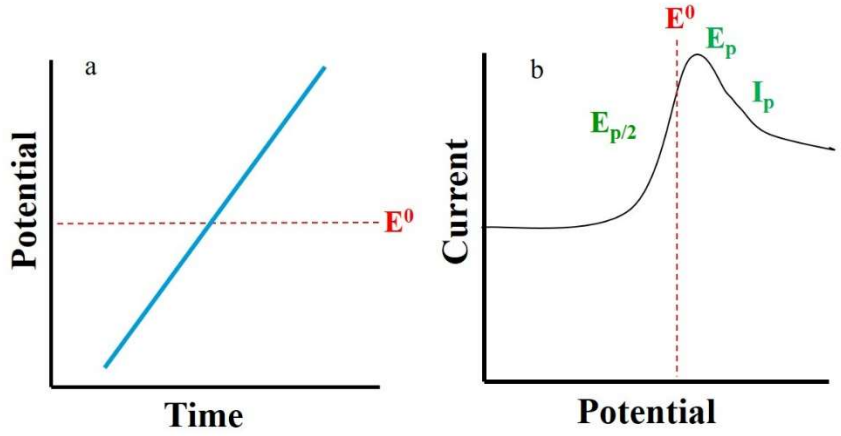

Figure 1.1. The LSV waveform (panel a) and the LSV voltammogram and measurable peak quantities (panel b).

A vast amount of theory work has been published on this technique. Of particular interest and relevance to this thesis was work by several notable people such as Laviron, Savéant, and Compton. Laviron contributed much theoretical development with LSV for many reaction mechanisms. Specifically, he investigated surface reactions with various isotherms describing the interactions between the surface molecules, varying degrees of the reversibility of the electron transfer, surface chemical reactions preceding or following the surface-confined electron transfer, autocatalysis, ohmic drop, and multi-layered structures which modify the electrode.[11-27] Laviron also studied diffusion-controlled reactions that may contain chemically-coupled reaction steps.[28, 29] Additionally, Savéant investigated many mechanisms and experimental conditions of LSV. Savéant examined chemically coupled mechanisms, kinetically controlled electron

transfers, homogeneous and heterogeneous electron transfers, uncompensated resistance, ohmic drop, bandpass limitations, and polarization.[30-38] Later, Compton introduced LSV for various configurations of channel and wall jet electrodes instead of the planar electrodes previously used.[39-42] The developments made within these works provide foundational work to other mechanistic electrochemistry techniques. Thus, both the development of the theoretical predictions of LSV and the experimental verification has been critical to the field of mechanistic electrochemistry.

Despite the ability to investigate current as it changes with time and potential and evaluate a host of mechanisms, LSV does not investigate the stability of the product of the electrochemical reaction. The measureable peak parameters only represent the reduction or oxidation of the electrochemically active species – not both. Furthermore, only two variables (sweep rate and analyte concentration) can be modified to identify the mechanism and determine any associated rates. Hence, even though the work regarding LSV provided great advancements in mechanistic electrochemistry, a technique which further probes the electrode reaction pathway is needed.

1.1.2 Cyclic Voltammetry

A technique similar to LSV is cyclic voltammetry or CV.[10] The significant difference is that CV sweeps the potential in two directions whereas LSV only sweeps in one direction as displayed in Figure 1.2a. Like LSV, mechanistic CV evaluates peak currents and peak potentials as a function of sweep rate (see Figure 1.2b). However, new measurable quantities peak ratio and peak separation provide further means to identify electrode reaction mechanisms and rates. Peak ratio is expressed as $I_{p,r}/I_{p,f}$ while peak separation is expressed as $\Delta E_p = E_{p,r} - E_{p,f}$. Experimenters can vary analyte

concentration, potential sweep rate, and the switching potential, which is the point at which the potential changes direction (see Figure 1.2a). Varying the switching potential dictates the length of the experiment and the time allotted for a reaction to proceed before reversing potential direction.

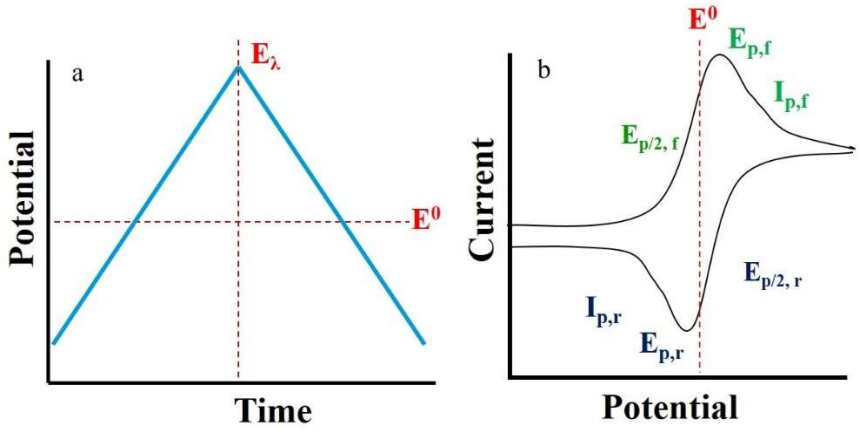

Figure 1.2. The CV waveform (panel a) and the CV voltammogram and measurable peak quantities (panel b).

Perhaps the most recognized work in theoretical CV was done by Nicholson and Shain.[43] In one publication, six different mechanisms were investigated. Namely, the reversible, quasireversible, chemically coupled mechanisms (with either preceding or following chemical reactions with varying degrees of reversibility), and the catalytic mechanism were investigated. Master plots containing six mechanisms were generated for peak currents, peak ratio, and peak potential as a function of scan rate. These plots easily and rapidly enable the user to match the reaction pathway for the analyte of interest to one of these mechanisms. This specific paper is the gold standard for mechanistic electrochemistry. Several publications from this group involved investigation of chemically coupled reactions, multi-step charge transfers, and those complicated by

adsorption or stripping.[44-52] Savéant also published noteworthy works as he investigated several other mechanisms also appearing in this thesis, specifically, asymmetric potential waveforms and chemically coupled mechanisms, and a host of other mechanisms.[53, 54] Thus, CV provides a fantastic basis for mechanistic electrochemistry.

In the years since LSV and CV were first reported, many advances have been made in the instrumentation used to acquire electrochemical data. LSV and CV are no longer taken with analog devices with a potential sweep rate that is truly linear. Instead, instrumentation is now digital and data is acquired at discrete points. What was once known as a true LSV or CV potential waveform is now a staircase waveform, perhaps better described as linear staircase voltammetry and cyclic staircase voltammetry. Unfortunately, most experimentalists, both frequent and infrequent users of electrochemical techniques, are unaware of this change. Much work has been done to show that the Nicholson and Shain diagnostic criteria no longer holds true for the new instrumentation; peak parameters depends greatly on the sampling point used and may require a correction factor after data analysis.[55-64] Digitally acquiring data is not the same as its analog counterpart without corrections. Thus, with advances in technology, diagnostic criteria sets must be updated to match the present instrumentation.

1.1.3 Square Wave Voltammetry

Shortly after linear sweep techniques, several pulse techniques emerged in the electrochemistry realm as a compliment to chronoamperometry and chronopotentiometry. These techniques include normal pulse voltammetry, differential pulse voltammetry, and most importantly square wave voltammetry (SWV).[65] The SWV potential waveform is the addition of an alternating up and down pulse to a linear ramp like LSV displayed in

Figure 1.3. The waveform has several characteristics known as empirical parameters as shown in the Figure 1.3 inset. The height of the pulse is known as amplitude, E_{SW}. The length of time required to complete an up and down pulse is known as period, τ, or frequency, $f = 1/\tau$. The rise in the potential waveform is the increment, δE. Comparisons to LSV in sweep rate can be made via the effective potential sweep rate = $\delta E/\tau$ though as stated above, a correction factor is needed.

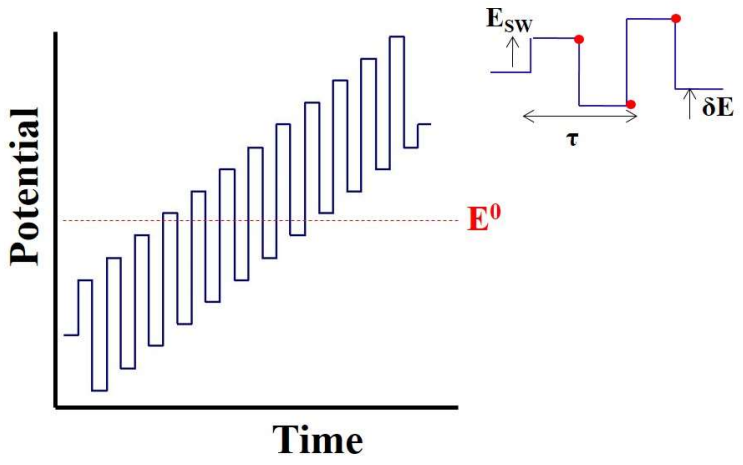

Figure 1.3. The square wave potential waveform and the empirical parameters used to generate the square wave potential waveform (inset).

As the potential is applied, the current decays after the onset of a potential pulse and is sampled at discrete points along each pulse. Typically, the last data point on each pulse prior to the next pulse is stored via the software controlling the potentiostat. The currents corresponding to the forward pulses, or the pulses in the direction of the sweep, comprise the forward individual current (red dots in Figure 1.4a). Similarly, currents corresponding to the pulses in the opposite direction of the sweep comprise the reverse individual current (green dots in Figure 1.4a). The reverse current is subtracted from the forward current to yield a difference current. The potentials corresponding to the

difference current are the average of the two potential pulses on which the current was sampled. The SWV voltammogram is the plot of difference current versus the average potential as displayed in Figure 1.4b. By varying the empirical parameters, the shape of the SWV voltammogram changes like the effect of sweep rate on the LSV voltammogram. The measureable quantities are peak current and peak potential as shown in Figure 1.4b.

SWV has many advantages over LSV. SWV has lower detection limits by several orders of magnitude due in part to the difference current and the manner in which the current is sampled.[66,67] SWV measures current at the end of each potential pulse, which should be dominated by faradaic current as the capacitance current should have decayed more rapidly than the faradaic.[67] Additionally, taking the difference in currents resulting from two pulses further reduces the impact of capacitance current as the charging current should be equal and subtracted.[67] From a diagnostic standpoint, in varying three empirical parameters, (period, increment, and amplitude) much more information can be gained about the mechanism of interest than in LSV when only the sweep rate can be varied.

The seminal work of O'Dea, Osteryoung and Osteryoung established SWV as a mechanistic tool.[66, 68, 69] Extensive work originated from the Osteryoung group regarding surface reactions, chemically coupled reactions, and kinetically controlled reactions.[67, 70-82] Since, others have contributed to the body of theoretical knowledge and experimental verification for SWV. These works investigated the mechanisms involving adsorption[83-92], quasireversible electron transfers[93-95], stripping[96-99], chemically coupled reactions[100-112], adsorbed and chemically coupled reactions[113-117], and protein films[118-120]. Several

experimental conditions have also been evaluated.[121-131] Mirčeski and coworkers published a book detailing the theoretical development and experimental verification for a host of mechanisms.[132] Unfortunately, though there have been great advancements in SWV, seldom is it used by experimentalists who occasionally need an electrochemistry technique. With the exception of a few reports, most plots available in the literature present only the variation of period (or frequency). Though this is a critical component of identifying reaction mechanisms, it does not provide as much information as the variation of all empirical parameters. Moreover, sweeping only in one direction does not provide information regarding the stability of the electrochemical reaction product. Furthermore, the experimenter may incorrectly assign the formal potential whereas the experimenter would gain information about the formal potential by scanning in both directions as the formal potential would lie between the forward and reverse peak. Thus, there is a demand for a technique that possesses qualities of both CV and SWV.

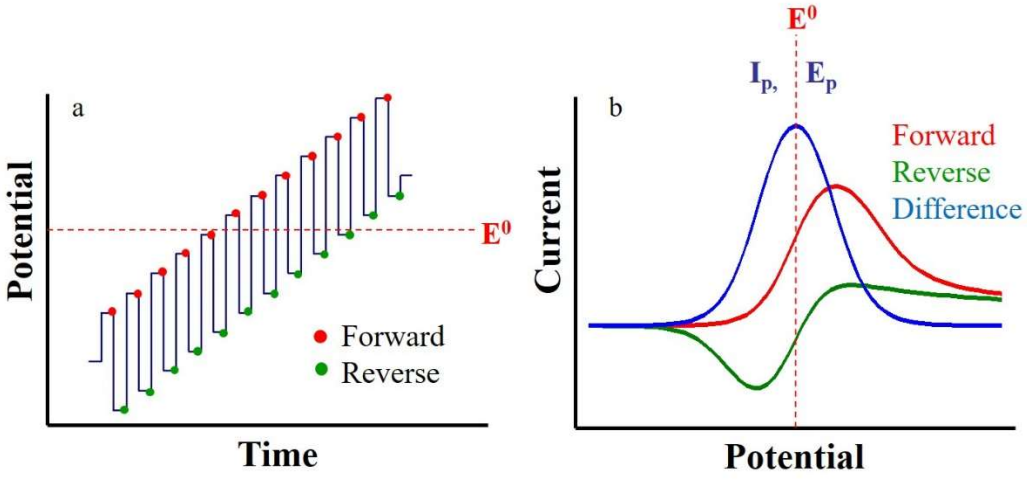

Figure 1.4. The square wave potential waveform with the sampling of the forward and reverse currents (panel a) and the individual and difference currents with measureable quantities (panel b).

1.1.4 Cyclic Square Wave Voltammetry

Cyclic square wave voltammetry (CSWV) is a technique that comprises all of the features of SWV with the ability to scan in two directions like CV. CSWV has the same empirical parameters that control the waveform as SWV (period, amplitude, increment), but also has switching potential as displayed in Figure 1.5. Experimenters can vary these empirical parameters in addition to analyte concentration to gain information about the electrode reaction mechanism and rate of a reaction. The effect of the empirical parameters is measured in the peak parameters (peak current, peak potential, peak ratio, and peak separation).

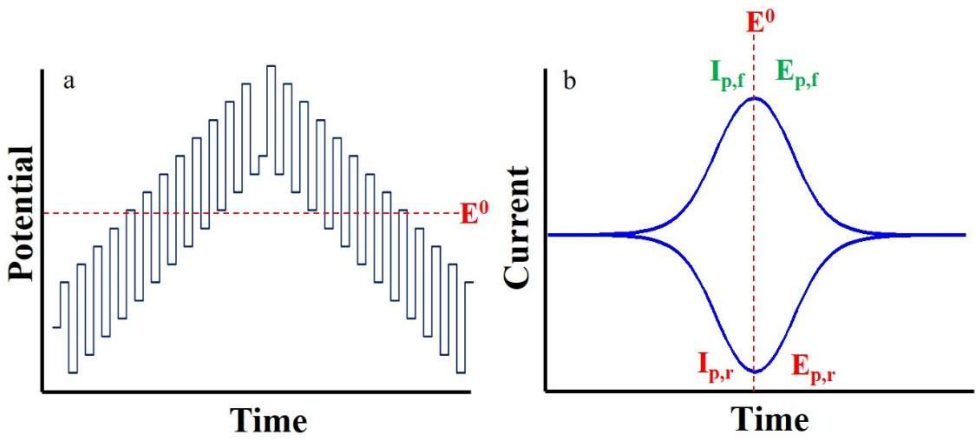

Figure 1.5. The CSWV waveform (panel a) and the CSWV voltammogram with measurable peak quantities (panel b).

CSWV is a critical advancement in electrochemistry because it has the benefits of SWV and CV combined. CSWV is capable of lower detection limits than CV, but the manner in which the voltammogram is interpreted is similar. This feature makes it easier for the experimenter to readily transition between the use of CV and CSWV. In a parallel

advancement in CV over LSV, CSWV enables the experimentalist to investigate the product of the electrochemical reaction whereas SWV which contains only one potential sweep. As a result, other measurable peak quantities such as peak ratio, reverse peak potential, and peak separation provide additional information about the electrode reaction. These added peak parameters contribute to the identification of mechanisms and determination reaction rates.

The utility of CSWV as a mechanistic tool has been established. Theory for the experimental examination of the reversible[133-136], quasireversible [137], irreversible [138, 139], EC [140], and catalytic mechanisms[141-143] have been presented. Noteworthy experimental applications include complexation reactions in immiscible liquids[144], catalytic processes involving surface adsorbates[145], amalgamations[146] and nitro-containing compounds[147]. Previous mechanistic work using CSWV has been presented by Helfrick.[148, 149] Helfrick added a reverse sweep to SWV to create CSWV by using mathematical framework available in the literature[43, 150, 151], codes written by O'Dea [68], and reports emanating from the Osteryoung group[66, 69]. He simulated voltammograms for a variety of electrode reaction mechanisms, namely the reversible, quasireversible, EE, EEE, EC, CE, EC_{cat}, and ECE mechanisms using CSWV. Furthermore, he varied empirical parameters, identified trends for each mechanism, and experimentally verified the trends. His work proved that many electrode reaction mechanisms could be identified with CSWV and that rates could be determined experimentally from some of the working curves that he simulated. Futur modified O'Deas's/Helfrick's derivations to include the E_qC, CE_q, and E_qC_{cat} mechanisms.

Helfrick and Futur's mathematical methods, codes, and results were used as a basis for the work within this thesis. Unfortunately, the treatment of current and dimensionless kinetic parameters generated by O'Dea[66, 68, 69] and subsequently Helfrick are misleading, difficult to interpret by experimentalists, and do not represent what is obtained experimentally. As a result and discussed in detail below, there is a great need to revisit mechanisms previously investigated by SWV and CSWV to revise these simulations. Furthermore, the variation of empirical parameters needs to be executed for the quasireversible and chemically coupled mechanisms so that the trends in empirical parameters can be compared to their reversible counterparts. Lastly, the diagnostic criteria for each mechanism investigated needs to be clearly identified and compared to other electrode reaction mechanisms. Therefore, though much work has been done with CSWV as a mechanistic tool, there is a significant need for improvement.

1.2 Novel Contributions to Mechanistic Electrochemistry

The salient and unique qualities of CSWV as a technique for mechanistic electrochemistry provided in this thesis pertain to 1) the separation of kinetic parameters and time, 2) the treatment of normalized dimensionless current, and 3) the identification of the diagnostic criteria for each mechanism that matches commercially available, current instrumentation. Previously, in much of the mechanistic electrochemistry work with LSV, CV, SWV, and even CSWV, kinetic parameters like electron transfer rates and chemical reaction rates were combined with time (scan rate, frequency, or period as appropriate) and other constants to make a dimensionless kinetic parameter. Peak

parameters were often plotted against the dimensionless kinetic parameters as appearing in the substantial SWV work by O'Dea[66, 68] and Helfrick[148]. The figures presented in those works were intended to show the interplay between kinetic rates and period affecting measurable peak parameters. However, plotting data in this manner is misleading. A recreation of plots similar to those previously published is shown in Figure 1.6. For a fixed value of the electron transfer rate k^0, as period, τ, is increased, peak current increases. Experimentally, it is well known that peak currents decrease as time increases (i.e., slower scan rates in LSV and CV). Only under a very limited set of conditions should this occur, i.e. a catalytic mechanism in which electroactive species are regenerated. Otherwise, under no circumstances should current increase as time increases. There is a conceptual flaw in presenting data in this manner which desperately needs to be addressed.

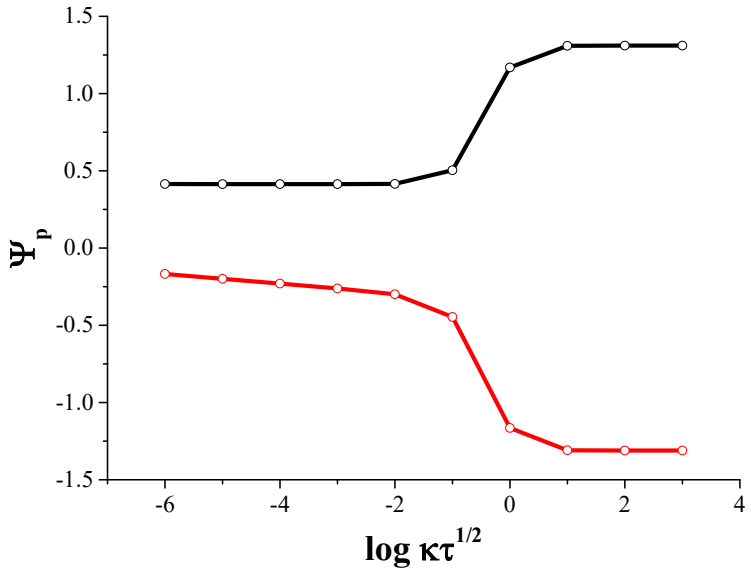

Figure 1.6. The effect of $k^0\tau^{1/2}$ on peak current, Ψ_p where κ contains k^0, the heterogeneous electron transfer rate and the diffusion coefficient, and τ is the period in the CSWV waveform.

The work contained within this thesis separates kinetic parameters from time parameters so that the effect of each can be considered independently. More specifically, when period is varied, the plots presented within this work match what the experimenter would observe in the laboratory setting.

Secondly, within this work, the treatment of dimensionless current as a function of time is treated differently than in other theory publications. Previous works from the Osteryoung group and Mirčeski and coworkers plot dimensionless current versus the dimensionless kinetic parameter containing period (or frequency). However, these plots do not match what is observed experimentally even after the kinetic and time terms are separated. Similarly, plots generated by Helfrick for the variation of period do not match experimental observations either. The experimental observation for SWV and CSWV should be in agreement with CV. For instance, it is well known from CV that peak current versus the square root of scan rate should yield a linear relationship if the analyte is diffusion controlled. This should be true for plotting peak current as a function of the square root of period for CSWV. This relationship is only true if dimensionless peak current is converted to one that accounts for current as it behaves with time, a normalized faradaic current, which is further discussed in Chapter 2. The relationship between normalized faradaic current and the square root of period is addressed for every mechanism in this thesis to parallel trends in CV.

Thirdly, the manner in which the data is presented is quite different than other SWV or CSWV reports present in the literature. Oftentimes in theoretical electrochemistry, reports are brief; mechanistic information not presented in a manner that is easily understood by the scientific community. Useful working curves are not available to

experimentalists. This body of works aims to make the process of data analysis and rate determination easier for both those outside of the electrochemistry specialty and those within the electrochemistry community who are not familiar with the technique. Each chapter investigates a different mechanism and provides a discussion of the diagnostic criteria for that mechanism, a protocol for assessing any associated rates, and summarizes the results in a table. The concluding chapter compares a collection of mechanisms in a manner similar to the plots originally published by Nicholson and Shain[43] but updated for CSWV and instrumentation available in the 21st century. Such a presentation is the first of its kind in decades and most certainly the first for CSWV.

Lastly, there are several mechanisms investigated in this thesis that have not been explored by CSWV, which are the surface-confined, E_qC, CE_q, and E_qC_{cat} mechanisms. The surface-confined mechanism is examined so that the experimentalist can differentiate between a process that is controlled by diffusion and one where no diffusion occurs. The quasireversible and chemically coupled mechanisms are complimentary to their reversible counterparts, which are also investigated in this thesis. The study of these mechanisms and diagnostic criteria are presented. Furthermore, the trends in peak parameters that can be used to discern a between two mechanisms, e.g., EC versus E_qC and E_{quasi} versus E_qC, are identified.

1.3 Conclusion

This chapter has provided insight into the history of mechanistic electrochemistry for LSV, CV, and SWV. In doing so, it has been demonstrated that there is a great need for a

technique which elegantly provides the experimenter with the ability to easily, rapidly, and correctly identify the reaction mechanism and any associated rates of electron transfers or chemical reactions. CSWV has the capability to do so as it possesses the added benefits of CV and SWV combined. Additionally, this chapter has identified the novel contributions to the field of mechanistic electrochemistry contained in this thesis, namely, the separation of the dimensionless kinetic parameter and time, the treatment of a normalized peak current, investigations of mechanisms that have not previously been addressed by CSWV, identification of the diagnostic criteria for each mechanism, and the manner in which the diagnostic criteria for the specified mechanisms are presented to the scientific community.

1.4 References

1. Delahay, P. *Anal. Chim. Acta*, **1947**. 1, 19-32.

2. Delahay, P., *New Instrumental Methods in Electrochemistry*. **1954**, Interscience Publishers: New York.

3. Reilley, C.N., G.W. Everett, and R.H. Johns. *Anal. Chem.*, **1955**. 27, 483-491.

4. Reilley, C.N. and W.G. Scribner. *Anal. Chem.*, **1955**. 27, 1210-1215.

5. King, R.M. and C.N. Reilley. *J. Electroanal. Chem. (1959-1966)*, **1960**. 1, 434-442.

6. Murray, R.W. and C.N. Reilley. *J. Electroanal. Chem. (1959-1966)*, **1962**. 3, 182-202.

7. Murray, R.W. and C.N. Reilley. *J. Electroanal. Chem. (1959-1966)*, **1962**. 3, 64-77.

8. Murray, R.W. *Anal. Chem.*, **1963**. 35, 1784-1789.

9. Murray, R.W. *J. Electroanal. Chem. (1959-1966)*, **1964**. 7, 242-245.

10. Bard, A.J. and L.R. Faulkner, *Electrochemical Methods: Fundamentals and Applications*. **2000**, Wiley: New York.

11. Laviron, E. *Bull. Soc. Chim. Fr.*, **1967**. 10, 3717-3721.

12. Laviron, E. *Bull. Soc. Chim. Fr.*, **1968**. 5, 2256-2260.

13. Laviron, E. *Electrochim. Acta*, **1971**. 16, 409-421.

14. Laviron, E. *J. Electroanal. Chem. Interfacial Electrochem.*, **1972**. 39, 1-23.

15. Laviron, E. *J. Electroanal. Chem. Interfacial Electrochem.*, **1972**. 35, 333-342.

16. Laviron, E. *Chem.-Ing.-Tech.*, **1972**. 44, 183-186.

17. Laviron, E. *J. Electroanal. Chem. Interfacial Electrochem.*, **1972**. 34, 463-473.

18. Laviron, E. *J. Electroanal. Chem. Interfacial Electrochem.*, **1973**. 42, 415-422.

19. Laviron, E. *J. Electroanal. Chem. Interfacial Electrochem.*, **1974**. 52, 395-402.

20. Laviron, E. *J. Electroanal. Chem. Interfacial Electrochem.*, **1974**. 52, 355-393.

21. Laviron, E. *J. Electroanal. Chem.*, **1979**. 101, 19-28.

22. Laviron, E., L. Roullier, and C. Degrand. *J. Electroanal. Chem. Interfacial Electrochem.*, **1980**. 112, 11-23.

23. Laviron, E. and L. Roullier. *J. Electroanal. Chem. Interfacial Electrochem.*, **1980**. 115, 65-74.

24. Laviron, E. *J. Electroanal. Chem. Interfacial Electrochem.*, **1981**. 122, 37-44.

25. Vallat, A., M. Person, and E. Laviron. *Electrochim. Acta*, **1982**. 27, 485-493.

26. Roullier, L. and E. Laviron. *J. Electroanal. Chem. Interfacial Electrochem.*, **1983**. 157, 193-203.

27. Laviron, E. and L. Roullier. *J. Electroanal. Chem.*, **1998**. 443, 195-207.

28. Laviron, E. and A. Vallat. *J. Electroanal. Chem. Interfacial Electrochem.*, **1976**. 74, 297-307.

29. Plichon, V. and E. Laviron. *J. Electroanal. Chem. Interfacial Electrochem.*, **1976**. 71, 143-156.

30. Mastragostino, M., L. Nadjo, and J.M. Savéant. *Electrochim. Acta*, **1968**. 13, 721–749.

31. Savéant, J.M. and J.C. Imbeaux. *J. Electroanal. Chem. Interfacial Electrochem.*, **1970**. 28, 327-340.

32. Imbeaux, J.C. and J.M. Savéant. *J. Electroanal. Chem. Interfacial Electrochem.*, **1971**. 31, 183-192.

33. Nadjo, L. and J.M. Savéant. *J. Electroanal. Chem. Interfacial Electrochem.*, **1973**. 48, 113-145.

34. Garreau, D. and J.M. Savéant. *J. Electroanal. Chem. Interfacial Electrochem.*, **1974**. 50, 1-22.

35. Amatore, C. and J.M. Savéant. *J. Electroanal. Chem. Interfacial Electrochem.*, **1977**. 85, 27-46.

36. Amatore, C., M. Gareil, and J.M. Savéant. *J. Electroanal. Chem. Interfacial Electrochem.*, **1983**. 147, 1-38.

37. Savéant, J.M. and K.B. Su. *J. Electroanal. Chem. Interfacial Electrochem.*, **1985**. 196, 1-22.

38. Savéant, J.M. and F. Xu. *J. Electroanal. Chem. Interfacial Electrochem.*, **1986**. 208, 197-217.

39. Compton, R.G. and P.R. Unwin. *J. Electroanal. Chem. Interfacial Electrochem.*, **1986**. 206, 57-67.

40. Compton, R.G. and P.R. Unwin. *J. Electroanal. Chem. Interfacial Electrochem.*, **1989**. 264, 27-36.

41. Fisher, A.C. and R.G. Compton. *J. Appl. Electrochem.*, **1992**. 22, 38-42.

42. Compton, R.G., A.C. Fisher, M.H. Latham, C.M.A. Brett, and A.M.C.F.O. Brett. *J. Phys. Chem.*, **1992**. 96, 8363-8367.

43. Nicholson, R.S. and I. Shain. *Anal. Chem.*, **1964**. 36, 706-723.

44. Alberts, G.S. and I. Shain. *Anal. Chem.*, **1963**. 35, 1859-1866.

45. Nicholson, R.A. and I. Shain. *Anal. Chem.*, **1965**. 37, 178-190.

46. Underkofler, W.L. and I. Shain. *Anal. Chem.*, **1965**. 37, 218-222.

47. Polcyn, D.S. and I. Shain. *Anal. Chem.*, **1966**. 38, 370-375.

48. Polcyn, D.S. and I. Shain. *Anal. Chem.*, **1966**. 38, 376-382.

49. Wopschall, R.H. and I. Shain. *Anal. Chem.*, **1967**. 39, 1535-1542.

50. Wopschall, R.H. and I. Shain. *Anal. Chem.*, **1967**. 39, 1514-1527.

51. Shuman, M.S. and I. Shain. *Anal. Chem.*, **1969**. 41, 1818-1825.

52. Hulbert, M.H. and I. Shain. *Anal. Chem.*, **1970**. 42, 162-171.

53. Saveant, J.M. *Electrochim. Acta*, **1967**. 12, 999-1030.

54. Savéant, J.M., *Elements of Molecular and Biomolecular Electrochemistry: An Electrochemical Approach to Electron Transfer Chemistry*. **2006**, Wiley-Interscience: Hoboken, NJ.

55. Miaw, L.H.L., P.A. Boudreau, M.A. Pichler, and S.P. Perone. *Anal. Chem.*, **1978**. 50, 1988-1996.

56. Bilewicz, R., R.A. Osteryoung, and J. Osteryoung. *Anal. Chem.*, **1986**. 58, 2761-2765.

57. Seralathan, M., R. Osteryoung, and J. Osteryoung. *J. Electroanal. Chem. Interfacial Electrochem.*, **1986**. 214, 141-156.

58. Seralathan, M., R.A. Osteryoung, and J.G. Osteryoung. *J. Electroanal. Chem. Interfacial Electrochem.*, **1987**. 222, 69-100.

59. Bilewicz, R., K. Wikiel, R. Osteryoung, and J. Osteryoung. *Anal. Chem.*, **1989**. 61, 965-972.

60. Bott, A.W. *Curr. Sep.*, **1997**. 16, 23-26.

61. Heering, H.A., M.S. Mondal, and F.A. Armstrong. *Anal. Chem.*, **1999**. 71, 174-182.

62. Barnes, A.S., I. Streeter, and R.G. Compton. *J. Electroanal. Chem.*, **2008**. 623, 129-133.

63. Fatouros, N., D. Krulic, and H. Groult. *J. Electroanal. Chem.*, **2009**. 625, 1-6.

64. Batchelor-McAuley, C., M. Yang, E.M. Hall, and R.G. Compton. *J. Electroanal. Chem.*, **2015**. 758, 1-6.

65. Ramaley, L. and M.S. Krause, Jr. *Anal. Chem.*, **1969**. 41, 1362-1365.

66. O'Dea, J.J., J. Osteryoung, and R.A. Osteryoung. *Anal. Chem.*, **1981**. 53, 695-701.

67. Osteryoung, J.G. and R.A. Osteryoung. *Anal. Chem.*, **1985**. 57, 101A-102A, 105A-106A, 108A, 110A.

68. O'Dea, J.J., *Ph.D. Dissertation*, in *Chemistry*. 1979, Colorado State University: Fort Collins, CO.

69. Osteryoung, J.G. and J.J. O'Dea, *Square-Wave Voltammetry*, *Electroanalytical chemistry: a series of advances*. **1986**, Marcel Dekker, Inc: New York. 209-308

70. O'Dea, J.J., J. Osteryoung, and R.A. Osteryoung. *J. Phys. Chem.*, **1983**. 87, 3911-3918.

71. Kounaves, S.P., J.J. O'Dea, P. Chandresekhar, and J. Osteryoung. *Anal. Chem.*, **1986**. 58, 3199-3202.

72. O'Dea, J.J., J. Osteryoung, and T. Lane. *J. Phys. Chem.*, **1986**. 90, 2761.

73. Whelan, D.P., J.J. O'Dea, and J. Osteryoung. *J. Electroanal. Chem.*, **1986**. 202, 23-36.

74. Zeng, J. and R.A. Osteryoung. *Anal. Chem.*, **1986**. 58, 2766-2771.

75. O'Dea, J.J., K. Wikiel, and J. Osteryoung. *J. Phys. Chem.*, **1990**. 94, 3628-3636.

76. Nuwer, M.J., J.J. O'Dea, and J. Osteryoung. *Anal. Chim. Acta*, **1991**. 251, 13-25.

77. Osteryoung, J. *Chemometr. Intell. Lab. Syst.*, **1991**. 10, 141-154.

78. O'Dea, J.J. and J. Osteryoung. *Anal. Chem.*, **1993**. 65, 3090-3097.

79. O'Dea, J.J., A. Ribes, and J. Osteryoung. *J. Electroanal. Chem.*, **1993**. 345, 287-301.

80. Xu, G., J.J. O'Dea, L.A. Mahoney, and J. Osteryoung. *Anal. Chem.*, **1994**. 66, 808-812.

81. Xu, G., J.J. O'Dea, and J. Osteryoung. *Dyes and Pigments*, **1996**. 30, 201-223.

82. O'Dea, J.J. and J. Osteryoung. *Anal. Chem.*, **1997**. 69, 650--658.

83. Lovrić, M. and M. Branica. *J. Electroanal. Chem. Interfacial Electrochem.*, **1987**. 226, 239-251.

84. Reeves, J.H., S. Song, and E.F. Bowden. *Anal. Chem.*, **1993**. 65, 683-688.

85. Komorsky-Lovrić, Š. and M. Lovrić. *J. Electroanal. Chem.*, **1995**. 384, 115-122.

86. Mirčeski, V. and M. Lovrić. *Electroanalysis*, **1997**. 9, 1283-1287.

87. Barros, A.A., J.A. Rodrigues, P.J. Almeida, P.G. Rodrigues, and A.G. Fogg. *Anal. Chim. Acta*, **1999**. 385, 315-323.

88. Gulaboski, R. and B. Jordanoski. *Glasnik na Hemicarite i Tehnolozite na Makedonija*, **2000**. 19, 177-181.

89. Mirčeski, V., R. Gulaboski, B. Jordanoski, and Š. Komorsky-Lovrić. *J. Electroanal. Chem.*, **2000**. 490, 37-47.

90. Mirčeski, V., M. Lovrić, and R. Gulaboski. *J. Electroanal. Chem.*, **2001**. 515, 91-100.

91. Mirčeski, V. and R. Gulaboski. *Croatica Chemica Acta*, **2003**. 76, 37-48.

92. Lovrić, M. and Š. Komorsky-Lovrić. *Cent. Eur. J. Chem.*, **2010**. 8, 513-518.

93. Brookes, B.A. and R.G. Compton. *J. Phys. Chem. B*, **1999**. 103, 9020-9028.

94. Mirčeski, V., R. Gulaboski, and I. Kuzmanovski. *Glasnik na Hemicarite i Tehnolozite na Makedonija*, **1999**. 18, 57-64.

95. Mirčeski, V., E. Laborda, D. Guziejewski, and R.G. Compton. *Anal. Chem.*, **2013**. 85, 5586-5594.

96. Stojanova, K., R. Gulaboski, V. Mireceski, and S. Petrovska-Jovanovic. *Anal. Lett.*, **1999**. 32, 2937-2950.

97. Gulaboski, R., V. Mirčeski, and Š. Komorsky-Lovrić. *Electroanalysis*, **2002**. 14, 345-355.

98. Mirčeski, V. and R. Gulaboski. *Mikrochimica Acta*, **2002**. 138, 33-42.

99. Gulaboski, R., V. Mirčeski, Š. Komorsky-Lovrić, and M. Lovrić. *Electroanalysis*, **2004**. 16, 832-842.

100. Correia dos Santos, M.M., M.L. Simoes Goncalves, and J.C. Romao. *J. Electroanal. Chem.*, **1996**. 413, 97-103.

101. Miles, A.B. and R.G. Compton. *J. Phys. Chem. B*, **2000**. 104, 5331-5342.

102. Molina, A., C. Serna, and F. Martinez-Ortiz. *J. Electroanal. Chem.*, **2000**. 486, 9-15.

103. Mirčeski, V., R. Gulaboski, and F. Scholz. *Electrochemistry Communications*, **2002**. 4, 814-819.

104. Garay, F. and M. Lovric. *J. Electroanal. Chem.*, **2002**. 518, 91-102.

105. Garay, F. and M. Lovric. *Electroanalysis*, **2002**. 14, 1635-1643.

106. Fatouros, N., D. Krulic, and N. Larabi. *J. Electroanal. Chem.*, **2004**. 568, 55-64.

107. Krulic, D., N. Larabi, and N. Fatouros. *J. Electroanal. Chem.*, **2005**. 579, 239-242.

108. Gulaboski, R., C.M. Pereira, M.N.D.S. Cordeiro, I. Bogeski, E. Ferreira, D. Ribeiro, M. Chirea, and A.F. Silva. *J. Phys. Chem. B*, **2005**. 109, 12549-12559.

109. Mirceski, V., A. Bobrowski, J. Zarebski, and F. Spasovski. *Electrochim. Acta*, **2010**. 55, 8696-8703.

110. Molina, A., J. Gonzalez, E. Laborda, Y.-J. Wang, and R.G. Compton. *Phys. Chem. Chem. Phys.*, **2011**. 13, 16748-16755.

111. Komorsky-Lovrić, S. and M. Lovrić. *Anal. Bioanal. Electrochem.*, **2013**. 5, 291-304.

112. Olmos, J.M., A. Molina, E. Laborda, and F. Martínez-Ortiz. *Electrochim. Acta*, **2015**. 176, 1044–1053.

113. Mirčeski, V. and R. Gulaboski. *Electroanalysis*, **2001**. 13, 1326-1334.

114. Mirčeski, V. and R. Gulaboski. *J. Solid State Electrochem.*, **2003**. 7, 157-165.

115. Gulaboski, R., V. Mirčeski, M. Lovrić, and I. Bogeski. *Electrochemistry Communications*, **2005**. 7, 515-522.

116. Mirceski, V. and F. Quentel. *J. Electroanal. Chem.*, **2005**. 578, 25-35.

117. Mirceski, V., S. Skrzypek, W. Ciesielski, and A. Sokolowski. *J. Electroanal. Chem.*, **2005**. 585, 97-104.

118. Gulaboski, R., M. Lovrić, V. Mirčeski, I. Bogeski, and M. Hoth. *Biophysical Chemistry*, **2008**. 137, 49-55.

119. Gulaboski, R. *J. Solid State Electrochem.*, **2009**. 13, 1015-1024.

120. Gulaboski, R. and L. Mihajlov. *Biophys. Chem.*, **2011**. 155, 1-9.

121. Jordanoski, B., V. Mirčeski, and R. Gulaboski. *Portugaliae Electrochim. Acta*, **1999**. 17, 243-253.

122. Spirevska, I., L. Soptrajanova, and R. Gulaboski. *Anal. Lett.*, **2000**. 33, 919-928.

123. Gulaboski, R., I. Spirevska, L. Soptrajanova, and R. Slavevska. *Anal. Lett.*, **2001**. 34, 1719-1731.

124. Mirčeski, V., R. Gulaboski, S. Petrovska-Jovanovic, and K. Stojanova. *Portugaliae Electrochim. Acta*, **2001**. 19, 25-41.

125. Scholz, F., R. Gulaboski, V. Mirčeski, and P. Langer. *Electrochemistry Communications*, **2002**. 4, 659-662.

126. Scholz, F., R. Gulaboski, and K. Caban. *Electrochemistry Communications*, **2003**. 5, 929-934.

127. Mirčeski, V., R. Gulaboski, and F. Scholz. *J. Electroanal. Chem.*, **2004**. 566, 351-360.

128. Gulaboski, R., V. Mirčeski, C.M. Pereira, M.N.D.S. Cordeiro, A.F. Silva, F. Quentel, M. L'Her, and M. Lovrić. *Langmuir*, **2006**. 22, 3404-3412.

129. Mirčeski, V. and R. Gulaboski. *J. Phys. Chem. B*, **2006**. 110, 2812-2820.

130. Mirceski, V., F. Quentel, M. L'Her, and C. Elleouet. *J. Phys. Chem. C*, **2007**. 111, 8283-8290.

131. Gulaboski, R., M. Lovrić, V. Mirčeski, I. Bogeski, and M. Hoth. *Biophysical Chemistry*, **2008**. 138, 130-137.

132. Mirčeski, V., Š. Komorsky-Lovrić, and M. Lovrić, *Square Wave Voltammetry: Theory and Application*, *Monographs in Electrochemistry*. **2007**, Springer-Verlag: Berlin.

133. Pu, G., S. Wu, and X. Cheng. *Zhongguo Kexue Jishu Daxue Xuebao*, **1986**. 16, 365-366, 364.

134. Chen, X. and G. Pu. *Anal. Lett.*, **1987**. 20, 1511-1519.

135. Pu, G., X. Cheng, and E. Wang. *Yingyong Huaxue*, **1987**. 4, 31-36.

136. Mo, J., P. Cai, Z. Lu, R. Zhang, and Y. Zou. *Fenxi Huaxue*, **1995**. 23, 250-254.

137. Pu, G., X. Cheng, and E. Wang. *Yingyong Huaxue*, **1988**. 5, 32-37.

138. Miao, W., J. Mo, P. Cai, and R. Zhang. *Fenxi Ceshi Xuebao*, **1995**. 14, 1-5.

139. Mo, J., W. Miao, P. Cai, and R. Zhang. *Fenxi Ceshi Xuebao*, **1993**. 12, 16-20.

140. Jadreško, D. and M. Zelić. *J. Electroanal. Chem.*, **2014**. 714-715, 30-37.

141. Mo, J., W. Miao, P. Cai, and R. Zhang. *Fenxi Ceshi Xuebao*, **1995**. 14, 1-6.

142. Mo, J., R. Zhang, Z. Lu, P. Cai, and Y. Zou. *Fenxi Huaxue*, **1995**. 23, 255-258.

143. Cai, P., W. Miao, J. Mo, and R. Zhang. *Fenxi Ceshi Xuebao*, **1995**. 14, 33-38.

144. Molina, A., E. Torralba, C. Serna, and J.A. Ortuno. *Electrochim. Acta*, **2013**. 106, 244-257.

145. Gonzalez, J., C.M. Soto, and A. Molina. *Open Electrochem. J.*, **2009**. 1, 37-41.

146. Camacho, L., J.J. Ruiz, C. Serna, A. Molina, and J. Gonzalez. *J. Electroanal. Chem.*, **1997**. 422, 55-60.

147. Galik, M., A.M. O'Mahony, and J. Wang. *Electroanalysis*, **2011**. 23, 1193-1204.

148. Helfrick, J.C., Jr., *Cyclic square wave voltammetry*, in *Chemistry*. 1989, Georgia Inst. Technol.: Atlanta, GA, USA. p. 408.

149. Helfrick, J.C., Jr. and L.A. Bottomley. *Anal. Chem.*, **2009**. 81, 9041-9047.

150. Smith, D.E. *Anal. Chem.*, **1963**. 35, 602-609.

151. Nicholson, R.S. and M.L. Olmstead, *Electrochemistry: Calculations, Simulation and Instrumentation,*. **1972**, Marcel Dekker: New York. Ch. 5

CHAPTER 2

THE CSWV MATHEMATICAL DERIVATION METHOD AND THEORETICAL PEAK PARAMETER NOMENCLATURE

2.1 Introduction

The simulation of each mechanism investigated in this thesis required a mathematical derivation to predict current as a function of time and potential. The manner in which the final equation is derived for each mechanism is similar. The general method used is provided in detail in this chapter. First, the derivation of the surface-confined mechanism is shown as an example for all of the mechanisms within this thesis. Next, the diffusion controlled electrode reactions are addressed. The reactions and conditions that define each mechanism can be found in Tables 2.1-2.3. The final equation used to generate voltammograms is located both in Table 2.4 and within the chapter for the respective mechanism. The method for the variation of empirical parameters and the nomenclature used to describe peak parameters throughout this thesis is also described in this chapter.

2.2 Surface-Confined Process

Chapter 4 investigates the case in which both the reactant and product of the electron transfer are confined to the surface. This mechanism excludes all three types of mass transport, can be applied to spherical or planar electrodes, and does not consider interactions between molecules. This is the simplest mechanism presented in this thesis as Fick's laws of diffusion were excluded. Therefore, it will be used as an example for other more complicated diffusion-controlled mechanisms.

The derivation began by writing a reaction for the two electroactive species:

$$Ox_{(ads)} + ne^- \rightleftharpoons Red_{(ads)} \tag{2.1}$$

Next, the initial conditions are written. At time t = 0, only $Ox_{(ads)}$ is present on the electrode surface for the surface-confined mechanism.

$$\Gamma_{Ox} = \Gamma^*$$

$$\Gamma_{Red} = 0$$

Then, the boundary conditions are written. At time t > 0, $Ox_{(ads)}$ is converted to $Red_{(ads)}$, as expressed by the equations below.

$$\Gamma^* = \Gamma_{Ox} + \Gamma_{Red}$$

$$\Gamma_{Red} = \int_0^t \frac{i(\tau)}{nFA} d\tau$$

The boundary conditions are applied, and the concentration of $Ox_{(ads)}$ at the electrode surface can be rewritten as

$$\Gamma_{Ox} = \Gamma^* - \Gamma_{Red} \tag{2.2}$$

$$\Gamma_{Ox} = \Gamma^* - \int_0^t \frac{i(\tau)}{nFA} d\tau \tag{2.3}$$

For ease, the following substitutions are made:

$$\text{Let } H = \frac{1}{nFA} \tag{2.4}$$

and $I = \int_0^t i(\tau)d\tau$ (2.5)

So that expressions for Γ_{Ox} and Γ_{Red} become

$$\Gamma_{Ox} = \Gamma^* - HI \tag{2.6}$$

$$\Gamma_{Red} = HI \tag{2.7}$$

At this point, the surface excess concentrations of each species can be inserted into an equation which relates the concentration to potential and current. A form of the Butler-Volmer equation is used for electroactive species confined to the electrode surface:

$$i = nFAk^0\left[\Gamma_{Ox}e^{-\alpha\phi} - \Gamma_{Red}e^{(1-\alpha)\phi}\right] \tag{2.8}$$

where $\phi = \frac{nF}{RT}\left(E^0 - E_{applied}\right)$, α is the transfer coefficient, n is the number of electrons transferred, R is the gas constant, T is temperature, F is the Faraday constant, E^0 is the formal potential for the redox reaction, $E_{applied}$ is the applied potential, and k^0 is the electron transfer rate constant.

Substituting Equations 2.6 and 2.7 into 2.8 yields

$$i = nFAk^0\left[\left(\Gamma^* - \mathrm{HI}\right)e^{-\alpha\phi} - \mathrm{HI}e^{(1-\alpha)\phi}\right] \tag{2.9}$$

The current in Equation 2.9 is dependent on the area of the electrode and Γ^*. To convert the current to a dimensionless current that eliminates these two variables and is more generalized, the following transformation can be used

$$i(t) = \frac{nFA\Gamma^*}{\tau}\Psi(t) \qquad \text{or} \qquad i(t) = \frac{\Gamma^*}{H\tau}\Psi(t) \tag{2.10}$$

Combination of Equations 2.9 and 2.10 yields

$$\Psi(t)\frac{nFA\Gamma^*}{\tau} = nFAk^0\left[\left(\Gamma^* - \Psi(t)\frac{\Gamma^*}{\tau}\right)e^{-\alpha\phi} - \Psi(t)\frac{\Gamma^*}{\tau}e^{(1-\alpha)\phi}\right] \tag{2.11}$$

Equation 11 can be simplified as:

$$\Psi(t) = \frac{k^0\tau}{\Gamma^*}\left[\left(\Gamma^* - \Psi(t)\frac{\Gamma^*}{\tau}\right)e^{-\alpha\varphi} - \Psi(t)\frac{\Gamma^*}{\tau}e^{(1-\alpha)\varphi}\right] \tag{2.12}$$

And further reduced as:

$$\Psi(t) = \left(k^0\tau - k^0\Psi(t)\right)e^{-\alpha\varphi} - k^0\Psi(t)e^{(1-\alpha)\varphi} \tag{2.13}$$

To approximate the integrals in the dimensionless current, a numerical summation can be used by dividing each time step into subintervals. The numerical solution for Equation 2.13 can be written using a variation of the Nicholson and Olmstead method[1] for all mechanisms.

$$\Psi_m = \left(k^0\tau - \frac{k^0\tau}{2L}\sum_{i=1}^{m}\Psi_i\right)e^{-\alpha\phi} - \frac{k^0\tau}{2L}\sum_{i=1}^{m}\Psi_i e^{(1-\alpha)\phi} \tag{2.14}$$

Separating the first term in the summation yields

$$\Psi_m + \frac{k^0\tau}{2L}\Psi_m e^{-\alpha\phi} + \frac{k^o\tau}{2L}\Psi_m e^{(1-\alpha)\phi} = \left(k^0\tau - \frac{k^0\tau}{2L}\sum_{i=1}^{m-1}\Psi_i\right)e^{-\alpha\phi} - \frac{k^0\tau}{2L}\sum_{i=1}^{m-1}\Psi_i e^{(1-\alpha)\phi} \tag{2.15}$$

Solving for Ψ_m yields

$$\Psi_m = \frac{\left(k^0\tau - \frac{k^0\tau}{2L}\sum_{i=1}^{m-1}\Psi_i\right)e^{-\alpha\phi} - \frac{k^0\tau}{2L}\sum_{i=1}^{m-1}\Psi_i e^{(1-\alpha)\phi}}{1 + \frac{k^0\tau}{2L}e^{-\alpha\phi} + \frac{k^0\tau}{2L}e^{(1-\alpha)\phi}} \tag{2.16}$$

The recursive calculation of current Ψ_m on each step for every step in the potential waveform was performed in MATLAB. From this, voltammograms representing the surface-confined mechanism and the impact of the variation of empirical parameters on the waveshape were investigated. Trends in peak parameters were examined as a function of the empirical parameter varied. From these trends, diagnostic criteria for this mechanism can be established as well as a means to determine kinetic parameters like the electron transfer coefficient and electron transfer rate. Furthermore, a protocol for an experimentalist to identify the surface-confined mechanism and ascertain kinetic parameters can be elucidated.

2.3 Diffusion-Controlled Processes

Molecules can be transported to the electrode surface by convection, migration, and/or diffusion. Convection occurs when there is a physical disturbance to the analyte/electrolyte solution such as a stirrer being used to constantly bring new species to the electrode surface from the bulk solution or a rotating working electrode acting in the same manner. Migration is an electrostatic interaction that occurs when a charged species in solution is attracted to an electrode of opposite charge or repelled from an electrode of similar charge. Diffusion occurs as a result of unequal distribution of species in the analyte/electrolyte solution, i.e., a concentration gradient. Species in high concentration areas move to areas in the solution with low concentrations of that species, namely, the working electrode. The mechanisms investigated in Chapters 3 and 5-10

only consider diffusion as the mode of mass transport in most electrochemical experiments are not performed under stirring conditions and have sufficient concentrations of electrolyte to negate the effects of migration. Furthermore, these mechanisms were derived for the case of planar working electrode and semi-infinite linear diffusion.

The overall approach to deriving an equation that predicts current as a function of time and potential for the diffusion controlled case is similar to that for the surface-confined case. The derivation for these mechanisms began by writing a reaction for all species involved in the electrode reaction sequence, including both electroactive and electro-inactive species as shown in column 2 in Tables 2.1-2.3. Next, expressions of Fick's laws of diffusion were written for each species as shown in column 3 of Table 2.1. These equations are used to describe the concentration of each species as a function of distance from the electrode and time. These expressions were solved by using Laplace transformations and application of appropriate boundary conditions for each case as shown in columns 4-6 in Table 2.1-2.3. The resultant concentrations of the electroactive components are plugged into either the Nernst equation for reversible electron transfers (mechanisms 5-8) or the Erdey-Gruz and Volmer equation for kinetically-controlled electron transfers (mechanisms 3, 7, 9, and 10). From this, numerical approximations of the resultant integrals representing current as a function of time and potential were performed in the same manner previously established by Nicholson and Olmstead.[1] Like the surface-confined case, voltammograms are generated in MATLAB by using the final equations listed in Table 2.4. Empirical parameters are varied so that the diagnostic trends for each mechanism can be identified.

2.4 Specifics of Empirical Parameter Variation and Nomenclature

The empirical parameters used to describe the CSWV waveform are presented in Figure 2.1. The systematic variation of period (τ), amplitude (E_{sw}), and increment (δE) is executed over the following intervals: 1 ms $\leq \tau \leq$ 5 s, 10 mV $\leq E_{sw} \leq$ 90 mV, 1 mV $\leq \delta E \leq$ 25 mV, and L = 20 over each period. Switching potential is varied by extending the sweep past E^0 by 100 mV per sweep. Period limits were set in consideration of typical potentiostat rise times, commonly encountered solution resistances and electrode double layer capacitances as well as the time duration required per scan. Amplitude limits were set in accordance with the range typically used in SWV. Increment limits were set in consideration of the number of points to define the peak. Specific parameter levels for simulated data are denoted by open circles and listed in the figure captions.

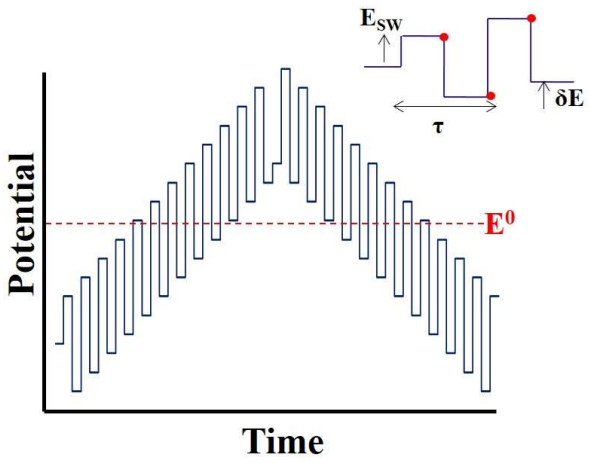

Figure 2.1. The CSWV waveform and the empirical parameters used to describe the waveform (inset).

Voltammograms were calculated for the singular case where the number of electrons

is always one. The predicted difference current, $\Delta\Psi$, is computed from $\Psi_{\text{forward pulse}}$ - $\Psi_{\text{reverse pulse}}$. The corresponding potential for $\Delta\Psi$ is the average of the corresponding forward and reverse potential pulses. The forward difference current, $\Delta\Psi_f$ denotes the difference currents acquired over the interval $E_{initial}$ to the switching potential E_λ, and the difference current, $\Delta\Psi_r$, denotes difference currents acquired over the reverse potential sweep from E_λ to the final potential, E_{final}. To capture the effect of period as it relates to current, $\Delta\Psi^+$ is used to describe diffusion-controlled processes where

$$\Delta\Psi^+ = \Delta\Psi \Big/ \sqrt{\tau} \tag{2.17}$$

For the surface-confined process, $\Delta\Psi^s$ is used where

$$\Delta\Psi^s = \Delta\Psi \Big/ \tau \tag{2.18}$$

The physical meaning of $\Delta\Psi^+$ and $\Delta\Psi^s$ are the normalized faradaic current emanating from the electron transfer. The plotting convention used herein treats reduction currents as positive and oxidative currents as negative values. Figures of merit that describe the shape of the voltammogram are: $\Delta\Psi^+_{p,f}$ and $\Delta\Psi^+_{p,r}$ the net peak currents on the forward and reverse sweep, peak ratio $\Delta\Psi^+_{p,r} \Big/ \Delta\Psi^+_{p,f}$, $E_{p,f}$ and $E_{p,r}$ the peak potentials on the forward and reverse sweep, ΔE_p the peak separation defined as $E_{p,r} - E_{p,f}$, and $W_{1/2,f}$ and $W_{1/2,r}$ the peak widths measured at half peak maximum. For the surface-confined case, all figures of merit are the same except for the net peak currents, $\Delta\Psi^s_{p,f}$ and $\Delta\Psi^s_{p,r}$, and peak ratio $\Delta\Psi^s_{p,r} \Big/ \Delta\Psi^s_{p,f}$.

2.5. Summary

This chapter has outlined the method used to derive the final equations for each mechanism investigated in this thesis. This chapter includes tables containing the reactions for each mechanism as well as the diffusion equations (where applicable), the initial and boundary conditions, and the final equations coded in MATLAB. Furthermore, the nomenclature used to describe the peak parameters throughout this thesis.

Table 2.1. The reactions, diffusion equations, and boundary conditions for kinetically controlled mechanisms.

Chapter	Reaction	Diffusion Equations	Initial Conditions	Boundary Conditions	
				$t > 0$ & $x \rightarrow \infty$	$t > 0$ & $x = 0$
3 – Quasi-reversible	$Ox + ne^- \underset{k_2}{\overset{k_1}{\leftrightarrow}} Red$	$\frac{\partial C_{Ox}(x,t)}{\partial t} = D_{Ox}\frac{\partial^2 C_{Ox}(x,t)}{\partial x^2}$ $\frac{\partial C_{Red}(x,t)}{\partial t} = D_{Red}\frac{\partial^2 C_{Red}(x,t)}{\partial x^2}$	$C_{Ox}(x,0) = C^*_{Ox}$ $C_{Red}(x,0) = 0$	$C_{Ox}(\infty,t) \rightarrow C^*_{Ox}$ $C_{Red}(\infty,t) \rightarrow 0$	$D_{Ox}\frac{\partial C_{Ox}(x,t)}{\partial x} = -D_{Red}\frac{\partial C_{Red}(x,t)}{\partial x} = \frac{i(t)}{nFA}$
4 – Surface-Confined	$Ox_{(ads)} + ne^- \underset{k_2}{\overset{k_1}{\leftrightarrow}} Red_{(ads)}$	Not applicable	$\Gamma_{Ox} = \Gamma^*$ $\Gamma_{Red} = 0$	Not applicable	$\Gamma^* = \Gamma_{Ox} + \Gamma_{Red}$ $\Gamma_{Red} = \int_0^t \frac{i(\tau)}{nFA} d\tau$

Table 2.2. The reactions, diffusion equations, and boundary conditions for chemically coupled mechanisms.

Chapter	Reaction	Diffusion Equations	Initial Conditions	Boundary Conditions	
				$t > 0$ & $x \rightarrow \infty$	$t > 0$ & $x = 0$
5 – EC	$Ox + ne^- \leftrightarrow Red$ $Red \underset{k_b}{\overset{k_f}{\leftrightarrow}} Z$ $K = k_f / k_b$	$\frac{\partial C_{Ox}(x,t)}{\partial t} = D_{Ox}\frac{\partial^2 C_{Ox}(x,t)}{\partial x^2}$ $\frac{\partial C_{Red}(x,t)}{\partial t} = D_{Red}\frac{\partial^2 C_{Red}(x,t)}{\partial x^2} + k_b[C_z - KC_{Red}]$ $\frac{\partial C_z(x,t)}{\partial t} = D_z\frac{\partial^2 C_z(x,t)}{\partial x^2} + k_b[C_z - KC_{Red}]$	$C_{Ox}(x,0) = C^*_{Ox}$ $C_{Red}(x,0) = 0$ $C_Z(x,0) = 0$	$C_{Ox}(\infty,t) \rightarrow C^*_{Ox}$ $C_{Red}(\infty,t) \rightarrow 0$ $C_Z(\infty,t) \rightarrow 0$	$D_{Ox}\frac{\partial C_{Ox}(x,t)}{\partial x} = -D_{Red}\frac{\partial C_{Red}(x,t)}{\partial x} = \frac{i(t)}{nFA}$ $D_Z\frac{\partial C_Z(x,t)}{\partial x} = 0$
6 – CE	$Y \underset{k_b}{\overset{k_f}{\leftrightarrow}} Ox$ $Ox + ne^- \leftrightarrow Red$ $K = k_f / k_b$	$\frac{\partial C_Y(x,t)}{\partial t} = D_Y\frac{\partial^2 C_Y(x,t)}{\partial^2 x} - k_f[C_Y - C_{Ox}/K]$ $\frac{\partial C_{Ox}(x,t)}{\partial t} = D_{Ox}\frac{\partial^2 C_{Ox}(x,t)}{\partial^2 x} + k_f[C_Y - C_{Ox}/K]$ $\frac{\partial C_{Red}(x,t)}{\partial t} = D_{Red}\frac{\partial^2 C_{Red}(x,t)}{\partial^2 x}$	$C_{Ox}(x,0) +$ $C_Y(x,0) = C^T$ $\frac{C_{Ox}(x,0)}{C_Y(x,0)} = K$ $C_{Red}(x,0) = 0$	$C_{Ox}(\infty,t) +$ $C_Y(\infty,t) \rightarrow C^T$ $\frac{C_{Ox}(\infty,t)}{C_Y(\infty,t)} \rightarrow K$ $C_{Red}(\infty,t) \rightarrow 0$	$D_{Ox}\frac{\partial C_{Ox}(x,t)}{\partial x} = -D_{Red}\frac{\partial C_{Red}(x,t)}{\partial x} = \frac{i(t)}{nFA}$ $D_Y\frac{\partial C_Y(x,t)}{\partial x} = 0$
7 - EC_{cat}	$Ox + ne^- \leftrightarrow Red$ $Red \xrightarrow{k_{apparent}} Ox$	$\frac{\partial C_{Ox}(x,t)}{\partial t} = D_{Ox}\frac{\partial^2 C_{Ox}(x,t)}{\partial x^2} + kC_{Red}(x,t)$ $\frac{\partial C_{Red}(x,t)}{\partial t} = D_{Red}\frac{\partial^2 C_{Red}(x,t)}{\partial x^2} - kC_{Red}(x,t)$	$C_{Ox}(x,0) = C^*_{Ox}$ $C_{Red}(x,0) = 0$	$C_{Ox}(\infty,t) \rightarrow C^*_{Ox}$ $C_{Red}(\infty,t) \rightarrow 0$	$D_{Ox}\frac{\partial C_{Ox}(x,t)}{\partial x} = -D_{Red}\frac{\partial C_{Red}(x,t)}{\partial x} = \frac{i(t)}{nFA}$
8 – ECE	$Ox_1 + n_1e^- \leftrightarrow Red_1$ $Red_1 \underset{k_b}{\overset{k_f}{\leftrightarrow}} Ox_2$ $Ox_2 + n_2e^- \leftrightarrow Red_2$ $K = k_f / k_b$	$\frac{\partial C_{Ox_1}(x,t)}{\partial t} = D_{Ox_1}\frac{\partial^2 C_{Ox_1}(x,t)}{\partial^2 x}$ $\frac{\partial C_{Red_1}(x,t)}{\partial t} = D_{Red_1}\frac{\partial^2 C_{Red_1}(x,t)}{\partial^2 x} + k_b[C_{Ox_2} - KC_{Red_1}]$ $\frac{\partial C_{Ox_2}(x,t)}{\partial t} = D_{Ox_2}\frac{\partial^2 C_{Ox_2}(x,t)}{\partial^2 x} - k_b[C_{Ox_2} - KC_{Red_1}]$ $\frac{\partial C_{Red_2}(x,t)}{\partial t} = D_{Red_2}\frac{\partial^2 C_{Red_2}(x,t)}{\partial^2 x}$	$C_{Ox_1}(x,0) = C^*_{Ox_1}$ $C_{Red_1}(x,0) = 0$ $C_{Ox_2}(x,0) = 0$ $C_{Red_2}(x,0) = 0$	$C_{Ox_1}(\infty,t) = C^*_{Ox_1}$ $C_{Red_1}(\infty,t) = 0$ $C_{Ox_2}(\infty,t) = 0$ $C_{Red_2}(\infty,t) = 0$	$D_{Ox_1}\frac{\partial C_{Ox_1}(x,t)}{\partial x} = -D_{Red_1}\frac{\partial C_{Red_1}(x,t)}{\partial x} = \frac{i_1(t)}{n_1FA}$ $D_{Ox_2}\frac{\partial C_{Ox_2}(x,t)}{\partial x} = -D_{Red_2}\frac{\partial C_{Red_2}(x,t)}{\partial x} = \frac{i_2(t)}{n_2FA}$

Table 2.3. The reactions, diffusion equations, and boundary conditions for chemically coupled and kinetically controlled mechanisms.

Chapter	Reaction	Diffusion Equations	Initial Conditions	Boundary Conditions	
				$t > 0$ & $x \rightarrow \infty$	$t > 0$ & $x = 0$
7 – E_qC_{cat}	$Ox + ne^- \underset{k_2}{\overset{k_1}{\leftrightarrow}} Red$ $Red \xrightarrow{k_{apparent}} Ox$	Same as EC_{cat}	Same as EC_{cat}	Same as EC_{cat}	Same as EC_{cat}
9 – E_qC	$Ox + ne^- \underset{k_2}{\overset{k_1}{\leftrightarrow}} Red$ $Red \underset{k_b}{\overset{k_f}{\leftrightarrow}} Z$	Same as EC	Same as EC	Same as EC	Same as EC
10 - CE_q	$Y \underset{k_b}{\overset{k_f}{\leftrightarrow}} Ox$ $Ox + ne^- \underset{k_2}{\overset{k_1}{\leftrightarrow}} Red$	Same as CE	Same as CE	Same as CE	Same as CE

Table 2.4. The final equations coded in MATLAB for all mechanisms in this thesis.

Chapter	Final Equation	References in Agreement with Final Equation
3 – Quasi-reversible	$\Psi_m = \frac{\kappa\sqrt{\pi\tau}\exp(-\alpha\varphi)\left[\left(1-\frac{1}{\pi}\sqrt{\frac{2}{L}}\sum_{i=1}^{m-1}\Psi_i S_j\right)-\exp(\varphi)\frac{1}{\pi}\sqrt{\frac{2}{L}}\sum_{i=1}^{m-1}\Psi_i S_j\right]}{1+\kappa\sqrt{\pi\tau}\exp(-\alpha\varphi)\frac{1}{\pi}\sqrt{\frac{2}{L}}+\kappa\sqrt{\pi\tau}\exp(-\alpha\varphi)\exp(\varphi)\frac{1}{\pi}\sqrt{\frac{2}{L}}}$	2-8
4 – Surface-Confined	$\Psi_m = \frac{\left(k^0\tau-\frac{k^0\tau}{2L}\sum_{i=1}^{m-1}\Psi_i\right)e^{-\alpha\varphi}-\frac{k^0\tau}{2L}\sum_{i=1}^{m-1}\Psi_i e^{(1-\alpha)\varphi}}{1+\frac{k^0\tau}{2L}e^{-\alpha\varphi}+\frac{k^0\tau}{2L}e^{(1-\alpha)\varphi}}$	7, 8
5 – EC	$\Psi_m = \frac{\frac{(k\pi\tau)^{1/2}}{\varepsilon}-\left(\frac{1}{K+1}+\frac{1}{\varepsilon}\right)\left(\frac{2k\tau}{L\pi}\right)^{1/2}\sum_{i=1}^{i=m-1}\Psi_i S_j-\left(\frac{K}{K+1}\right)\sum_{i=1}^{i=m-1}\Psi_i R_j}{\left(\frac{1}{K+1}+\frac{1}{\varepsilon}\right)\left(\frac{2k\tau}{L\pi}\right)^{1/2}+\left(\frac{K}{K+1}\right)R_1}$	3, 5, 7, 9
6 – CE	$\Psi_m = \frac{\left(\frac{K(k\pi\tau)^{1/2}}{K+1}\right)-\left[\varepsilon+\left(\frac{K}{K+1}\right)\right]\left(\frac{2k\tau}{\pi L}\right)^{1/2}\sum_{i=1}^{i=m-1}\Psi_i S_j-\frac{1}{K+1}\sum_{i=1}^{i=m-1}\Psi_i R_j}{\left[\varepsilon+\left(\frac{K}{K+1}\right)\right]\left(\frac{2k\tau}{\pi L}\right)^{1/2}+\frac{1}{K+1}R_1}$	3, 5, 7
7 - EC_{cat}	$\Psi_m = \frac{\frac{(\pi k_{apparent}\tau)^{1/2}}{(1+\varepsilon)}-\sum_{i=1}^{m-1}\Psi_i R_j}{R_1}$	3, 5, 7
7 - E_qC_{cat}	$\Psi_m = \frac{\sqrt{\pi}-\sqrt{\frac{1}{k_{apparent}\tau}}\sum_{i=1}^{m-1}\Psi_i R_j-\varepsilon\sqrt{\frac{1}{k_{apparent}\tau}}\sum_{i=1}^{m-1}\Psi_i R_j}{\frac{1}{\kappa\varepsilon^{-\alpha}\sqrt{\tau}}+\frac{1}{\sqrt{k_{apparent}\tau}}R_1+\frac{\varepsilon}{\sqrt{k_{apparent}\tau}}R_1}$	7

Table 2.4. Continued

Chapter	Final Equation	References in Agreement with Final Equation
8 – ECE	$\Psi_{m1} = \dfrac{\pi\left(\frac{L}{2}\right)^{1/2} - \sum_{i=1}^{i=m-1}\Psi_{i1}S_j - \varepsilon_1\left(\frac{\pi L}{2k_f\tau}\right)^{1/2}\sum_{i=1}^{i=m-1}\Psi_{i1}R_j}{S_1 + R_1\varepsilon_1\left(\frac{\pi L}{2k_f\tau}\right)^{1/2}}$ $\Psi_{m2} = \dfrac{\sum_{i=1}^{i=m}\Psi_{i1}S_j - \sum_{i=1}^{i=m-1}\Psi_{i2}S_j - \left(\frac{\pi L}{2k_f\tau}\right)^{1/2}\sum_{i=1}^{i=m}\Psi_{i1}R_j - \varepsilon_2\sum_{i=1}^{i=m-1}\Psi_{i2}S_j}{\varepsilon_2 + S_1}$ $\Psi_{total} = n_1\Psi_{m1} + n_2\Psi_{m2}$	5, 7, 9, 10
9 – E_qC	$\Psi_m = \dfrac{\sqrt{\pi} - \left(\frac{2}{\pi L}\right)^{1/2}\left(1+\left(\frac{\varepsilon}{(K+1)}\right)\right)\sum_{i=1}^{i=m-1}\Psi_i S_j - \left(\frac{K\varepsilon}{(K+1)\sqrt{k\tau}}\right)\sum_{i=1}^{i=m-1}\Psi_i R_j}{\frac{1}{\kappa\varepsilon^{-\alpha}\sqrt{\tau}} + \left(\frac{2}{\pi L}\right)^{1/2}\left(1+\left(\frac{\varepsilon}{(K+1)}\right)\right) + \left(\frac{K\varepsilon}{(K+1)\sqrt{k\tau}}\right)R_1}$	7, 8
10 - CE_q	$\Psi_m = \dfrac{\frac{K\sqrt{\pi}}{K+1} - \left(\varepsilon + \frac{K}{(K+1)}\right)\left(\frac{2}{\pi L}\right)^{1/2}\sum_{i=1}^{i=m-1}\Psi_i S_j - \left(\frac{1}{(K+1)}\right)\left(\frac{1}{k\tau}\right)^{1/2}\sum_{i=1}^{i=m-1}\Psi_i R_j}{\frac{1}{\kappa\varepsilon^{-\alpha}\tau^{1/2}} + \left(\frac{1}{(K+1)}\right)\left(\frac{1}{k\tau}\right)^{1/2}R_1 + \left(\varepsilon + \frac{K}{(K+1)}\right)\left(\frac{2}{\pi L}\right)^{1/2}}$	7

2.6 References

1. Nicholson, R.S. and M.L. Olmstead, *Electrochemistry: Calculations, Simulation and Instrumentation,*. **1972**, Marcel Dekker: New York. Ch. 5

2. O'Dea, J.J., *Ph.D. Dissertation*, in *Chemistry*. 1979, Colorado State University: Fort Collins, CO.

3. O'Dea, J.J., J. Osteryoung, and R.A. Osteryoung. *Anal. Chem.*, **1981**. 53, 695-701.

4. Osteryoung, J.G. and J.J. O'Dea, *Square-Wave Voltammetry*, *Electroanalytical chemistry: a series of advances*. **1986**, Marcel Dekker, Inc: New York. 209-308

5. Helfrick, J.C., Jr., *Cyclic square wave voltammetry*, in *Chemistry*. 1989, Georgia Inst. Technol.: Atlanta,GA,USA. p. 408.

6. Nuwer, M.J., J.J. O'Dea, and J. Osteryoung. *Anal. Chim. Acta*, **1991**. 251, 13-25.

7. Mirčeski, V., Š. Komorsky-Lovrić, and M. Lovrić, *Square Wave Voltammetry: Theory and Application*, *Monographs in Electrochemistry*. **2007**, Springer-Verlag: Berlin.

8. Mirčeski, V., E. Laborda, D. Guziejewski, and R.G. Compton. *Anal. Chem.*, **2013**. 85, 5586-5594.

9. Miles, A.B. and R.G. Compton. *J. Phys. Chem. B*, **2000**. 104, 5331-5342.

10. O'Dea, J.J., K. Wikiel, and J. Osteryoung. *J. Phys. Chem.*, **1990**. 94, 3628-3636.

CHAPTER 3

THE QUASIREVERSIBLE MECHANISM

3.1 Introduction

The quasireversible mechanism is often referred to as irreversible or kinetically-controlled as the homogeneous electron transfer kinetics are sluggish in comparison to a reversible reaction. Over the years, the quasireversible mechanism has been considered by a variety of electrochemical techniques. [1-12] Additionally, the quasireversible mechanism has been investigated by SWV.[13-20] These collective developments have presented the identification of the mechanism and determination of the electron transfer rate.

Though much theory describing the quasireversible mechanism has been presented in the literature, the literature associated with CV does not account for the recent advances in instrumentation, i.e., the conversion from analog to digital. Furthermore, even though a vast amount of literature is present for SWV, seldom is the information used by non-electrochemists. Oftentimes, improper assignment of the formal potential may happen when using SWV as the peak potential may be displaced from the formal potential. Including the reverse sweep by using CSWV allows to experimentalist to more accurately determine E^0. The goals of this chapter are to 1) develop the diagnostic criteria for the

diffusional, quasireversible mechanism using CSWV, 2) provide a protocol in which experimenters can identify their reaction mechanism and determine the kinetic parameters, and 3) provide experimental verification of the diagnostic criteria in which the formal potential and electron transfer parameters have been determined via CSWV for a well-known quasireversible reaction.

3.2 Experimental

Experimental verification was obtained using a Pine Instruments WaveNow USB Potentiostat. Voltammograms were acquired at a static mercury drop electrode (EG&G PARC Model 303A), an Ag/AgCl reference electrode with 0.5 M KCl filling solution, and a Pt counter electrode. All solutions were sparged with N_2 to remove dissolved O_2. The analytes were reagent grade and used as received from Sigma Aldrich.

3.3 Results and Discussion

3.3.1 Theory

For the reaction generalized quasireversible reaction

$$Ox + ne^- \underset{k_2}{\overset{k_1}{\leftrightarrow}} Red \tag{3.1}$$

the rate of formation of Red = $k_1 C_{Ox}(0,t)$, and the rate of formation of Ox = $k_2 C_{Red}(0,t)$ where k_1 is the forward rate constant (cm/sec), k_2 is the reverse rate constant (cm/sec), $C_{Ox}(0,t)$ is the surface concentration of Ox (mol/cm^3), and $C_{Red}(0,t)$ is the surface concentration of Red (mol/cm^3). Both rate constants are dependent on the applied potential:

$$k_1 = k^0 \exp\left[\frac{-\alpha nF(E_{applied} - E^0)}{RT}\right] \tag{3.2}$$

$$k_2 = k^0 \exp\left[\frac{(1-\alpha)nF(E_{applied} - E^0)}{RT}\right] \tag{3.3}$$

where k^0 is the standard rate constant (cm/sec), α is the transfer coefficient, F is the Faraday constant, $E_{applied}$ is the applied potential, E^0 is the formal potential, and n is the number of electrons transferred. Equations 3.2 and 3.3 implicitly assume that α is independent of potential. For a quasireversible electron transfer, the current, potential, and surface concentrations of Ox and Red are related through the Erdey-Gruz and Volmer equation[13, 21]:

$$i(t) = \frac{nFA}{D_{Ox}^{(1-\alpha)/2} D_{Red}^{\alpha/2}} k^0 \exp\left[\left(\frac{-\alpha nF}{RT}\right)\left(E_{applied} - E^0\right)\right]\left[\sqrt{D_{Ox}} C_{Ox}(0,t) - \exp\left[\left(\frac{nF}{RT}\right)\left(E_{applied} - E^0\right)\right]\sqrt{D_{Red}} C_{Red}(0,t)\right] \tag{3.4}$$

where D_{Ox} = diffusion coefficient of Ox (cm^2/sec), and D_{Red} = diffusion coefficient of Red (cm^2/sec). To provide a current that is independent of electrode area and concentration of the electroactive species, the current is made dimensionless by using the following form of Erdey-Gruz and Volmer equation:

$$\Psi(t) = \left[\frac{\sqrt{\pi\tau}}{\sqrt{D_{Ox}} C_{Ox}^*}\right] \frac{k^0}{D_{Ox}^{(1-\alpha)/2} D_{Red}^{\alpha/2}} \exp(-\alpha\phi)\left[\sqrt{D_{Ox}} C_{Ox}(0,t) - \exp(\phi)\sqrt{D_{Red}} C_{Red}(0,t)\right] \tag{3.5}$$

where $\phi = \left[\left(\frac{nF}{RT}\right)\left(E_{applied} - E^0\right)\right]$ and τ = period (sec).

Integrals representing the current as a function of time and potential are replaced with summations and solved by using numerical methods.[22] The final equation coded in MATLAB to generate voltammograms for the quasireversible mechanism is:

$$\Psi_m = \frac{\kappa\sqrt{\pi\tau}\exp(-\alpha\phi)\left[\left(1-\frac{1}{\pi}\sqrt{\frac{2}{L}}\sum_{i=1}^{m-1}\Psi_i S_j\right)-\exp(\phi)\frac{1}{\pi}\sqrt{\frac{2}{L}}\sum_{i=1}^{m-1}\Psi_i S_j\right]}{1+\kappa\sqrt{\pi\tau}\exp(-\alpha\phi)\frac{1}{\pi}\sqrt{\frac{2}{L}}+\kappa\sqrt{\pi\tau}\exp(-\alpha\phi)\exp(\phi)\frac{1}{\pi}\sqrt{\frac{2}{L}}} \tag{3.6}$$

In the following sections, the results of simulations for the variation of empirical parameters for the quasireversible mechanism are presented, first holding $\alpha = 0.5$ and log $k^0 = -3$. Later, the effects of k^0 and α are examined, followed by a description of diagnostic criteria that can be used to identify a kinetically controlled reaction. This chapter concludes with experimental verification of the diagnostic criteria, a protocol for evaluating data, and a comparison with the diagnostic criteria for the reversible mechanism.

3.3.2 Effect of period (τ)

A series of voltammograms in which period is varied is shown in Figure 3.1. As period increases, $\Delta\Psi^{+}_{p,f}$ and $\Delta\Psi^{+}_{p,r}$ magnitudes decrease and both $E_{p,f}$ and $E_{p,r}$ shift towards the formal potential, resulting in peak separation that approaches zero (see inset of Figure 3.1). As peak separation approaches zero, peak ratios increasing toward a value of one. Peak widths also depend on period. For both the forward and reverse sweeps, the peak widths decrease with increasing period until they approach the peak widths observed for reversible electron transfers.

Comparison of the trends for $\Delta\Psi^{+}_{p}$ and E_p as a function of period reveals several differences between the reversible and quasireversible mechanisms. Peak currents are proportional to the period$^{-1/2}$ for both the reversible and quasireversible mechanisms, but with differing proportionalities (*vide infra*). Peak ratios remain constant for the

reversible mechanism whereas peak ratios increase with period for the quasireversible mechanism. Peak potentials and peak separation are unchanged by the variation of period for the reversible mechanism whereas peak potentials shift toward the formal potential (and thereby decrease peak separation) as period is increased for the quasireversible mechanism.

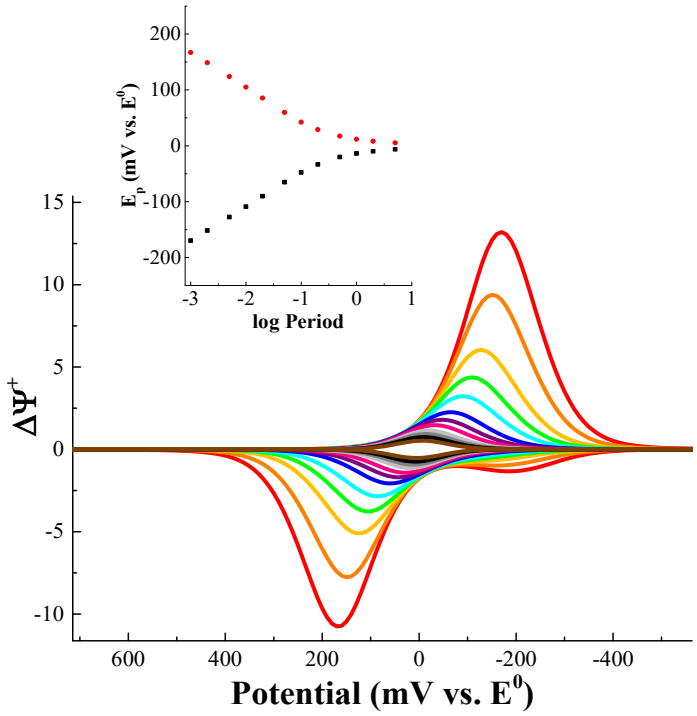

Figure 3.1. The effect of period on the shape of the voltammogram when log k^0 = -3, α = 0.5, $D_{Ox} = D_{Red} = 5 \times 10^{-6}$ cm^2s^{-1}, amplitude = 50 mV, increment = 10 mV, and period = 1 ms (red), 2 ms (orange), 5 ms (gold), 10 ms (green), 20 ms (cyan), 50 ms (blue), 100 ms (purple), 200 ms (magenta), 0.5 s (light gray), 1 s (gray), 2 s (black), and 5 s (brown). The inset presents peak potentials versus log period for the voltammograms depicted in this figure ($E_{p,f}$ represented by black squares and $E_{p,r}$ represented by red circles).

These trends are consistent with the notion that as period lengthens the electrode reaction transitions from being kinetically controlled to mass transfer controlled. Thus, systematic variation in period is useful in discriminating between the two mechanisms.

3.3.3 Effect of increment (δE)

A series of voltammograms in which the increment is varied is shown in Figure 3.2. With increasing increment, ΔE_p and $\Delta\Psi_p^+$ values increase while the peak ratio decreases from one. The cause of the increase in $\Delta\Psi_p^+$ is seen by examining the currents on each individual pulse. The currents on the odd numbered pulses increase more than the currents on the even numbered pulses with increment (see Figure 3.3). The same trend holds on the reverse sweep but the magnitude of the currents on each pulse are smaller. Thus, the difference current increases with increment but the peak ratio decreases. Since ΔE_p and $\Delta\Psi_p^+$ values also depend on period, trends in peak currents, peak ratio, peak potentials, peak separation, and peak width with increment and period for the quasireversible mechanism can be found in Figures 3.4 through 3.6.

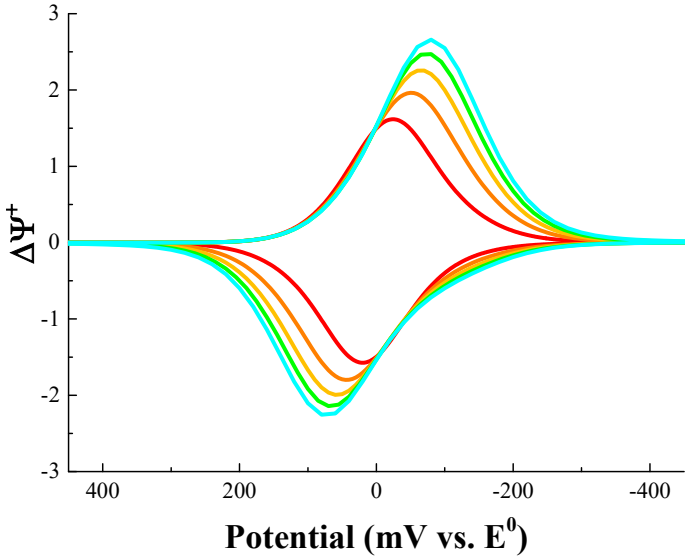

Figure 3.2. The effect of increment on the shape of the voltammogram when $\log k^0 = -3$, $\alpha = 0.5$, $D_{Ox} = D_{Red} = 5 \times 10^{-6}$ cm^2s^{-1}, period = 50 ms, amplitude = 50 mV, and the increment = 1 mV (red), 5 mV (orange), 10 mV (gold), 15 mV (green), and 20 mV (cyan).

Comparison of the trends for $\Delta\Psi_p^+$ and E_p as a function of increment reveals several differences between the reversible and quasireversible mechanisms. Peak currents decrease with increment for the reversible mechanism whereas they increase for the quasireversible mechanism. Peak potentials remain at the formal potential for the reversible mechanism whereas they shift away from the formal potential for the quasireversible mechanism. Thus, systematic variation in increment is useful in discriminating between these two mechanisms.

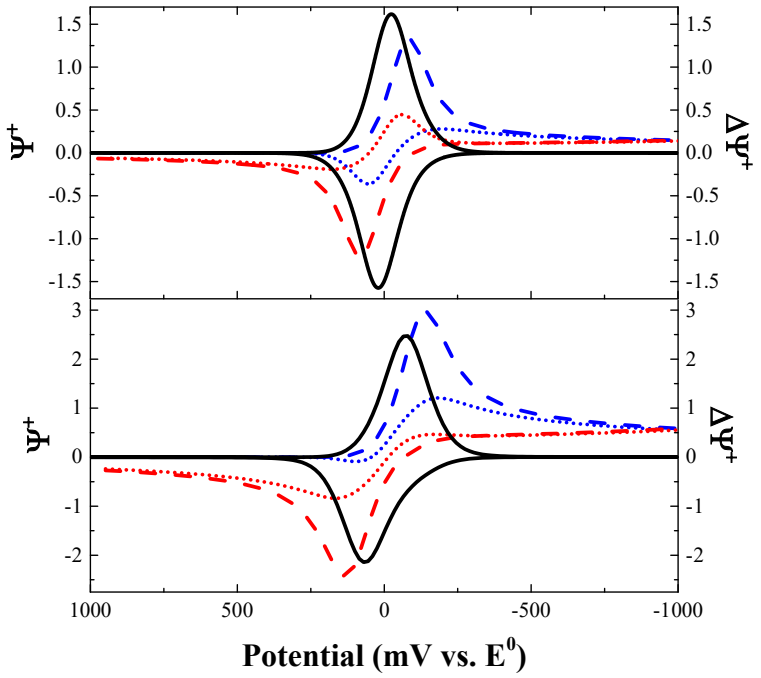

Figure 3.3. The effect of increment on the shape of the voltammogram when log k^0 = -3, period = 50 ms, $D_{Ox} = D_{Red}$ = 5 x 10^{-6} cm^2s^{-1}, α = 0.5, amplitude = 50 mV, and the increment is 1 mV (upper panel) and 15 mV (lower panel). The currents on the odd pulses (dashed line) and on the even pulses (dotted line) are associated with the primary Y-axis; the solid trace denotes the net current and is associated with the secondary Y-axis.

It is interesting to note that the trends observed for period are the inverse of those

observed for increment. For example, $\Delta\Psi_p^+$ values decrease with period but increase with increment. Similarly, while E_p values shift towards E^0 with period, they shift away from E^0 with increment. The effective potential sweep rate is increment divided by period. Thus increasing the potential sweep rate is achieved by either increasing increment or shortening period.

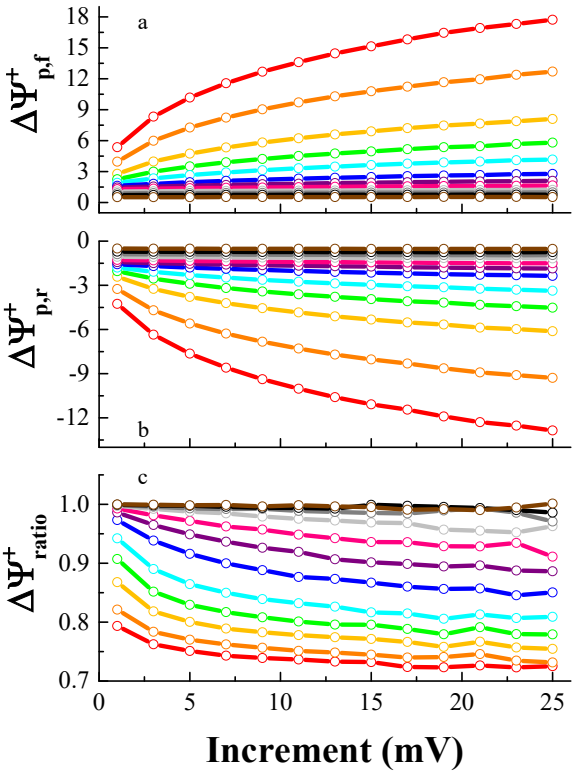

Figure 3.4. The dependence of net peak current on increment: a) $\Delta\Psi^+_{p,f}$, b) $\Delta\Psi^+_{p,r}$, and c) peak ratio when $\alpha = 0.5$, amplitude = 50 mV, $\log k^0 = -3$, $D_{Ox} = D_{Red} = 5 \times 10^{-6}$ cm^2s^{-1}, and period = 1 ms (red), 2 ms (orange), 5 ms (gold), 10 ms (green), 20 ms (cyan), 50 ms (blue), 100 ms (purple), 200 ms (magenta), 0.5 s (light gray), 1 s (gray), 2 s (black), and 5 s (brown). Note: open circles indicate the specific increments where simulation was performed.

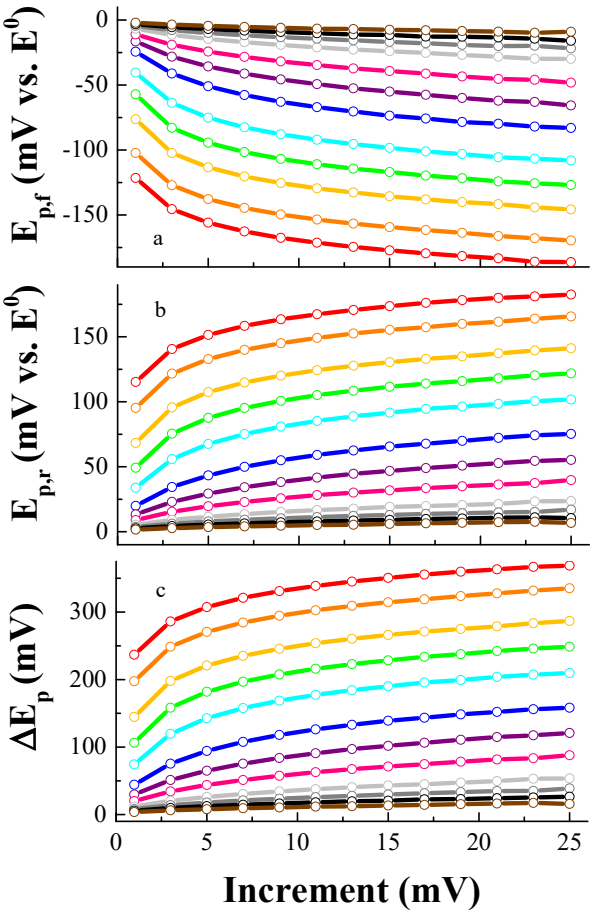

Figure 3.5. The dependence of a) $E_{p,f}$, b) $E_{p,r}$, and c) ΔE_p on increment when $\alpha = 0.5$, amplitude = 50 mV, $\log k^0 = -3$, $D_{Ox} = D_{Red} = 5 \times 10^{-6}$ cm^2s^{-1}, and period = 1 ms (red), 2 ms (orange), 5 ms (gold), 10 ms (green), 20 ms (cyan), 50 ms (blue), 100 ms (purple), 200 ms (magenta), 0.5 s (light gray), 1 s (gray), 2 s (black), and 5 s (brown). Note: open circles indicate increments where simulations were performed.

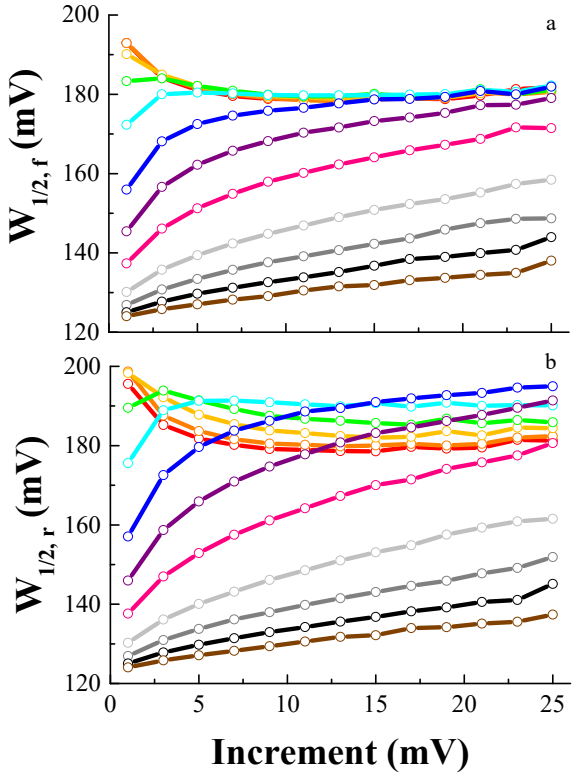

Figure 3.6. The dependence of peak width on increment: a) $W_{1/2,f}$ and b) $W_{1/2,r}$ when α = 0.5, amplitude = 50 mV, $\log k^0 = -3$, $D_{Ox} = D_{Red} = 5 \times 10^{-6}$ cm^2s^{-1}, and period = 1 ms (red), 2 ms (orange), 5 ms (gold), 10 ms (green), 20 ms (cyan), 50 ms (blue), 100 ms (purple), 200 ms (magenta), 0.5 s (light gray), 1 s (gray), 2 s (black), and 5 s (brown). Note: open circles indicate the specific increments where simulation was performed.

3.3.4 Effect of switching potential (E_λ)

A series of voltammograms in which the switching potential is varied is shown in Figure 3.7. As the switching potential moves from 200 to 1000 mV past E^0, $E_{p,f}$ and $\Delta\Psi^+_{p,f}$ remain constant but $\Delta\Psi^+_{p,r}$ increases in magnitude and $E_{p,r}$ shifts but only by a few millivolts. The dependence of peak currents and peak ratio on switching potential and period is shown in Figure 3. Changes in reverse sweep peak width are only seen when switching potential occurs before the forward sweep peak returns to baseline.

Comparison of the trends for $\Delta\Psi_p^+$ and E_p as a function of switching potential reveals minor differences between the reversible and quasireversible mechanisms. Forward peak currents and potentials remain unchanged for both mechanisms. Reverse peak currents and potentials are invariant for the reversible mechanism but decrease as the switching potential is shifted towards the formal potential for the quasireversible mechanism. As a result, peak ratio for the quasireversible mechanism decreases as the switching potential approaches the formal potential. However, the magnitude of this decrease is not large enough to be a reliable discriminator for these two mechanisms.

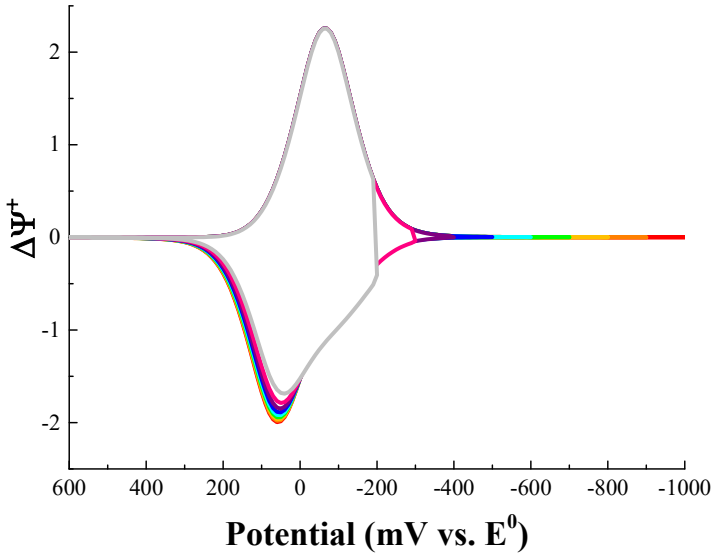

Figure 3.7. The effect of switching potential on the shape of the voltammogram when log $k^0 = -3$, $\alpha = 0.5$, $D_{Ox} = D_{Red} = 5 \times 10^{-6}$ cm^2s^{-1}, amplitude = 50 mV, increment = 10 mV, period = 50 ms, and the switching potential was varied from 200 (light gray) to 1000 (red) mV past E^0 in 100 mV steps.

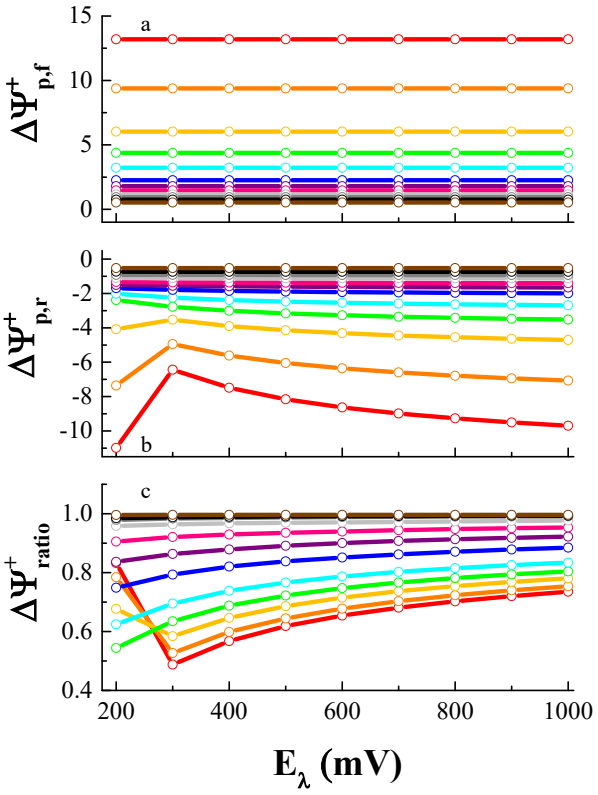

Figure 3.8. The dependence of net peak current on switching potential: a) $\Delta\Psi^+_{p,f}$, b) $\Delta\Psi^+_{p,r}$, and c) peak ratio when $\alpha = 0.5$, amplitude = 50 mV, increment = 10 mV, log k^0 = -3, $D_{Ox} = D_{Red} = 5 \times 10^{-6}$ cm^2s^{-1}, and period = 1 ms (red), 2 ms (orange), 5 ms (gold), 10 ms (green), 20 ms (cyan), 50 ms (blue), 100 ms (purple), 200 ms (magenta), 0.5 s (light gray), 1 s (gray), 2 s (black), and 5 s (brown). Note: open circles indicate the specific values of E_λ where simulation was performed.

3.3.5 Effect of amplitude (E_{SW})

The utility of systematic variation in amplitude in determining electrode reaction mechanisms by square wave voltammetry has recently been reported.[19] The effects of amplitude on the cyclic square wave voltammogram are visualized in Figure 3.9. Both $E_{p,f}$ and $E_{p,r}$ shift towards E^0 as the amplitude increases from 10 to 90 mV. The magnitude of the potential shift and the resultant ΔE_p depends on period (see Figure 3.10). Peak currents also increase with amplitude with a magnitude that depends on the

period (see Figure 3.11). The peak ratio for the set of voltammograms depicted in Figure 3.9 increases from 0.85 to 0.95. Period impacts the change in peak ratio with amplitude (also shown in Figure 3.11). Similarly, peak widths increase with amplitude (Figure 3.12).

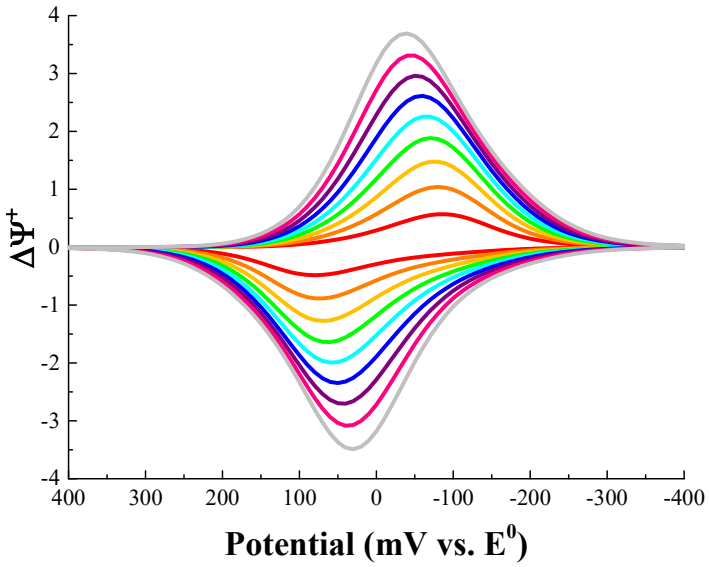

Figure 3.9. The effect of amplitude on the shape of the voltammogram when log k^0 = -3, α = 0.5, $D_{Ox} = D_{Red}$ = 5 x 10^{-6} cm^2s^{-1}, increment = 10 mV, and period = 50 ms, and the amplitude varied from 10 (red) to 90 mV (gray) in 10 mV steps.

Comparison of the trends for $\Delta\Psi_p^+$ and E_p as a function of amplitude reveals several differences between the reversible and quasireversible mechanisms. Peak currents and peak widths increase with amplitude for both mechanisms; the magnitude depends on period. Peak potentials are invariant for the reversible mechanism but shift toward the formal potential with increasing amplitude for the quasireversible case. Therefore, systematic variation of amplitude provides a means for discerning between the two mechanisms.

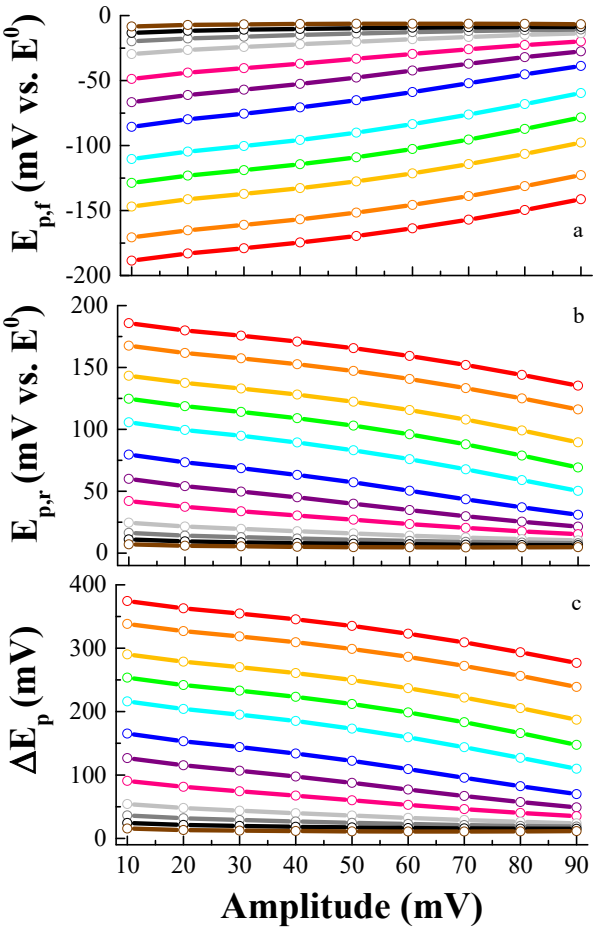

Figure 3.10. The dependence of peak potential on amplitude: a) $E_{p,f}$, b) $E_{p,r}$, and c) ΔE_p when $\alpha = 0.5$, increment = 10 mV, $\log k^0 = -3$, $D_{Ox} = D_{Red} = 5 \times 10^{-6}$ cm^2s^{-1}, and period = 1 ms (red), 2 ms (orange), 5 ms (gold), 10 ms (green), 20 ms (cyan), 50 ms (blue), 100 ms (purple), 200 ms (magenta), 0.5 s (light gray), 1 s (gray), 2 s (black), and 5 s (brown). Note: open circles indicate simulated amplitudes.

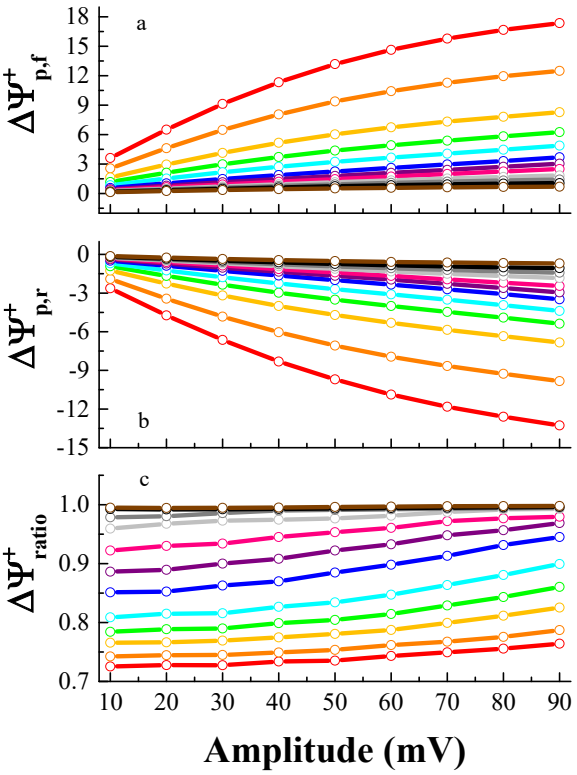

Figure 3.11. The dependence of net peak current on amplitude: a) $\Delta\Psi^{+}_{p,f}$, b) $\Delta\Psi^{+}_{p,r}$, and c) peak ratio when $\alpha = 0.5$, increment = 10 mV, $\log k^0 = -3$, $D_{Ox} = D_{Red} = 5 \times 10^{-6}$ cm^2s^{-1}, and period = 1 ms (red), 2 ms (orange), 5 ms (gold), 10 ms (green), 20 ms (cyan), 50 ms (blue), 100 ms (purple), 200 ms (magenta), 0.5 s (light gray), 1 s (gray), 2 s (black), and 5 s (brown). Note: open circles indicate the specific amplitudes where simulation was performed.

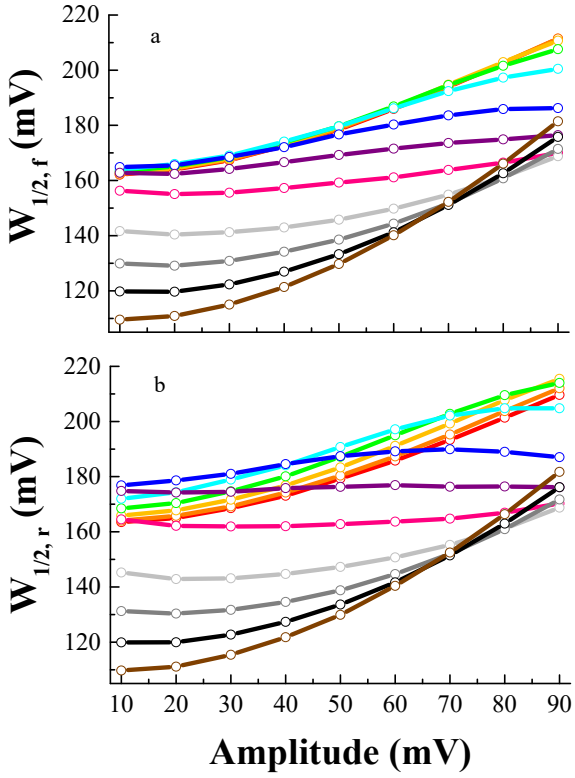

Figure 3.12. The dependence of peak width on amplitude: a) $W_{1/2,f}$ and b) $W_{1/2,r}$ when $\alpha = 0.5$, increment = 10 mV, $\log k^0 = -3$, $D_{Ox} = D_{Red} = 5 \times 10^{-6}$ cm^2s^{-1}, and period = 1 ms (red), 2 ms (orange), 5 ms (gold), 10 ms (green), 20 ms (cyan), 50 ms (blue), 100 ms (purple), 200 ms (magenta), 0.5 s (light gray), 1 s (gray), 2 s (black), and 5 s (brown). Note: open circles indicate the specific amplitudes where simulation was performed.

3.3.6 Effect of k^0

The impact of heterogeneous kinetics on the shape of the voltammogram depends upon the magnitude of k^0 relative to period. The values of α, k^0, D_{ox} and D_{red} are quantities intrinsic to the analyte undergoing an electron transfer reaction at a particular electrode immersed in a specific electrolyte. While in practice one varies period and determines k^0 from changes in the shape of the voltammograms, it is informative to examine changes in the voltammogram when the value of k^0 is systematically varied. Computational variation of k^0 at a fixed value of period is, in effect, predicting responses

for different analytes and/or different electrode/electrolyte combinations.

Figure 3.13 illustrates the impact of varying k^0 on the shape of the voltammogram. The voltammograms displayed in this figure were computed based on fixed values of α, period, D_{ox} and D_{red} allowing k^0 to vary over nine orders of magnitude. Note that at small values of k^0, a second peak on the reverse sweep is observed at a peak potential value similar to that of $E_{p,f}$. The difference current for this peak is hereafter referred to as the leak-over peak as identified by $\Delta\Psi^*_{p,r}$. The cause of the leak-over peak is seen by examining the currents on each individual pulse. It results from differences in the magnitude of the currents on the odd and even potential steps acquired on the reverse sweep. The magnitudes of $E^*_{p,r}$ and $\Delta\Psi^*_{p,r}$ depend on amplitude as well as the separation between $E_{p,f}$ and the switching potential. The presence of a leak-over peak depends upon the rate of electron transfer (*vide infra*).

Figure 3.14 presents plots of the figures of merit from the voltammograms as a function of k^0. For each panel in this figure, three regimes can be identified. For $\log k^0 \leq -3$, $E_{p,f}$ and $E_{p,r}$ are proportional to k^0. For $\log k^0 \geq -1$, $E_{p,f} = E_{p,r}$ and both are independent of k^0. For $-3 < \log k^0 < -1$, $E_{p,f}$ and $E_{p,r}$ are curvilinearly related to k^0 (see Figure 3.14a). Similarly, ΔE_p is proportional to $\log k^0$ up to -3, curvilinearly related to $\log k^0$ over the range -3 to -1, and independent of $\log k^0$ at values greater than -1 (see Figure 3.14b). Figure 3.14c presents the sigmoidal relationship between $\Delta\Psi^+_{p,f}$, $\Delta\Psi^+_{p,r}$, and $\log k^0$. Over the range $\log k^0 < -3$, $\Delta\Psi^+_{p,f} = 1.8$. Over the range $-3 < \log k^0 < -1$, $\Delta\Psi^+_{p,f}$ increases from 1.8 to 5.9, the value of $\Delta\Psi^+_{p,f}$ at $\log k^0 > -1$. In comparison, over

the range $-6 \leq \log k^0 < -3$, $\Delta\Psi^+_{p,r}$ increases in magnitude from -1 to -2. Over the range $-3 < \log k^0 < -1$, $\Delta\Psi^+_{p,r}$ increases from -2 to -5.9, the value of $\Delta\Psi^+_{p,r}$ at $\log k^0 > -1$.

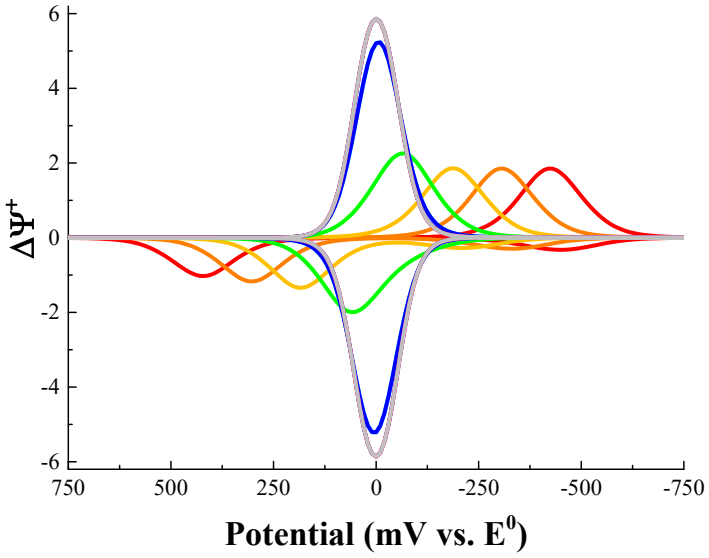

Figure 3.13. The effect of k^0 on the shape of the voltammogram when $\alpha = 0.5$, $D_{Ox} = D_{Red} = 5 \times 10^{-6}$ cm^2s^{-1}, amplitude = 50 mV, increment = 10 mV, period = 50 ms, and $\log k^0 =$ -6 (red), -5 (orange), -4 (gold), -3 (green), -2 (cyan), -1 (blue), 0 (purple), 1 (magenta), and 2 (light gray).

The dependence of peak width on k^0 also displays a sigmoidal shape (see Figure 3.14d). When $\log k^0 \leq -4$, $W_{1/2,f} = 179$ mV. When $\log k^0 \geq -1$, $W_{1/2,f}$ remains constant at 126 mV. Over the range $-4 < \log k^0 < -1$, $W_{1/2,f}$ decreases from 179 mV to 126 mV. Similarly, $W_{1/2,r} = 177$ mV when $\log k^0 \leq -4$ and equals 126 mV when $\log k^0 \geq -1$. However, $W_{1/2,r}$ increases from 179 mV at $\log k^0 = -4$ to 191 mV at $\log k^0 = -3$ as the leakover peak merges with the true peak. When $-3 < \log k^0 < -1$, $W_{1/2,r}$ decreases with a sigmoidal shape from 191 mV to 126 mV.

For all four measurable quantities, when $\log k^0 \geq -1$, the voltammogram features are identical to those obtained for a reversible mechanism. Indeed, in the limit of reversible

electron transfer kinetics, the simulations converge on the values for a reversible electrode reaction, *i.e.* are limited by mass transport of Ox to the electrode surface. Below this threshold, the voltammogram features and appearance are very sensitive to the rate of electron transfer. The transition from reversible to quasireversible wave shapes depends upon the magnitude of k^0 relative to period. Figures 3.15 and 3.16 present the relationships between of peak currents and potentials on both period and k^0. Thus, variation in period for CSWV is an important parameter for gaining insight to the rate and reversibility of an electron transfer.

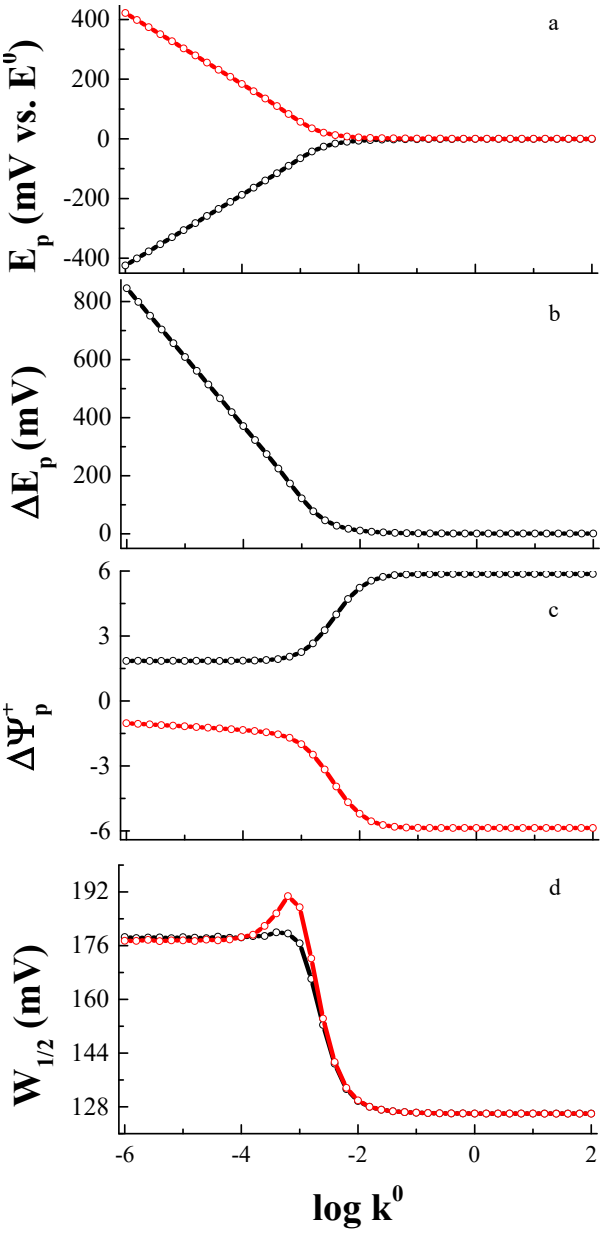

Figure 3.14. The effect of k^0 on the figures of merit: a) $E_{p,f}$ (black) and $E_{p,r}$ (red), b) ΔE_p, c) $\Delta\Psi^+_{p,f}$ (black) and $\Delta\Psi^+_{p,r}$ (red), and d) $W_{1/2,f}$ (black) and $W_{1/2,r}$ (red) when amplitude = 50 mV, increment = 10 mV, period = 50 ms, $\alpha = 0.5$, $D_{Ox} = D_{Red} = 5 \times 10^{-6}$ cm^2s^{-1}, and log k^0 = -6 to 2. Note: open circles denote values were simulations were performed.

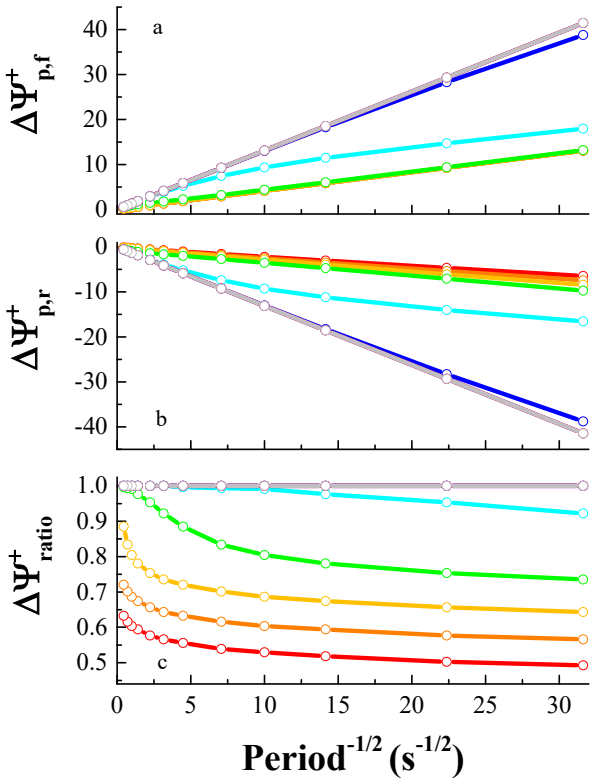

Figure 3.15. The dependence of net peak current on period and log k^0: a) $\Delta\Psi^{+}_{p,f}$, b) $\Delta\Psi^{+}_{p,r}$, and c) peak ratio when amplitude = 50 mV, increment = 10 mV, $\alpha = 0.5$, $D_{Ox} = D_{Red} = 5 \times 10^{-6}$ cm^2s^{-1}, and log k^0 = -6 (red), -5 (orange), -4 (gold), -3 (green), -2 (cyan), -1 (blue), 0 (purple), 1 (magenta), and 2 (light gray). Note: open circles indicate the specific periods where simulation was performed.

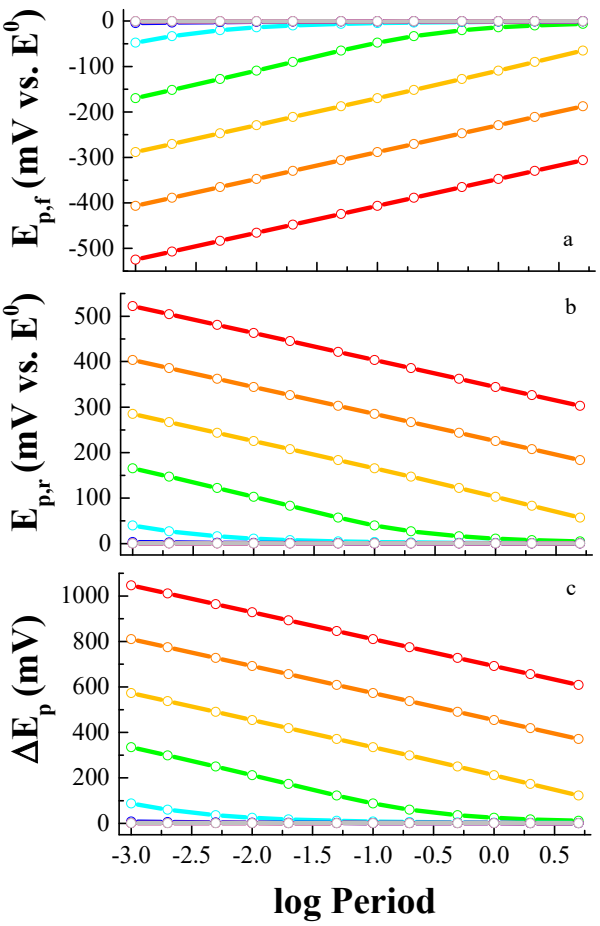

Figure 3.16. The dependence of peak potential on period and k^0: a) $E_{p,f}$, b) $E_{p,r}$, and c) ΔE_p when amplitude = 50 mV, increment = 10 mV, $\alpha = 0.5$, $D_{Ox} = D_{Red} = 5 \times 10^{-6}$ cm^2s^{-1}, and log k^0 = -6 (red), -5 (orange), -4 (gold), -3 (green), -2 (cyan), -1 (blue), 0 (purple), 1 (magenta), and 2 (light gray). Note: open circles indicate the specific periods where simulation was performed.

3.3.7 Effect of alpha (α)

The electron transfer coefficient, α, describes the symmetry of the overlap of the two potential wells of the reaction coordinate for electron transfer. An α value of 0.5 denotes a perfectly symmetrical overlap. Since α ranges from 0 to 1, values other than 0.5 indicate that the overlap of the potential energy – reaction coordinate curves leans towards the potential well of the reactant ($\alpha < 0.5$) or the product ($\alpha > 0.5$). Alpha is

inherent to a particular species reacting at a given electrode; hence, it cannot be varied by an experimenter. However, CSWV experiments can be executed to determine its value for a given electrode reaction performed under a specific set of conditions.

The shape of the voltammogram is strongly dependent upon α (see Figure 3.17). As α decreases, both $E_{p,f}$ and $E_{p,r}$ shift to more negative potentials but with differing magnitudes. In addition, $\Delta\Psi^{+}_{p,f}$ decreases whereas $\Delta\Psi^{+}_{p,r}$ increases with decreasing α.

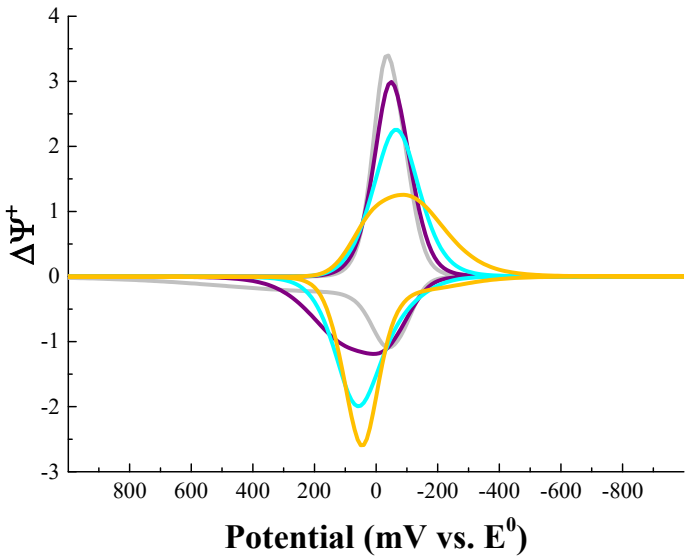

Figure 3.17. The effect of α on the shape of the voltammogram when log k^0 = -3, D_{Ox} = D_{Red} = 5 x 10^{-6} cm^2s^{-1}, period = 50 ms, amplitude = 50 mV, increment = 10 mV, and α is a) 0.9 (gray), b) 0.7 (purple), c) 0.5 (cyan), d) 0.3 (gold).

Figure 3.18 presents the simultaneous variation of α and period when log k^0 = -3. When α = 0.5 (Figure 3.18e), $E_{p,f}$ and $E_{p,r}$ are symmetrically displaced from E^0 by a value determined by k^0 and period (*vide supra*). Peak shapes are similar; *i.e.* $W_{1/2,f} \sim W_{1/2,r}$. When α < 0.5 (Figure 3.18a-d), both $E_{p,f}$ and $E_{p,r}$ are shifted negatively and the forward peak is broader compared to values for α = 0.5. When α > 0.5 (Figure 3.18f-i), both $E_{p,f}$ and $E_{p,r}$ are shifted positively and the reverse peak is broader compared to values for α =

0.5. For all values of α, as the period is lengthened, both peak potentials converge to E^0. Thus, when $\alpha \neq 0.5$, the peak potentials are asymmetrically displaced from E^0; the magnitude of displacement depends on period, k^0 and α (Figures 3.19 and 3.20 for E_p and ΔE_p, respectively). Note that the peak separation for $\alpha = 0.4$ is identical to that for $\alpha = 0.6$. In fact, α pairs of 0.3 and 0.7, 0.2 and 0.8, and 0.1 and 0.9 will also overlap except when the leak-over peak merges with the reverse peak.

The relationship between $\Delta\Psi_p^+$ and α is qualitatively presented in Figure 3.18. Peak currents are proportional to period$^{-1/2}$ but with a slope that depends upon α. Further details of the relationship between α, period, peak potentials, currents, and peak ratios are presented in Figures 3.21 through 3.23.

The results presented in Figures 3.18 and 3.19 suggests a straightforward means for determining α, *i.e.* examining forward and reverse peak potential shifts as a function of period. A plot of $E_{p,f}$ vs. $E_{p,r}$ acquired from the systematic variation of period is shown in Figure 3.24 for $\log k^0 = -3$. When $\Delta E_p \geq 100$ mV, a linear relationship between $E_{p,f}$ vs. $E_{p,r}$ is observed. For $\alpha = 0.5$, the slope of the line = 1 as both the forward and reverse sweeps are equally displaced from the formal potential.

For $\alpha < 0.5$, the slope of the line < 1 whereas for $\alpha > 0.5$, the slope of the line > 1. Thus, the slope of $E_{p,f}$ vs. $E_{p,r}$, plotted exactly as in Figure 3.24, can be used with Equation 3.7 to determine α even for intermediate values of α that are not displayed in this figure.

$$\text{slope of } E_{p,f} \text{ vs. } E_{p,r} = \frac{\alpha}{1-\alpha} \tag{3.7}$$

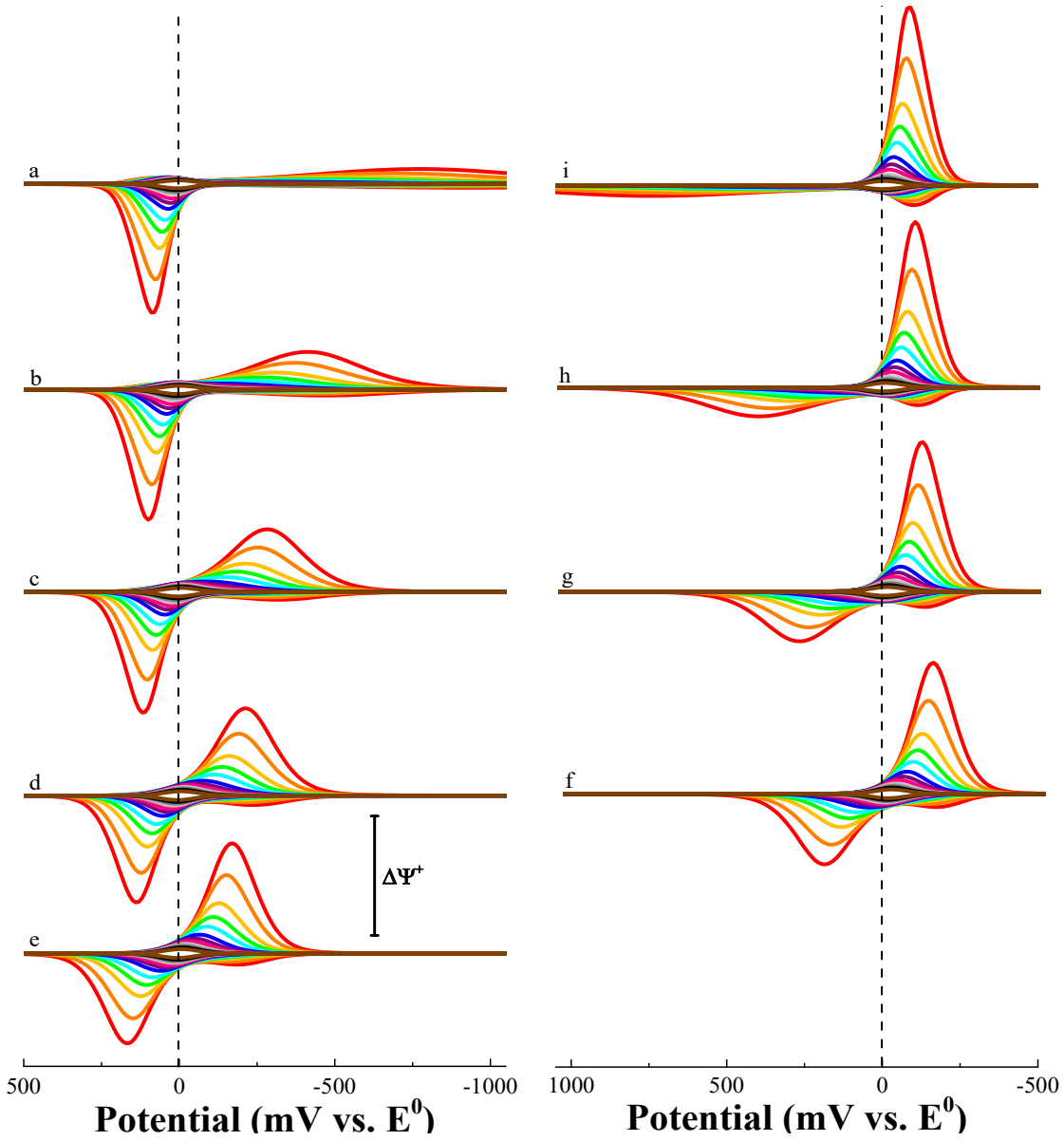

Figure 3.18. Effect of α and period on the shape of the voltammogram: log k^0 = -3, D_{Ox} = D_{Red} = 5 x 10^{-6} cm^2s^{-1}, amplitude = 50 mV, increment = 10 mV, α is a) 0.1 through i) 0.9 in steps of 0.1, and period = 1 ms (red), 2 ms (orange), 5 ms (gold), 10 ms (green), 20 ms (cyan), 50 ms (blue), 100 ms (purple), 200 ms (magenta), 0.5 s (light gray), 1 s (gray), 2 s (black), and 5 s (brown). The y-axis scale bar denotes $\Delta\Psi^+$ = 15. Note: the range in the potential axis differs between panels for clarity.

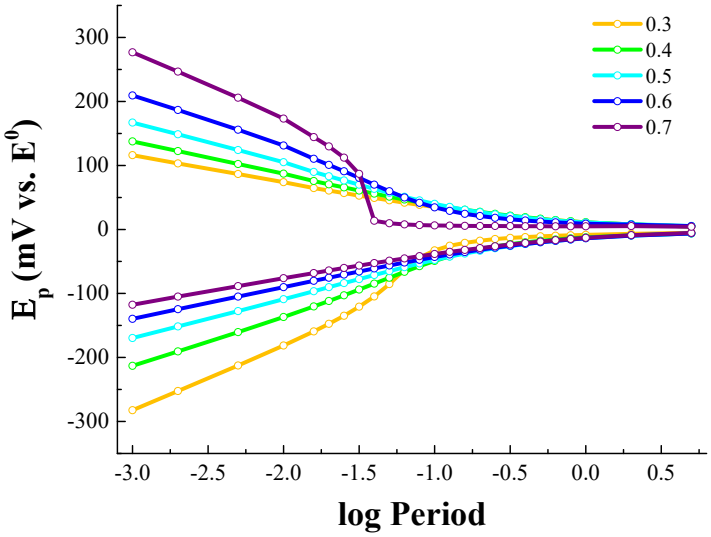

Figure 3.19. Plot of peak potential versus log period as a function of α when log k^0 = -3, $D_{Ox} = D_{Red}$ = 5 x 10^{-6} cm^2s^{-1}, amplitude = 50 mV, increment = 10 mV, and where α is 0.3 (gold), 0.4 (green), , 0.5 (cyan), 0.6 (blue)and 0.7 (purple). Note: open circles indicate the specific periods where simulation was performed.

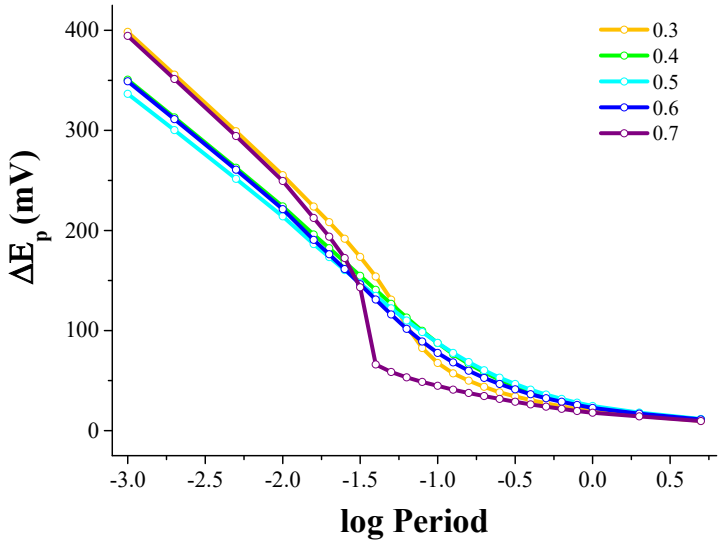

Figure 3.20. The dependence of peak potential on amplitude for ΔE_p when amplitude = 50 mV, increment = 10 mV, log k^0 = -3, $D_{Ox} = D_{Red}$ = 5 x 10^{-6} cm^2s^{-1}, and α = 0.3 (gold), 0.4 (green), 0.5 (cyan), 0.6 (blue), and 0.7 (purple). Note: open circles indicate the specific periods where simulation was performed.

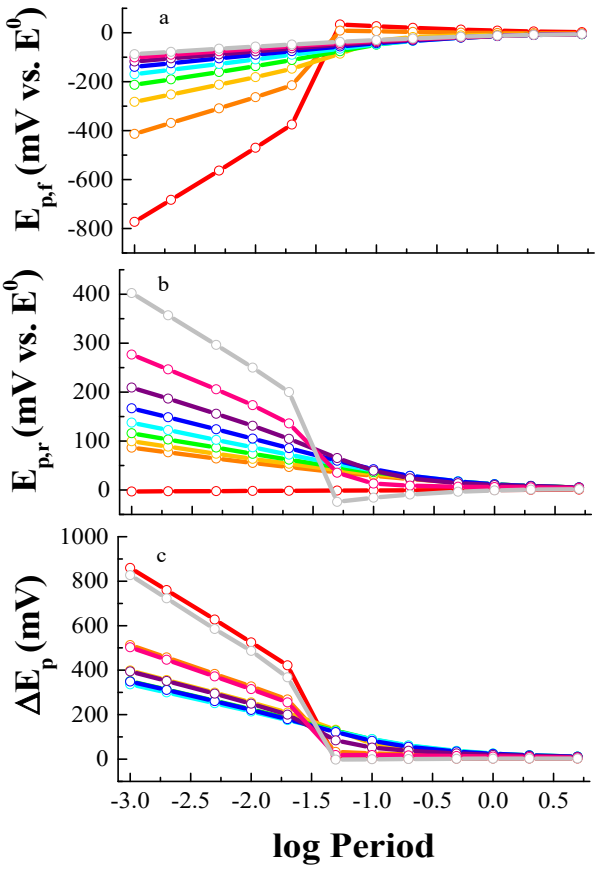

Figure 3.21. The dependence of peak potential on amplitude: a) $E_{p,f}$, b) $E_{p,r}$, and c) ΔE_p when amplitude = 50 mV, increment = 10 mV, log k^0 = -3, $D_{Ox} = D_{Red}$ = 5 x 10^{-6} cm^2s^{-1}, and α = 0.1 (red), 0.2 (orange), 0.3 (gold), 0.4 (green), 0.5 (cyan), 0.6 (blue), 0.7 (purple), 0.8 (magenta), and 0.9 (light gray). Note: open circles indicate the specific periods where simulation was performed.

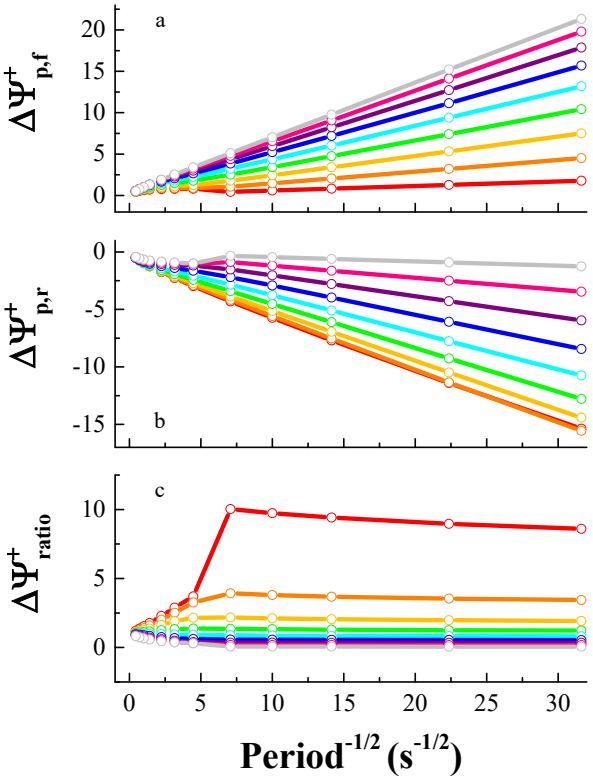

Figure 3.22. The dependence of net peak current on period: a) $\Delta\Psi^{+}_{p,f}$, b) $\Delta\Psi^{+}_{p,r}$, and c) peak ratio when amplitude = 50 mV, increment = 10 mV, log k^0 = -3, $D_{Ox} = D_{Red}$ = 5 x 10^{-6} cm^2s^{-1}, and α = 0.1 (red), 0.2 (orange), 0.3 (gold), 0.4 (green), 0.5 (cyan), 0.6 (blue), 0.7 (purple), 0.8 (magenta), and 0.9 (light gray). Note: open circles indicate the specific periods where simulation was performed.

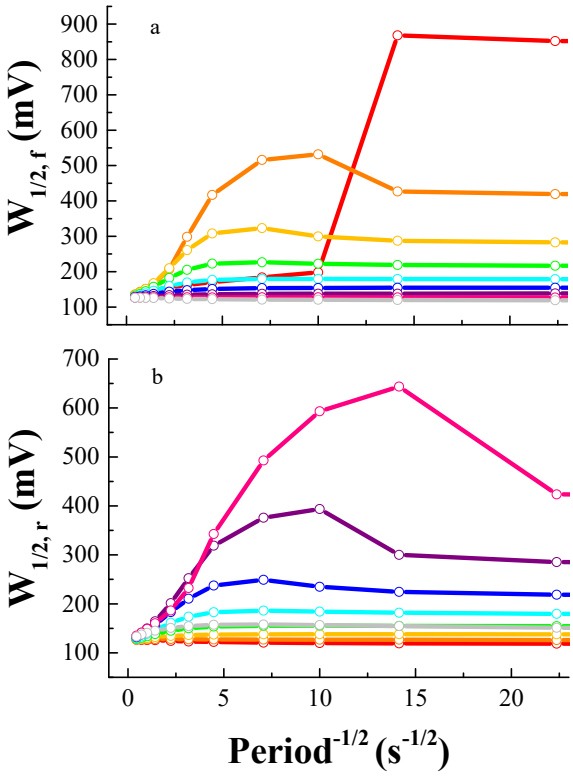

Figure 3.23. The dependence of net peak width on period: a) $W_{1/2,f}$ and b) $W_{1/2,r}$ when amplitude = 50 mV, increment = 10 mV, $\log k^0 = -3$, $D_{Ox} = D_{Red} = 5 \times 10^{-6}$ cm^2s^{-1}, and α = 0.1 (red), 0.2 (orange), 0.3 (gold), 0.4 (green), 0.5 (cyan), 0.6 (blue), 0.7 (purple), 0.8 (magenta), and 0.9 (light gray). Note: open circles indicate the specific periods where simulation was performed.

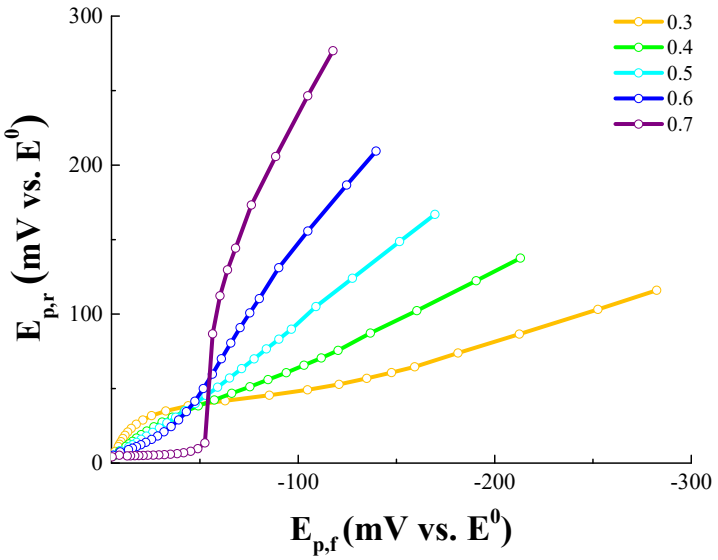

Figure 3.24. Plot of $E_{p,f}$ versus $E_{p,r}$ as a function of period when log k^0 = -3, $D_{Ox} = D_{Red}$ = 5 x 10^{-6} cm^2s^{-1}, amplitude = 50 mV, increment = 10 mV and where α is 0.3 (gold), 0.4 (green), 0.5 (blue), 0.6 (cyan), and 0.7 (purple). Note: open circles denote values were simulations were performed.

The cause of the apparent discontinuity when α = 0.7 is revealed by inspection of the voltammograms presented in Figure 3.18g. As the period is elongated and the true reverse peak shifts towards the formal potential, its peak current falls below that of the leak-over peak when the two peaks merge. As a result, the combined peak suddenly shifts negatively and its peak potential remains relatively constant as the leak-over peak occurs at the same potential as the forward peak.

3.3.8 Protocol for assigning mechanism and evaluating kinetic parameters

Europium(III) chloride hexahydrate was the analyte chosen to experimentally validate the trends predicted above and to demonstrate how to apply them in evaluating experimental data. The experiments were conducted in 0.5 M KCl. Classification of the $Eu^{3+/2+}$ redox couple system as quasireversible has been well documented.[23-25] The

protocol for assigning an electrode reaction as quasireversible is given in Table 3.1.

Figure 3.25a presents a set of voltammograms obtained on Eu^{3+} when the period was systematically varied from 10 to 200 ms. As shown in the remaining panels of this figure, $E_{p,f}$, $E_{p,r}$, and ΔE_p were linearly related to log period. A plot of $E_{p,f}$ versus $E_{p,r}$ was also linear (data not shown); the experimentally determined value of α from the slope of the line was 0.47 ± 0.03. The colored lines behind the individual data points in Figure 3.25b-d are the predicted trends for selected values of k^0. From the peak potentials and peak separation we conclude that $k^0 = 3.5 \pm 0.5 \times 10^{-4}$ cm s^{-1}. A linear relationship between $\Delta I_{p,f}$ and $\Delta I_{p,r}$ with period$^{-1/2}$ was obtained (see Figure 3.26) that was consistent with expected trends for quasireversible reactions (see Figure 3.22). Within experimental uncertainty, the peak ratio was constant at 0.60 ± 0.05 over the range in period from 10 to 200 ms.

Figure 3.27a presents a set of voltammograms obtained on Eu^{3+} when the increment was systematically varied from 1 to 19 mV. As shown in the remaining panels of this figure, $E_{p,f}$, $E_{p,r}$, and ΔE_p are curvilinearly related to increment. The colored lines behind the individual data points are the predicted trends for selected values of k^0. Relatively good agreement is found between the measured values and those predictor for $k^0 = 3.5 \pm 0.5 \times 10^{-4}$ cm s^{-1} at increments ≥ 5 mV. We attribute the difference between experimental and predicted values to the fact that the simulated values are for planar diffusion whereas the experimental data was acquired at a hanging mercury drop electrode. Alternatively, these differences could also be due to convective currents originating from mechanical vibrations. A curvilinear relationship between ΔI_p and increment was obtained (see Figure 3.28) that was consistent with expected trends for quasireversible reactions (see

Figure 3.4).

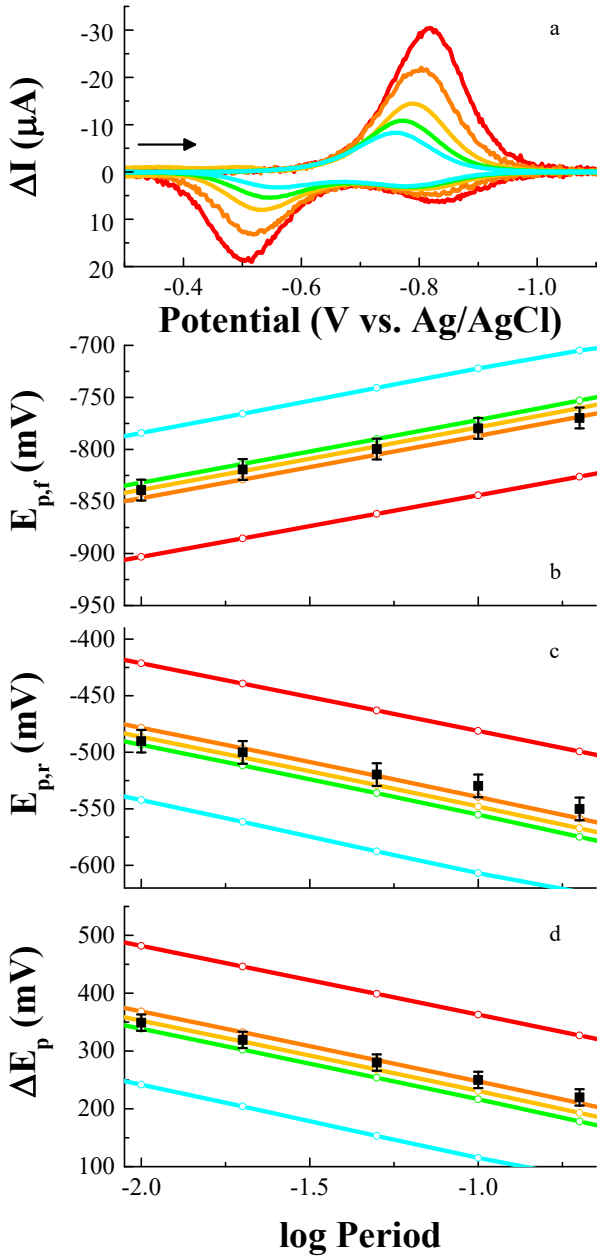

Figure 3.25. Effect of period on the $Eu^{3+/2+}$ redox couple: a) voltammograms with period variation = 10 ms (red), 20 ms (orange), 50 ms (gold), 100 ms (green), and 200 ms (cyan), and b-d) experimentally measured $E_{p,f}$, $E_{p,r}$, and ΔE_p (black squares) and predicted values for $E_{p,f}$, $E_{p,r}$, and ΔE_p when k^0 = 1 x 10^{-4} cm s^{-1}(red), 3 x 10^{-4} cm s^{-1} (orange), 3.5 x 10^{-4} cm s^{-1} (gold), 4 x 10^{-4} cm s^{-1} (green), and 1 x 10^{-3} cm s^{-1} (cyan). Note: open circles are simulated results; closed squares are experimental results.

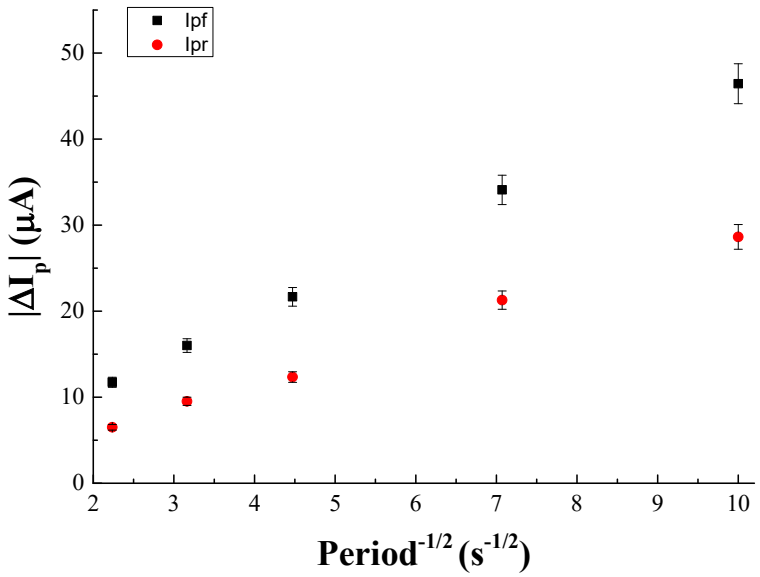

Figure 3.26. Effect of period on $|\Delta I_{p,f}|$ (black squares) and $|\Delta I_{p,r}|$ (red circles) for the $Eu^{3+/2+}$ redox couple. Note: closed circles indicate the specific periods where experiments were performed.

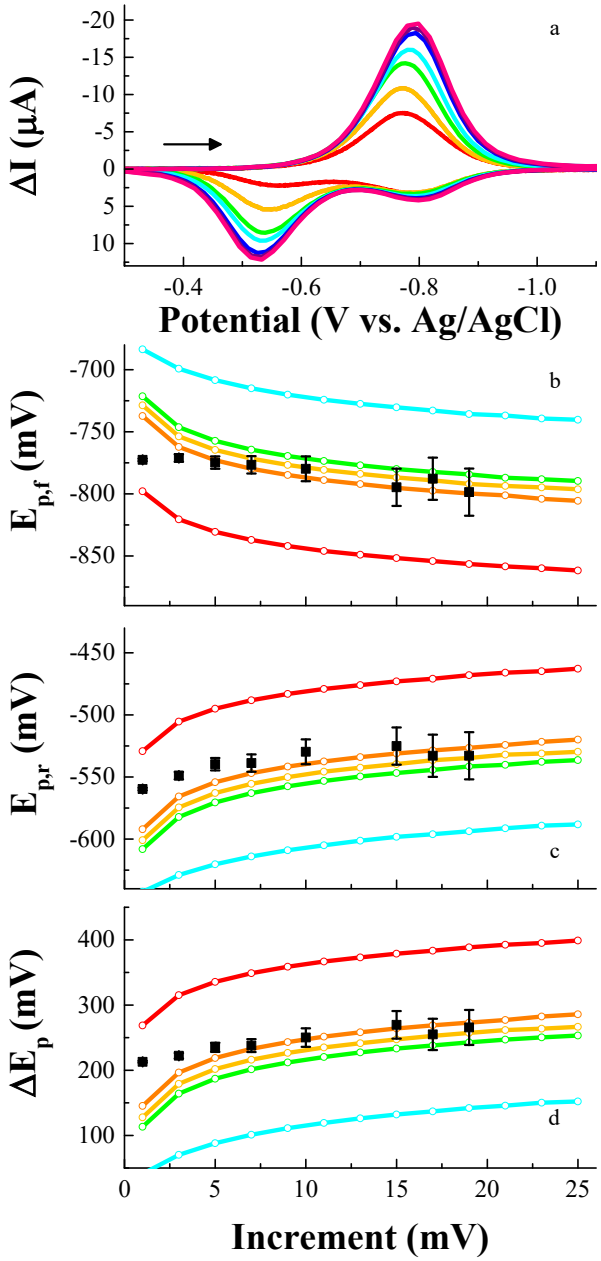

Figure 3.27. Effect of increment on the $Eu^{3+/2+}$ redox couple: a) voltammograms with increment variation = 1 mV (red), 3 mV (orange), 5 mV (gold), 7 mV (green), 10 mV (cyan), 15 mV (blue), 17 mV (purple), and 19 mV (magenta), and b-d) experimentally measured $E_{p,f}$, $E_{p,r}$, and ΔE_p (black squares) and predicted values for $E_{p,f}$, $E_{p,r}$, and ΔE_p when $k^0 = 1 \times 10^{-4}$ cm s^{-1}(red), 3×10^{-4} cm s^{-1} (orange), 3.5×10^{-4} cm s^{-1} (gold), 4×10^{-4} cm s^{-1} (green), and 1×10^{-3} cm s^{-1} (cyan). Note: open circles are simulated results; closed squares are experimental results.

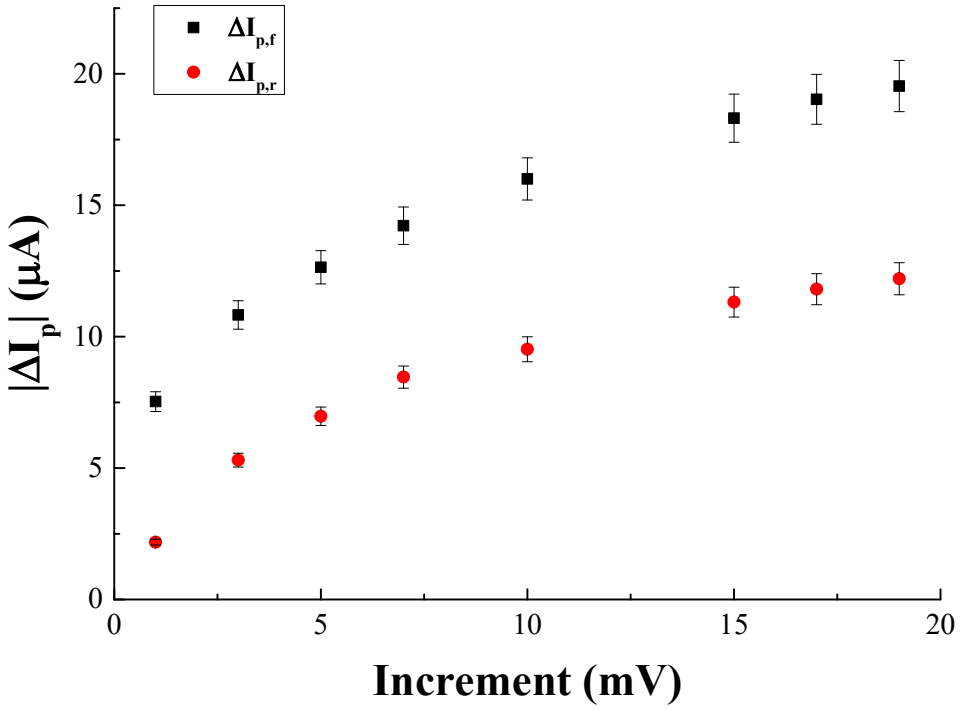

Figure 3.28. Effect of increment on $|\Delta I_{p,f}|$ (black squares) and $|\Delta I_{p,r}|$ (red circles) for the $Eu^{3+/2+}$ redox couple. Note: closed circles indicate the specific periods where experiments were performed.

Figure 3.29a presents a set of voltammograms obtained on Eu^{3+} when the amplitude was systematically varied from 10 to 90 mV. As shown in the remaining panels of this figure, $E_{p,f}$, $E_{p,r}$, and ΔE_p are curvilinearly related to amplitude. The colored lines behind the individual data points are the predicted trends for selected values of k^0. From the peak potentials and peak separation we again conclude that $k^0 = 3.5 \pm 0.5 \times 10^{-4}$ cm s^{-1}. A curvilinear relationship between ΔI_p and amplitude was obtained (see Figure 3.30) that was consistent with expected trends for quasireversible reactions (see Figure 3.11). Taken collectively, the agreement between theory and experiment is excellent.

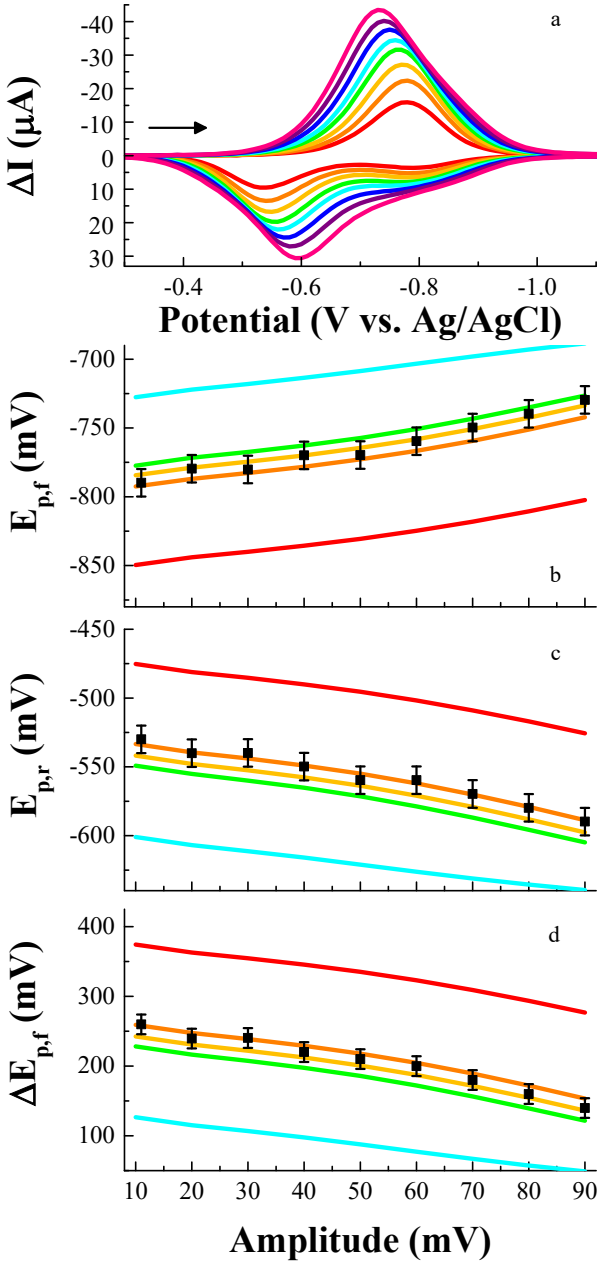

Figure 3.29. Effect of amplitude on the $Eu^{3+/2+}$ redox couple: a) voltammograms with amplitude variation = 10 mV (red), 20 mV (orange), 30 mV (gold), 40 mV (green), 50 mV (cyan), 60 mV (blue), 70 mV (purple), 80 mV (magenta), and 90 mV (light gray), and b-d) experimentally measured $E_{p,f}$, $E_{p,r}$, and ΔE_p (black squares) and predicted values for $E_{p,f}$, $E_{p,r}$, and ΔE_p when $k^0 = 1 \times 10^{-4}$ cm s^{-1}(red), 3×10^{-4} cm s^{-1} (orange), 3.5×10^{-4} cm s^{-1} (gold), 4×10^{-4} cm s^{-1} (green), and 1×10^{-3} cm s^{-1} (cyan). Note: open circles are simulated results; closed squares are experimental results.

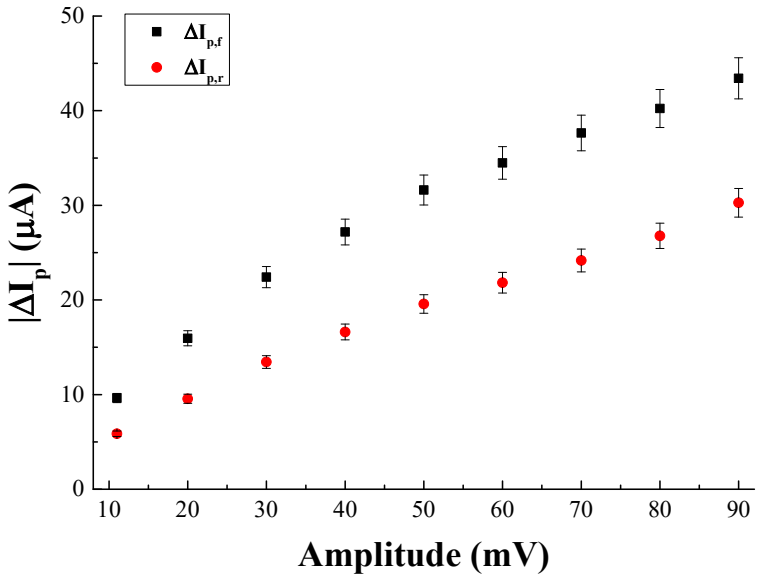

Figure 3.30. Effect of amplitude on $|\Delta I_{p,f}|$ (black squares) and $|\Delta I_{p,r}|$ (red circles) for the $Eu^{3+/2+}$ redox couple.

3.4 Conclusion

The peak currents, potentials and shapes of cyclic square wave voltammograms have been shown to be a complex function α, k^0 increment, period, switching potential and amplitude. Trends in empirical parameters enabled determination of kinetic parameters for the $Eu^{3+/2+}$ redox pair. The effects of these various parameters on the voltammograms of a quasireversible mechanism are summarized in Table 3.1. The diagnostic criteria presented in this table will enable rapid identification of quasireversible electron transfer reactions with CSWV.

Table 3.1. Diagnostic Plots and Protocol for Assessing a Quasireversible Electrode Reaction by CSWV

Waveform parameters	Empirical variables							
	Period, τ		***Increment, δE***		***Switching potential, E_λ***		***Amplitude, E_{SW}***	
	Plot	**Trace**	**Plot**	**Trend**	**Plot**	**Trend**	**Plot**	**Trend**
Peak currents	ΔI_p vs. $(period)^{-1/2}$	Linear with slope dependent upon α, k^0, n, and D (see Figures 3.15 & 3.22)	ΔI_p vs. δE	Increase[a] curvilinearly with δE (see Figure 3.4)	ΔI_p vs. E_λ	$\Delta I_{p,f}$ is independent of E_λ while $\Delta I_{p,r}$ increases in magnitude[a] with E_λ (see Figure 3.8)	ΔI_p vs. E_{SW}	$\Delta I_{p,f}$ and $\Delta I_{p,r}$ increase[a] curvilinearly with E_{SW}; (see Figure 3.11)
Peak ratio	Peak ratio vs. $(period)^{-1/2}$	Curvilinear with shape dependent on α (see Figures 3.15 & 3.22)	Peak ratio vs. δE	Decreases[a] curvilinearly with increasing δE (see Figure 3.4)	Peak ratio vs. E_λ	Increase with increasing E_λ; the magnitude[a] depends upon period (see Figure 3.8)	Peak ratio vs. E_{SW}	Increases[a] with E_{SW} (see Figure 3.11)
Peak potentials	E_p vs. log period	Linear with slope[b] dependent on α (see Figure 3.21)	E_p vs. δE	Shifts[a] curvilinearly away from E^0 with increasing δE (see Figure 3.5)	E_p vs. E_λ	Independent of E_λ	E_p vs. E_{SW}	Shifts[a] linearly towards E^0 with E_{SW} (see Figure 3.10)
	$E_{p,f}$ vs. $E_{p,r}$	Linear or curvilinear depending on α and k^0 (see Figure 3.24)						
Peak separation	ΔE_p vs. log period	Linear with slope[b] depending on α (see Figure 3.20)	ΔE_p vs. δE	Increases[a] curvilinearly with increasing δE (see Figure 3.5)	ΔE_p vs. E_λ	Independent of E_λ	ΔE_p vs. E_{SW}	Decreases[a] linearly with increasing E_{SW} (see Figure 3.10)
Peak widths	$W_{1/2}$ vs. $(period)^{-1/2}$	Complex relationship (see Figure 3.23)	$W_{1/2}$ vs. δE	Complex relationship (see Figure 3.6)	$W_{1/2}$ vs. E_λ	Independent of E_λ	$W_{1/2}$ vs. E_{SW}	$W_{1/2}$ generally increases with E_{SW}; trend depends on period (see Figure 3.12)

a) Trend magnitudes are dependent upon both period and k^0.

b) Note: zero slope indicates reversible reaction.

3.5 References

1. Bard, A.J. and L.R. Faulkner, *Electrochemical Methods: Fundamentals and Applications*. **2000**, Wiley: New York.

2. Nicholson, R.S. and I. Shain. *Anal. Chem.*, **1964**. 36, 706-723.

3. Chen, X. and G. Pu. *Anal. Lett.*, **1987**. 20, 1511-1519.

4. Pu, G., X. Cheng, and E. Wang. *Yingyong Huaxue*, **1988**. 5, 32-37.

5. Abrantes, L.M., J. Gonzalez, A. Molina, and F. Saavedra. *Electrochim. Acta*, **1999**. 45, 457-468.

6. Neudeck, A., F. Marken, and R.G. Compton. *Electroanalysis*, **1999**. 11, 1149-1154.

7. Prasad, M.A. and M.V. Sangaranarayanan. *Electrochim. Acta*, **2004**. 49, 2569-2579.

8. Prasad, M.A. and M.V. Sangaranarayanan. *Chem. Phys. Lett.*, **2004**. 387, 317-321.

9. Molina, A., F. Martinez-Ortiz, E. Laborda, and R.G. Compton. *Electrochim. Acta*, **2010**. 55, 5163-5172.

10. Laborda, E., M.C. Henstridge, A. Molina, F. Martinez-Ortiz, and R.G. Compton. *J. Electroanal. Chem.*, **2011**. 660, 169-177.

11. Jadreško, D. and M. Zelić. *J. Electroanal. Chem.*, **2013**. 707, 20-30.

12. Molina, A. and J. González, *Pulse Voltammetry in Physical Electrochemistry and Electroanalysis: Theory and Applications*, *Monographs in Electrochemistry*. **2016**, Springer: Heidelberg.

13. O'Dea, J.J., J. Osteryoung, and R.A. Osteryoung. *Anal. Chem.*, **1981**. 53, 695-701.

14. Osteryoung, J.G. and J.J. O'Dea, *Electroanalytical Chemistry*. **1986**, Marcel Dekker: New York. 209-224

15. Nuwer, M.J., J.J. O'Dea, and J. Osteryoung. *Anal. Chim. Acta*, **1991**. 251, 13-25.

16. Mirčeski, V., R. Gulaboski, and I. Kuzmanovski. *Glasnik na Hemicarite i Tehnolozite na Makedonija*, **1999**. 18, 57-64.

17. Mirčeski, V., Š. Komorsky-Lovrić, and M. Lovrić, *Square Wave Voltammetry: Theory and Application*, *Monographs in Electrochemistry*. **2007**, Springer-Verlag: Berlin.

18. Lovrić, M. and D. Jadreško. *Electrochim. Acta*, **2010**. 55, 948-951.

19. Mirčeski, V., E. Laborda, D. Guziejewski, and R.G. Compton. *Anal. Chem.*, **2013**. 85, 5586-5594.

20. Mirceski, V., D. Guziejewski, and R. Gulaboski. *Maced. J. Chem. Chem. Eng.*, **2015**. 34, 181-188.

21. Erdey-Gruz, T., *Kinetics of Electrode Processes*. **1972**, Wiley-Interscience Division: New York.

22. Nicholson, R.S. and M.L. Olmstead, *Electrochemistry: Calculations, Simulation and Instrumentation,*. **1972**, Marcel Dekker: New York. Ch. 5

23. Wang, Y., E. Laborda, M.C. Henstridge, F. Martinez-Ortiz, A. Molina, and R.G. Compton. *J. Electroanal. Chem.*, **2012**. 668, 7-12.

24. Henstridge, M.C., Y. Wang, J.G. Limon-Petersen, E. Laborda, and R.G. Compton. *Chem. Phys. Lett.*, **2011**. 517, 29-35.

25. Henstridge, M.C., E. Laborda, Y. Wang, D. Suwatchara, N. Rees, A. Molina, F. Martinez-Ortiz, and R.G. Compton. *J. Electroanal. Chem.*, **2012**. 672, 45-52.

CHAPTER 4

THE QUASIREVERSIBLE SURFACE-CONFINED MECHANISM

4.1 Introduction

Redox active adsorbates have been studied for over five decades. The impetus for these studies included: 1) gaining insight into monolayer formation and the associated isotherm for its formation, 2) exploring the reason(s) behind preferential accumulation of the adsorbate on the surface of one electrode material over another, 3) pre-concentration of analyte on the electrode for quantitative purposes, as well as 4) measuring kinetic parameters associated with the surface-confined species.[1, 2] Voltammetric methods have been employed to characterize this family of electrode reactions.[3-6] Recent interest has focused on the application of pulse voltammetric techniques for characterizing redox active adsorbates.[7-11] The reason for moving to the pulse techniques is straightforward. The diagnostic criteria put forth by originally by Randles,[12] Ševčik,[13] Nicholson and Shain[14] for identifying electrode reactions was developed when analog instrumentation was commonplace. Current instrumentation is digital; cyclic voltammograms acquired with digital instruments are actually cyclic staircase voltammograms. The applicability of theory developed for analog instruments to data acquired with digital instruments depends upon when the current is sampled during the potential pulse.[15] The "correct" sampling point depends upon the electrode reaction mechanism.[16, 17] This leads to the

experimental conundrum of what sampling point to select if one doesn't know the electrode reaction mechanism.

SWV has been shown to be particularly useful in identifying kinetically-controlled surface-confined redox active analytes.[18-24] Even though a strong theoretical basis for using SWV to identify the electrode reaction exists, the application of this theory has been limited to a small number of electrochemists. The goals of this chapter are: to develop diagnostic criteria for surface-confined electron transfer processes, to experimentally verify these criteria in determining kinetic parameters for a strongly adsorbed redox active analyte, and to compare the criteria with that for a non-surface confined quasireversible reaction. For this mechanism, CSWV enables accurate measures of E^0 and k^0 and the electron transfer coefficient, α, compared with SWV.

4.2 Experimental

Two analytes were used to validate the diagnostic criteria presented below: (15-mercapto-N-pentadecyl)ferrocenecarboxamide hereafter abbreviated as $(Fc)CONH(CH_2)_{15}SH$ and the disodium salt of anthraquinone disulfonic acid hereafter abbreviated as AQDS. This compound was used as received from Sigma-Aldrich (St. Louis, MO). A monolayer of $(Fc)CONH(CH_2)_{15}SH$ was assembled onto a gold electrode (area = 0.20 cm^2) via a previously established method.[25-28] A Pt mesh served as the counter electrode; the reference electrode was $Ag/AgClO_4$ located behind a frit filled with 0.1 M $NaClO_4$. The electrolyte used for all CV and CSWV experiments was 0.1 M $HClO_4$.

A monolayer of AQDS was assembled onto the surface of a hanging mercury drop connected to a PerkinElmer 303A SMDE (Waltham, MA) by exposing a fresh drop (area = 0.027 cm^2) to 5 μM AQDS in 0.1 M acetate buffer (pH = 4.5). A Pt wire served as the counter electrode and the reference electrode was Ag/AgCl located behind a frit filled with a saturated KCl solution. A new mercury drop was used for each scan; the potential was held at 150 mV (vs. Ag/AgCl) for 30 s before each scan. CSWV data was acquired using a Pine Instruments (Durham, NC) WaveNano potentiostat. No solution resistance compensation was used as this capability is not an option on the WaveNano potentiostat. Pine Instruments software program *Aftermath* was used to set experimental parameters, record voltammograms, and analyze the data. Oxygen was removed from all solutions by sparging with N_2.

4.3 Results and Discussion

4.3.1 Theory

The generalized reaction for a surface-confined redox active species is

$$Ox_{(ads)} + ne^- \rightleftharpoons Red_{(ads)} \quad (4.1)$$

The surface concentrations of the oxidized and reduced forms are potential and time dependent. Underlying assumptions in this work are that no interactions exist between redox moieties on the electrode surface and that the electroactive molecules may be present as a either a single or multiple monolayers so long as no concentration gradient exists within the layer(s) on the time scale of the voltammetric experiment.[29] Derivation of an equation for predicting current as a function of potential and time begins by

applying appropriate boundary conditions for this electrode reaction. The resultant expressions for surface concentrations were inserted into the Butler-Volmer relationship

$$i = nFAk^0\left[\Gamma_{Ox}e^{-\alpha\phi} - \Gamma_{Red}e^{(1-\alpha)\phi}\right] \tag{4.2}$$

where $\phi = \frac{nF}{RT}\left(E^0 - E_{applied}\right)$, α is the transfer coefficient, Γ_{Ox} and Γ_{Red} represent the surface excess at equilibrium for the oxidized and reduced forms, n is the number of electrons transferred, F is the Faraday constant, and k^0 is the standard heterogeneous electron transfer rate constant in units of s^{-1}. The current response was converted into a dimensionless current to remove the electrode area and the surface excess magnitude using the equation

$$i(t) = \frac{nFA\Gamma^*}{\tau}\Psi(t) \tag{4.3}$$

where Γ^* = the total surface concentration of $Ox_{(ads)}$ and $Red_{(ads)}$ and A is the electrode area. The Nicholson-Olmstead method was used to replace the integrals with summations expressing the dimensionless current equation numerically.[30] The final equation is:

$$\Psi_m = \frac{\left(k^0\tau - \frac{k^0\tau}{2L}\sum_{i=1}^{m-1}\Psi_i\right)e^{-\alpha\phi} - \frac{k^0\tau}{2L}\sum_{i=1}^{m-1}\Psi_i e^{(1-\alpha)\phi}}{1 + \frac{k^0\tau}{2L}e^{-\alpha\phi} + \frac{k^0\tau}{2L}e^{(1-\alpha)\phi}} \tag{4.4}$$

where τ is the period, L is the number subintervals on the step, and Ψ_m is the dimensionless current for each time increment with the serial number m. A detailed explanation of this derivation is provided in Appendix 1.

To capture the effect of period as it relates to current, $\Delta\Psi^s$ is used throughout this chapter is shown in Equation 4.5.

$$\Delta\Psi^{s} = \Delta\Psi / \tau = \frac{i(t)}{nFA\Gamma^{*}} \tag{4.5}$$

The physical meaning of $\Delta\Psi^{s}$ is the normalized real current emanating from the electron transfer.

In the following sections, the impact of each empirical parameter on the shape of the voltammogram is examined and compared to the diffusional quasireversible mechanism for the specific case where n = 1. Then, a protocol for discerning this mechanism from empirical data is provided followed by experimental validation of this protocol using two redox active, surface-confined analytes. Note that the theoretical trends delineated below are applicable to both planar and spherical electrodes.[29] Also note that trends for the forward sweep are identical to those one would obtain using conventional SWV.[18-24]

4.3.2 Effect of Period, τ

A series of voltammograms in which the period is varied is shown in Figure 4.1. Determination of the mechanism using cyclic voltammetry requires variation in the potential sweep rate. In SWV and CSWV, the effective potential sweep rate is increment divided by period. Thus, increasing period is equivalent to decreasing the potential sweep rate. As period increases, $E_{p,f}$ and $E_{p,r}$ shift toward the formal potential (see inset of Figure 4.1) and $\Delta\Psi_{p}^{s}$ decreases linearly with period^{-1} while peak ratio remains constant at unity. ΔE_{p} approaches zero as the period is elongated. Peak widths remain constant, increase to a maximum, and then decrease as period is increased.

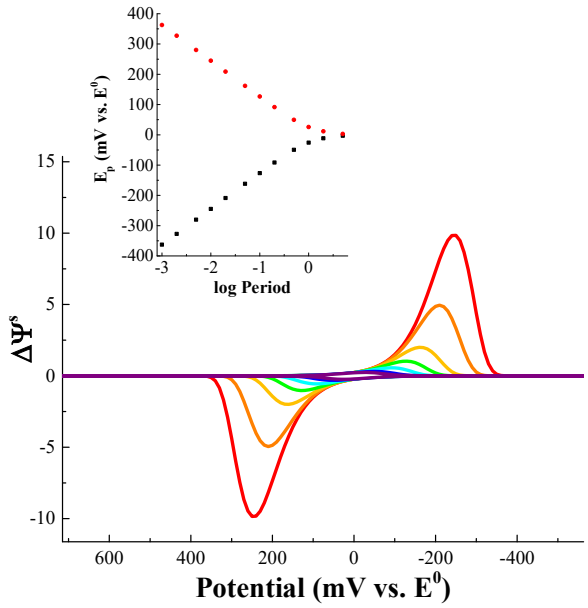

Figure 4.1. The effect of period on the shape of the voltammogram when log k^0 = -1, α = 0.5, amplitude = 50 mV, increment = 10 mV, and period = 1 ms (red), 2 ms (orange), 5 ms (gold), 10 ms (green), 20 ms (cyan), 50 ms (blue), 100 ms (purple), 200 ms (magenta), 500 ms (light gray), 1 s (gray), 2 s (black), and 5 s (brown). The inset presents peak potentials versus log period for the voltammograms depicted in this figure (black squares represent $E_{p,f}$ and red circles represent $E_{p,r}$).

Comparison of the trends for $\Delta\Psi_p^s$ and E_p as a function of period reveals several differences between the surface-confined and diffusional mechanisms. Trends in peak potentials with period are similar between these two mechanisms whereas peak currents and peak ratios differ. As period increases, $\Delta\Psi_p^s$ decreases linearly with period^{-1}. For the diffusional case, $\Delta\Psi_p^+$ decreases linearly with period$^{-1/2}$ (where $\Delta\Psi^+ = \Delta\Psi/\tau^{1/2}$). Peak ratios increase to unity as period is increased for the diffusional case but remain constant at unity for the surface-confined case. Thus, trends in peak currents and peak ratios with period can be used to discern a diffusional from a surface-confined quasireversible mechanism.

4.3.3 Effect of Increment, δE

The effect of increment on the shape and magnitude of the voltammogram is shown in Figure 4.2. For comparison with cyclic voltammetry, the effective potential sweep rate is increment divided by period. Thus, an increase in increment is equivalent to increasing the potential sweep rate. However, the number of points defining the voltammogram decreases as the increment increases. As a consequence, the peaks become less rounded and more jagged. As increment increases, $\Delta\Psi_p^s$ and $W_{1/2}$ increase, and $E_{p,f}$ and $E_{p,r}$ shift away from E^0. As a result, ΔE_p increases with increment. $\Delta\Psi_{ratio}^s$ remains at unity throughout the variation of increment. As reported in the previous section, peak currents, potentials, and widths depend on period. The variation of both period and increment and the resultant peak currents, peak ratios, peak potentials, peak separations, and peak widths are shown in Figure 4.3 to 4.5.

Several key differences in the effect of increment on voltammograms for the diffusional and surface-confined cases can be identified. Peak currents slightly increase in a curvilinear fashion for the diffusional case whereas they increase in a linear fashion for the surface-confined case. Peak ratios decrease with increasing increment for the diffusional mechanism while peak ratios are invariant with increasing increment for the surface-confined case. Though peak potentials shift away from the formal potential for both mechanisms, the magnitude of the shift differs for each mechanism. The shift is also dependent upon period. Thus, the systematic variation of increment on resultant peak currents and potentials can be used to distinguish the diffusional and surface-confined mechanisms.

It is interesting to note that the trends observed for period are the inverse of those observed for increment. For example, $\Delta\Psi_p^s$ values decrease with period but increase with increment. Similarly, while E_p values shift towards E^0 with period, they shift away from E^0 with increment.

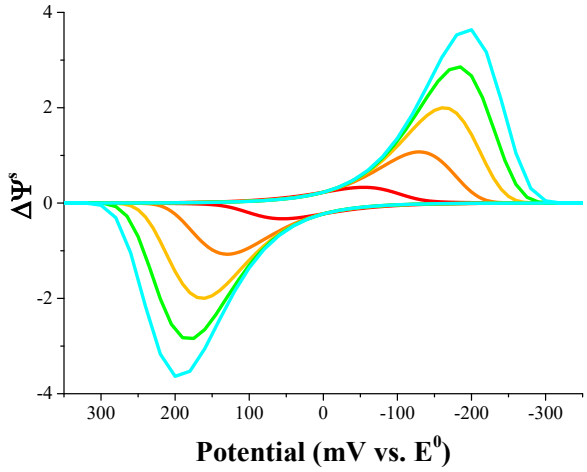

Figure 4.2. The effect of increment on the shape of the voltammogram when $\log k^0 = -1$, $\alpha = 0.5$, period = 50 ms, amplitude = 50 mV, and the increment = 1 mV (red), 5 mV (orange), 10 mV (gold), 15 mV (green), and 20 mV (cyan).

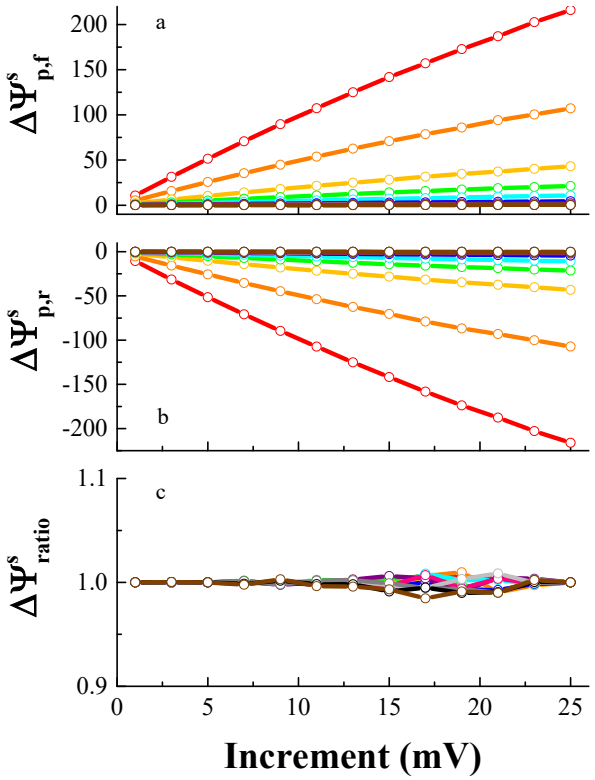

Figure 4.3. The dependence of net peak current on increment: a) $\Delta\Psi^s_{p,f}$, b) $\Delta\Psi^s_{p,r}$, and c) peak ratio when $\alpha = 0.5$, amplitude = 50 mV, $\log k^0 = -1$, and period = 1 ms (red), 2 ms (orange), 5 ms (gold), 10 ms (green), 20 ms (cyan), 50 ms (blue), 100 ms (purple), 200 ms (magenta), 500 ms (light gray), 1 s (gray), 2 s (black), and 5 s (brown).

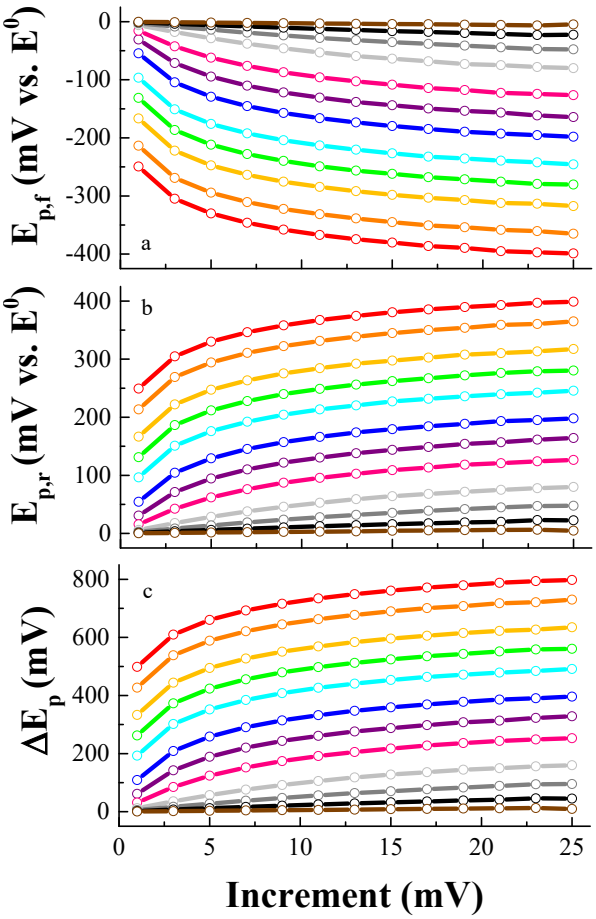

Figure 4.4. The dependence of peak potential on increment: a) $E_{p,f}$, b) $E_{p,r}$, and c) ΔE_p when $\alpha = 0.5$, amplitude = 50 mV, $\log k^0 = -1$, and period = 1 ms (red), 2 ms (orange), 5 ms (gold), 10 ms (green), 20 ms (cyan), 50 ms (blue), 100 ms (purple), 200 ms (magenta), 500 ms (light gray), 1 s (gray), 2 s (black), and 5 s (brown).

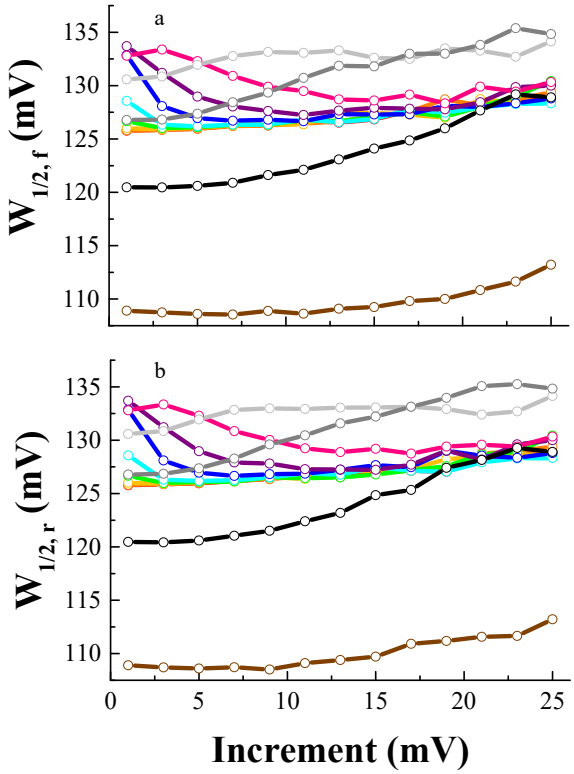

Figure 4.5. The dependence of peak width on increment: a) $W_{1/2,f}$ and b) $W_{1/2,r}$ when α = 0.5, amplitude = 50 mV, log k^0 = -1, period = 1 ms (red), 2 ms (orange), 5 ms (gold), 10 ms (green), 20 ms (cyan), 50 ms (blue), 100 ms (purple), 200 ms (magenta), 500 ms (light gray), 1 s (gray), 2 s (black), and 5 s (brown).

4.3.4 Effect of Switching Potential, E_λ

The effect of switching potential on voltammograms for the surface-confined mechanism is shown in Figure 4.6. As the switching potential is shifted positively, peak currents and potentials remain constant until the switching potential occurs before the current can return to the baseline. Peak ratio decreases at this point, and peak separation is slightly decreased. Similarly, peak widths are unaffected until the switching potential occurs before the current can to return to baseline. At this point, peak widths decrease. Further inspection of the effect of switching potential and period on voltammograms is shown in Figures 4.7 to 4.9.

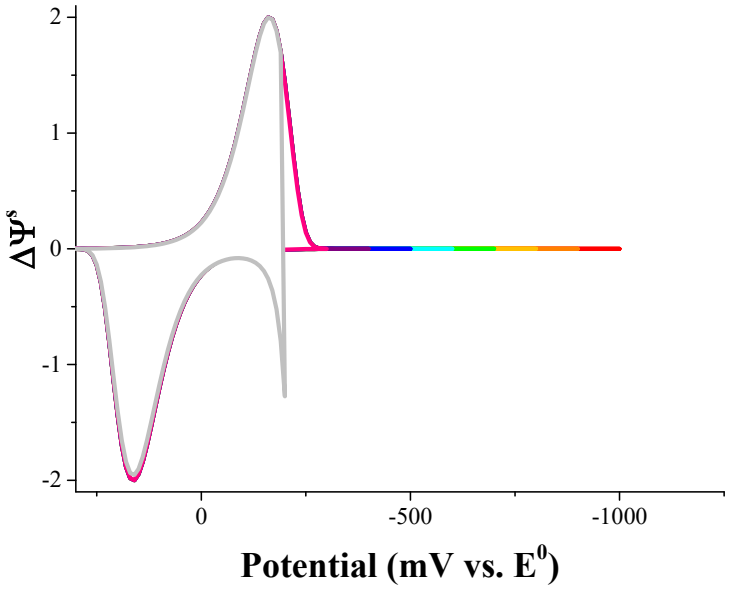

Figure 4.6. The effect of switching potential on the shape of the voltammogram when log $k^0 = -1$, $\alpha = 0.5$, amplitude = 50 mV, increment = 10 mV, period = 50 ms, and the switching potential was varied from 200 (light gray) to 1000 (red) mV negative of E^0 in 100 mV steps.

The effect of switching potential on the voltammogram for the surface-confined mechanism is very similar to that of the diffusional case. Peak currents and peak potentials are only affected when the switching potential occurs prior to the current to baseline. Thus, the variation of switching potential cannot be used to distinguish between these two electrode reaction mechanisms.

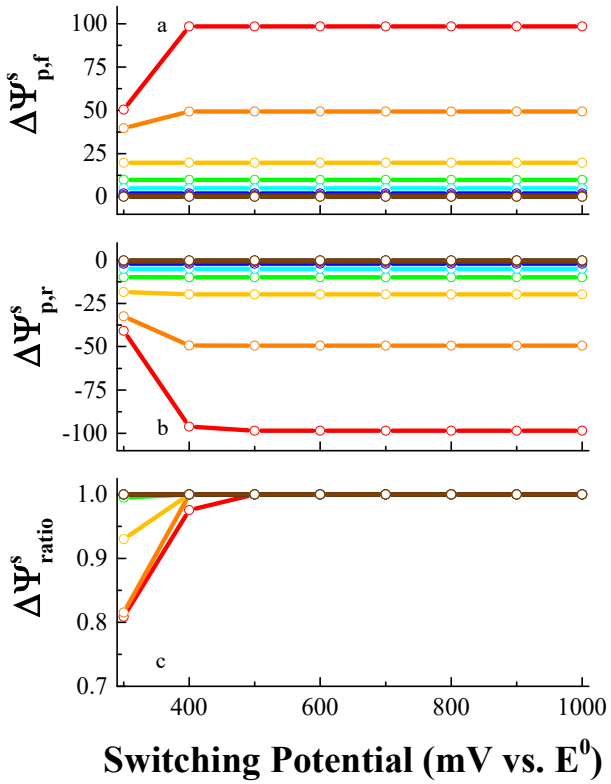

Figure 4.7. The dependence of net peak current on switching potential: a) $\Delta\Psi^s_{p,f}$, b) $\Delta\Psi^s_{p,r}$, and c) peak ratio when $\alpha = 0.5$, amplitude = 50 mV, increment = 10 mV, $\log k^0 = -1$, and period = 1 ms (red), 2 ms (orange), 5 ms (gold), 10 ms (green), 20 ms (cyan), 50 ms (blue), 100 ms (purple), 200 ms (magenta), 500 ms (light gray), 1 s (gray), 2 s (black), and 5 s (brown).

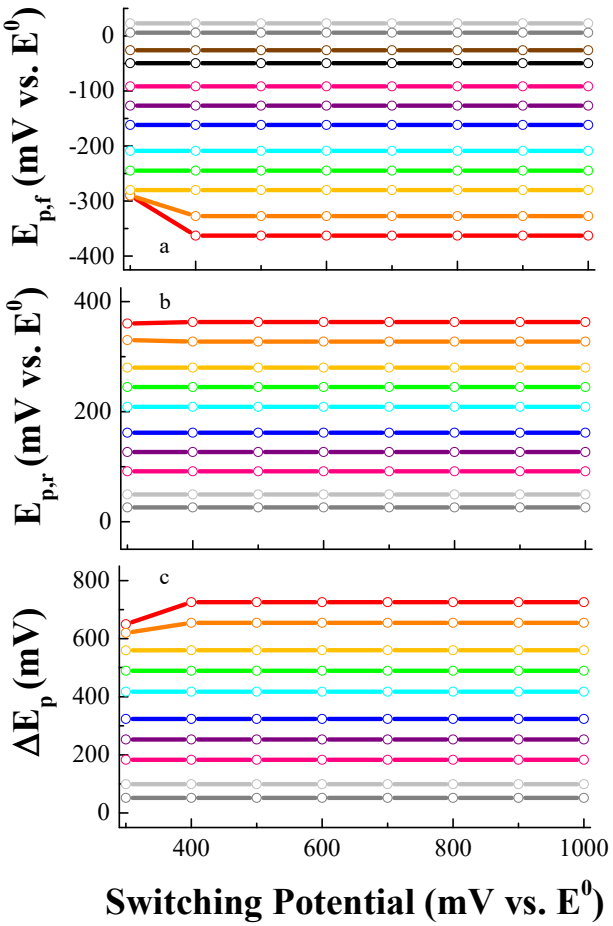

Figure 4.8. The dependence of peak potential on switching potential: a) $E_{p,f}$, b) $E_{p,r}$, and c) ΔE_p when $\alpha = 0.5$, amplitude = 50 mV, increment = 10 mV, log $k^0 = -1$, and period = 1 ms (red), 2 ms (orange), 5 ms (gold), 10 ms (green), 20 ms (cyan), 50 ms (blue), 100 ms (purple), 200 ms (magenta), 500 ms (light gray), 1 s (gray), 2 s (black), and 5 s (brown).

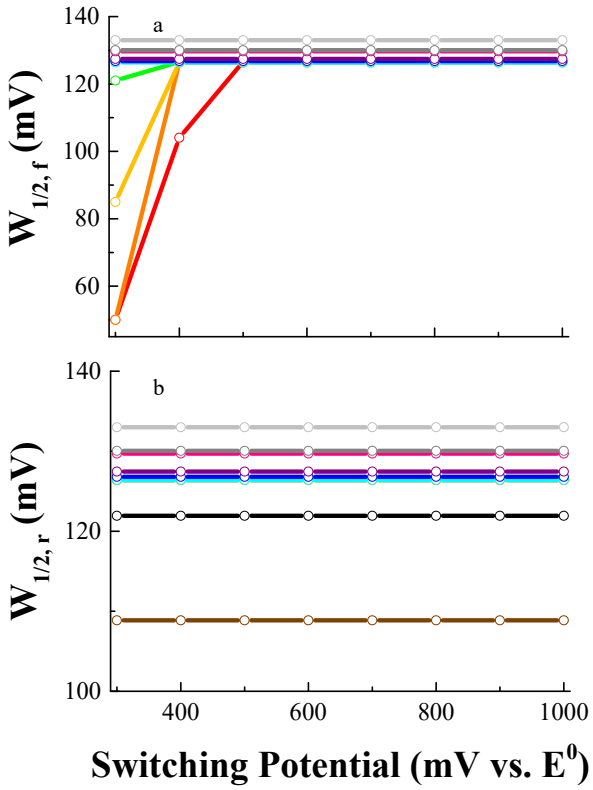

Figure 4.9. The dependence of peak width on switching potential: a) $W_{1/2,f}$ and b) $W_{1/2,r}$ when $\alpha = 0.5$, amplitude = 50 mV, increment = 10 mV, log $k^0 = -1$, and period = 1 ms (red), 2 ms (orange), 5 ms (gold), 10 ms (green), 20 ms (cyan), 50 ms (blue), 100 ms (purple), 200 ms (magenta), 500 ms (light gray), 1 s (gray), 2 s (black), and 5 s (brown).

4.3.5 Effect of Amplitude, E_{SW}

Figure 4.10a presents the effect of amplitude on the shape of the voltammogram for the surface-confined mechanism. Mirčeski et al.[22] have established that the voltammetric response depends on the product nE_{SW}. This section presents a discussion of the effect of amplitude for n = 1. Readers encountering systems with n > 1 should refer to Mirčeski's text. As amplitude increases, $\Delta\Psi^s_{p,f}$ and $\Delta\Psi^s_{p,r}$ increase curvilinearly, and both $E_{p,f}$ and $E_{p,r}$ shift toward E^0. Peak ratio remains constant at unity and ΔE_p decreases as amplitude increases. $W_{1/2}$ increases with amplitude. The effect of both period and amplitude on waveform parameters can be found in 4.11 to 4.13.

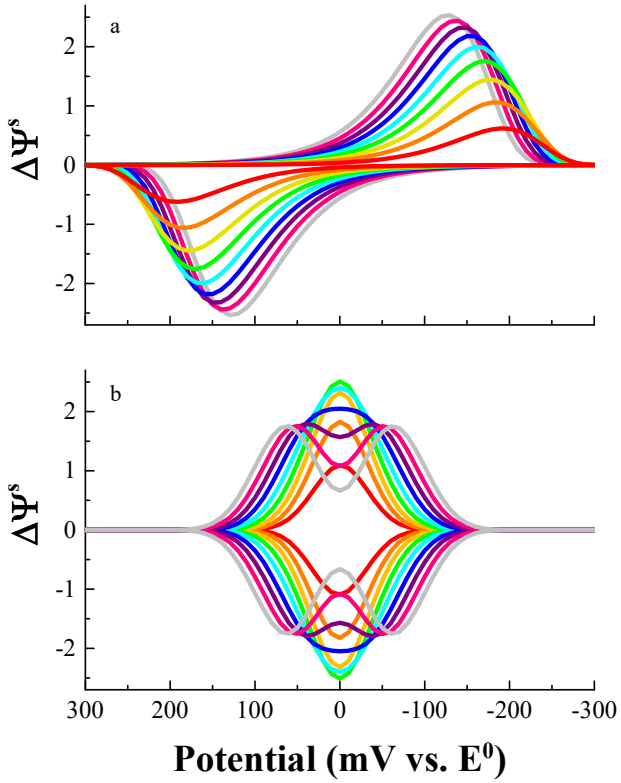

Figure 4.10. The effect of amplitude on the shape of the voltammogram when $\alpha = 0.5$, increment = 10 mV, and amplitude varied from 10 (red) to 90 mV (gray) in 10 mV steps. a) log $k^0 = -1$ and period = 50 ms; b) log $k^0 = 1$ and period = 200 ms.

Systematic variation of amplitude leads to several similar trends for the surface-confined and diffusional mechanisms. Peak potentials shift toward E^0 while ΔE_p decreases for both cases. However, the magnitude of the shift differs for each mechanism. Peak currents and peak widths increase with amplitude for both cases. However, peak ratios for the surface-confined case remain constant at unity while peak ratios increase with amplitude for the diffusional case. Thus, examining the effect of amplitude on peak ratio and the magnitude of peak potential shift can be used for the identification of surface-confined mechanisms.

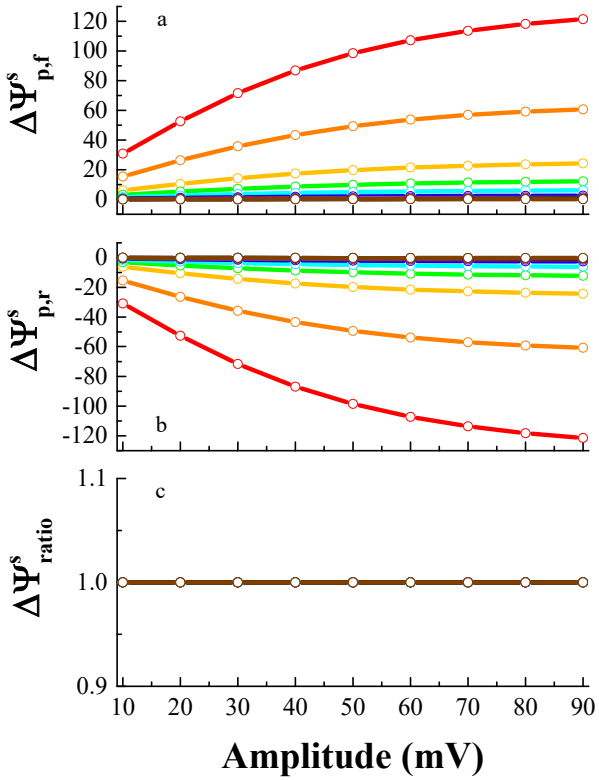

Figure 4.11. The dependence of net peak current on amplitude: a) $\Delta\Psi^s_{p,f}$, b) $\Delta\Psi^s_{p,r}$, and c) peak ratio when $\alpha = 0.5$, increment = 10 mV, $\log k^0 = -1$, and period = 1 ms (red), 2 ms (orange), 5 ms (gold), 10 ms (green), 20 ms (cyan), 50 ms (blue), 100 ms (purple), 200 ms (magenta), 500 ms (light gray), 1 s (gray), 2 s (black), and 5 s (brown).

In some instances, when amplitude is varied a different trend emerges. As shown in Figure 10b, $\Delta\Psi^s_{p,f}$ and $\Delta\Psi^s_{p,r}$ increase with amplitude, reach a maximum, and then decrease and split into two separate peaks. This phenomenon is unique to a quasireversible surface-confined mechanism.[22] Amplitude, k^0, and period values determine when the peak split will occur. Splitting is observed at small k^0 values when using long periods and high amplitudes. It is also observed at large k^0 values when using short periods and low amplitudes but the peak currents under these conditions are quite low (see section below on effects of k^0). Thus, peak splitting is an additional indicator of a surface-confined mechanism.

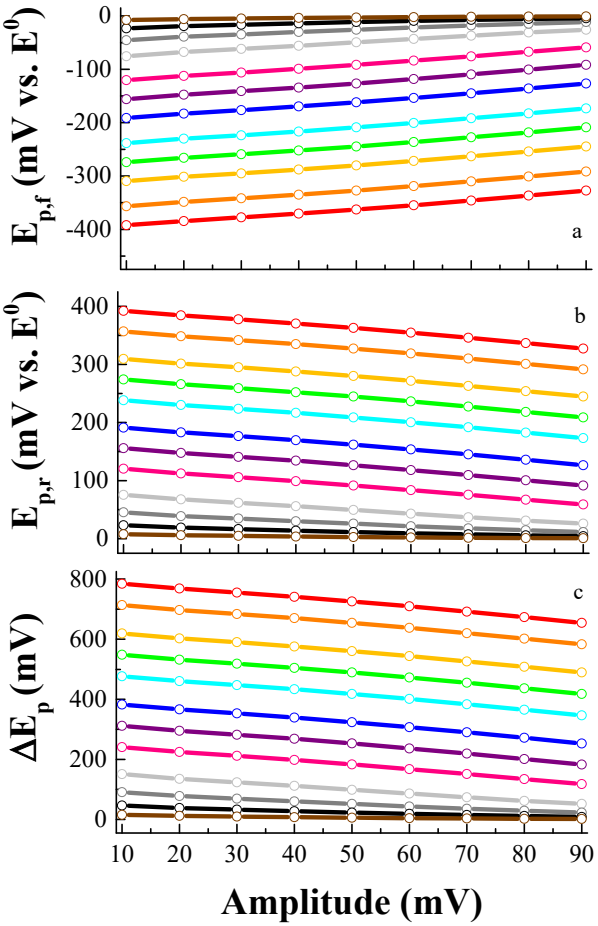

Figure 4.12. The dependence of peak potential on amplitude: a) $E_{p,f}$, b) $E_{p,r}$, and c) ΔE_p when $\alpha = 0.5$, increment = 10 mV, $\log k^0 = -1$, and period = 1 ms (red), 2 ms (orange), 5 ms (gold), 10 ms (green), 20 ms (cyan), 50 ms (blue), 100 ms (purple), 200 ms (magenta), 500 ms (light gray), 1 s (gray), 2 s (black), and 5 s (brown).

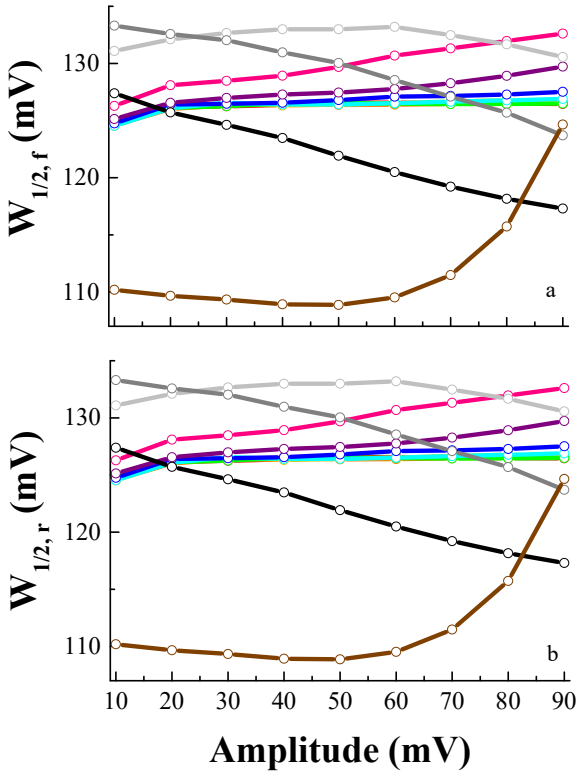

Figure 4.13. The dependence of peak width on amplitude: a) $W_{1/2,f}$ and b) $W_{1/2,r}$ when $\alpha = 0.5$, increment = 10 mV, $\log k^0 = -1$, and period = 1 ms (red), 2 ms (orange), 5 ms (gold), 10 ms (green), 20 ms (cyan), 50 ms (blue), 100 ms (purple), 200 ms (magenta), 500 ms (light gray), 1 s (gray), 2 s (black), and 5 s (brown).

4.3.6 Effect of k^0

The impact of heterogeneous kinetics on the shape of the voltammogram depends upon the magnitude of k^0 relative to τ. Previous investigators have treated the effects of SWV frequency and k^0 (or period and k^0) as a single dimensionless kinetic parameter. [18, 20, 22-24] These quantities are treated individually to assist non-specialists in interpreting the voltammetric trends and assigning the proper mechanism. In practice, one varies τ and determines k^0 from changes in the shape of the voltammograms. The kinetic parameter k^0 is intrinsic to the analyte undergoing an electron transfer reaction at a

particular electrode immersed in a specific electrolyte. Therefore, varying k^0 at a fixed value of τ is, in effect, comparing responses for different analytes and/or different electrode/electrolyte combinations.

Figure 4.14 depicts a set of calculated voltammograms for which period is held constant at 100 ms and log k^0 is varied from -6 to 2 in decades. These limits encompass the range historically associated with an irreversible and reversible process.

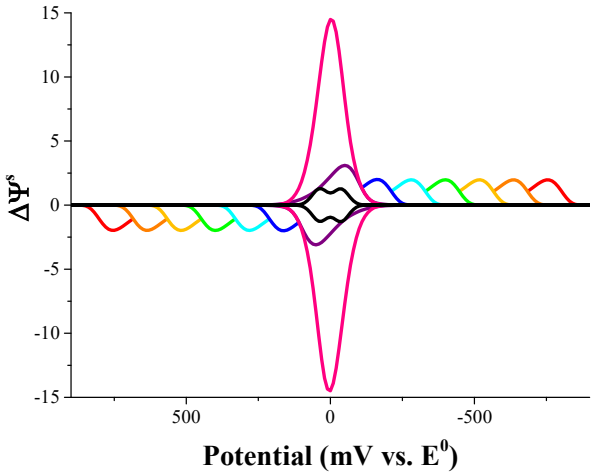

Figure 4.14. The effect of k^0 on the shape of the voltammogram when $\alpha = 0.5$, amplitude = 50 mV, increment = 10 mV, period = 50 ms, and log k^0 = -6 (red), -5 (orange), -4 (gold), -3 (green), -2 (cyan), -1 (blue), 0 (purple), 1 (magenta), and 2 (light gray).

Figure 4.15 presents the dependence of peak potentials on log k^0. Peak potentials shift toward E^0 as log k^0 increases linearly from -6 to 0 and then curvilinearly from 0 to 1. Peak potentials equal E^0 over the range $1 \geq \log k^0 \geq 1.7$. At $\log k^0 > 1.7$, the peak in each scan direction splits into two. Consequently, peak potential separations decrease with increasing log k^0 reaching zero at $\log k^0 = 1$. After the peak splitting occurs, ΔE_p for each pair remains at zero.

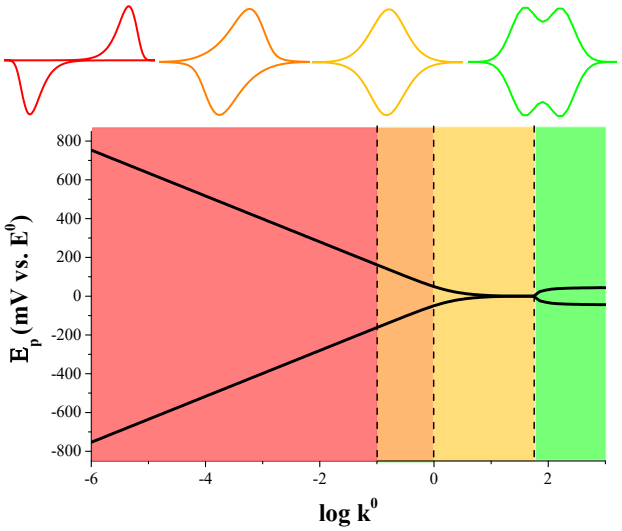

Figure 4.15. The effect of k^0 on $E_{p,f}$ and $E_{p,r}$ and voltammogram shape when amplitude = 50 mV, increment = 10 mV, period = 50 ms, $\alpha = 0.5$, and log k^0 = -6 to 2. Note: the current magnitudes for voltammograms depicted on top of the plot are normalized for display purposes. They are not indicative of the variation of current with k^0.

Figure 4.16a presents the dependence of peak currents on log k^0. Peak currents remain unchanged up to log k^0 equal -0.7. At higher values of log k^0, peak currents increase to a maximum at log k^0 = 1.2. After the maximum, the peak current decreases until it splits into two (*vide supra*) and then falls rapidly into the baseline. As the rate of electron transfer increases, the time required to convert Ox_{ads} to Red_{ads} at a given potential decreases. When the period is longer than the time required for this conversion, peak currents will approach zero. Previous reports have established the quasireversible maximum in SWV as an indicator of a surface-confined process.[22, 31-33] This trend is in sharp contrast with CV. In CV using analog instrumentation, a peak is observed regardless of k^0 and its magnitude is proportional to the potential sweep rate. However, in cyclic staircase voltammetry (*i.e.* CV with digital instrumentation), the peak magnitude depends markedly on when the current is sampled on the step.

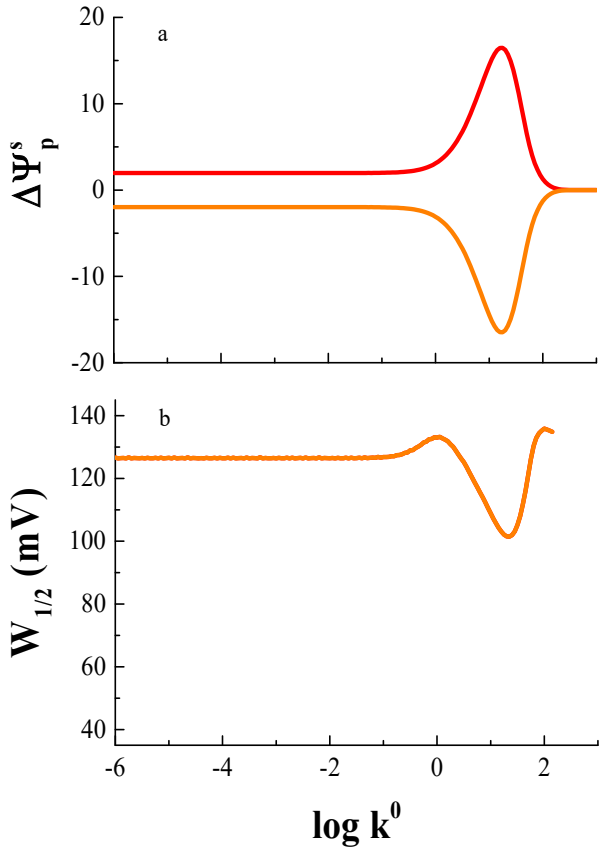

Figure 4.16. The effect of k^0 on $\Delta\Psi^s_{p,f}$ (black) and $\Delta\Psi^s_{p,r}$ (red), and d) $W_{1/2,f}$ (black) and $W_{1/2,r}$ (red) when amplitude = 50 mV, increment = 10 mV, period = 50 ms, $\alpha = 0.5$, and log k^0 = -6 to 2.

Figure 4.16b presents the dependence of peak widths on log k^0. Peak widths are equal to 127 mV and remain constant over the range $-6 < \log k^0 < -1$. They increase to 133 mV as log k^0 increases from -1 to 0 and then decrease to 101 mV at log $k^0 = 1.3$. At log $k^0 >$ 1.3, the peak widths rise as a result of peak splitting.

Several differences in the effect of k^0 on the voltammogram for quasireversible diffusional and surface-confined cases can be identified. Peak potentials and peak separation are dependent upon log k^0 for both mechanisms but with slightly differing slopes. Quasireversible diffusional processes have leak-over peaks[34] at small values of k^0 whereas surface-confined processes never have leak-over peaks. For diffusional

processes, peak currents increase with log k^0 in a sigmoidal fashion whereas peak currents reach a maximum and then fall with a surface-confined process. Peak splitting is only observed with surface-confined processes; the point at which peak splitting occurs depends upon period, amplitude, and k^0. Peak widths decrease with increasing log k^0 in a sigmoidal fashion for diffusional processes but both increase and decrease with increasing log k^0 for surface-confined processes. Thus, log k^0 affects the shape and magnitude of the voltammogram differently for diffusional and surface-confined processes. The range in log k^0 accessible with CSWV is limited by the range in τ and whether the experimenter is using peak separation or peak current maxima.

4.3.7 Effect of the Transfer Coefficient

The transfer coefficient, α, describes the symmetry of the overlap of the two potential wells of the reaction coordinate for electron transfer. The transfer coefficient is a property that is inherent to a particular electron transfer process. Hence, this value cannot be varied by an experimenter, but CSWV experiments can be executed to identify the transfer coefficient for a given reaction. An α value of 0.5 denotes a perfectly symmetrical overlap. Since α ranges from 0 to 1, values other than 0.5 indicate that the overlap of the potential energy – reaction coordinate curves leans towards one well or the other.

Figure 4.17 presents the effect of α on the shape of a voltammogram. As α increases, $\Delta\Psi^s_{p,f}$ increases while $\Delta\Psi^s_{p,r}$ decreases. $\Delta\Psi^s_{ratio}$ decreases with increasing α. $E_{p,f}$ shifts positively towards E^0 with increasing α whereas $E_{p,r}$ shifts negatively away from E^0. $W_{1/2,f}$ decreases with increasing α; $W_{1/2,r}$ increases with α. Thus, α strongly affects the shape and magnitude of the voltammogram.

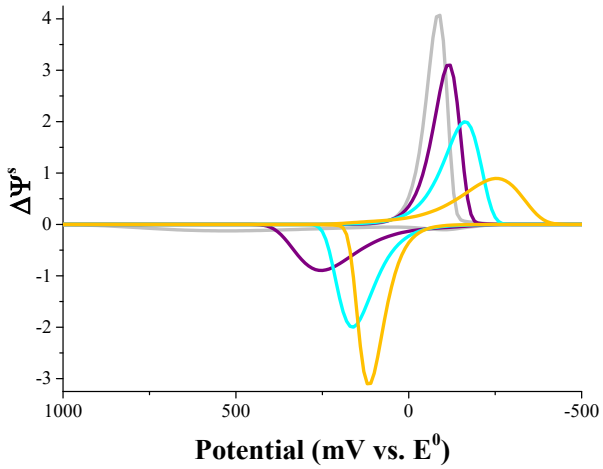

Figure 4.17. The effect of α on the shape of the voltammogram when log k^0 = -1, period = 50 ms, amplitude = 50 mV, increment = 10 mV, and α is a) 0.9 (gray), b) 0.7 (purple), c) 0.5 (cyan), d) 0.3 (gold).

Figure 4.18 presents the combined effect of α and period on the shape of the voltammogram. For α = 0.5 (Figure 4.18c), peak potentials are symmetrically displaced from the formal potential; peak currents are of equal and opposite magnitude while $W_{1/2,f} = W_{1/2,r}$. For α < 0.5 (Figure 4.18a and 4.18b), peak potentials are shifted negatively compared to values for α = 0.5. $\Delta\Psi^s_{p,f}$ values are smaller for α < 0.5 compared to α = 0.5; $\Delta\Psi^s_{p,f}$ values are greater than values expected for α = 0.5. $W_{1/2,f}$ are greater than the values obtained for α = 0.5, and $W_{1/2,r}$ values are smaller than the values obtained for α = 0.5. For α > 0.5 (Figure 4.18d and 4.18e), peak potentials are shifted positively compared to values for α = 0.5. $\Delta\Psi^s_{p,f}$ values are larger for α < 0.5 compared to α = 0.5; $\Delta\Psi^s_{p,f}$ values are smaller than values expected for α = 0.5. $W_{1/2,f}$ are smaller than the values obtained for α = 0.5, and $W_{1/2,r}$ values are greater than the values obtained for α = 0.5.

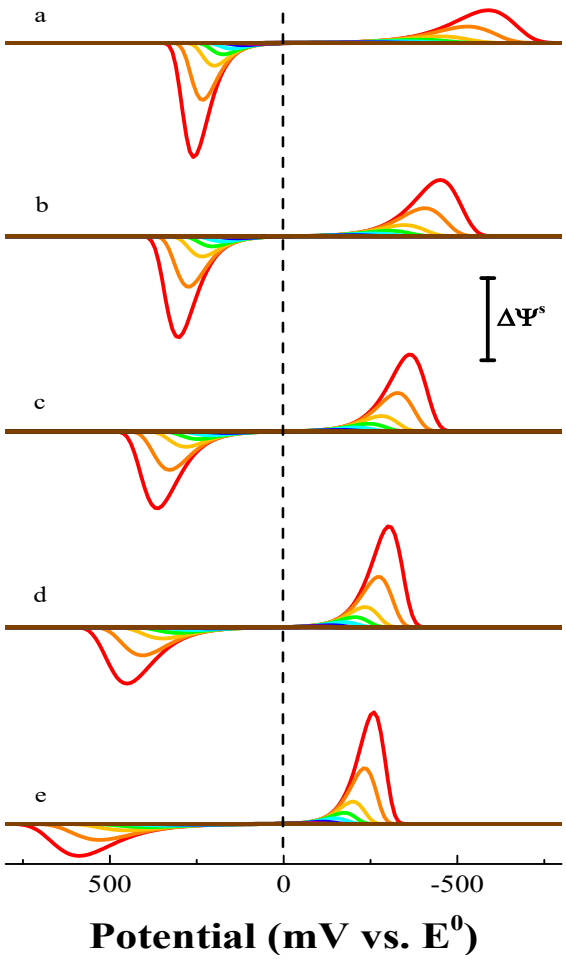

Figure 4.18. The effect of α and period on the shape of the voltammogram when log k^0 = -1, amplitude = 50 mV, increment = 10 mV, α is a) 0.3, b) 0.4, c) 0.5, d) 0.6 and e) 0.7 and period = 1 ms (red), 2 ms (orange), 5 ms (gold), 10 ms (green), 20 ms (cyan), 50 ms (blue), 100 ms (purple), 200 ms (magenta), 500 ms (light gray), 1 s (gray), 2 s (black), and 5 s (brown).

Interested readers are referred to Figure 4.19 for a further analysis of peak widths as a function of α and period.

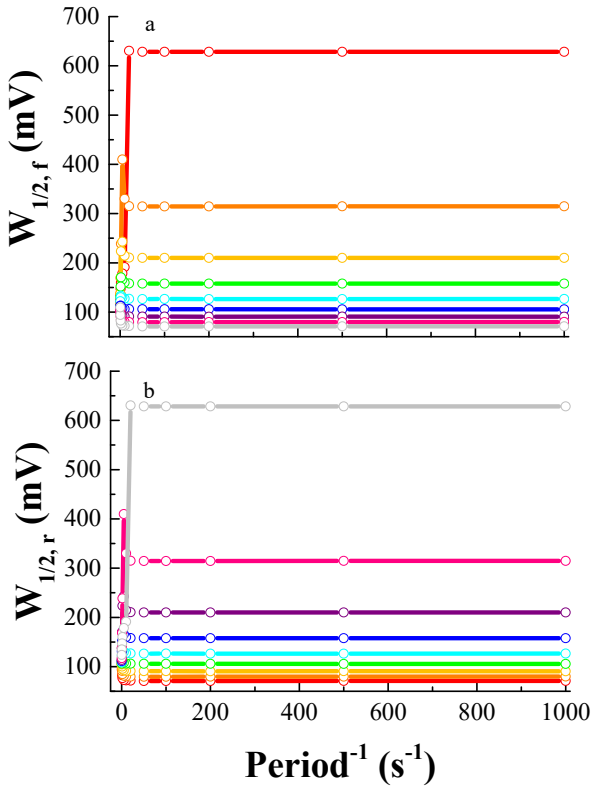

Figure 4.19. The dependence of net peak current on period: a) $W_{1/2,f}$ and b) $W_{1/2,r}$ when amplitude = 50 mV, increment = 10 mV, log k^0 = -1, and α = 0.1 (red), 0.2 (orange), 0.3 (gold), 0.4 (green), 0.5 (cyan), 0.6 (blue), 0.7 (purple), 0.8 (magenta), and 0.9 (light gray).

Figure 4.20a displays peak potentials as a function of α and log period corresponding to the voltammograms found in Figure 4.18. Peak potentials are linearly related to period so long as log period ≤ -0.5. For log period > -0.5, peak potentials curvilinearly approach zero and remain constant as period is increased. Similarly, peak potential separation depends on both α and period (see Figure 4.21). Note that the trace for α = 0.4 in Figure 4.21 is identical to that for α = 0.6. The traces for α = 0.3 and 0.7, 0.2 and 0.8, as well as 0.1 and 0.9 overlap as well.

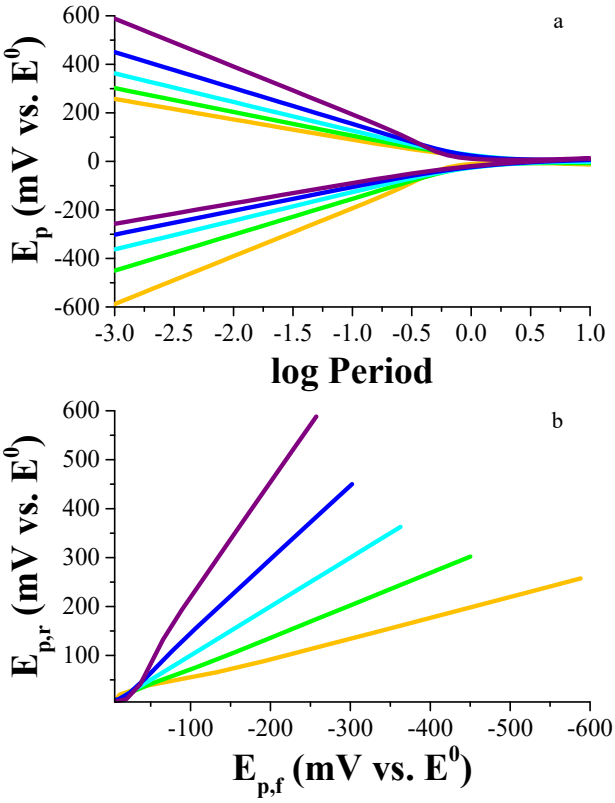

Figure 4.20. Plot of a) peak potential versus log period and b) $E_{p,f}$ versus $E_{p,r}$ as a function of α when log k^0 = -1, amplitude = 50 mV, increment = 10 mV, and where α is 0.3 (gold), 0.4 (green), 0.5 (cyan), 0.6 (blue), and 0.7 (purple).

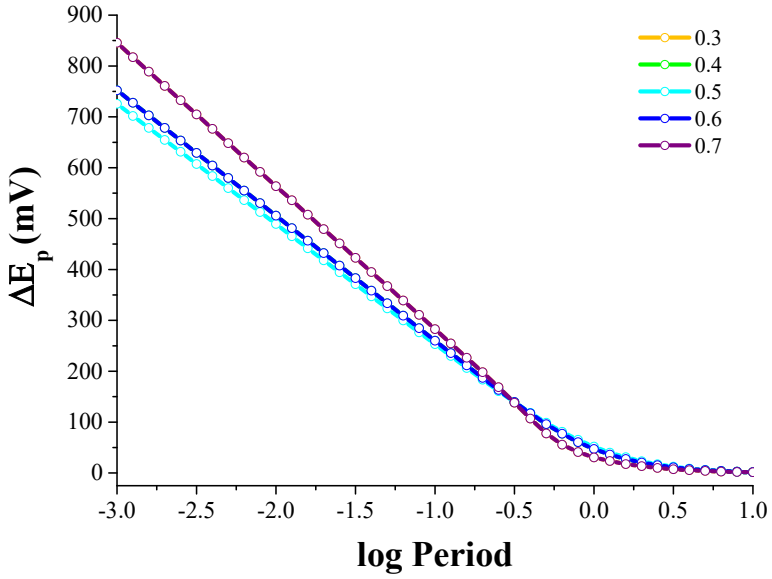

Figure 4.21. Plot of peak separation versus log period as a function of α when log k^0 = -1, amplitude = 50 mV, increment = 10 mV, and where α is 0.3 (gold), 0.4 (green), , 0.5 (cyan), 0.6 (blue)and 0.7 (purple).

It has been previously shown that the value of α for a diffusional quasireversible electrode reaction can be determined from systematic variation of period.[34] A plot of $E_{p,f}$ vs. $E_{p,r}$ constructed from measurements made over a range in period (while keeping amplitude, increment and switching potential constant) provides a straightforward means for calculating α. This method is also applicable to the surface-confined reaction. Figure 4.20b illustrates that a linear relationship is obtained between $E_{p,f}$ vs. $E_{p,r}$ (when $\Delta E_p \geq$ 100 mV) and the marked dependence of the slope on α. Thus the slope of the line can be used to calculate α

$$\text{slope of } E_{p,f} \text{ vs. } E_{p,r} = \frac{\alpha}{1-\alpha} \tag{4.6}$$

For all of the voltammograms depicted in Figure 4.18, $\Delta\Psi_p^s$ decreases with increasing period. Figure 4.22 shows that $\Delta\Psi_p^s$ is linearly related to 1/period; the slope of this trace

depends upon α. This contrasts with the diffusional quasireversible mechanism where $\Delta\Psi_p^+$ decreases with the square root of period. Thus plots of peak currents versus period^{-1} and period$^{1/2}$ are diagnostic indicators of each reaction mechanism and the value of α.

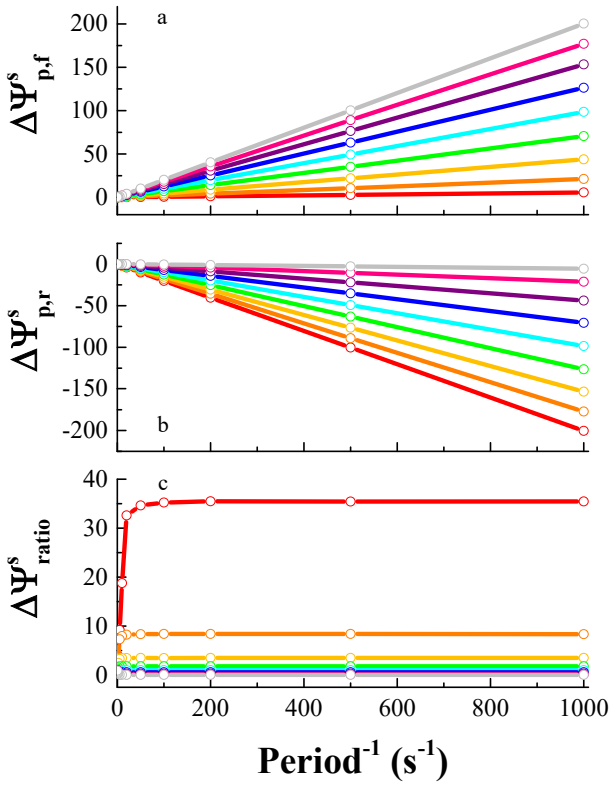

Figure 4.22. The dependence of net peak current on period: a) $\Delta\Psi^s_{p,f}$, b) $\Delta\Psi^s_{p,r}$, and c) peak ratio when amplitude = 50 mV, increment = 10 mV, log k^0 = -1, and α = 0.1 (red), 0.2 (orange), 0.3 (gold), 0.4 (green), 0.5 (cyan), 0.6 (blue), 0.7 (purple), 0.8 (magenta), and 0.9 (light gray).

4.3.8 Diagnostic Criteria for Identifying a Surface-Confined Reaction

The peak currents, potentials and shapes of cyclic square wave voltammograms have been shown to be a complex function α, k^0, increment, period, switching potential and amplitude. The effects of these various parameters on the voltammograms for a surface-confined electrode reaction have enabled the discovery of diagnostic criteria for this

mechanism. These are listed in Table 4.1. Also included in this table are diagnostic plots that will enable rapid identification of electrode reaction using CSWV.

4.3.9 Experimental Verification of Predicted Trends for a Surface-Confined Mechanism

To experimentally validate the trends delineated above, the oxidation of $(Fc)CONH(CH_2)_{15}SH$ adsorbed on a gold electrode was investigated by CSWV. This molecule was selected because it is well established that the molecule chemisorbs to the gold surface through a Au-S-C linkage and remains bound to the surface when the ferrocenyl moiety is oxidized at least over the potential range -0.2 to 0.45 V vs $Ag/AgClO_4$.[25-28] Voltammograms were acquired with systematic variation in period, increment, switching potential and amplitude. The following trends in peak currents and potentials were obtained. As period increased, peak current decreased. Figure 4.23 presents a plot of peak current vs. the reciprocal of period; the expected linear relationship is obtained (compare Figure 4.23 with Figure 4.22). As period increased, peak potentials shifted toward an $E^0 = 0.25$ V vs. $Ag/AgClO_4$ with a corresponding decrease in peak separation. As increment was increased, peak currents increased in a manner consistent with theory (compare Figure 4.24 with Figure 4.3). As increment increased, peak potentials shifted away from E^0 with a corresponding increase in peak separation. Peak currents and potentials were not affected by variation of switching potential (data not shown).

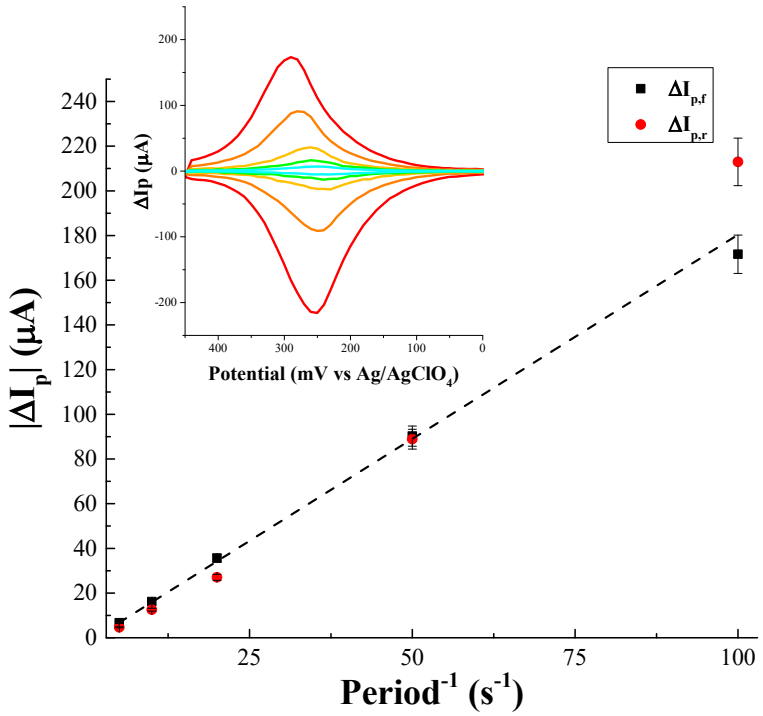

Figure 4.23. Effect of period on ΔI_p for (Fc)CONH$(CH_2)_{15}$SH when amplitude = 20 mV, increment = 10 mV, and period is 10 (red) , 20 (orange), 50 (yellow), 100 (green), and 200 ms (cyan).

Trends in amplitude were dependent upon period. At a period of 20 ms, peak currents increased curvilinearly while $E_{p,f}$ and $E_{p,r}$ shifted negatively with amplitude (see Figures 4.25 and 4.26). The peak widths significantly broaden with increasing amplitude. The peak current and $E_{p,r}$ trends align with theory; the apparent $E_{p,f}$ trend did not. At a period of 200 ms, peak currents increased to a maximum, decreased slightly, and then split into two peaks in each scan direction, *i.e.* $E_{p,f1}$, $E_{p,r1}$, $E_{p,f2}$, and $E_{p,r2}$ (see Figures 4.27 and 4.28). As expected, peak widths at half maximum broadened with increasing amplitude. Prior to the peak splitting, $E_{p,f}$ and $E_{p,r}$ shifted negatively with amplitude. After the peak splitting occurred, the separation between $E_{p,f1}$ and $E_{p,f2}$ as well as $E_{p,r1}$ and $E_{p,r2}$ increased with amplitude (see Figure 4.28). The predicted trend is that the peak potentials remain

at or near the E^0 until peak splitting occurs. It is possible that the apparent negative shift in $E_{p,f}$ at low amplitude is due to inaccuracies in peak potential measurement caused by unresolvable split peaks.

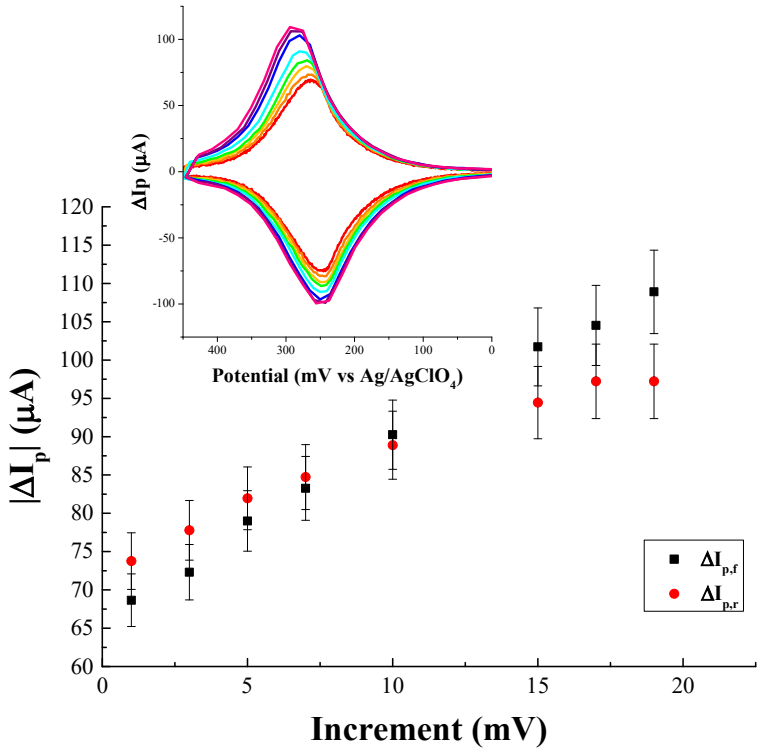

Figure 4.24. Effect of increment on ΔI_p for $(Fc)CONH(CH_2)_{15}SH$ when amplitude = 20 mV, period = 20 ms, and increment is 1 (red), 3 (orange), 5 (yellow), 7 (green), 10 (cyan), 15 (blue), 17 (purple), and 19 mV (pink).

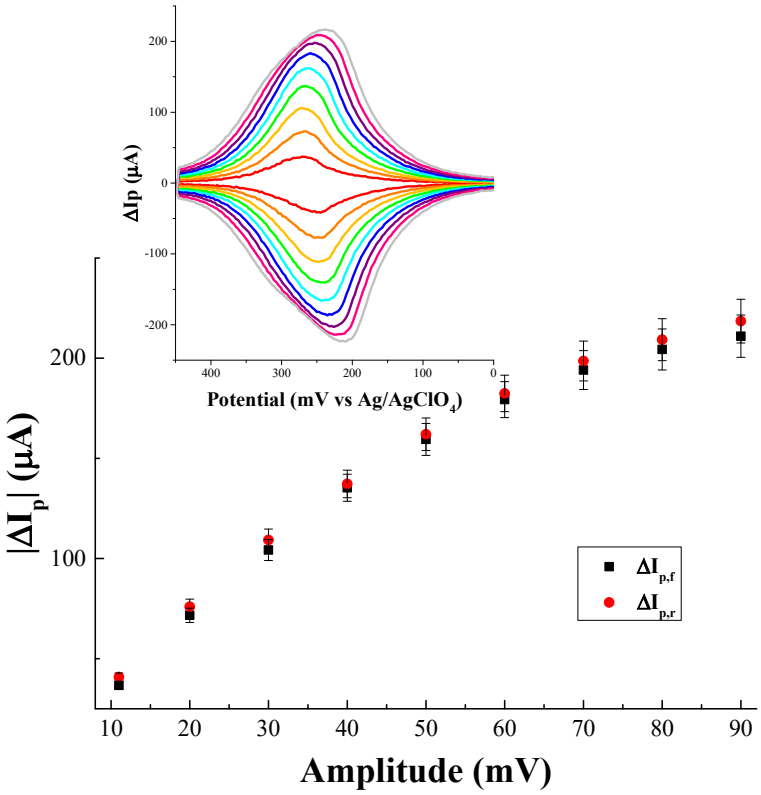

Figure 4.25. Effect of amplitude on ΔI_p for (Fc)CONH$(CH_2)_{15}$SH when period = 20 ms, increment = 3 mV, and amplitude is varied from 10 (red) to 90 mV (light gray) in 10 mV steps.

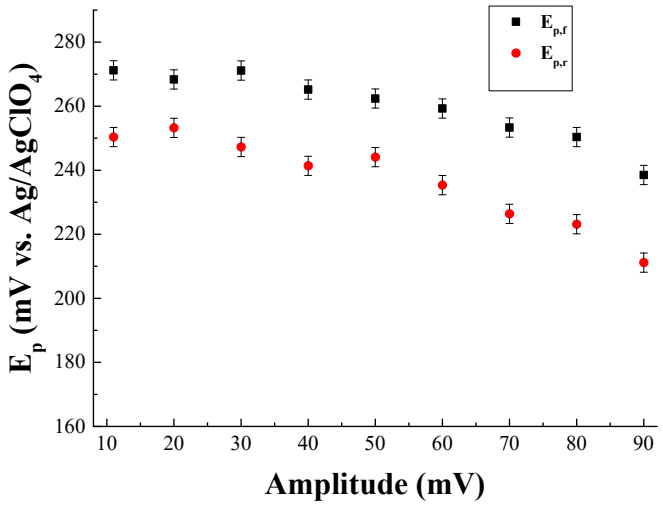

Figure 4.26. Effect of amplitude on E_p for (Fc)CONH$(CH_2)_{15}$SH when when period = 20 ms, increment = 3 mV, and amplitude is varied from 10 to 90 mV in 10 mV steps.

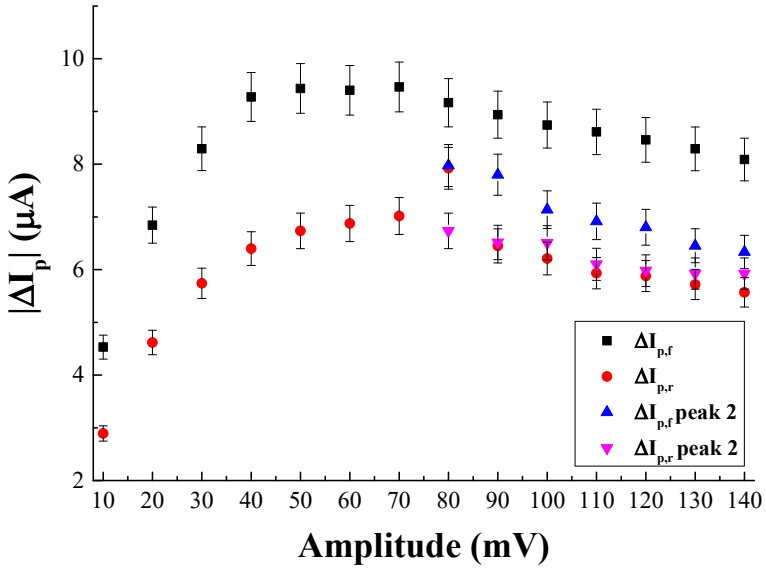

Figure 4.27. Effect of amplitude on ΔI_p for (Fc)CONH$(CH_2)_{15}$SH when period = 200 ms, increment = 10 mV, and amplitude is varied from 10 to 140 mV in 10 mV steps.

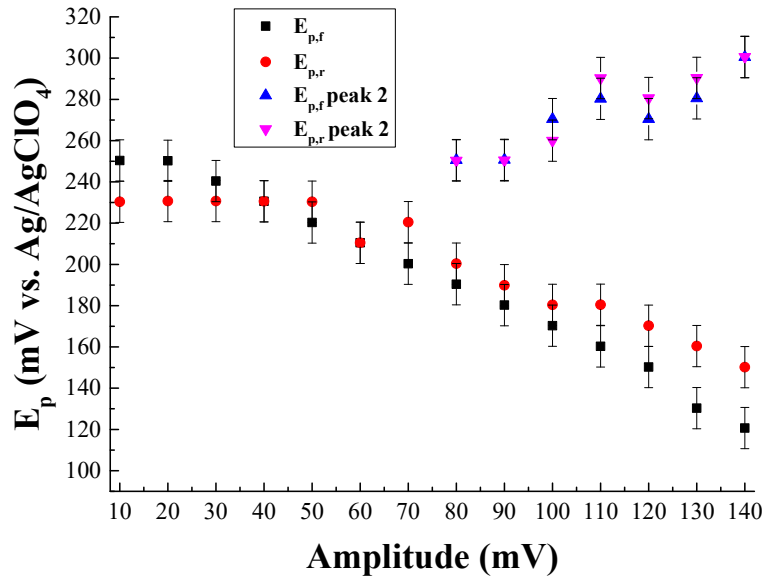

Figure 4.28. Effect of amplitude on E_p for (Fc)CONH$(CH_2)_{15}$SH when when period = 200 ms, increment = 10 mV, and amplitude is varied from 10 to 140 mV in 10 mV steps.

Earlier, a method for determining α from peak potentials as a function of period was presented. This method is most applicable when $\Delta E_p \geq 100$ mV. The maximum peak separation observed for $(Fc)CONH(CH_2)_{15}SH$ was only 50 mV for parameter combinations investigated. Mirčeski and coworkers[22] have also presented a method for determining α from square wave voltammetry data for a surface confined analyte. Their method scans the potential in one direction and plots the individual anodic and cathodic currents versus potential. For oxidative electrode reactions, they compute the ratio of the maximum cathodic current over the maximum anodic current to determine α. Note: these currents are different than the net peak currents discussed above. Using this method, α was determined to be 0.49 ± 0.01 for oxidation of a monolayer of $(Fc)CONH(CH_2)_{15}SH$ on gold, a value consistent with literature.[25]

A method for determining k^0 from peak potentials as a function of period was also presented earlier. Again, this method is most applicable when $\Delta E_p \geq 100$ mV. Since the observed ΔE_p for $(Fc)CONH(CH_2)_{15}SH$ was only 50 mV, this method is inapplicable in this instance. Komorsky-Lovrić and Lovrić[31] have an alternative method for determining k^0 from SWV data. Their method involves plotting net peak current versus the log of square wave frequency to determine the eponymous quasireversible maximum. From the frequency at maximum current, k^0 can be determined. Unfortunately, this method is not applicable here since there was no quasireversible maximum observed over the range in period investigated. Instead, the current decay on each and every pulse was examined over the potential range 0.210 to 0.300 V vs. $Ag/AgClO_4$. Plots of ln(I) vs. time on each pulse were constructed. As shown in Figure 4.29a, curvature was observed consistent with previous report on electroactive monolayers.[35-37] Creager and Weber's example was

used to compute $k_f + k_b$ from the linear portion over the second half of each pulse.[37] A plot of $k_f + k_b$ vs. E_{pulse} was constructed (see Figure 4.29b) analogous to a Tafel plot. An asymmetric curve was observed with the slope of the cathodic portion being less steep than that of the anodic portion. Creager and Weber[37] have also observed this asymmetry. They attribute this to the following phenomena: the chemisorbed monolayer is almost completely uncharged through the cathodic branch and almost completely charged through the anodic branch. The minimum on this curve represents the point where the monolayer is undergoing large changes in surface charge. It is important to note that the minima depend on period and amplitude as observed experimentally. For example, at an increment of 3 mV and a period of 20 ms, $(k_f + k_b)_{min}$ equal to 98.3, 111, and 116 s^{-1} were measured at amplitudes of 10, 20, and 30 mV, respectively. In comparison, at a period of 50 ms, a $(k_f + k_b)_{min}$ of 64.4 s^{-1} was measured for a 20 mV amplitude at an increment of 3 mV. These rates are in close agreement with those previously reported for complete monolayer of $(Fc)CONH(CH_2)_{15}SH$.[37] Lower rates have been reported for submonolayer coverage of this ferrocene alkanethiol.[25-28]

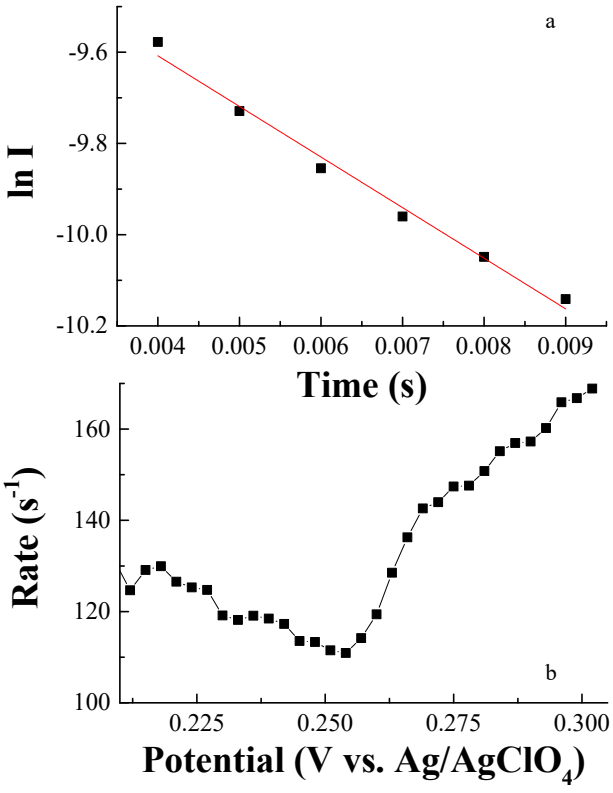

Figure 4.29. The relationship between a) ln I and potential measured at E_{pulse} = 0.254 (V vs. $Ag/AgClO_4$) when amplitude = 20 mV, increment = 3 mV, and period = 20 ms where the slope of the best line of fit yields the rate and b) rate as a function of E_{pulse} for the same empirical parameters given in Figure 4.28a for $(Fc)CONH(CH_2)_{15}SH$.

Variation of empirical parameters should have resulted in peak ratios of 1 for the surface-confined process modeled in this work. However, this trend was not obtained. Since a peak ratio of unity over a wide range of scan rate was obtained from cyclic voltammetry on the same monolayer, this deviation from theory can be attributed to non-ideal behavior, *i.e.*, interactions between the surface-confined molecules, ion-solvation energies, and ion spatial distribution that result from our use of a full monolayer of $(Fc)CONH(CH_2)_{15}SH$.[28, 37-47]

AQDS, another well characterized surface-confined analyte, was also investigated.[8, 11, 48-52] Even though the AQDS electrode reaction is complicated by pH-dependent

chemical reactions,[53, 54] it was selected to highlight how variation of amplitude distinguishes a surface-confined process. Note: a linear relationship between current and scan rate was observed by CV (results not shown) confirming surface confinement of both the oxidized and reduced forms. With increasing CSWV amplitude, peak currents grew to a maximum, began to decrease and broaden, and finally, split into two separate peaks as shown in Figures 4.30 and 4.31. This peak split is in agreement with theory, as reported in this manuscript (see Figure 10b) and by others.[22, 31] Peak ratios ranged from 1.0 to 1.2 (see Figure 4.32) which is indicative of coupled chemical reactions.

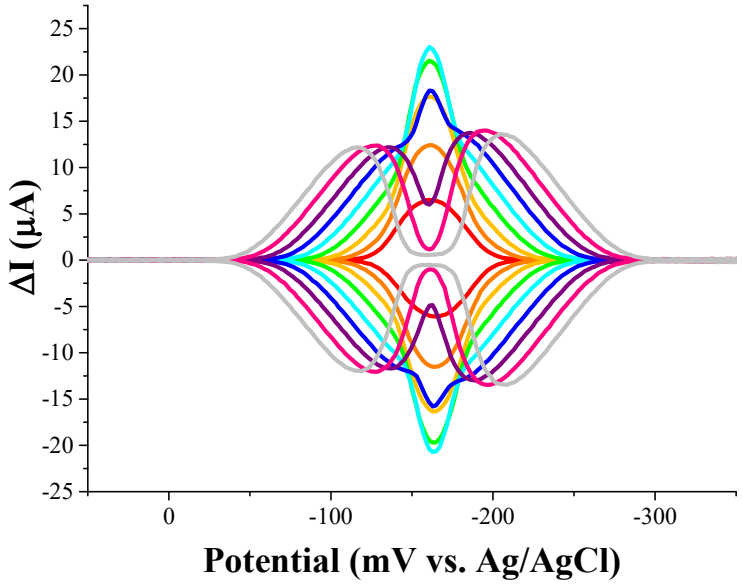

Figure 4.30. The effect of amplitude on the AQDS experimental system when increment = 2 mV, period = 30 ms, and amplitude is varied from 10 (red) to 90 mV (gray) in 10 mV steps.

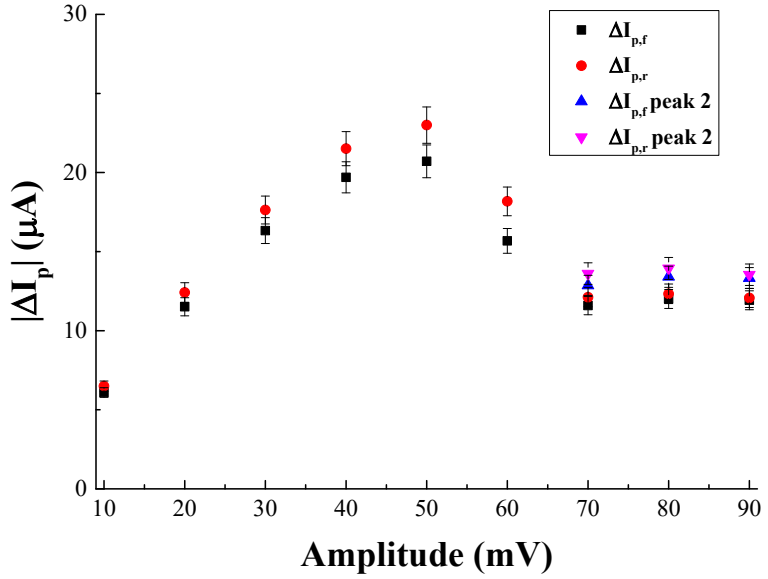

Figure 4.31. The effect of amplitude on peak current for AQDS when period = 30 ms and increment = 2 mV.

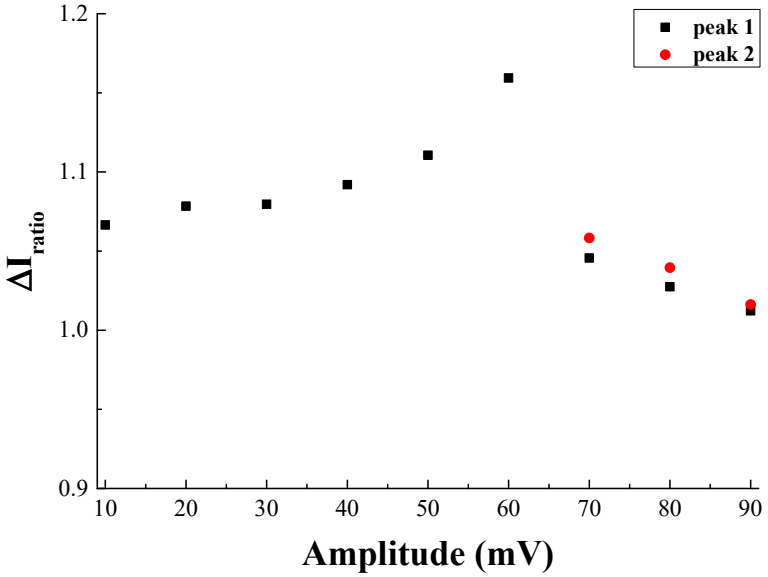

Figure 4.32. The effect of amplitude on peak ratio for AQDS when period = 30 ms and increment = 2 mV.

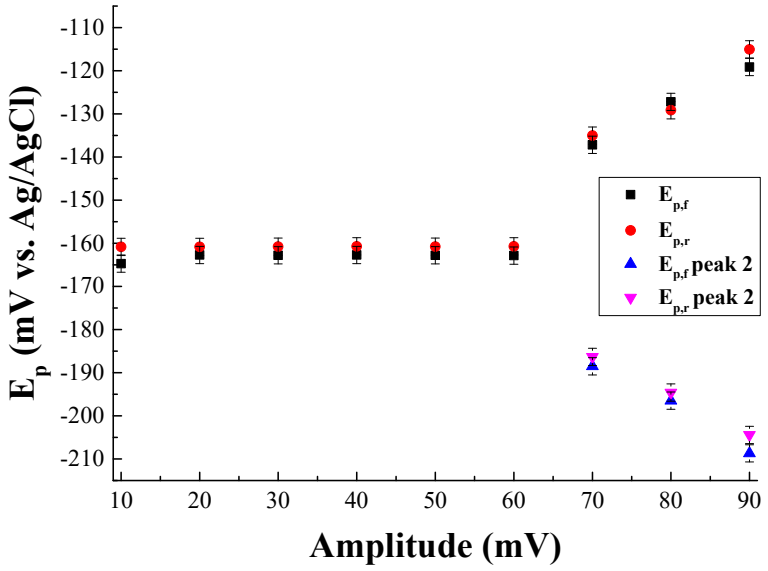

Figure 4.33. The effect of amplitude on peak potential for AQDS when period = 30 ms and increment = 2 mV.

Diagnostic criteria for chemically-coupled electrode reactions will be addressed in detail in a forthcoming manuscript. Peak potentials remained at the formal potential until the peaks split, and peak separation was less than the increment (see Figure 4.34). All trends with amplitude are consistent with a fast, surface-confined electron transfer.

From the peak currents after peak splitting has occurred, α can be calculated using Mirčeski and coworkers' previously established method.[22] Using this method, it was determined that $\alpha = 0.53$ for AQDS for the specific pH, electrolyte and electrode examined. This value is in agreement with previous reports.[48]

4.4 Conclusion

In this chapter, theory for a surface-confined, kinetically-controlled electrode reaction has been developed for CSWV. This theory is applicable to both planar and spherical electrodes. Diagnostic criteria to assist experimenters in identifying this mechanism from

CSWV data have been presented (see Table 4.1). These criteria were experimentally verified using two well-characterized surface-confined analytes. For this particular mechanism, the trends observed for CSWV are comparable to those obtainable with SWV coupled with reverse scan SWV. However, this is not the case for chemically-coupled electron transfer reactions.

Table 4.1. Diagnostic Plots and Protocol for Assessing a Quasireversible Surface-Confined Electrode Reaction by CSWV

	Empirical variables							
Waveform parameters	***Period,* τ**		***Increment,* δE**		***Switching potential,* E_λ**		***Amplitude,* E_{SW}**	
	Plot	**Trend**	**Plot**	**Trend**	**Plot**	**Trend**	**Plot**	**Trend**
Peak currents	ΔI_p vs. τ^{-1}	ΔI_p decrease with τ; plot trace is linear with slope dependent upon α, k^0, and n (see Figure 4.22)	ΔI_p vs. δE	ΔI_p increase curvilinearly with δE; magnitudes are dependent upon both period and k^0 (see Figure 4.3)	ΔI_p vs. E_λ	ΔI_p is independent of E_λ (see Figure 4.7)	ΔI_p vs. E_{SW}	ΔI_p increase curvilinearly with E_{SW} (see Figure 4.11) or increase to a maximum, decrease, and split[a] (see Figure 4.10) depending on k^0 relative to τ
Peak ratio	Peak ratio vs. τ^{-1}	Independent of τ, with value dependent on α (see Figure 4.22)	Peak ratio vs. δE	Independent of δE and equal to unity (see Figure 4.3)	Peak ratio vs. E_λ	Independent of E_λ and equal to unity (see Figure 4.7)	Peak ratio vs. E_{SW}	Independent of E_{SW} and equal to unity (see Figure 4.11)
Peak potentials	E_p vs. log τ	$E_{p,f}$ shifts positively and $E_{p,r}$ shifts negatively with τ until both converge on E^0. Plot trace is linear with slope[a] dependent on α (see Figure 4.1 and 4.20a)	E_p vs. δE	$E_{p,f}$ shifts negatively and $E_{p,r}$ shifts positively in a curvilinear fashion with increasing δE. (see Figure 4.4)	E_p vs. E_λ	Independent of E_λ (see Figure 4.8)	E_p vs. E_{SW}	$E_{p,f}$ shifts positively and $E_{p,r}$ shifts negatively with E_{SW}; the slope magnitudes are dependent upon both τ and k^0 (see Figure 4.12)
	$E_{p,f}$ vs. $E_{p,r}$	Trace is linear or curvilinear dependent on α and k^0 (see Figure 4.20b)						
Peak separation	ΔE_p vs. log τ	Decreases with increasing τ. Plot trace is linear with slope[a] dependent on α (see Figure 4.21)	ΔE_p vs. δE	Increases curvilinearly with increasing δE (see Figure 4.4) Trend magnitudes are dependent upon both period and k^0.	ΔE_p vs. E_λ	Independent of E_λ (see Figure 4.8)	ΔE_p vs. E_{SW}	Decreases linearly with increasing E_{SW} depending on k^0 relative to τ (see Figure 4.12)
Peak widths	$W_{1/2}$ vs. τ^{-1}	Independent of τ but dependent upon α (see Figure 4.19)	$W_{1/2}$ vs. δE	Complex relationship; see Figure 4.5	$W_{1/2}$ vs. E_λ	Independent of E_λ (see Figure 4.9)	$W_{1/2}$ vs. E_{SW}	Complex relationship (see Figure 4.13)

[a] Note: zero slope indicates reversible reaction.

4.5 References

1. Shoesmith, D.W. and R.G. Barradas. *Rev. Anal. Chem.*, **1974**. 2, 83-127.

2. Kalvoda, R. *Stud. Surf. Sci. Catal.*, **1999**. 120B, 111-134.

3. Brown, A.P. and F.C. Anson. *Anal. Chem.*, **1977**. 49, 1589-1595.

4. Laviron, E. *J. Electroanal. Chem. Interfacial Electrochem.*, **1974**. 52, 395-402.

5. Laviron, E. *J. Electroanal. Chem.*, **1979**. 101, 19-28.

6. Rubinstein, I. *J. Electroanal. Chem. Interfacial Electrochem.*, **1985**. 183, 379-386.

7. Brown, A.P. and F.C. Anson. *J. Electroanal. Chem. Interfacial Electrochem.*, **1978**. 92, 133-145.

8. Forster, R.J. *Langmuir*, **1995**. 11, 2247-2255.

9. Komorsky-Lovrić, Š. and M. Lovrić. *Electroanalysis*, **1996**. 8, 959-962.

10. Molina, A. and J. Gonzalez. *Electrochim. Acta*, **2004**. 49, 1349-1360.

11. Molina, A., J. Gonzalez, and N. Abenza. *Electrochim. Acta*, **2007**. 52, 4351-4362.

12. Randles, J.E.B. *Trans. Faraday Soc.*, **1948**. 44, 327-338.

13. Ševčík, A. *Collect. Czech. Chem. Commun.* , **1948**. 13, 349-377.

14. Nicholson, R.S. and I. Shain. *Anal. Chem.*, **1964**. 36, 706-723.

15. Miaw, L.-H.L., P.A. Boudreau, M.A. Pichler, and S.P. Perone. *Anal. Chem.*, **1978**. 50, 1988-1996.

16. Bilewicz, R., R.A. Osteryoung, and J. Osteryoung. *Anal. Chem.*, **1986**. 58, 2761-2765.

17. Bilewicz, R., K. Wikiel, R. Osteryoung, and J. Osteryoung. *Anal. Chem.*, **1989**. 61, 965-972.

18. O'Dea, J.J. and J.G. Osteryoung. *Anal. Chem.*, **1993**. 65, 3090-3097.

19. Reeves, J.H., S. Song, and E.F. Bowden. *Anal. Chem.*, **1993**. 65, 683-688.

20. Mirčeski, V. and M. Lovrić. *Electroanalysis*, **1997**. 9, 1283-1287.

21. Barros, A.A., J.A. Rodrigues, P.J. Almeida, P.G. Rodrigues, and A.G. Fogg. *Anal. Chim. Acta*, **1999**. 385, 315-323.

22. Mirčeski, V., Š. Komorsky-Lovrić, and M. Lovrić, *Square Wave Voltammetry: Theory and Application*, *Monographs in Electrochemistry*. **2007**, Springer-Verlag: Berlin.

23. Lovrić, M. and Š. Komorsky-Lovrić. *Cent. Eur. J. Chem.*, **2010**. 8, 513-518.

24. Mirčeski, V., E. Laborda, D. Guziejewski, and R.G. Compton. *Anal. Chem.*, **2013**. 85, 5586-5594.

25. Liu, B., A.J. Bard, M.V. Mirkin, and S.E. Creager. *J. Am. Chem. Soc.*, **2004**. 126, 1485-1492.

26. Hockett, L.A. and S.E. Creager. *Langmuir*, **1995**. 11, 2318-2321.

27. Weber, K.S. and S.E. Creager. *J. Electroanal. Chem.*, **1998**. 458, 17-22.

28. Weber, K. and S.E. Creager. *Anal. Chem.*, **1994**. 66, 3164-3172.

29. Leddy, J. *J. Electroanal. Chem. Interfacial Electrochem.*, **1991**. 300, 295-307.

30. Nicholson, R.S. and M.L. Olmstead, *Electrochemistry: Calculations, Simulation and Instrumentation,*. **1972**, Marcel Dekker: New York. Ch. 5

31. Komorsky-Lovrić, Š. and M. Lovrić. *Anal. Chim. Acta*, **1995**. 305, 248-255.

32. Komorsky-Lovrić, Š. and M. Lovrić. *Electrochim. Acta*, **1995**. 40, 1781-1784.

33. Komorsky-Lovrić, Š. and M. Lovrić. *J. Electroanal. Chem.*, **1995**. 384, 115-122.

34. Mann, M.A., J.C. Helfrick, Jr., and L.A. Bottomley. *Anal. Chem.*, **2014**. 86, 8183-8191.

35. Chidsey, C.E.D. *Science,* **1991**. 251, 919-922.

36. Finklea, H.O. and D.D. Hanshew. *J. Am. Chem. Soc.*, **1992**. 114, 3173–3181.

37. Creager, S.E. and K. Weber. *Langmuir*, **1993**. 9, 844-850.

38. Chidsey, C.E.D., C.R. Bertozzi, T.M. Putvinski, and A.M. Mujsce. *J. Am. Chem. Soc.*, **1990**. 112, 4301-4306.

39. Creager, S.E. and G.K. Rowe. *Anal. Chim. Acta*, **1991**. 246, 233-239.

40. Rowe, G.K. and S.E. Creager. *J. Phys. Chem.*, **1994**. 98, 5500-5507.

41. Creager, S.E. and G.K. Rowe. *J. Electroanal. Chem.*, **1997**. 420, 291-299.

42. Fujii, S., K. Murase, and H. Sugimura. *Electrochemistry (Tokyo, Jpn.)*, **2007**. 75, 523-527.

43. Guo, Y., J. Zhao, and J. Zhu. *Thin Solid Films*, **2008**. 516, 3051-3057.

44. Eggers, P.K., D.B. Hibbert, M.N. Paddon-Row, and J.J. Gooding. *J. Phys. Chem. C*, **2009**. 113, 8964-8971.

45. Rudnev, A.V., U. Zhumaev, T. Utsunomiya, C. Fan, Y. Yokota, K.-i. Fukui, and T. Wandlowski. *Electrochim. Acta*, **2013**. 107, 33-44.

46. Rudnev, A.V., K. Yoshida, and T. Wandlowski. *Electrochim. Acta*, **2013**. 87, 770-778.

47. Tian, H., Y. Dai, H. Shao, and H.-Z. Yu. *J. Phys. Chem. C*, **2013**. 117, 1006-1012.

48. Chen, X., J. Zhuang, and P. He. *J. Electroanal. Chem. Interfacial Electrochem.*, **1989**. 271, 257-268.

49. He, P., R.M. Crooks, and L.R. Faulkner. *J. Phys. Chem.*, **1990**. 94, 1135-1141.

50. Kano, K. and B. Uno. *Anal. Chem.*, **1993**. 65, 1088-1093.

51. Xu, J., Q. Chen, and G.M. Swain. *Anal. Chem.*, **1998**. 70, 3146-3154.

52. Bechtold, T., C. Fitz-Binder, and A. Turcanu. *Dyes Pigm.*, **2010**. 87, 194-203.

53. Batchelor-McAuley, C., Q. Li, S.M. Dapin, and R.G. Compton. *J. Phys. Chem. B*, **2010**. 114, 4094-4100.

54. Batchelor-McAuley, C., B.R. Kozub, D. Menshykau, and R.G. Compton. *J. Phys. Chem. C*, **2011**. 115, 714-718.

CHAPTER 5

THE EC MECHANISM

Submitted to *Electrochimica Acta*

5.1 Introduction

Electron transfer reactions that generate an unstable product are commonly referred to as an EC mechanism when the product of the chemical reaction following the electron transfer is electroinactive over the potential range examined. The chemical reaction may be reversible or irreversible; the electron transfer may be fast or kinetically-controlled. The EC mechanism can be identified with a variety of electrochemical techniques.[1-8] While theory to guide the experimentalist in identifying this electrode reaction using SWV has been reported,[9-18] very few applications of this theory have been published.[19-22]

In this chapter, theory of CSWV for the $E_{rev}C$ mechanism is presented. Signature trends resulting from systematic variation of the empirical parameters for CSWV, *i.e.* period, increment, switching potential, and amplitude are identified and used to establish diagnostic criteria for the identification of these mechanisms. When properly applied, these trends enable the experimentalist to identify an EC mechanism and calculate the rate of the following reaction as well as thermodynamic parameters.

5.2 Results and Discussion

5.2.1 Theory

The general reaction pathway for an electron transfer followed by a chemical reaction

is:

$$Ox + ne^- \leftrightarrow Red \underset{k_b}{\overset{k_f}{\rightleftarrows}} Z \qquad (5.1)$$

where Ox is the reactant, Red is the initial product of the electron transfer, Z is the electroinactive product of the following chemical reaction, k_f is the rate constant for the conversion of Red to Z in s^{-1}, and k_b is the rate constant for conversion of Z to Red in s^{-1}. All chemical reactions are treated herein as first order. The derivation of an equation that enables calculation of current at each applied potential for this electrode reaction starting from Fick's laws of diffusion. Expressions for the concentrations of Ox and Red as a function of time and distance from the electrode are found using Laplace transformations following application of the boundary conditions. These expressions are related by the Nernst equation for a reversible electron transfer:

$$E_{applied} = E^0 + \left(\frac{RT}{nF}\right)\ln\left(\frac{C_{Ox}(0,t)}{C_{Red}(0,t)}\right) \qquad (5.2)$$

where n = number of electrons transferred, F = Faraday constant, A = area of the electrode, R = gas constant, T = temperature in Kelvin, E = applied potential, E^0 = formal potential for the electron transfer reaction, D_{Ox} = diffusion coefficient of Ox (cm^2/sec), D_{Red} = diffusion coefficient of Red (cm^2/sec), C_{Ox} (0, t) = concentration of Ox at the electrode surface and any time t, C_{Red} (0, t) = concentration of Red at the electrode surface and any time t. Numerical approximation of the resultant integral equations were performed in the same manner put forth by Nicholson and Olmstead.[23] The final equation used to compute theoretical voltammograms for the $E_{rev}C$ mechanism is

$$\Psi_m = \frac{\frac{(k\tau\,\pi)^{1/2}}{\varepsilon} - \left(\frac{1}{K+1} + \frac{1}{\varepsilon}\right)\left(\frac{2k\tau}{L\pi}\right)^{1/2} \sum_{i=1}^{i=m-1} \Psi_i S_j - \left(\frac{K}{K+1}\right) \sum_{i=1}^{i=m-1} \Psi_i R_j}{\left(\frac{1}{K+1} + \frac{1}{\varepsilon}\right)\left(\frac{2k\tau}{L\pi}\right)^{1/2} + \left(\frac{K}{K+1}\right) R_1} \tag{5.3}$$

where L = number of subintervals on each potential, K = the equilibrium constant for the following chemical reaction and equal to k_f/k_b, Ψ_m = dimensionless current for each time increment with the serial number m, m = number of discrete potentials that comprise the waveform, τ = period, k = the sum of the forward and reverse rate constants for the chemical reaction following the electron transfer, i.e. $k_f + k_b$, and

$$\varepsilon = \exp\left[\frac{nF}{RT}\left(E_{applied} - E^0\right)\right] \tag{5.4}$$

Cyclic square wave voltammograms were calculated to examine the impact of the empirical parameters period, increment, and amplitude on the characteristic features of the voltammogram for the singular case where the number of electrons transferred equals one.

5.2.2 Effect of K and k_f.

The shape of the voltammogram depends upon the magnitude of K as shown in Figure 5.1a. When the equilibrium favors Red (log K < -1), the voltammogram resembles that obtained for a reversible process (*e.g.* peak separation is ~ 0 mV, peak ratio is unity, etc.). The reader is referred to a previous publication for further details regarding reversible process characteristics.[24] When the equilibrium favors Z (log K ≥ -1), the shape of the voltammogram significantly departs from that of a reversible process. The peak parameters ($\Delta\Psi_p^+$, E_p, and $W_{1/2}$) for both the forward and reverse sweep depend upon K, k_f, and k_b.

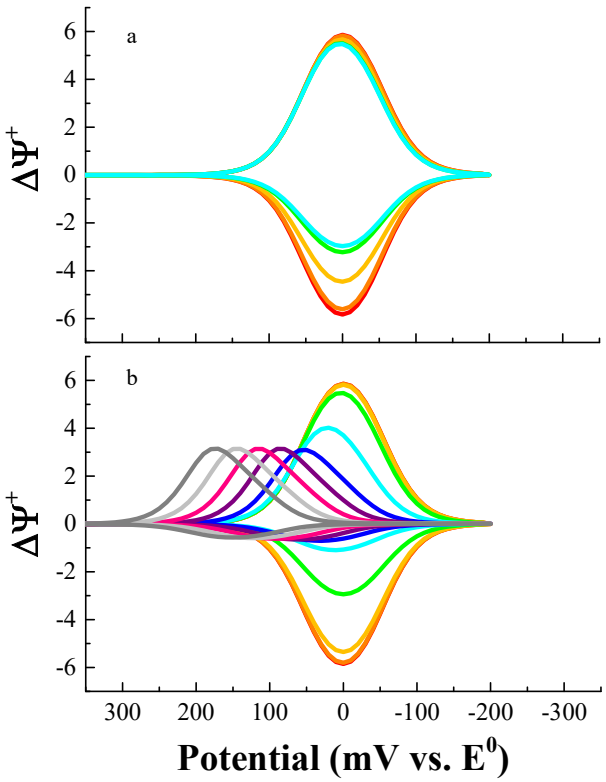

Figure 5.1. The impact of a) K and b) $k_f + k_b$ on the shape of the voltammogram when amplitude = 50 mV, period = 50 ms, E_λ = -200 mV, and increment is 10 mV. In panel a, log K ranges from -2 (red) to 2 (cyan) in steps of 1 when log ($k_f + k_b$) = 0. In panel b, log ($k_f + k_b$) ranges from -3 (red) to 6 (dark gray) in steps of 1 when log K = 6.

The shape of the voltammogram also depends upon the magnitude of k_f as shown in Figure 5.1b. At log $k_f \leq$ -2, the peak currents are commensurate with a reversible process. At -2 < log $k_f \leq$ 2, both $\Delta\Psi^+_{p,f}$ and $\Delta\Psi^+_{p,r}$ decrease; the resultant peak ratio drops from 1.0 to 0.2. At log $k_f >$ 2, the peak currents remain constant and the peak ratio equals 0.2. In contrast, peak potentials remain constant at log $k_f \leq$ 0. At larger values, both $E_{p,f}$ and $E_{p,r}$ shift positively. The peak separation is 19 mV for log $k_f >$ 2.

Figure 5.2a presents the dependence of $\Delta\Psi^+_{p,f}$ on both log ($k_f + k_b$) and K. This plot is similar to that presented as indicative of an EC mechanism.[9, 15] For all values of log K ≥ -1, $\Delta\Psi^+_{p,f}$ decreases, reaches a minimum, and then increases with increasing $k_f + k_b$. The

magnitude of the decrease and the span in $k_f + k_b$ values where $\Delta\Psi^+_{p,f}$ remains below the value for a reversible voltammogram depend upon K. At low values of $k_f + k_b$, there is no appreciable chemical reaction following the electron transfer. Thus, the process appears reversible. As k_f increases, $\Delta\Psi^+_{p,f}$ decreases until a minimum is reached. $\Delta\Psi^+_{p,f}$ begins to increase when k_b becomes sufficiently large for conversion of Z back to Red within the time of the pulse.

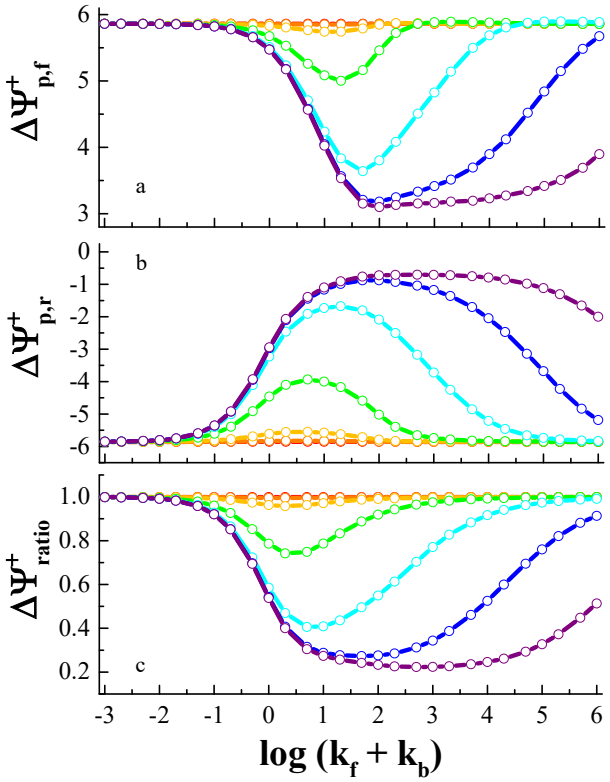

Figure 5.2. The impact of K, k_f, and k_b on a) $\Delta\Psi^+_{p,f}$, b) $\Delta\Psi^+_{p,r}$, and c) peak ratio when amplitude = 50 mV, period = 50 ms, E_λ = -200 mV, and increment = 10 mV. Log K ranges from -3 (red) to 3 (purple) in steps of 1.

Figure 5.2b presents the dependence of $\Delta\Psi^+_{p,r}$ versus log $(k_f + k_b)$ for various values of K. In comparison to $\Delta\Psi^+_{p,f}$, the impact of K, k_f, and k_b on $\Delta\Psi_{p,r}$ is more pronounced.

The onset of the decrease in $\Delta\Psi^{+}_{p,r}$ magnitude occurs at lower values of $k_f + k_b$ and the magnitude of $\Delta\Psi^{+}_{p,r}$ at its minimum is much lower than $\Delta\Psi^{+}_{p,f}$ at its lowest value. The point at which $\Delta\Psi^{+}_{p,r}$ begins to increase in magnitude, however, occurs at the same the same $k_f + k_b$ value for $\Delta\Psi^{+}_{p,f}$. Figure 5.2c presents the dependence of peak ratio versus log ($k_f + k_b$) for various values of K. The trend in peak ratio with K, k_f, and k_b reflects the greater impact on the peak parameters for the reverse sweep relative to those on the forward sweep.

Figure 5.3 presents the dependence of $E_{p,f}$, $E_{p,r}$, and ΔE_p versus log ($k_f + k_b$) for various values of K.

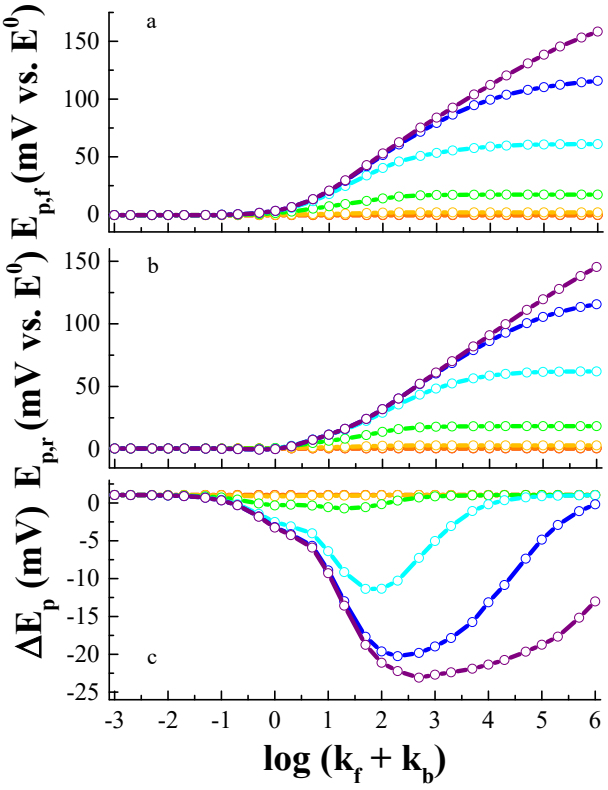

Figure 5.3. The impact of K, k_f, and k_b on a) $E_{p,f}$, b) $E_{p,r}$, and c) peak separation when amplitude = 50 mV, period = 50 ms, E_λ = -200 mV, and increment = 10 mV. Log K ranges from -3 (red) to 3 (purple) in steps of 1.

For log K ≤ -1, both $E_{p,f}$ and $E_{p,r}$ are equal to E^0 and are thus independent of k_f and k_b. When log K > -1, both $E_{p,f}$ and $E_{p,r}$ shift positively by an amount that depends upon K, k_f, and k_b. Peak widths vary somewhat over the range in K, k_f, and k_b investigated herein (see Figure 5.4). While the trends in $\Delta\Psi_p^+$ and E_p as a function of K and $k_f + k_b$ suggest the utility of CSWV in identifying the presence of a chemical reaction following the electron transfer, they do not provide a means for determining the rate constants or equilibrium constant from analysis of a set of voltammograms.

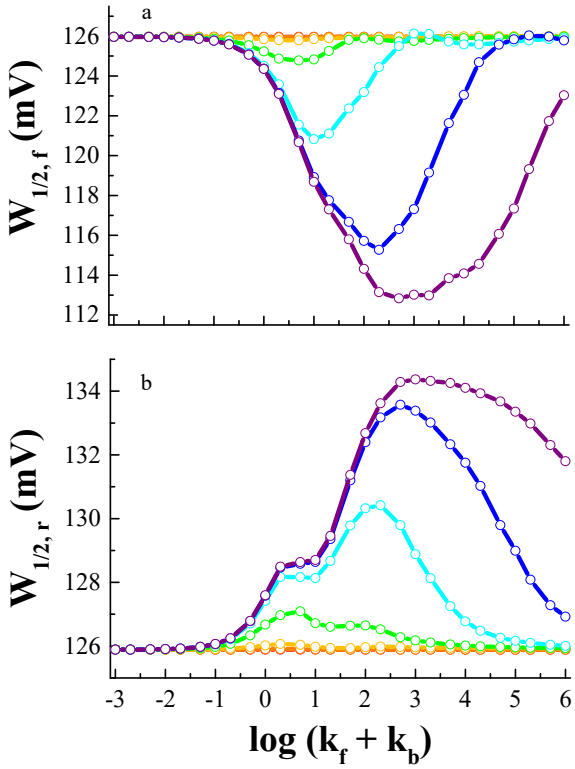

Figure 5.4. The impact of K, k_f, and k_b on a) $W_{1/2,f}$ and b) $W_{1/2,r}$ when amplitude = 50 mV, period = 50 ms, E_λ = -200 mV, and increment = 10 mV. Log K ranges from -3 (red) to 3 (purple) in steps of 1.

5.2.3 Effect of Period (τ)

A set of voltammograms in which period alone is varied is depicted in Figure 5.5a. $E_{p,f}$ and $E_{p,r}$ are ~ E^0 at short periods but shift positively with increasing period; peak potential separation is initially zero increasing to 19 mV (Figure 5.5b). $\Delta\Psi^{+}_{p,f}$ and $\Delta\Psi^{+}_{p,r}$ decrease as period increases. A characteristic of a diffusion controlled, reversible process is that peak currents are proportional to period$^{-1/2}$.[25] As shown in Figure 5.5c, a linear relationship was found for $\Delta\Psi^{+}_{p,f}$ but not for $\Delta\Psi^{+}_{p,r}$. Curvilinearity is indicative of a following chemical reaction (*vide infra*). Figure 5.5d presents the dependence of peak ratio on period. As period increases, the peak ratio decreases from 1.0 to 0.2. This trend is comparable to that observed in cyclic voltammetry since increasing period decreases the potential sweep rate and lengthens the time window for the conversion of Red to Z.[2]

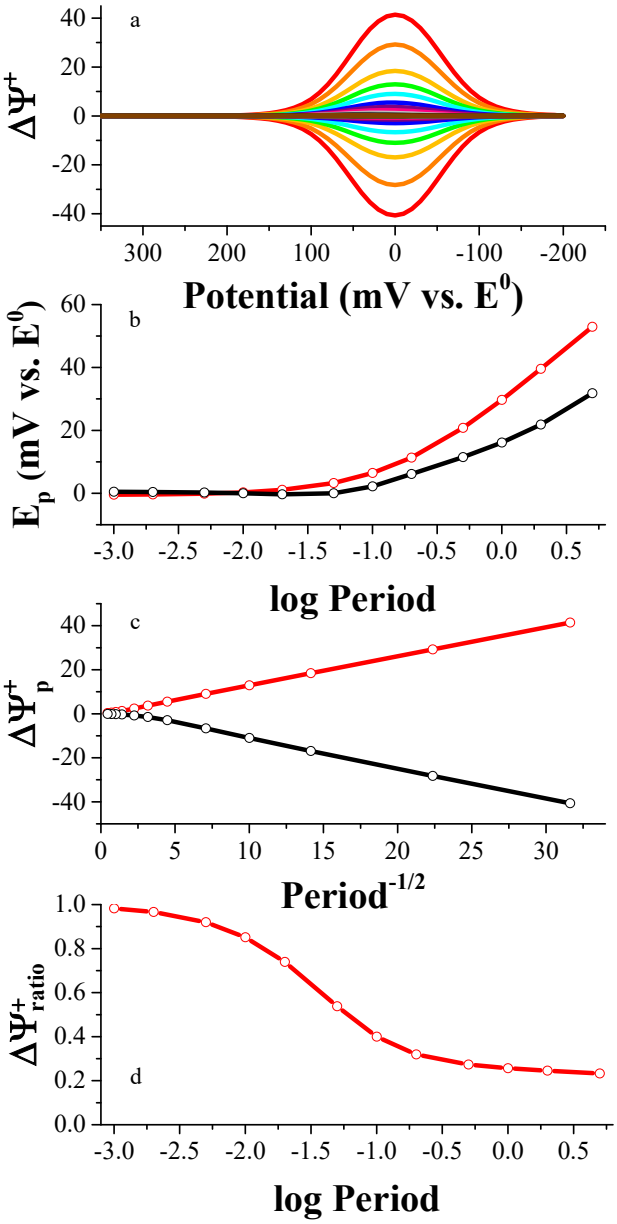

Figure 5.5. The impact of period on the shape of the voltammogram when amplitude = 50 mV, increment = 10 mV, E_λ = -200 mV, log K = 3, and log ($k_f + k_b$) = 0. Panel a): Period ranges from 1 ms (red) to 5 s (brown). Panel b): $E_{p,f}$ (red) and $E_{p,r}$ (black). Panel c): $\Delta\Psi^+_{p,f}$ (red) and $\Delta\Psi^+_{p,r}$ (black). Panel d): Peak ratio (red).

Figure 5.6a presents the peak ratio as a function of both period and K when log ($k_f + k_b$) = 0. At log K ≤ -2, the peak ratio is equal to unity and independent of period. This reflects little to no conversion of Red to Z within the time window determined by period.

Over the range $-2 < \log K \leq 1$, the peak ratio decreases then increases with period; the span in peak ratio depends upon log K. A drop in peak ratio occurs because of increased conversion of Red to Z within the time window of the pulse. At longer periods, the peak ratio begins to rise with increasing conversion of Z back to Red and subsequently to Ox within the time window. Finally, at $\log K > 1$, the peak ratio drops from 1.0 to 0.2 indicative of little to no conversion of Z back to Red to Ox within the time window determined by period.

Figure 5.6b presents the relationship between $\Delta\Psi^{+}_{ratio}$ and log period as $\log (k_f + k_b)$ is varied from -3 to 6 and $\log K = 1$ (the cyan trace in panel a). Vertical sectioning of this contour plot at any value of period reveals that as $\log (k_f + k_b)$ increases, $\Delta\Psi^{+}_{ratio}$ falls from 1 to a minimum before rising back to 1. Similarly, horizontal sectioning of this contour plot reveals that as period increases $\Delta\Psi^{+}_{ratio}$ may increase, decrease, or fall to a minimum before rising, depending upon on $\log (k_f + k_b)$.

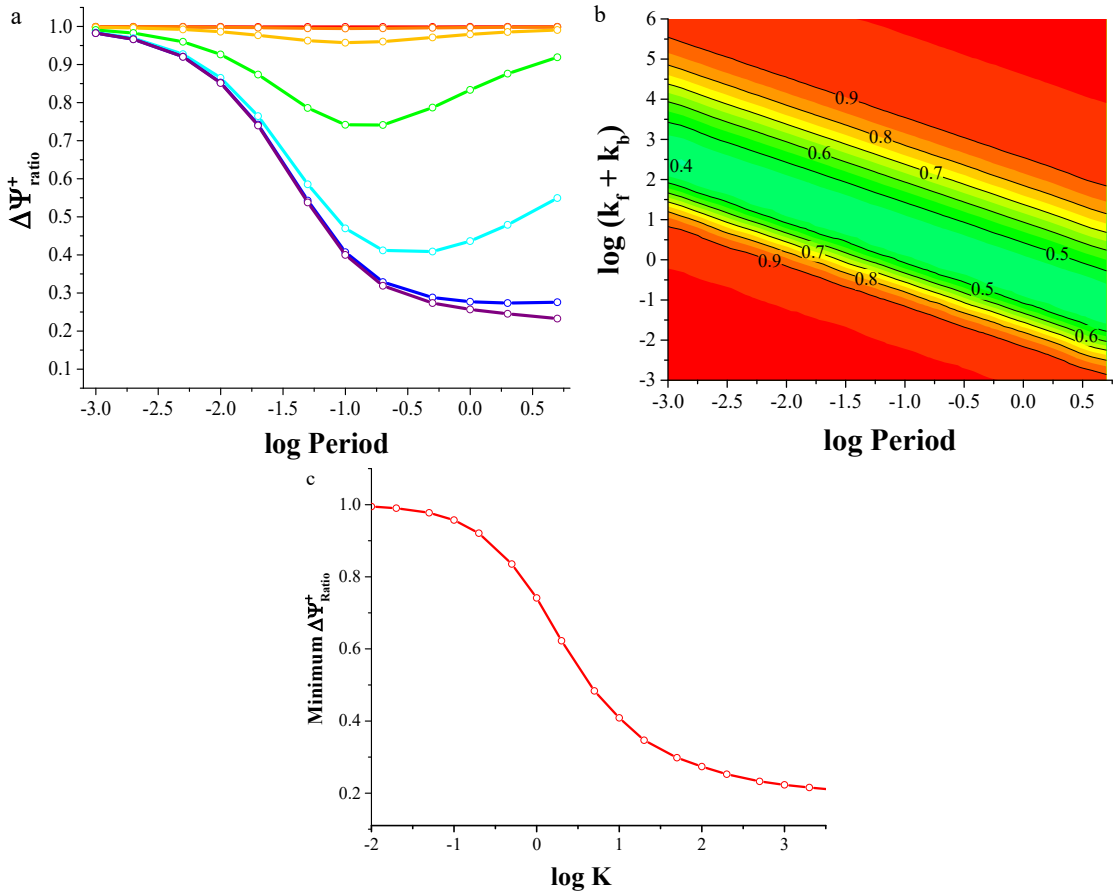

Figure 5.6. The impact of period on the peak ratio as a function of log K and log ($k_f + k_b$) when amplitude = 50 mV, increment = 10 mV, and switching potential = -200 mV. Panel a illustrates the relationship between $\Delta\Psi^+_{ratio}$ and period as log K is varied from -3 (red) to 3 (purple) and log ($k_f + k_b$) = 0. Panel b presents the relationship between $\Delta\Psi^+_{ratio}$ and period as log ($k_f + k_b$) is varied from -3 to 6 and log K = 1 (the cyan trace in panel a). Panel c relates the minimum in $\Delta\Psi^+_{ratio}$ versus log K.

Figure 5.7 demonstrates that the minimum in $\Delta\Psi^+_{ratio}$ versus log period trace depends both on log K and log ($k_f + k_b$). Note: to facilitate the reader's review of the evidence supporting this statement, two versions of Figure 5.7 are provided; one that presents $\Delta\Psi^+_{ratio}$ vs. log period traces for specific $k_f + k_b$ values in an overlay format (Figure 5.7) and the other in contour plot format (Figure 5.8). At large K values, *i.e.*, $k_f >> k_b$, peak ratio decreases with period in proportion to amount of Red converting to Z. For log $k_f >$

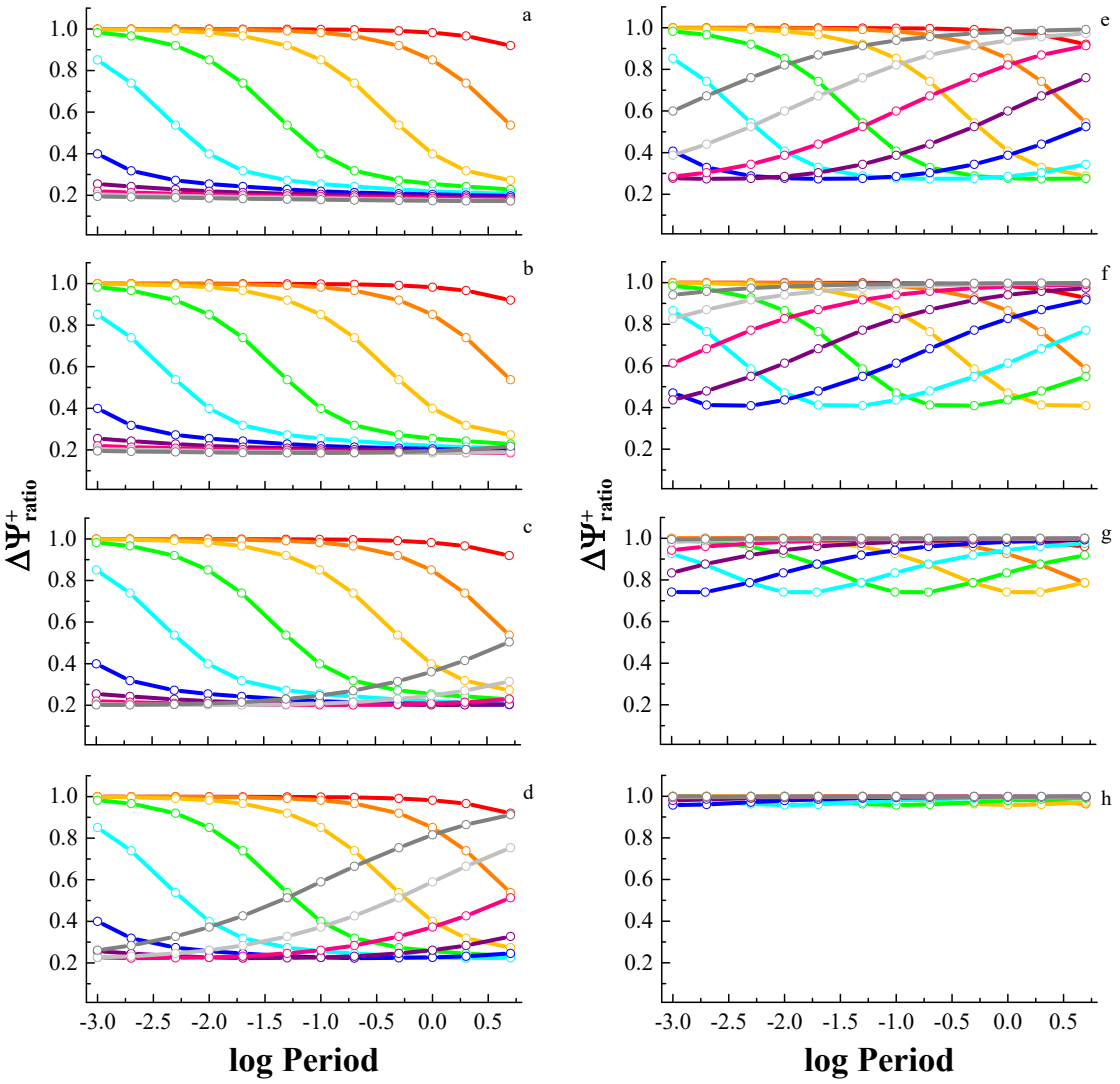

Figure 5.7. The impact of period on peak ratio over the log ($k_f + k_b$) range -3 (red) to 6 (dark gray) for log K = 6 (panel a) to -1 (panel h) when amplitude = 50 mV, E_λ = -200 mV, and increment = 10 mV.

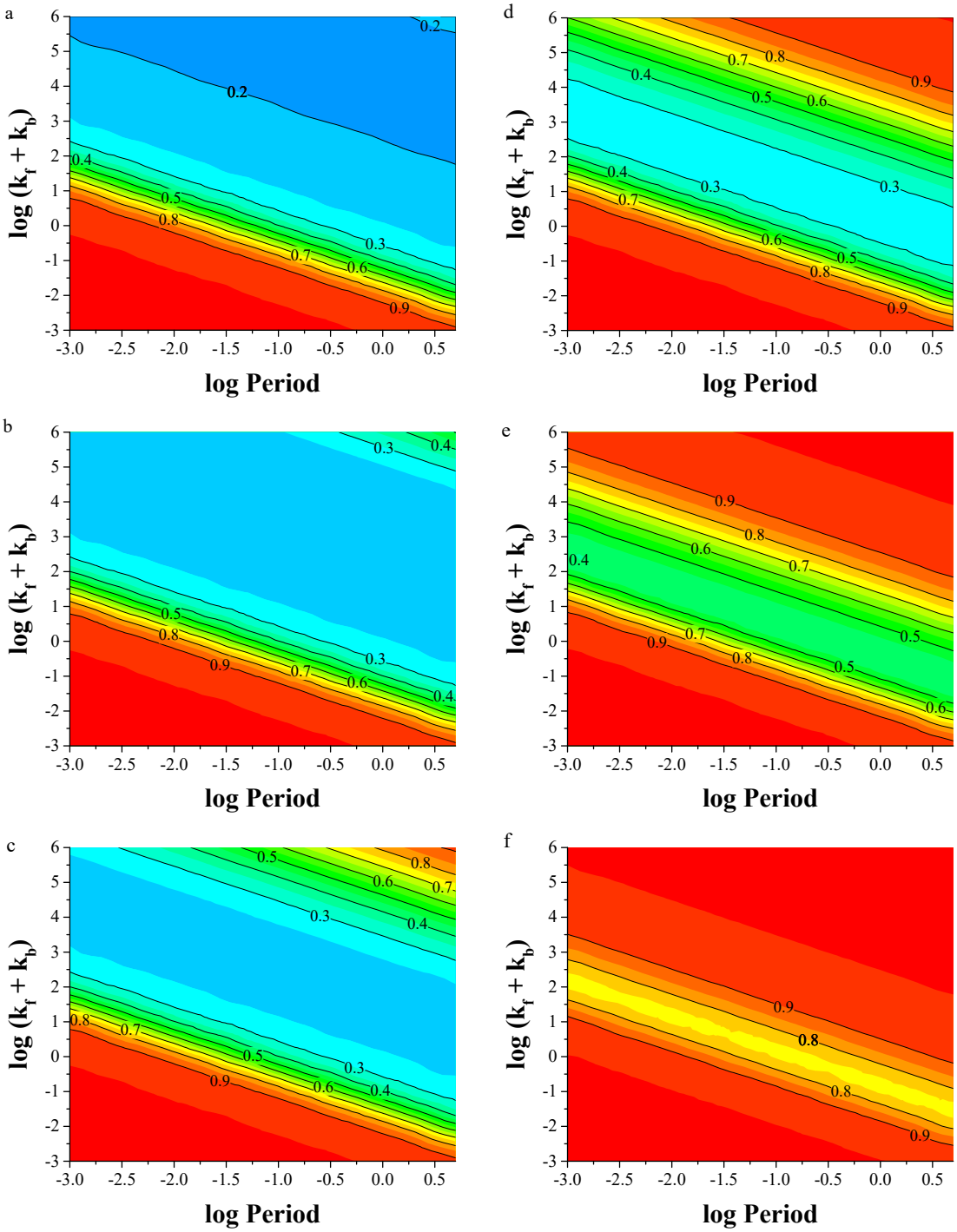

Figure 5.8. The impact of period on peak ratio over the log ($k_f + k_b$) range -3 to 6 for for log K = 5 (panel a) to 0 (panel f) when amplitude = 50 mV, E_λ = -200 mV, and increment = 10 mV. Note: the range in log K included in this format does not directly compare with Figure 5.7.

2, the reaction proceeds so quickly that the peak ratio is 0.2 and independent of period. At intermediate K values (panels c-f in Figure 5.7) although $k_f > k_b$, peak ratio drops and then rises with increasing period. The minimum value for peak ratio ranges from 0.2 (at log K = 4) to 0.4 (at log K = 1). A similar trend in peak ratio is observed at log K = 0 (panel g in Figure 5.7). At this K, $k_f \sim k_b$ and the minimum value for peak ratio is 0.7. At log K ≤ -1 (panel h), the peak ratio is essentially unity and independent of period and log $(k_f + k_b)$.

Clearly, the dependence of peak ratio on period is an important indicator of an EC mechanism. This mechanism is indicated when the peak ratio ≤ 1 and varies with period. To experimentally determine K and $k_f + k_b$, a plot of peak ratio versus log period should be constructed and examined. If a minimum in the $\Delta\Psi^+_{ratio}$ - log period curve is observed, the value of K is directly obtained from the working curve presented in Figure 5.6c. The value of log $(k_f + k_b)$ is then determined by identifying the period at which the apex occurs in the appropriate panel in Figure 5.7 or Figure 5.8. Note that extrapolation between minima presented in a given panel or between panels may be necessary. If a minimum in the $\Delta\Psi^+_{ratio}$ - log period curve is not observed, both K and $k_f + k_b$ can be estimated from overlaying the trace onto the best fitting trace in Figure 5.7. In this situation, additional simulations at other log K and log $(k_f + k_b)$ values than those reported in Figure 5.7 may be required for refinement of initial estimates.

A second indicator of an EC mechanism is the relationship between $\Delta\Psi^+_{p,f}$ and period$^{-1/2}$ (see Figure 5.9). At log K = 6 and low values of k_f, the slope is identical to that found for a reversible mechanism. At high values of k_f, the slope approximately half the value found for the reversible case. At intermediate values, the trace is curvilinear. Similarly,

the relationship between $\Delta\Psi^{+}_{p,r}$ follows the same trend as $\Delta\Psi^{+}_{p,f}$ except that at high values of k_f, the slope approaches zero reflecting that conversion of Red to Z is essentially complete. Again, at intermediate values, the trace is curvilinear but with a larger bowing compared to $\Delta\Psi^{+}_{p,f}$.

A third indicator of an EC mechanism is the shift in peak potentials with period. The magnitude of shifts in $E_{p,f}$ (Figure 5.10) and $E_{p,r}$ (Figure 5.11) depend on K and $k_f + k_b$. At log $K \leq 0$, the peak potentials remain essentially unchanged as period is varied. At $0 <$ log $K < 4$, the peak potential versus log period trace is curvilinear with slopes approaching 30 mV.

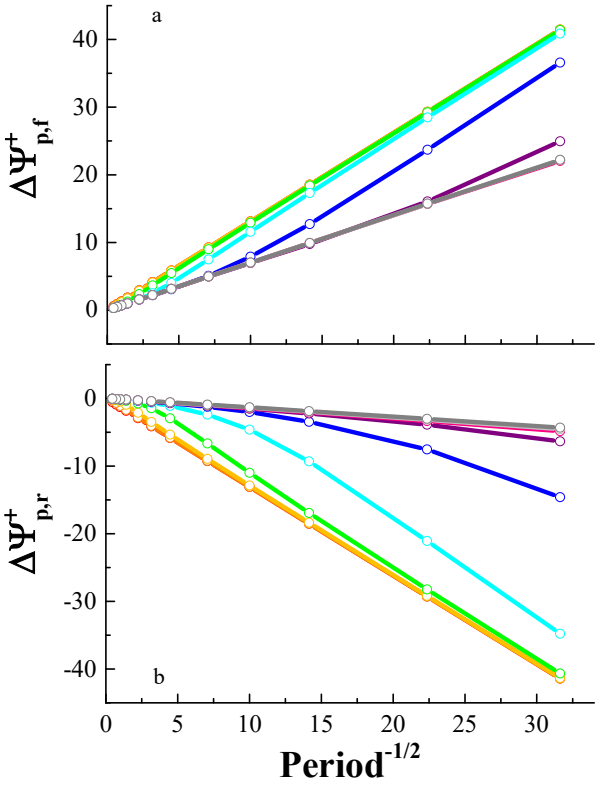

Figure 5.9. The impact of period on $\Delta\Psi^{+}_{p,f}$ and $\Delta\Psi^{+}_{p,r}$ when amplitude = 50 mV, increment = 10 mV, E_λ = -200 mV, log K = 6, and log ($k_f + k_b$) ranges from -3 (red) to 6 (dark gray).

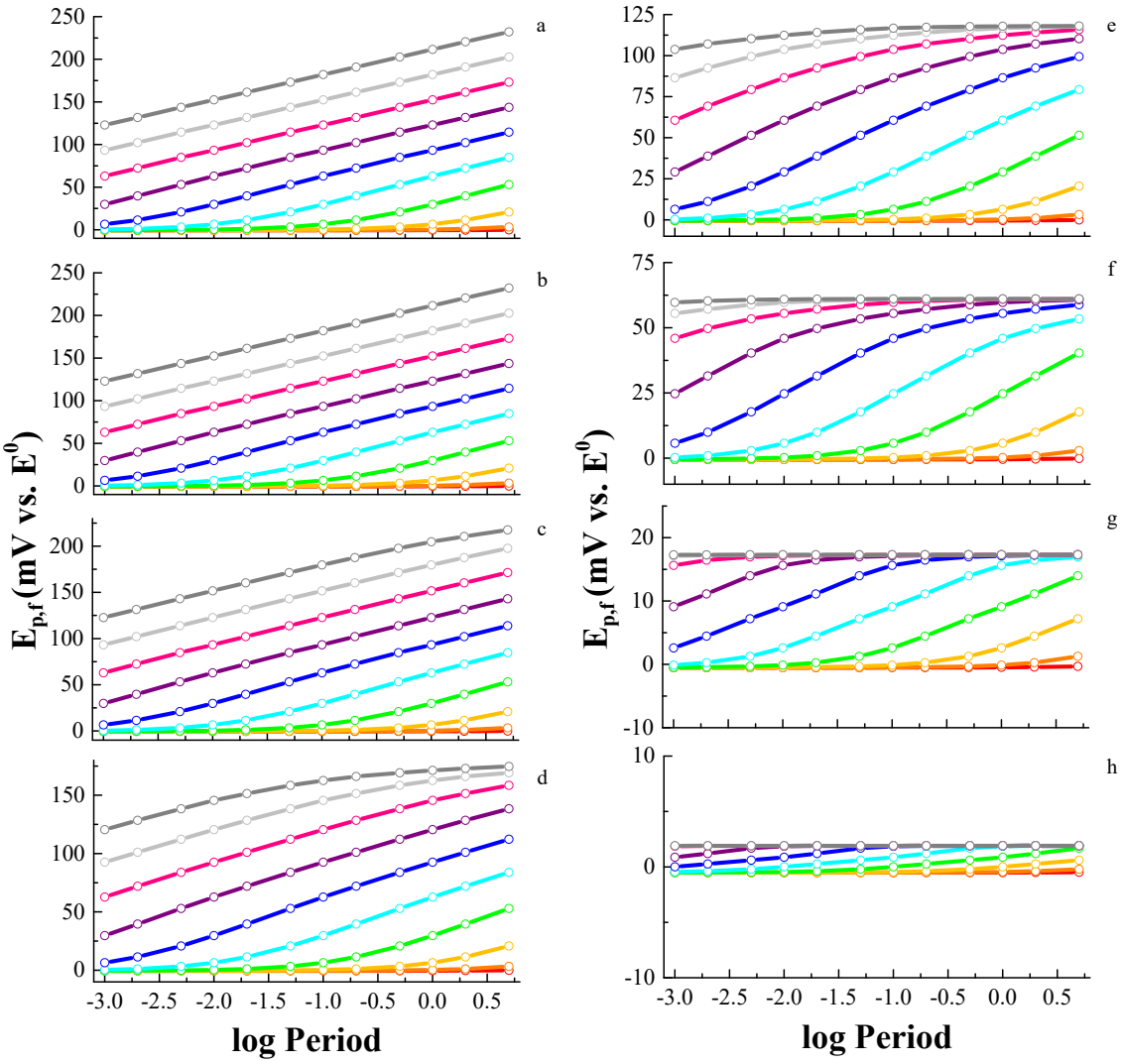

Figure 5.10. The impact of period on $E_{p,f}$ over the log ($k_f + k_b$) range -3 (red) to 6 (dark gray) for log K = 6 (panel a) to -1 (panel h) when amplitude = 50 mV, E_λ = -200 mV, and increment = 10 mV.

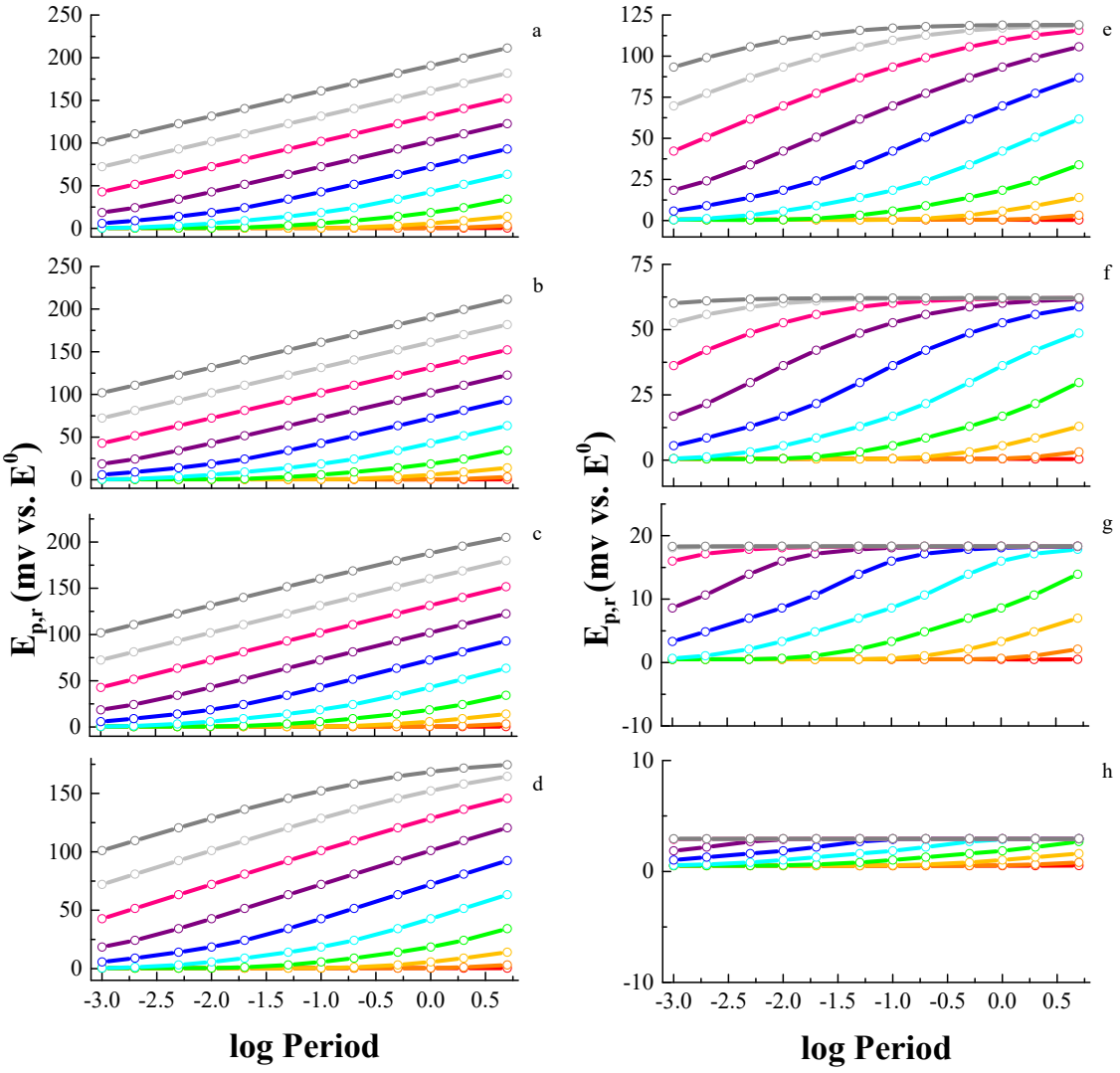

Figure 5.11. The impact of period on $E_{p,r}$ over the log ($k_f + k_b$) range -3 (red) to 6 (dark gray) for log K = 6 (panel a) to -1 (panel h) when amplitude = 50 mV, E_λ = -200 mV, and increment = 10 mV.

At log K ≥ 4, the slope is 30 mV, consistent with the trend in peak potentials with scan rate found by Nicholson and Shain for cyclic voltammetry.[2]

When varying period, several differences can be identified between the EC and reversible cases. Peak potentials shift positively from E^0 with period for the EC case and remain at E^0 for the reversible case. Current is curvilinearly related to period$^{-1/2}$ for the

EC case and linearly related to period$^{-1/2}$ reversible case. Peak ratios vary with period for the EC case but are always unity for the reversible case. Readers are reminded that all trends for the EC case are dependent on K, k_f, and k_b. Thus, given these differences in the trends for the two mechanisms, variation of period can be used to distinguish between the reversible and EC mechanisms.

5.2.4 Effect of Increment (δE)

A set of voltammograms in which increment alone is varied is depicted in Figure 5.12a for log K = 3 and log ($k_f + k_b$) = 0. Peak potentials shift toward the formal potential with increment (see Figure 5.12b). The change in $\Delta\Psi^{+}_{p,r}$ with increment is greater than that for $\Delta\Psi^{+}_{p,f}$ though both values increase (see Figure 5.12c). Peak ratio increases with increment from 0.25 to 0.7 as shown in Figure 5.12d.

Figure 5.13 shows the effects of increment on peak ratio for selected values of K. For log K ≤ -2, the peak ratio is independent of increment. At greater values of log K, the peak ratio increases with increment. This trend is comparable to that observed in cyclic voltammetry since increasing increment increases the potential sweep rate and shortens the time window for the conversion of Red to Z.

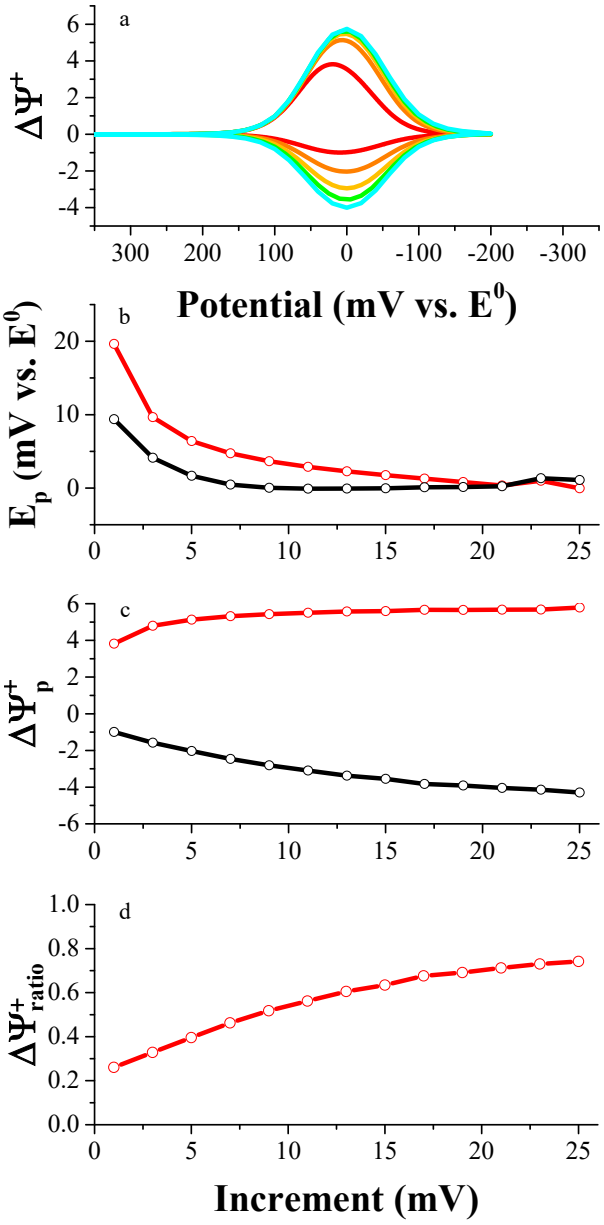

Figure 5.12. The impact of increment on the shape of the voltammogram when amplitude = 50 mV, period = 50 ms, E_λ = -200 mV, log K = 3, and log ($k_f + k_b$) = 0. Panel a): Increment ranges from 1 mV (red), 5 mV (orange), 10 mV (yellow), 15 mV (green), and 20 mV (cyan). Panel b): $E_{p,f}$ (red) and $E_{p,r}$ (black). Panel c): $\Delta\Psi^+_{p,f}$ (red) and $\Delta\Psi^+_{p,r}$ (black). Panel d): Peak ratio (red).

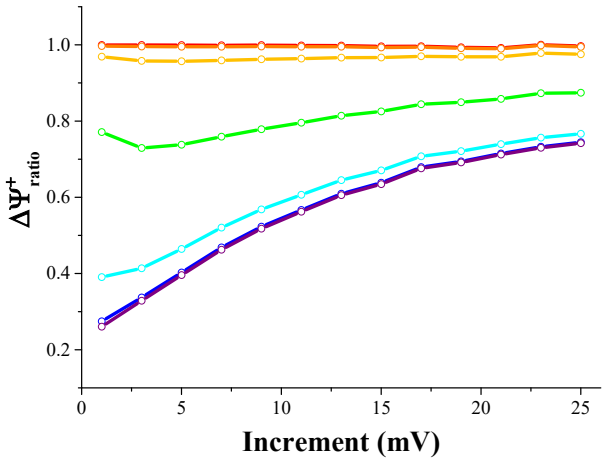

Figure 5.13. The impact of increment on the peak ratio as log K is varied from -3 (red) to 3 (purple) in steps of 1 when amplitude = 50 mV, period = 50 ms, E_λ = -200 mV, and log ($k_f + k_b$) = 0.

The relationship of peak ratio with increment is markedly dependent upon $k_f + k_b$ and K. The complex dependency is shown in Figure 5.14. At log K ≥ 5 (panels a & b), the effect of $k_f + k_b$ and increment on peak ratio is similar. When log ($k_f + k_b$) = -3, the trend for peak ratio vs. increment mirrors that for a reversible reaction. When -2 ≤ log ($k_f + k_b$) ≤ 0, peak ratio increases with increment. When log ($k_f + k_b$) > 0, peak ratio remains constant and independent of increment.

For intermediate values of K (panels c-e), the effects of increment log ($k_f + k_b$) ≤ 0 remain the same as in panels a & b. For log ($k_f + k_b$) > 0, peak ratio decreases as increment is increased with a magnitude dependent upon the value of log ($k_f + k_b$). For 0 ≤ log K ≤ 1 (panels f & g), trends in peak ratio with increment and log ($k_f + k_b$) match those obtained for log K = 2 but over a smaller span in peak ratio. When log K ≤ -1 (shown for log K = -1 in panel h), the peak ratio is independent of increment and very slightly dependent on log ($k_f + k_b$).

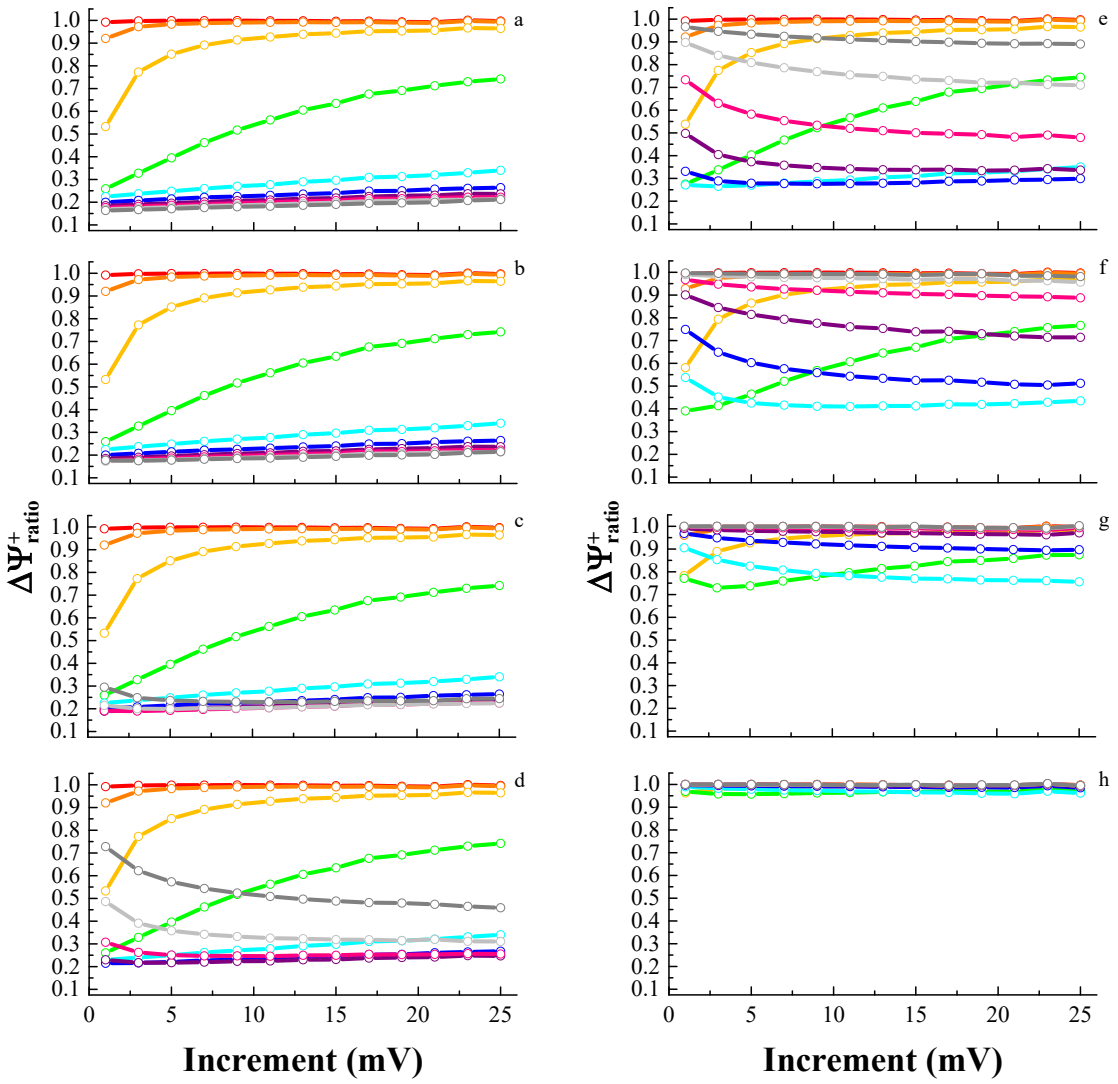

Figure 5.14. The impact of increment on peak ratio over the log ($k_f + k_b$) range -3 (red) to 6 (dark gray) for log K = 6 (panel a) to -1 (panel h) when amplitude = 50 mV, E_λ = -200 mV, and period = 50 ms.

Figure 5.15 presents the impact of increment on $\Delta\Psi^+_{p,f}$ (panel a) and $\Delta\Psi^+_{p,r}$ (panel b) as a function of $k_f + k_b$. Detailed inspection of this figure provides insight into the trends shown in Figure 5.14a. When log ($k_f + k_b$) > 2, both $\Delta\Psi^+_{p,f}$ and $\Delta\Psi^+_{p,r}$ increase in magnitude curvilinearly with increment; the slope depends upon log ($k_f + k_b$). But, for given value of log ($k_f + k_b$) $\Delta\Psi^+_{p,f}$ and $\Delta\Psi^+_{p,r}$ are not mirror images of each other. The

difference reflects the rate of conversion of Red to Z.

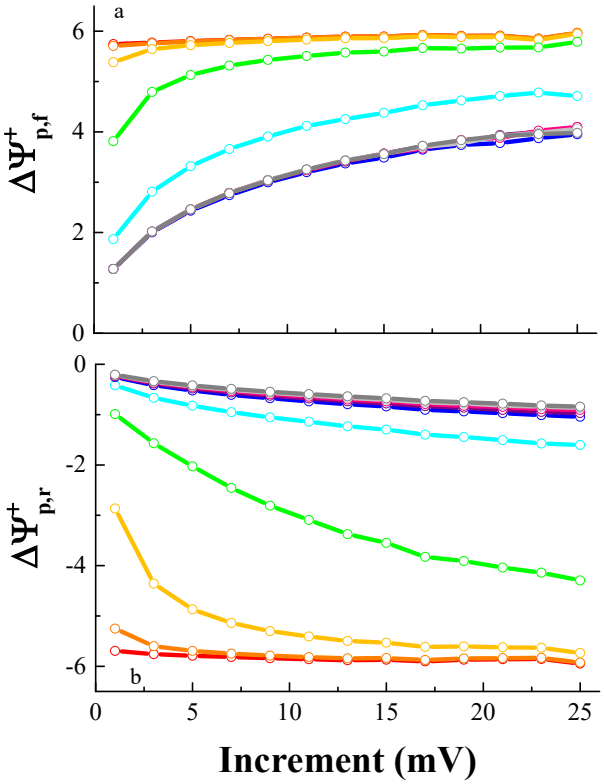

Figure 5.15. The impact of increment on $\Delta\Psi^{+}_{p,f}$ and $\Delta\Psi^{+}_{p,r}$ when amplitude = 50 mV, period = 50 ms, E_λ = -200 mV, log K = 6, and log ($k_f + k_b$) ranges from -3 (red) to 6 (dark gray).

The impact of increment, K, and $k_f + k_b$ on peak potentials is shown in Figures 5.16 and 5.17. Regardless of the value of K, when the rate of the following reaction is slow (i.e. log ($k_f + k_b$) ≤ -1) $E_{p,f}$ and $E_{p,r} = E^0$ and are independent of increment. At faster rates of the reaction (i.e. log ($k_f + k_b$) > -1) when the equilibrium lies strongly in favor of Z (i.e. log K ≥ 1, panels a-f), E_p values shift curvilinearly toward E^0 with increment. The displacement of both peak potentials from E^0 depends strongly on $k_f + k_b$. When the equilibrium begins to favor Red (i.e. log K < 1, panels g & h), the shift in E_p with increment is ≤ 10 mV over the range in increment from 1 to 25 mV and collapses on E^0

when log K ≤ -1.

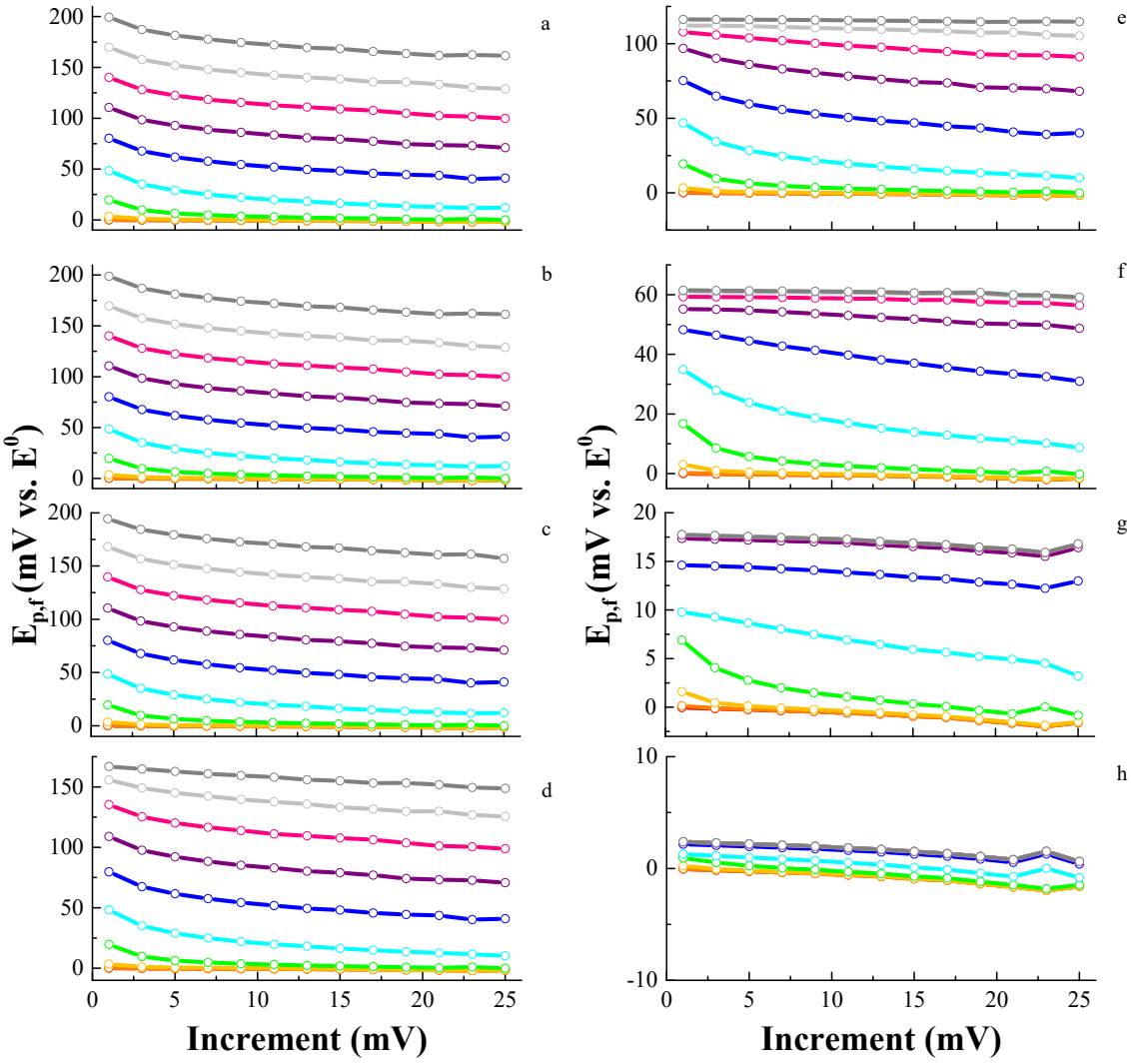

Figure 5.16. The impact of increment on $E_{p,f}$ over the log ($k_f + k_b$) range -3 (red) to 6 (dark gray) for log K = 6 (panel a) to -1 (panel h) when amplitude = 50 mV, E_λ = -200 mV, and period = 50 ms.

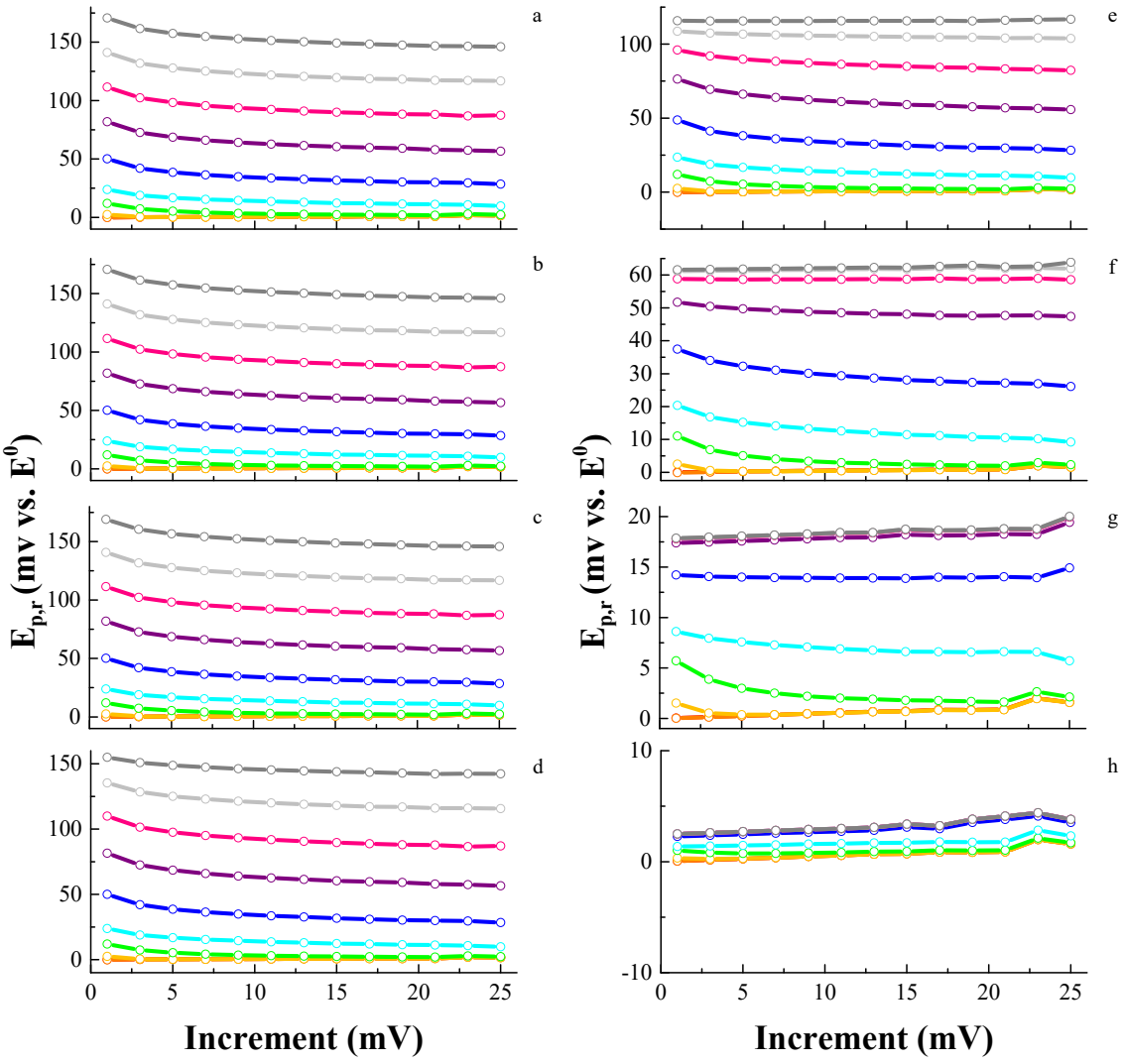

Figure 5.17. The impact of increment on $E_{p,r}$ over the log ($k_f + k_b$) range -3 (red) to 6 (dark gray) for log K = 6 (panel a) to -1 (panel h) when amplitude = 50 mV, E_λ = -200 mV, and period = 50 ms.

In comparing the trends for the EC and reversible cases as a function of increment, several differences can be identified. Peak potentials shift negatively towards E^0 with increment for the EC case but remain at E^0 for the reversible case; the magnitude of the shift depends on K, k_f, and k_b. Peak currents increase with increment for the EC case but are unaffected by increment for the reversible. Peak ratios vary with increment for the

EC case but are unity regardless of increment for the reversible case; the trend is dependent upon K, k_f, and k_b. Hence, the systematic variation of increment can be used to discern between the reversible and EC mechanisms.

5.2.5 Effect of Switching Potential (E_λ)

The dramatic effect of switching potential on the wave shape for an EC mechanism is shown in Figure 5.18 for log K = 3 and log ($k_f + k_b$) = 0. While $\Delta\Psi^+_{p,f}$, $E_{p,f}$, and $E_{p,r}$ are unaffected, $\Delta\Psi^+_{p,r}$ is greatly affected by E_λ (Figures 5.18b&c). As E_λ approaches E^0, $\Delta\Psi^+_{p,r}$ increases and consequently, the peak ratio increases (Figure 5.18d). This occurs as less time is allowed for Red to convert to Z when E_λ is closer to the formal potential. The trends in $\Delta\Psi^+_{p,r}$ and peak ratio with E_λ distinguishes the EC mechanism from others.

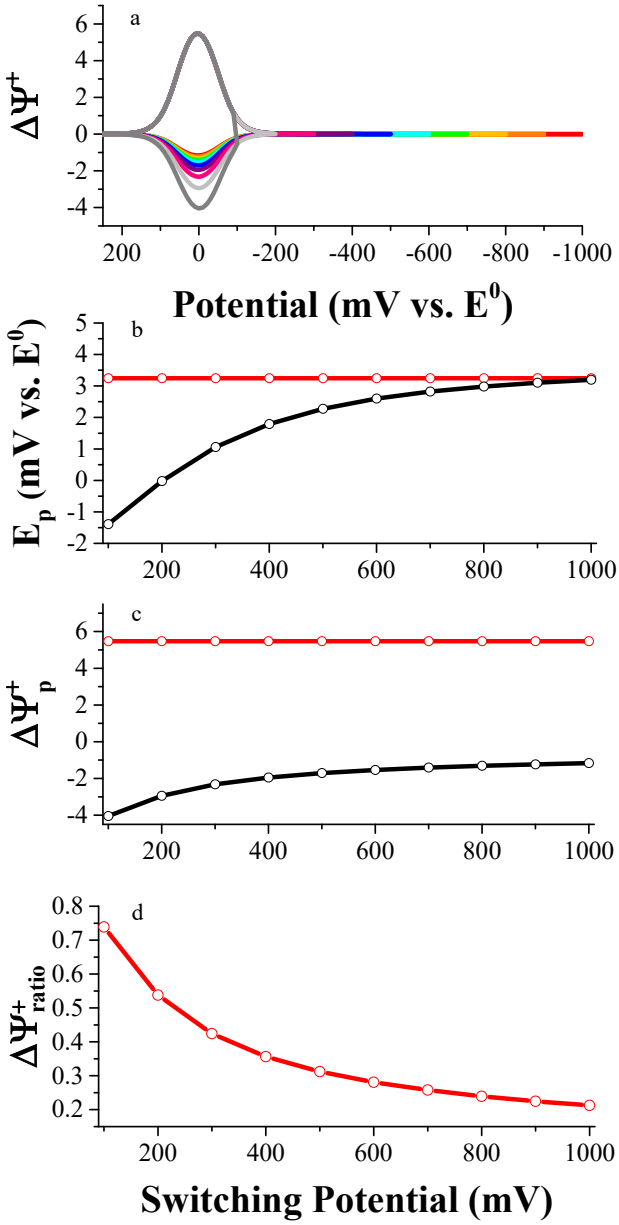

Figure 5.18. The impact of switching potential on the shape of the voltammogram when amplitude = 50 mV, increment = 10 mV, period = 50 ms, log K = 3, and log ($k_f + k_b$) = 0. Panel a): Switching potentials: 1000 mV (red), 900 mV (orange), 800 mV (yellow), 700 mV (green), 600 mV (cyan), 500 mV (blue), 400 mV (purple), 300 mV (magenta), 200 mV (light gray), and 100 mV (dark gray). Panel b): $E_{p,f}$ (red) and $E_{p,r}$ (black). Panel c): $\Delta\Psi^+_{p,f}$ (red) and $\Delta\Psi^+_{p,r}$ (black). Panel d): Peak ratio (red).

The impact of K on the relationship between peak ratio and E_λ is shown in Figure 5.19 for log ($k_f + k_b$) = 0. At low K values where the equilibrium favors Red, peak ratio is

unaffected by the switching potential just as in the reversible electron transfer mechanism. At higher K values, peak ratio decreases with increasing E_λ. The magnitude of the decrease is proportional to K.

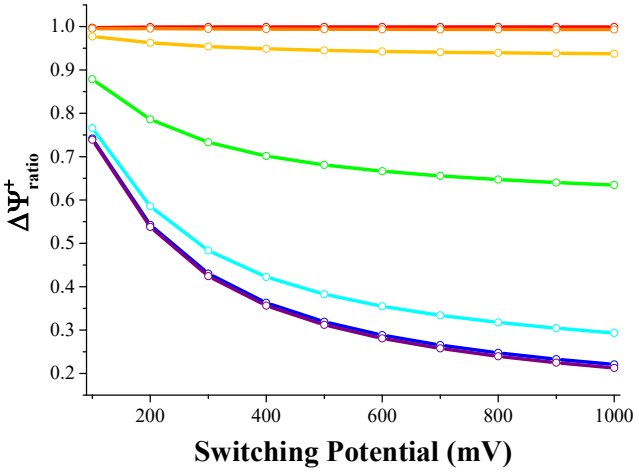

Figure 5.19. The impact of switching potential on the peak ratio as log K is varied from -3 (red) to 3 (purple) in steps of 1 when increment = 10 mV, period = 50 ms, and log ($k_f + k_b$) = 0.

The impact of $k_f + k_b$ on the peak ratio vs. E_λ is quite complex as shown in Figure 5.20. At low values of log ($k_f + k_b$) (i.e. $\leq$ -2), peak ratios are independent of E_λ and equal to unity regardless of log K. The rate of the following reaction is too slow to impact the current within the time window of the period. At intermediate values (i.e. -2 < log ($k_f + k_b$) $\leq$ 2), peak ratios decrease curvilinearly with E_λ; the span in peak ratio over the range in E_λ depends upon log K. At high rates (log ($k_f + k_b$) > 2), the span in peak ratio is only 0.1 with increasing E_λ. The magnitude of peak ratio at a given E_λ increases with decreasing K. For example, at log ($k_f + k_b$) = 6 and E_λ equal to 400 mV, the peak ratio is 0.5 for log K =3 and 0.9 for log K =2.

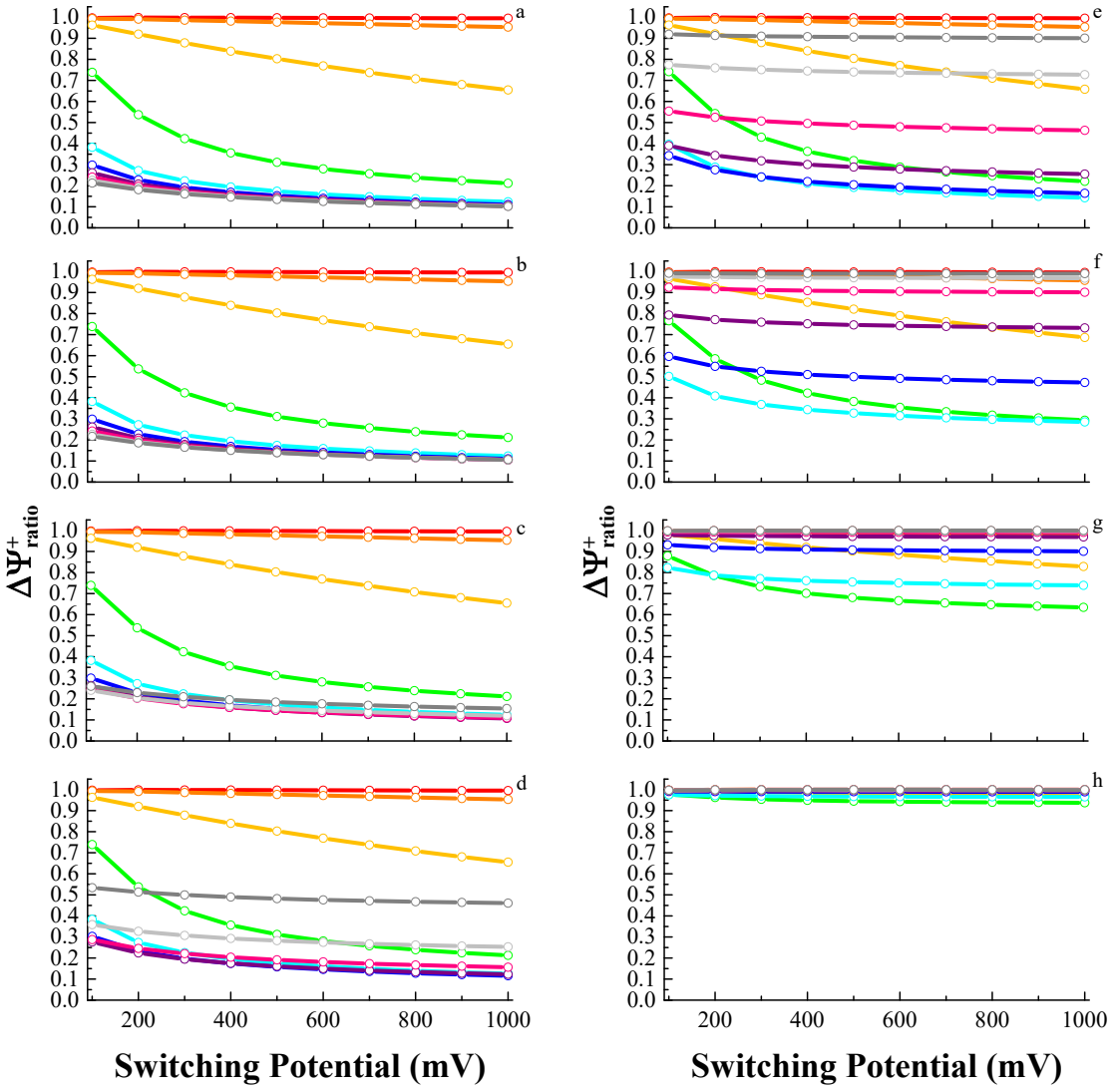

Figure 5.20. The impact of switching potential on peak ratio over the log ($k_f + k_b$) range -3 (red) to 6 (dark gray) for log K = 6 (panel a) to -1 (panel h) when increment = 10 mV and period = 50 ms.

The relationship between peak currents and E_λ depends upon both K (*vide supra*) and log ($k_f + k_b$) as shown in Figure 5.21. $\Delta\Psi^{+}_{p,f}$ remains constant while switching potential is varied though the value of $\Delta\Psi^{+}_{p,f}$ is dependent upon log ($k_f + k_b$). Similarly, $\Delta\Psi^{+}_{p,r}$ is unaffected by E_λ when log ($k_f + k_b$) $\leq$ -2. At higher values of $k_f + k_b$, $\Delta\Psi^{+}_{p,r}$ increases dramatically as switching potential decreases. When log ($k_f + k_b$) $\geq$ 1, $\Delta\Psi^{+}_{p,r}$ approaches

zero and remains relatively constant as switching potential is varied.

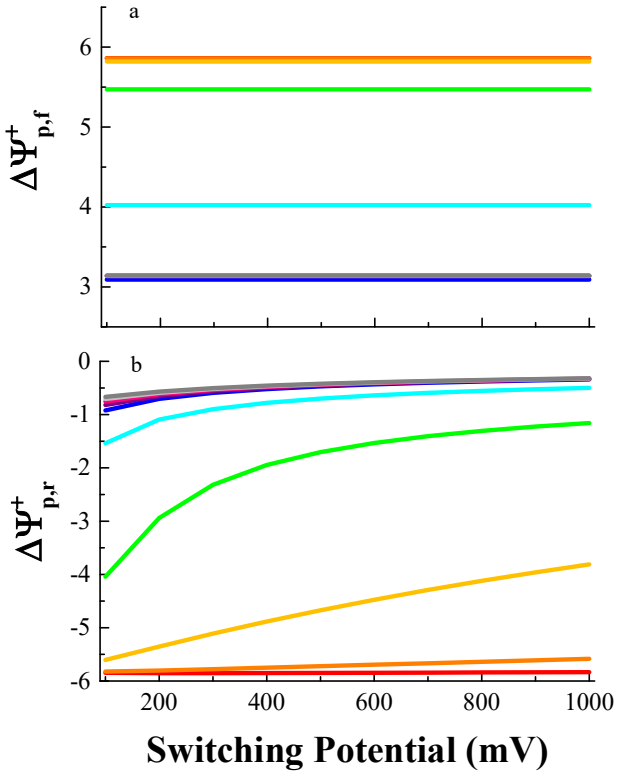

Figure 5.21. The impact of switching potential on $\Delta\Psi^{+}_{p,f}$ and $\Delta\Psi^{+}_{p,r}$ when increment = 10 mV, period = 50 ms, log K = 6, and log ($k_f + k_b$) ranges from -3 (red) to 6 (dark gray).

The effect of $k_f + k_b$ on the relationship between peak potentials and E_λ is shown in Figures 5.22 and 5.23. $E_{p,f}$ and $E_{p,r}$ are unaffected by switching potential though their values are characteristic of K and $k_f + k_b$.

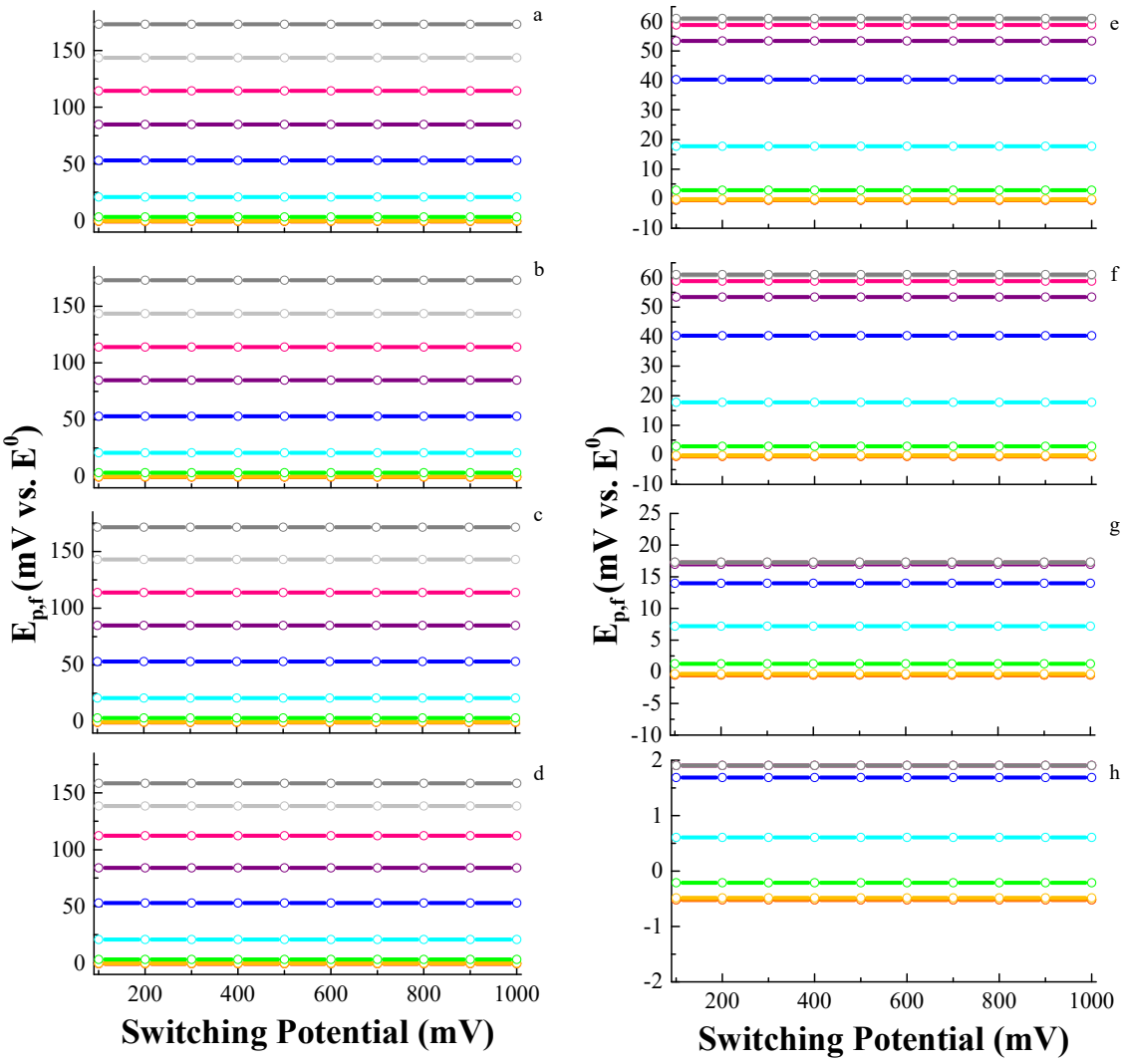

Figure 5.22. The impact of switching potential on $E_{p,f}$ over the log ($k_f + k_b$) range -3 (red) to 6 (dark gray) for log K = 6 (panel a) to -1 (panel h) when increment = 10 mV and period = 50 ms.

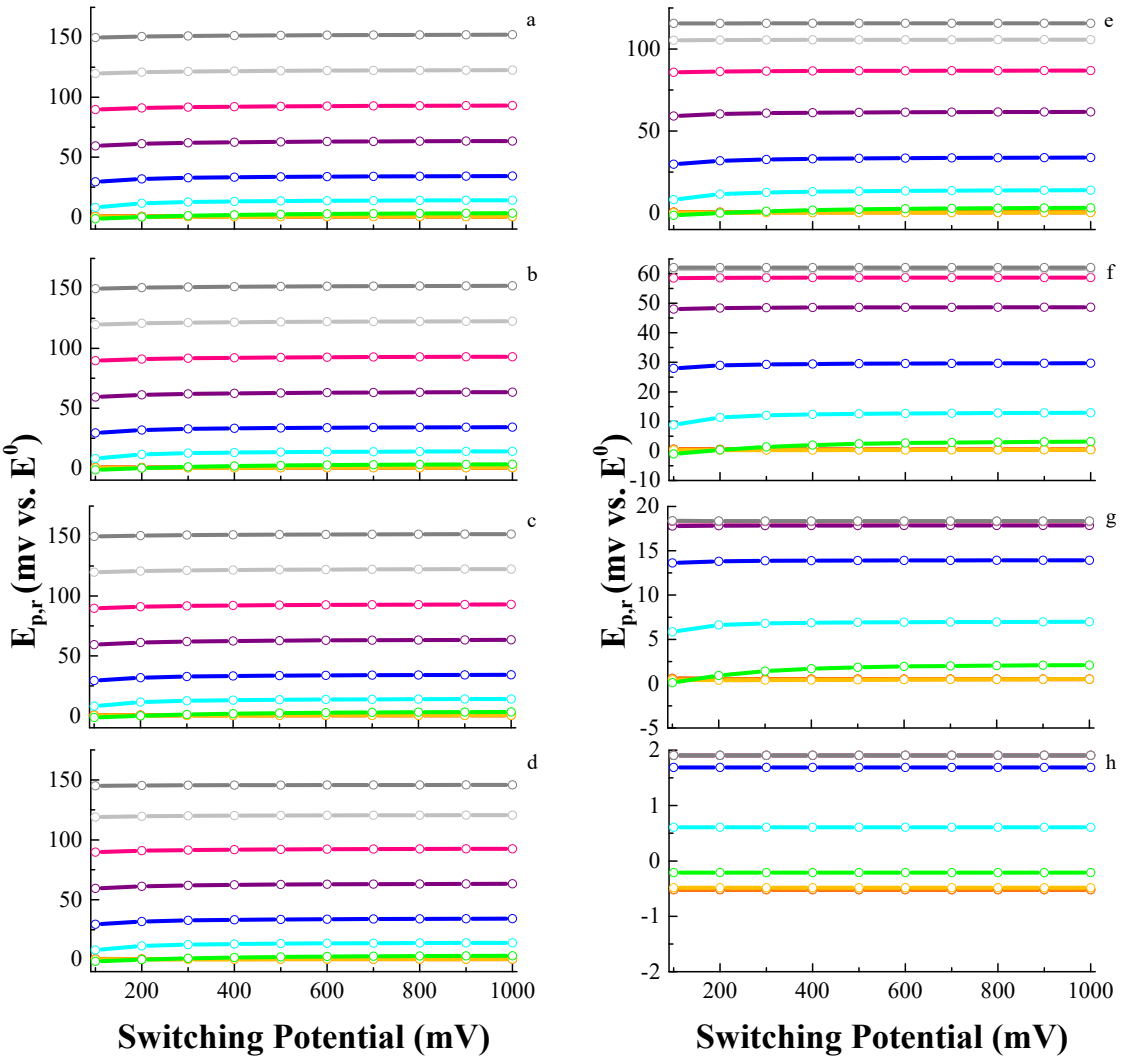

Figure 5.23. The impact of switching potential on $E_{p,r}$ over the log ($k_f + k_b$) range -3 (red) to 6 (dark gray) for log K = 6 (panel a) to -1 (panel h) when increment = 10 mV and period = 50 ms.

There are contrasting trends for the effect of switching potential on the voltammograms of the reversible and EC cases. $E_{p,f}$ and $E_{p,r}$ are displaced from E^0 but remain essentially constant with variation in switching potential for the EC mechanism whereas $E_{p,f}$ and $E_{p,r}$ remain at E^0 for the reversible case. $\Delta\Psi^+_{p,f}$ is unaffected by switching potential for the EC case but $\Delta\Psi^+_{p,r}$ increases as switching potential approaches

E^0. The magnitude of both $\Delta\Psi^+_{p,f}$ and $\Delta\Psi^+_{p,r}$ depend on K, k_f, and k_b. Peak currents are unaffected by switching potential for the reversible case. Subsequently, peak ratio increases as the switching potential approaches E^0 for the EC case while peak ratio is invariant of switching potential for the reversible case. Thus, the effect of switching potential on the peak properties can be used to identify EC vs. reversible mechanisms.

5.2.6 Effect of Amplitude (E_{SW})

The effect of amplitude on the voltammogram is illustrated in Figure 5.24a and explored in detail in Figures 5.24b-d for log K = 3 and log ($k_f + k_b$) = 0. Peak potentials shift slightly with amplitude (Figure 5.24b). Both $\Delta\Psi^+_{p,f}$ and $\Delta\Psi^+_{p,r}$ increase with amplitude though the effect on $\Delta\Psi^+_{p,f}$ is more drastic (Figure 5.24c). Amplitude has a negligible effect on peak ratio as shown in Figure 5.24d where the peak ratio increases by only 0.06 when the amplitude is increased from 10 to 90 mV.

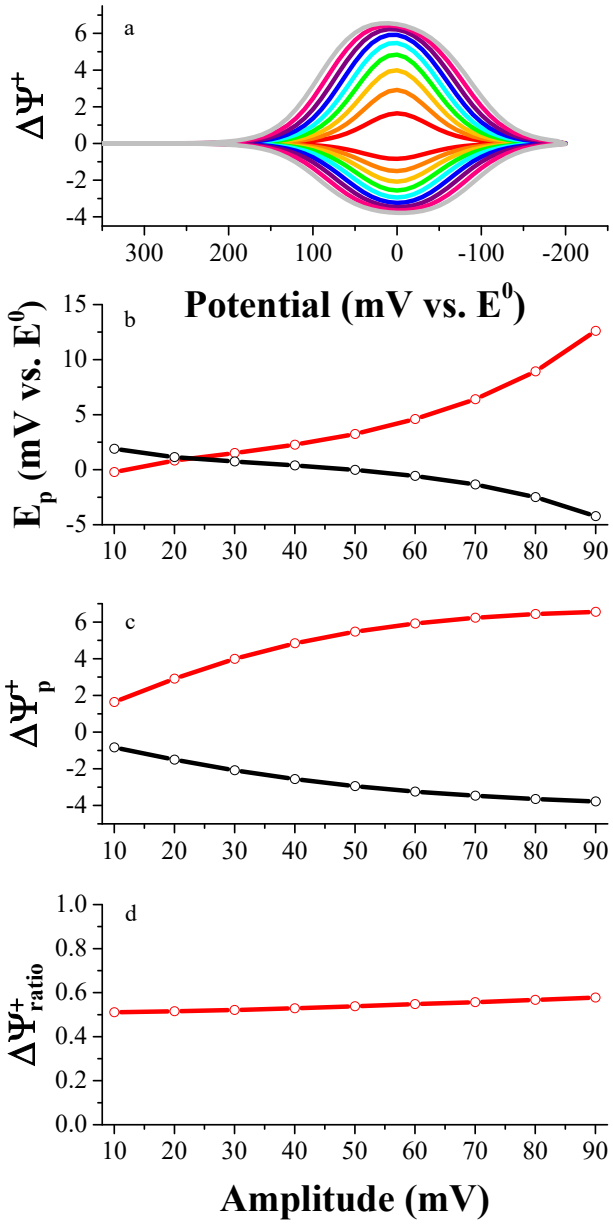

Figure 5.24. The impact of amplitude on the shape of the voltammogram when increment = 10 mV, period = 50 ms, E_λ = -200 mV, log K = 3, and log ($k_f + k_b$) = 0. Panel a): Amplitude ranges from 10 mV (red), 20 mV (orange), 30 mV (yellow), 40 mV (green), 50 mV (cyan), 60 mV (blue), 70 mV (purple), 80 mV (magenta), and 90 mV (light gray). Panel b): $E_{p,f}$ (red) and $E_{p,r}$ (black). Panel c): $\Delta\Psi^+_{p,f}$ (red) and $\Delta\Psi^+_{p,r}$ (black). Panel d): Peak ratio (red).

The value of peak ratio is governed by log K and log ($k_f + k_b$) (Figure 5.25). Figure 5.26 provides insight into the peak ratio-amplitude trends shown in Figure 5.25a. Both

$\Delta\Psi^{+}_{p,f}$ and $\Delta\Psi^{+}_{p,r}$ increase curvilinearly with amplitude however the effect of amplitude on $\Delta\Psi^{+}_{p,f}$ is greater than that on $\Delta\Psi^{+}_{p,r}$.

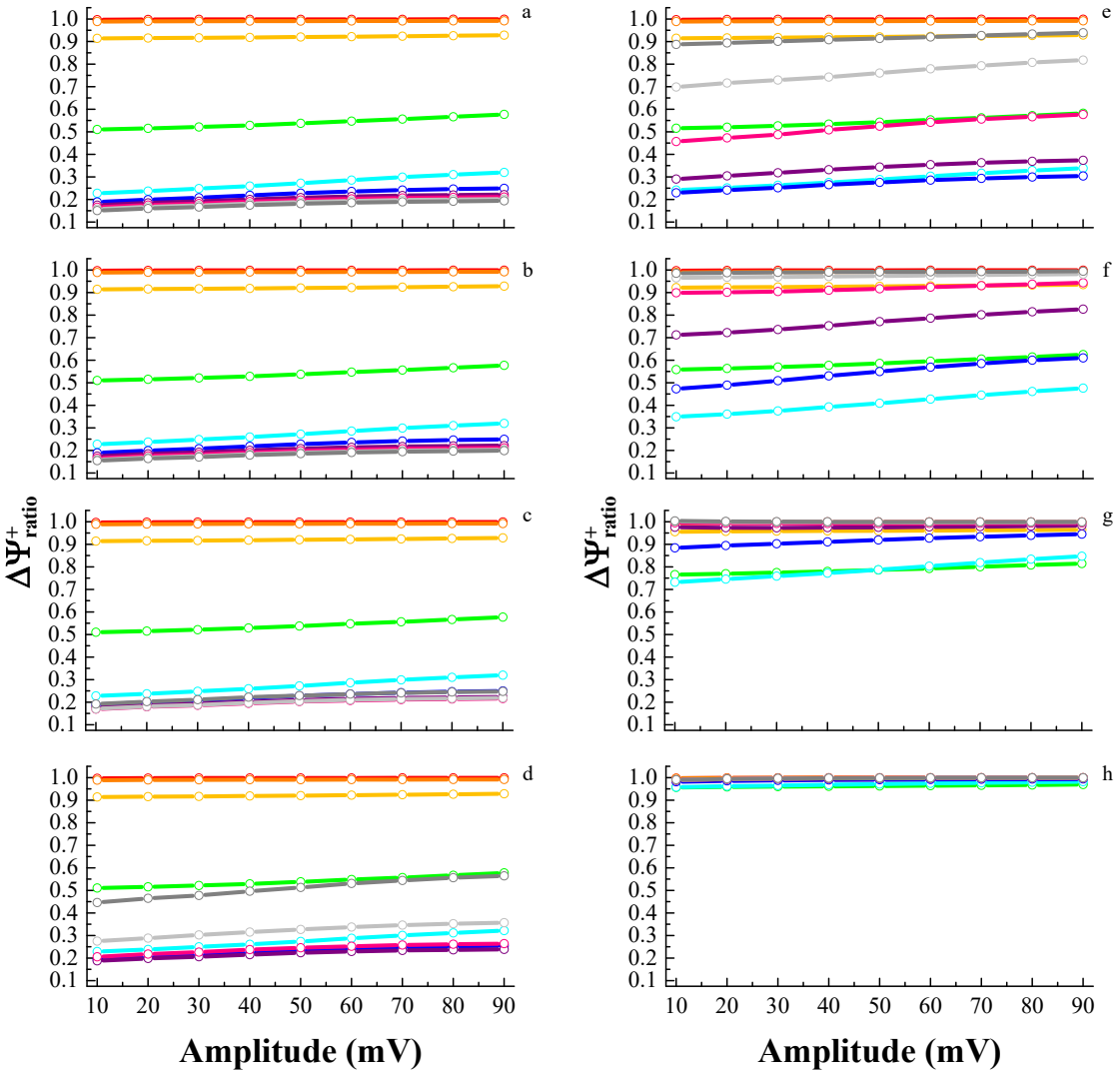

Figure 5.25. The impact of amplitude on peak ratio over the log ($k_f + k_b$) range -3 (red) to 6 (dark gray) for log K = 6 (panel a) to -1 (panel h) when increment = 10 mV, E_λ = -200 mV, and period = 50 ms.

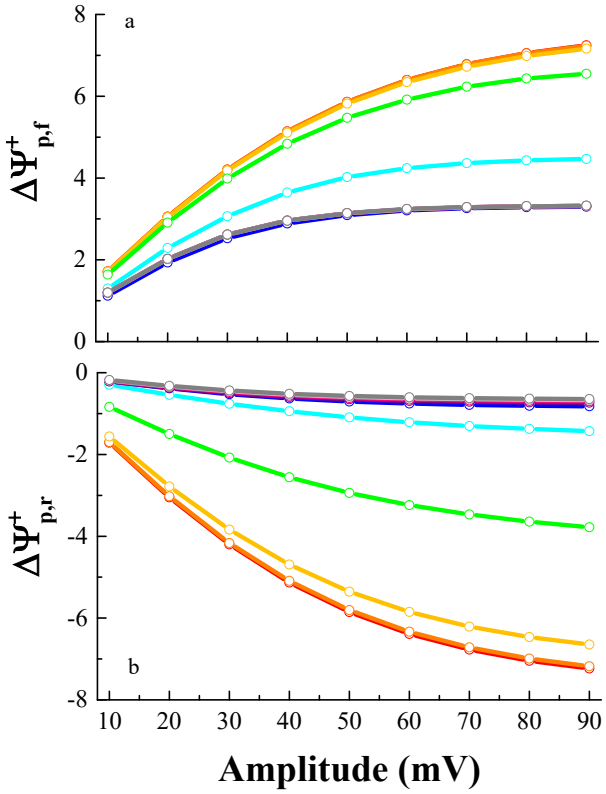

Figure 5.26. The impact of amplitude on $\Delta\Psi^{+}_{p,f}$ and $\Delta\Psi^{+}_{p,r}$ when increment = 10 mV, period = 50 ms, E_λ = -200 mV, log K = 6, and log ($k_f + k_b$) ranges from -3 (red) to 6 (dark gray).

Figures 5.27 and 5.28 present the impact of amplitude on peak potentials as a function of log ($k_f + k_b$) and log K. When log ($k_f + k_b$) ≤ -1 (red, orange and yellow traces in both figures), both peak potentials are essentially at E^0, regardless of log K and amplitude. When log ($k_f + k_b$) ≥ 0 and log K ≥ 3, both $E_{p,f}$ and $E_{p,r}$ shift positively with amplitude; peak potentials values and magnitude of change depends on log ($k_f + k_b$) (see panels a-d in both figures). As K becomes smaller (panels e-g in both figures), larger log ($k_f + k_b$) values are invariant with amplitude while intermediate vales of log ($k_f + k_b$) shift positively with amplitude. When log K ≤ -1, peak potentials become invariant of amplitude, regardless of $k_f + k_b$.

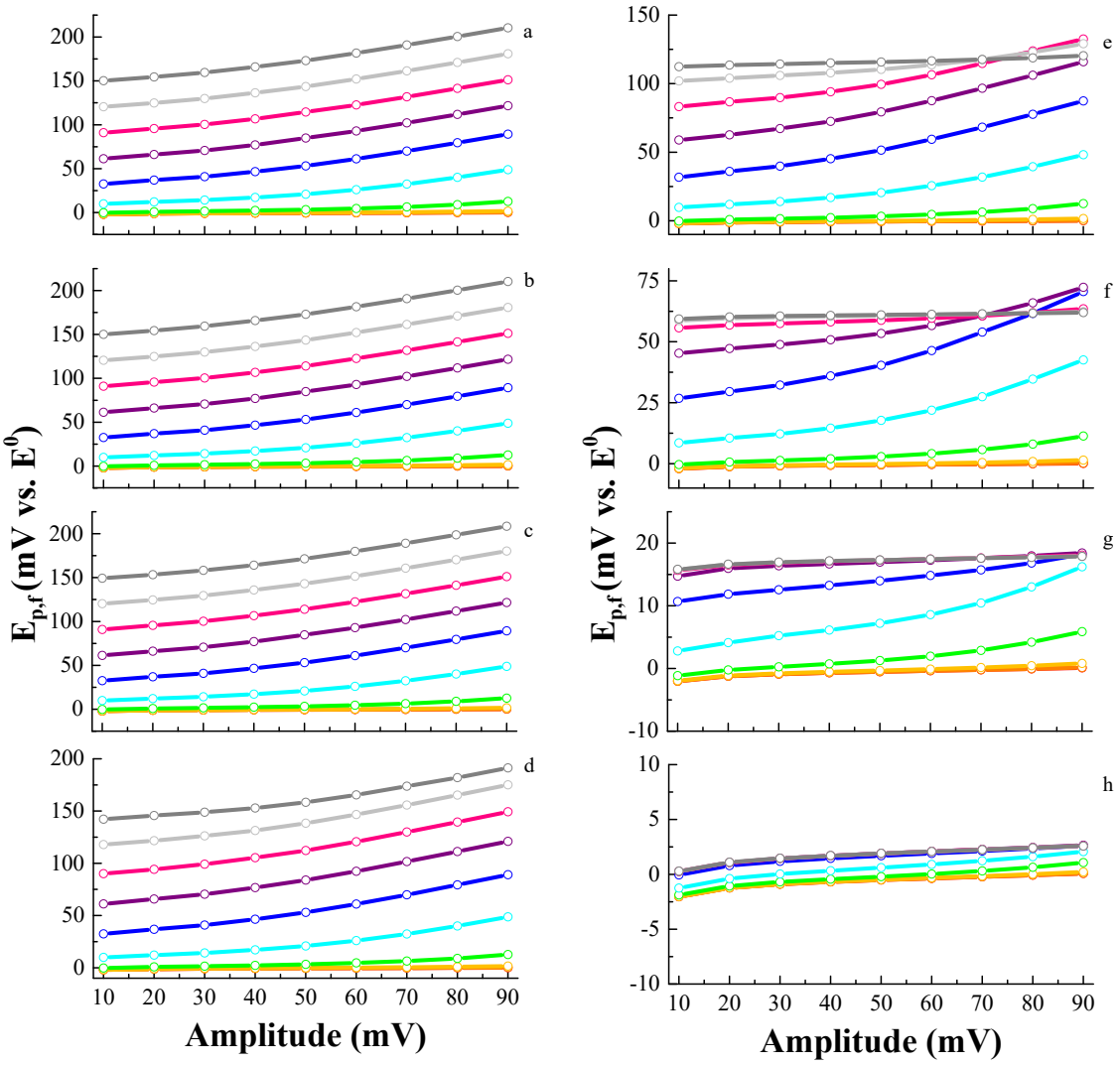

Figure 5.27. The impact of amplitude on $E_{p,f}$ over the log ($k_f + k_b$) range -3 (red) to 6 (dark gray) for log K = 6 (panel a) to -1 (panel h) when increment = 10 mV, E_λ = -200 mV, and period = 50 ms.

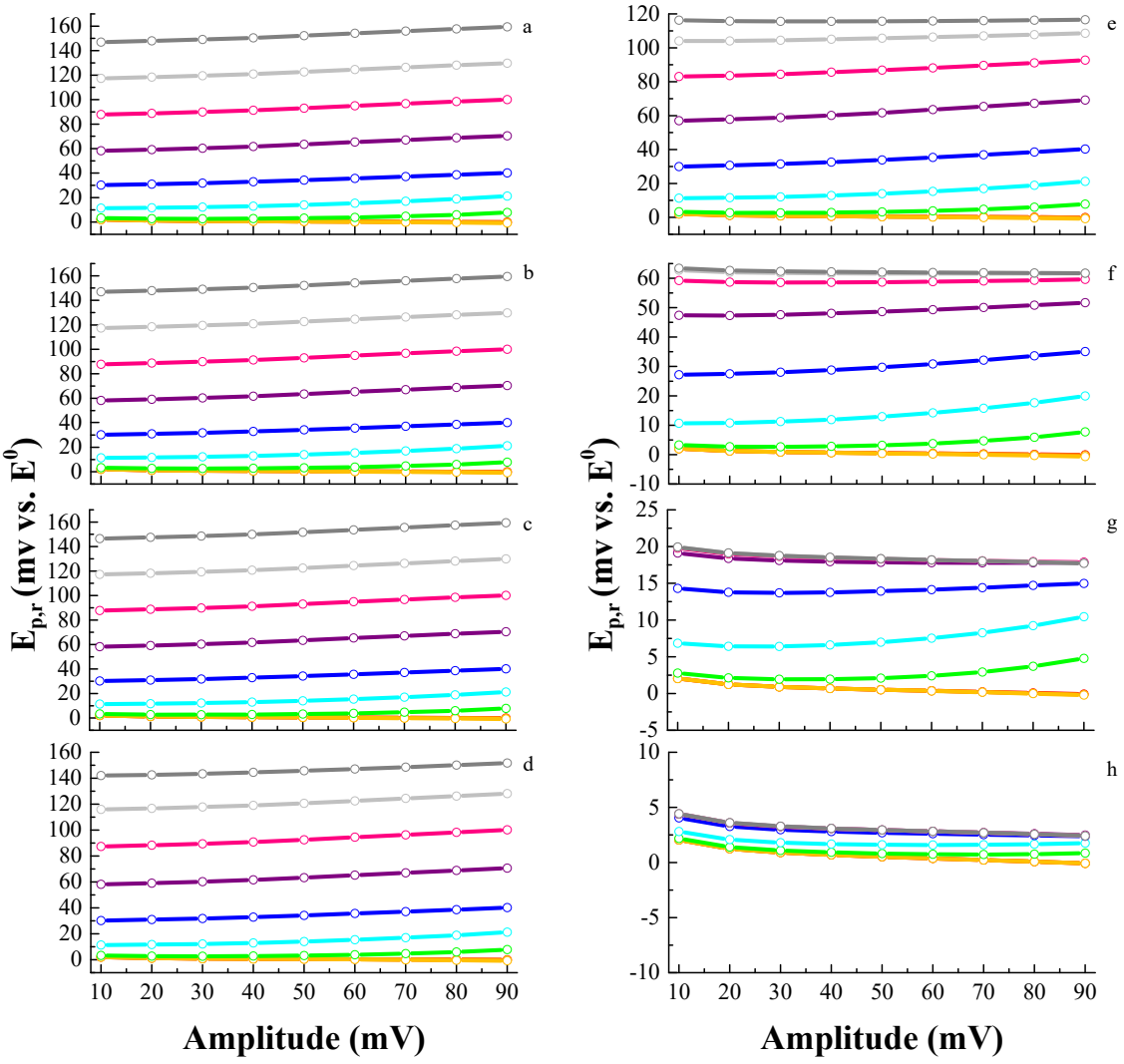

Figure 5.28. The impact of amplitude on $E_{p,r}$ over the log ($k_f + k_b$) range -3 (red) to 6 (dark gray) for log K = 6 (panel a) to -1 (panel h) when increment = 10 mV, E_λ = -200 mV, and period = 50 ms.

Several contrasting trends can be identified when comparing the EC and reversible mechanisms. For the EC mechanism, peak potentials shift positively from E^0 with amplitude. For the reversible mechanism, peak potentials are independent of amplitude. Peak currents increase with amplitude for both cases, but the increase is dependent upon K, k_f, and k_b for the EC mechanism. Peak ratios are either less than unity or increase towards unity for the EC mechanism but are always unity for the reversible case. Thus,

the variation of amplitude can be used to distinguish between the reversible and EC mechanisms.

5.3 Conclusion

The peak currents, potentials, and shapes of cyclic square wave voltammograms for the EC mechanism have been shown to be a complex function K, ($k_f + k_b$), increment, period, switching potential and amplitude. The effects of these empirical parameters on the voltammograms for this mechanism are summarized in Table 5.1. The diagnostic criteria presented in this table will enable rapid identification of EC mechanisms using CSWV. Close examination of the trends presented in the figures throughout this chapter reveals the following limits. When the following chemical reaction is irreversible, i.e. $\log K \geq 3$, measureable $\log k_f$ values are limited to the range $-2 < \log k_f < 2$. When the following chemical reaction is reversible, i.e. $0 \leq \log K < 3$, measureable $\log (k_f + k_b)$ values span a much broader range $-2 < \log (k_f + k_b) < 6$.

Table 5.1. Diagnostic Plots and Protocol for Assessing an EC Electrode Reaction by CSWV

	Empirical variables							
Waveform parameters	***Period,* τ**		***Increment,* δE**		***Switching potential,* E_λ**		***Amplitude,* E_{SW}**	
	Plot	**Trace**	**Plot**	**Trend**	**Plot**	**Trend**	**Plot**	**Trend**
Peak currents	ΔI_p vs. $(\text{period})^{-1/2}$	Decrease linearly or curvilinearly with increasing period (see Figure 5.5c and 5.9)	ΔI_p vs. δE	Increases in magnitude with increment (see Figure 5.12c and 5.15)	ΔI_p vs. E_λ	$\Delta I_{p,f}$ is independent of E_λ $\Delta I_{p,r}$ increases with E_λ approaching E^0 (see Figure 5.18c and 5.21)	ΔI_p vs. E_{SW}	ΔI_p increases with E_{SW} though $\Delta I_{p,f}$ increases more than $\Delta I_{p,r}$ (see Figure 5.24c and 5.26)
Peak ratio	Peak ratio vs. log period	Decreases or increases with increasing period depending upon magnitude of K and $k_f + k_b$ (see Figure 5.5d, 5.6, 5.7, and 5.8)	Peak ratio vs. δE	Increase with increment; magnitude depends upon K and $k_f + k_b$ (see Figure 5.12d, 5.13, and 5.14)	Peak ratio vs. E_λ	Increases with E_λ approaching E^0 (see Figure 5.18d, 5.19, and 5.20)	Peak ratio vs. E_{SW}	Increases slightly with E_{SW} (see Figure 5.24d and 5.25)
Peak potentials	E_p vs. log period	Shift positively with increasing period (see Figure 5.5b, 5.10, and 5.11)	E_p vs. δE	Shift negatively with increment (see Figure 5.12b, 5.16, and 5.17)	E_p vs. E_λ	Invariant with E_λ approaching E^0 (see Figure 5.18b, 5.22, and 5.23)	E_p vs. E_{SW}	Shift positively with E_{SW} (see Figure 5.24b, 5.27, and 5.28)
Peak separation	ΔE_p vs. log period	Complex relationship, may increase or decrease with increasing period depending upon magnitude of K and $k_f + k_b$ (compare Figures 5.10 and 5.11)	ΔE_p vs. δE	Complex relationship, may increase or decrease with increasing increment depending upon magnitude of K and $k_f + k_b$ (compare Figures 5.16 and 5.17)	ΔE_p vs. E_λ	Invariant with E_λ approaching E^0	ΔE_p vs. E_{SW}	Complex relationship, may increase or decrease with increasing E_{SW} depending upon magnitude of K and $k_f + k_b$ (compare Figures 5.27 and 5.28)
Peak widths	$W_{1/2}$ vs. $(\text{period})^{-1/2}$	Generally varies by ~10 mV	$W_{1/2}$ vs. δE	Generally varies by ~10 mV	$W_{1/2}$ vs. E_λ	Invariant with E_λ approaching E^0	$W_{1/2}$ vs. E_{SW}	$W_{1/2}$ increases with E_{SW}

5.4 References

1. Smith, D.E. *Anal. Chem.*, **1963**. 35, 602-609.

2. Nicholson, R.S. and I. Shain. *Anal. Chem.*, **1964**. 36, 706-723.

3. Laviron, E. *J. Electroanal. Chem. Interfacial Electrochem.*, **1972**. 39, 1-23.

4. Nadjo, L. and J.M. Saveant. *J. Electroanal. Chem. Interfacial Electrochem.*, **1973**. 48, 113-145.

5. Kim, M.-H., L. Yan, R.L. Birke, and M.-Z. Czae. *Electroanalysis*, **2003**. 15, 1541-1553.

6. Gulaboski, R., E.S. Ferreira, C.M. Pereira, M.N.D.S. Cordeiro, A. Garau, V. Lippolis, and A.F. Silva. *J. Phys. Chem. C*, **2008**. 112, 153-161.

7. Laborda, E., F. Martinez-Ortiz, and A. Molina. *Electroanalysis*, **2010**. 22, 1857-1866.

8. Mozo, J.D., J. Carbajo, J.C. Sturm, L.J. Nunez-Vergara, R. Moscoso, and J.A. Squella. *Anal. Chim. Acta*, **2011**. 699, 33-43.

9. O'Dea, J.J., J. Osteryoung, and R.A. Osteryoung. *Anal. Chem.*, **1981**. 53, 695-701.

10. Osteryoung, J.G. and J.J. O'Dea, *Square-Wave Voltammetry*, *Electroanalytical chemistry: a series of advances*. **1986**, Marcel Dekker, Inc: New York. 209-308

11. Mirceski, V. and M. Lovric. *Croat. Chem. Acta*, **2000**. 73, 305-329.

12. Garay, F. and M. Lovrić. *J. Electroanal. Chem.*, **2002**. 518, 91-102.

13. Miles, A.B. and R.G. Compton. *J. Phys. Chem. B*, **2000**. 104, 5331-5342.

14. Mirceski, V. and M. Lovric. *J. Electroanal. Chem.*, **2004**. 565, 191-202.

15. Mirčeski, V., Š. Komorsky-Lovrić, and M. Lovrić, *Square Wave Voltammetry: Theory and Application*, *Monographs in Electrochemistry*. **2007**, Springer-Verlag: Berlin.

16. Mirčeski, V., E. Laborda, D. Guziejewski, and R.G. Compton. *Anal. Chem.*, **2013**. 85, 5586-5594.

17. Jadreško, D. and M. Zelić. *J. Electroanal. Chem.*, **2014**. 714-715, 30-37.

18. Cizmek, L., S. Komorsky-Lovric, and M. Lovric. *ChemElectroChem*, **2015**. 2, 2027-2031.

19. Stone, D.L. and D.K. Smith. *Polyhedron*, **2003**. 22, 763-768.

20. Gu, J.-S., D.-B. Chu, X.-F. Zhou, and G.-X. Shen. *Huaxue Xuebao*, **2003**. 61, 1405-1409.

21. Farias, P.A.M. and M.B.R. Bastos. *Int. J. Electrochem. Sci.*, **2009**. 4, 458-470.

22. Yola, M.L. and N. Ozaltin. *Rev. Chim. (Bucharest, Rom.)*, **2011**. 62, 420-426.

23. Nicholson, R.S. and M.L. Olmstead, *Electrochemistry: Calculations, Simulation and Instrumentation,*. **1972**, Marcel Dekker: New York. Ch. 5

24. Helfrick, J.C., Jr. and L.A. Bottomley. *Anal. Chem.*, **2009**. 81, 9041-9047.

25. Mann, M.A., J.C. Helfrick, Jr., and L.A. Bottomley. *Anal. Chem.*, **2014**. 86, 8183-8191.

CHAPTER 6

THE CE MECHANISM

Helfrick, J.C., Jr., M.A. Mann, and L.A. Bottomley: Diagnostic Criteria for the Characterization of Electrode Reactions with Chemically-Coupled Reactions Preceding the Electron Transfer by Cyclic. *ChemPhysChem*. **2016**. Accepted.

6.1 Introduction

The CE mechanism has been investigated by electrochemists over the past five decades.[1-9] The continuing interest reflects the advent of new mathematical approaches for modeling the electrode reaction sequence and new electrochemical techniques to identify short lived intermediates and quantify reaction rates. This mechanism frequently occurs in electrode reactions of coordination compounds,[10-14] carboxylic acids in aprotic media,[15, 16] as well as benzoic acid and protonated amines and sulfonamides in ionic liquids.[17, 18] With various examples of the CE or CEC square mechanisms present in the literature, a need for a technique that provides a means for mechanistic assignment and rate determination is imperative. This chapter examines the effect of empirical parameters on peak parameters for the CE mechanism. From this, the diagnostic criteria for the CE mechanism using CE and a protocol for an experimentalist to determine the rate of the chemical reaction and the equilibrium constant are provided.

6.2 Results and Discussion

6.2.1 Theory

This CE mechanism is characterized by a chemical reaction that precedes an electron transfer, as shown in Equation 6.1.

$$Y \underset{k_b}{\overset{k_f}{\rightleftarrows}} Ox + ne^- \leftrightarrow Red \tag{6.1}$$

where Ox is the reactant, Red is the product of the electron transfer, Y is the electroinactive reactant in the reaction preceding the electron transfer step, k_f is the rate constant for the conversion of Y to Ox in s^{-1}, and k_b is the rate constant for conversion of Ox to Y in s^{-1}. The forward and reverse chemical reactions have been treated as first order and the electron transfer is diffusion limited. The derivation of an equation that enables calculation of current at each applied potential for this electrode reaction begins with Fick's laws of diffusion. Expressions for the concentrations of Ox and Red as a function of time and distance from the electrode are found using Laplace transformations following application of the boundary conditions. These expressions are related by the Nernst equation for a reversible electron transfer:

$$E_{applied} = E^0 + \left(\frac{RT}{nF}\right)\ln\left(\frac{C_{Ox}(0,t)}{C_{Red}(0,t)}\right) \tag{6.2}$$

where n = number of electrons transferred, F = Faraday constant, A = area of the electrode, R = gas constant, T = temperature in Kelvin, $E_{applied}$ = applied potential, E^0 = formal potential for the electron transfer reaction, D_{Ox} = diffusion coefficient of Ox (cm^2/sec), D_{Red} = diffusion coefficient of Red (cm^2/sec), C_{Ox} (x, t) = concentration of Ox

at the electrode surface and any time t, C_{Red} (x, t) = concentration of Red at the electrode surface and any time t. Numerical approximation of the resultant integral equations were performed in the same manner put forth by Nicholson and Olmstead.[19] The final equation used to compute theoretical voltammograms for the CE mechanism is

$$\Psi_m = \frac{\left(\frac{K(k\tau\pi)^{1/2}}{K+1}\right) - \left[\varepsilon + \left(\frac{K}{K+1}\right)\right]\left(\frac{2k\tau}{\pi L}\right)^{1/2} \sum_{i=1}^{i=m-1} \Psi_i S_j - \frac{1}{K+1} \sum_{i=1}^{i=m-1} \Psi_i R_j}{\left[\varepsilon + \left(\frac{K}{K+1}\right)\right]\left(\frac{2k\tau}{\pi L}\right)^{1/2} + \frac{1}{K+1} R_1} \tag{6.3}$$

where L = number of subintervals on each potential, K = equilibrium constant for the following chemical reaction and equal to k_f/k_b, Ψ_m = dimensionless current for each time increment with the serial number m, τ = period, k = the sum of the forward and reverse homogeneous first order rate constants for the chemical reaction preceding the electron transfer, i.e. $k_f + k_b$, and

$$\varepsilon = \exp\left[\frac{nF}{RT}\left(E_{applied} - E^0\right)\right] \tag{6.4}$$

6.2.2 Effect of K, k_f, and k_b

K and $k_f + k_b$ greatly affect the shape of the voltammogram for the CE mechanism. Figure 6.1a shows the effect of K at a fixed value of $k_f + k_b$ on peak parameters and voltammogram shape.

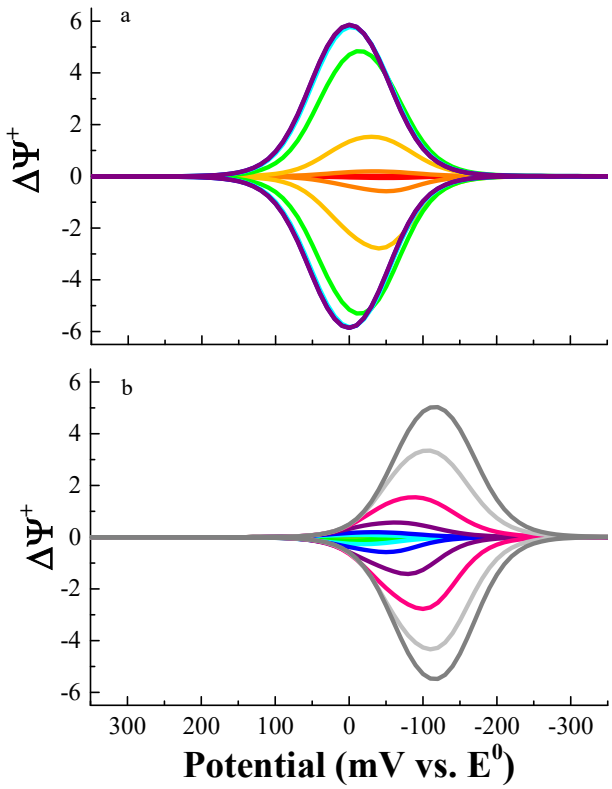

Figure 6.1. The impact of a) K and b) $k_f + k_b$ on the shape of the voltammogram when amplitude = 50 mV, period = 50 ms, and increment is 10 mV. For panel a, log K ranges from -3 (red) to 3 (purple) in steps of 1 when log ($k_f + k_b$) = 2. For panel b, log ($k_f + k_b$) ranges from -3 (red) to 6 (dark gray) in steps of 1 when log K = -2.

When the equilibrium lies in favor of Y (log K = 0), the current for reduction of Ox is small, peak potentials are negative of the formal potential, and peak ratio > 1. When the equilibrium lies in favor of Ox (log K > 0), peak currents increase, peak potentials approach the formal potential, and peak ratio approaches unity.

The effect of $k_f + k_b$ on the voltammogram for the CE mechanism is shown in Figure 6.1b for log K = -2, where Y is the predominant species in solution. Under this condition, the peak currents reflect the amount of conversion from Y to Ox during the time of the potential pulse. At small values of log ($k_f + k_b$), *i.e.*, log ($k_f + k_b$) $\leq$ 2, the current is extremely small due to negligible conversion from Y to Ox. As log ($k_f + k_b$)

increases, current increases, peak potentials shift negatively, and peak ratio is > 1. When $\log (k_f + k_b) > 5$, the wave shape appears reversible as peak ratio approaches unity; however, peak potentials remain shifted negative of the formal potential.

The dependence of peak currents and peak ratio on both K and $k_f + k_b$ is further illustrated in Figure 6.2. Figure 6.2a shows how $\Delta\Psi^{+}_{p,f}$ scales with $\log (k_f + k_b)$ and log K. Figure 6.2b shows that $\Delta\Psi^{+}_{p,r}$ scales with $\log (k_f + k_b)$ and log K as well but the change in magnitude starts at a lower $\log (k_f + k_b)$ value. When log K > 1, $\Delta\Psi^{+}_{p,f}$ and $\Delta\Psi^{+}_{p,r}$ are independent of $\log (k_f + k_b)$ and are equal to the value expected for a reversible process. Figure 6.2c illustrates the peak ratios for a CE process are ≥ 1 and sensitive to $\log (k_f + k_b)$ at log K ≤ 0. It is important to note that Figure 6.2a is identical to previously reported trends for SWV.[2, 7] The data presented in Figures 6.2b and 6.2c are only available with CSWV.

The effect of $\log (k_f + k_b)$ and log K on peak potentials and peak separation for the CE mechanism is shown in Figure 6.3. When the equilibrium favors Ox (i.e. log K ≥ 0), peak potentials remain at the formal potential and $\Delta E_p = 0$. When the equilibrium favors Y (i.e. log K < 0) and $\log (k_f + k_b) > 0$, peak potentials shift negatively with $\log (k_f + k_b)$; the magnitude is dependent upon K and $k_f + k_b$. Subsequently, for the same values of K and $k_f + k_b$, ΔE_p increases to a maximum and then decreases with $\log (k_f + k_b)$; the magnitude is dependent upon K.

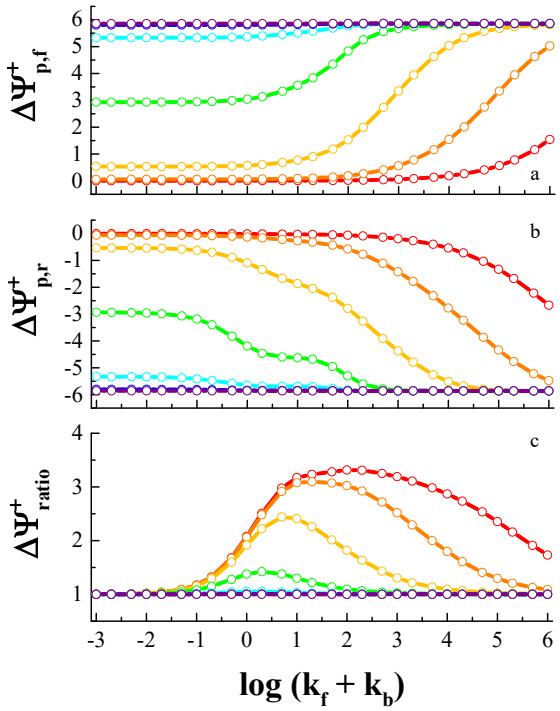

Figure 6.2. The impact of K, k_f, and k_b on a) $\Delta\Psi^+_{p,f}$, b) $\Delta\Psi^+_{p,r}$, and c) peak ratio when amplitude = 50 mV, period = 50 ms, and increment = 10 mV. Log K ranges from -3 (red) to 3 (purple) in steps of 1.

Figure 6.4 presents the impact of K and $k_f + k_b$ on peak width. For $K \geq 1$, both $W_{1/2,\,f}$ and $W_{1/2,\,r}$ are independent of log ($k_f + k_b$) and equal to the value for a reversible mechanism. When $K < 1$, $W_{1/2,\,f}$ increases to a maximum and decreases with log ($k_f + k_b$); the magnitude is dependent upon log K. In contrast, $W_{1/2,\,r}$ decreases to a minimum and increases with log ($k_f + k_b$) where the magnitude is dependent on K. While the trends in $\Delta\Psi^+_p$ and E_p as a function of K and $k_f + k_b$ suggest the utility of CSWV in identifying the presence of a chemical reaction preceding the electron transfer, they do not provide a means for determining the rate constants or equilibrium constant from analysis of a set of voltammograms.

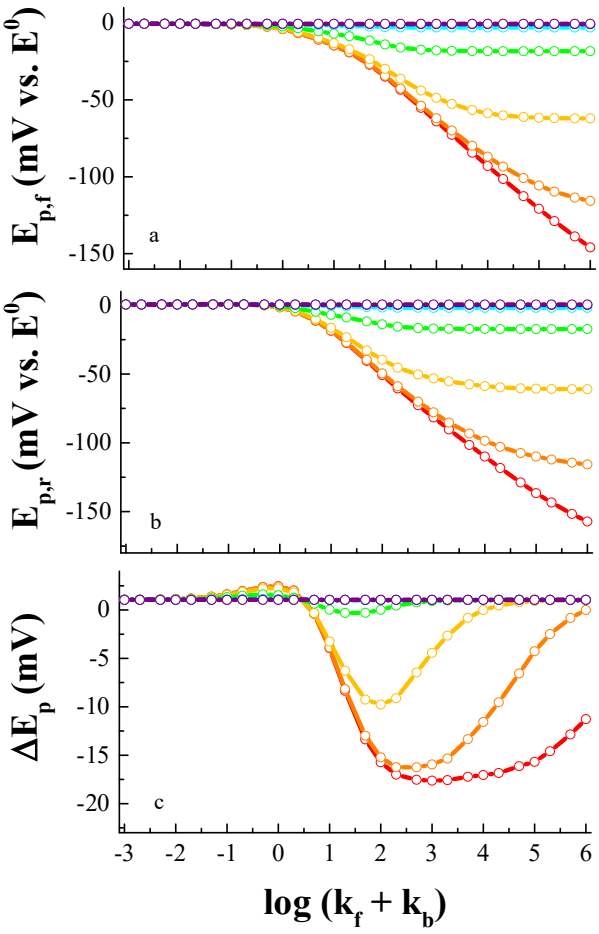

Figure 6.3. The impact of K, k_f, and k_b on a) $E_{p,f}$, b) $E_{p,r}$, and c) peak separation when amplitude = 50 mV, period = 50 ms, and increment = 10 mV. Log K ranges from -3 (red) to 3 (purple) in steps of 1.

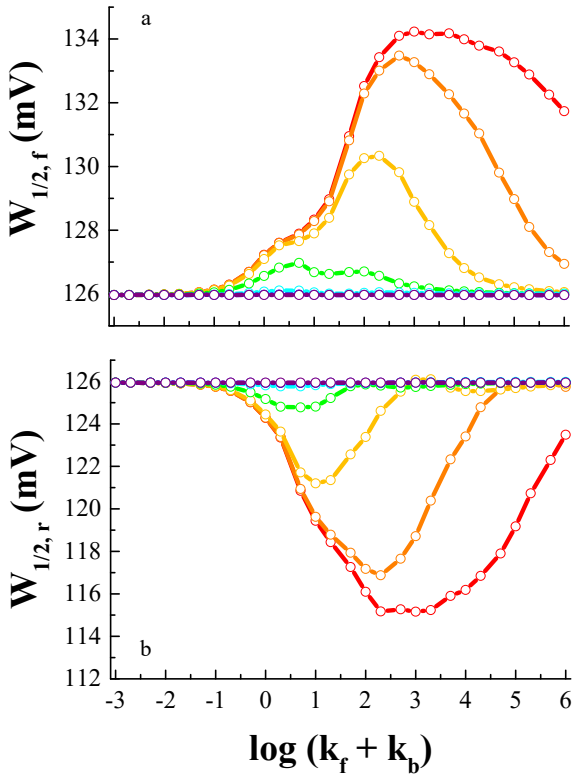

Figure 6.4. The impact of K, k_f, and k_b on a) $W_{1/2,f}$ and b) $W_{1/2,r}$ when amplitude = 50 mV, period = 50 ms, and increment = 10 mV. Log K ranges from -3 (red) to 3 (purple) in steps of 1.

6.2.3 Effect of Period (τ)

The effect of period on the voltammogram for the CE mechanism is shown in Figure 6.5. As period increases, peak currents decrease, and peak potentials shift negatively (Figure 6.5a). $E_{p,f}$ and $E_{p,r}$ are ~ E^0 at short periods but shift negatively with increasing period; peak potential separation is initially zero increasing to ~10 mV and then collapses back to zero (Figure 6.5b).

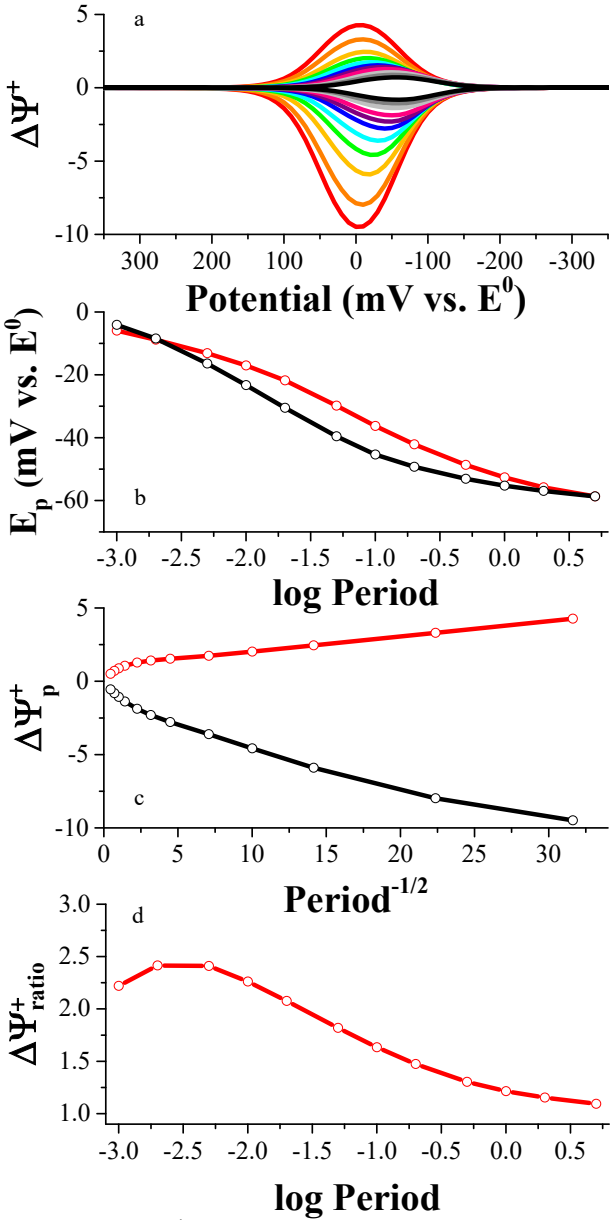

Figure 6.5. The impact of period on the shape of the voltammogram when amplitude = 50 mV, increment = 10 mV, log K = -1, and log ($k_f + k_b$) = 2. Panel a): Period ranges from 1 ms (red) to 5 s (brown). Panel b): $E_{p,f}$ (red) and $E_{p,r}$ (black). Panel c): $\Delta\Psi^+_{p,f}$ (red) and $\Delta\Psi^+_{p,r}$ (black). Panel d): Peak ratio (red).

$\Delta\Psi^+_{p,r}$ is decreases more rapidly than $\Delta\Psi^+_{p,f}$ though both decrease curvilinearly with period$^{-1/2}$ (Figure 6.5c). Figure 6.5d presents the dependence of peak ratio on period.

As period increases, the peak ratio increases from 2.0 to 2.4 before decreasing to unity. This trend is similar to that observed in CV since increasing period decreases the potential sweep rate and lengthens the time window for the conversion of Y to Ox.[1]

The impact of K on the relationship between peak ratio and period is shown in Figure 6.6a for log ($k_f + k_b$) equal to 2. When log $K \geq 1$, peak ratio is unity and independent of period. Over these log K values, the equilibrium lies in favor of Ox, and the peak ratio is identical to that for reversible mechanism. When log K = 0, peak ratio decreases with period. When log K < 0, peak ratio increases to a maximum and then decreases with period; the apex of the curve is dependent upon K. Figure 6.6b presents the relationship between $\Delta\Psi^{+}_{ratio}$ and log period as log ($k_f + k_b$) is varied from -3 to 6 and log K = -2 (the orange trace in panel a). Vertical sectioning of this contour plot at any value of period reveals that as log ($k_f + k_b$) increases, $\Delta\Psi^{+}_{ratio}$ rises from 1 to a maximum before falling back to 1. Similarly, horizontal sectioning of this contour plot reveals that as period increases, $\Delta\Psi^{+}_{ratio}$ may increase, decrease, or rise to a maximum before falling, depending upon on the log ($k_f + k_b$).

Figure 6.7 demonstrates that the apex in $\Delta\Psi^{+}_{ratio}$ versus log period trace depends both on log K and log ($k_f + k_b$). To facilitate the review of the evidence supporting this statement, two variations of Figure 6.7 are provided; one that overlays $\Delta\Psi^{+}_{ratio}$ vs. log period traces for specific $k_f + k_b$ values (Figure 6.7) and another presenting the same evidence in contour plot format (Figure 6.8). Close inspection of these figures reveals that an apex in the $\Delta\Psi^{+}_{ratio}$ - log period trace is observed over all values of log K except when the equilibrium lies heavily in favor of Ox (i.e. log K > 1, panels e & f). From the

results presented in these figure, it is demonstrated that the magnitude of the $\Delta\Psi^{+}_{ratio}$ apex depends only on K; the period value at which the apex is observed depends upon $k_f + k_b$. Figure 6.6c presents the correlation of the apex magnitude in $\Delta\Psi^{+}_{ratio}$ with log K.

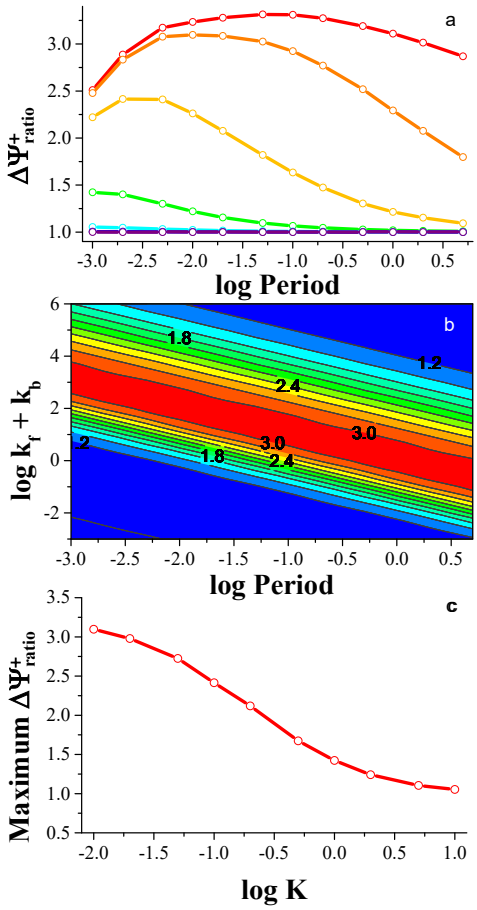

Figure 6.6. The impact of period on the peak ratio as a function of log K and log ($k_f + k_b$) when amplitude = 50 mV, increment = 10 mV. Panel a illustrates the relationship between $\Delta\Psi^{+}_{ratio}$ and period as log K is varied from -3 (red) to 3 (purple), and log ($k_f + k_b$) = 2. Panel b presents the relationship between $\Delta\Psi^{+}_{ratio}$ and period as log ($k_f + k_b$) is varied from -3 to 6 and log K = -2 (the orange trace in panel a). Panel c relates the maximum in $\Delta\Psi^{+}_{ratio}$ versus log K. This panel is a working curve enabling determination of log K from $\Delta\Psi^{+}_{ratio}$ versus period data.

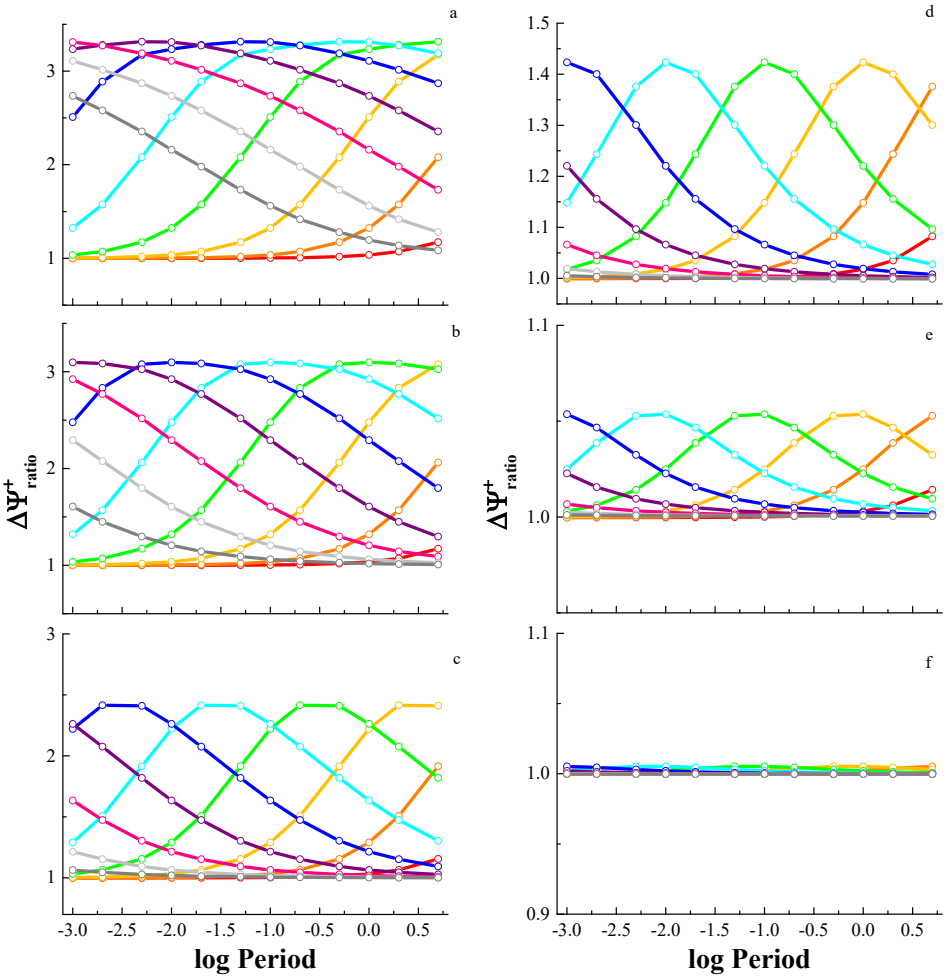

Figure 6.7. The impact of period on peak ratio over the log ($k_f + k_b$) range -3 (red) to 6 (dark gray) for log K = -3 (panel a) to 2 (panel f) when amplitude = 50 mV and increment = 10 mV.

Clearly, the dependence of peak ratio on period is an important indicator of a CE mechanism. This mechanism is indicated when the peak ratio ≥ 1 and varies with period. To experimentally determine K and $k_f + k_b$, a plot of peak ratio versus log period should be constructed and examined. If an apex in the $\Delta\Psi^{+}_{ratio}$ - log period curve is observed, the value of K is directly obtained from the magnitude of the apex using the working curve presented in Figure 6.6c.

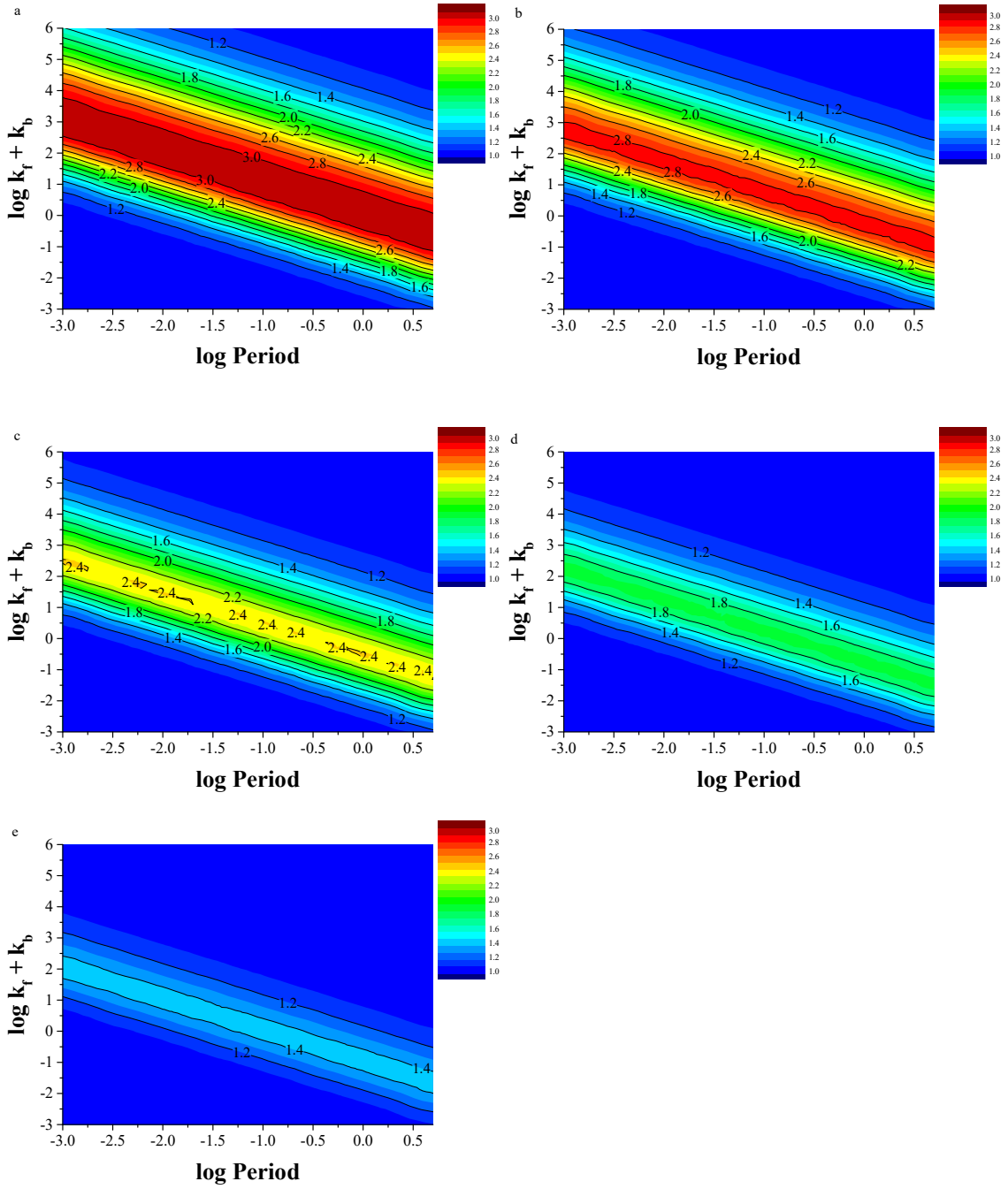

Figure 6.8. The impact of period on peak ratio over the log ($k_f + k_b$) range -3 to 6 for log K = -2 (panel a), -1.5 (panel b), -1 (panel c), -0.5 (panel d), and 0 (panel e) when amplitude = 50 mV and increment = 10 mV.

Log ($k_f + k_b$) is then determined by identifying the period at which the apex occurs in the appropriate panel in Figures 6.7 and 6.8. Note that extrapolation between maxima

presented in a given panel or between panels may be necessary. If an apex in the $\Delta\Psi^{+}_{ratio}$ - log period curve is not observed, both K and $k_f + k_b$ can be estimated from overlaying the trace onto the best fitting trace in Figure 6.7. In this situation, additional simulations at other log K and log ($k_f + k_b$) values than those reported in Figure 6.7 may be required for refinement of initial estimates.

The effect of period on peak current for a fixed value of K while $k_f + k_b$ is varied is shown in Figure 6.9. When the rate of conversion of Y to Ox is slow, both $\Delta\Psi^{+}_{p,f}$ and $\Delta\Psi^{+}_{p,r}$ are small and linearly related to period$^{-1/2}$.

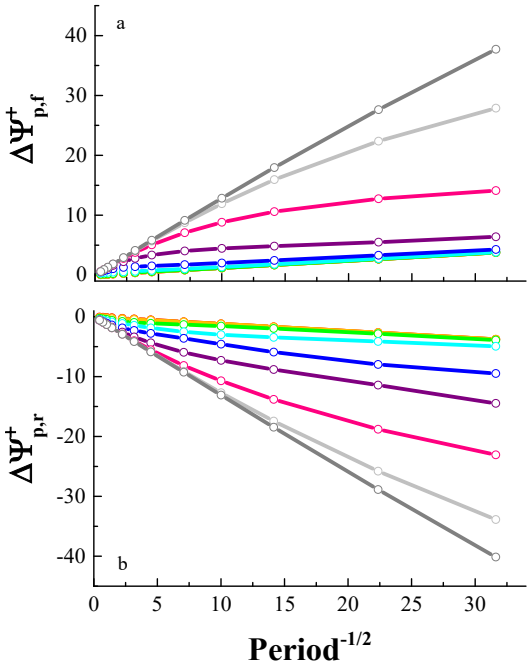

Figure 6.9. The impact of period on $\Delta\Psi^{+}_{p,f}$ and $\Delta\Psi^{+}_{p,r}$ when amplitude = 50 mV, increment = 10 mV, log K = -1, and log ($k_f + k_b$) ranges from -3 (red) to 6 (dark gray).

When the rate of conversion of Y to Ox is very fast (e.g. log ($k_f + k_b$) = 6), peak currents are linear with period$^{-1/2}$ and approach the value for a reversible process. At intermediate

rates of conversion, peak currents are curvilinearly related to period$^{-1/2}$ and increase with log ($k_f + k_b$). Thus, a curvilinear relationship between peak current and period$^{-1/2}$ is a second indicator of a coupled chemical reaction.

The effect of K, $k_f + k_b$, and period on $E_{p,f}$ and $E_{p,r}$ is shown in Figures 6.10 and 6.11, respectively. When the equilibrium lies heavily in favor of Y, i.e. log K ≤ -2, (see panels a & b) and when log ($k_f + k_b$) ≤ -2, peak potentials equal E^0 and are unaffected by period. When log ($k_f + k_b$) > -2, $E_{p,f}$ and $E_{p,r}$ shift negatively with period; the magnitude of the shift is dependent upon $k_f + k_b$. When -1 ≤ log K ≤ 0, (see panels c & d) and at slow rates of conversion, $E_{p,f}$ and $E_{p,r}$ remain at E^0 and are independent of period. At intermediate rates of conversion i.e. -2 ≤ log ($k_f + k_b$) ≤ 4, peak potentials shift negatively with period; the magnitude of the shift is dependent upon $k_f + k_b$. At fast rates of conversion, i.e., when log ($k_f + k_b$) ≥ 5, both $E_{p,f}$ and $E_{p,r}$ become invariant with period and are shifted negatively from E^0 by an amount determined by K. When the equilibrium lies heavily in favor of Ox, i.e. log K ≥ 1, (panels e & f), peak potentials equal E^0 regardless of period and the magnitude of log ($k_f + k_b$). Thus, a third indicator of a CE mechanism is the negative shift in peak potentials with period.

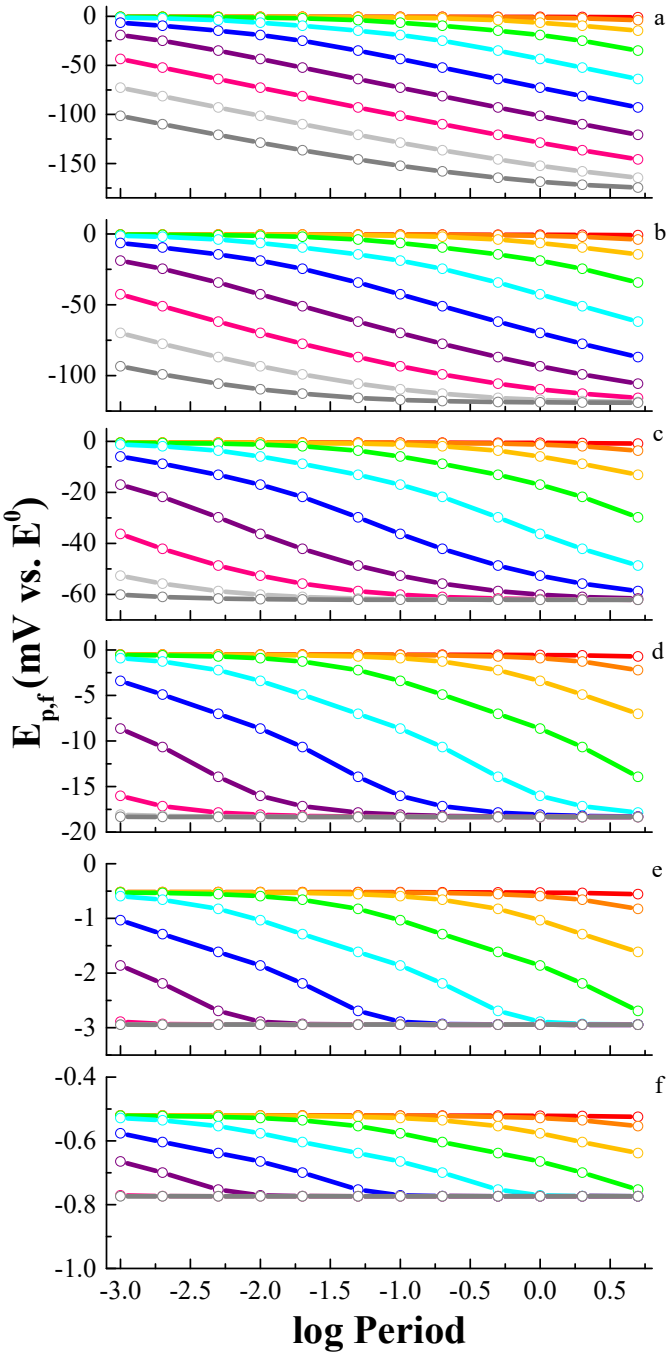

Figure 6.10. The impact of period on $E_{p,f}$ over the log ($k_f + k_b$) range -3 (red) to 6 (dark gray) for log K = -3 (panel a) to 2 (panel f) when amplitude = 50 mV and increment = 10 mV.

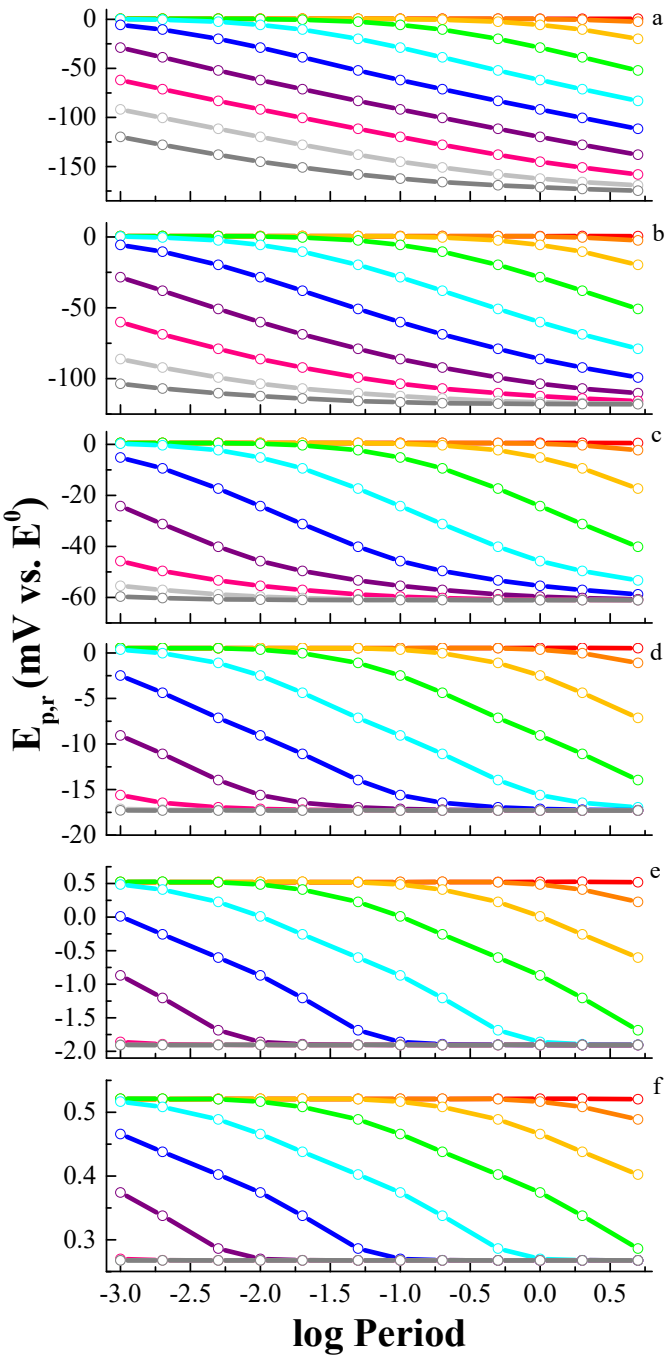

Figure 6.11. The impact of period on $E_{p,r}$ over the log ($k_f + k_b$) range -3 (red) to 6 (dark gray) for log K = -3 (panel a) to 2 (panel f) when amplitude = 50 mV and increment = 10 mV.

When varying period, several differences can be identified between the CE and reversible cases. Peak potentials shift negatively from E^0 with period for the CE case

(except when the equilibrium lies in favor of Ox) and remain at E^0 for the reversible case. Current is curvilinearly related to period$^{-1/2}$ for the CE case and linearly related to period$^{-1/2}$ reversible case. Peak ratios are ≥ 1 with period for the CE case but are always unity for the reversible case. Readers are reminded that all trends for the CE case are dependent on K, k_f, and k_b. Thus, given these differences in the trends for the two mechanisms, variation of period can be used to distinguish between the reversible and CE mechanisms.

Similarly, when varying period, several differences can be identified between a coupled chemical reaction preceding (CE) and following (EC) the electron transfer. Peak potentials shift negatively from E^0 with period for the CE case and positively for the EC case. Current is curvilinearly related to period$^{-1/2}$ for both cases. Peak ratios vary with period for both mechanisms; peak ratios are ≥ 1 for the CE case and ≤ 1 for the EC case. Thus, systematic variation in period affords ready differentiation between a CE and EC mechanism.

6.2.4 Effect of Increment (δE)

The effect of increment on the voltammogram for a CE mechanism is shown in Figure 6.12a. $E_{p,f}$ and $E_{p,r}$ are both negative of E^0 and shift positively with increasing increment though $E_{p,f}$ shifts less than $E_{p,r}$ (Figure 6.12b). Thus, the peak separation is initially 10 mV and decreases with increasing increment. $\Delta\Psi^{+}_{p,f}$ decreases slightly with increment while $\Delta\Psi^{+}_{p,r}$ increases with increment (Figure 6.12c). Relative changes in peak currents result in an increase in peak ratio with increment (Figure 6.12d). This trend is

comparable to that observed in CV since the effective potential sweep rate scales with increment and shortens the time window for the conversion of Y to Ox.

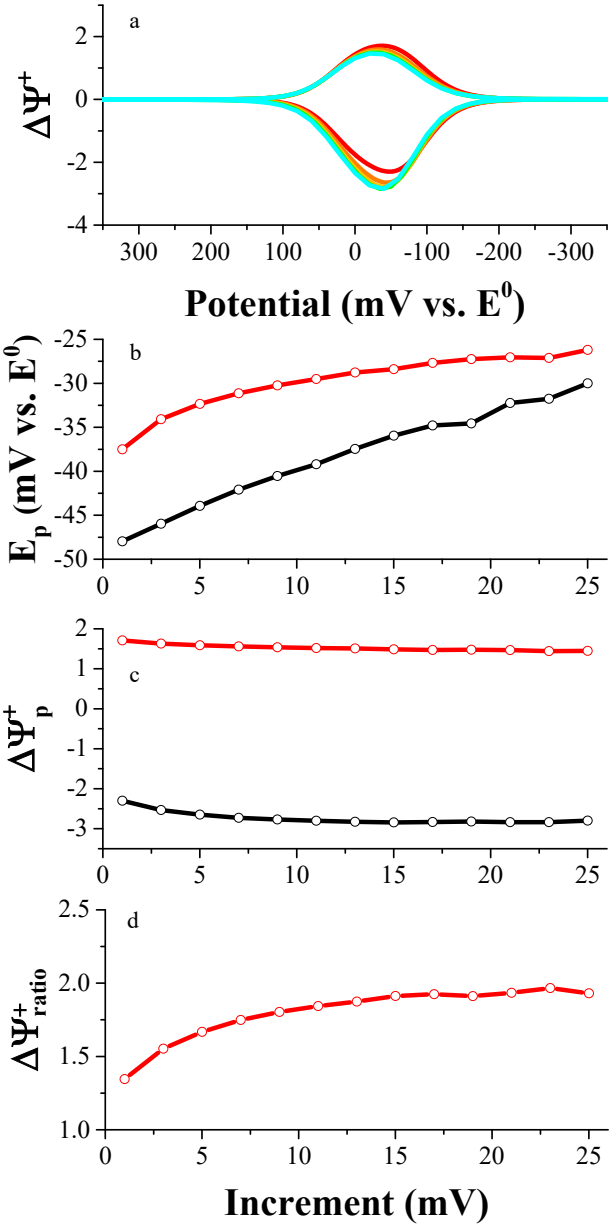

Figure 6.12. The impact of increment on the shape of the voltammogram when amplitude = 50 mV, period = 50 ms, log K = -1, and log ($k_f + k_b$) = 2. Panel a): Increment ranges from 1 mV (red), 5 mV (orange), 10 mV (yellow), 15 mV (green), and 20 mV (cyan). Panel b): $E_{p,f}$ (red) and $E_{p,r}$ (black). Panel c): $\Delta\Psi^+_{p,f}$ (red) and $\Delta\Psi^+_{p,r}$ (black). Panel d): Peak ratio (red).

Figure 6.13 presents the effect of increment and K on peak ratio when $k_f + k_b$ is held constant. When log K = -3, peak ratio decreases slightly with increment. For $-2 \leq \log K \leq 0$, peak ratio increases with increment though the value of peak ratio depends on K. When log K > 0, peak ratio is unaffected by increment as the equilibrium favors Ox, appearing as a reversible reaction.

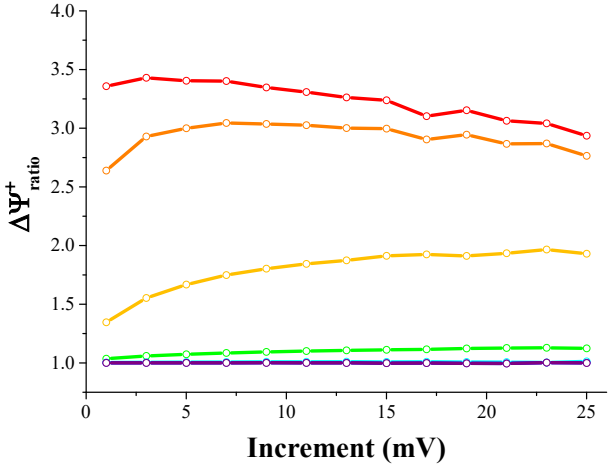

Figure 6.13. The impact of increment on the peak ratio as log K is varied from -3 (red) to 3 (purple) in steps of 1 when amplitude = 50 mV, period = 50 ms, and log $(k_f + k_b) = 2$.

The effect of K, $k_f + k_b$, and increment on peak ratio is shown in Figure 6.14. When the equilibrium lies heavily in favor of Y, i.e. log $K \leq -2$ (panels a & b) peak ratio ranges from 1 to 3.5 depending upon increment and log $(k_f + k_b)$. At slow rates of conversion from Y to Ox, the peak ratio is unaffected by increment. At intermediate rates i.e. $-1 \leq \log (k_f + k_b) \leq 2$, peak ratio decreases with increment but scales with k_f. At fast rates of conversion i.e. log $(k_f + k_b) > 2$, peak ratio increases with increment but decreases with increasing log $(k_f + k_b)$. For $-1 \leq \log K \leq 1$ (panels c to d) and log $(k_f + k_b) \leq -2$ or when log $(k_f + k_b) > 3$ peak ratio is unaffected by increment. At $-2 < \log (k_f + k_b) \leq 3$, the trend and magnitude of peak ratio with increment depend upon $k_f + k_b$. When the equilibrium

lies heavily in favor of Ox, i.e. log $K \geq 1$ (panels e & f), peak ratio is unaffected by increment regardless of K and $k_f + k_b$.

The effect of increment on peak current as a function of $k_f + k_b$ is shown in Figure 6.15. The magnitudes of both $\Delta\Psi^{+}_{p,f}$ and $\Delta\Psi^{+}_{p,r}$ increase in proportion to $k_f + k_b$. $\Delta\Psi^{+}_{p,f}$ is invariant of increment over all values of $k_f + k_b$ whereas $\Delta\Psi^{+}_{p,r}$ increases slightly with increment for log $(k_f + k_b) \geq 2$ and either decreases slightly or is unaffected by increment for log $(k_f + k_b) < 2$ (Figure 6.15b).

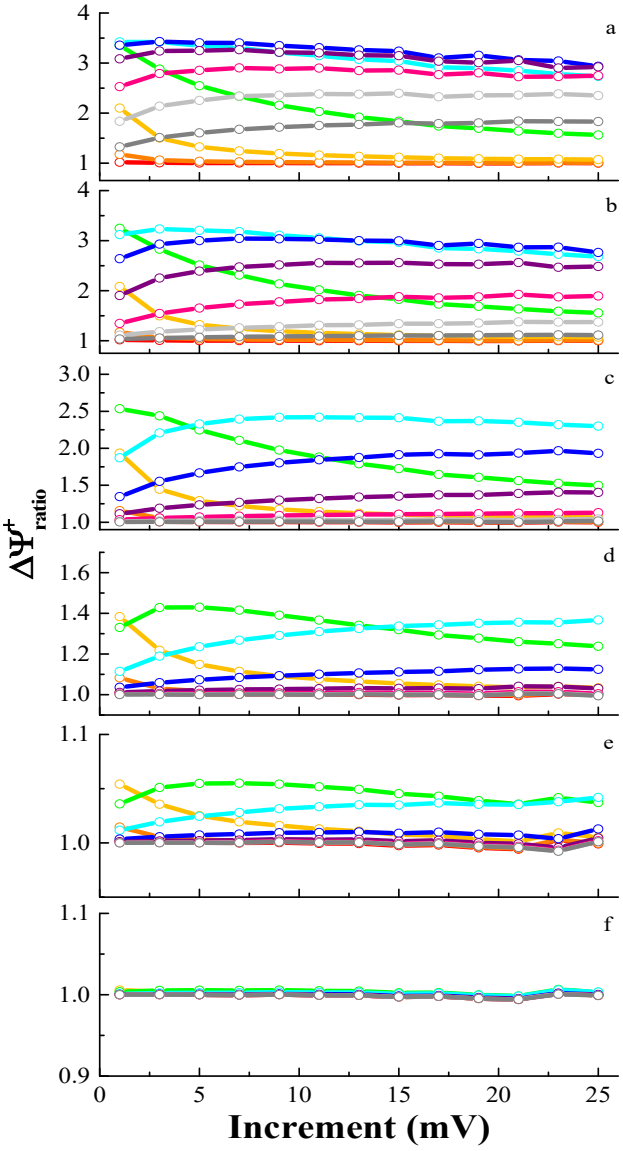

Figure 6.14. The impact of increment on peak ratio over the log ($k_f + k_b$) range -3 (red) to 6 (dark gray) for log K = -3 (panel a) to 2 (panel f) when amplitude = 50 mV and period = 50 ms.

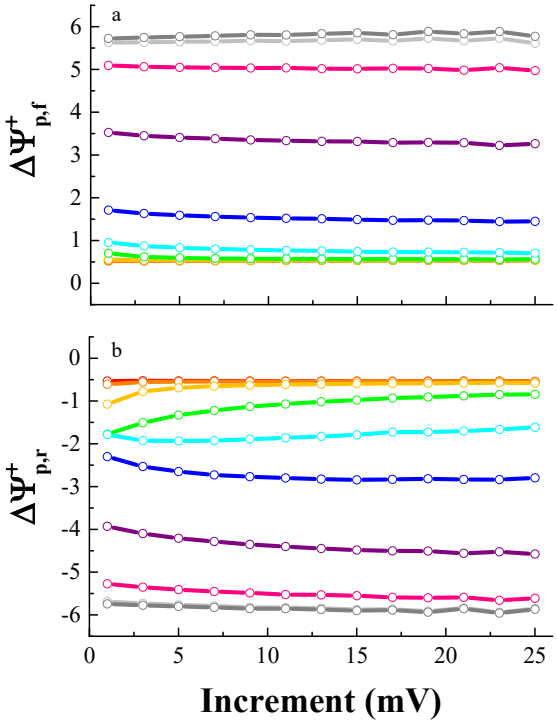

Figure 6.15. The impact of increment on $\Delta\Psi^{+}_{p,f}$ and $\Delta\Psi^{+}_{p,r}$ when amplitude = 50 mV, period = 50 ms, log K = -1, and log ($k_f + k_b$) ranges from -3 (red) to 6 (dark gray).

$E_{p,f}$ and $E_{p,r}$ are related K, $k_f + k_b$, and increment as shown in Figures 6.16 and 6.17. When the equilibrium lies heavily in favor of Y, i.e. log K = -3 & -2 (panels a & b in both figures) and log ($k_f + k_b$) ≥ -2, peak potentials shift positively with increment; the magnitude and the shift depends on $k_f + k_b$. When -2 ≤ log K ≤ -1 (panels c & d in both figures), peak potential is invariant with increment when log ($k_f + k_b$) ≤ -1 and when log ($k_f + k_b$) ≥ 5 at values dictated by log ($k_f + k_b$). Intermediate values shift positively with increment though the magnitude and shift depend on ($k_f + k_b$). When the equilibrium lies heavily in favor of Ox, i.e. log K ≥ 1 (panels e & f in both figures), peak potential remains essentially constant with increment regardless of $k_f + k_b$.

In comparing the trends for the CE and reversible cases as a function of increment, several differences can be identified. Peak potentials shift positively towards E^0 with increment for the CE case but remain at E^0 for the reversible case; the magnitude of the shift depends on K, k_f, and k_b.

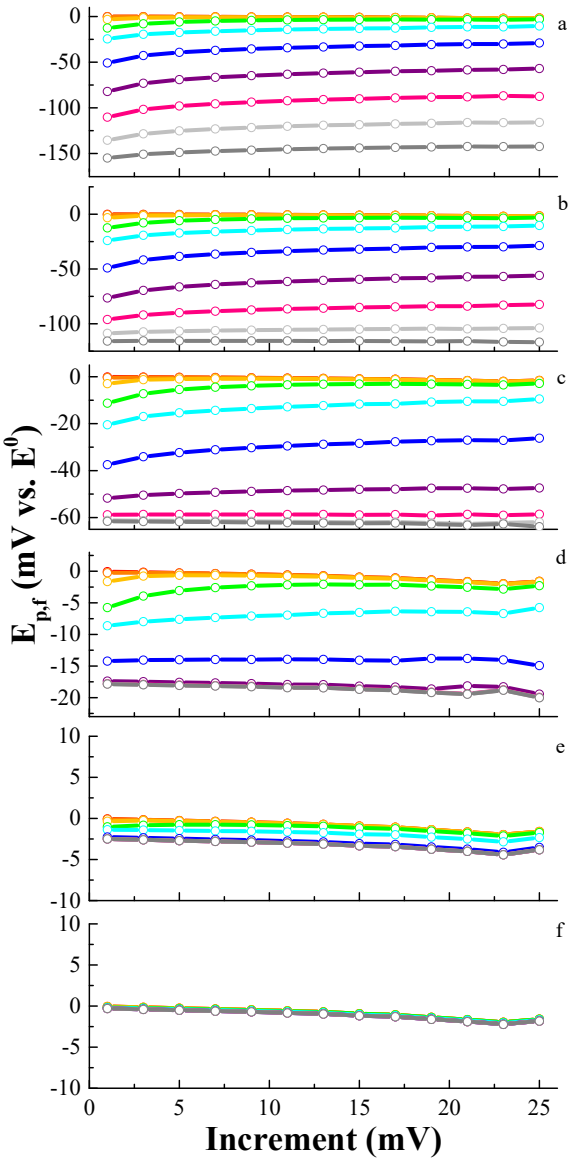

Figure 6.16. The impact of increment on $E_{p,f}$ over the log (k_f + k_b) range -3 (red) to 6 (dark gray) for log K = -3 (panel a) to 2 (panel f) when amplitude = 50 mV and period = 50 ms.

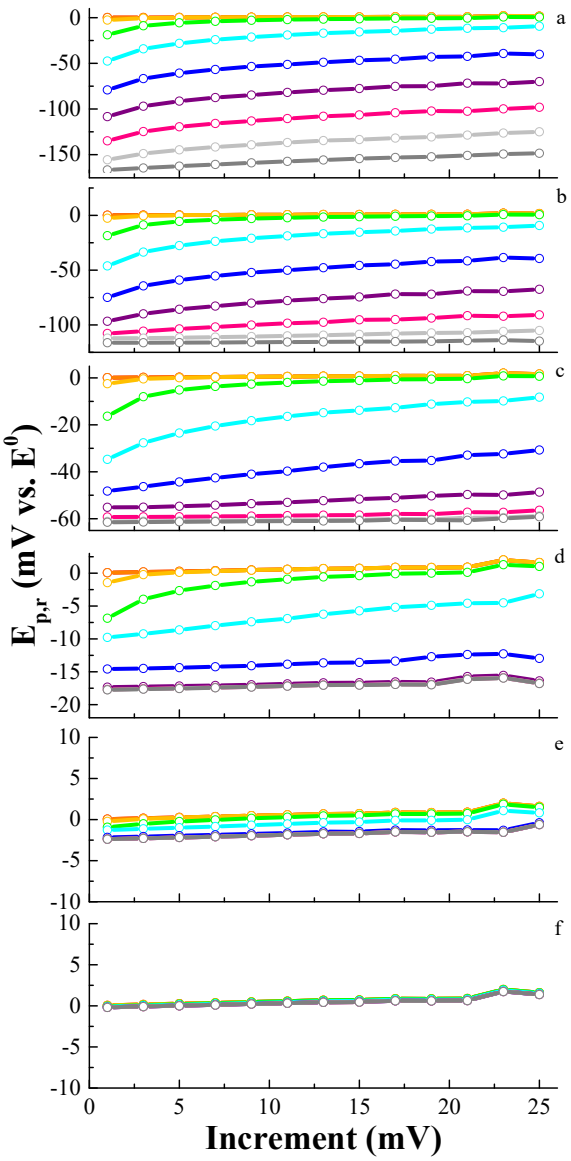

Figure 6.17. The impact of increment on $E_{p,r}$ over the log ($k_f + k_b$) range -3 (red) to 6 (dark gray) for log K = -3 (panel a) to 2 (panel f) when amplitude = 50 mV and period = 50 ms.

Peak currents increase slightly with increment for the CE case but are unaffected by increment for the reversible. Peak ratios are ≥ 1 and vary with increment for the CE case but are unity regardless of increment for the reversible case; the trend is dependent upon

K, k_f, and k_b. Hence, the systematic variation of increment can be used to discern between the reversible and CE mechanisms.

Similarly, when varying increment, several differences can be identified between a CE and EC mechanism. Peak potentials shift positively towards E^0 with increment for the CE case and negatively for the EC case. Peak currents increase to a small extent with increment for the CE case and to a much larger extent for the EC case. Peak ratios vary with increment for both mechanisms; peak ratios are ≥ 1 for the CE case and ≤ 1 for the EC case. Thus, systematic variation in increment enables discrimination between a CE and EC mechanism.

6.2.5 Effect of Switching Potential (E_λ)

Switching potential (relative to E^0) greatly affects the voltammogram for a CE mechanism as shown in Figure 6.18a. $E_{p,f}$ remains constant as E_λ is varied though $E_{p,r}$ shifts slightly positive as E_λ approaches E^0 (Figure 6.18b). $\Delta\Psi^+_{p,f}$ is unaffected by E_λ - while $\Delta\Psi^+_{p,r}$ decreases as E_λ approaches E^0 (Figure 6.18c). Subsequently, peak ratio decreases as E_λ approaches E^0 (Figure 6.18d).

The effect of K and E_λ on peak ratio is shown in Figure 6.19. For cases in which the equilibrium favors Y, i.e., $K \leq -1$, peak ratio decreases as E_λ approaches E^0. When log K ≥ 0, peak ratio is invariant with switching potential.

The effect of K, $k_f + k_b$, and E_λ on peak ratio is shown in Figure 6.20. When the equilibrium lies heavily in favor of Y, i.e. log $K \leq -3$ (panel a) and log $(k_f + k_b) \leq -2$, peak ratio is unaffected by E_λ. Peak ratio decreases as E_λ approaches E^0 log $(k_f + k_b) > -2$. For $-2 \leq$ log $K \leq 0$ (panels b to d), extreme values of log $(k_f + k_b)$ are invariant with E_λ

whereas intermediate values of log ($k_f + k_b$) cause peak ratios to decrease as E_λ - approaches E^0.

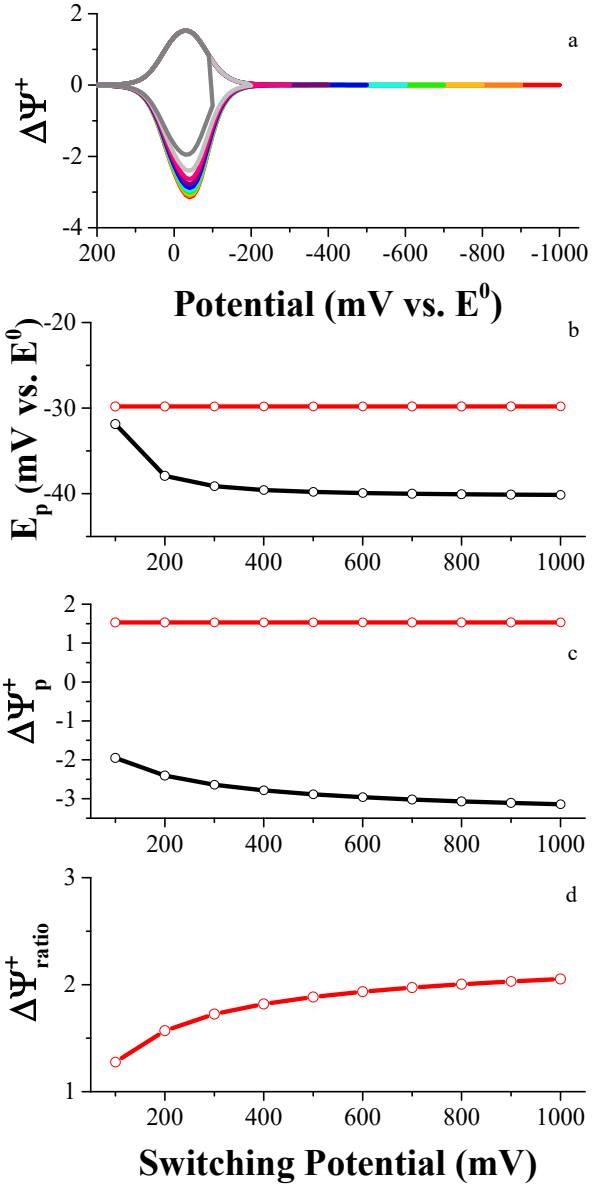

Figure 6.18. The impact of switching potential on the shape of the voltammogram when amplitude = 50 mV, increment = 10 mV, period = 50 ms, log K = -1, and log ($k_f + k_b$) = 2. Panel a): Switching potential ranges from 1000 mV (red), 900 mV (orange), 800 mV (yellow), 700 mV (green), 600 mV (cyan), 500 mV (blue), 400 mV (purple), 300 mV (magenta), 200 mV (light gray), and 100 mV (dark gray). Panel b): $E_{p,f}$ (red) and $E_{p,r}$ (black). Panel c): $\Delta\Psi^+_{p,f}$ (red) and $\Delta\Psi^+_{p,r}$ (black). Panel d): Peak ratio (red).

When the equilibrium lies heavily in favor of Ox, i.e. log K ≥ 1 (panels e & f), peak ratio is nearly unaffected by E_λ.

Figure 6.21 presents the effects of E_λ and $k_f + k_b$ on peak currents when log K is constant. $\Delta\Psi^+_{p,f}$ (Figure 6.21a) is invariant of E_λ unless E_λ occurs before the current returns to baseline; the magnitude of $\Delta\Psi^+_{p,f}$ depends on $k_f + k_b$. $\Delta\Psi^+_{p,r}$ (Figure 6.21b) decreases as E_λ approaches E^0 with some values of $\Delta\Psi^+_{p,r}$ approaching zero. Like $\Delta\Psi^+_{p,f}$, the magnitude of current depends on $k_f + k_b$.

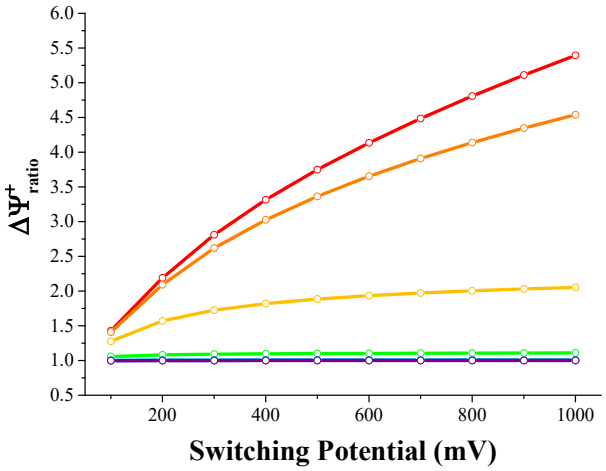

Figure 6.19. The impact of switching potential on the peak ratio as log K is varied from -3 (red) to 3 (purple) in steps of 1 when increment = 10 mV, period = 50 ms, and log ($k_f + k_b$) = 2.

Peak potential trends with E_λ, K, and $k_f + k_b$ are shown in Figures 6.22 and 6.23. $E_{p,f}$ is invariant of E_λ unless E_λ occurs before the current returns to baseline. The value of $E_{p,f}$ depends on $k_f + k_b$ and K. $E_{p,r}$ remains at E^0 regardless of K and E_λ for log ($k_f + k_b$) ≤ 1 (Figure 6.23 all panels). $E_{p,r}$ approaches E^0 as E_λ approaches E^0 when log K < 1 and log ($k_f + k_b$) > 1 (panels a to d); the value of $E_{p,r}$ depends on $k_f + k_b$ and K. When log K ≥ 1 (panels e & f), $E_{p,r}$ is invariant of E_λ and remains at E^0 for all values of $k_f + k_b$.

There are contrasting trends for the effect of switching potential on the voltammograms of the reversible and CE cases. Peak potentials are displaced from E^0 but remain essentially constant with the variation of switching potential CE mechanism; $E_{p,f}$ and $E_{p,r}$ remain at E^0 for the reversible case.

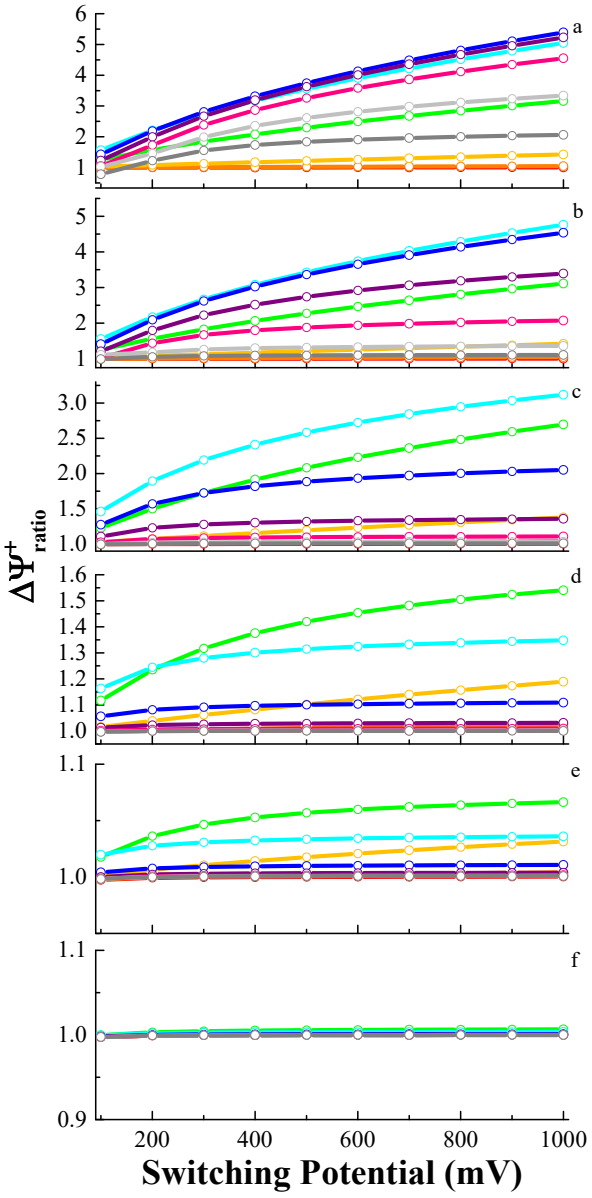

Figure 6.20. The impact of switching potential on peak ratio over the log ($k_f + k_b$) range -3 (red) to 6 (dark gray) for log K = -3 (panel a) to 2 (panel f) when amplitude = 50 mV, increment = 10 mV, and period = 50 ms.

Peak currents are unaffected by switching potential for the reversible case.

$\Delta\Psi^{+}_{p,f}$ is unaffected by switching potential for the CE case but the magnitude of depends on K, k_f, and k_b. $\Delta\Psi^{+}_{p,r}$ may increase with E_λ. Subsequently, peak ratio increases with switching potential for the CE case while it is invariant for the reversible case. This trend is observed because as E_λ increases, the number of potential steps past E^0 increases. Conversion of Y to Ox to Red occurs on each step past E^0 and consequently the net current on the reverse sweep grows with E_λ. Thus, the effect of switching potential on the peak properties can be used to identify CE vs. reversible mechanisms.

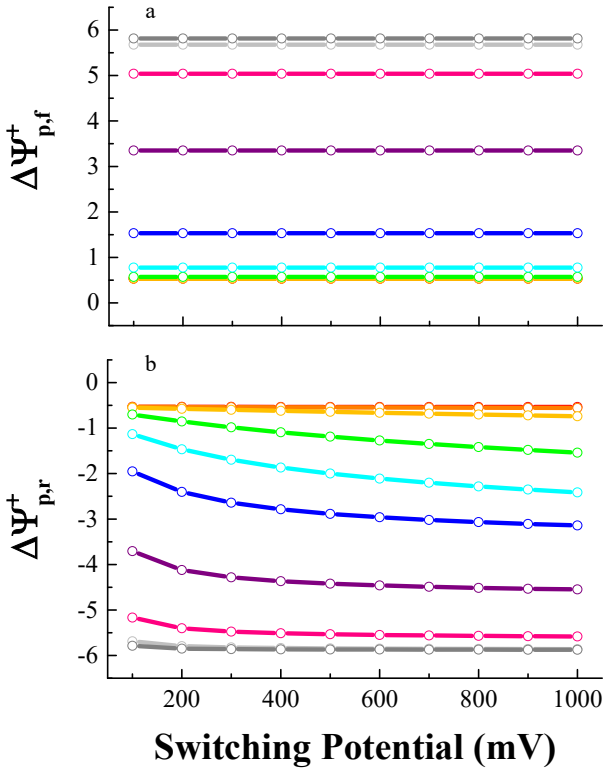

Figure 6.21. The impact of switching potential on $\Delta\Psi^{+}_{p,f}$ and $\Delta\Psi^{+}_{p,r}$ when amplitude = 50 mV, increment = 10 mV, period = 50 ms, log K = -1, and log ($k_f + k_b$) ranges from -3 (red) to 6 (dark gray).

Varying switching potential also affords discrimination between a CE and EC mechanism. Peak potentials are displaced from E^0 but remain essentially constant with the variation of switching potential for both mechanisms.

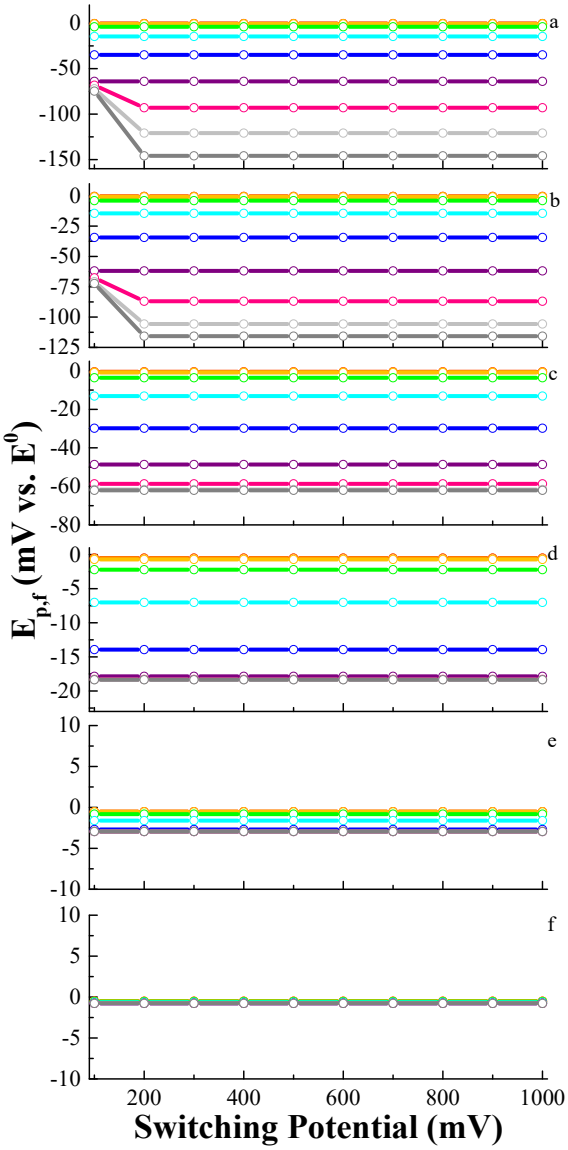

Figure 6.22. The impact of switching potential on $E_{p,f}$ over the log ($k_f + k_b$) range -3 (red) to 6 (dark gray) for log K = -3 (panel a) to 2 (panel f) when amplitude = 50 mV, increment = 10 mV and period = 50 ms.

$\Delta\Psi^{+}_{p,f}$ is unaffected by switching potential for both CE and EC. However, $\Delta\Psi^{+}_{p,r}$ decreases as the switching potential moves towards E^0 for the CE case and increases for the EC case.

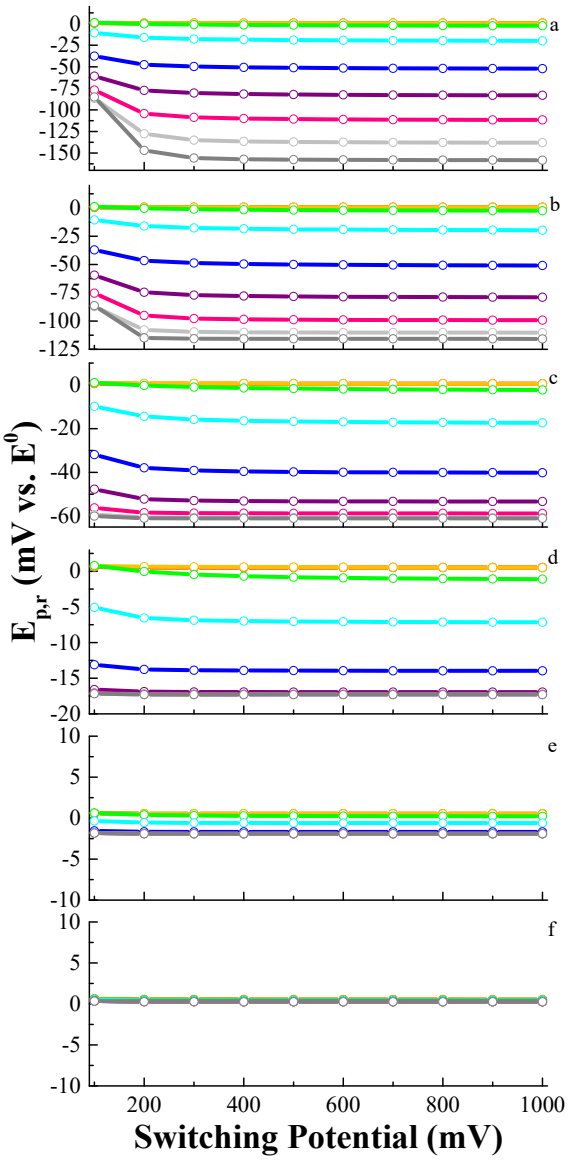

Figure 6.23. The impact of switching potential on $E_{p,r}$ over the log (k_f + k_b) range -3 (red) to 6 (dark gray) for log K = -3 (panel a) to 2 (panel f) when amplitude = 50 mV, increment = 10 mV and period = 50 ms.

Peak ratios are ≥ 1 for the CE case and decrease as E_λ approaches E^0 whereas peak ratios ≤ 1 for the EC case and increase as E_λ approaches E^0. Thus, systematic variation in switching potential distinguishes a CE from an EC mechanism.

It should be noted that for the CE mechanism, the results obtained by CSWV will not be equivalent to those obtained by conventional SWV followed by a reverse scan. Significant differences in the magnitude of the reverse peak (and consequently, peak ratio) will occur with any delay between the completion of the forward and the initiation of the reverse scans in SWV or if the working electrode potential is momentarily uncontrolled in between the two scans. The former will result in an increase in the effective switching potential. The latter will cause changes in the concentrations of Red and Ox at the electrode surface prior to the initiation of the reverse scan. In either case, significant differences in the reverse peak current and peak current ratios will be obtained.

6.2.6 Effect of Amplitude (E_{SW})

The effect of amplitude on the shape of the voltammogram is shown in Figure 6.24a. As amplitude increases, $E_{p,f}$ shifts negatively by a few mV while $E_{p,r}$ shifts negatively by more than 40 mV (see Figure 6.24b). Both $\Delta\Psi^+_{p,f}$ and $\Delta\Psi^+_{p,r}$ increase with amplitude though $\Delta\Psi^+_{p,r}$ increases more rapidly than $\Delta\Psi^+_{p,f}$ (Figure 6.24c). As a result, peak ratio decreases with amplitude, as shown in Figure 6.24d.

The relationship between peak ratio and amplitude depends on K. This is shown in Figure 6.25 for an intermediate rate of conversion of Y to Ox. When the equilibrium favors Y, i.e. log K < 0, peak ratio decreases with amplitude; the range and magnitude of

peak ratio depends on K. When the equilibrium favors Ox i.e. $K \geq 0$, peak ratio is nearly unity, remaining constant and unaffected by amplitude.

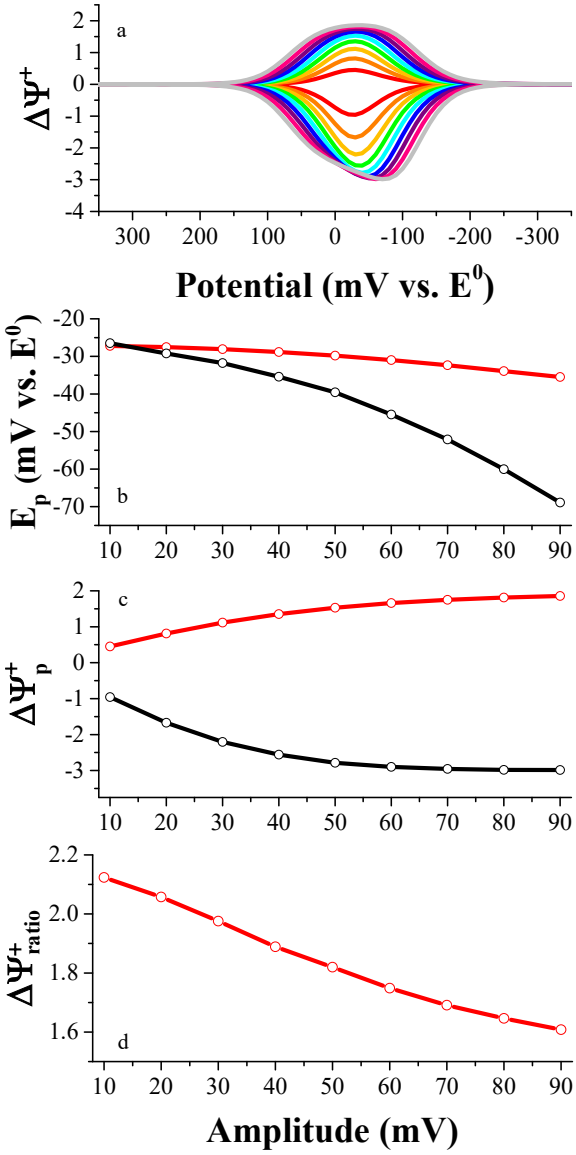

Figure 6.24. The impact of amplitude on the shape of the voltammogram when increment = 10 mV, period = 50 ms, log K = -1, and log ($k_f + k_b$) = 2. Panel a): Amplitude ranges from 10 mV (red), 20 mV (orange), 30 mV (yellow), 40 mV (green), 50 mV (cyan), 60 mV (blue), 70 mV (purple), 80 mV (magenta), and 90 mV (light gray). Panel b): $E_{p,f}$ (red) and $E_{p,r}$ (black). Panel c): $\Delta\Psi^+_{p,f}$ (red) and $\Delta\Psi^+_{p,r}$ (black). Panel d): Peak ratio (red).

The effect of K, $k_f + k_b$, and amplitude on peak ratio is shown in Figure 6.26. When Y is favored in the equilibrium, i.e., when log K ≤ 0 (panels a-d), peak ratios decrease or remain constant, dependent upon $k_f + k_b$. When the equilibrium favors Ox, i.e. log K ≥ 1, peak ratio is unaffected by $k_f + k_b$.

The impact of amplitude and $k_f + k_b$ on $\Delta\Psi^+_{p,f}$ and $\Delta\Psi^+_{p,r}$ are shown in Figure 6.27a and 6.27b, respectively. Both peak currents increase with amplitude; however, the magnitude of the peak current and the span of the current range depend markedly on $k_f + k_b$.

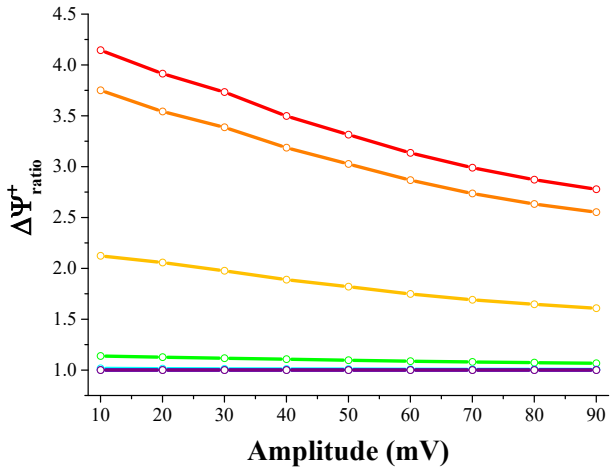

Figure 6.25. The impact of amplitude on the peak ratio as log K is varied from -3 (red) to 3 (purple) in steps of 1 when increment = 10 mV, period = 50 ms, and log ($k_f + k_b$) = 2.

Figures 6.28 and 6.29 present the impact of amplitude on peak potentials as a function of log ($k_f + k_b$) and log K. Over the entire range in log K and log ($k_f + k_b$), $E_{p,f}$ shifts negatively by less than 15 mV with increasing amplitude. However, the position of $E_{p,f}$ relative to E^0 depends on log ($k_f + k_b$) and log K (see Figure 6.28). For a given log K, $E_{p,f}$ shifts negative of E^0 with increasing log ($k_f + k_b$). Similarly, for a given log ($k_f + k_b$), $E_{p,f}$ shifts back towards E^0 with increasing log K. In comparison, $E_{p,r}$ shifts negatively by as

much as 60 mV with increasing amplitude. The position of $E_{p,r}$ relative to E^0 also depends on log ($k_f + k_b$) and log K (see Figure 6.29).

Several contrasting trends can be identified when comparing the CE and reversible mechanisms. For a reversible mechanism peak potentials occur at E^0 and are independent of amplitude. For the CE mechanism, peak potentials are negatively shifted from E^0 by an amount that depends on log ($k_f + k_b$) and log K; the shift in $E_{p,r}$ is greater than the shift in $E_{p,f}$ with amplitude.

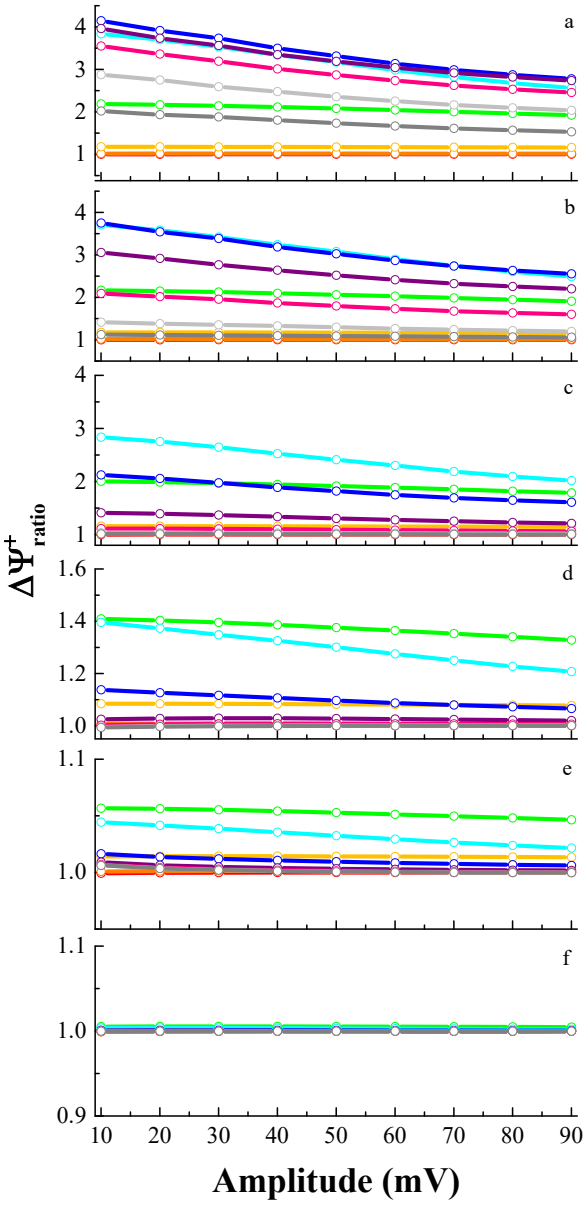

Figure 6.26. The impact of amplitude on peak ratio over the log ($k_f + k_b$) range -3 (red) to 6 (dark gray) for log K = -3 (panel a) to 2 (panel f) when increment = 10 mV and period = 50 ms.

Peak currents increase with amplitude for both cases, but the increase is dependent upon K, k_f, and k_b for the CE mechanism. Peak ratios are greater than one for the CE mechanism and decrease towards unity with increasing amplitude whereas they are

always unity for the reversible case. Thus, the reversible and CE mechanisms can be distinguished by variation of amplitude.

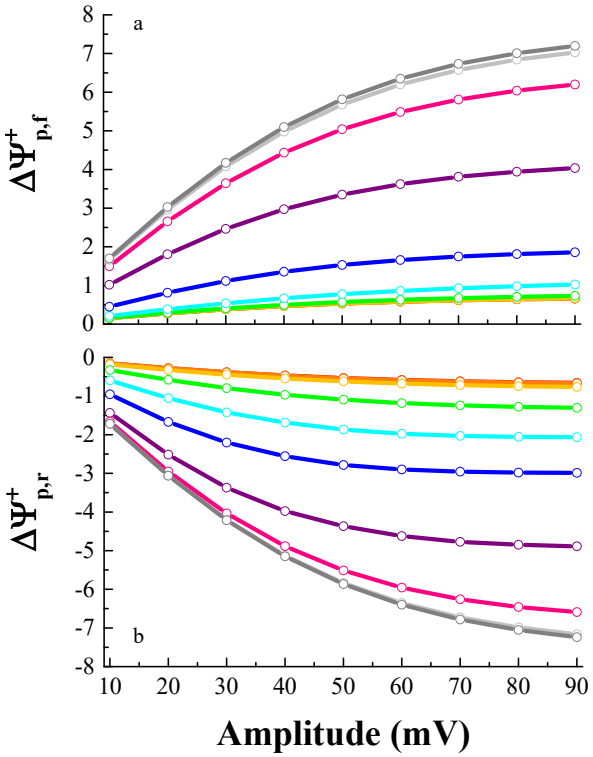

Figure 6.27. The impact of amplitude on $\Delta\Psi^{+}_{p,f}$ and $\Delta\Psi^{+}_{p,r}$ when increment = 10 mV, period = 50 ms, log K = -1, and log ($k_f + k_b$) ranges from -3 (red) to 6 (dark gray).

Varying amplitude also affords discrimination between a CE and EC mechanism because the peak potentials shift in opposite directions (positively from E^0 for EC and negatively for CE). Peak ratios are greater than one for the CE mechanism and decrease towards unity with increasing amplitude whereas they are either less than unity or increase towards unity for the EC mechanism. Thus, systematic variation of amplitude enables one to discern between coupled chemical reactions that precede or follow the electron transfer step.

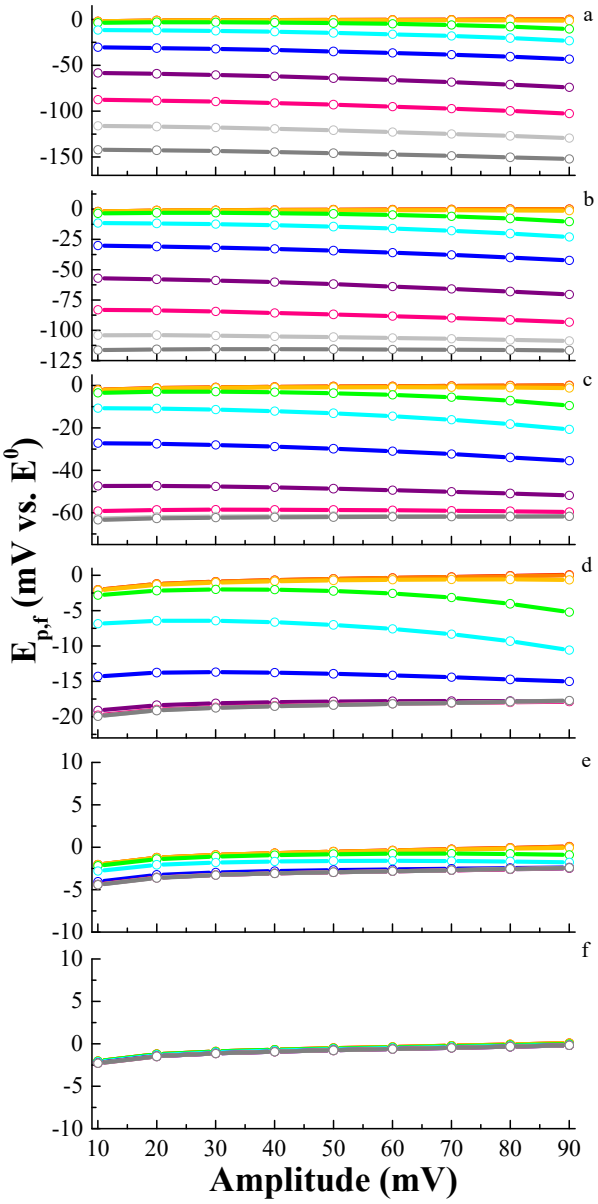

Figure 6.28. The impact of amplitude on $E_{p,f}$ over the log ($k_f + k_b$) range -3 (red) to 6 (dark gray) for log K = -3 (panel a) to 2 (panel f) when increment = 10 mV and period = 50 ms.

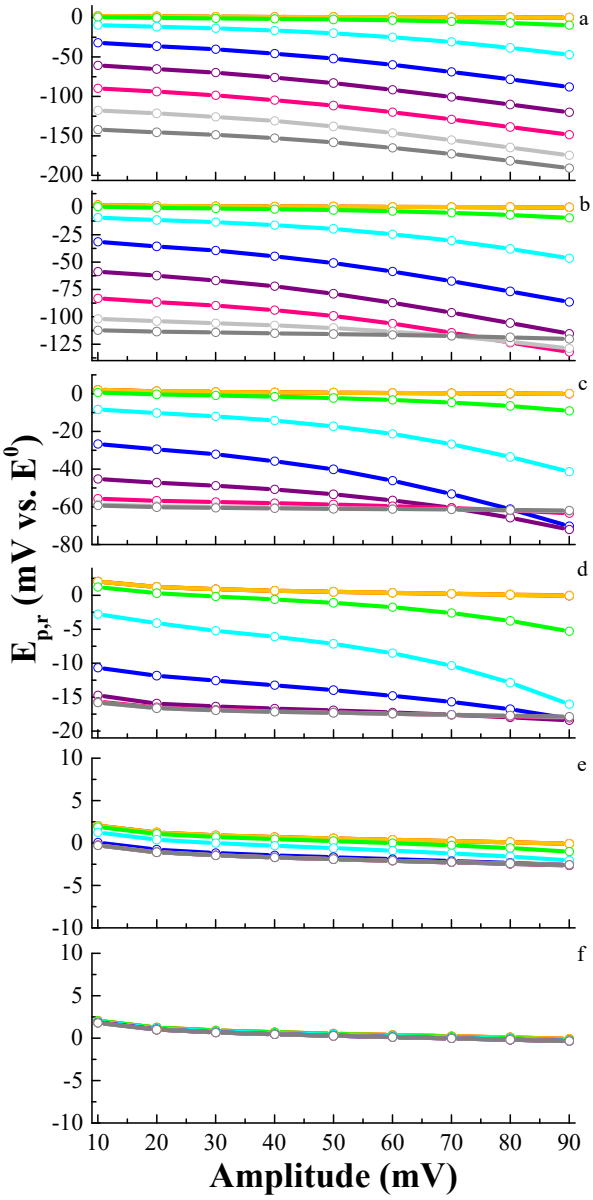

Figure 6.29. The impact of amplitude on $E_{p,r}$ over the log ($k_f + k_b$) range -3 (red) to 6 (dark gray) for log K = -3 (panel a) to 2 (panel f) when increment = 10 mV and period = 50 ms.

6.3 Conclusion

The peak currents, potentials and shapes of cyclic square wave voltammograms for the CE mechanism have been shown to be a complex function K, $k_f + k_b$, increment, period, switching potential and amplitude. The effects of these empirical parameters on the voltammograms for this mechanism are summarized in Table 6.1. The diagnostic criteria presented in this table will enable rapid identification of CE mechanisms (with both reversible and irreversible coupled chemical reactions) using CSWV so long as the equilibrium $[Y] \geq [Ox]$, i.e. $-3 < \log K \leq 0$. Within this range, peak current, peak ratio, and peak potential variation with the empirical parameters investigated herein afford measure of the rate of conversion from Y to Ox within the time period of the potential pulse.

Table 6.1. Diagnostic Plots and Protocol for Assessing a CE Electrode Reaction by CSWV

	Empirical variables							
Waveform parameters	***Period,* τ**		***Increment,* δE**		***Switching potential,* E_λ**		***Amplitude,* E_{SW}**	
	Plot	**Trace**	**Plot**	**Trend**	**Plot**	**Trend**	**Plot**	**Trend**
Peak currents	ΔI_p vs. $\tau^{-1/2}$	Decreases linearly or curvilinearly with increasing period (see Figures 6.5c and 6.9)	ΔI_p vs. δE	$\Delta I_{p,f}$ is invariant with δE; $\Delta I_{p,r}$ may increase or be invariant with δE depending upon log K and log $(k_f + k_b)$ (see Figure 6.12c and 6.15)	ΔI_p vs. E_λ	$\Delta I_{p,f}$ is invariant with E_λ; $\Delta I_{p,r}$ decreases as E_λ approaches E^0 (see Figure 6.18c and 6.21)	ΔI_p vs. E_{SW}	$\Delta I_{p,f}$ and $\Delta I_{p,r}$ increase with E_{SW} (see Figure 6.24c and 6.27)
Peak ratio	Peak ratio vs. $\tau^{-1/2}$	Is greater than or equal to unity. May be curvilinearly related to period depending upon log K and log $(k_f + k_b)$ (see Figures 6.5d, 6.6, 6.7, and 6.8)	Peak ratio vs. δE	Is greater than or equal to unity. May be curvilinearly related to increment depending upon log K and log $(k_f + k_b)$. (see Figure 6.12d, 6.13, and 6.14)	Peak ratio vs. E_λ	Decreases or invariant as E_λ approaches E^0 depending upon log K and log $(k_f + k_b)$. (see Figures 6.18d, 6.19, and 6.20)	Peak ratio vs. E_{SW}	Decreases or is invariant with E_{SW} depending upon log K and log $(k_f + k_b)$. (see Figure 6.24d and 6.26)
Peak potentials	E_p vs. log τ	Shifts negatively with increasing period (see Figure 6.5b, 6.10, and 6.11); Magnitude of displacement of E_p from E^0 depends upon log K and log $(k_f + k_b)$.	E_p vs. δE	Shifts positively towards E^0 or is invariant with increasing δE; Magnitude of displacement of E_p from E^0 depends upon log K and log $(k_f + k_b)$. (see Figure 6.12b, 6.16, and 6.17)	E_p vs. E_λ	$E_{p,f}$ is unaffected by E_λ; $E_{p,r}$ shifts slightly positive (see Figure 6.18b, 6.22, and 6.23) Magnitude of displacement of E_p from E^0 depends upon log K and log $(k_f + k_b)$.	E_p vs. E_{SW}	E_p shifts negatively with E_{SW}; shift magnitude depends on log K and log $(k_f + k_b)$. (see Figure 6.24b, 6.28, and 6.29)
Peak separation	ΔE_p vs. log τ	Generally unaffected by period (see Figure 6.5b)	ΔE_p vs. δE	Slight decrease for low δE values but generally invariant with δE	ΔE_p vs. E_λ	Generally unaffected or slight decrease as E_λ approaches E^0	ΔE_p vs. E_{SW}	Increases with E_{SW} for some values of log $(k_f + k_b)$ but otherwise is invariant with E_{SW}
Peak widths	$W_{1/2}$ vs. $\tau^{-1/2}$	Generally unaffected by period	$W_{1/2}$ vs. δE	Generally unaffected by δE	$W_{1/2}$ vs. E_λ	Generally invariant as E_λ approaches E^0	$W_{1/2}$ vs. E_{SW}	Increases with E_{SW}

6.4 References

1. Nicholson, R.S. and I. Shain. *Anal. Chem.*, **1964**. 36, 706-723.

2. O'Dea, J.J., J. Osteryoung, and R.A. Osteryoung. *Anal, Chem.*, **1981**. 53, 695-701.

3. Savéant, J.M. and F. Xu. *J. Electroanal. Chem. Interfacial Electrochem.*, **1986**. 208, 197-217.

4. Bilewicz, R., K. Wikiel, R. Osteryoung, and J. Osteryoung. *Anal. Chem.*, **1989**. 61, 965-972.

5. El-Hallag, I.S., M.M. Ghoneim, and E. Hammam. *Anal. Chim. Acta*, **2000**. 414, 173-180.

6. Moharram, Y.I. *J. Electroanal. Chem.*, **2004**. 563, 283-290.

7. Mirčeski, V., Š. Komorsky-Lovrić, and M. Lovrić, *Square Wave Voltammetry: Theory and Application*, *Monographs in Electrochemistry*. **2007**, Springer-Verlag: Berlin.

8. Molina, A. and I. Morales. *Int. J. Electrochem. Sci.*, **2007**. 2, 386-405.

9. Molina, A., F. Martinez-Ortiz, E. Laborda, and I. Morales. *J. Electroanal. Chem.*, **2009**. 633, 7-14.

10. Taube, H., *Electron Transfer Reactions of Complex Ions in Solution*. **1970**, Academic Press: New York.

11. Lexa, D. and J.M. Saveant. *Acc. Chem. Res.*, **1983**. 16, 235-243.

12. Lexa, D., P. Rentien, J.M. Saveant, and F. Xu. *J. Electroanal. Chem. Interfacial Electrochem.*, **1985**. 191, 253-279.

13. Orsini, J. and W.E. Geiger. *Organometallics*, **1999**. 18, 1854-1861.

14. Fatouros, N., D. Krulic, and N. Larabi. *J. Electroanal. Chem.*, **2003**. 549, 81-90.

15. Daniele, S., M.A. Baldo, and F. Simonetto. *Anal. Chim. Acta*, **1996**. 331, 117-123.

16. Kurek, S.S., B.J. Laskowska, and A. Stoklosa. *Electrochim. Acta*, **2006**. 51, 2306-2314.

17. Meng, Y., S. Norman, C. Hardacre, and R.G. Compton. *Phys. Chem. Chem. Phys.*, **2013**. 15, 2031-2036.

18. Bentley, C.L., A.M. Bond, A.F. Hollenkamp, P.J. Mahon, and J. Zhang. *J. Phys. Chem. C*, **2015**. 119, 21828-21839.

19. Nicholson, R.S. and M.L. Olmstead, *Electrochemistry: Calculations, Simulation and Instrumentation,*. **1972**, Marcel Dekker: New York. Ch. 5

CHAPTER 7

THE EC_{cat} AND E_qC_{cat} MECHANISMS

7.1 Introduction

Electrocatalysis is foundational to solving current challenges in sequestration oxidation of CO, improving fuel cell efficiency, and the transformation of CO_2 into useful organic chemicals.[1-4] The term electrocatalysis describes several different processes.[1, 5] In some instances, the term refers to electrode reactions in which the electrode material is chemically involved in the catalytic process. An example of this is oxygen reduction at a platinum electrode.[4] The term also refers to electrode materials or coatings that increase the rate of reaction that involves an exchange of electrons. Fuel cells are an example of this as electrocatalysts are needed at both the anode and the cathode to carry out the oxidation of H_2 (and reduction of O_2) at a reasonable rate. Electrocatalytic reactions include homogeneous[2] or heterogeneous[6] and inner or outer sphere charge transfer reactions.[7, 8] In this chapter, the term is used to describe a chemical reaction in which a homogeneous irreversible chemical reaction regenerates a species undergoing a heterogeneous electron transfer at an electrode surface.

This electrocalytic mechanism has been the subject of considerable interest by electrochemists over the past five decades.[9-22] Though many reports have been published, seldom is it used in the greater scientific community for mechanistic identification. In this chapter, CSWV is used for the analysis of an electrocatalytic or

EC_{cat} mechanism as well as the case where the heterogeneous electron transfer step is kinetically limiting, i.e. E_qC_{cat} mechanism. This evaluation involves examination of theoretical voltammograms following systematic variation of empirical parameters for CSWV, *i.e*. period, increment, switching potential, and amplitude. Changes in the voltammogram characteristic of this electrode reaction are identified and form the basis of diagnostic criteria for recognition of an electrocatalytic mechanism.

7.2 Results and Discussion

7.2.1 Theory

The general reaction pathway for an electrocatalytic mechanism, $EC_{cat,}$ is:

$$Ox + ne^- \leftrightarrow Red \tag{7.1}$$

$$Red + Z \leftrightarrow Ox + Z' \tag{7.2}$$

where Red, the product of the electron transfer, undergoes a homogeneous electron transfer reaction with Z to regenerate Ox.[6, 23-28] In chapter work, the concentration of Z is assumed to be at least three orders of magnitude higher than the concentration of Ox so that the reaction can be treated as a pseudo-first order following chemical reaction,[19] *i.e.*

$$Ox + ne^- \leftrightarrow Red \tag{7.3}$$

$$Red \xrightarrow{k_{apparent}} Ox \tag{7.4}$$

The rate of the reaction can be expressed as

$$rate = k_{apparent}[Red] \tag{7.5}$$

where the apparent rate constant $k_{apparent} = k_{catalytic}[Z]^n$ in L $mol^{-1}sec^{-1}$, and $k_{catalytic}$ is the rate constant for the catalytic reaction in sec^{-1}. The derivation of an equation that enables calculation of current at each applied potential begins with Fick's laws of diffusion.

Expressions for the concentrations of Ox and Red as a function of time and distance from the electrode are found using Laplace transformations following application of the boundary conditions. These expressions are related by the Nernst equation for a reversible electron transfer:

$$E_{applied} = E^0 + \left(\frac{RT}{nF}\right)\ln\left(\frac{C_{Ox}(0,t)}{C_{Red}(0,t)}\right) \tag{7.6}$$

where n = number of electrons transferred, F = Faraday constant, A = area of the electrode, R = gas constant, T = temperature in Kelvin, E = applied potential, E^0 = formal potential for the electron transfer reaction, D_{Ox} = diffusion coefficient of Ox (cm^2/sec), D_{Red} = diffusion coefficient of Red (cm^2/sec), C_{Ox} (0, t) = concentration of Ox at the electrode surface and any time t, and C_{Red} (0, t) = concentration of Red at the electrode surface and any time t. Numerical approximation of the resultant integral equations were performed in the same manner put forth by Nicholson and Olmstead.[29] The final equation used to compute theoretical voltammograms for the EC_{cat} mechanism is

$$\Psi_m = \frac{\frac{(\pi k_{apparent}\tau)^{1/2}}{(1+\varepsilon)} - \sum_{i=1}^{m-1}\Psi_i R_j}{R_1} \tag{7.7}$$

where τ = period in s, Ψ_m is the dimensionless current for each time increment with the serial number m, and

$$\varepsilon = \exp\left[\frac{nF}{RT}\left(E_{applied} - E^0\right)\right] \tag{7.8}$$

When the electron transfer step is kinetically controlled, the general reaction pathway for the electrocatalytic mechanism changes to

$$Ox + ne^- \underset{k_2}{\overset{k_1}{\leftrightarrow}} Red \tag{7.9}$$

$$\text{Red} \xrightarrow{k_{apparent}} \text{Ox} \tag{7.10}$$

where k_1 is the forward rate constant (cm/sec), k_2 is the reverse rate constant (cm/sec), and k^0 is rate constant for heterogeneous electron transfer (cm s^{-1}).

$$k_1 = k^0 \exp\left[\frac{-\alpha nF(E_{applied} - E^0)}{RT}\right] \tag{7.11}$$

$$k_2 = k^0 \exp\left[\frac{(1-\alpha)nF(E_{applied} - E^0)}{RT}\right] \tag{7.12}$$

The derivation of the equation used to compute theoretical voltammograms for this E_qC_{cat} mechanism followed similar lines as above except that the surface concentrations of Ox and Red are related by the Erdy-Gruz and Volmer equation for a quasi-reversible electron transfer [28, 30]:

$$i(t) = \frac{nFA}{D_{Ox}^{(1-\alpha)/2} D_{Red}^{\alpha/2}} k^0 \varepsilon^{-\alpha}\left[\sqrt{D_{Ox}} C_{Ox}(0,t) - \varepsilon\sqrt{D_{Red}} C_{Red}(0,t)\right] \tag{7.13}$$

where α = electron transfer coefficient. Based on this equation and the numerical approximation of Nicholson and Olmstead[29] the following final equation used to compute theoretical voltammograms is

$$\Psi_m = \frac{\sqrt{\pi} - \sqrt{\frac{1}{k_{apparent}\tau}}\sum_{i=1}^{m-1}\Psi_i R_j - \varepsilon\sqrt{\frac{1}{k_{apparent}\tau}}\sum_{i=1}^{m-1}\Psi_i R_j}{\frac{1}{\kappa\varepsilon^{-\alpha}\sqrt{\tau}} + \frac{1}{\sqrt{k_{apparent}\tau}} R_1 + \frac{\varepsilon}{\sqrt{k_{apparent}\tau}} R_1} \tag{7.14}$$

where

$$\kappa = \frac{k^0}{D_{Ox}^{(1-\alpha)/2} D_{Red}^{\alpha/2}} \tag{7.15}$$

7.2.2 Effect of $k_{apparent}$

The voltammetric features characteristic of a reversible reaction are: $E_{p,f} = E_{p,r} = E^0$, $\Delta E_p = 0$, $\Delta\Psi^+_{p,f} = \Delta\Psi^+_{p,r}$, $\Delta\Psi^+_{p,r} / \Delta\Psi^+_{p,f}$ = unity, $W_{1/2,f} = W_{1/2,r} = 126$ mV/n. In contrast, when the electron transfer reaction is coupled to a following irreversible reaction, i.e. an EC_{irrev} mechanism, the characteristic voltammetric features are $E_{p,f}$ and $E_{p,r}$ are shifted positively from E^0, $\Delta\Psi^+_{p,f} \geq \Delta\Psi^+_{p,r}$, and $\Delta\Psi^+_{p,r} / \Delta\Psi^+_{p,f} \leq$ unity. Figure 7.1a illustrates the effect of the rate of the catalytic reaction following electron transfer on the shape of the voltammogram. Regardless of the magnitude of $k_{apparent}$, peak potentials remain at E^0, $\Delta E_p = 0$ mV and peak widths ~ 126 mV. While peak currents depend upon the rate of the catalytic reaction, peak ratios are equal to unity and independent of $k_{apparent}$. Thus, when compared to the voltammogram for a reversible reaction, the presence of the following catalytic reaction impacts the magnitude of $\Delta\Psi^+_{p,f}$ and $\Delta\Psi^+_{p,r}$. When compared to the voltammogram for an EC_{irrev} reaction, the peak ratio being equal to unity is the major distinguishing feature.

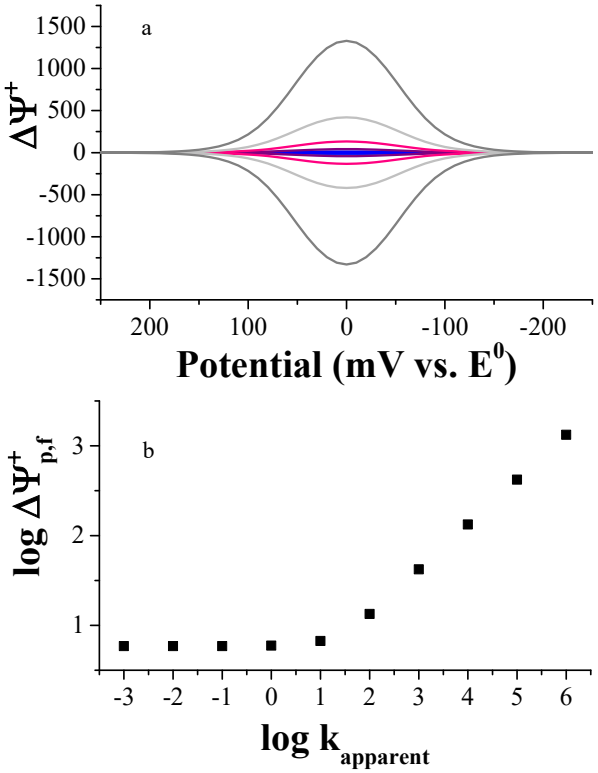

Figure 7.1. Panel a: The effect of $k_{apparent}$ on the shape of the voltammogram when period = 50 ms, amplitude = 50 mV, increment = 10 mV, and log $k_{apparent}$ = -3 (red) to 6 (dark gray) in decades. Panel b: log $\Delta\Psi^{+}_{p,f}$ vs. log $k_{apparent}$.

Figure 7.1b presents a correlation of $\Delta\Psi^{+}_{p,f}$ with $k_{apparent}$ under a fixed set of empirical parameters (τ = 50 ms, δE = 10 mV, and E_{SW} = 50 mV). For log $k_{apparent} \leq 0$, $\Delta\Psi^{+}_{p,f}$ is equivalent to the value observed for the reversible mechanism. For log $k_{apparent} > 0$, $\Delta\Psi^{+}_{p,f}$ increases exponentially. An identical trend is observed for $\Delta\Psi^{+}_{p,r}$. Thus, the experimenter has but two choices in distinguishing the catalytic reaction from the reversible reaction: by comparing voltammograms acquired in the presence and absence of Z and/or by comparing currents at the end of the individual potential pulses.[23-28, 31-35] Discriminating between these two mechanisms by the latter comparison is illustrated in Figure 7.2. As $k_{apparent}$ increases, the currents at the end of each pulse plotted versus step

potential transition into a superimposable sigmoidal wave. The sigmoidal wave shape is characteristic for a catalytic electrode reaction.[11, 19, 20, 36]

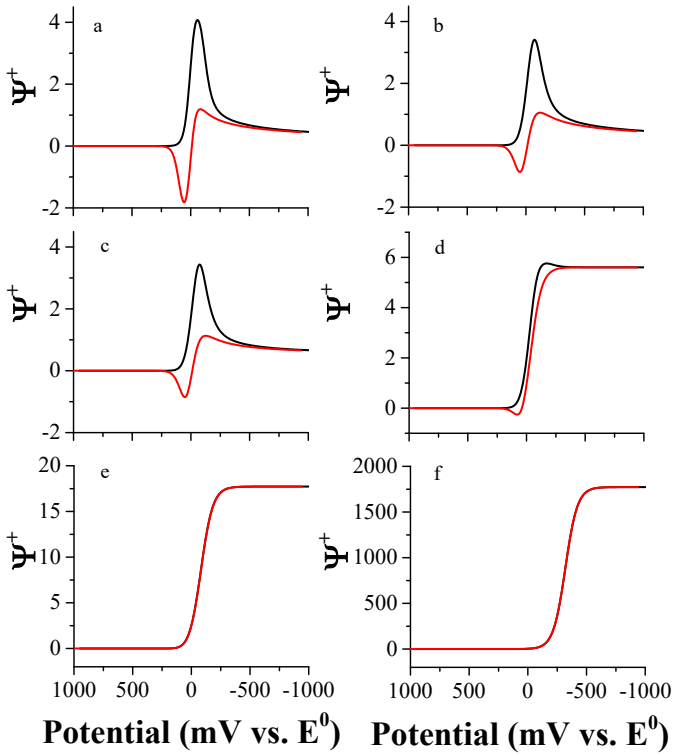

Figure 7.2. The effect of $k_{apparent}$ on the individual currents on the forward sweep. Black trace denotes the current at the end of the cathodic potential pulse; red trace denotes the current at the end of the anodic potential pulse when amplitude = 50 mV, increment = 10 mV, and period = 50 ms. Panel a presents the individual pulse voltammograms for a reversible mechanism. Panel b through f presents the corresponding voltammogram when log $k_{apparent}$ = -3, -1, 1, 2, 6, respectively.

7.2.3 Effect of Period (τ)

In SWV and CSWV, the effective potential sweep rate is increment divided by period. Thus, increasing period is equivalent to decreasing the potential sweep rate and consequently, increasing the time window for the catalytic reaction to occur. The effect of period on the voltammogram for the EC_{cat} mechanism is shown in Figure 7.3a for log $k_{apparent}$ = 2. As period is varied, E_p, ΔE_p, and $W_{1/2}$ are unaffected; $E_{p,f} = E_{p,r} = E^0$, $\Delta E_p = 0$

mV, and peak widths are ~ 126 mV/n. The peak currents diminish with increasing period while the peak ratio is constant and equal to unity. Figure 7.3b presents the dependence of $\Delta\Psi_p^+$ on both period and $k_{apparent}$. When log $k_{apparent} \geq 4$, $\Delta\Psi_p^+$ is invariant with period.

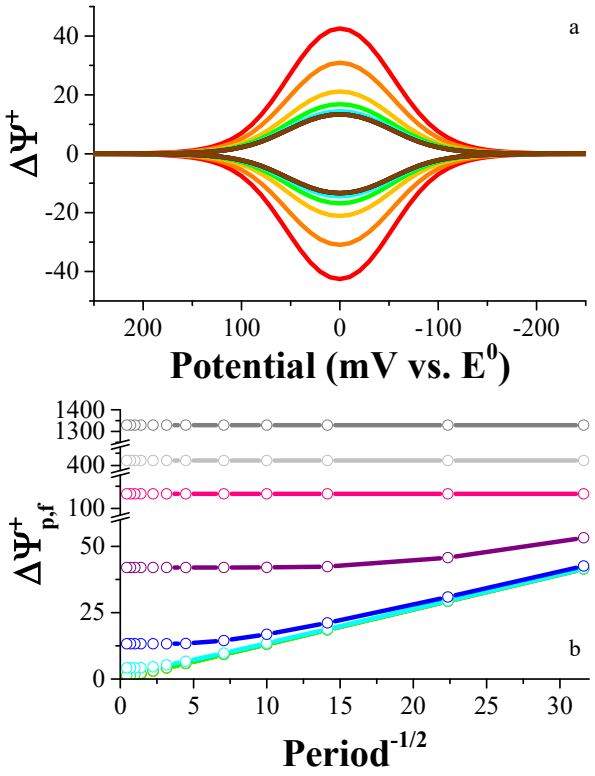

Figure 7.3. Panel a: The effect of period on the shape of the voltammogram when amplitude = 50 mV, increment = 10 mV, log $k_{apparent}$ = 2, and period = 1 ms (red), 2 ms (orange), 5 ms, 10 ms, 20 ms, 50 ms, 100 ms, 200 ms, 500 ms, 1 s, 2 s, and 5 s (dark gray). Panel b: The effect of $k_{apparent}$ on the relationship between $\Delta\Psi_p^+$ and period$^{-1/2}$ and log $k_{apparent}$ = -3 (red) to 6 (dark gray) in decades.

When 1 < log $k_{apparent}$ < 4, $\Delta\Psi_p^+$ is linear with period$^{-1/2}$ at short periods and invariant at long periods. $\Delta\Psi_p^+$ becomes invariant with period when the shape of the forward and reverse pulse voltammograms is sigmoidal (see Figure 7.2). For comparison, $\Delta\Psi_p^+$ is linearly related to period$^{-1/2}$ for reversible electrode reactions. Thus, Figure 7.3b

illustrates how systematic variation in period provides a second way to distinguish the EC_{cat} from the reversible mechanism.

The trends associated with systematic variation of period for the EC_{irrev} mechanism are: both $E_{p,f}$ and $E_{p,r}$ shift positively with period. $\Delta\Psi^{+}_{p,f}$ is linear with period$^{-1/2}$ and $\Delta\Psi^{+}_{p,r}$ is curvilinear with period$^{-1/2}$ and peak ratio decreases with period. Hence, variation of period can be used to discern between EC_{cat} and EC_{irrev} mechanisms.

7.2.4 Effect of Increment (δE)

Figure 7.4 shows the effect of increment on the voltammogram for the EC_{cat} mechanism. As increment is increased, E_p remains at E^0, and $\Delta E_p = 0$ mV. $\Delta\Psi^{+}_{p}$ is constant with increment though the magnitude is dependent upon $k_{apparent}$. Peak ratio remains constant at unity with the variation of increment. $W_{1/2}$ increases with increment but by no more than 5 mV, which is within the error of the increment values used in the simulation.

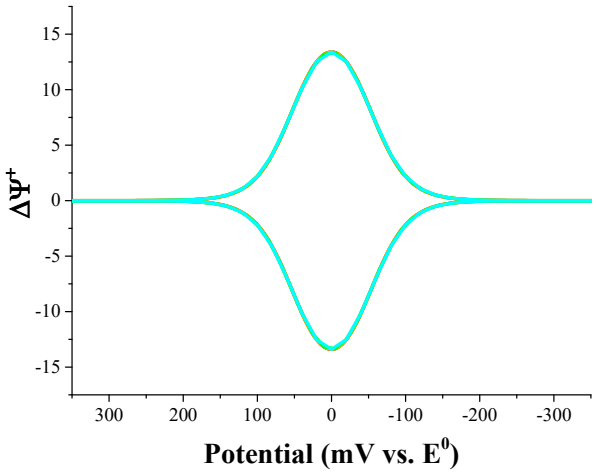

Figure 7.4. The effect of increment on the shape of the voltammogram when period = 50 ms, amplitude = 50 mV, log $k_{apparent}$ = 2, and increment = 1 (red), 5 (orange), 10 (yellow), 15 (green), and 20 mV (cyan).

Unfortunately, increment cannot be used to discern between the EC_{cat} and the reversible mechanism as peak parameter trends for two mechanisms are the same. However, increment can be used to discriminate between the EC_{cat} and EC_{irrev} cases. Peak potentials remain at E^0 for the EC_{cat} mechanism while peak potentials shift negatively toward E^0 for the EC_{irrev} case. $\Delta E_p = 0$ mV for the EC_{cat} mechanism while ΔE_p decreases with increment for the EC_{irrev} mechanism. $\Delta\Psi_p^+$ is invariant with increment for the EC_{cat} mechanism while $\Delta\Psi_p^+$ increases with increment for the EC_{irrev} case. Thus, variation of increment can be used to differentiate between the EC_{cat} and EC_{irrev} mechanisms.

7.2.5 Effect of Switching Potential (E_λ)

Switching potential has little effect on the voltammogram for an EC_{cat} mechanism as shown in Figure 7.5. Again, E_p remains at E^0, and $\Delta E_p = 0$ mV as switching potential approaches the formal potential. $W_{1/2}$ is invariant with switching potential. $\Delta\Psi_p^+$ is constant with switching potential though the magnitude of $\Delta\Psi_p^+$ depends upon $k_{apparent}$. Switching potential cannot be used to distinguish between the EC_{cat} and reversible mechanisms as the trends for peak parameters with E_λ are the same.

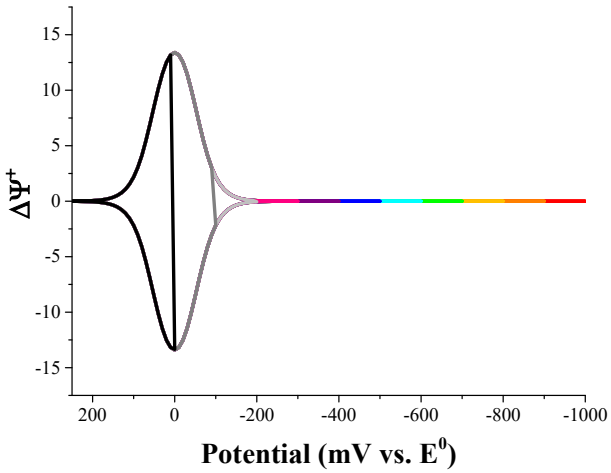

Figure 7.5. The effect of switching potential on the shape of the voltammogram when period = 50 ms, amplitude = 50 mV, increment = 10 mV, and the switching potential is moved from 1000 to 0 mV past E^0.

Several differences in the effect of switching potential on the voltammogram for the EC_{cat} and EC_{irrev} mechanisms can be noted. For both mechanisms, $\Delta\Psi^+_{p,f}$, $E_{p,f}$, and $E_{p,r}$ are unaffected by switching potential. ΔE_p is also invariant of switching potential for both mechanisms. However, $\Delta\Psi^+_{p,r}$ is unaffected by switching potential for the EC_{cat} case whereas it increases in magnitude as the switching potential approaches E^0 for the EC_{irrev} case. Peak ratio remains constant at unity for the EC_{cat} case whereas peak ratio decreases the switching potential goes further negative of E^0. Thus, by inspection of $\Delta\Psi^+_{p,r}$ and peak ratio, differences in the EC_{cat} and the EC_{irrev} mechanism can be used to discern these mechanisms.

7.2.6 Effect of Amplitude (E_{SW})

The effect of amplitude on the voltammogram for the EC_{cat} mechanism is shown in Figure 7.6. As with other empirical parameters, when amplitude is increased, E_p remains at E^0, and $\Delta E_p = 0$ mV. $\Delta\Psi^+_p$ increases with amplitude though the magnitude and extent

of the increase depend upon $k_{apparent}$. Peak ratio is independent of amplitude and remains at unity. $W_{1/2}$ increases from 94 to 188 mV as amplitude is increased from 10 to 90 mV for all values of $k_{apparent}$. Amplitude cannot be used to discern between the EC_{cat} mechanism and the reversible mechanism as trends in peak parameters for each mechanism are identical.

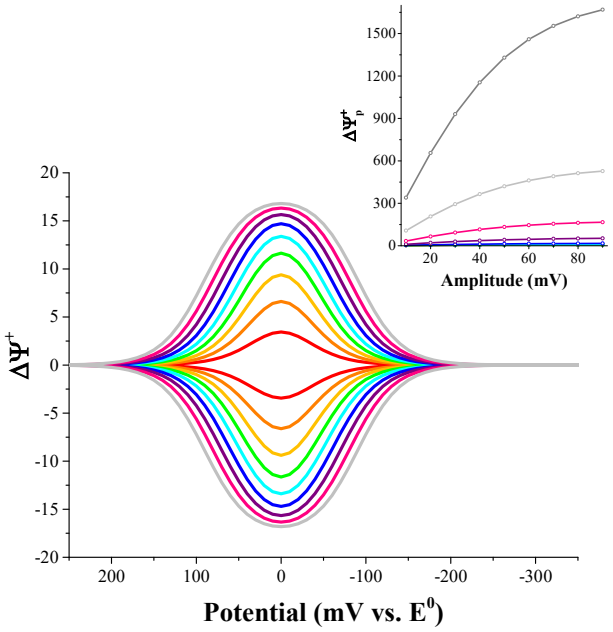

Figure 7.6. The effect of amplitude on the shape of the voltammogram when period = 50 ms, increment = 10 mV, log $k_{apparent}$ = 2, and amplitude = 10 to 90 mV in 10 mV steps. Inset: The effect of $k_{apparent}$ on the relationship between $\Delta\Psi^+_p$ and amplitude.

Differences in effect of amplitude on the voltammograms enable discrimination between the EC_{cat} and EC_{irrev} mechanisms. E_p remains at E^0 for the EC_{cat} case but shifts positively with amplitude for the EC_{irrev} case. $\Delta E_p = 0$ mV for all amplitudes in the EC_{cat} case but $\Delta E_p > 0$ mV for the EC_{irrev} case. $\Delta\Psi^+_{p,f}$ and $\Delta\Psi^+_{p,r}$ increase equally with amplitude for the EC_{cat} case; however, $\Delta\Psi^+_{p,f}$ increases more than $\Delta\Psi^+_{p,r}$ with amplitude for the EC_{irrev} case. Peak ratio remains constant at unity for the EC_{cat} case. However,

peak ratio ≤ 1 and increases with amplitude for the EC_{irrev} case. Thus, the variation of amplitude can lead to discerning between the EC_{cat} and EC_{irrev} mechanisms.

7.2.7 Effect of Heterogeneous Kinetics (k^0)

The impact of heterogeneous kinetics on the shape of the voltammogram depends upon the magnitude of k^0 relative to τ. Previous investigators have treated the effects of SWV frequency and k^0 (or period and k^0) as a single dimensionless kinetic parameter.[23, 28, 37] The work within this thesis deliberately treats these quantities individually to assist non-specialists in interpreting the voltammetric trends and assigning the proper mechanism. In practice, one varies τ and determines k^0 from changes in the shape of the voltammograms. The kinetic parameter k^0 is intrinsic to the analyte undergoing an electron transfer reaction at a particular electrode immersed in a specific electrolyte. It cannot be experimentally varied without changing the electrode and/or electrolyte. Theoretically, varying k^0 at a fixed value of τ enables one to assess its impact on the shape of the voltammogram.

The effect of k^0 on the E_qC_{cat} mechanism is shown in Figure 7.7. When the rate of the catalytic reaction is slow (e.g. Figure 7.7a), the voltammogram is identical to the quasireversible mechanism. At $\log k^0 \geq -2$, the voltammogram is identical to that obtained for a reversible process. At $\log k^0 < -2$, $E_{p,f}$ shifts negatively from E^0, $E_{p,r}$ shifts positively from E^0, and thus the peak separation increases. Similarly, $\Delta\Psi_p^+$ decreases and then levels off with decreasing k^0. The symmetry in peak potential shifts and peak current diminution is a function of alpha. The reader is referred to Chapter 3 and a previous report on the quasireversible mechanism for further details.[38]

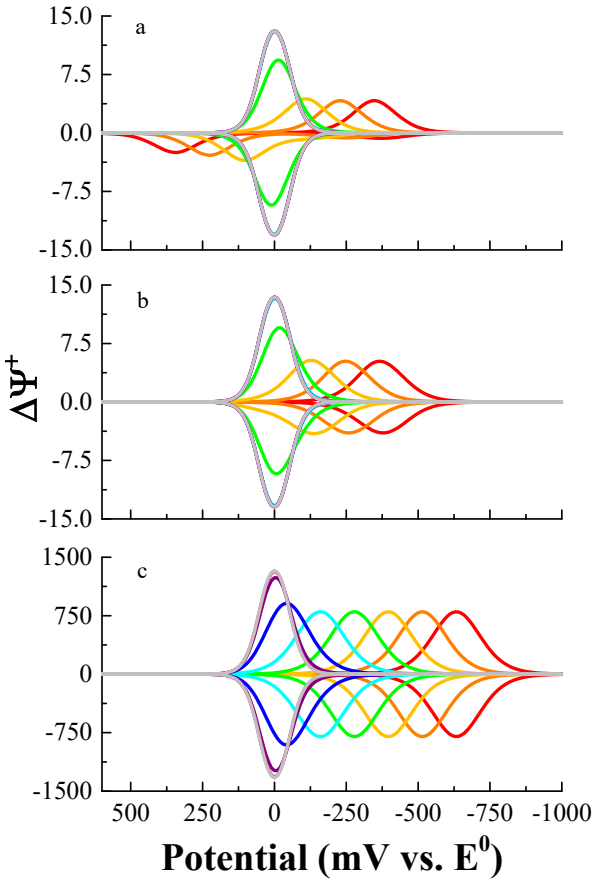

Figure 7.7. The effect of log k^0 on the shape of the voltammogram when period = 50 ms, amplitude = 50 mV, increment = 10 mV, log $k_{apprent}$ = -3 (panel a), 1 (panel b), and 6 (panel c) and log k^0 varies from -6 (red) to 2 (light gray) in steps of 1.

At intermediate rates of the catalytic reaction (Figure 7.7b) and at log $k^0 \geq -2$, the voltammogram is identical to that obtained for a reversible process. At log $k^0 < -2$, $E_{p,f}$ and $E_{p,r}$ shift negatively from E^0 while $\Delta\Psi_p^+$ decreases and then levels off with decreasing k^0. Similar trends exist at fast rates of the catalytic reaction (Figure 7.7c) except that shift in peak potentials commence at log $k^0 < 0$ and shift negatively by 120 mV per decade in k^0. $\Delta\Psi_p^+$ is proportional to log $k_{apparent}$ (see Figure 7.8) but remains constant at log $k^0 < 0$.

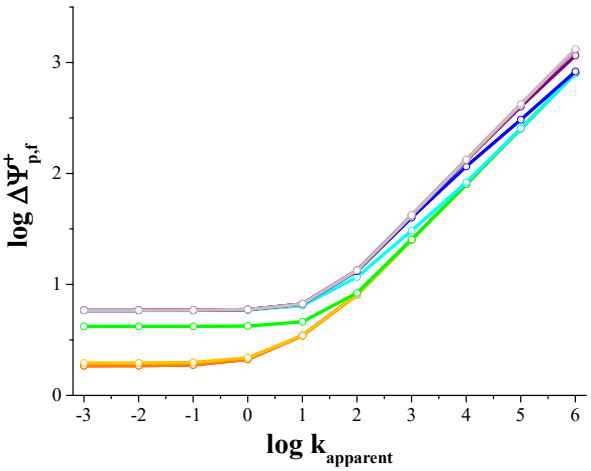

Figure 7.8. Plot of log $\Delta\Psi^+_{p,f}$ versus log $k_{apparent}$ as log k^0 varies from -6 (red) to 2 (light gray) in decades when period = 50 ms, amplitude = 50 mV, and increment = 10 mV.

The effect of increment, switching potential and amplitude on the shape of the voltammogram for kinetically-controlled electron transfers essentially mirrors that described above when the rate of the electron transfer step is fast. However, systematic variation in period provides a straightforward means for distinguishing between the two mechanisms and measurement of k^0.

The effect of period on peak currents for the E_qC_{cat} mechanism is shown in Figure 7.9. The trends are qualitatively similar to that shown in Figure 7.3b. $\Delta\Psi_p^+$ decreases linearly with period$^{-1/2}$ for log $k_{apparent} \leq 0$. When $0 <$ log $k_{apparent} \leq 3$, $\Delta\Psi_p^+$ is linearly related to period$^{-1/2}$ at short times and invariant with period$^{-1/2}$ at long times. When log $k_{apparent} > 3$, $\Delta\Psi_p^+$ is independent of period. Over the entire range in log $k_{apparent}$, $\Delta\Psi_p^+$ is proportional to log k^0 as shown in Figures 7.7 and 7.9. Peak ratio is unity and invariant with both period over the entire range in $k_{apparent}$.

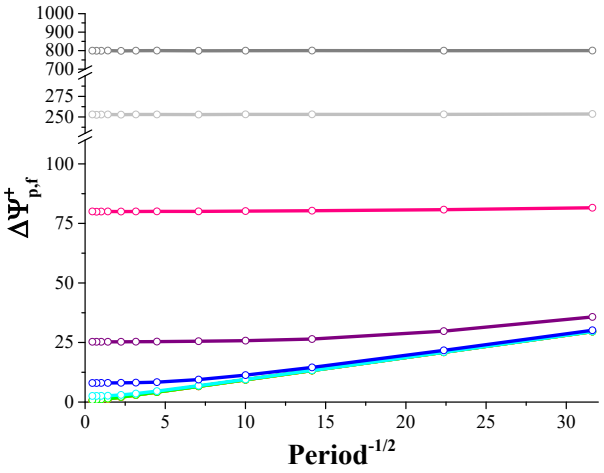

Figure 7.9. The effect of $k_{apparent}$ on the relationship between $\Delta\Psi^{+}_{p}$ and period$^{-1/2}$ when amplitude = 50 mV, increment = 10 mV, log k^0 = -3, and log $k_{apparent}$ = -3 (red) to 6 (dark gray) in decades.

The effect of period on peak potentials is a distinguishing feature between the EC_{cat} and E_qC_{cat} mechanisms. In the former case, peak potentials are independent of period. In the latter case, E_p is independent of period only when log $k_{apparent} \leq -2$. When $-2 <$ log $k_{apparent} \leq 2$, $E_{p,f}$ and $E_{p,r}$ shift negatively in a curvilinear fashion with log period (see Figure 7.10). When log $k_{apparent} > 2$, $E_{p,f}$ and $E_{p,r}$ shift negatively and linearly with log period. Consequently, ΔE_p decreases with log period for $-1 \leq$ log $k_{apparent} < 2$; otherwise, ΔE_p is constant at 25 mV or 0 mV for log $k_{apparent} < -1$ and ≥ 2, respectively (see Figure 7.10c).

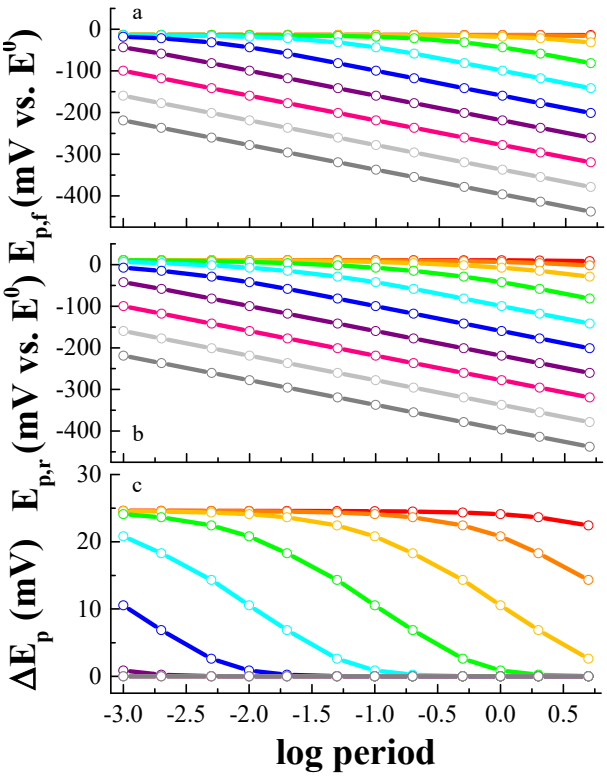

Figure 7.10. The effect of $k_{apparent}$ on the relationship between peak potential and period when amplitude = 50 mV, increment = 10 mV, log k^0 = -3, and log $k_{apparent}$ = -3 (red) to 6 (dark gray) in decades.

Several comparisons between the E_qC_{cat} mechanism and the E_{quasi} mechanism[38] can be made. The relationship between $\Delta\Psi_p^+$ and period$^{-1/2}$ depends on $k_{apparent}$ for the E_qC_{cat} mechanism whereas $\Delta\Psi_p^+$ is always linear with period$^{-1/2}$ for the E_{quasi} mechanism. Peak ratio is invariant at unity with period for log $k^0 \geq -3$ for the E_qC_{cat} mechanism whereas peak ratio increases with period for the E_{quasi} case. Both peak potentials shift negatively with period (in a manner dependent on $k_{apparent}$) for the E_qC_{cat} case whereas both peak potentials shift toward E^0 for the E_{quasi} case. ΔE_p decreases for both mechanisms though the values for E_qC_{cat} tend to be smaller for those obtained for E_{quasi}.

E_qC_{cat} and EC_{cat} have similar trends in $\Delta\Psi_p^+$ as a function of period though the magnitude of $\Delta\Psi_p^+$ is smaller for the E_qC_{cat} case. Peak ratio is invariant at unity with period for both cases so long as $\log k^0 \geq -3$ for the E_qC_{cat} mechanism. Peak potentials shift negatively with log period for the E_qC_{cat} case but remain at E^0 for the EC_{cat} case. Furthermore, dependent on $\log k_{apparent}$, ΔE_p may change for E_qC_{cat} whereas ΔE_p is always 0 for the EC_{cat} case. Thus, the variation of period and its effect on peak parameters provides insight into identifying the E_qC_{cat} mechanism. The effects of the various parameters on the peaks for the EC_{cat} and E_qC_{cat} mechanisms are summarized in Tables 7.1 and 7.2.

7.3 Conclusion

In this work, the effect of variation of empirical parameters on the shape and magnitude of voltammograms using CSWV was completed for the EC_{cat} mechanism. Trends in the peak parameters were identified and experimentally verified. Furthermore, trends in peak parameters for the EC_{cat} case were compared to that of the EC_{irrev} case. Unfortunately, all trends in empirical parameters for the EC_{cat} mechanism are identical to the reversible mechanism except when $\log k_{apparent}$ is sufficiently large or the individual currents are analyzed. When the electron transfer step is kinetically controlled, the presence of a chemical reaction following the electron transfer that catalytically regenerates Ox is identified by analyzing peak potential shifts as a function of period. While CSWV has limited value in the characterization of an EC_{cat} mechanism, it is incredibly useful in identifying for chemically coupled mechanisms, e.g. EC, CE, and ECE mechanisms, and quantifying rates of reaction.[39-41]

Table 7.1. Diagnostic Plots and Protocol for Assessing an EC_{cat} Electrode Reaction by CSWV

	Empirical variables							
Waveform parameters	***Period, τ***		***Increment, δE***		***Switching potential, E_λ***		***Amplitude, E_{SW}***	
	Plot	**Trend**	**Plot**	**Trend**	**Plot**	**Trend**	**Plot**	**Trend**
Peak currents	ΔI_p vs. $(period)^{-1/2}$	ΔI_p is dependent on log $k_{apparent}$** (see Figure 7.3)	ΔI_p vs. δE	Independent of δE	ΔI_p vs. E_λ	Independent of E_λ	ΔI_p vs. E_{SW}	ΔI_p increases with E_{SW}
Peak ratio	Peak ratio vs. log period	Unity for all periods	Peak ratio vs. δE	Unity for all δE	Peak ratio vs. E_λ	Unity for all E_λ	Peak ratio vs. E_{SW}	Unity for all E_{SW}
Peak potentials	E_p vs. log period	Independent of period; remains at E^0	E_p vs. δE	Independent of δE; remains at E^0	E_p vs. E_λ	Independent of E_λ; remains at E^0	E_p vs. E_{SW}	Independent of E_{SW}; remains at E^0
Peak separation	ΔE_p vs. log period	Independent of period; $\Delta E_p = 0$	ΔE_p vs. δE	Independent of δE; $\Delta E_p = 0$	ΔE_p vs. E_λ	Independent of E_λ; $\Delta E_p = 0$	ΔE_p vs. E_{SW}	Independent of E_{SW}; $\Delta E_p = 0$
Peak widths	$W_{1/2}$ vs. log period	Independent of period	$W_{1/2}$ vs. δE	Independent of δE	$W_{1/2}$ vs. E_λ	Independent of E_λ	$W_{1/2}$ vs. E_{SW}	$W_{1/2}$ increases with E_{SW}

** When $\log k_{apparent} \leq -1$, ΔI_p is linear with $period^{-1/2}$. When $-1 < \log k_{apparent} < 4$, ΔI_p is linear with $period^{-1/2}$ at short periods and invariant at long periods. When $\log k_{apparent} \geq 4$, ΔI_p is independent of period.

Table 7.2. Diagnostic Plots and Protocol for Assessing an E_qC_{cat} Electrode Reaction by CSWV

	Empirical variables							
Waveform parameters	***Period, τ***		***Increment, δE***		***Switching potential, E_λ***		***Amplitude, E_{SW}***	
	Plot	**Trend**	**Plot**	**Trend**	**Plot**	**Trend**	**Plot**	**Trend**
Peak currents	ΔI_p vs. $(\text{period})^{-1/2}$	ΔI_p is dependent on log $k_{apparent}$** (see Figure 7.9)	ΔI_p vs. δE	Slight increase with δE for log $k_{apparent} \leq 0$ and invariant otherwise; magnitude depends on $k_{apparent}$	ΔI_p vs. E_λ	Independent of E_λ; magnitude depends on log $k_{apparent}$	ΔI_p vs. E_{SW}	ΔI_p increases with E_{SW}; magnitude depends on log $k_{apparent}$
Peak ratio	Peak ratio vs. log period	Unity for all periods	Peak ratio vs. δE	Unity for all δE	Peak ratio vs. E_λ	Unity for all E_λ	Peak ratio vs. E_{SW}	Unity for all E_{SW}
Peak potentials	E_p vs. log period	Invariant when log $k_{apparent} \leq -2$ and shifts negatively with period when log $k_{apparent} > -2$; magnitude of shift and displacement from E^0 depends on log $k_{apparent}$ (see Figure 7.10)	E_p vs. δE	$E_{p,f}$ shifts negatively while $E_{p,r}$ shifts slightly positive with δE for log $k_{apparent} \leq 0$; both are invariant with δE for log $k_{apparent} \geq 1$. Displacement from E^0 for both depends on $k_{apparent}$	E_p vs. E_λ	$E_{p,f}$ is independent of E_λ while $E_{p,r}$ shifts slightly negative for log $k_{apparent} \leq 0$; displacement from E^0 depends on $k_{apparent}$	E_p vs. E_{SW}	$E_{p,f}$ shifts slightly positive and $E_{p,r}$ shifts slightly negative for log $k_{apparent} \leq 0$; both are independent of E_{SW} for log $k_{apparent} \geq 1$. Displacement from E^0 depends on $k_{apparent}$
Peak separation	ΔE_p vs. log period	Decreases with period for $-1 \leq$ log $k_{apparent} \leq 1$ and invariant otherwise; magnitude depends on $k_{apparent}$ (see Figure 7.10)	ΔE_p vs. δE	Increases negatively with δE for log $k_{apparent} \leq 0$; independent of δE and zero for log $k_{apparent} \geq 1$	ΔE_p vs. E_λ	Decreases with E_λ and negative for log $k_{apparent} \leq 0$; independent and zero for log $k_{apparent} \geq 1$	ΔE_p vs. E_{SW}	Slight decrease with E_{SW} and negative for log $k_{apparent} \leq 0$; independent of E_{SW} and zero for log $k_{apparent} \geq 1$
Peak widths	$W_{1/2}$ vs. log period	Increases with period for $-1 \leq$ log $k_{apparent} \leq 3$ and independent otherwise; magnitude depends on $k_{apparent}$	$W_{1/2}$ vs. δE	Increases with δE for log $k_{apparent} \leq 0$ and invariant otherwise; magnitude depends on log $k_{apparent}$	$W_{1/2}$ vs. E_λ	Independent of E_λ; magnitude depends on $k_{apparent}$	$W_{1/2}$ vs. E_{SW}	$W_{1/2}$ increases with E_{SW}; magnitude depends on $k_{apparent}$

** When log $k_{apparent} \leq 0$, ΔI_p is linear with $\text{period}^{-1/2}$. When $0 <$ log $k_{apparent} \leq 3$, ΔI_p is linear with $\text{period}^{-1/2}$ at short periods and invariant at long periods. When log $k_{apparent} > 3$, ΔI_p is independent of period. The magnitude of ΔI_p depends on $k_{apparent}$.

7.4 References

1. Koper, M.T.M. *Faraday Discuss.*, **2009**. 140, 11-24.

2. Rountree, E.S., B.D. McCarthy, T.T. Eisenhart, and J.L. Dempsey. *Inorg. Chem.*, **2014**. 53, 9983-10002.

3. Kortlever, R., J. Shen, K.J.P. Schouten, F. Calle-Vallejo, and M.T.M. Koper. *J. Phys. Chem. Lett.*, **2015**. 6, 4073-4082.

4. Jaksic, J.M., F. Nan, G.D. Papakonstantinou, G.A. Botton, and M.M. Jaksic. *J. Phys. Chem. C*, **2015**. 119, 11267-11285.

5. Saveant, J.-M. *Chem. Rev.*, **2008**. 108, 2348–2378.

6. Mirceski, V., F. Quentel, M. L'Her, and C. Elleouet. *J. Phys. Chem. C*, **2007**. 111, 8283-8290.

7. Taube, H., *Electron Transfer Reactions of Complex Ions in Solution*. **1970**, Academic Press: New York.

8. Bard, A.J. *J. Am. Chem. Soc.*, **2010**. 132, 7559–7567.

9. Smith, D.E. *Anal. Chem.*, **1963**. 35, 602-609.

10. Smith, D.E. *Anal. Chem.*, **1963**. 35, 610-614.

11. Nicholson, R.S. and I. Shain. *Anal. Chem.*, **1964**. 36, 706-723.

12. Saveant, J.M. and E. Vianello. *Electrochim. Acta*, **1965**. 10, 905-920.

13. Polcyn, D.S. and I. Shain. *Anal. Chem.*, **1966**. 38, 376-382.

14. Kim, M.H. and R.L. Birke. *Anal. Chem.*, **1983**. 55, 522-527.

15. Compton, R.G., M.J. Day, M.E. Laing, R.J. Northing, J.I. Penman, and A.M. Waller. *J. Chem. Soc., Faraday Trans. 1*, **1988**. 84, 2013-2025.

16. Molina, A., C. Serna, and J. Gonzalez. *J. Electroanal. Chem.*, **1998**. 454, 15-31.

17. Serna, C., A. Molina, F. Martinez-Ortiz, and J. Gonzalez. *J. Electroanal. Chem.*, **1999**. 468, 158-169.

18. Molina, A. and I. Morales. *J. Electroanal. Chem.*, **2005**. 583, 193-202.

19. Feldberg, S.E. and J.E. Campbell. *Anal. Chem.*, **2009**. 81, 8797-8800.

20. Molina, A., J. Gonzalez, E. Laborda, Y. Wang, and R.G. Compton. *Phys. Chem. Chem. Phys.*, **2011**. 13, 14694-14704.

21. Pasti, I.A., N.M. Gavrilov, and S.V. Mentus, *Voltammetric techniques in electrocatalytic studies*, *Voltammetry: Theory, Types and Applications*. **2014**, Nova Science Publishers, Inc.: Hauppauge, NY. 1-42

22. Costentin, C. and J.-M. Saveant. *J. Phys. Chem. C*, **2015**. 119, 12174-12182.

23. Zeng, J. and R.A. Osteryoung. *Anal. Chem.*, **1986**. 58, 2766-2771.

24. Molina, A., C. Serna, and F. Martinez-Ortiz. *J. Electroanal. Chem.*, **2000**. 486, 9-15.

25. Mirceski, V., A. Bobrowski, J. Zarebski, and F. Spasovski. *Electrochim. Acta*, **2010**. 55, 8696-8703.

26. Molina, A., J. Gonzalez, E. Laborda, Y.-J. Wang, and R.G. Compton. *Phys. Chem. Chem. Phys.*, **2011**. 13, 16748-16755.

27. Gulaboski, R. and V. Mirceski. *Electrochim. Acta*, **2015**. 167, 219-225.

28. O'Dea, J.J., J. Osteryoung, and R.A. Osteryoung. *Anal. Chem.*, **1981**. 53, 695-701.

29. Nicholson, R.S. and M.L. Olmstead, *Electrochemistry: Calculations, Simulation and Instrumentation,*. **1972**, Marcel Dekker: New York. Ch. 5

30. Erdey-Gruz, T., *Kinetics of Electrode Processes*. **1972**, Wiley-Interscience Division: New York.

31. Mirčeski, V. and R. Gulaboski. *Electroanalysis*, **2001**. 13, 1326-1334.

32. Mirčeski, V. and R. Gulaboski. *J. Solid State Electrochem.*, **2003**. 7, 157-165.

33. Mirceski, V. and F. Quentel. *J. Electroanal. Chem.*, **2005**. 578, 25-35.

34. Gulaboski, R. and L. Mihajlov. *Biophys. Chem.*, **2011**. 155, 1-9.

35. Gonzalez, J., A. Molina, F. Martinez Ortiz, and E. Laborda. *J. Phys. Chem. C*, **2012**. 116, 11206−11215.

36. Soto, C.M., A. Molina, and J. Gonzalez. *Electroanalysis*, **2010**. 22, 106-112.

37. Mirčeski, V., Š. Komorsky-Lovrić, and M. Lovrić, *Square Wave Voltammetry: Theory and Application*, *Monographs in Electrochemistry*. **2007**, Springer-Verlag: Berlin.

38. Mann, M.A., J.C. Helfrick, Jr., and L.A. Bottomley. *Anal. Chem.*, **2014**. 86, 8183-8191.

39. Helfrick, J.C., Jr., M.A. Mann, and L.A. Bottomley. *ChemPhysChem*, **2015**. submitted.

40. Helfrick, J.C., Jr., M.A. Mann, and L.A. Bottomley. *Electrochim. Acta*, **2015.** submitted for publication.

41. Mann, M.A., J. Helfrick, J. C., and L.A. Bottomley. *J. Electrochem. Soc.*, **2015**. 163, H3101-H3109.

CHAPTER 8

THE ECE MECHANISM

Reproduced from *J. Electrochem. Soc.* 2016, 163(4), H3101-H3109.

8.1 Introduction

The ECE mechanism has been the subject of considerable interest by electrochemists over the past five decades.[1-13] The continuing interest reflects: (1) the challenge in mathematically modeling the complex electrode reaction sequence involving two sequential heterogeneous electron transfer reactions coupled by a homogeneous kinetically-controlled chemical reaction(s) that may or may not involve homogeneous electron transfer, and (2) the advent of new electrochemical techniques to identify short lived intermediates and quantify reaction rates.[14-19] The primary motivation educes from the fact that this mechanism is quite common in organic electrochemistry.[20-22] Hence, there is a need for an electrochemical technique which provides experimenters with an efficient and straightforward means to identify an ECE mechanism. This chapter investigates the effect of empirical parameters on the peak parameters for the ECE mechanism. From this investigation, the diagnostic criteria for an ECE mechanism are presented as well as a protocol for experimentalists to identify the ECE mechanism and determine the rate of the chemical reaction.

8.2 Results and Discussion

8.2.1 Theory

The generalized ECE electrode reaction sequence is:

$$Ox_1 + n_1e^- \leftrightarrow Red_1$$
$$Red_1 \xrightarrow{k_f} Ox_2$$
$$Ox_2 + n_2e^- \leftrightarrow Red_2$$

where E_1^0 is the formal potential for reduction of Ox_1 and E_2^0 is the formal potential for the reduction of Ox_2. For simplicity, $E_1^0 = 0$ and all other potential values are referenced to it. This work only considers the situation where $E_2^0 \leq E_1^0$ and denotes the difference in formal potentials as $\Delta E^0 = E_1^0 - E_2^0$. This restriction enables discussion of the mechanism without considering the complication of homogeneous electron transfer (disproportionation[4-7, 9, 23, 24]) reaction, i.e. $Ox_1 + Red_2 \rightleftarrows Red_1 + Ox_2$.

Derivation of an equation for predicting current as a function of potential and time began by solving Fick's laws of diffusion using Laplace transformations following application of appropriate boundary conditions for each case. Expressions for the concentrations of Ox_1, Red_1, Ox_2, and Red_2 are related by the Nernst equation for a reversible electron transfer for each redox pair:

$$E_{applied} = E_1^0 + \frac{RT}{nF}\ln\frac{C_{Ox_1}(0,t)}{C_{Red_1}(0,t)} \tag{8.1}$$

$$E_{applied} = E_2^0 + \frac{RT}{nF}\ln\frac{C_{Ox_2}(0,t)}{C_{Red_2}(0,t)} \tag{8.2}$$

where n = number of electrons transferred, F = Faraday constant, A = area of the electrode, R = gas constant, T = temperature in Kelvin, $E_{applied}$ = applied potential, E^0 = formal potential for the designated electron transfer reaction, $C_{Ox1}(x, t)$, $C_{Ox2}(x, t)$, $C_{Red1}(x, t)$, $C_{Red2}(x, t)$ are concentrations of Ox_1, Ox_2, Red_1, and Red_2, respectively at the electrode surface and any time t. Numerical approximation of the resultant integral equations were performed in the same manner put forth by Nicholson and Olmstead.[25] The final equations used to compute theoretical voltammograms are:

$$\Psi_{m1} = \frac{\pi\left(\frac{L}{2}\right)^{1/2} - \sum_{i=1}^{i=m-1}\Psi_{i1}S_j - \varepsilon_1\left(\frac{\pi L}{2k_f\tau}\right)^{1/2}\sum_{i=1}^{i=m-1}\Psi_{i1}R_j}{S_1 + R_1\varepsilon_1\left(\frac{\pi L}{2k_f\tau}\right)^{1/2}} \tag{8.3}$$

$$\Psi_{m2} = \frac{\sum_{i=1}^{i=m}\Psi_{i1}S_j - \sum_{i=1}^{i=m-1}\Psi_{i2}S_j - \left(\frac{\pi L}{2k_f\tau}\right)^{1/2}\sum_{i=1}^{i=m}\Psi_{i1}R_j - \varepsilon_2\sum_{i=1}^{i=m-1}\Psi_{i2}S_j}{\varepsilon_2 + S_1} \tag{8.4}$$

$$\Psi_{total} = n_1\Psi_{m1} + n_2\Psi_{m2} \tag{8.5}$$

where L = number of subintervals on each potential, k_f is the rate of the chemical reaction in s^{-1}, Ψ_m = dimensionless current for each time increment with the serial number m, and

$$\varepsilon_1 = \exp\left[\frac{nF}{RT}\left(E_{applied} - E_1^0\right)\right] \tag{8.6}$$

$$\varepsilon_2 = \exp\left[\frac{nF}{RT}\left(E_{applied} - E_2^0\right)\right] \tag{8.7}$$

The final expressions are in agreement with those previously presented by Miles and Compton.[11]

8.2.2 Effect of k_f.

The impact of chemical reactions on voltammetric features depends upon the extent of the reaction within the time window of the measurement. The overall effect is usually evaluated using a dimensionless kinetic parameter. In cyclic voltammetry (CV) this parameter is k_f/v where v is the potential sweep rate. In CSWV, the effective sweep rate is the increment ÷ period; the dimensionless kinetic parameter is $k_f\tau$. The k_f and τ variables have been separated to enable consideration of the empirical parameters. In doing so, the theoretical trends presented directly match what experimentalists observe from systematic variation in period.

At the onset, an ECE mechanism can be readily distinguished from case where the analyte undergoes two sequential electron transfers, i.e. the EE mechanism. Two separate reversible processes are observed in the voltammogram for the EE mechanism so long at the $\Delta E^0 \geq 150$ mV. The peak potentials for each process remain at E^0, peak currents scale linearly with $\tau^{-1/2}$, and peak ratios for both processes are unity.[26] In cyclic voltammetry and CSWV, the number and magnitude of peaks observed for the ECE mechanism is a function of the rate of the chemical reaction interposed between the two electron transfers, the difference in formal potentials, and the effective potential sweep rate.[3] Figure 8.1 presents the impact of log k_f and ΔE^0 on the voltammogram. For very slow rates of reaction, the voltammogram is comprised of a single peak on each sweep direction whose shape and magnitude resembles that found for a reversible electron transfer reaction. At intermediate rates (e.g. $-2 < \log k_f < 4$), the number of peaks observed on each sweep depends on E_2^0 relative to E_1^0. Two peaks are observed on each sweep direction when $E_2^0 = -300$ mV. At $E_2^0 = -100$ mV, on the forward sweep the first

peak broadens and splits into two peaks while only one peak is observed on the reverse sweep with increasing k_f. When $E_2^0 = E_1^0$, only one peak is observed on each sweep. At fast rates (e.g. $\log k_f \geq 4$), two peaks are observed on the forward sweep and only one peak on the reverse sweep when $E_2^0 \leq E_1^0$.

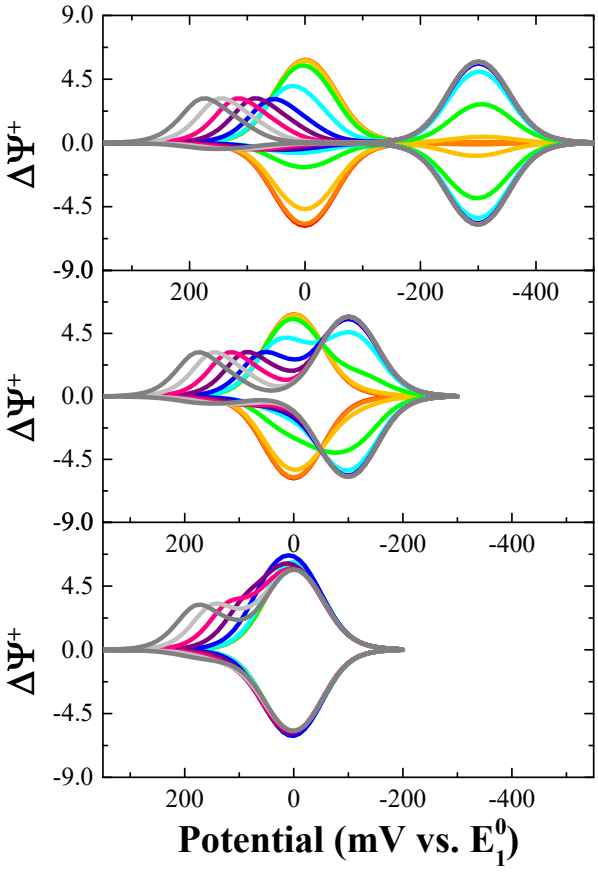

Figure 8.1. Effect of k_f and E_2^0 on the shape of the voltammogram when E_2^0 is -300 mV relative to E_1^0 (top panel), -100 mV (middle panel), and equal to E_1^0 (bottom panel) and $\log k_f$ is -3 (red), -2 (orange), -1 (yellow), 0 (green), 1 (cyan), 2 (blue), 3 (purple), 4 (magenta), 5 (light gray) and 6 (dark gray). Parameter values are: period = 50 ms, amplitude = 50 mV, increment = 10 mV. The switching potential is 200 mV negative of E_2^0.

Comparison of the voltammograms when $E_2^0 < E_1^0$ reveals that the peak potentials for the first electron transfer step shift positively as $\log k_f$ is increased from -3 to 6 whereas

the peak potentials for the second remain constant at E_2^0 as shown in Figure 8.1 and more quantitatively in Figure 8.2.

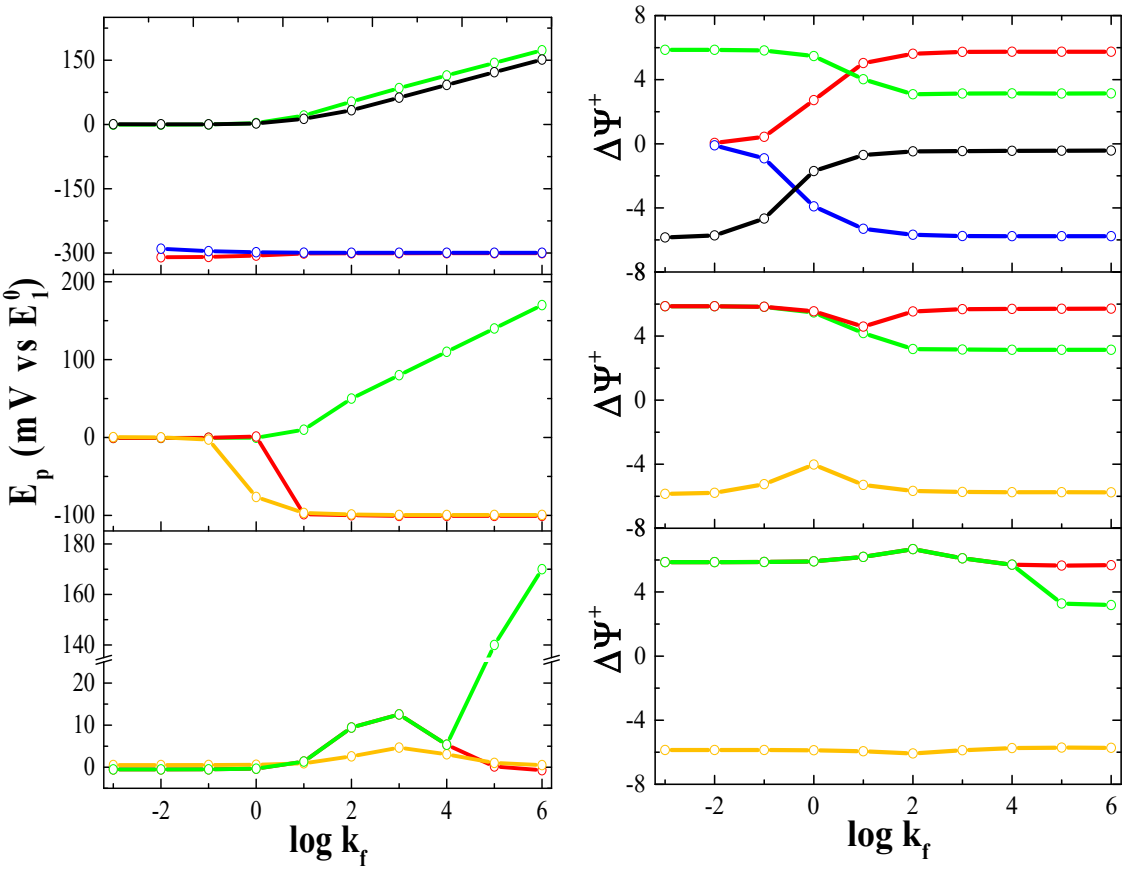

Figure 8.2. Dependence of peak currents and peak potentials on log k_f for E_2^0 = -300 mV (top panels), -100 mV (middle panels), and 0 mV (bottom panels). Parameter values are: period = 50 ms, amplitude = 50 mV, increment = 10 mV. The switching potential is 200 mV negative of E_2^0. For the top panels: $\Delta\Psi^+_{p,f1}$ and $E_{p,f1}$ (green), $\Delta\Psi^+_{p,f2}$ and $E_{p,f2}$ (red), $\Delta\Psi^+_{p,r1}$ and $E_{p,r1}$ (black), $\Delta\Psi^+_{p,r2}$ and $E_{p,r2}$ (blue). For the middle and bottom panels: $\Delta\Psi^+_{p,f1}$ and $E_{p,f1}$ (green), $\Delta\Psi^+_{p,f2}$ and $E_{p,f2}$ (red), $\Delta\Psi^+_{p,r}$ and $E_{p,r}$ (gold). Open circles denote the specific parameter levels for simulated data.

The peak currents for the first process (both $\Delta\Psi^+_{p,f1}$ and $\Delta\Psi^+_{p,r1}$) diminish in magnitude before holding constant with increasing log k_f. In contrast, the peak currents for the

second process (both $\Delta\Psi^{+}_{p,f2}$ and $\Delta\Psi^{+}_{p,r2}$) increase in magnitude before holding constant with increasing log k_f (see Figure 8.2). Similarly, comparison of the voltammograms when $E^0_2 = E^0_1$ (bottom panels in Figure 8.1 and Figure 8.2) reveals that at low to moderate values of log k_f, one peak is observed on each sweep. At log $k_f > 3$, a second peak emerges at potentials positive of E^0_1. The peak current for this process remains constant with increasing log k_f.

A qualitative tool for identifying an ECE process with cyclic voltammetry involves performing multiple scans over the potential range. The same holds true for CSWV. For a reversible mechanism, there is no difference in the shape of the voltammogram on the first and second cycle. However, in the presence of coupled chemical reactions, the difference in peak currents between the first and second scans is a function of log k_f and ΔE^0.[4, 6, 10, 11, 13] This is illustrated in Figure 8.3. When $E^0_2 \leq$ -100 mV, measurable differences in $\Delta\Psi^{+}_{p,f1}$ for the second relative to the first scan at log $k_f \geq$ -1; at $E^0_2 = 0$, measurable differences are observed at log $k_f \geq 3$.

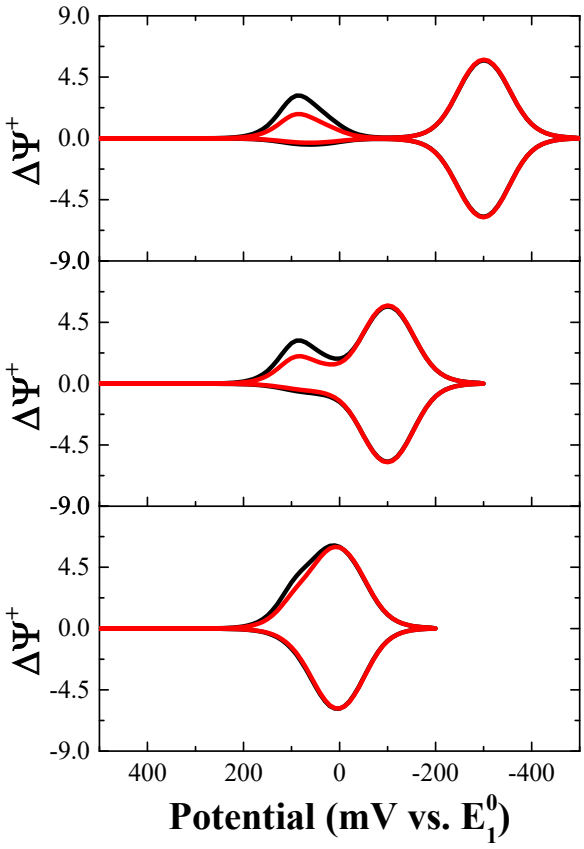

Figure 8.3. Comparison of voltammograms acquired on the first (black) and second (red) scans for E_2^0 = -300 mV (top panel), -100 mV (middle panel), and 0 mV (bottom panel). Parameter values are: log k_f = 3; period = 50 ms, amplitude = 50 mV, increment = 10 mV; switching potential is 200 mV negative of E_2^0.

8.2.3 Effect of Period (τ)

The effect of period on the shape of the voltammogram is a complex function of the separation between E_2^0 and E_1^0 and log k_f. Figure 8.4 presents the impact of varying period on the shape of the voltammogram as a function of E_2^0 for log k_f = 3. On both the forward and reverse sweeps, the peak potential for the first process shifts positively with increasing period while the second process (at E_2^0) is invariant for E_2^0 = -300 and -100

mV. In contrast, when $E_2^0 = 0$, the peak potentials on both the forward and reverse sweeps are invariant with period at this particular value of log k_f.

Figure 8.5 presents a detailed description of the relationships between peak potentials and currents on period and log k_f when $E_2^0 = -300$ mV. Both $E_{p,f1}$ and $E_{p,r1}$ shift positively by 30 mV per decade with increasing period (for log $k_f \geq 0$) whereas $E_{p,f2}$ and $E_{p,r2}$ remain essentially constant at E_2^0. Peak currents are proportional to the $\tau^{-1/2}$ over a wide range in log k_f. The $\Delta\Psi^+_{p,f1}$ vs. $\tau^{-1/2}$ trace is linear at log $k_f \leq 1$, curvilinear over the range $2 \leq \log k_f \leq 3$, and again linear at log $k_f \geq 4$. The slopes of the linear traces decrease with increasing log k_f. The ratio of $\Delta\Psi^+_{p,r1} / \Delta\Psi^+_{p,f1}$ ranges from 0.1 to 1 depending upon log k_f and period. This is shown in the upper right panel of Figure 8.5 and is comparable to the trend for an EC mechanism.[27] Similarly, the ratio of $\Delta\Psi^+_{p,r2} / \Delta\Psi^+_{p,f2}$ ranges between 1 and 2 depending upon log k_f and period. At log $k_f \leq 0$, this ratio increases to a value of two and then decreases to a value of one. At $0 < \log k_f \leq 2$, the peak ratio decreases to a value of one over the range in period investigated herein. For log $k_f > 2$, the ratio is invariant at unity. The trend shown in $\Delta\Psi^+_{p,r2} / \Delta\Psi^+_{p,f2}$ is comparable to the trend for a CE mechanism where peak ratios > 1 reflect the amount of conversion of Red_1 to Ox_2 and subsequent reduction to Red_2 over the period of the potential pulse.[28]

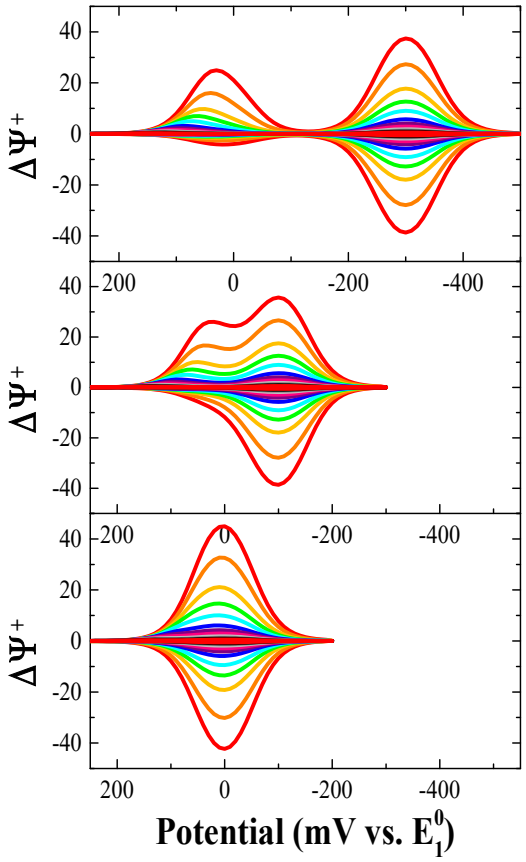

Figure 8.4. Effect of period and E_2^0 on the shape of the voltammogram when E_2^0 is -300 mV relative to E_1^0 (top panel), -100 mV (middle panel), and equal to E_1^0 (bottom panel) and log k_f = 3. Parameter values are: amplitude = 50 mV, increment = 10 mV, switching potential is 200 mV negative of E_2^0, and period is varied from 1 ms (red), 2 ms (orange), 5 ms (yellow), 10 ms (green), 20 ms (cyan), 50 ms (blue), 100 ms (purple), 200 ms (magenta), 500 ms (dark gray), 1 s (dark gray), 2 s (black), and 5 s (brown).

Finally, the ratio of $\Delta\Psi^+_{p,r2}/\Delta\Psi^+_{p,f2}$ ranges from 0 to 1.8 depending upon log k_f and period as shown in Figure 8.5. The slope of the linear portions of the traces depicted in this panel of the figure are consistently 0.778. Note that peak ratios presented in Figure 8.5 are specific to the increment, amplitude and switching potential values given in the caption. At switching potentials further negative of E_2^0, each trace shifts to the left.

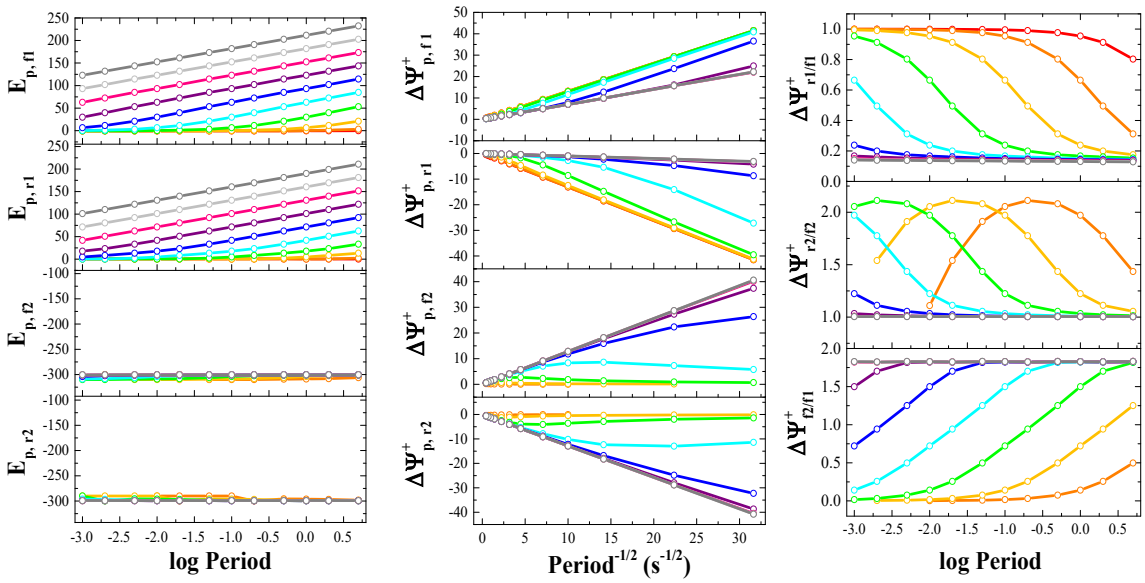

Figure 8.5. Plots of peak current versus $\tau^{-1/2}$ and peak potentials and peak ratios versus log period for E_2^0 = -300 mV as a function of log k_f ranging from -3 (red) to 6 (dark gray) using the color scheme described in the caption of Figure 8.1. Parameter values are: amplitude = 50 mV, increment = 10 mV, and switching potential is 200 mV negative of E_2^0. Open circles denote the specific parameter levels for simulated data.

Figure 8.6 presents the relationships between peak potentials and currents on period and log k_f when E_2^0 = -100 mV. $E_{p,f1}$ shifts positively by 30 mV per decade increase in period (for log $k_f \geq 0$). $E_{p,f2}$ emerges when log $k_f \geq 0$, and remains essentially constant at E_2^0. This trend is not observed for $E_{p,r}$. At log $k_f \geq 3$, the peak is located at E_2^0 over all periods. At log $k_f < 3$, the peak moves from E_1^0 to E_2^0 as period increases. Peak currents are linearly or curvilinearly related to $\tau^{-1/2}$ depending upon log k_f. The $\Delta\Psi^+_{p,f1}$ and $\Delta\Psi^+_{p,r}$ vs. $\tau^{-1/2}$ traces are linear at log $k_f \leq 1$, curvilinear over the range $2 \leq \log k_f \leq 3$, and again linear at log $k_f \geq 4$. At log $k_f \leq 0$, the ratio of $\Delta\Psi^+_{p,r} / \Delta\Psi^+_{p,f1}$ diminishes from 1 to ~0.7 with increasing period until the $E_{p,r}$ shifts to E_2^0 whereupon the ratio begins to increase to ~1.15. At log $k_f > 0$, the shift in $E_{p,r}$ to -100 mV occurs at shorter periods and

the forward peak separates into two. When this occurs, the ratio $\Delta\Psi^{+}_{p,r}/\Delta\Psi^{+}_{p,f1}$ increases from 1.15 to 1.8 whereas the ratio $\Delta\Psi^{+}_{p,r}/\Delta\Psi^{+}_{p,f2}$ decreases from 1.15 to unity with increasing period. Thus, the transition in the shape of the voltammogram from one to two peaks on the forward sweep occurs for all log k_f values but at different periods; the higher the log k_f value, the shorter the period at which the transition occurs. Figure 8.7 provides insight into this transition by presenting the individual and difference currents (i.e. Ψ and $\Delta\Psi$) as a function of period for log $k_f = 1$.

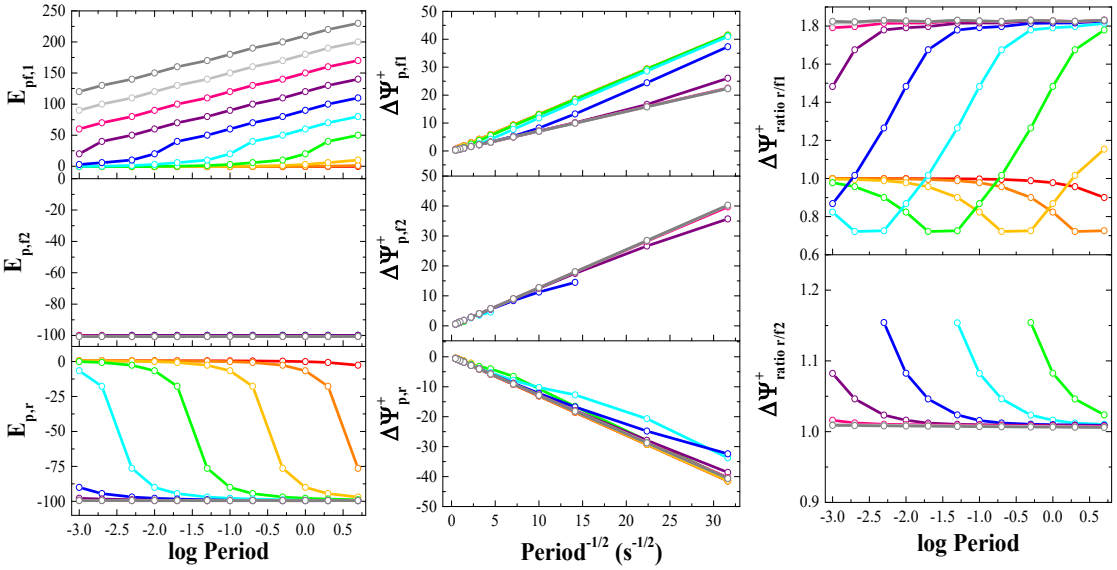

Figure 8.6. Plots of peak current versus $\tau^{-1/2}$ and peak potentials and peak ratios versus log period for E_2^0 = -100 mV as a function of log k_f ranging from -3 (red) to 6 (dark gray) using the color scheme described in the caption of Figure 8.1. Parameter values are: amplitude = 50 mV, increment = 10 mV, and switching potential is 200 mV negative of E_2^0. Open circles denote the specific parameter levels for simulated data.

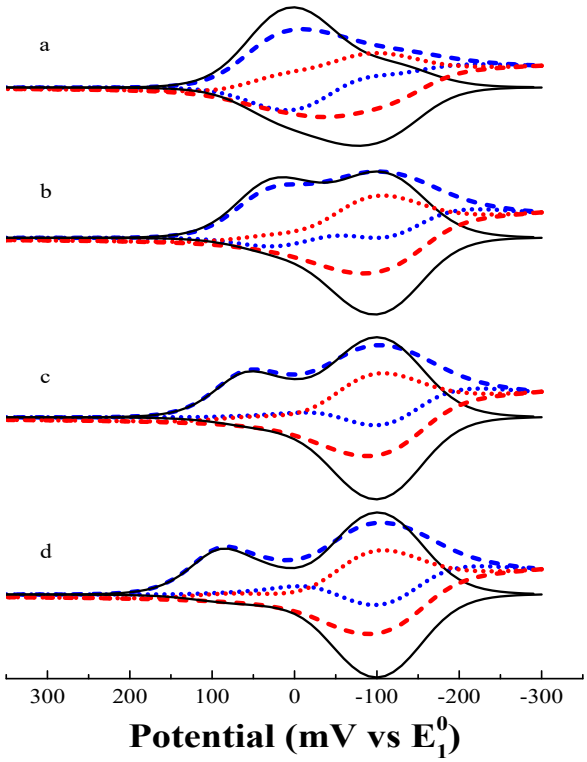

Figure 8.7. The effect of period on the individual and difference currents when log k_f = 1, E_2^0 = -100 mV, amplitude = 50 mV, increment = 10 mV, switching potential is -300 mV, and period: a) 5 ms, b) 50 ms, c) 500 ms, and d) 5000 ms. Difference currents (black); individual currents: forward sweep (blue), reverse sweep (red); odd numbered pulses (dashed), even numbered pulses (dotted).

Figure 8.8 presents the relationships between peak potentials and currents on period and log k_f when E_2^0 = 0 mV. $E_{p,f}$ remains at E_1^0 until log $k_f \geq 3$ when both $E_{p,f1}$ and $E_{p,f2}$ are resolved. At this point, $E_{p,f1}$ shifts positively by 30 mV per decade with increasing period. $E_{p,f2}$ remains at E_2^0. $E_{p,r}$ remains essentially constant at 0 mV over the entire range in log k_f. $\Delta\Psi^+_{p,f1}$ vs. $\tau^{-1/2}$ is linear for all log k_f values. However, the slopes of the traces marginally vary with log k_f. The ratio of $\Delta\Psi^+_{p,r}/\Delta\Psi^+_{p,f1}$ ranges from 0.9 to 1.0 depending upon log k_f and period until $E_{p,f1}$ and $E_{p,f2}$ are resolved. At this point, the ratio jumps to a value between 1.7 and 1.8 and the ratio of $\Delta\Psi^+_{p,r}/\Delta\Psi^+_{p,f2}$ is unity. At -3 ≤ log

$k_f \leq -1$, the peak width is invariant with period and equivalent to that for a reversible process. At all other values of log k_f, the $W_{1/2,f}$ increases with period with a magnitude dependent on k_f until two processes are resolved along the potential axis (see Figure 8.9).

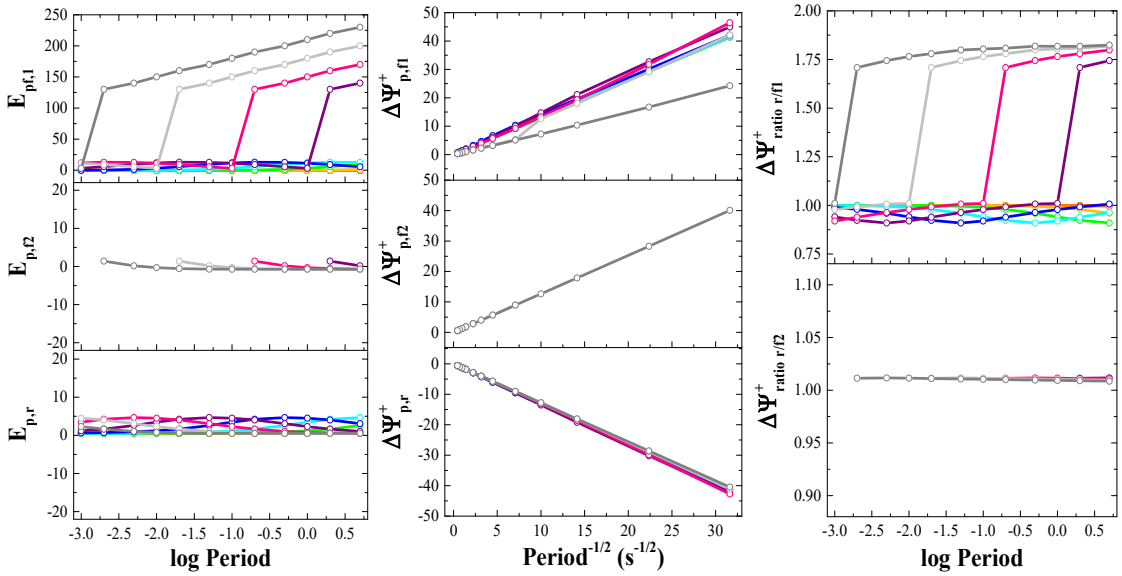

Figure 8.8. Plots of peak current versus $\tau^{-1/2}$ and peak potentials and peak ratios versus log period for E_2^0 = 0 mV as a function of log k_f ranging from -3 (red) to 6 (dark gray). Parameter values are: amplitude = 50 mV, increment = 10 mV, and switching potential is 200 mV negative of E_2^0. Open circles denote the specific parameter levels for simulated data.

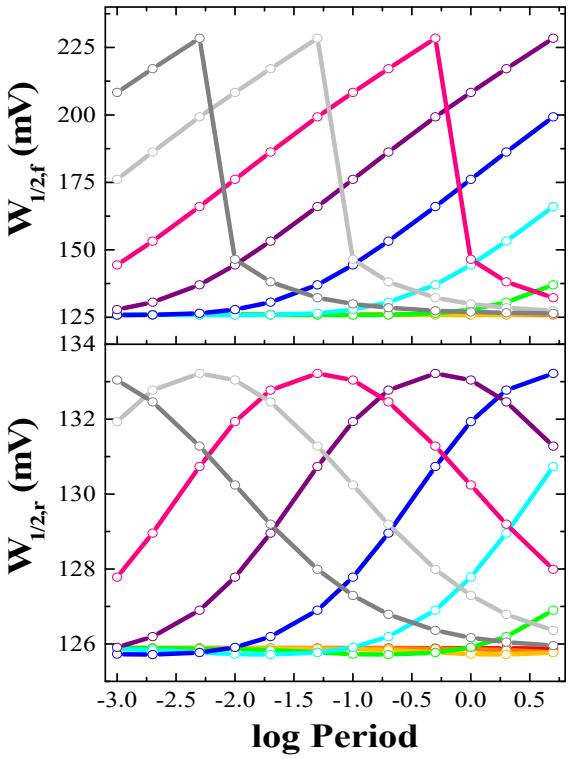

Figure 8.9. Plots of peak width versus log period for E_2^0 = 0 mV as a function of log k_f ranging from -3 (red) to 6 (dark gray). Parameter values are: amplitude = 50 mV, increment = 10 mV, and switching potential is -200 mV. Open circles denote the specific parameter levels for simulated data.

Thus, key indicators of an ECE mechanism are the differential dependences of peak potentials, currents, and current ratios with period. The shift in peak potential with period is diagnostic for the presence of a chemical reaction following the first reduction process.[3] A plot of peak current versus $\tau^{-1/2}$ confirms that the electrode reaction is diffusional rather than surface-confined[29-31] and identifies the presence of a chemical reaction following the first reduction process. Peak ratios deviate from unity and are indicative of both a following and preceding chemical reaction.[3] It is interesting to note that the trends for the first process mirror those for an EC mechanism;[27] however, the trends for the second process are unlike the trends for a CE mechanism.[28] Taken

collectively, systematic variation of period provides a diagnostic trend characteristic of the ECE mechanism from which the magnitude of k_f can be determined.

8.2.4 Effect of Increment (δE)

The effect of increment on the shape of the voltammogram depends on the separation between E_2^0 and E_1^0 and log k_f. Figure 8.10 presents the impact of varying increment on the shape of the voltammogram as a function of E_2^0 for log k_f = 3 and 1. On the forward scan, $E_{p,f1}$ shifts negatively and $\Delta\Psi^+_{p,f1}$ increases with increment while $E_{p,f2}$ and $\Delta\Psi^+_{p,f2}$ are invariant of E_2^0 = -300 and -100 mV and log k_f = 3 and 1. When E_2^0 = 0 mV at log k_f = 3, $E_{p,f}$ and $E_{p,r}$ are essentially unchanged, $\Delta\Psi^+_p$ increases slightly, and the apparent peak width increases with increment. At log k_f = 1, $E_{p,f} = E_{p,r}$, and the peak currents are independent of increment. The effective scan rate is increment divided by period. Thus, increasing increment versus increasing period shifts $E_{p,1}$ in opposite directions (see Figures 7.4 and 7.10).

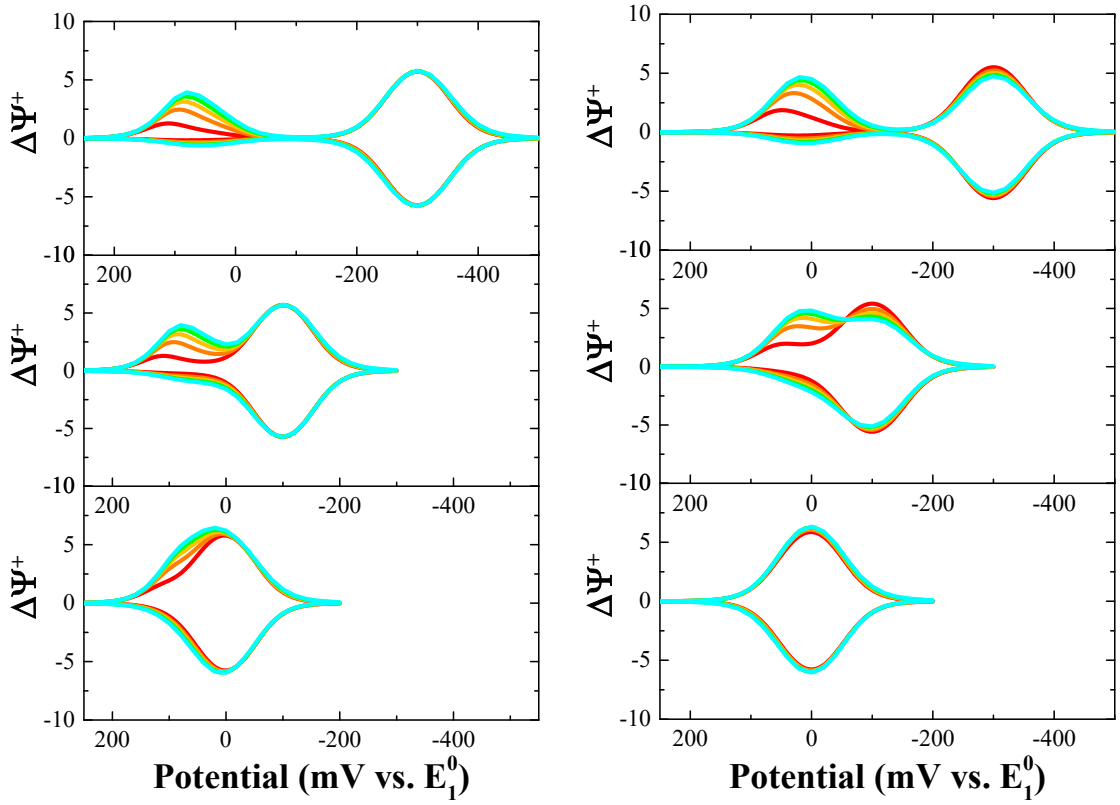

Figure 8.10. Effect of increment and E_2^0 on the shape of the voltammogram when E_2^0 is -300 mV relative to E_1^0 (top panel), -100 mV (middle panel), and equal to E_1^0 (bottom panel) and log k_f = 3 (left column) and log k_f = 1 (right column). Parameter values are: period = 50 ms, amplitude = 50 mV, switching potential is 200 mV negative of E_2^0, and increment is varied from 1 mV (red), 5 mV (orange), 10 mV (yellow), 15 mV (green), and 20 mV (cyan).

Figure 8.11 presents the dependence of peak potentials, currents, and current ratios on increment as a function of log k_f when E_2^0 = -300 mV. $E_{p,f1}$ and $E_{p,r2}$ shifts negatively ~28 mV per decade in increment whereas $E_{p,f2}$ and $E_{p,r2}$ remain constant at E_2^0. At log $k_f \leq$ -2, $\Delta\Psi^+_{p,f1}$ and $\Delta\Psi^+_{p,r1}$ are independent of increment. At higher k_f values, $\Delta\Psi^+_{p,f1}$ and $\Delta\Psi^+_{p,r1}$ increase curvilinearly with increment whereas $\Delta\Psi^+_{p,f2}$ and $\Delta\Psi^+_{p,r2}$ decrease with increment at low values of k_f but become independent of increment at log $k_f \geq 2$. The ratio of

$\Delta\Psi^{+}_{p,r1}/\Delta\Psi^{+}_{p,f1}$ ranges from 0.1 to 1 whereas the ratio of $\Delta\Psi^{+}_{p,r2}/\Delta\Psi^{+}_{p,f2}$ ranges between 1 and 2.2 depending upon log k_f and increment. Finally, the ratio $\Delta\Psi^{+}_{p,r2}/\Delta\Psi^{+}_{p,f2}$ decreases with increment for log $k_f \geq -1$. This trend is comparable to that observed in cyclic voltammetry[3] where increasing the potential sweep rate shortens the time window for the conversion of Red_1 to Ox_2.

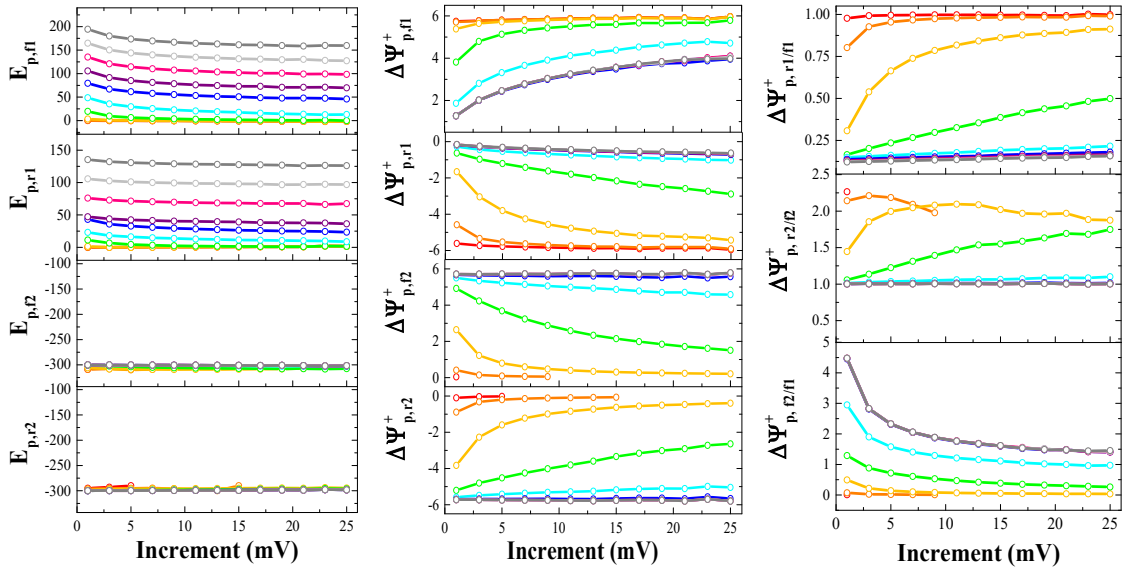

Figure 8.11. Plots of peak currents, potentials, and ratios versus increment for E_2^0 = -300 mV as a function of log k_f ranging from -3 (red) to 6 (dark gray) using the color scheme described in the caption of Figure 8.1. Parameter values are: period = 50 ms, amplitude = 50 mV, and switching potential is -500 mV. Open circles denote the specific parameter levels for simulated data.

Figure 8.12 presents the dependence of peak potentials, currents, and current ratios on increment as a function of log k_f when E_2^0 = -100 mV. $E_{p,f1}$ shifts negatively ~28 mV per decade in increment whereas $E_{p,f2}$, when it emerges, remains constant at E_2^0. At log k_f < 1, $E_{p,r}$ moves from E_2^0 to E_1^0 as increment increases whereas at log $k_f \geq 1$, $E_{p,r}$ is located at E_2^0 over all increments. At log $k_f \leq -2$, $\Delta\Psi^{+}_{p,f1}$ and $\Delta\Psi^{+}_{p,r1}$ are independent of increment.

At higher k_f values, $\Delta\Psi^+_{p,f1}$ and $\Delta\Psi^+_{p,r1}$ increase curvilinearly with increment whereas $\Delta\Psi^+_{p,f2}$ decreases with increment at low values of k_f but become independent of increment at log $k_f \geq 2$. The ratio of $\Delta\Psi^+_{p,r} / \Delta\Psi^+_{p,f1}$ ranges from 0.75 to 4 whereas the ratio of $\Delta\Psi^+_{p,r} / \Delta\Psi^+_{p,f2}$ ranges between 1 and 1.5 depending upon log k_f and increment.

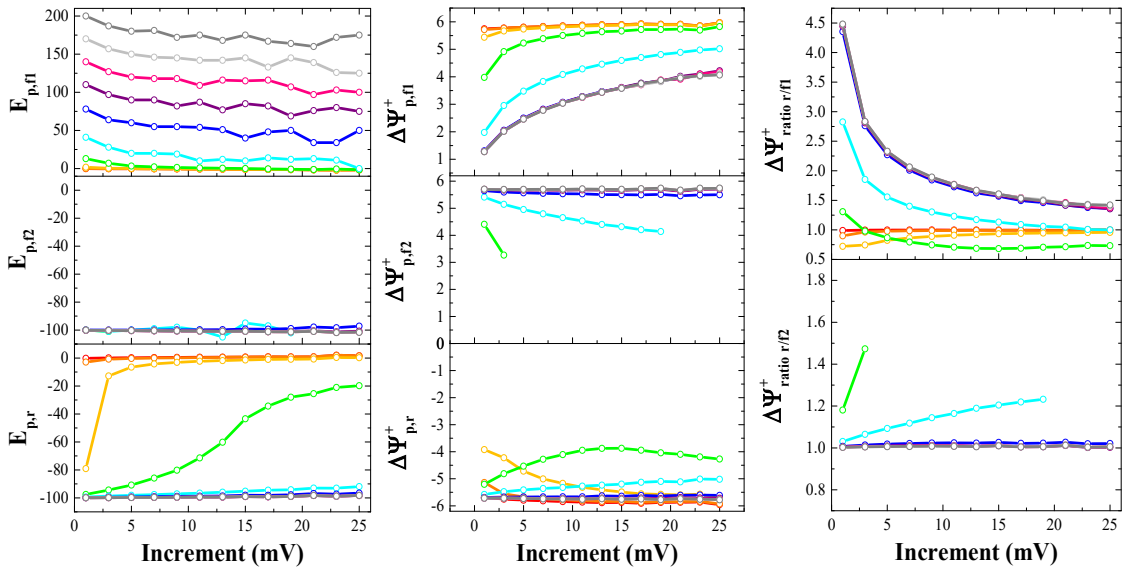

Figure 8.12. Plots of peak currents, potentials, and ratios versus increment for E^0_2 = -100 mV as a function of log k_f ranging from -3 (red) to 6 (dark gray). Parameter values are: period = 50 ms, amplitude = 50 mV, and switching potential is -300 mV. Open circles denote the specific parameter levels for simulated data.

Figure 8.13 presents the dependence of peak potentials, currents, and current ratios on increment as a function of log k_f when E^0_2 = 0 mV. $E_{p,f1}$ remains constant (within the value of the increment) until it becomes resolved from $E_{p,f2}$. Then, $E_{p,f1}$ shifts negatively by ~28 mV per decade in increment whereas $E_{p,f2}$ remains constant at E^0_2. $E_{p,r}$ remains constant at E^0_1 (within the value of the increment) over all increments. $\Delta\Psi^+_{p,f1}$ and $\Delta\Psi^+_{p,r}$ increase with increment whereas $\Delta\Psi^+_{p,f2}$ remains constant when present. The ratios $\Delta\Psi^+_{p,r}$

$/\Delta\Psi^{+}_{p,f1}$ and $\Delta\Psi^{+}_{p,r}/\Delta\Psi^{+}_{p,f2}$ are equal to unity except when $E_{p,f2}$ is resolved from $E_{p,f1}$. Then $\Delta\Psi^{+}_{p,r}/\Delta\Psi^{+}_{p,f1}$ drops curvilinearly from 4.5 to 1.5 with increment.

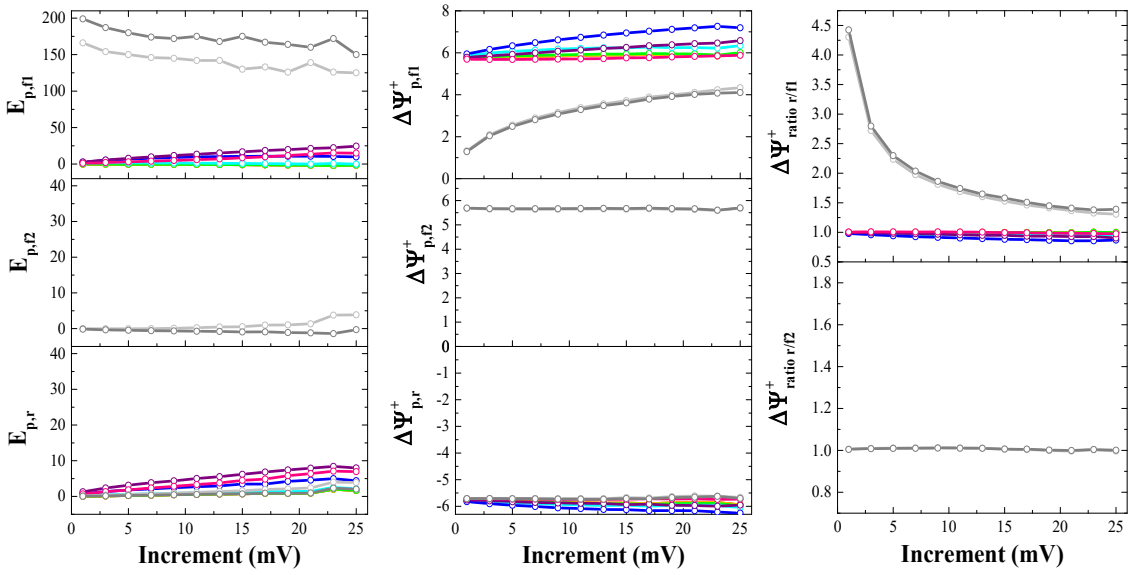

Figure 8.13. Plots of peak currents, potentials, and ratios versus increment for $E^0_2 = 0$ mV as a function of log k_f ranging from -3 (red) to 6 (dark gray). Parameter values are: period = 50 ms, amplitude = 50 mV, and switching potential is -200 mV. Open circles denote the specific parameter levels for simulated data.

The differential dependences of peak potentials and current ratios with increment are also indicators of an ECE mechanism. When the two processes are sufficient separated along the potential axis, $E_{p,f1}$ and $E_{p,r1}$ shift negatively towards E^0 with increment similar to an EC mechanism.[3] In contrast to the CE mechanism, $E_{p,f2}$ and $E_{p,r2}$ are independent of increment.[28] Peak ratios for the first process are ≤ 1 (similar to an EC mechanism) and for the second process ≥ 1 (similar to a CE process).[12,13] Peak potential dependence on increment can provide a measure of k_f if E^0_1 is known. When the two processes are not resolved along the potential axis, trends in peak potentials and peak current ratios

distinguish this mechanism from a reversible, quasireversible, EC, and CE mechanism (*vide supra*).

8.2.5 Effect of Amplitude (E_{SW})

The effect of amplitude on the shape of the voltammogram also depends on the separation between E_2^0 and E_1^0 and log k_f. Figure 8.14 presents the impact of varying amplitude on the shape of the voltammogram as a function of E_2^0 for log $k_f = 3$. On both the forward and reverse sweeps, the peak potentials for the first process shifts positively with amplitude while the peak potentials for the second process (at E_2^0) are invariant for all three E_2^0 values investigated herein.

The dependence of peak potentials, currents, and current ratios on amplitude is also indicative of log k_f. When $E_2^0 = -300$ mV, $E_{p,f1}$ and $E_{p,r1}$ shift positively whereas $E_{p,f2}$ and $E_{p,r2}$ remain constant with increasing amplitude (see Figure 8.15). The peak current magnitudes increase curvilinearly with amplitude; the degree of curvature depends upon log k_f. In contrast, peak ratios are almost always independent of amplitude but the value changes with log k_f.

When $E_2^0 = -100$ mV, $E_{p,f1}$ shifts positively when log $k_f \geq 2$ whereas $E_{p,f2}$ remains essentially constant with increasing amplitude (see Figure 8.16). Note that at log $k_f \leq -2$ $E_{p,r}$ remains at E_1^0 and at log $k_f \geq 2$ $E_{p,r}$ remains at E_2^0. In between these limits in log k_f, $E_{p,r}$ shifts with amplitude (see Figure 8.16). The peak current magnitudes increase curvilinearly with amplitude; the degree of curvature depends somewhat upon log k_f.

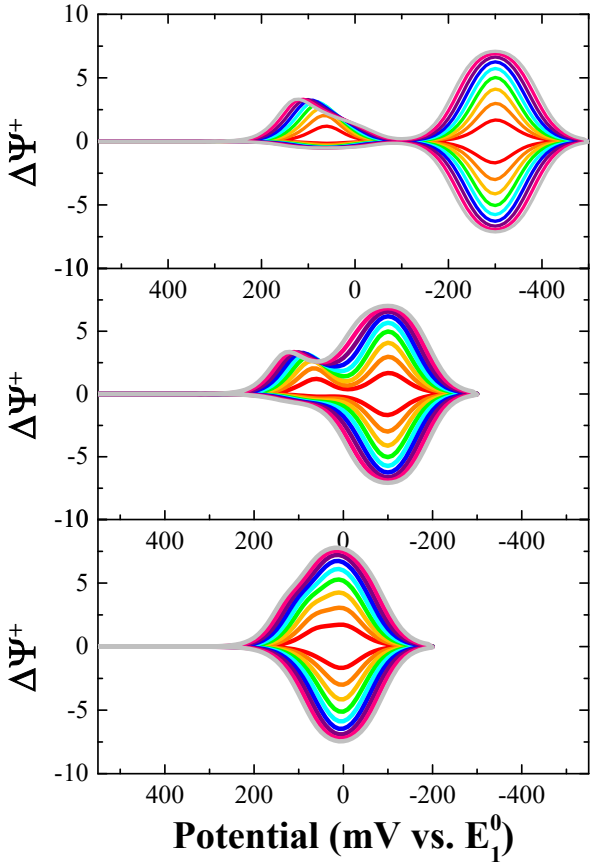

Figure 8.14. Effect of amplitude and E_2^0 on the shape of the voltammogram when E_2^0 is -300 mV relative to E_1^0 (top panel), -100 mV (middle panel), and equal to E_1^0 (bottom panel) and log k_f = 3. Parameter values are: period = 50 ms, increment = 10 mV, switching potential is 200 mV negative of E_2^0, and amplitude is varied from 10 mV (red) to 90 mV (light gray) in steps of 10 mV.

In contrast to when E_2^0 = -300 mV, the peak ratio $\Delta\Psi^+_{p,r}/\Delta\Psi^+_{p,fl}$ depends upon both amplitude and log k_f. At log $k_f \leq$ -2, $\Delta\Psi^+_{p,r}/\Delta\Psi^+_{p,fl}$ equals unity at all amplitudes. At -2 < log $k_f \leq 0$, $\Delta\Psi^+_{p,r}/\Delta\Psi^+_{p,fl}$ is less than unity and increases towards unity with amplitude. At log k_f = 1, two forward peaks are resolved along the potential axis at amplitudes ≤ 50 mV. At log $k_f \geq 2$, $\Delta\Psi^+_{p,r}/\Delta\Psi^+_{p,fl}$ increases from 1.4 to 2.2 with amplitude.

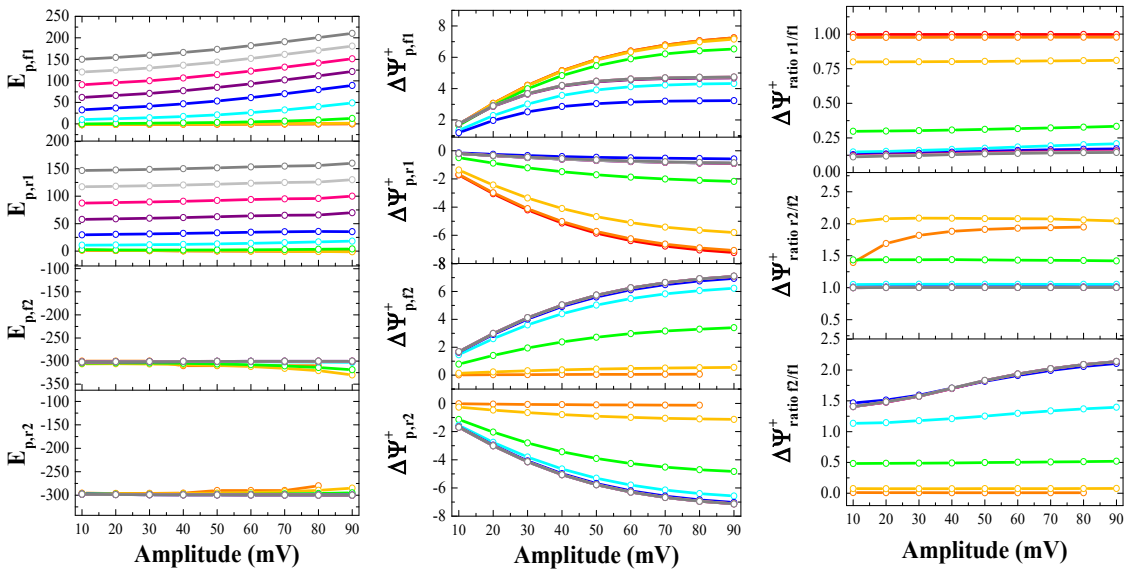

Figure 8.15. Plots of peak currents, potentials, and ratios versus amplitude for E_2^0 = -300 mV as a function of log k_f ranging from -3 (red) to 6 (dark gray) using the color scheme described in the caption of Figure 8.1. Parameter values are: period = 50 ms, increment = 10 mV, and switching potential is -500 mV. Open circles denote the specific parameter levels for simulated data.

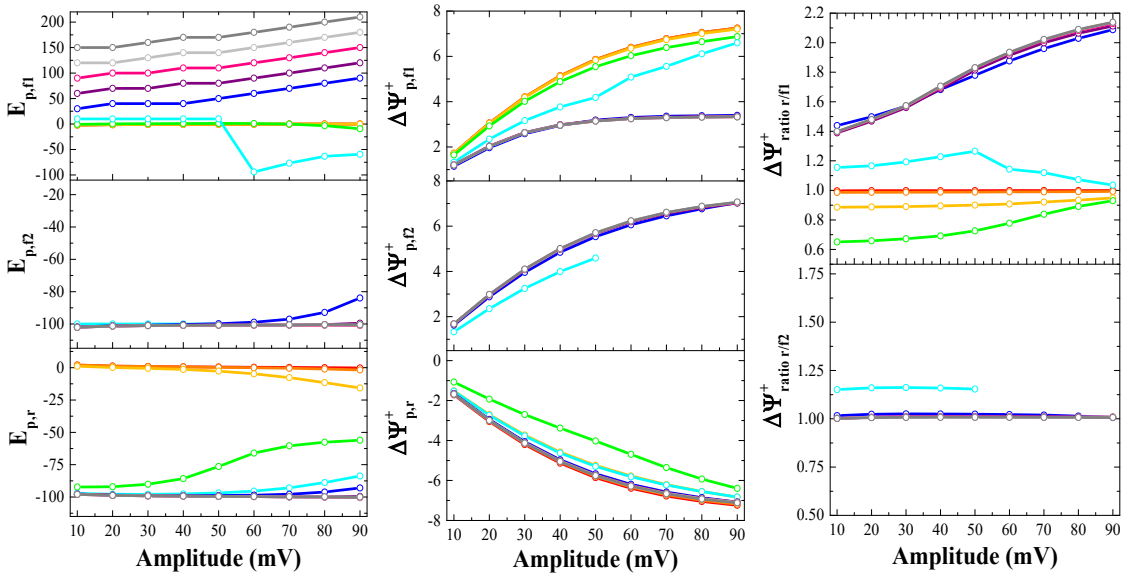

Figure 8.16. Plots of peak currents, potentials, and ratios versus amplitude for E_2^0 = -100 mV as a function of log k_f ranging from -3 (red) to 6 (dark gray). Parameter values are: period = 50 ms, increment = 10 mV, and switching potential is -300 mV. Open circles denote the specific parameter levels for simulated data.

When $E_{p,f2}$ is resolved from $E_{p,f1}$, the ratio $\Delta\Psi^{+}_{p,r} / \Delta\Psi^{+}_{p,f2}$ is measureable and equal to unity except with log $k_f = 1$ (see Figure 8.16).

Figure 8.17 presents the dependence of peak potentials, currents, and current ratios on amplitude as a function of log k_f when $E_2^0 = 0$ mV. $E_{p,f1}$ remains essentially constant with increasing amplitude up to log $k_f \leq 3$. When log $k_f = 4$, $E_{p,f2}$ becomes resolved from $E_{p,f1}$ at low amplitudes. At log $k_f > 4$, $E_{p,f2}$ is resolved from $E_{p,f1}$ at all amplitudes and both shift positively with increasing amplitude but with differing slopes. In contrast, $E_{p,r}$ remains essentially constant at E_1^0 regardless of k_f and amplitude. The peak current magnitudes increase curvilinearly with amplitude; the degree of curvature depends somewhat upon log k_f and whether the two processes are resolved.

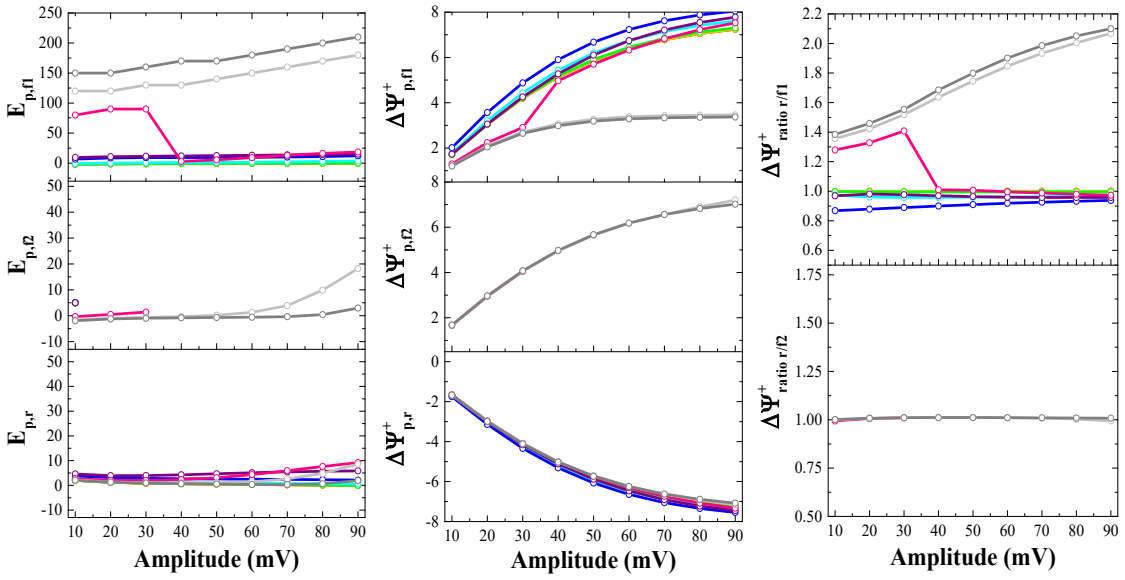

Figure 8.17. Plots of peak currents, potentials, and ratios versus amplitude for $E_2^0 = 0$ mV as a function of log k_f ranging from -3 (red) to 6 (dark gray). Parameter values are: period = 50 ms, increment = 10 mV, and switching potential is -200 mV. Open circles denote the specific parameter levels for simulated data.

The dependence of peak ratios on amplitude mirrors that presented above for E_2^0 = -100 mV (see Figure 8.17). Thus, the shift in peak potentials and the magnitude of peak ratios as a function of amplitude can be used to identify the value of k_f.

8.3 Conclusion

In this chapter, theory for an ECE mechanism has been developed for CSWV. The peak currents, potentials, and shapes of cyclic square wave voltammograms for the ECE mechanism have been shown to be a complex function k_f, increment, period, and amplitude. The effects of these empirical parameters on the voltammograms for this mechanism are summarized in Table 8.1. It is anticipated that experimenters seeking to identify the mechanism of the electrode reaction under investigation will prepare the diagnostic plots listed in this table. If the trends observed match those listed in Table 8.1, then assignment of the electrode reaction as an ECE mechanism is appropriate. If not, then the experimenter should consult other chapters in this thesis, other publications[26-28, 31-33], or the text by Mirčeski[34] to identify the electrode reaction pathway. The magnitude of k_f can then be determined by comparison of the observed trends in the diagnostic plots with those presented in figures both in this chapter. If the mechanism is properly assigned, the k_f value obtained from the trend in peak potentials will be consistent with that obtained from peak current and peak ratio data. Note that the range in measureable log k_f values is a function of ΔE^0 and whether an independent measure of E_1^0 is available (i.e. at low temperatures or fast scan rates). If $\Delta E^0 \geq 100$ mV, the range in log k_f extends from -2 to 6 if E_1^0 is known and from -2 to 2 if it isn't. When $\Delta E^0 < 100$ mV, only fast rates of reaction can be determined (i.e. log $k_f > 4$).

Table 8.1. Diagnostic Plots and Protocol for Assessing an ECE Electrode Reaction by CSWV

	Empirical variables					
Waveform parameters	***Period,* τ**		***Increment,* δE**		***Amplitude,* E_{SW}**	
	Plot	**Trace**	**Plot**	**Trend**	**Plot**	**Trend**
Peak currents	ΔI_p vs. $\tau^{-1/2}$	All ΔI_p decrease linearly or curvilinearly with increasing period regardless of separation between E_1^0 and E_2^0 (see Figures 8.5, 8.6, and 8.8)	ΔI_p vs. δE	$\Delta I_{p,1}$ increase whereas $\Delta I_{p,2}$ decrease with increment; the magnitude depends upon log k_f and E_2^0 relative to E_1^0 (see Figures 8.11, 8.12, and 8.13)	ΔI_p vs. E_{SW}	All ΔI_p values increase with E_{SW} with magnitude and curvature dependent on log k_f and E_2^0 relative to E_1^0 (see Figures 8.15, 8.16, and 8.17)
Peak ratio	Peak ratio vs. log τ	Complex behavior that depends on log k_f and E_2^0 relative to E_1^0 (see Figures 8.5, 8.6, and 8.8)	Peak ratio vs. δE	Either independent of or curvilinearly related to increment; trend depends on log k_f and E_2^0 relative to E_1^0 (see Figures 8.11, 8.12, and 8.13)	Peak ratio vs. E_{SW}	Either independent of or curvilinearly related to amplitude; trend depends on log k_f and E_2^0 relative to E_1^0 (see Figures 8.15, 8.16, and 8.17)
Peak potentials	$E_{p,f}$ vs. log τ	When two processes are observed on the forward sweep, $E_{p,f1}$ shifts positively by 30 mV per decade in increasing period (see Figure 8.4). $E_{p,f2} = E_2^0$. For one process observed on the forward sweep, $E_{p,f}$ may be at E_1^0 or E_2^0, depending upon k_f. (see Figures 8.5, 8.6, and 8.8)	$E_{p,f}$ vs. δE	Trend depends upon whether $E_{p,f1}$ and $E_{p,f2}$ are resolved: when only one peak is present $E_{p,f}$ remains essentially constant; when two peaks are present $E_{p,f1}$ shifts negatively whereas $E_{p,f2}$ is generally constant (see Figures 8.11, 8.12, and 8.13)	E_p vs. E_{SW}	Trend depends on whether $E_{p,f1}$ and $E_{p,f2}$ are resolved: when only one peak is present $E_{p,f}$ remains essentially constant; when two peaks are present $E_{p,f1}$ shifts with E_{SW} whereas $E_{p,f2}$ is generally constant (see Figures 8.15, 8.16, and 8.17)
	$E_{p,r}$ vs. log τ	When two processes are observed on the reverse sweep, $E_{p,r1}$ shifts positively by 30 mV per decade in period while $E_{p,r2}$ remains constant at E_2^0. When one process is observed on the reverse sweep, $E_{p,r}$ may be at E_1^0 or E_2^0, depending upon k_f when $E_2^0 < E_1^0$. (see Figures 8.5, 8.6, and 8.8)	$E_{p,r}$ vs. δE	$E_{p,r1}$ shifts negatively whereas $E_{p,r2}$ is generally constant; if only 1 peak exists, $E_{p,r}$ is generally constant but may transition from between E_2^0 and E_1^0 (see Figures 8.11, 8.12, and 8.13)		$E_{p,r1}$ shifts with E_{SW} whereas $E_{p,r2}$ is generally constant; magnitude dependent upon log k_f and E_2^0 relative to E_1^0. If only 1 peak exists, $E_{p,r}$ generally constant but may transition from between E_2^0 and E_1^0 (see Figures 8.15, 8.16, and 8.17)
Peak widths	$W_{1/2}$ vs. log τ	General increase when $E_1^0 = E_2^0$ (see Figure 8.9)	$W_{1/2}$ vs. δE	Small increase in $W_{1/2}$ with δE	$W_{1/2}$ vs. E_{SW}	$W_{1/2}$ increases with E_{SW}

8.4 References

1. Alberts, G.S. and I. Shain. *Anal. Chem.*, **1963**. 35, 1859-1866.

2. Saveant, J.M. and E. Vianello. *Electrochim. Acta*, **1965**. 10, 905-920.

3. Nicholson, R.A. and I. Shain. *Anal. Chem.*, **1965**. 37, 178-190.

4. Hawley, M.D. and S.W. Feldberg. *J. Phys. Chem.*, **1966**. 70, 3459-3464.

5. Mastragostino, M., L. Nadjo, and J.M. Saveant. *Electrochim. Acta*, **1968**. 13, 721–749.

6. Feldberg, S.W. and L. Jeftic. *J. Phys. Chem.*, **1972**. 76, 2439-2446.

7. Amatore, C. and J.M. Saveant. *J. Electroanal. Chem. Interfacial Electrochem.*, **1977**. 85, 27-46.

8. Amatore, C. and J.M. Saveant. *J. Electroanal. Chem. Interfacial Electrochem.*, **1978**. 86, 227-232.

9. Amatore, C. and J.M. Saveant. *J. Electroanal. Chem.*, **1979**. 102, 21-40.

10. O'Dea, J.J., K. Wikiel, and J. Osteryoung. *J. Phys. Chem.*, **1990**. 94, 3628-3636.

11. Miles, A.B. and R.G. Compton. *J. Phys. Chem. B*, **2000**. 104, 5331-5342.

12. Sanecki, P., C. Amatore, and P. Skital. *J. Electroanal. Chem.*, **2003**. 546, 109-121.

13. Komorsky-Lovrić, S. and M. Lovrić. *Anal. Bioanal. Electrochem.*, **2013**. 5, 291-304.

14. Smith, D.E. *Anal. Chem.*, **1963**. 35, 602-609.

15. Herman, H.B. and A.J. Bard. *J. Phys. Chem.*, **1966**. 70, 396-404.

16. Herman, H.B. and A.J. Bard. *J. Electrochem. Soc.*, **1968**. 115, 1028-1033.

17. Prater, K.B. and A.J. Bard. *J. Electrochem. Soc.*, **1970**. 117, 1517-1520.

18. Puglisi, V.J. and A.J. Bard. *J. Electrochem. Soc.*, **1972**. 119, 833-837.

19. Demaille, C., P.R. Unwin, and A.J. Bard. *J. Phys. Chem.*, **1996**. 100, 14137-14143.

20. Nadjo, L. and J.M. Saveant. *J. Electroanal. Chem. Interfac. Electrochem.*, **1971**. 33, 419-451.

21. Evans, D.H. *Chem. Rev.*, **1990**. 90, 739-751.

22. Moinet, C., J.-P. Hurvois, and A. Jutand. *Adv. Org. Synth.*, **2005**. 1, 403-453.

23. Adams, R.N., M.D. Hawley, and S.W. Feldberg. *J. Phys. Chem.*, **1967**. 71, 851-855.

24. Feldberg, S.W. *J. Phys. Chem.*, **1971**. 75, 2377-2380.

25. Nicholson, R.S. and M.L. Olmstead, *Electrochemistry: Calculations, Simulation and Instrumentation,*. **1972**, Marcel Dekker: New York. Ch. 5

26. Helfrick, J.C., Jr. and L.A. Bottomley. *Anal. Chem.*, **2009**. 81, 9041-9047.

27. Helfrick, J.C., Jr., M.A. Mann, and L.A. Bottomley. *Electrochim. Acta*, submitted for publication.

28. Helfrick, J.C., Jr., M.A. Mann, and L.A. Bottomley. *ChemPhysChem*, submitted for publication.

29. Komorsky-Lovrić, Š. and M. Lovrić. *J. Electroanal. Chem.*, **1995**. 384, 115-122.

30. Mirčeski, V. and M. Lovrić. *Electroanalysis*, **1997**. 9, 1283-1287.

31. Mann, M.A. and L.A. Bottomley. *Langmuir*, **2015**. 31, 9511-9520.

32. Mann, M.A., J.C. Helfrick, Jr., and L.A. Bottomley. *Anal. Chem.*, **2014**. 86, 8183-8191.

33. Mann, M.A., J.C. Helfrick, Jr., B. Manzoor, and L.A. Bottomley. *ACS Catalysis*, submitted for publication.

34. Mirčeski, V., Š. Komorsky-Lovrić, and M. Lovrić, *Square Wave Voltammetry: Theory and Application*, *Monographs in Electrochemistry*. **2007**, Springer-Verlag: Berlin.

CHAPTER 9

THE E_qC MECHANISM

9.1 Introduction

Electrode reactions with a chemical reaction occurring after an electron transfer, i.e., the EC mechanism, have been of interest for years.[1-15] When the electron transfer is kinetically controlled, the mechanism is known as the E_qC mechanism. The E_qC mechanism is far less common in the literature, and has been evaluated by cyclic voltammetry[16] and SWV[13, 17-19] Though previous reports have presented methods to identify the E_qC mechanism, it is rarely used by experimentalists. The significance of investigating the E_qC mechanism with CSWV is two-fold: 1) providing experimentalists with a rapid and fluid means for identifying the E_qC mechanism and determining any associated rates, and 2) providing experimentalists with diagnostic criteria to discern between the EC and E_qC mechanisms.

The work presented here investigated the E_qC mechanism using CSWV. The empirical parameters (period, increment, switching potential, and amplitude) were varied, and the trends in peak parameters were analyzed. From these trends, the diagnostic criteria for the E_qC mechanism were elucidated. The effects of the kinetic parameters (both the rate of the electron transfer and the rate of the chemical reaction) as well as the thermodynamics (the equilibrium constant) on peak parameters were also be considered. At the end of this chapter, the diagnostic criteria for the E_qC mechanism will be presented

in addition to a protocol for identifying the mechanism and determining any associated kinetic or thermodynamic values.

9.2 Results and Discussion

9.2.1 Theory

This work examines the E_qC mechanism in which a chemical reaction precedes a kinetically controlled electron transfer, as shown in Equation 9.1.

$$Ox + ne^- \overset{k^0}{\leftrightarrow} Red \underset{k_b}{\overset{k_f}{\rightleftarrows}} Z \tag{9.1}$$

where Ox is the reactant, Red is the product of the electron transfer, Z is the electroinactive product in the reaction following the electron transfer step, k_f is the rate constant for the conversion of Red to Z in s^{-1}, k_b is the rate constant for conversion of Z to Red in s^{-1}, and k^0 is the standard heterogeneous rate constant in cm/s. The forward and reverse chemical reactions have been treated as first order and the electron transfer is diffusion limited. The derivation of an equation that enables calculation of current at each applied potential for this electrode reaction begins with Fick's laws of diffusion. Expressions for the concentrations of Ox and Red as a function of time and distance from the electrode are found using Laplace transformations and application of the appropriate boundary conditions. For a quasireversible electron transfer, the current, potential, and surface concentrations of Ox and Red are related through the Erdey-Gruz and Volmer equation[9, 20]:

$$i(t) = \frac{nFA}{D_{Ox}^{(1-\alpha)/2} D_{Red}^{\alpha/2}} k^0 \exp\left[\left(\frac{-\alpha nF}{RT}\right)\left(E_{app} - E^0\right)\right]\left[\sqrt{D_{Ox}} C_{Ox}(0,t) - \exp\left[\left(\frac{nF}{RT}\right)\left(E_{app} - E^0\right)\right]\sqrt{D_{Red}} C_{Red}(0,t)\right] \quad (9.2)$$

where τ = period (sec), D_{Ox} = diffusion coefficient of Ox (cm^2/sec), and D_{Red} = diffusion coefficient of Red (cm^2/sec). To provide a current that is independent of electrode area and concentration of the electroactive species, the current is made dimensionless by using the following form of Erdey-Gruz and Volmer equation:

$$\Psi(t) = \left[\frac{\sqrt{\pi\tau}}{\sqrt{D_{Ox}} C_{Ox}^*}\right] \frac{k^0}{D_{Ox}^{(1-\alpha)/2} D_{Red}^{\alpha/2}} \exp(-\alpha\varphi)\left[\sqrt{D_{Ox}} C_{Ox}(0,t) - \exp(\varphi)\sqrt{D_{Red}} C_{Red}(0,t)\right] \quad (9.3)$$

where $\varphi = \left[\left(\frac{nF}{RT}\right)\left(E_{applied} - E^0\right)\right]$

Integrals representing the current as a function of time and potential are replaced with summations and solved by using previously established numerical methods. [21] The final equation coded in MATLAB to generate voltammograms for the E_qC mechanism is:

$$\Psi_m = \frac{\sqrt{\pi} - \left(\frac{2}{\pi L}\right)^{1/2}\left(1 + \left(\frac{\varepsilon}{(K+1)}\right)\right)\sum_{i=1}^{i=m-1}\Psi_i S_j - \left(\frac{K\varepsilon}{(K+1)\sqrt{k\tau}}\right)\sum_{i=1}^{i=m-1}\Psi_i R_j}{\frac{1}{\kappa\varepsilon^{-\alpha}\sqrt{\tau}} + \left(\frac{2}{\pi L}\right)^{1/2}\left(1 + \left(\frac{\varepsilon}{(K+1)}\right)\right) + \left(\frac{K\varepsilon}{(K+1)\sqrt{k\tau}}\right)R_1} \quad (9.4)$$

where L = number of subintervals on each potential, K = equilibrium constant for the following chemical reaction and equal to k_f/k_b, Ψ_m = dimensionless current for each time increment with the serial number m, τ = period, k = the sum of the forward and reverse homogeneous first order rate constants for the chemical reaction preceding the electron transfer, *i.e.* $k_f + k_b$.

In the following sections, the results of simulations for the effect of K and $k_f + k_b$ and the variation of empirical parameters for the E_qC mechanism are presented, first holding $\alpha = 0.5$ and $\log k^0 = -3$. Later, the effects of k^0, followed by a description of diagnostic

criteria that can be used to identify a kinetically controlled reaction are presented and comparisons to the EC mechanism are made. This work concludes with protocol for evaluating experimental data.

9.2.2 Effect of $k_f + k_b$ and K

The effect of K on the shape of the voltammogram is shown in Figure 9.1a. As log K increases, $\Delta\Psi^{+}_{p,r}$ decreases, and subsequently, peak ratio decreases. $\Delta\Psi^{+}_{p,f}$ and $E_{p,f}$ are unaffected by K for this particular scenario, and $E_{p,r}$ shifts within the error of the increment used.

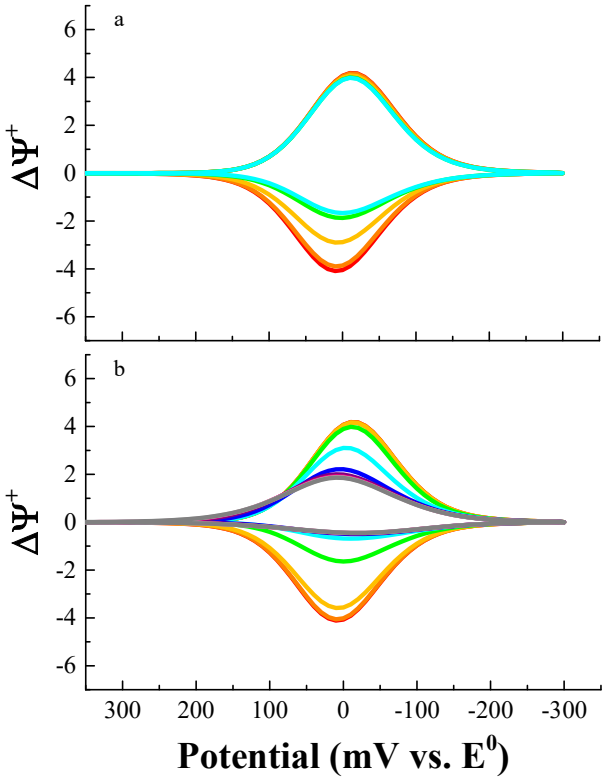

Figure 9.1. The impact of a) K and b) $k_f + k_b$ on the shape of the voltammogram when amplitude = 50 mV, period = 50 ms, E_λ = -300 mV, and increment is 10 mV. In panel a, log K ranges from -2 (red) to 2 (cyan) in steps of 1 when log ($k_f + k_b$) = 0. In panel b, log ($k_f + k_b$) ranges from -3 (red) to 6 (dark gray) in steps of 1 when log K = 6.

The effect of $k_f + k_b$ is presented in Figure 9.1b. As log ($k_f + k_b$) increases, $\Delta\Psi^+_{p,f}$ and $\Delta\Psi^+_{p,r}$ decrease and remains constant. Peak ratio decreases with increasing $k_f + k_b$. $E_{p,f}$ shifts positively with $k_f + k_b$ while $E_{p,r}$ shifts negatively.

Further examination of the effect of K and $k_f + k_b$ on $\Delta\Psi^+_{p,f}$, $\Delta\Psi^+_{p,r}$, and peak ratio are displayed in Figure 9.2. $\Delta\Psi^+_{p,f}$ is unaffected by K when log K ≤ -1 regardless of log ($k_f + k_b$). When log ($k_f + k_b$) > -0.5, K affects the magnitude of $\Delta\Psi^+_{p,f}$. As K and log ($k_f + k_b$) increase, $\Delta\Psi^+_{p,f}$ decreases and plateaus.

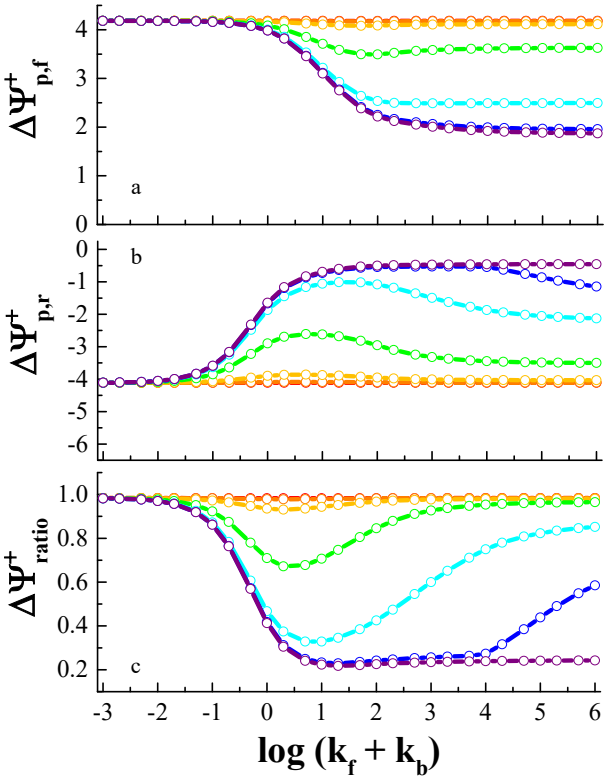

Figure 9.2. The impact of K, k_f, and k_b on a) $\Delta\Psi^+_{p,f}$, b) $\Delta\Psi^+_{p,r}$, and c) peak ratio when amplitude = 50 mV, period = 50 ms, E_λ = -300 mV, and increment = 10 mV. Log K ranges from -3 (red) to 3 (purple) in steps of 1.

Similarly, $\Delta\Psi^{+}_{p,r}$ is also unaffected when log K ≤ -1 regardless of log ($k_f + k_b$). At higher values of K, $\Delta\Psi^{+}_{p,r}$ decreases then increases with log ($k_f + k_b$) whereas $\Delta\Psi^{+}_{p,r}$ decreases then plateaus with log ($k_f + k_b$) when log K = 3. Peak ratio is unaffected by log ($k_f + k_b$) when log K ≤ -1. Peak ratio decreases then increases with log ($k_f + k_b$) when log K > -1 except for log K = 3 where peak ratio decreases then plateaus. The magnitude of the decrease and increase of peak ratio depends on K though log ($k_f + k_b$) value, i.e., log ($k_f + k_b$) = -1, where peak ratio begins to decrease is the same for all K.

The effect of K and $k_f + k_b$ on $E_{p,f}$, $E_{p,r}$, and ΔE_p is shown in Figure 9.3. $E_{p,f}$ is unaffected by K when log ($k_f + k_b$) ≤ 0. As log ($k_f + k_b$) increases, $E_{p,f}$ shifts positively then remains constant for log K > -1. $E_{p,r}$ behaves in a similar manner though the shift positive is much greater than that for $E_{p,f}$ when log K ≤ 0. At higher K values, $E_{p,r}$ shifts negatively with log ($k_f + k_b$) before shifting positively. This results from the chemical reaction rate increasing and becoming competitive with the electron transfer rate. As log ($k_f + k_b$) increases, the voltammogram appears like a typical EC mechanism with a reverse peak directly in line with the forward peak. At high values of log ($k_f + k_b$), i.e., when the electron transfer is the limiting step, a second reverse peak appears, and becomes the larger reverse peak. This is characteristic of a quasireversible mechanism.[22] Subsequently, ΔE_p changes with log ($k_f + k_b$) as a result of the shift by both peak potentials. ΔE_p is essentially constant when log K < 1. At higher values of log K, ΔE_p values become negative then positive with log ($k_f + k_b$) as the reverse peak shifts about the potential axis. For log K = 3, ΔE_p transitions from positive to negative values and then plateaus. Thus, K, k_f, and k_b greatly affect peak potentials for the E_qC mechanism.

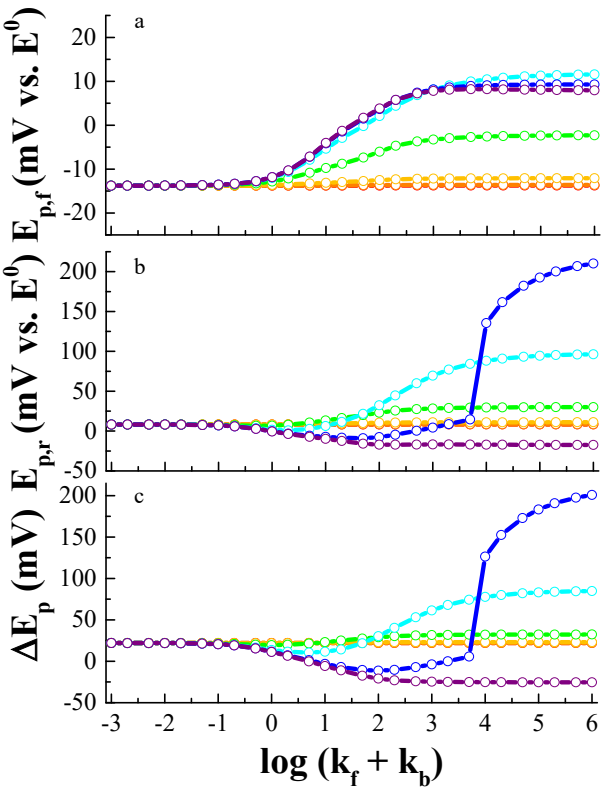

Figure 9.3. The impact of K, k_f, and k_b on a) $E_{p,f}$, b) $E_{p,r}$, and c) peak separation when amplitude = 50 mV, period = 50 ms, E_λ = -300 mV, and increment = 10 mV. Log K ranges from -3 (red) to 3 (purple) in steps of 1.

Peak width as it relates to $k_f + k_b$ and K is shown in Figure 9.4. $W_{1/2,\,f}$ is invariant for all $k_f + k_b$ values when log K ≤ -1. When log K > -1 and when log ($k_f + k_b$) > 1, $W_{1/2,\,f}$ increases with log ($k_f + k_b$) and then plateaus. The magnitude is of the increase is proportional to K though the same for log K > 1. Similarly, $W_{1/2,\,r}$ is invariant for all $k_f + k_b$ values when log K ≤ -1. When log K > -1, and when log ($k_f + k_b$) > 0, $W_{1/2,\,r}$ increases then decreases with log ($k_f + k_b$) though the magnitude is dependent on K. Again, the exception is for log K = 3 where $W_{1/2,r}$ increases with log ($k_f + k_b$). The reverse peak width is also evidence in the change in voltammogram shape that occurs with increasing $k_f + k_b$ and K. At high values of log K, i.e., log K > 0, $W_{1/2,r} > W_{1/2,f}$. This is again a

result of the reverse peak diminishing then transitioning into two reverse peaks as a result of the quasireversibility of the electron transfer. Thus, peak width is affected by K and $k_f + k_b$ and can indicative of a sluggish electron transfer rates.

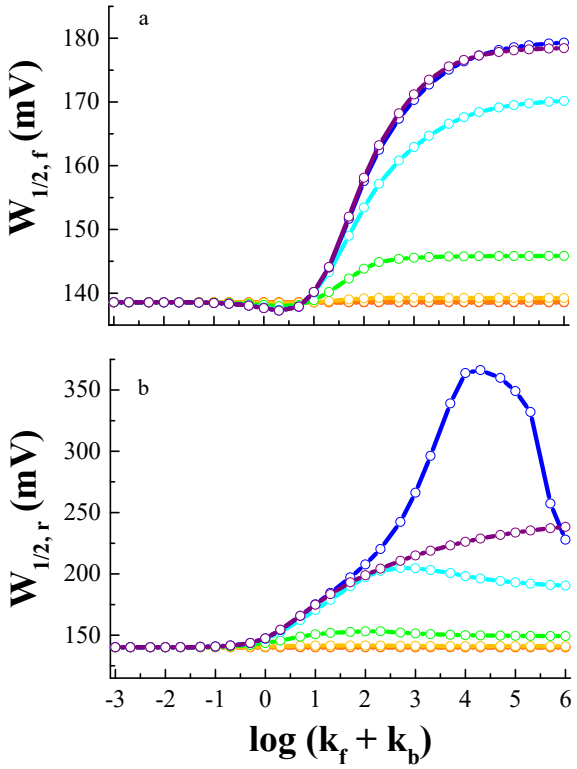

Figure 9.4. The impact of K, k_f, and k_b on a) $W_{1/2,f}$ and b) $W_{1/2,r}$ when amplitude = 50 mV, period = 50 ms, E_λ = -300 mV, and increment = 10 mV. Log K ranges from -3 (red) to 3 (purple) in steps of 1.

When comparing the effects of $k_f + k_b$ and K on the EC and E_qC mechanisms, several observations can be made. In general, peak currents are smaller for the E_qC case than for the EC. For the EC case, peak currents and peak ratio decrease and increase when log ($k_f + k_b$) when log K > -1. For the E_qC case over the same region of K, $\Delta\Psi^+_{p,f}$ decreases then plateaus with $k_f + k_b$ whereas $\Delta\Psi^+_{p,r}$ and peak ratio decreases then increases with the exception of log K = 3 which decreases and plateaus for both peak parameters. When log

$K > -1$ and $\log (k_f + k_b) > 0$, $E_{p,f}$ shifts positively with $k_f + k_b$ for both mechanisms though the magnitude of the shift is much greater for the EC case. Under the same kinetic conditions, $E_{p,r}$ shifts positively for both cases though moreso for the E_qC case for og $K < 3$. The trends in $E_{p,r}$ differ greatly when $\log K = 3$; $E_{p,r}$ shifts positively for the EC case and negatively with a plateau for the E_qC case. As a result, peak separation when $\log K > -1$ and $\log (k_f + k_b) > 0$ is larger and positive for the E_qC case and smaller and negative the EC case with the exceptions being the negative components in the trends for $\log K > 0$ for the E_qC case. Peak widths also differ between the two cases. Both mechanisms have peak widths that are invariant with $k_f + k_b$ when $\log K < 0$; however, the magnitudes are different. At higher values of K and $k_f + k_b$, $W_{1/2,f}$ decrease then increases with $k_f + k_b$ for the EC case and changing by no more than ~13 mV. In contrast, $W_{1/2,\,f}$ increases then plateaus with $k_f + k_b$ and K up to ~40 mV. Similarly, $W_{1/2,\,r}$ increases then decreases with $k_f + k_b$ for the EC mechanism by ~11 mV whereas it increases, then decreases and plateaus with $k_f + k_b$ for the E_qC case. The change in $W_{1/2,r}$ may be as large as 200 mV for the E_qC case and only increases with $\log (k_f + k_b)$ for $\log K = 3$. Thus, $k_f + k_b$ and K greatly impact peak shape for the E_qC mechanism in a manner different from the EC case and will be further investigated as a function of empirical parameters below.

9.2.3 Effect of Period (τ)

The length of the period greatly affects peak shape, and the variation of period provides insight into each electrode reaction mechanism. Figure 9.5 shows the effect of period on the E_qC mechanism when $k_f + k_b$ and K are held constant. $E_{p,f}$ shifts positively while $E_{p,r}$ shifts negatively with increasing period (see Figure 9.5b). $\Delta\Psi^{+}_{p,f}$ and $\Delta\Psi^{+}_{p,r}$ are

both linearly related to period$^{-1/2}$ (see figure 9.5c). Lastly, peak ratio decreases from 1.0 to 0.2 as period increases (see Figure 9.5d).

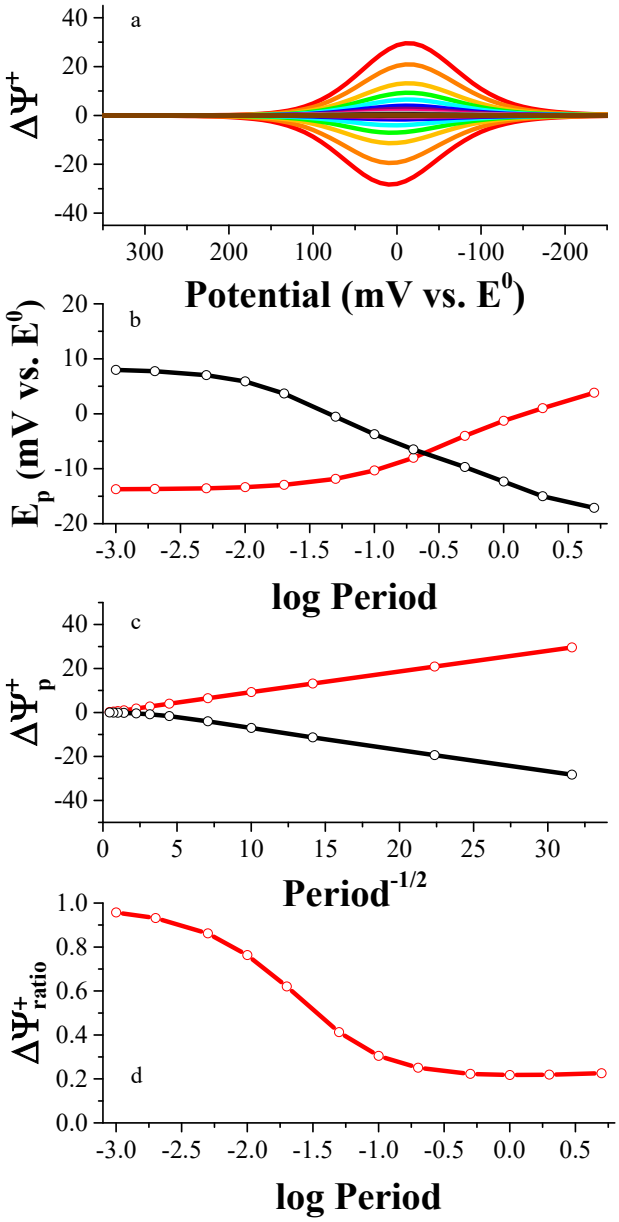

Figure 9.5. The impact of period on the shape of the voltammogram when amplitude = 50 mV, increment = 10 mV, E_λ = -300 mV, log K = 3, and log ($k_f + k_b$) = 0. Panel a): Period ranges from 1 ms (red) to 5 s (brown). Panel b): $E_{p,f}$ (red) and $E_{p,r}$ (black). Panel c): $\Delta\Psi^+_{p,f}$ (red) and $\Delta\Psi^+_{p,r}$ (black). Panel d): Peak ratio (red).

Figure 9.6 shows the relationship between peak ratio and K as a function of period for a specific value of log ($k_f + k_b$). Peak ratio is at or near unity when log K ≤ -1. Peak ratio decreases then increases for log K = 0 and 1 with increasing period. For log K > 1, peak ratio decreases then remains constant with increasing period.

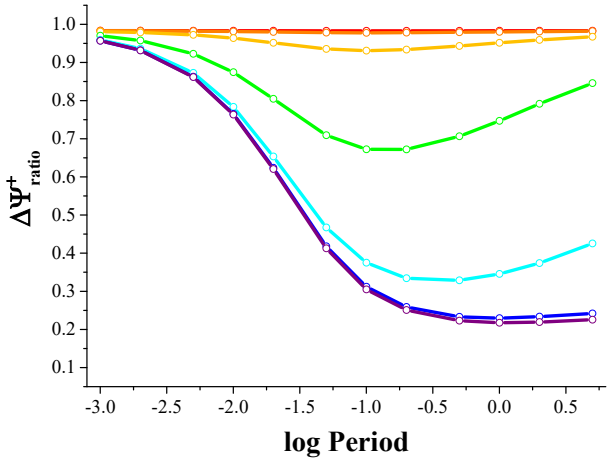

Figure 9.6. The impact of period on the peak ratio as log K is varied from -3 (red) to 3 (purple) when amplitude = 50 mV, increment = 10 mV, E_λ = -300 mV, and log ($k_f + k_b$) = 0.

A more detailed investigation of peak ratio, $k_f + k_b$, K, and period is presented in Figure 9.7. For log K ≥ 4 (panels a-c) and log ($k_f + k_b$) ≤ 1, peak ratio decreases with increasing period. For log ($k_f + k_b$) > 1, peak ratio is essentially invariant with period at ~0.2. When 3 ≤ log K ≤ 4, there are reverse small peaks located several hundred mV positive of E^0 at long periods and very fast $k_f + k_b$ values. The larger of the two reverse peaks is always used to peak ratio. For log K = 3 (panel d), peak ratio decreases with period for log ($k_f + k_b$) ≤ 1, is constant for 2 ≤ log ($k_f + k_b$) ≤ 4, and increases with period for log ($k_f + k_b$) > 4. Like higher K values, peak ratio decreases with period for log K = 2 (panel e) and log ($k_f + k_b$) ≤ 1 though it is constant for log ($k_f + k_b$) = 2 and increases for higher values of log ($k_f + k_b$). It should be noted that a shoulder exists on the reverse

peak when log K = 2. Similar trends occur for $0 \leq \log K \leq 1$ (panels f & g) though trends for $0 \leq \log (k_f + k_b) \leq 1$ may increase at long periods though only one peak exists on the reverse sweep. Peak ratio is ≥ 0.9 for log K = -1 (panel h). Thus, the effect of period on peak ratio is an indicator of an E_qC mechanism.

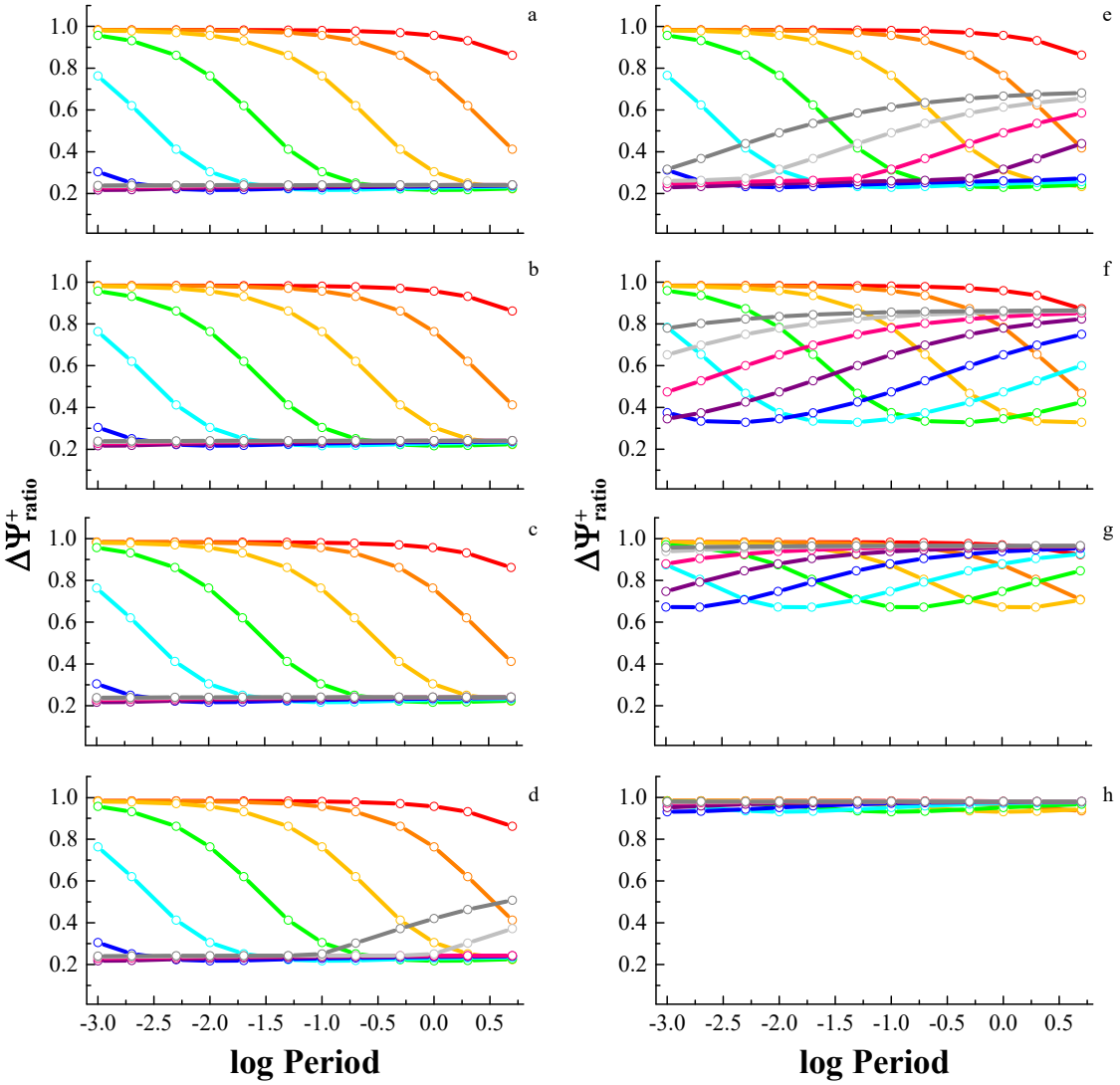

Figure 9.7. The impact of period on peak ratio over the log $(k_f + k_b)$ range -3 (red) to 6 (dark gray) for log K = 6 (panel a) to -1 (panel h) when amplitude = 50 mV, E_λ = -300 mV, and increment = 10 mV.

Figure 9.8 shows the relationship between $\Delta\Psi^{+}_{p,f}$ and $\Delta\Psi^{+}_{p,r}$ and period$^{-1/2}$. $\Delta\Psi^{+}_{p,f}$ is linearly related to period$^{-1/2}$ when log $(k_f + k_b) \leq 1$ and ≥ 4. Intermediate values are curvilinearly related to period$^{-1/2}$. Conversely, $\Delta\Psi^{+}_{p,r}$ is linearly related to period$^{-1/2}$ when log $(k_f + k_b) \leq -1$ and ≥ 4. Again, intermediate values are curvilinearly related to period$^{-1/2}$ though the bowing in the trend may occur at long periods.

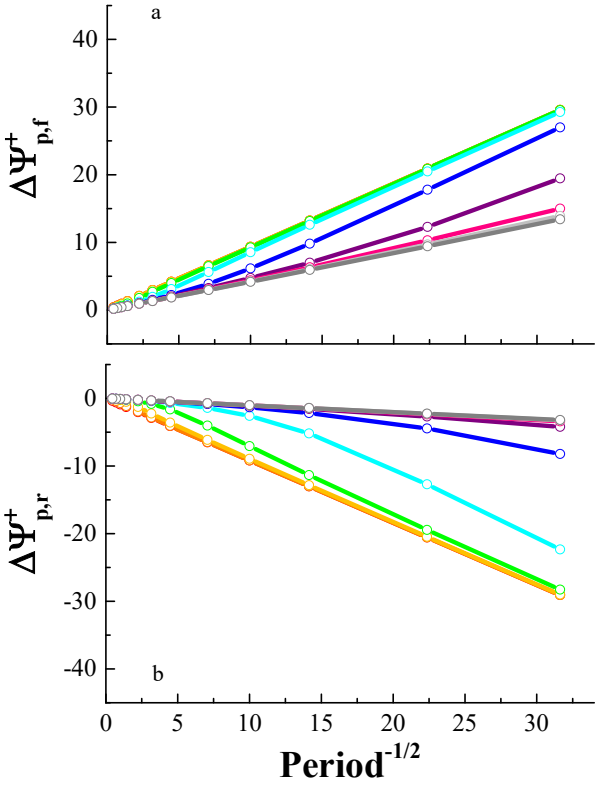

Figure 9.8. The impact of period on $\Delta\Psi^{+}_{p,f}$ and $\Delta\Psi^{+}_{p,r}$ when amplitude = 50 mV, increment = 10 mV, E_λ = -300 mV, log K = 6, and log $(k_f + k_b)$ ranges from -3 (red) to 6 (dark gray).

The relationship between $E_{p,f}$, $k_f + k_b$, K, and period is shown in Figure 9.9. Regardless of K and $k_f + k_b$, $E_{p,f}$ is within ± 20 mV of E^0. For log K ≥ 1, $E_{p,f}$ shifts positively by a 20 mV (twice the value of the increment) when $0 \leq \log (k_f + k_b) \leq 2$. $E_{p,f}$

does shift slightly for log ($k_f + k_b$) = -1 and 3 though it is within the error of the increment. Otherwise, $E_{p,f}$ is invariant with period. When log K < 2, $E_{p,f}$ behaves similarly to higher values of K; however, the magnitude of the $E_{p,f}$ shift is nearly the of the increment. When log K = -1, $E_{p,f}$ is invariant with period regardless of log ($k_f + k_b$).

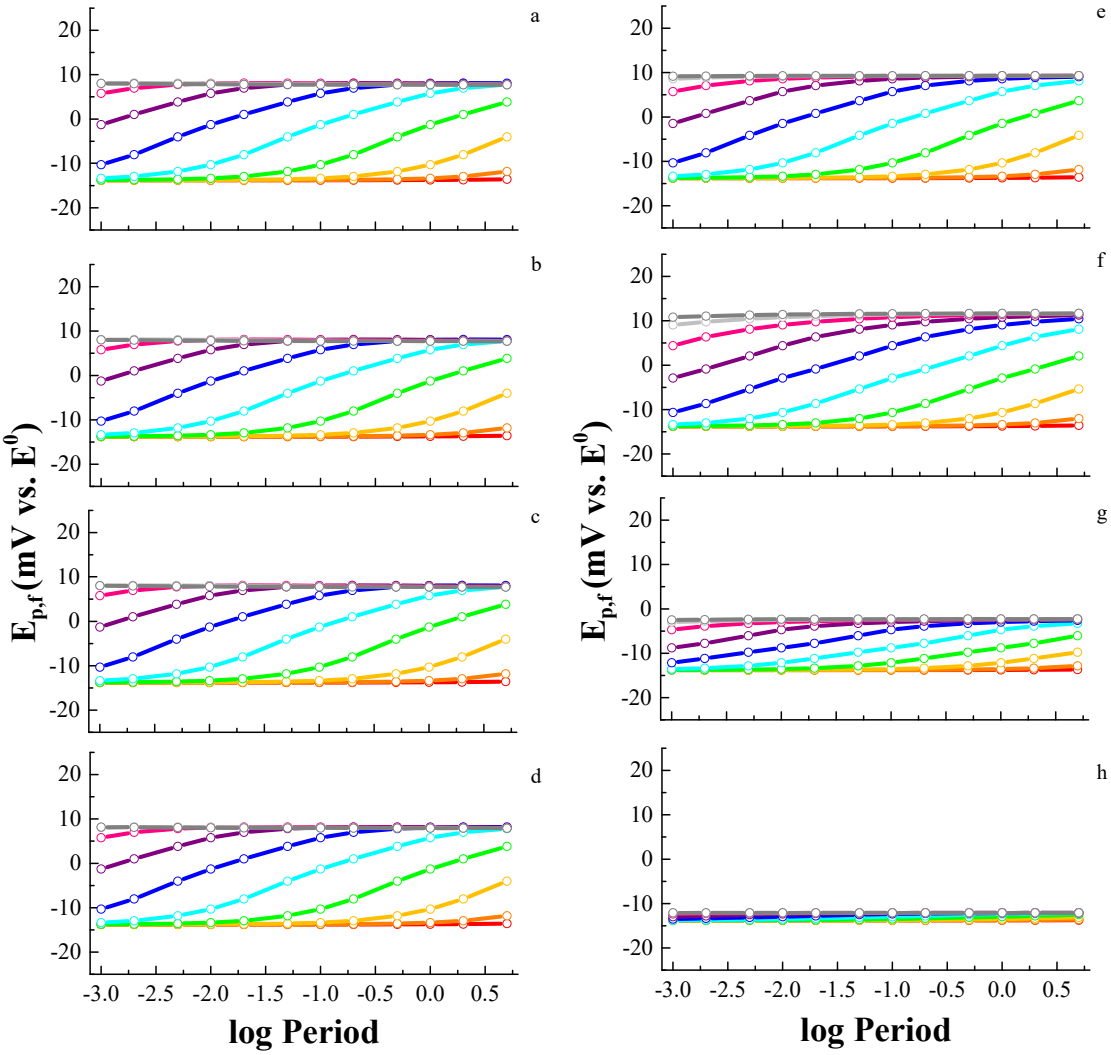

Figure 9.9. The impact of period on $E_{p,f}$ over the log ($k_f + k_b$) range -3 (red) to 6 (dark gray) for log K = 6 (panel a) to -1 (panel h) when amplitude = 50 mV, E_λ = -300 mV, and increment = 10 mV.

Figure 9.10 displays the relationship between $E_{p,r}$, $k_f + k_b$, K, and period. $E_{p,r}$ shifts negatively with period for log $K \geq 4$ and $-1 \leq \log (k_f + k_b) \leq 2$ (panels a-c). When $\log (k_f + k_b) < -1$ and when $\log (k_f + k_b) > 2$, $E_{p,r}$ either does not shift or does not shift by an amount greater than the increment. Similar trends hold for log K = 3 (panel d) except for $\log (k_f + k_b) \geq 5$ as a significant jump occurs as a second, larger peak emerges.

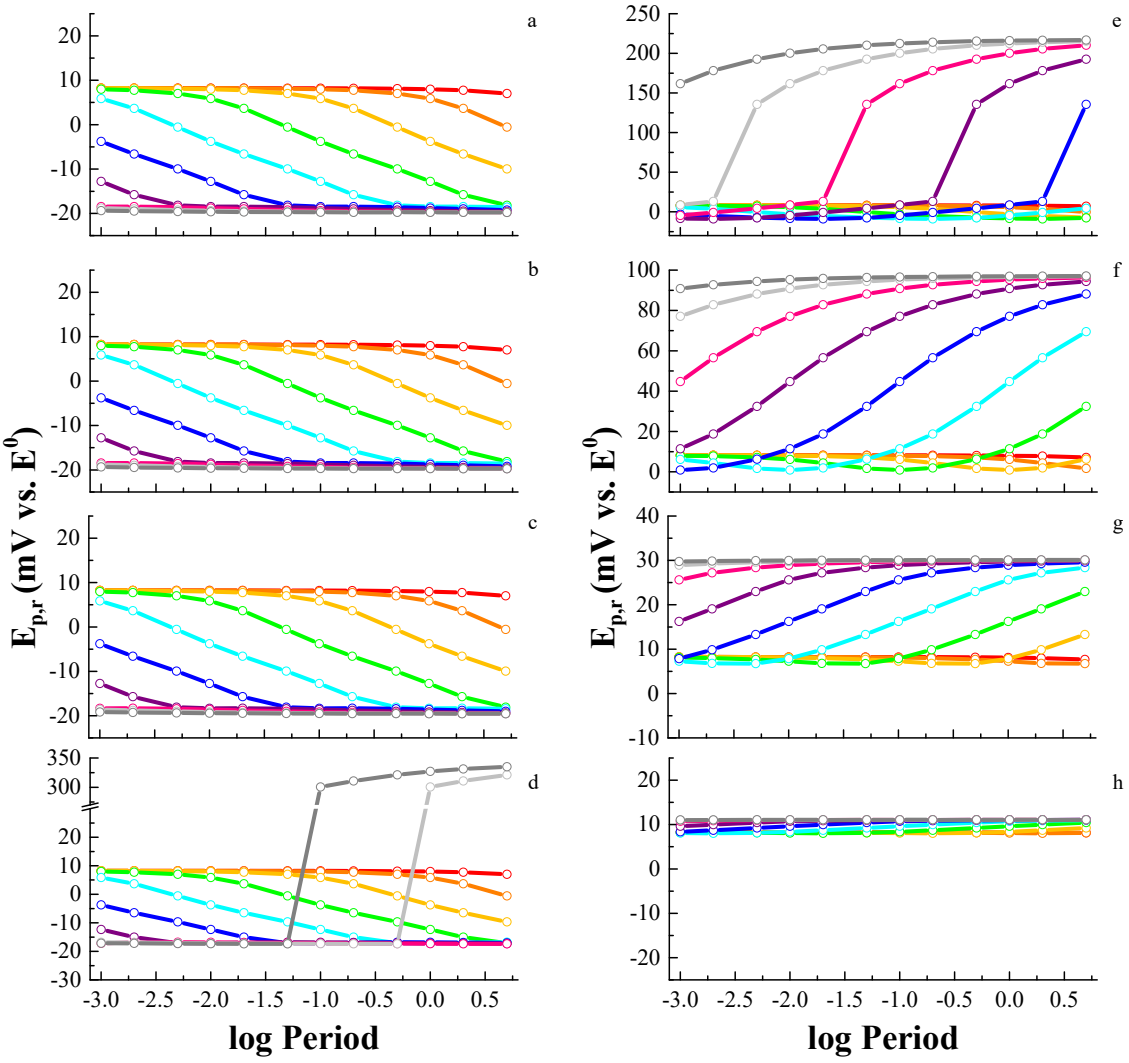

Figure 9.10. The impact of period on $E_{p,r}$ over the log $(k_f + k_b)$ range -3 (red) to 6 (dark gray) for log K = 6 (panel a) to -1 (panel h) when amplitude = 50 mV, E_λ = -300 mV, and increment = 10 mV.

When log K = 2 (panel e), $E_{p,r}$ is within 10 mV of E^0 for log $(k_f + k_b) \leq 1$. At higher values of log $(k_f + k_b)$ and with increasing period, $E_{p,r}$ jumps to values significantly displaced from E^0. This is again the result of a second peak emerging on the reverse sweep. When log K = 1 (panel f), $E_{p,r}$ shifts positively for log $(k_f + k_b) \geq 0$. The magnitude of the shift and the displacement from E^0 is determined by $k_f + k_b$. For log $(k_f + k_b) < 0$, $E_{p,r}$ remains constant with period. For log K = 0 (panel g), $E_{p,r}$ shifts positively with period for $0 \leq$ log $(k_f + k_b) \leq 3$ and is otherwise invariant with period. For log K = -1 (panel h), $E_{p,r}$ is invariant with period.

When comparing the effects of period on the EC and E_qC mechanisms, several differences can be identified. At extreme values of K, i.e. log K > 4 and when log $K \leq 0$, peak ratio for the EC and E_qC mechanisms is essentially identical for all $k_f + k_b$. At intermediate values of K, i.e., when $2 \leq$ log $K \leq 4$, trends are identical for the two mechanisms when log $(k_f + k_b) \leq 1$ and differ for higher values; the value of log $(k_f + k_b)$ where the two mechanisms depend on K. When log K = 1, and log $(k_f + k_b) < 3$, peak ratios are identical for the two mechanisms. However, when log $(k_f + k_b) \geq 3$, the magnitudes of the two peak ratio trends differ though the traces are similar in shape. Peak currents are similar in their relationship to period$^{-1/2}$, but the magnitude of the currents for the E_qC case are lower than that for the EC case.

$E_{p,f}$ trends differ drastically between the EC and E_qC cases even though $E_{p,f}$ shifts positively with log period for both cases. At large K values, i.e., log $K \geq 4$, $E_{p,f}$ shifts 30 mV/decade when log $(k_f + k_b) \geq 0$ with log period for the EC case whereas $E_{p,f}$ values for the E_qC case do not even shift by 30 mV for any value of K or $k_f + k_b$. Furthermore, the

beginning potentials prior to the shift for each mechanism are not the same; $E_{p,f}$ values for log $(k_f + k_b) > 1$ are located positive of E^0 for the EC case whereas the $E_{p,f}$ values for the E_qC case are located within ± 15 mV of E^0. The same trend holds true for intermediate K values, i.e., $2 \leq \log K \leq 4$ though the trends change slope for the EC mechanism. When log K = 1, and log $(k_f + k_b) \geq 0$, $E_{p,f}$ shifts by differing amounts for the two cases – more for the EC case than the E_qC case. At low values of K, i.e., log K ≤ 0, $E_{p,f}$ shifts by 15 mV of E^0 for both cases and is located within ± 15 mV of E^0. Thus, $E_{p,f}$ is indistinguishable for these cases for this low range in K.

Trends in $E_{p,r}$ are also drastically different between the two mechanisms. When log K ≥ 4 and log $(k_f + k_b) \geq 0$, $E_{p,r}$ shifts positively by 30 mV/decade with log period for the EC case whereas log $(k_f + k_b) = 1$ and 2 give rise to $E_{p,r}$ shifting negatively by 30 mV with period for the E_qC case. Similar trends hold true for log K = 3 though there is a significant jump in potentials for the E_qC mechanism when log $(k_f + k_b) \geq 5$. When log K = 2, trends are drastically different as $E_{p,r}$ jumps largely positive for the E_qC case for fast rates and shifts less so for the EC case. When log K = 1, trends for each $k_f + k_b$ value are similar for each case the but the magnitude of the shift is greater and potentials are located more positively of E^0 for the E_qC mechanism. When log K < 1, peak potentials shift positively for both mechanisms, and the trends for each mechanism are within the error of the increment of each other. Thus, trends in peak potential with period may be used to identify the EC versus the E_qC mechanism.

9.2.4 Effect of Increment (δE)

The effect of increment on the E_qC mechanism is shown in Figure 9.11. $E_{p,f}$ shifts negatively with increment while $E_{p,r}$ is essentially constant (see Figure 9.11b). Both

$\Delta\Psi^{+}_{p,f}$ and $\Delta\Psi^{+}_{p,r}$ increase with increment though more so for $\Delta\Psi^{+}_{p,r}$ (see Figure 9.11c).

Subsequently, peak ratio increases from 0.2 to 0.6 with increment (see Figure 9.11d).

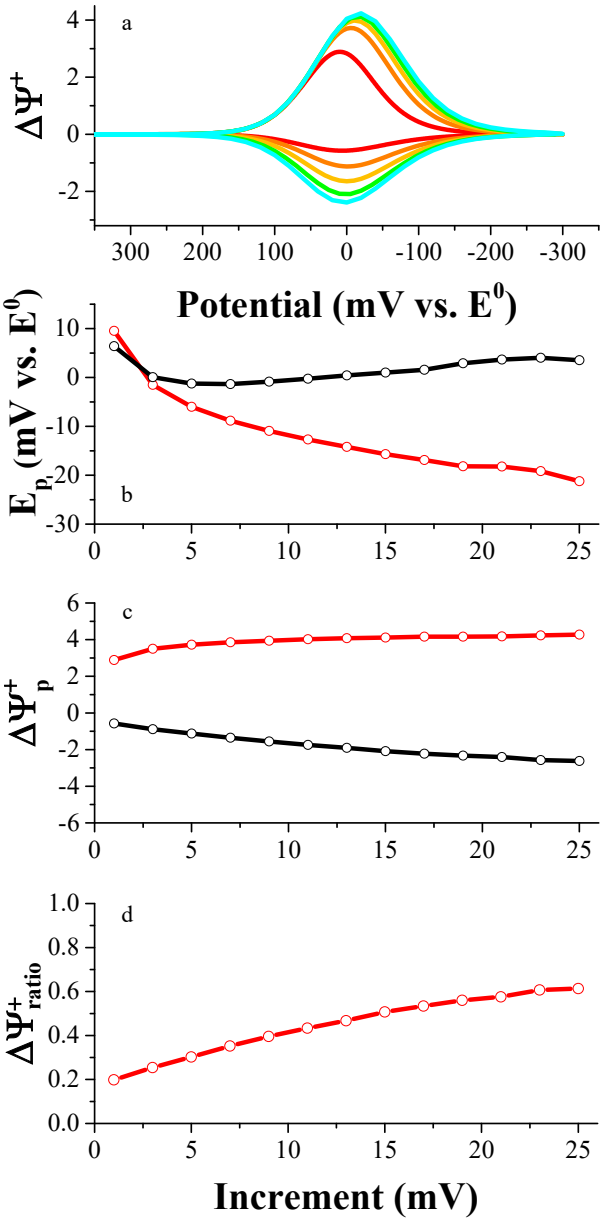

Figure 9.11. The impact of increment on the shape of the voltammogram when amplitude = 50 mV, period = 50 ms, E_λ = -300 mV, log K = 3, and log ($k_f + k_b$) = 0. Panel a): Increment ranges from 1 mV (red), 5 mV (orange), 10 mV (yellow), 15 mV (green), and 20 mV (cyan). Panel b): $E_{p,f}$ (red) and $E_{p,r}$ (black). Panel c): $\Delta\Psi^{+}_{p,f}$ (red) and $\Delta\Psi^{+}_{p,r}$ (black). Panel d): Peak ratio (red).

The relationship between K, peak ratio, and increment is shown in Figure 9.12. Peak ratio is near or at unity for log K ≤ -1. As K increases, peak ratio increases with increment though the magnitude is dependent on K.

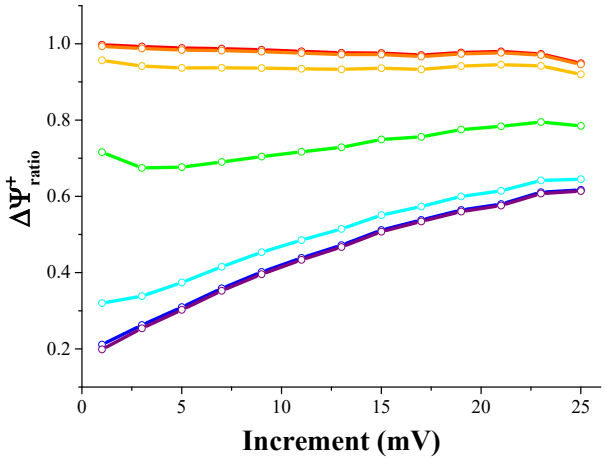

Figure 9.12. The impact of increment on the peak ratio as log K is varied from -3 (red) to 3 (purple) in steps of 1 when amplitude = 50 mV, period = 50 ms, E_λ = -300 mV, and log ($k_f + k_b$) = 0.

A more detailed investigation of K, peak ratio, and increment is presented in Figure 9.13. When log K ≥ 3, and log ($k_f + k_b$) = -3, the trend for peak ratio vs. increment mirrors that for a reversible reaction. When -2 ≤ log ($k_f + k_b$) ≤ 0, peak ratio increases with increment. When log ($k_f + k_b$) > 0, peak ratio remains constant at unity and independent of increment with the exception for log K = 3 and log ($k_f + k_b$) = 6. When 0 ≤ log K ≤ 2, the same trends for log ($k_f + k_b$) ≤ 0 are true. However, when log ($k_f + k_b$) > 0, peak ratio decreases with increment; the magnitude of the decrease is dependent on log ($k_f + k_b$). Readers are reminded that the reverse peak is the larger of the two peaks for log K = 3 and log K = 2. When log K = -1, peak ratio is invariant with increment and remains at unity. Thus, peak ratio may be useful in identifying the E_qC mechanism.

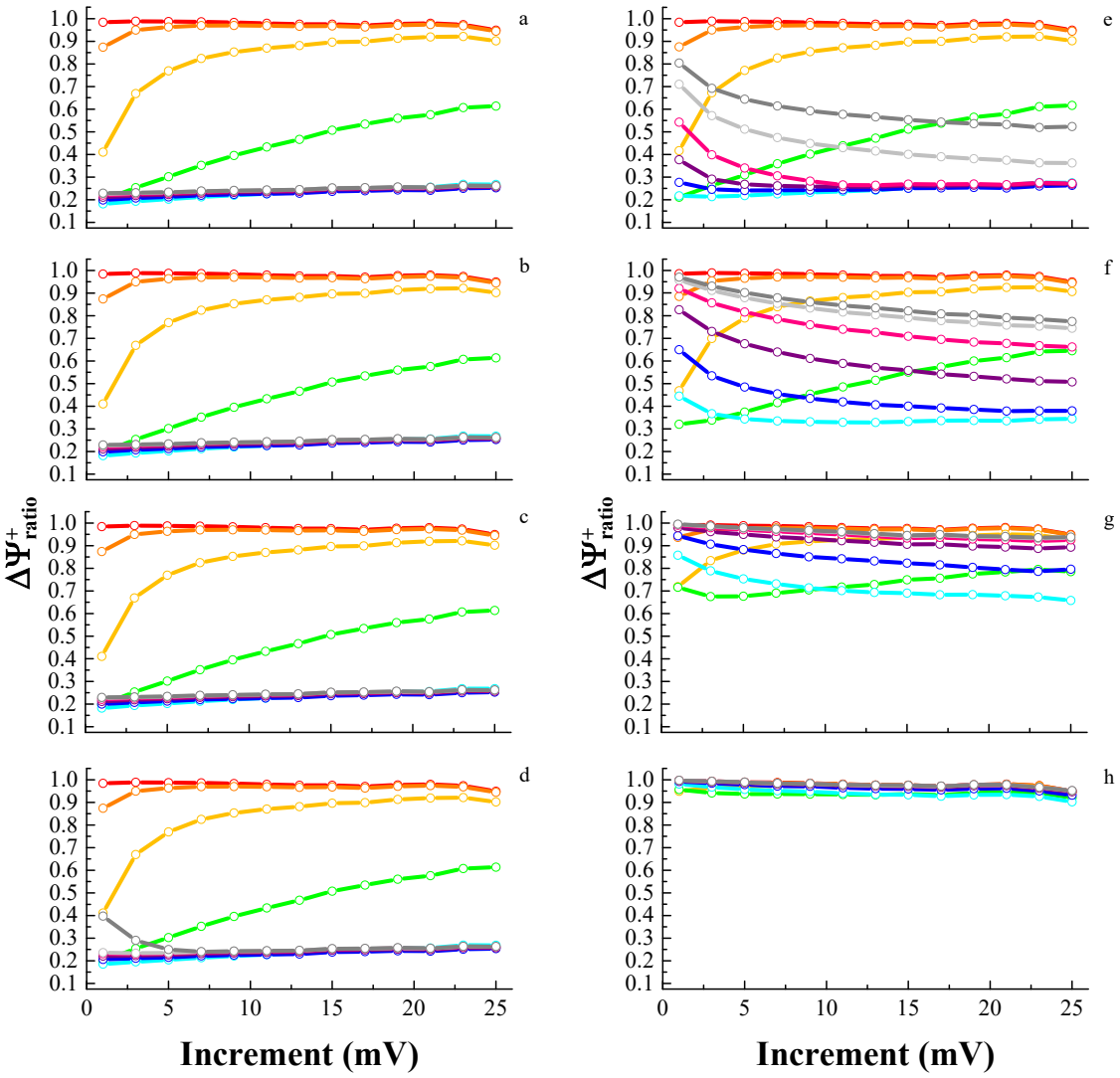

Figure 9.13. The impact of increment on peak ratio over the log ($k_f + k_b$) range -3 (red) to 6 (dark gray) for log K = 6 (panel a) to -1 (panel h) when amplitude = 50 mV, E_λ = -300 mV, and period = 50 ms.

Trends in peak ratio can be understood by evaluating peak currents. The relationship between peak current and increment is shown in Figure 9.14. $\Delta\Psi^+_{p,f}$ increases with increment for log ($k_f + k_b$) ≥ 0 whereas $\Delta\Psi^+_{p,r}$ increases with increment for log ($k_f + k_b$) ≥ -1. For both cases, current is invariant with increment below these thresholds in $k_f + k_b$.

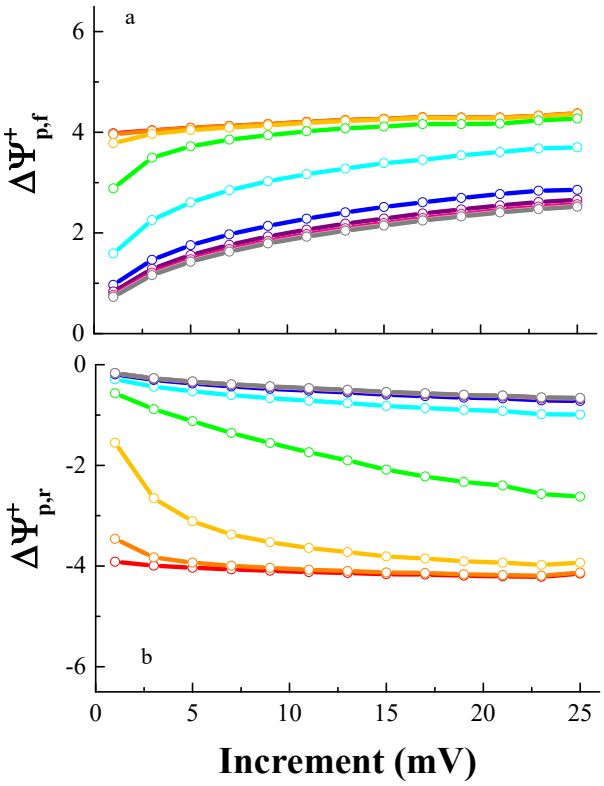

Figure 9.14. The impact of increment on $\Delta\Psi^{+}_{p,f}$ and $\Delta\Psi^{+}_{p,r}$ when amplitude = 50 mV, period = 50 ms, E_λ = -300 mV, log K = 6, and log ($k_f + k_b$) ranges from -3 (red) to 6 (dark gray).

The effect of increment on $E_{p,f}$ is shown in Figure 9.15. $E_{p,f}$ shifts negatively with increment though the offset from E^0 is dependent on K and $k_f + k_b$. $E_{p,f}$ may shift between 15 and 60 mV. A complex relationship exists between $E_{p,r}$, $k_f + k_b$, and K as shown in Figure 9.16. When log K ≥ 4 (panels a-c), $E_{p,r}$ shifts slightly positive for log ($k_f + k_b$) < 1 and shifts negatively for log ($k_f + k_b$) ≥ 1. The trends for log K = 3 (panel d) are similar to higher K values except at small increments for log ($k_f + k_b$) = 6. The trends in $E_{p,r}$ for log K = 2 (panel e) shift positively with increment for log ($k_f + k_b$) < 1 and shift negatively with increment for log ($k_f + k_b$) = 2 and 3. The trend for log ($k_f + k_b$) = 4 jumps in potential as the small positive reverse peak becomes the larger dominate peak

closer to E^0. When log ($k_f + k_b$) ≥ 5, $E_{p,r}$ shifts positively with increment. When log K = 1 and 0 (panels f & g), $E_{p,r}$ shifts positively with increasing when log ($k_f + k_b$) < 0 and > 3. Otherwise, $E_{p,r}$ shifts negatively with increment. The location of $E_{p,r}$ relative to E^0 depends on K and $k_f + k_b$. When log K = -1 (panel h), shifts positively by ~10 mV. Thus, the variation of increment can be used to identify an E_qC mechanism.

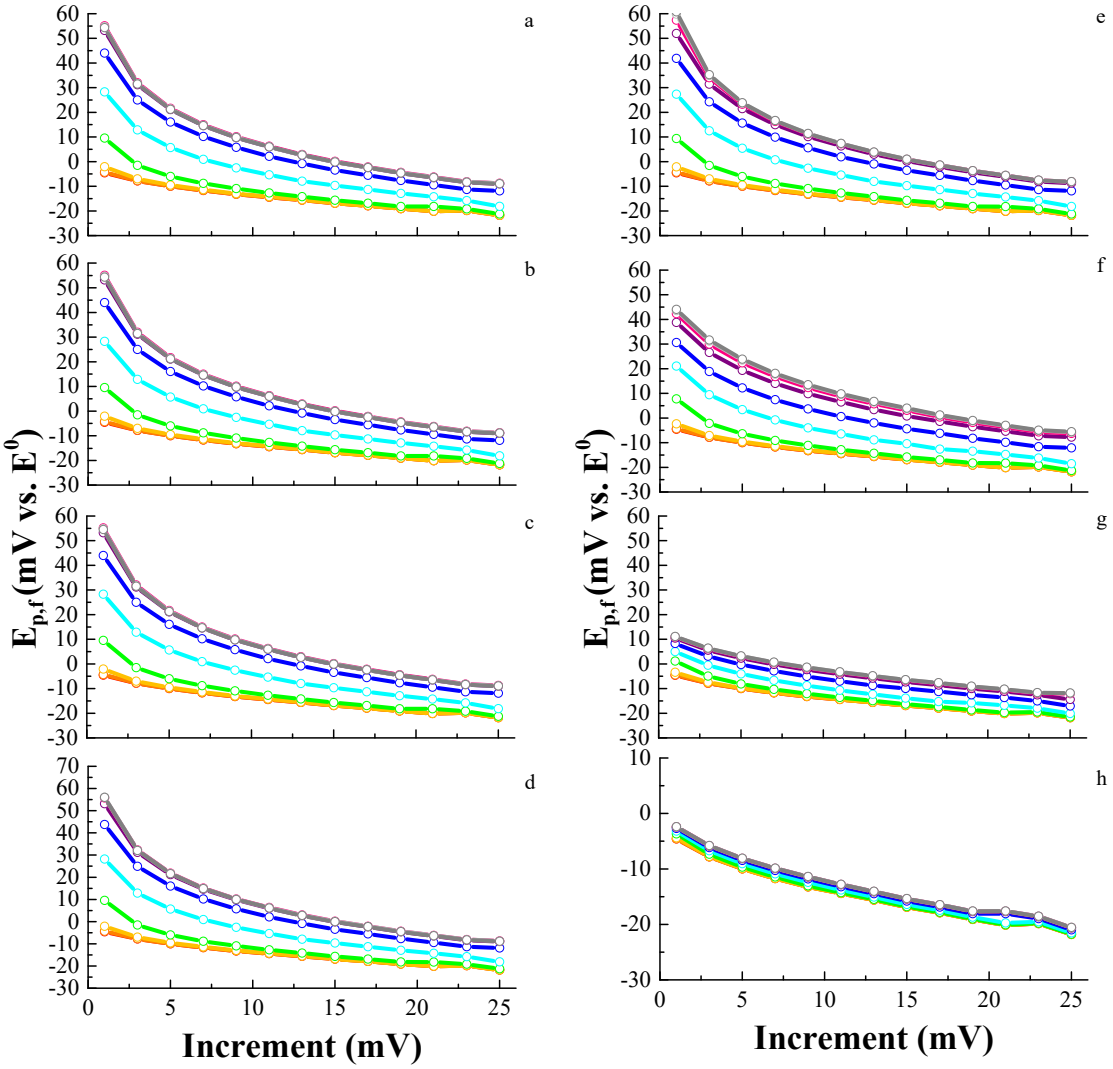

Figure 9.15. The impact of increment on $E_{p,f}$ over the log ($k_f + k_b$) range -3 (red) to 6 (dark gray) for log K = 6 (panel a) to -1 (panel h) when amplitude = 50 mV, E_λ = -300 mV, and period = 50 ms.

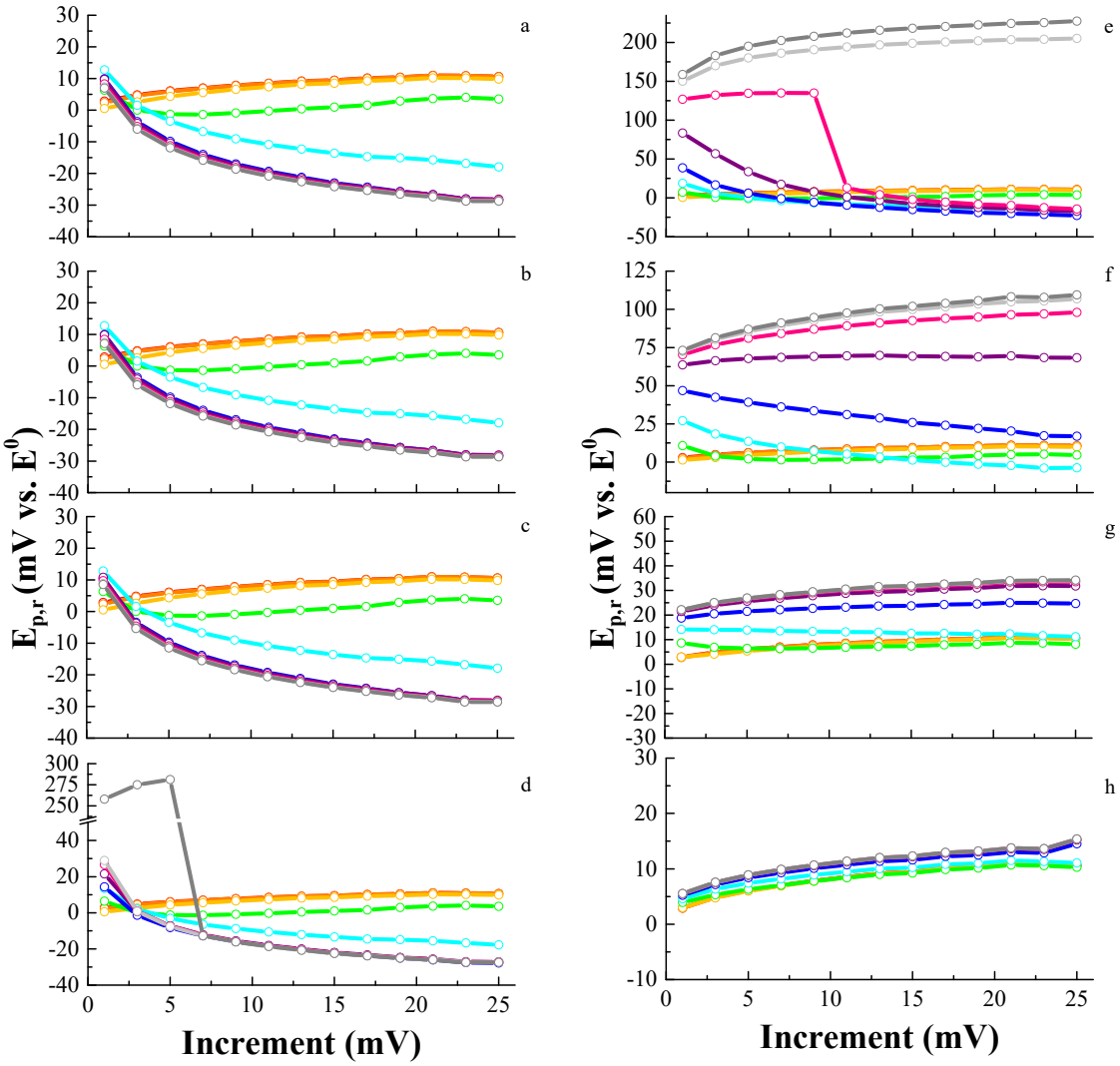

Figure 9.16. The impact of increment on $E_{p,r}$ over the log ($k_f + k_b$) range -3 (red) to 6 (dark gray) for log K = 6 (panel a) to -1 (panel h) when amplitude = 50 mV, E_λ = -300 mV, and period = 50 ms.

Comparing trends in increment for the EC and E_qC mechanism leads to several differences. Peak ratio trends with increment are essentially identical for the EC and E_qC cases. Trends in peak ratio may be discernable for the two mechanisms when $1 \leq \log K \leq 3$ and fast rates. Peak currents are smaller for the E_qC mechanism than for the EC case though they have the same relationship with period$^{-1/2}$ for both cases. $E_{p,f}$ may shift

negatively with increment for both mechanisms though the magnitude of the shift and the position relative to E^0 differs between the two for all values of K. For instance, when log $K \geq 5$, $E_{p,f}$ may be as far as 200 mV positive of E^0 for the EC case whereas it does not exceed 60 mV positive of E^0 for the E_qC case. $E_{p,r}$ trends are drastically different between the two mechanisms for all values of K both in magnitude and displacement from E^0. Thus, increment can be used as a means to differentiate between the two mechanisms.

9.2.5 Effect of Switching Potential (E_λ)

Switching potential provides great insight into chemically coupled mechanisms. The effect of switching potential on the E_qC mechanism is shown in Figure 9.17. As the switching potential approaches E^0, $E_{p,f}$ does not vary while $E_{p,r}$ varies within the error of the increment (see Figure 9.17b). $\Delta\Psi^+_{p,f}$ is invariant while $\Delta\Psi^+_{p,r}$ increases as switching potential approaches E^0 (see Figure 9.17c). Consequently, peak ratio increases as the switching potential approaches E^0 (see Figure 9.17d).

Switching potential affects peak ratio and is a function of K as shown in Figure 9.18. Peak ratio is unaffected and remains at or near unity when log $K < 0$. For greater values of K, peak ratio increases as E_λ approaches E^0. The magnitude of the increase depends on K. Further investigation of the relationship between peak ratio and switching potential as a function of K and $k_f + k_b$ is shown in Figure 9.19. When log $K \geq 3$, peak ratio is constant at unity for log $(k_f + k_b) < -1$ while peak ratio increases as switching potential approaches E^0 for log $(k_f + k_b) \geq -1$. The magnitude and the increase of peak ratio depends on log $(k_f + k_b)$. The only exception is for log $K = 3$ and log $(k_f + k_b) = 6$ where peak ratio decreases then increases as E_λ approaches E^0.

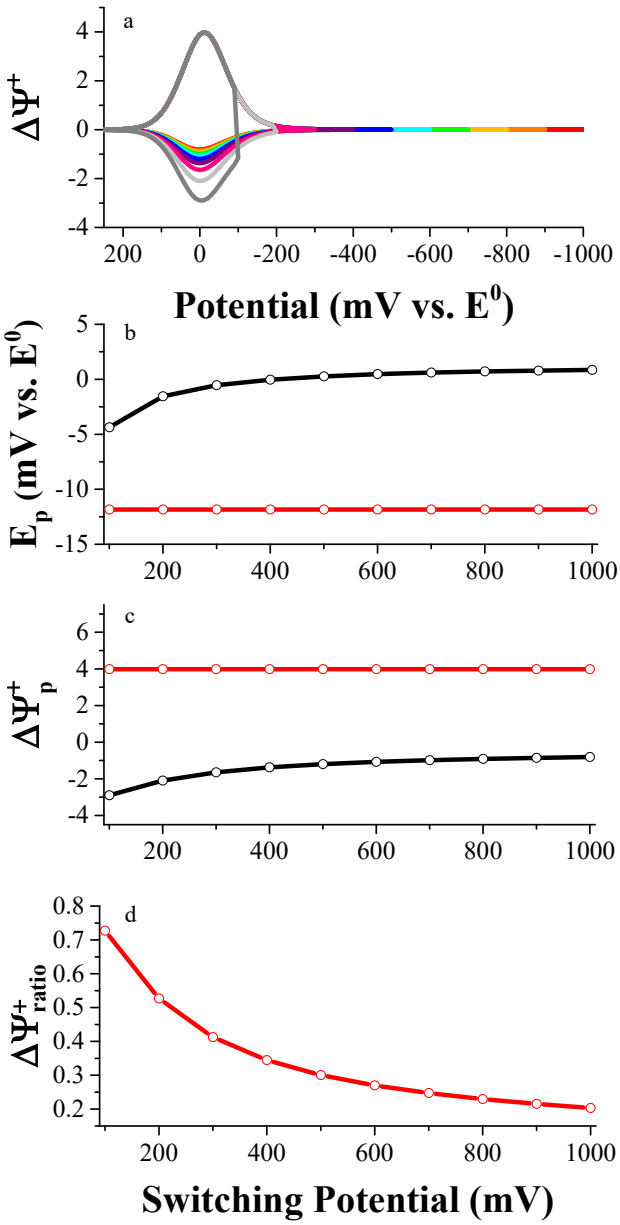

Figure 9.17. The impact of switching potential on the shape of the voltammogram when amplitude = 50 mV, increment = 10 mV, period = 50 ms, log K = 3, and log ($k_f + k_b$) = 0. Panel a): Switching potential ranges from 1000 mV (red), 900 mV (orange), 800 mV (yellow), 700 mV (green), 600 mV (cyan), 500 mV (blue), 400 mV (purple), 300 mV (magenta), 200 mV (light gray), and 100 mV (dark gray). Panel b): $E_{p,f}$ (red) and $E_{p,r}$ (black). Panel c): $\Delta\Psi^+_{p,f}$ (red) and $\Delta\Psi^+_{p,r}$ (black). Panel d): Peak ratio (red).

When log K = 2 (panel e), again, peak ratio is unaffected by switching potential for log ($k_f + k_b$) < -1 while peak ratio increases as switching potential approaches E^0 for log (k_f +

k_b) < 5. For log ($k_f + k_b$) ≥ 5, peak ratio decreases slightly as switching potential approaches E^0. When log K = 1 (panel f), peak ratio is unaffected at unity by switching potential when log ($k_f + k_b$) < -1. For -1 ≤ log ($k_f + k_b$) ≤ 2, peak ratio increases as switching potential approaches E^0. For log ($k_f + k_b$) = 3, peak ratio is unaffected. When log ($k_f + k_b$) > 3, peak ratio decreases slightly as switching potential approaches E^0. When log K = 0 (panel g), peak ratio decreases is unaffected at unity by switching potential when log ($k_f + k_b$) < -1 and increases as switching potential approaches E^0 when -1 ≤ log ($k_f + k_b$) ≤ 1. Peak ratio is essentially invariant for higher values of $k_f + k_b$. When log K = -1 (panel h), peak ratio is invariant at unity with switching potential.

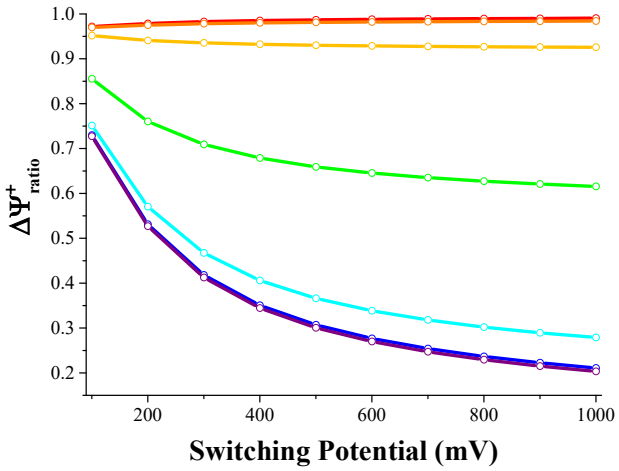

Figure 9.18. The impact of switching potential on the peak ratio as log K is varied from -3 (red) to 3 (purple) in steps of 1 when increment = 10 mV, period = 50 ms, and log ($k_f + k_b$) = 0.

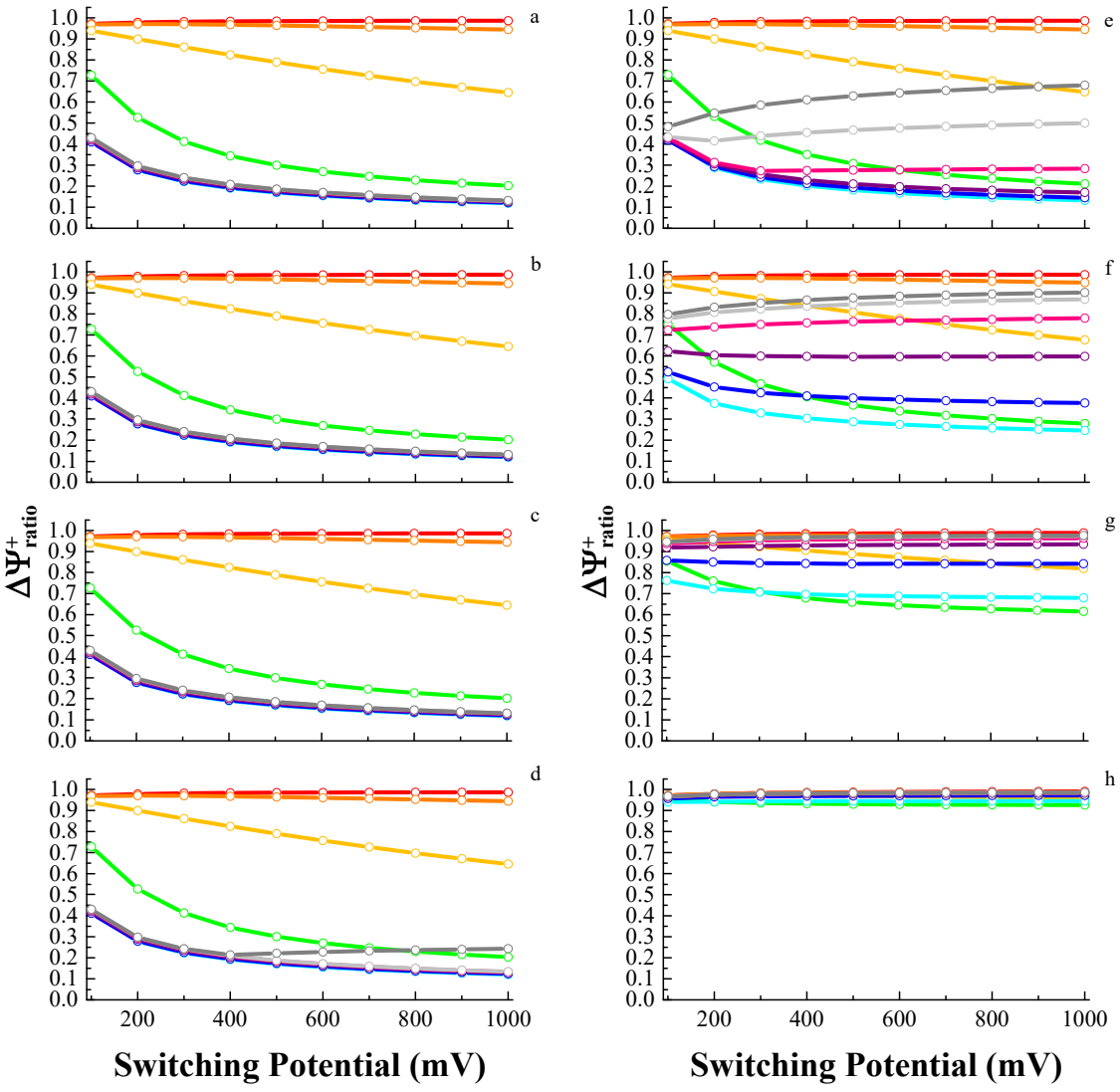

Figure 9.19. The impact of switching potential on peak ratio over the log ($k_f + k_b$) range -3 (red) to 6 (dark gray) for log K = 6 (panel a) to -1 (panel h) when increment = 10 mV and period = 50 ms.

The effect of switching potential on peak current is displayed in Figure 9.20. $\Delta\Psi^{+}_{p,f}$ is invariant while switching potential is varied though the magnitude depends on log ($k_f + k_b$). $\Delta\Psi^{+}_{p,r}$ is invariant with switching potential when log ($k_f + k_b$) < -1 whereas $\Delta\Psi^{+}_{p,r}$ increases as switching potential approaches E^0 for larger values of $k_f + k_b$. The magnitude of the increase depends on $k_f + k_b$.

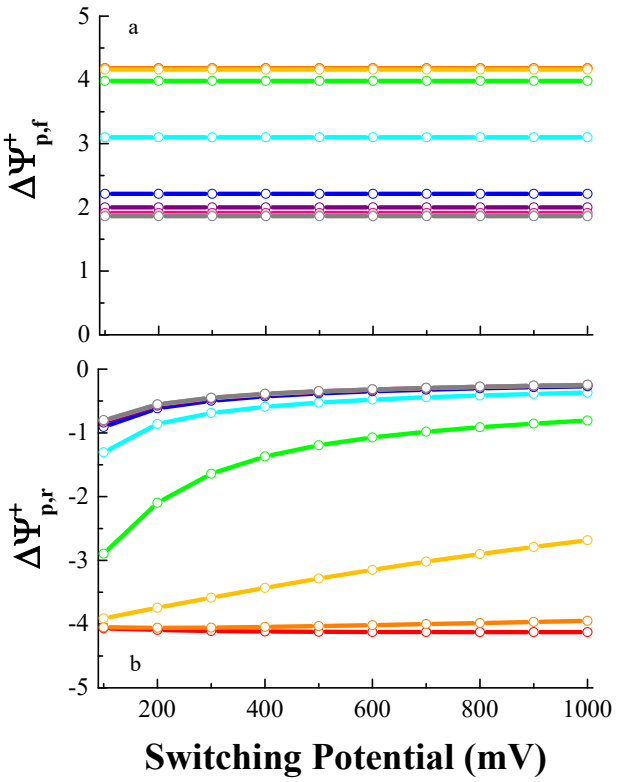

Figure 9.20. The impact of switching potential on $\Delta\Psi^{+}_{p,f}$ and $\Delta\Psi^{+}_{p,r}$ when increment = 10 mV, period = 50 ms, log K = 6, and log ($k_f + k_b$) ranges from -3 (red) to 6 (dark gray).

Peak potentials, $E_{p,f}$ and $E_{p,r}$, as they relate to switching potential, K, and $k_f + k_b$ are displayed in Figures 9.21 and 9.22, respectively. $E_{p,f}$ is only a function K and $k_f + k_b$ and is invariant with switching potential. $E_{p,r}$ shifts slightly negative when log K ≥ 3 (panels a-d) and when log K ≤ 0 (panels g & h) though the position of $E_{p,r}$ relative to E^0 is dependent on K and $k_f + k_b$. Again the exception to these trends is for log K = 3 and log ($k_f + k_b$) = 6 where a dramatic jump in peak potential occurs. When 1 ≤ log K ≤ 2, $E_{p,r}$ is near E^0 and shifts slightly negative for log ($k_f + k_b$) ≤ 1. For higher values of log ($k_f + k_b$), $E_{p,r}$ may be shifted greatly positive of E^0 with a magnitude and trend greatly dependent on K and log ($k_f + k_b$).

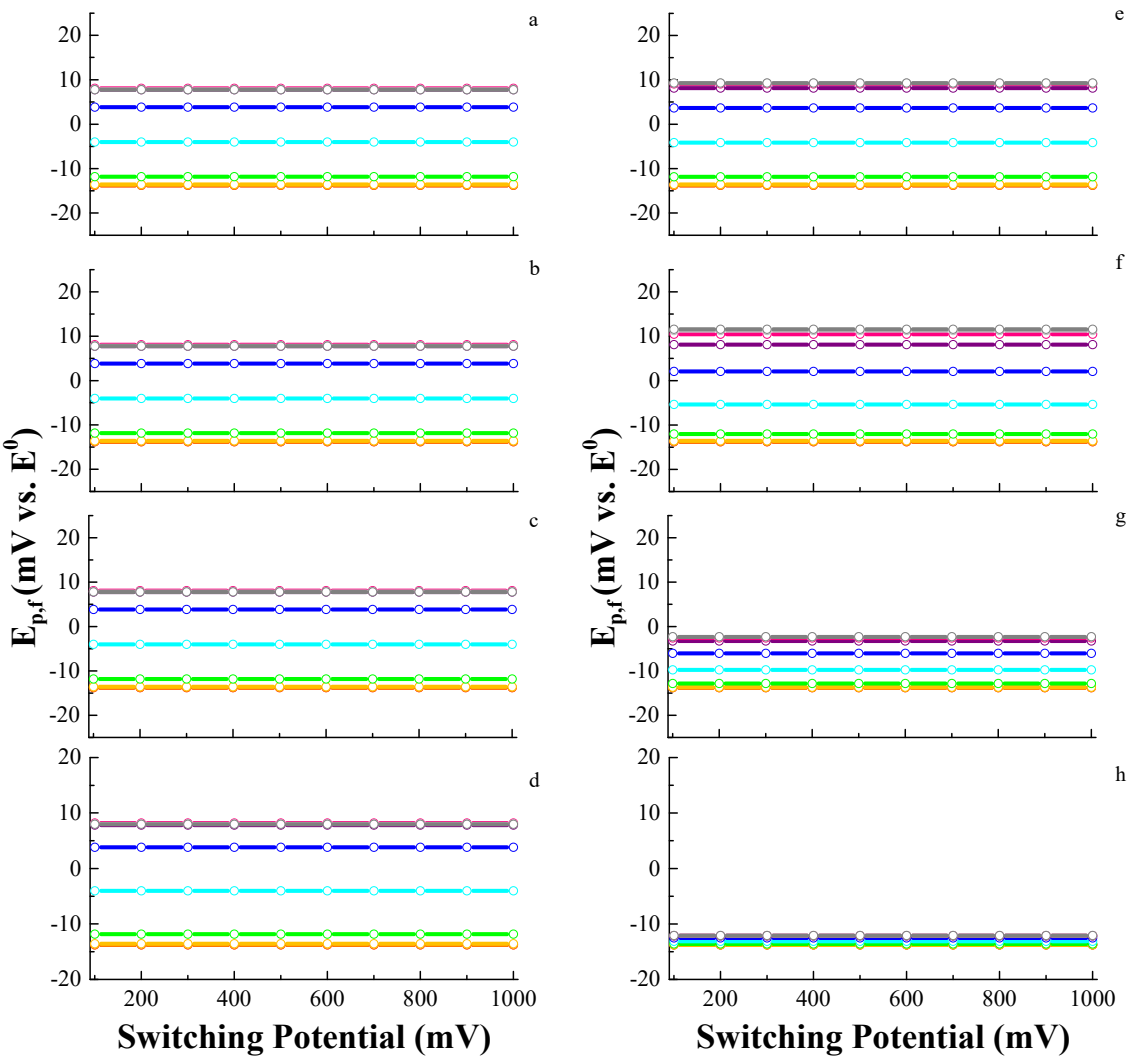

Figure 9.21. The impact of switching potential on $E_{p,f}$ over the log (k_f + k_b) range -3 (red) to 6 (dark gray) for log K = 6 (panel a) to -1 (panel h) when increment = 10 mV and period = 50 ms.

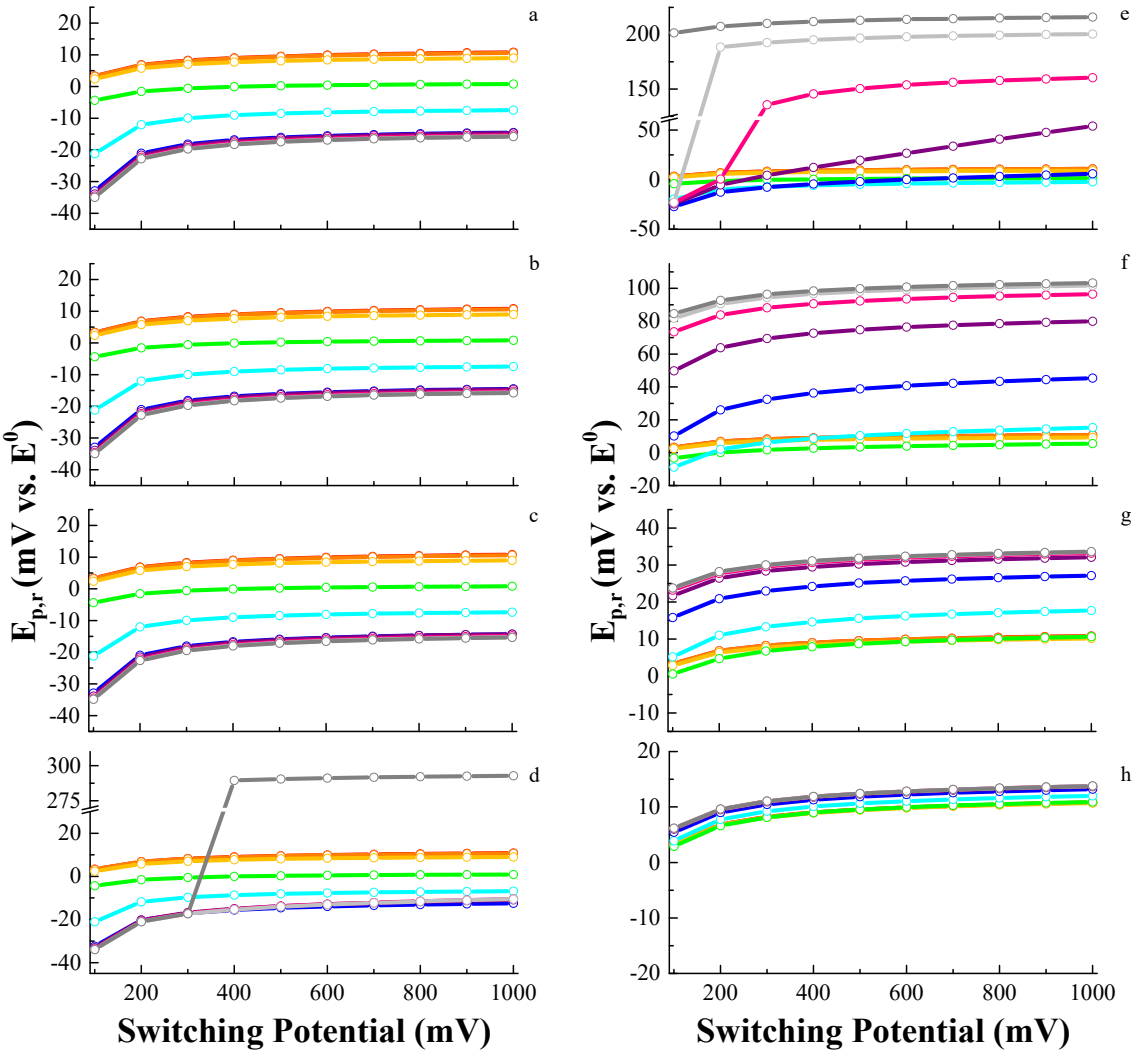

Figure 9.22. The impact of switching potential on $E_{p,r}$ over the log ($k_f + k_b$) range -3 (red) to 6 (dark gray) for log K = 6 (panel a) to -1 (panel h) when increment = 10 mV and period = 50 ms.

In comparing trends in switching potential for the E_qC and EC cases, several differences in the mechanism can be identified. $\Delta\Psi^+_{p,f}$ is invariant for both mechanisms while $\Delta\Psi^+_{p,r}$ increases as switching potential approaches E^0; the magnitude of both currents depends on K and $k_f + k_b$. When log K ≥ 4, trends in peak ratio are similar for the two mechanisms though the E_qC mechanism peak ratio is smaller than that of the EC

when log ($k_f + k_b$) ≥ 0. For intermediate values of log K, i.e., 2 ≤ log K ≤ 3, peak ratio trends are identical for small values of $k_f + k_b$ but differ in magnitude and trend for higher values of $k_f + k_b$, i.e., for log ($k_f + k_b$) > 4 for log K = 3 and for log ($k_f + k_b$) ≥ 3 for log K = 2. When log K = 1 and log ($k_f + k_b$) > 1, peak ratio differs in magnitude and trend as peak ratio decreases with increment for the EC case and increases with increment for the E_qC case. When log ($k_f + k_b$) ≤ 1 and when log K ≤ 0, peak ratio is identical for the two mechanisms. $E_{p,f}$ values are essentially constant with switching potential and only shift when as the switching potential approaches E^0. The location of $E_{p,f}$ relative to E^0 is a function of $k_f + k_b$ and K and is different for each mechanism. Similarly, $E_{p,r}$ trends are identical but differ in displacement from E^0 for both mechanisms except in the case when 1 ≤ log K ≤ 3. The magnitude of $E_{p,r}$ and displacement of $E_{p,r}$ from E^0 depends on K and $k_f + k_b$ for both mechanisms but is these properties and trends in $E_{p,r}$ drastically different in this range of K. Thus, switching potential is not useful in identifying the E_qC versus the EC mechanism but does identify a chemically-coupled mechanism.

9.2.6 Effect of Amplitude (E_{SW})

The effect of amplitude of on the shape of the voltammogram is shown in Figure 9.23. $E_{p,f}$ shifts positively with amplitude whereas $E_{p,r}$ shifts slightly negative with amplitude (see Figure 9.23b). Both $\Delta\Psi^+_{p,f}$ and $\Delta\Psi^+_{p,r}$ increase with amplitude though by differing amounts (see Figure 9.23c). Subsequently, peak ratio increases slightly with amplitude (see Figure 9.23d).

A more detailed investigation in the relationship between peak ratio and amplitude is displayed in Figure 9.24. When log K ≥ 3 (panels a-d), peak ratio only increases slightly with variation of amplitude. The magnitude of peak ratio depends on log ($k_f + k_b$).

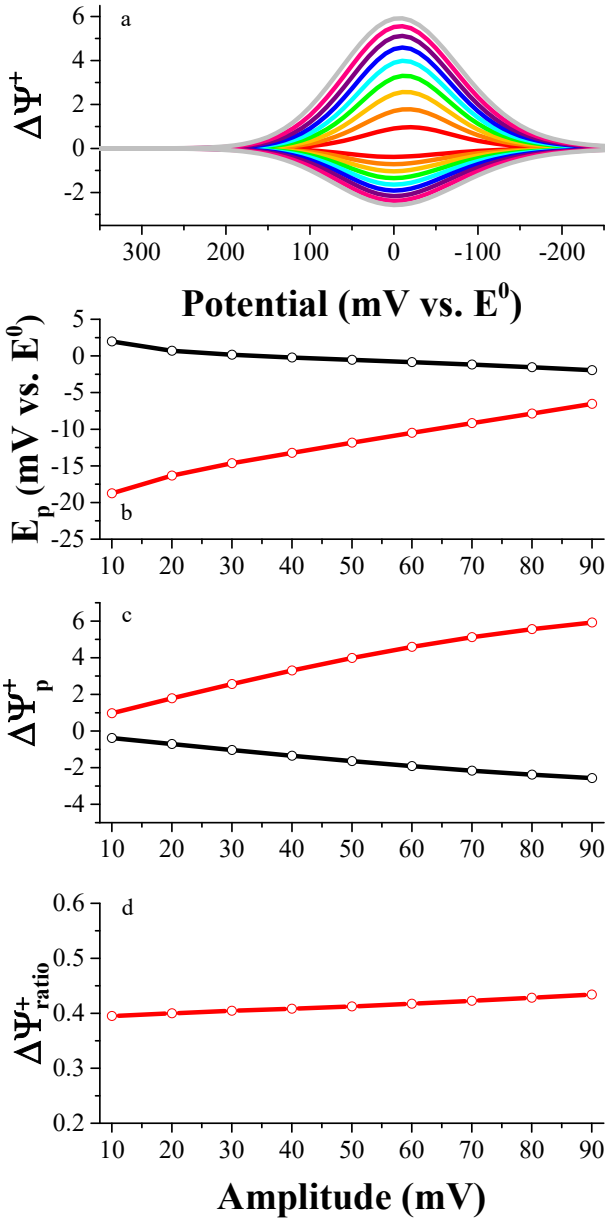

Figure 9.23. The impact of amplitude on the shape of the voltammogram when increment = 10 mV, period = 50 ms, E_λ = -300 mV, log K = 3, and log ($k_f + k_b$) = 0. Panel a): Amplitude ranges from 10 mV (red), 20 mV (orange), 30 mV (yellow), 40 mV (green), 50 mV (cyan), 60 mV (blue), 70 mV (purple), 80 mV (magenta), and 90 mV (light gray). Panel b): $E_{p,f}$ (red) and $E_{p,r}$ (black). Panel c): $\Delta\Psi^+_{p,f}$ (red) and $\Delta\Psi^+_{p,r}$ (black). Panel d): Peak ratio (red).

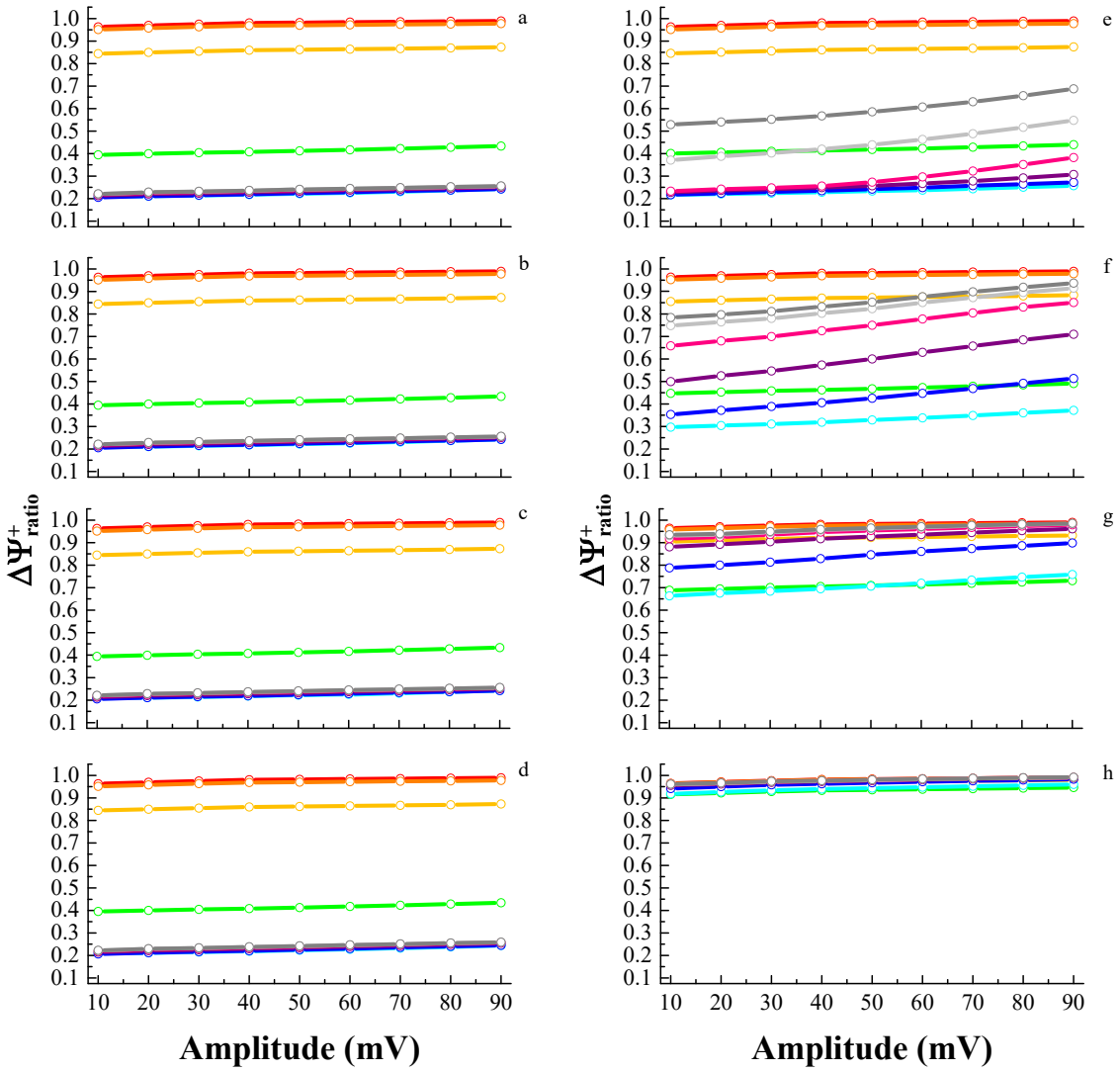

Figure 9.24. The impact of amplitude on peak ratio over the log ($k_f + k_b$) range -3 (red) to 6 (dark gray) for log K = 6 (panel a) to -1 (panel h) when increment = 10 mV, E_λ = -300 mV, and period = 50 ms.

The reader is reminded that the largest reverse peak is used to calculate peak ratio for scans in which there are two reverse peaks (log K = 3). The case in which log K = 2 (panel e) is special. At low amplitudes and fast rates, i.e., $E_{SW} \leq 50$ mV and log ($k_f + k_b$) ≥ 4, two peaks appear on the reverse sweep. As amplitude increases for these cases of $k_f + k_b$, the two peaks merge together. The larger peak of the two is used to calculate peak

ratio, and its corresponding peak potentials are identified below. The trends for log K = 2 are identical to higher values of K when log $(k_f + k_b) \leq 3$ and increase with amplitude when log $(k_f + k_b) \geq 4$. When log K = 1 and 0 (panels f & g), peak ratio is invariant and at unity with amplitude for log $(k_f + k_b) < -1$. For $-1 \leq \log (k_f + k_b) \leq 0$, peak ratio is nearly constant at a value less than unity. For larger $k_f + k_b$ values, peak ratio increases with amplitude and approaches unity. The magnitude of each trend depends on K. When log K = -1 (panel h), peak ratio is invariant with amplitude and near unity for all values of $k_f + k_b$. The effect of amplitude on peak currents is shown in Figure 9.25. Both $\Delta\Psi^{+}_{p,f}$ and $\Delta\Psi^{+}_{p,r}$ increase with amplitude; the magnitude of each is dependent on log $(k_f + k_b)$.

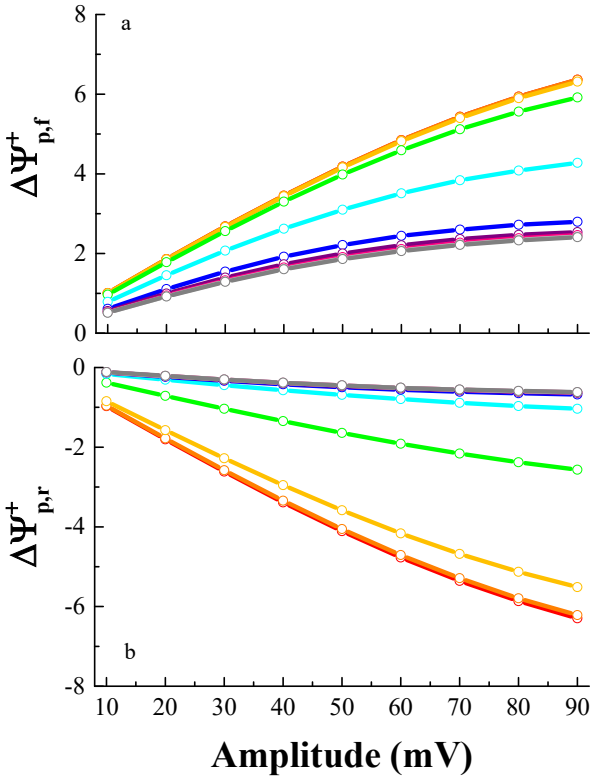

Figure 9.25. The impact of amplitude on $\Delta\Psi^{+}_{p,f}$ and $\Delta\Psi^{+}_{p,r}$ when increment = 10 mV, period = 50 ms, E_λ = -300 mV, log K = 6, and log $(k_f + k_b)$ ranges from -3 (red) to 6 (dark gray).

The relationship between $E_{p,f}$, $k_f + k_b$, K, and amplitude is shown in Figure 9.26. $E_{p,f}$ shifts positively with amplitude thought the magnitude of the shift and the displacement from E^0 depends on $k_f + k_b$ and K. Some cases may only shift by 10 mV whereas others are as large as 50 mV.

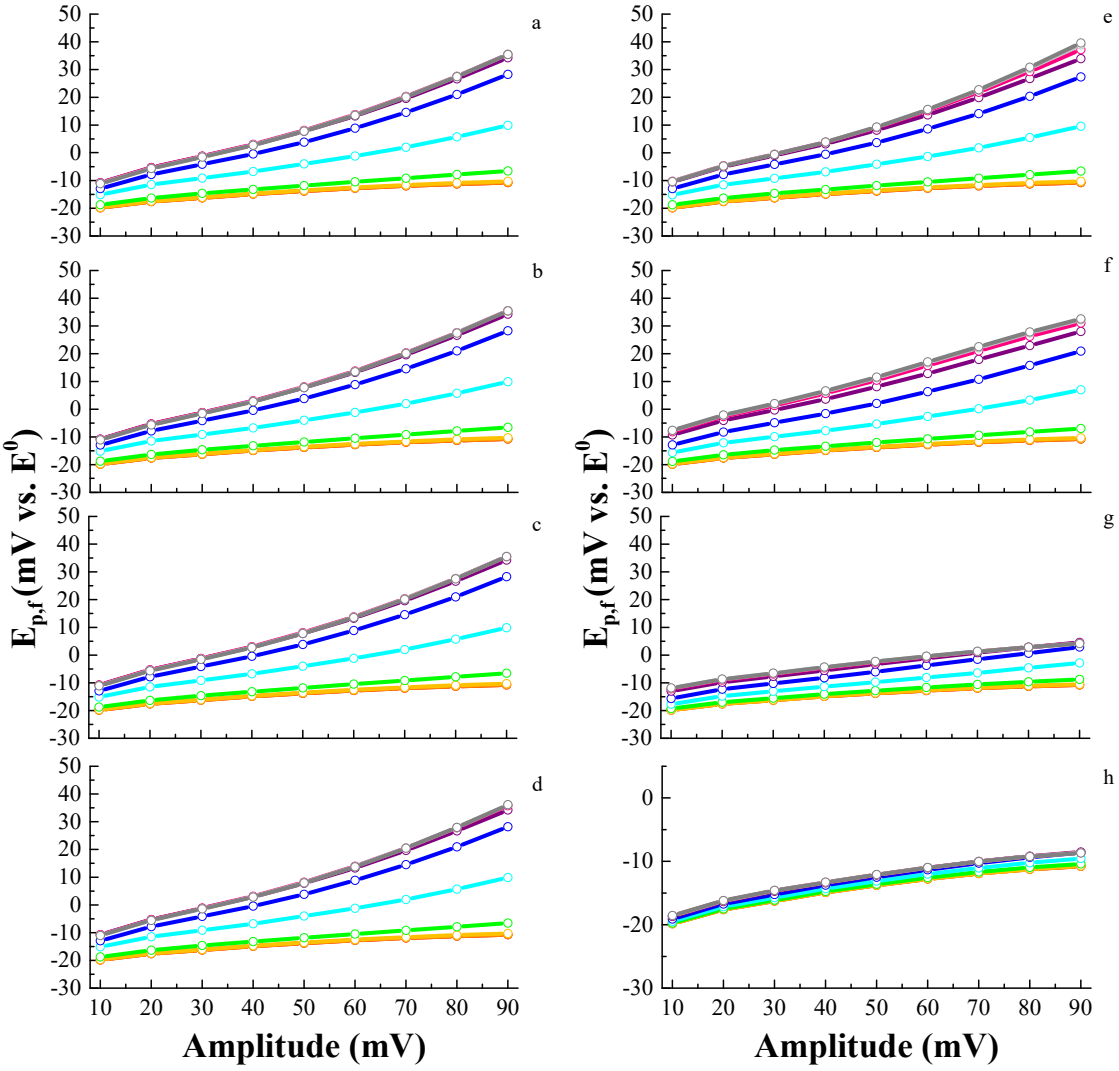

Figure 9.26. The impact of amplitude on $E_{p,f}$ over the log ($k_f + k_b$) range -3 (red) to 6 (dark gray) for log K = 6 (panel a) to -1 (panel h) when increment = 10 mV, E_λ = -300 mV, and period = 50 ms.

In contrast, $E_{p,r}$ has a complex relationship with amplitude as displayed in Figure 9.27 $E_{p,r}$ may shift positively, negatively, or be invariant with amplitude depending on K and $k_f + k_b$. Some shifts are 10 mV whereas other shifts may be 30 mV. Trends in $E_{p,r}$ for log $K \geq 3$ (panels a-d) are identical, and shifts occur by no more than 20 mV.

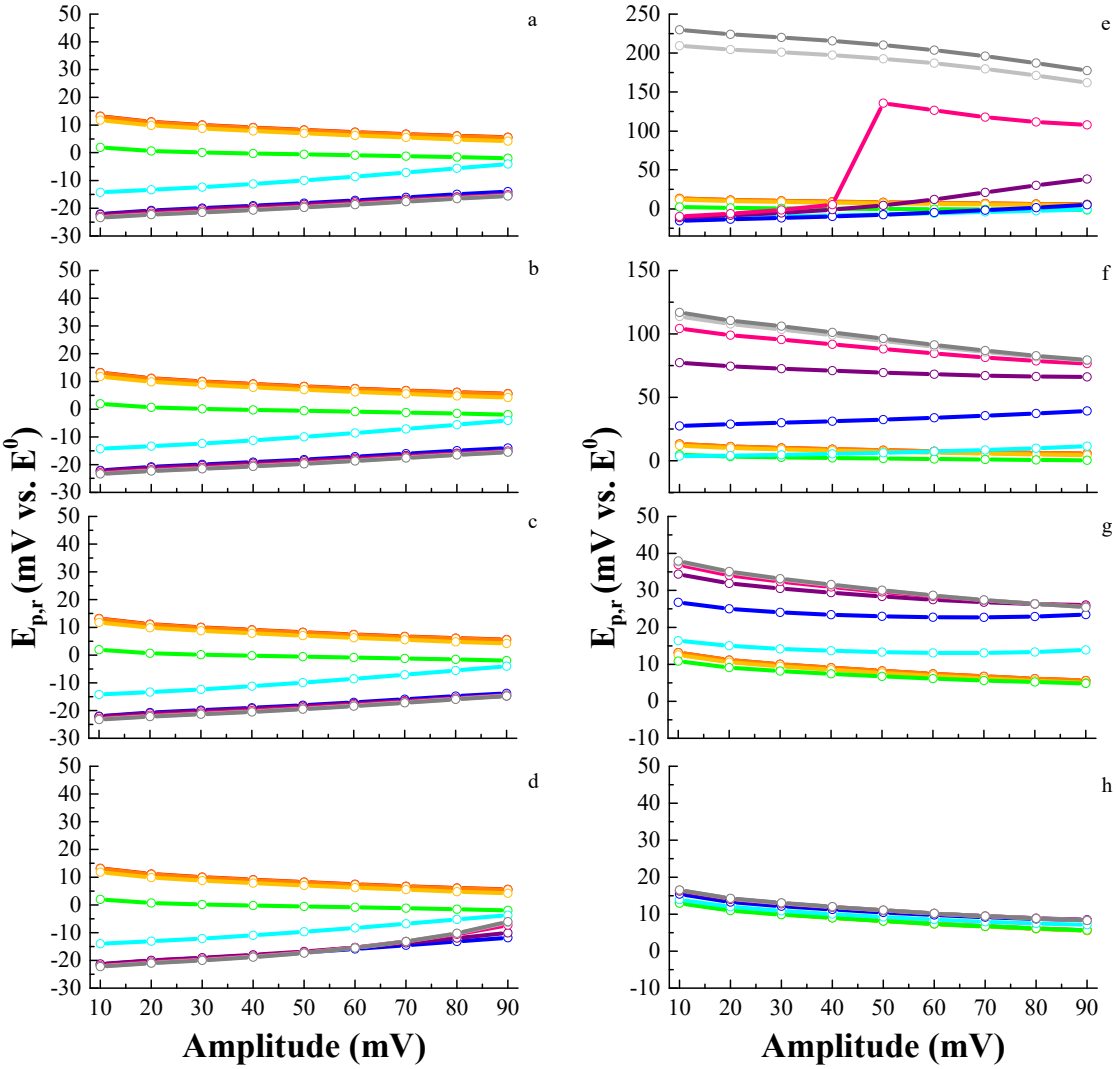

Figure 9.27. The impact of amplitude on $E_{p,r}$ over the log ($k_f + k_b$) range -3 (red) to 6 (dark gray) for log K = 6 (panel a) to -1 (panel h) when increment = 10 mV, E_λ = -300 mV, and period = 50 ms.

The special case exists for log K = 2 (panel e) where at fast rates, such as log $(k_f + k_b) \geq$ 4, two peaks are present at low amplitudes and converge into one at high amplitudes. There is a significant jump in $E_{p,r}$ when this occurs for log $(k_f + k_b) = 4$ whereas $E_{p,r}$ is located more than 150 mV positive of E^0 for log $(k_f + k_b) \geq 5$. Dramatic shifts from E^0 in $E_{p,r}$ occur for log $(k_f + k_b) > 1$ when log K = 1 (panel f), and the trend is dependent on log $(k_f + k_b)$. $E_{p,r}$ shifts slightly negative, e.g. by no more than 10 mV, for log K = 0 (panel g) and log K = 1 (panel h) though $E_{p,r}$ is located positive of E^0 for fast rates when log K = 0. Thus, the effect of amplitude on peak potential may provide insights into identification of the E_qC mechanism.

Comparison of the effect of amplitude on the EqC and EC mechanisms lead to several differences in the trends. Peak ratio trends are nearly identical with only small differences in magnitude for the two mechanisms when log $K \geq 4$. In this intermediate range in K, the following scenarios result in trends with differing magnitudes: log K = 3 and log $(k_f + k_b) \geq 5$, log K = 2 and log $(k_f + k_b) \geq 3$, and log K = 1 and log $(k_f + k_b) \geq -1$. Peak ratios are also identical for log $K \leq 0$. Peak current trends are similar for both mechanisms though the magnitude of the trends for the E_qC mechanism is lower than that for the EC mechanism. $E_{p,f}$ shifts positively with amplitude for both mechanisms, but the magnitude of the shift and the location of the peak relative to E^0 are quite different for all values of log K. $E_{p,f}$ trends corresponding to low K values with fast rates shift for the E_qC case whereas shifts in this kinetic region do not occur for the EC case. $E_{p,r}$ trends and displacement from E^0 are quite different between the two mechanisms for all values of K and most significantly for log K = 2. Thus, the relationship between peak potentials and amplitude may be used to discern between the EC and E_qC mechanisms.

9.2.7 Effect of k^0

Experimentally, k^0 is intrinsic to a given analyte/electrolyte/electrode combination. However, changing either the electrode and/or electrolyte may change the reversibility of an electron transfer for a given analyte. Furthermore, different analytes in the same electrode/electrolyte conditions may follow the E_qC reaction pay with differing values of k^0. Simulating the variation of k^0 is in essence evaluating a host of analyte/electrode/electrolyte conditions. The range in k^0 investigated here predicts how changing these experimental variables affects the voltammogram for the E_qC mechanism. Furthermore, the variation of k^0 and empirical parameters provides a means for determining the value of k^0 experimentally.

The effect of k^0 on the shape of the voltammogram is shown in Figure 9.28. At low values of k^0, i.e., $\log k^0 \leq -4$, one peak appears on the forward sweep, and two peaks appear on the reverse sweep. The peaks are asymmetrically displaced from E^0.

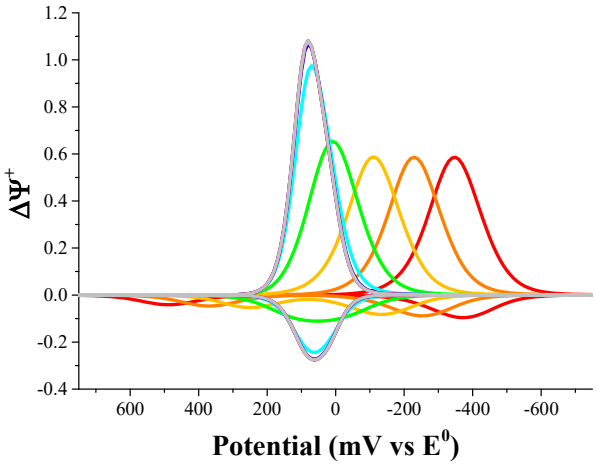

Figure 9.28. The effect of k^0 on the shape of the voltammogram when, amplitude = 50 mV, period = 50 ms, increment = 10 mV, E_λ = -1000 mV, log K = 2 and log ($k_f + k_b$) = 2, and log k^0 is varied from -6 (red), -5 (orange), -4 (yellow), -3 (green), -2 (cyan), -1 (blue), 0 (purple), 1 (pink), and 2 (light gray).

As k^0 increases, only one peak exists on the reverse sweep, and the peak potentials approach E^0 then shift positive of E^0. Regardless of k^0, the forward peak is larger than the reverse peak.

The range that CSWV is sensitive to the E_qC mechanism for determination of k^0 is best investigated by examining the effect of simultaneous variation of k^0 and period. As shown in Figure 9.29a, $\Delta\Psi^+_{p,f}$ decreases linearly with period$^{-1/2}$, and the slope of the relationship increases with k^0. Slopes approach those of a reversible process for log $k^0 \geq$ -2.

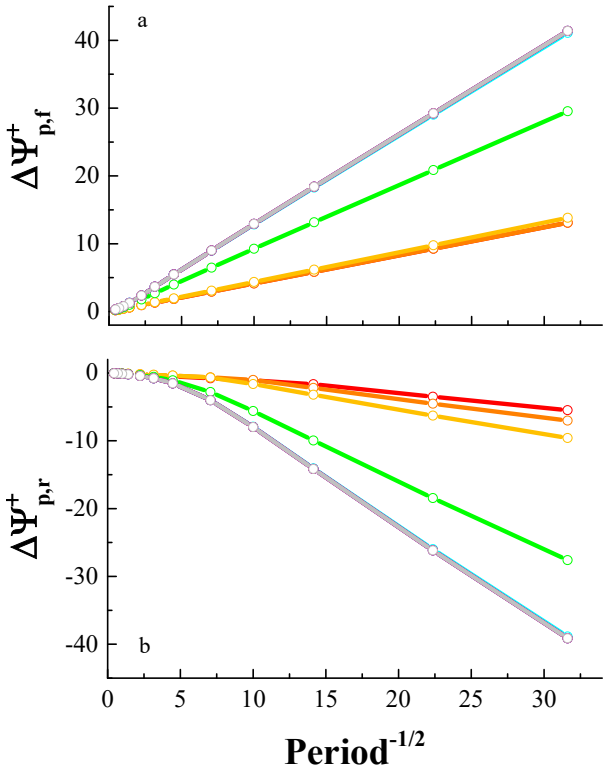

Figure 9.29. The effect of period and k^0 on $\Delta\Psi^+_{p,f}$ (panel a) and $\Delta\Psi^+_{p,r}$ (panel b) when amplitude = 50 mV, increment = 10 mV, E_λ = -600 mV, log K = 3, log ($k_f + k_b$) = 0, and log k^0 is varied from -6 (red), -5 (orange), -4 (yellow), -3 (green), -2 (cyan), -1 (blue), 0 (purple), 1 (pink), and 2 (light gray).

Similarly, in Figure 9.29b, $\Delta\Psi^{+}_{p,r}$ decreases linearly with period$^{-1/2}$ at short periods and becomes curvilinear for long periods. As result of these changes in peak current, trends in peak ratio as a function of period and k^0 are shown in Figure 9.30. Peak ratio decreases with increasing period as expected for the EC mechanism. However, the magnitude of peak ratio depends on k^0; for $k^0 \leq -4$, peak ratio trends are lower than the corresponding trends for higher k^0 values. Readers are reminded that the largest reverse peak is used to calculate peak ratio when two peaks may exist on the reverse sweep.

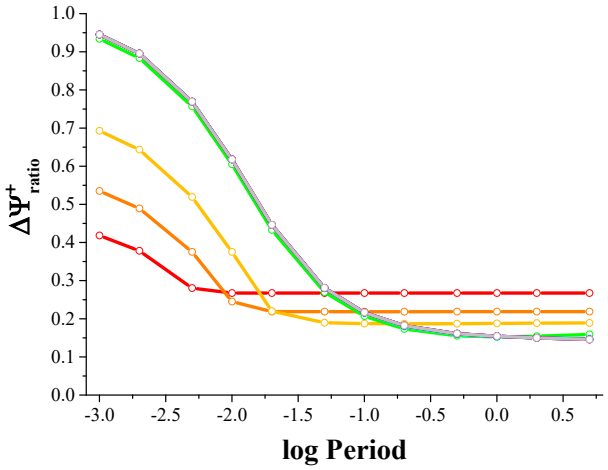

Figure 9.30. The effect of period and k^0 on peak ratio when amplitude = 50 mV, increment = 10 mV, E_λ = -600 mV, log K = 3, log ($k_f + k_b$) = 0, and log k^0 is varied from -6 (red), -5 (orange), -4 (yellow), -3 (green), -2 (cyan), -1 (blue), 0 (purple), 1 (pink), and 2 (light gray).

The effect of k^0 and period on peak potentials is displayed in Figure 9.31. $E_{p,f}$ (panel a) is constant with period when log $k^0 \leq -4$, shifts slightly positive with period when log $k^0 = -3$, and shifts positively by ~50 mV at long periods for log $k^0 \geq -2$. The effect of period and k^0 on $E_{p,r}$ (panel b) is interesting. For log $k^0 \leq -4$, a several hundred mV jump is observed in $E_{p,r}$ as the magnitude of the two reverse peaks change with period. At short periods, the reverse peak positive of E^0 is the dominant peak. At period elongates,

the more positive of the two reverse peaks diminishes, and the reverse peak located negative of E^0 becomes the dominant peak. $E_{p,r}$ for log k^0 = -3 shifts slightly negative by ~ 20 mV with period whereas trends for log $k^0 \geq$ -2 shift positively by ~30 mV with period. Subsequently, ΔE_p decreases rapidly and changes sign for log $k^0 \leq$ -4. A similar but smaller trend in ΔE_p occurs for log k^0 = -3. For larger values of k^0, ΔE_p increases negatively with period. Thus, peak parameters for the E_qC mechanism are affected by both k^0 and period.

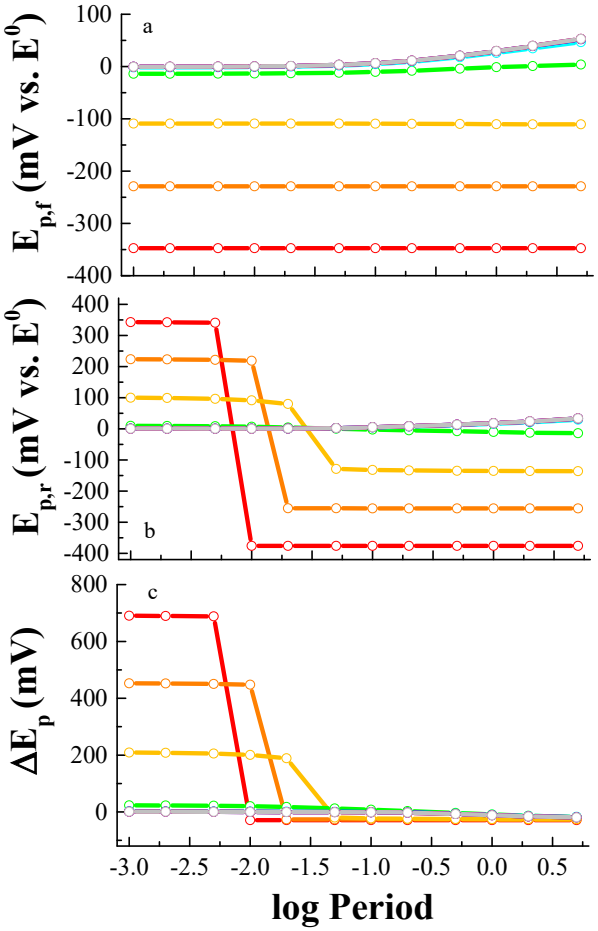

Figure 9.31. The effect of period and k^0 on a) $E_{p,f}$, b) $E_{p,r}$, and c) ΔE_p when amplitude = 50 mV, increment = 10 mV, E_λ = -600 mV, log K = 3, log ($k_f + k_b$) = 0, and log k^0 is varied from -6 (red), -5 (orange), -4 (yellow), -3 (green), -2 (cyan), -1 (blue), 0 (purple), 1 (pink), and 2 (light gray).

Several comparisons to distinguish the E_qC and EC mechanisms have been made throughout this chapter. What has yet to be addressed is the ability to discern between the E_qC and the E_{quasi} mechanisms. Peak currents are linearly or curvilinearly related to period$^{-1/2}$ for both mechanisms, and the slope of the relationship is dependent on k^0. However, the trends in peak ratio, period, and k^0 differ drastically. Peak ratio increases and may approach unity for the E_{quasi} mechanism though peak ratio decreases then plateaus for the E_qC mechanism as shown in Figure 9.32. It should be noted that for each mechanism, peak ratio has s a dependence on the magnitude on k^0 and that one value was chosen to highlight the differences in the two mechanisms.

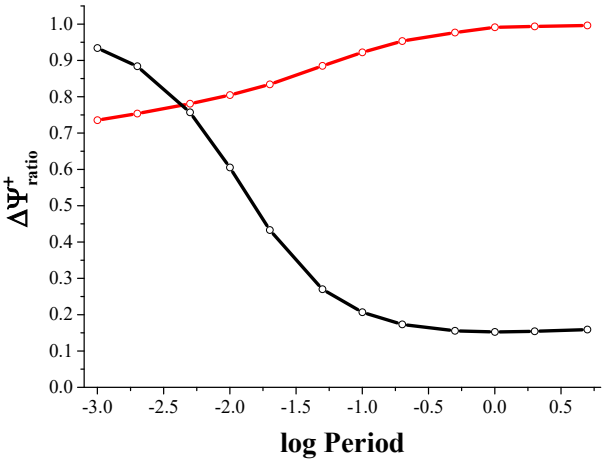

Figure 9.32. The effect of period on peak ratio for the E_{quasi} mechanism (red) and the E_qC mechanism (black) when amplitude = 50 mV, increment = 10 mV, and log k^0 = -3. For the E_qC mechanism, E_λ = -600 mV, log K = 3, and log ($k_f + k_b$) = 0.

Furthermore, trends in peak potential differ markedly as displayed in Figure 9.33. Peak potentials approach E^0 with increasing period, and peak separation decreases for the E_{quasi} mechanism. In contrast, $E_{p,f}$ is constant or shifts positively (away from E^0) with period, and $E_{p,r}$ transitions between the reverse peaks or shifts positively (away from E^0) with period for the E_qC mechanism. Subsequent trends in ΔE_p differ from the E_{quasi}

mechanism as the trend for E_qC does not decrease with period and depends on k^0. Again, it should be noted that peak potentials for both mechanisms depend on k^0. Thus, the variation of period using CSWV can be used to discriminate between the E_qC and E_{quasi} mechanisms.

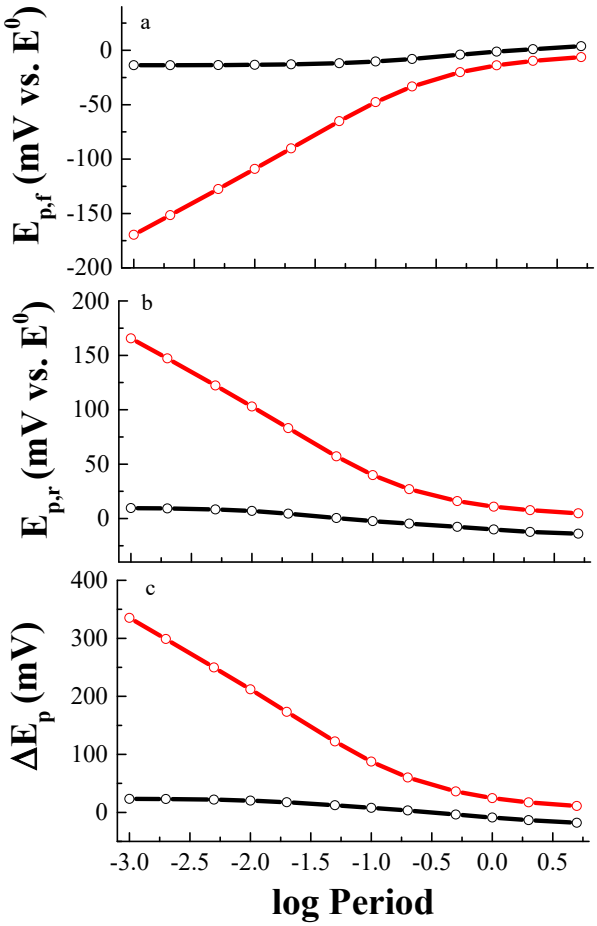

Figure 9.33. The effect of period on a) $E_{p,f}$, b) $E_{p,r}$, and c) ΔE_p for the E_{quasi} mechanism (red) and the E_qC mechanism (black) when amplitude = 50 mV, increment = 10 mV, and log k^0 = -3. For the E_qC mechanism, E_λ = -600 mV, log K = 3, and log ($k_f + k_b$) = 0.

9.3 Conclusion

This chapter presented an investigation of the E_qC mechanism using CSWV. The effects of the rates of the electron transfer and chemical reaction were considered. The

empirical parameters were varied, and key trends in peak parameters were identified. Examination of these trends was used to generate the diagnostic criteria for the E_qC mechanism. The effect of rates in combination with the variation of empirical parameters led to the protocol for experimentalists to assign the E_qC mechanism to an analyte of interest and determine any associated kinetic or thermodynamic properties. The protocol is presented in Table 9.1. Comparisons between the diagnostic criteria for EC and E_qC mechanisms were also presented.

Table 9.1. Diagnostic Plots and Protocol for Assessing an E_qC Electrode Reaction by CSWV

	Empirical variables							
Waveform parameters	***Period,* τ**		***Increment,* δE**		***Switching potential,* E_λ**		***Amplitude,* E_{SW}**	
	Plot	**Trace**	**Plot**	**Trend**	**Plot**	**Trend**	**Plot**	**Trend**
Peak currents	ΔI_p vs. $\tau^{-1/2}$	ΔI_p is linearly or curvilinearly related to period$^{-1/2}$ dependent upon K and $k_f + k_b$ (see Figures 9.5c and 9.8)	ΔI_p vs. δE	ΔI_p may increase or be invariant with δE dependent on K and $k_f + k_b$ (see Figures 9.11c and 9.14)	ΔI_p vs. E_λ	$\Delta I_{p,f}$ is independent of E_λ while $\Delta I_{p,r}$ may be invariant or increase as E_λ approaches E^0 (see Figures 9.17c and 9.20)	ΔI_p vs. E_{SW}	ΔI_p increases with E_{SW} with a magnitude dependent on K and $k_f + k_b$ (see Figure 9c and S-16)
Peak ratio	Peak ratio vs. log τ	Peak ratio $\leq$ unity and may increase, decrease or be invariant with period dependent on K and $k_f + k_b$ (see Figures 9.5d, 9.6, and 9.7)	Peak ratio vs. δE	Peak ratio may increase, decrease or remain constant; trend and magnitude depends upon K and $k_f + k_b$ (see Figures 9.11d, 9.12, and 9.13)	Peak ratio vs. E_λ	Peak ratio may increase, decrease, or be invariant with E_λ dependent upon K and $k_f + k_b$ (see Figures 9.17d, 9.18, and 9.19)	Peak ratio vs. E_{SW}	Peak ratio either increases or is invariant as E_{SW} increases; the magnitude and trend depend on K and $k_f + k_b$ (see Figures 9.23d and 9.24)
Peak potentials	E_p vs. log τ	$E_{p,f}$ either shifts positive or is invariant with period; Ep,r may shift positively, negatively, or be invariant with period. Both depend greatly on K and $k_f + k_b$ (see Figures 9.5b, 9.9, and 9.10)	E_p vs. δE	$E_{p,f}$ shifts negatively with δE while $E_{p,r}$ has a complex relationship with δE; magnitude and trend depend on K and $k_f + k_b$ (see Figures 9.11b, 9.15, and 9.16)	E_p vs. E_λ	$E_{p,f}$ is invariant with E_λ though the location relative to E^0 depends on K and $k_f + k_b$; $E_{p,r}$ may be invariant or shift negatively with E_λ dependent on K and $k_f + k_b$ (see Figures 9.17b, 9.21, and 9.22)	E_p vs. E_{SW}	$E_{p,f}$ may shift in small or large amounts positively with E_{SW} whereas $E_{p,r}$ may shift positive, negative, or be invariant with E_{SW}; both potentials depend on K and $k_f + k_b$ (see Figures 9.23b, 9.26, and 9.27)
Peak separation	ΔE_p vs. log τ	ΔE_p may increase, decrease, or remain constant with period	ΔE_p vs. δE	ΔE_p may increase or decrease with increasing δE	ΔE_p vs. E_λ	Generally ΔE_p is invariant but may decrease slightly	ΔE_p vs. E_{SW}	ΔE_p may increase or decrease with increasing E_{SW}
Peak widths	$W_{1/2}$ vs. log τ	Generally $W_{1/2}$ increases or is invariant with period	$W_{1/2}$ vs. δE	$W_{1/2}$ may increase or decrease slightly with increasing δE	$W_{1/2}$ vs. E_λ	$W_{1/2}$ is invariant with E_λ unless E_λ occurs before current returns to the baseline	$W_{1/2}$ vs. E_{SW}	Generally, $W_{1/2}$ increases with E_{SW}

9.4 References

1. Smith, D.E. *Anal. Chem.*, **1963**. 35, 602-609.

2. Nicholson, R.S. and I. Shain. *Anal. Chem.*, **1964**. 36, 706-723.

3. Laviron, E. *J. Electroanal. Chem. Interfacial Electrochem.*, **1972**. 39, 1-23.

4. Nadjo, L. and J.M. Saveant. *J. Electroanal. Chem. Interfacial Electrochem.*, **1973**. 48, 113-145.

5. Kim, M.-H., L. Yan, R.L. Birke, and M.-Z. Czae. *Electroanalysis*, **2003**. 15, 1541-1553.

6. Laborda, E., F. Martinez-Ortiz, and A. Molina. *Electroanalysis*, **2010**. 22, 1857-1866.

7. Mozo, J.D., J. Carbajo, J.C. Sturm, L.J. Nunez-Vergara, R. Moscoso, and J.A. Squella. *Anal. Chim. Acta*, **2011**. 699, 33-43.

8. O'Dea, J.J., J. Osteryoung, and R.A. Osteryoung. *Anal. Chem.*, **1981**. 53, 695-701.

9. Osteryoung, J.G. and J.J. O'Dea, *Square-Wave Voltammetry*, *Electroanalytical chemistry: a series of advances*. **1986**, Marcel Dekker, Inc: New York. 209-308

10. Miles, A.B. and R.G. Compton. *J. Phys. Chem. B*, **2000**. 104, 5331-5342.

11. Mirceski, V. and M. Lovric. *Croat. Chem. Acta*, **2000**. 73, 305-329.

12. Mirceski, V. and M. Lovric. *J. Electroanal. Chem.*, **2004**. 565, 191-202.

13. Mirčeski, V., Š. Komorsky-Lovrić, and M. Lovrić, *Square Wave Voltammetry: Theory and Application*, *Monographs in Electrochemistry*. **2007**, Springer-Verlag: Berlin.

14. Jadreško, D. and M. Zelić. *J. Electroanal. Chem.*, **2014**. 714-715, 30-37.

15. Cizmek, L., S. Komorsky-Lovric, and M. Lovric. *ChemElectroChem*, **2015**. 2, 2027-2031.

16. Evans, D.H. *J. Phys. Chem.*, **1972**. 76, 1160-1165.

17. Garay, F. and M. Lovric. *J. Electroanal. Chem.*, **2002**. 518, 91-102.

18. Garay, F. and M. Lovrić. *J. Electroanal. Chem.*, **2002**. 518, 91-102.

19. Mirčeski, V., E. Laborda, D. Guziejewski, and R.G. Compton. *Anal. Chem.*, **2013**. 85, 5586-5594.

20. Erdey-Gruz, T., *Kinetics of Electrode Processes*. **1972**, Wiley-Interscience Division: New York.

21. Nicholson, R.S. and M.L. Olmstead, *Electrochemistry: Calculations, Simulation and Instrumentation,*. **1972**, Marcel Dekker: New York. Ch. 5

22. Mann, M.A., J.C. Helfrick, Jr., and L.A. Bottomley. *Anal. Chem.*, **2014**. 86, 8183-8191.

CHAPTER 10

THE CE_q MECHANISM

10.1 Introduction

The CE mechanism (Chapter 6) has been the subject of many theoretical electrochemical investigations for decades.[1-10] Less frequent in the literature is the CE_q mechanism in which the electron transfer is quasireversible or irreversible.[5, 8, 11-13] An analyte that exhibits CE properties may exhibit CE_q properties for another electrode and/or electrolyte. Thus, it is essential to explore the CE_q mechanism with CSWV.

This work inspects the effect of the kinetics and equilibrium of the chemical reaction as well as the effect of the kinetically controlled electron transfer on the peak parameters. Furthermore, the effect of the empirical parameters on the peak parameters is considered. Also included in this report is the diagnostic criteria for the CE_q mechanism, a protocol to assign the CE_q mechanism, and comparisons to the CE mechanism so that the experimenter can discern between the two.

10.2 Results and Discussion

10.2.1 Theory

This work examines the CE_q mechanism in which a chemical reaction precedes a kinetically controlled electron transfer, as shown in Equation 10.1.

$$Y \underset{k_b}{\overset{k_f}{\rightleftarrows}} Ox + ne^- \overset{k^0}{\leftrightarrow} Red \tag{10.1}$$

where Ox is the reactant, Red is the product of the electron transfer, Y is the electroinactive reactant in the reaction preceding the electron transfer step, k_f is the rate constant for the conversion of Y to Ox in s^{-1}, k_b is the rate constant for conversion of Ox to Y in s^{-1}, and k^0 is the standard heterogeneous rate constant in cm/s. The forward and reverse chemical reactions have been treated as first order and the electron transfer is diffusion limited. The derivation of an equation that enables calculation of current at each applied potential for this electrode reaction begins with Fick's laws of diffusion. Expressions for the concentrations of Ox and Red as a function of time and distance from the electrode are found using Laplace transformations and application of the appropriate boundary conditions. For a quasireversible electron transfer, the current, potential, and surface concentrations of Ox and Red are related through the Erdey-Gruz and Volmer equation[2, 14]:

$$i(t) = \frac{nFA}{D_{Ox}^{(1-\alpha)/2} D_{Red}^{\alpha/2}} k^0 \exp\left[\left(\frac{-\alpha nF}{RT}\right)\left(E_{app} - E^0\right)\right]\left[\sqrt{D_{Ox}} C_{Ox}(0,t) - \exp\left[\left(\frac{nF}{RT}\right)\left(E_{app} - E^0\right)\right]\sqrt{D_{Red}} C_{Red}(0,t)\right] \tag{10.2}$$

where τ = period (sec), D_{Ox} = diffusion coefficient of Ox (cm^2/sec), and D_{Red} = diffusion coefficient of Red (cm^2/sec). To provide a current that is independent of electrode area and concentration of the electroactive species, the current is made dimensionless by using the following form of Erdey-Gruz and Volmer equation[2, 14]:

$$\Psi(t) = \left[\frac{\sqrt{\pi\tau}}{\sqrt{D_{Ox}} C_{Ox}^*}\right] \frac{k^0}{D_{Ox}^{(1-\alpha)/2} D_{Red}^{\alpha/2}} \exp(-\alpha\varphi)\left[\sqrt{D_{Ox}} C_{Ox}(0,t) - \exp(\varphi)\sqrt{D_{Red}} C_{Red}(0,t)\right] \tag{10.3}$$

where $\varphi = \left[\left(\frac{nF}{RT}\right)\left(E_{applied} - E^0\right)\right]$

Integrals representing the current as a function of time and potential are replaced with summations and solved by using numerical methods.[15] The final equation coded in MATLAB to generate voltammograms for the CE_q mechanism is:

$$\Psi_m = \frac{\frac{K\sqrt{\pi}}{K+1} - \left(\varepsilon + \frac{K}{(K+1)}\right)\left(\frac{2}{\pi L}\right)^{1/2} \sum_{i=1}^{i=m-1} \Psi_i S_j - \left(\frac{1}{(K+1)}\right)\left(\frac{1}{k\tau}\right)^{1/2} \sum_{i=1}^{i=m-1} \Psi_i R_j}{\frac{1}{\kappa\varepsilon^{-\alpha}\tau^{1/2}} + \left(\frac{1}{(K+1)}\right)\left(\frac{1}{k\tau}\right)^{1/2} R_1 + \left(\varepsilon + \frac{K}{(K+1)}\right)\left(\frac{2}{\pi L}\right)^{1/2}} \tag{10.4}$$

where L = number of subintervals on each potential, K = equilibrium constant for the following chemical reaction and equal to k_f/k_b, Ψ_m = dimensionless current for each time increment with the serial number m, τ = period, k = the sum of the forward and reverse homogeneous first order rate constants for the chemical reaction preceding the electron transfer, *i.e.* $k_f + k_b$.

In the following sections, the results of simulations for the effect of K and $k_f + k_b$ and the variation of empirical parameters for the CE_q mechanism are presented, first holding $\alpha = 0.5$ and $\log k^0 = -3$. Later, the effects of k^0, followed by a description of diagnostic criteria that can be used to identify a kinetically controlled reaction are presented and comparisons to the CE mechanism are made. This work concludes with protocol for evaluating experimental data.

10.2.2 Effect of K and $k_f + k_b$

The effect of K on the shape of the voltammogram is shown in Figure 10.1a. At low values of K, peak current is quite small, and the peaks are hard to distinguish from the baseline current as equilibrium likes in favor of Y, and little to no Ox is available for reduction. As K increases, the voltammogram takes on the classic CE appearance where the reverse peak is larger than that of the forward peak as the equilibrium begins to shift toward Ox. At large values of K, the peak appears reversible as equilibrium lies in favor

of Ox. The effect of $k_f + k_b$ on the shape of the voltammogram is shown in Figure 10.1b. At low values of $k_f + k_b$, little to no current exists as the rate of conversion of Y to Ox is slow, and thus, there is no Ox available to reduce within the period. As $k_f + k_b$ is increases, peak current increases as more Ox becomes available during each period. The waveshape appears quasireversible, i.e., there is a large separation between the forward and reverse peaks, and at very high $k_f + k_b$ values, two peaks appear on the reverse sweep.[16]

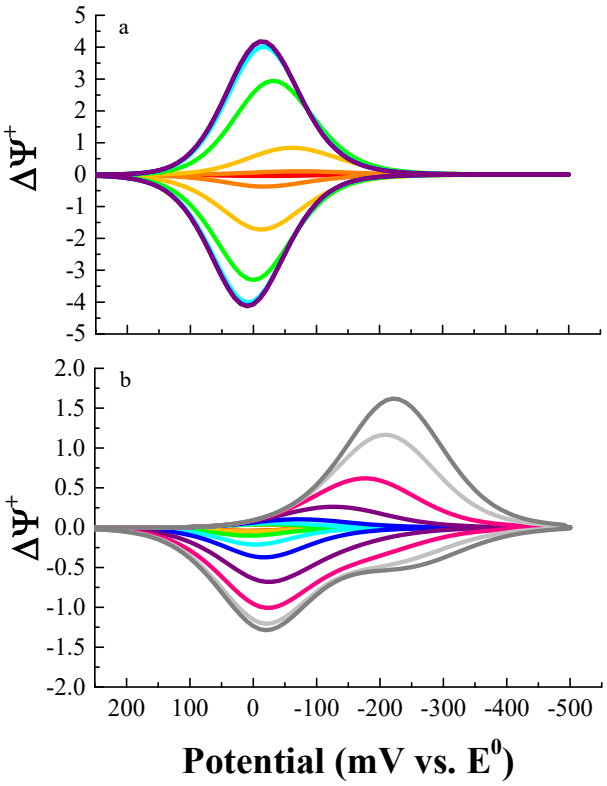

Figure 10.1. The impact of a) K and b) $k_f + k_b$ on the shape of the voltammogram when amplitude = 50 mV, period = 50 ms, increment = 10 mV, switching potential = -500 mV, log k^0 = -3, and $D_{Ox} = D_{Red} = 5 \times 10^{-6}$. For panel a, log K ranges from -3 (red) to 3 (purple) in steps of 1 when log ($k_f + k_b$) = 2. For panel b, log ($k_f + k_b$) ranges from -3 (red) to 6 (dark gray) in steps of 1 when log K = -2.

Peak currents and peak ratio are further investigated as a function of k_f, k_b, and K in Figure 10.2. $\Delta\Psi^+_{p,f}$ and $\Delta\Psi^+_{p,r}$ are invariant with $k_f + k_b$ when log K ≥ 1. Lower values of K increases with $k_f + k_b$ with a manner and magnitude dependent on $k_f + k_b$. Similarly, peak ratio is invariant and equal to unity when log K ≥ 1. Peak ratio increases to a maximum then decreases with $k_f + k_b$ for all other K values. The magnitude of the trend and the $k_f + k_b$ value that the maximum occurs depends on K.

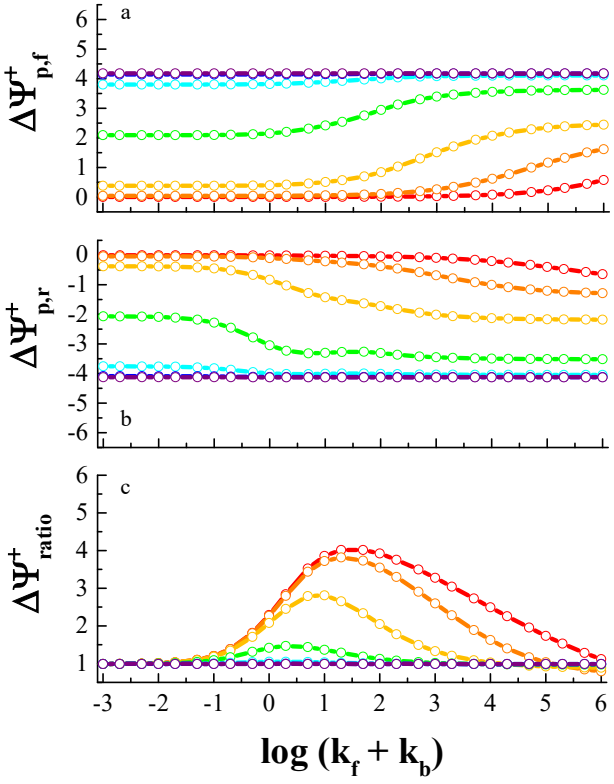

Figure 10.2. The impact of K, k_f, and k_b on a) $\Delta\Psi^+_{p,f}$, b) $\Delta\Psi^+_{p,r}$, and c) peak ratio when amplitude = 50 mV, period = 50 ms, increment = 10 mV, switching potential = -500 mV, log k^0 = -3, and $D_{Ox} = D_{Red}$ = 5 x 10^{-6}. Log K ranges from -3 (red) to 3 (purple) in steps of 1.

Peak potentials are investigated as a function of k_f, k_b, and K in Figure 10.3. $E_{p,f}$ is unaffected by $k_f + k_b$ when log K ≥ 1. $E_{p,f}$ shifts negative with log ($k_f + k_b$) when log K <

1 and log ($k_f + k_b$) ≥ 0. The magnitude of the shift decreases as log ($k_f + k_b$) increases. Similarly, $E_{p,r}$ is in variant with $k_f + k_b$ when log K ≥ 1. $E_{p,r}$ shifts negatively then plateaus when log K < 1 and log ($k_f + k_b$) ≥ 0. The extent of the shift is dependent on $k_f + k_b$. Subsequently, ΔE_p is independent of $k_f + k_b$ when log K ≥ 1. ΔE_p increases when log K < 1 and log ($k_f + k_b$) ≥ 0. The magnitude of ΔE_p decreases as log ($k_f + k_b$) increases.

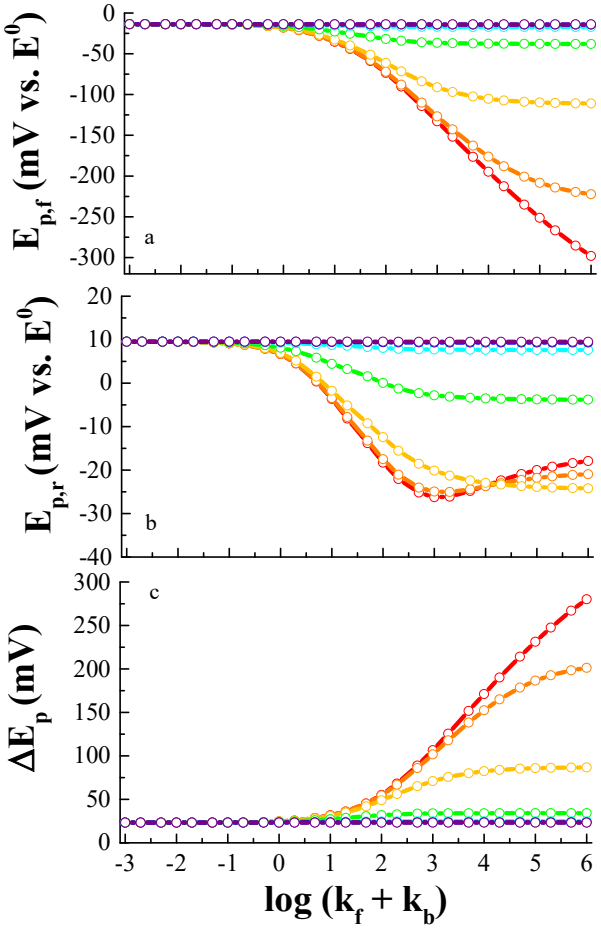

Figure 10.3. The impact of K, k_f, and k_b on a) $E_{p,f}$, b) $E_{p,r}$, and c) peak separation when amplitude = 50 mV, period = 50 ms, increment = 10 mV, log k^0 = -3, $D_{Ox} = D_{Red}$ = 5 x 10^{-6}, and switching potential = -500 mV. Log K ranges from -3 (red) to 3 (purple) in steps of 1.

$W_{1/2}$ increases then decreases with $k_f + k_b$ when log $(k_f + k_b) \geq -1$ and log $K < 1$, and the magnitude is dependent on $k_f + k_b$. $W_{1/2}$ is invariant with $k_f + k_b$ when log $K \geq 1$ (see Figure 10.4).

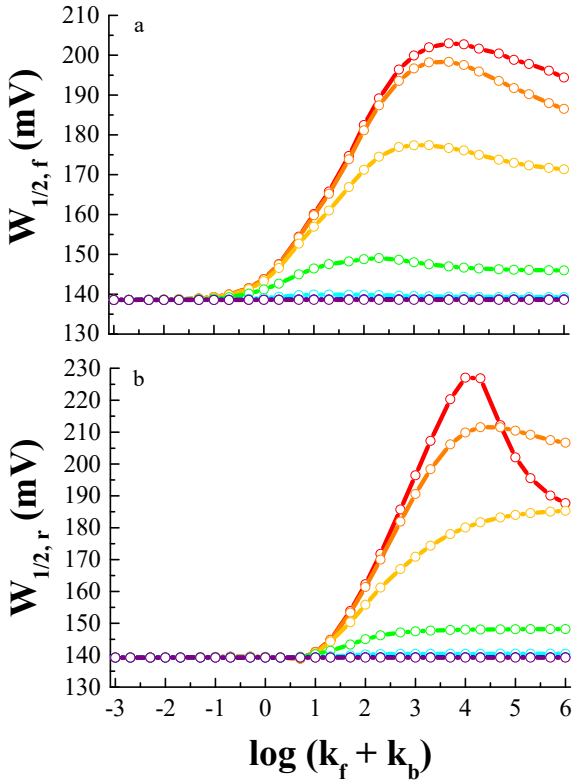

Figure 10.4. The impact of K, k_f, and k_b on a) $W_{1/2,f}$ and b) $W_{1/2,r}$ when amplitude = 50 mV, period = 50 ms, increment = 10 mV, switching potential = -500 mV, log $k^0 = -3$, and $D_{Ox} = D_{Red} = 5 \times 10^{-6}$. Log K ranges from -3 (red) to 3 (purple) in steps of 1.

In comparing the effect of $k_f + k_b$ and K on the CE_q and CE mechanisms, several differences can be identified. $\Delta\Psi^+_{p,f}$ and $\Delta\Psi^+_{p,r}$ have similar trends with both mechanisms, but the magnitude for the CE_q mechanism is lower than that for CE. Peak ratio values are greater for CE_q than for CE when log $K < 1$. Peak potentials and peak separation only change with $k_f + k_b$ when log $K < 1$ for both mechanisms. Trends in peak potentials are similar, however, the magnitudes differ greatly. $E_{p,f}$ shifts more

negatively with $k_f + k_b$ for the CE_q mechanism than the CE case. $E_{p,r}$ shifts more negatively for the CE mechanism than the CE_q. Peak separations are negative and less than 20 mV for the CE mechanism whereas peak separation is positive and may approach 300 mV for the CE_q mechanism. Thus, $k_f + k_b$ and K affect peak potentials differently for the CE_q and CE mechanisms.

10.2.3 Effect of Period (τ)

The effect of period on the voltammogram is shown in Figure 10.5. As period is elongated, peak magnitude decreases and shifts negatively. As shown in Figure 10.5b, $E_{p,f}$ shifts more negatively with period than $E_{p,r}$. $\Delta\Psi^{+}_{p,f}$ is linearly related to period$^{-1/2}$ while $\Delta\Psi^{+}_{p,r}$ is curvilinearly related to period$^{-1/2}$ (see Figure 10.5c). Peak ratio increases then decreases to unity with log period (see Figure 10.5d).

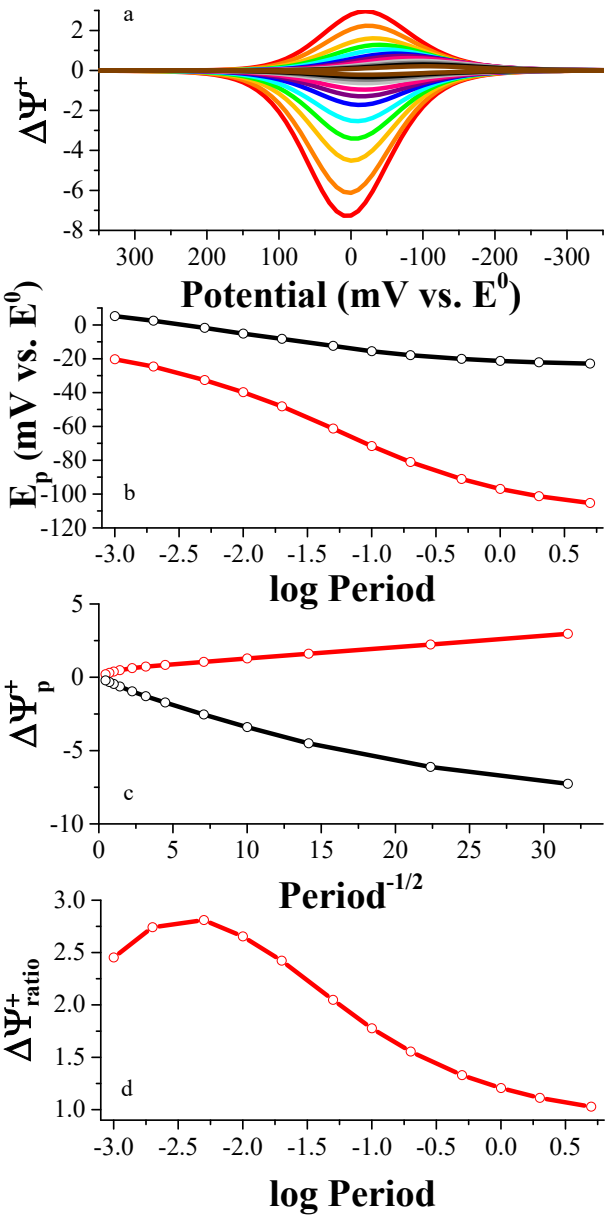

Figure 10.5. The impact of period on the shape of the voltammogram when amplitude = 50 mV, increment = 10 mV, switching potential = -500 mV, log K = -1, log ($k_f + k_b$) = 2, log k^0 = -3, and $D_{Ox} = D_{Red} = 5 \times 10^{-6}$. Panel a): Period ranges from 1 ms (red) to 5 s (brown). Panel b): $E_{p,f}$ (red) and $E_{p,r}$ (black). Panel c): $\Delta\Psi^+_{p,f}$ (red) and $\Delta\Psi^+_{p,r}$ (black). Panel d): Peak ratio (red).

The effect of K on peak ratio as period is varied is shown in Figure 10.6. When log K < 1, peak ratio increases then decreases with log period; the magnitude of the increase

and decrease depends on K. For log K ≥ 1, peak ratio is invariant at unity as period is varied.

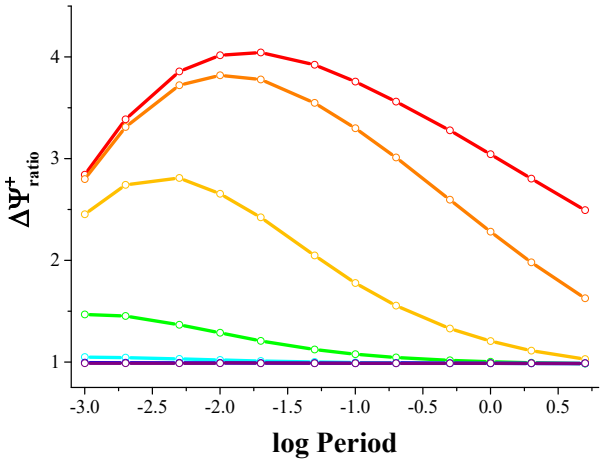

Figure 10.6. The impact of period on the peak ratio as log K is varied from -3 (red) to 3 (purple) when amplitude = 50 mV, increment = 10 mV, switching potential = -500 mV, log ($k_f + k_b$) = 2, log k^0 = -3, and $D_{Ox} = D_{Red} = 5 \times 10^{-6}$.

Peak ratio is further investigated as a function of $k_f + k_b$, K, and period is investigated in Figure 10.7. Several trends in $k_f + k_b$ can be identified when log K ≤ 0. When log ($k_f + k_b$) = -3, peak ratio is essentially unity regardless of K or period. When log ($k_f + k_b$) = -2 and -1, peak ratio increases with period though the magnitude depends on K. When 0 ≤ log ($k_f + k_b$) ≤ 2, peak ratio increases then decreases with period where the magnitude and location of the apex depends on K. When log ($k_f + k_b$) ≥ 3, peak ratio decreases with period with the magnitude dependent on K; at some values of K, peak ratio may be unity dependent on K. When log K > 0, peak ratio is essentially unity and invariant with period.

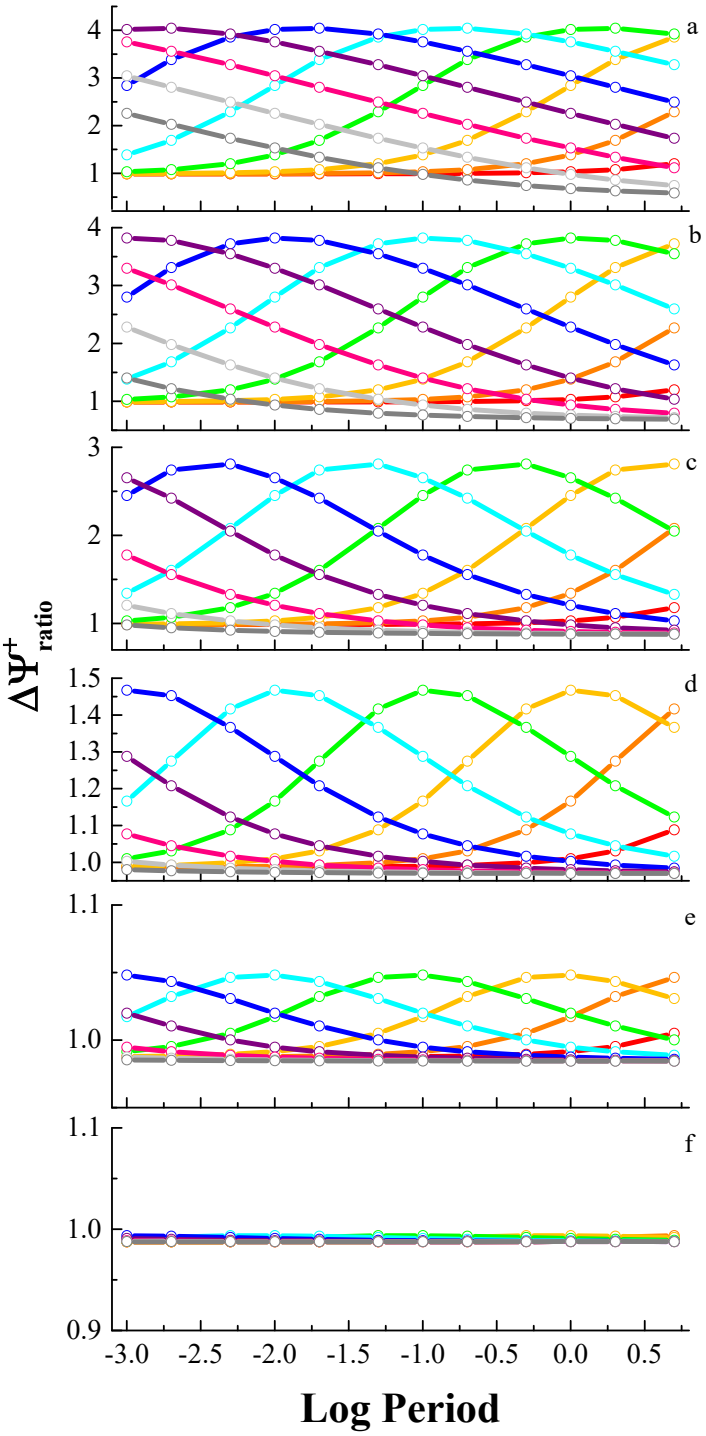

Figure 10.7. The impact of period on peak ratio over the log ($k_f + k_b$) range -3 (red) to 6 (dark gray) for log K = -3 (panel a) to 2 (panel f) when amplitude = 50 mV, increment = 10 mV, switching potential = -500 mV, log k^0 = -3, and $D_{Ox} = D_{Red} = 5 \times 10^{-6}$.

The effect of period on $\Delta\Psi^{+}_{p,f}$ and $\Delta\Psi^{+}_{p,r}$ is displayed in Figure 10.8 for a fixed value of K and the variation of $k_f + k_b$. $\Delta\Psi^{+}_{p,f}$ is linearly related to period$^{-1/2}$ when log ($k_f + k_b$) < 2 and > 5. Otherwise, $\Delta\Psi^{+}_{p,f}$ is curvilinearly related to period$^{-1/2}$. Similarly, $\Delta\Psi^{+}_{p,r}$ is linearly related to period$^{-1/2}$ when log ($k_f + k_b$) < 0 and > 5. Otherwise, $\Delta\Psi^{+}_{p,r}$ is curvilinearly related to period$^{-1/2}$.

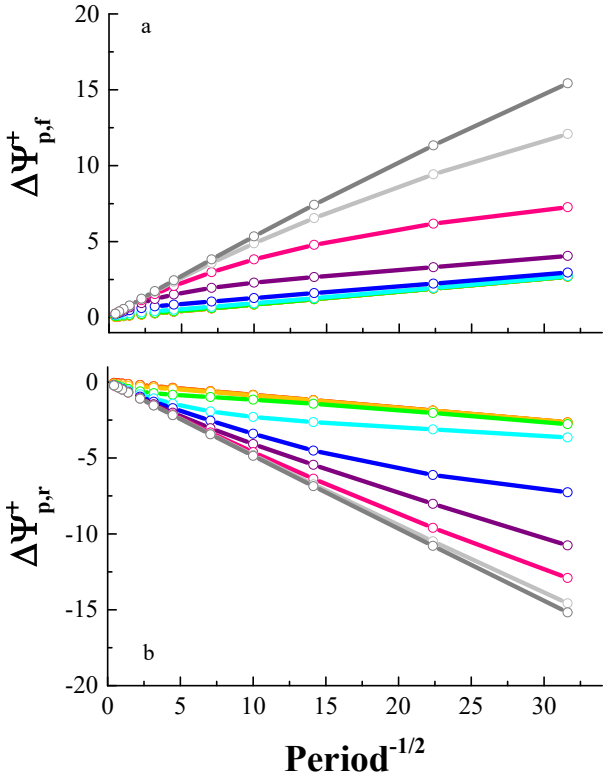

Figure 10.8. The impact of period on $\Delta\Psi^{+}_{p,f}$ and $\Delta\Psi^{+}_{p,r}$ when amplitude = 50 mV, increment = 10 mV, switching potential = -500 mV, log K = -1, log k^0 = -3, $D_{Ox} = D_{Red}$ = 5 x 10^{-6}, and log ($k_f + k_b$) ranges from -3 (red) to 6 (dark gray).

The effect of period on $E_{p,f}$ as a function of k_f, k_b, and K is shown in Figure 10.9. Regardless of K, $E_{p,f}$ is constant with period when log ($k_f + k_b$) < -1. $E_{p,f}$ shifts negative with period for log ($k_f + k_b$) > -1 when log K ≤ 0. The magnitude of the shift and whether

the starting potential is shifted from E^0 is dependent on $k_f + k_b$ and K. $E_{p,f}$ is slightly negative of E^0 by no more than 20 mV and essentially invariant with period when log K > 0.

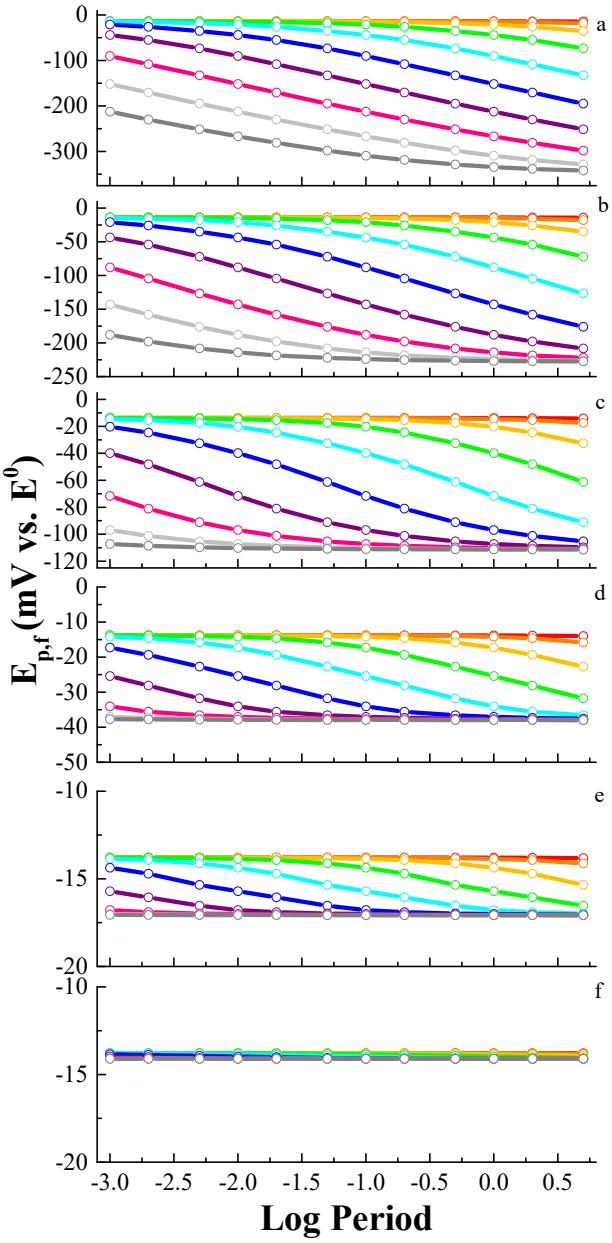

Figure 10.9. The impact of period on $E_{p,f}$ over the log ($k_f + k_b$) range -3 (red) to 6 (dark gray) for log K = -3 (panel a) to 2 (panel f) when amplitude = 50 mV, increment = 10 mV, switching potential = -500 mV, log k^0 = -3, and $D_{Ox} = D_{Red} = 5 \times 10^{-6}$.

The effect of period on $E_{p,r}$ as a function of $k_f + k_b$ and K is shown in Figure 10.10.

When log ($k_f + k_b$) < -1, $E_{p,r}$ is invariant with period regardless of K.

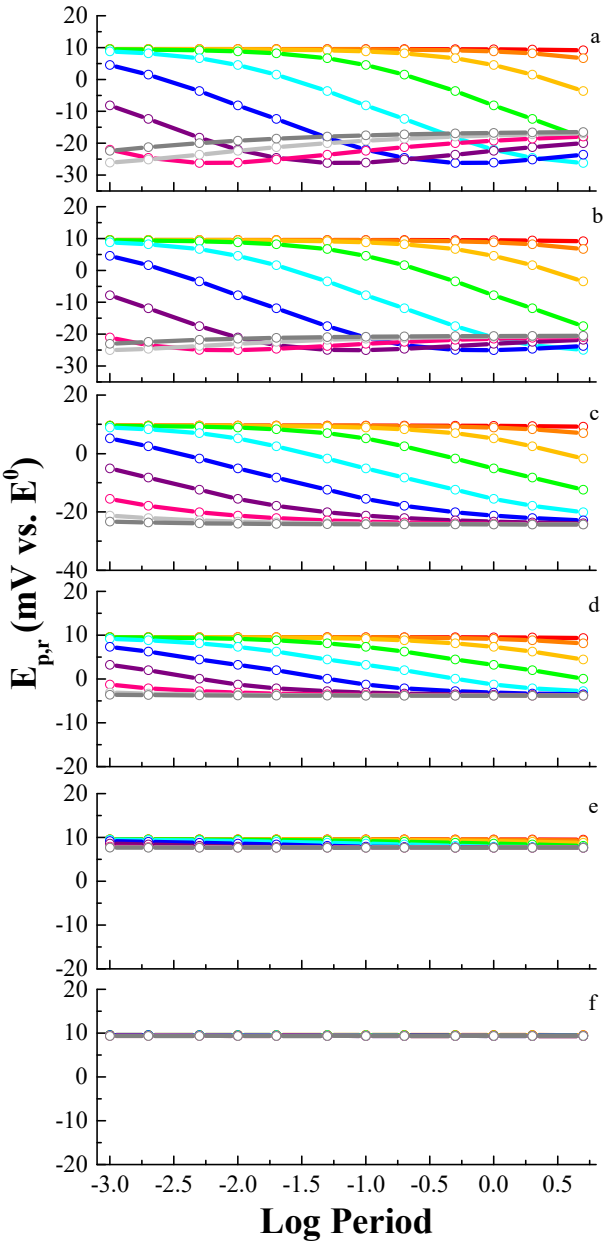

Figure 10.10. The impact of period on $E_{p,r}$ over the log ($k_f + k_b$) range -3 (red) to 6 (dark gray) for log K = -3 (panel a) to 2 (panel f) when amplitude = 50 mV, increment = 10 mV, switching potential = -500 mV, log k^0 = -3, and $D_{Ox} = D_{Red} = 5 \times 10^{-6}$.

$E_{p,r}$ shifts negative with period for log K < 0 and log -1 ≤ $k_f + k_b$ ≤ 3; the magnitude depends on $k_f + k_b$ and K. At higher values of log ($k_f + k_b$), $E_{p,r}$ is constant with period though the magnitude depends on K. When log K ≥ 0, $E_{p,r}$ is essentially invariant and shifted positive of E^0 by ~10 mV regardless of $k_f + k_b$.

Period affects both the CE_q and CE mechanisms. $\Delta\Psi^+_{p,f}$ and $\Delta\Psi^+_{p,r}$ trends with period$^{-1/2}$ are similar though the magnitude for peak currents in the CE_q case are lower than the CE mechanism. Peak ratio trends are similar for these mechanisms, but the magnitude is different; peak ratio values are larger for the CE_q case than CE. $E_{p,f}$ may shift negatively with period for both mechanisms though the magnitude of the shift and the relative position to E^0 is different. Generally, if $E_{p,f}$ shifts, it shifts more for the CE_q case than the CE case. $E_{p,r}$ may shift negatively for both mechanisms, but the location relative to E^0 and the magnitude of the shift differ between the mechanisms. If there is a shift in $E_{p,r}$, it is generally larger for the CE mechanism than the CE_q mechanism. Thus, the magnitude of peak ratio and trends in peak potentials with period may be used to discern between the CE_q and CE mechanisms.

10.2.4 Effect of Increment (δE)

The impact of increment on the CE_q voltammogram is shown in Figure 10.11. The reverse peak is more affected by increment than the forward peak. $E_{p,f}$ shifts negatively by ~10 mV with increment while $E_{p,r}$ shifts positively ~30 mV with increment (see Figure 10.11b). $\Delta\Psi^+_{p,f}$ decreases slightly with increment while $\Delta\Psi^+_{p,r}$ slightly increases with increment (see Figure 10.11c). Subsequently, peak ratio increases with increment for the CE_q case (see Figure 10.11d).

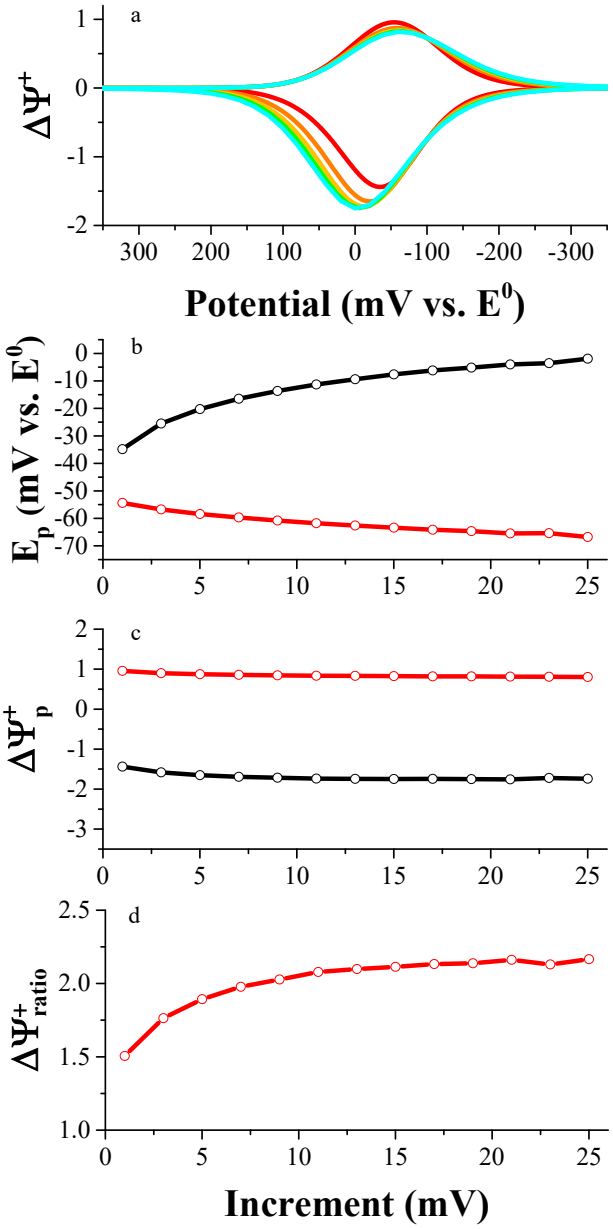

Figure 10.11. The impact of increment on the shape of the voltammogram when amplitude = 50 mV, period = 50 ms, switching potential = -500 mV, log K = -1, log ($k_f + k_b$) = 2, log k^0 = -3, and $D_{Ox} = D_{Red} = 5 \times 10^{-6}$. Panel a): Increment ranges from 1 mV (red), 5 mV (orange), 10 mV (yellow), 15 mV (green), and 20 mV (cyan). Panel b): $E_{p,f}$ (red) and $E_{p,r}$ (black). Panel c): $\Delta\Psi^+_{p,f}$ (red) and $\Delta\Psi^+_{p,r}$ (black). Panel d): Peak ratio (red).

The manner in which increment and K affect peak ratio is shown in Figure 10.12. Peak ratio is greater than unity when log K < 1. For this range in K, the response of peak ratio to increment depends on K. Peak ratio is invariant at unity when log K ≥ 1.

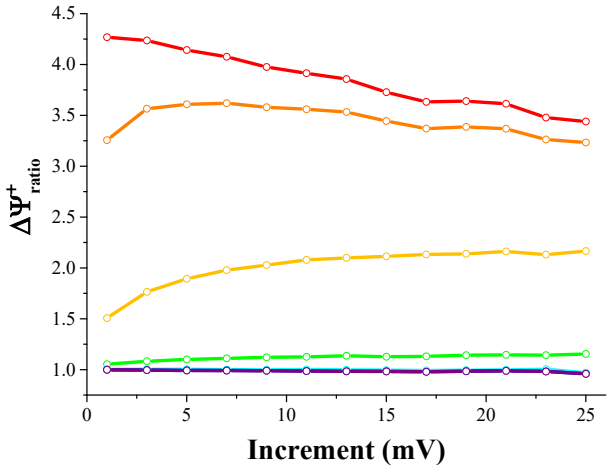

Figure 10.12. The impact of increment on the peak ratio as log K is varied from -3 (red) to 3 (purple) in steps of 1 when amplitude = 50 mV, period = 50 ms, switching potential = -500 mV, log ($k_f + k_b$) = 2, log k^0 = -3, and $D_{Ox} = D_{Red} = 5 \times 10^{-6}$.

Further investigation of peak ratio as a function of k_f, k_b, K, and increment is shown in Figure 10.13. Regardless of K, when log ($k_f + k_b$) ≤ -2 and when log ($k_f + k_b$) > 5, peak ratio is essentially unity and invariant with increment. When log K < 1 and -2 < log ($k_f + k_b$) ≤ 5, peak ratio is larger than unity, and the trend depends on both $k_f + k_b$ and K. When log K ≥ 1, peak ratio is essentially unity with increasing increment.

$\Delta\Psi^{+}_{p,f}$ and $\Delta\Psi^{+}_{p,r}$ are affected by increment as shown in Figure 10.14. $\Delta\Psi^{+}_{p,f}$ is essentially constant with increment when log ($k_f + k_b$) ≤ 3. At higher log ($k_f + k_b$) values, $\Delta\Psi^{+}_{p,f}$ is proportional to increment. $\Delta\Psi^{+}_{p,r}$ is invariant with increment when log ($k_f + k_b$)

< -1. $\Delta\Psi^{+}_{p,r}$ decreases with increment when -1 ≤ log ($k_f + k_b$) < 2 and increases slightly when log ($k_f + k_b$) = 2. $\Delta\Psi^{+}_{p,r}$ increases with increment when log ($k_f + k_b$) > 2.

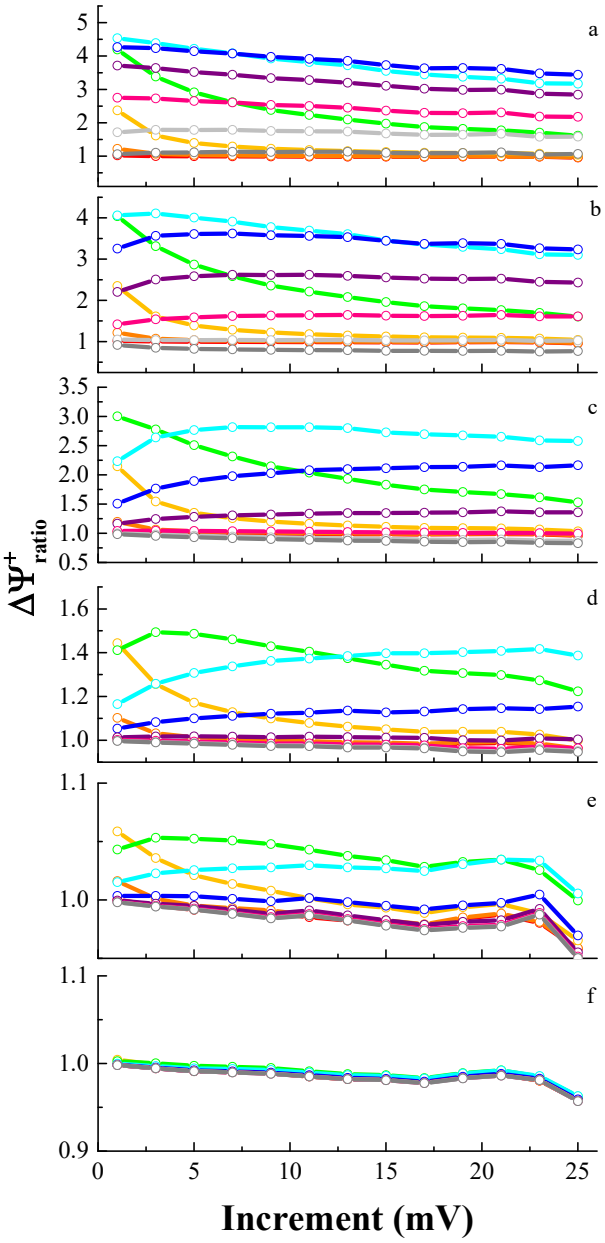

Figure 10.13. The impact of increment on peak ratio over the log ($k_f + k_b$) range -3 (red) to 6 (dark gray) for log K = -3 (panel a) to 2 (panel f) when amplitude = 50 mV, period = 50 ms, switching potential = -500 mV, log k^0 = -3, and $D_{Ox} = D_{Red} = 5 \times 10^{-6}$.

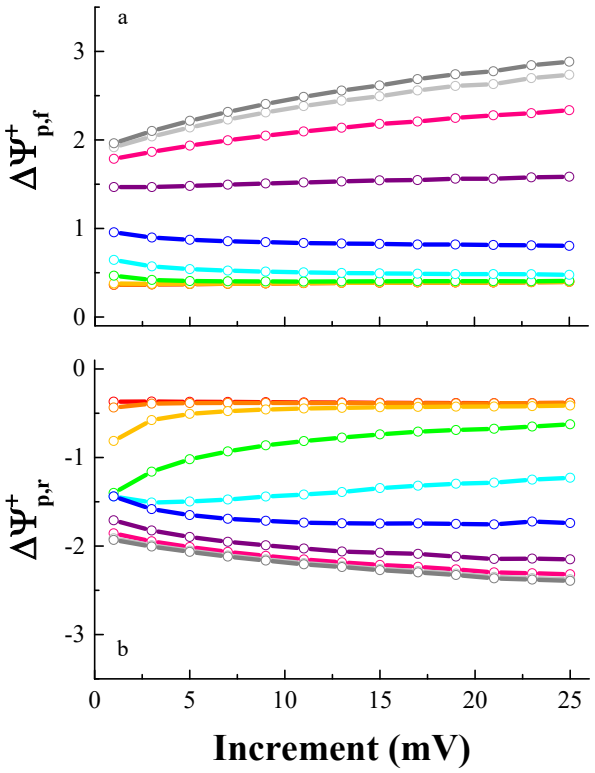

Figure 10.14. The impact of increment on $\Delta\Psi^{+}_{p,f}$ and $\Delta\Psi^{+}_{p,r}$ when amplitude = 50 mV, period = 50 ms, switching potential = -500 mV, log k^0 = -3, $D_{Ox} = D_{Red} = 5 \times 10^{-6}$, log K = -1, and log ($k_f + k_b$) ranges from -3 (red) to 6 (dark gray).

The relationship between peak potentials $E_{p,f}$ and $E_{p,r}$ and increment are shown in Figures 10.15 and 10.16, respectively. $E_{p,f}$ shifts negatively with increment for most combinations of K and $k_f + k_b$. When $E_{p,f}$ does shift, the offset from E^0 and the magnitude of the shift depends on $k_f + k_b$ and K. Conversely, $E_{p,r}$ shifts positively with increment. Again, the offset from E^0 and the magnitude of the shift depends on $k_f + k_b$ and K. For both peak potentials, when log K > 0, all $k_f + k_b$ trends are essentially identical with increment.

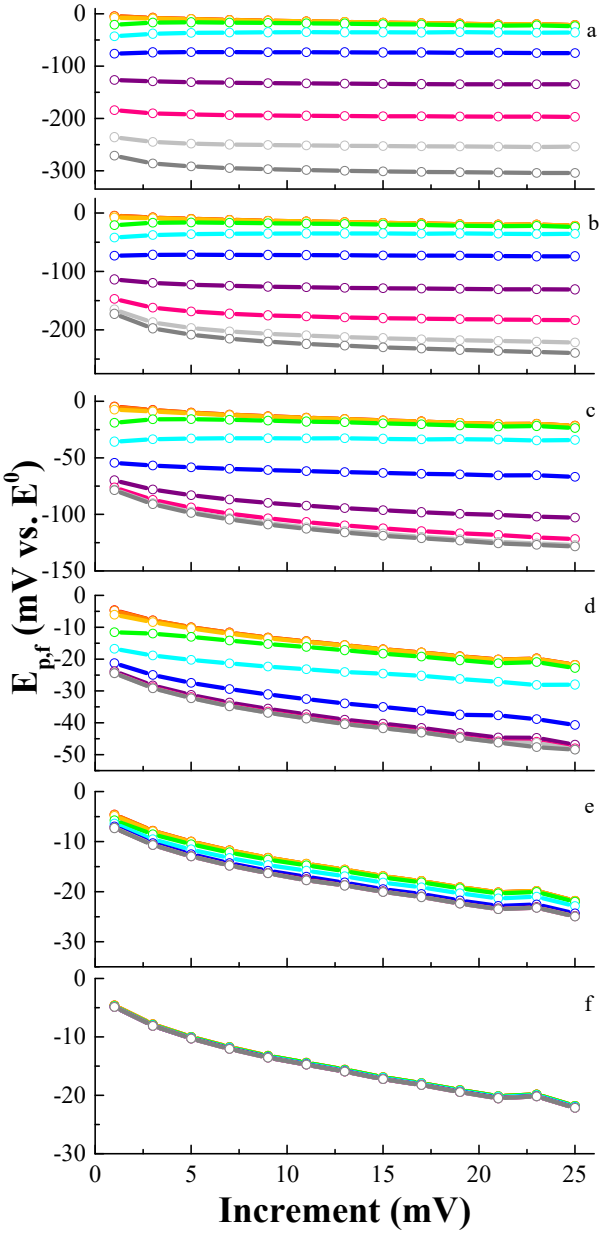

Figure 10.15. The impact of increment on $E_{p,f}$ over the log ($k_f + k_b$) range -3 (red) to 6 (dark gray) for log K = -3 (panel a) to 2 (panel f) when amplitude = 50 mV, period = 50 ms, switching potential = -500 mV, log k^0 = -3, and $D_{Ox} = D_{Red} = 5 \times 10^{-6}$.

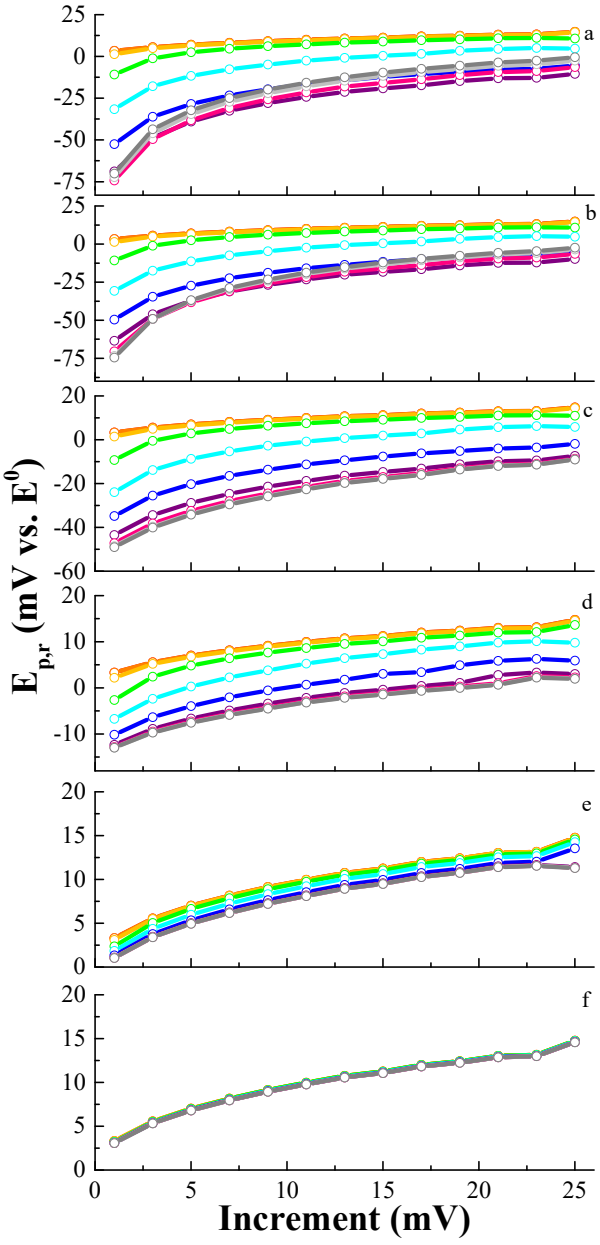

Figure 10.16. The impact of increment on $E_{p,r}$ over the log ($k_f + k_b$) range -3 (red) to 6 (dark gray) for log K = -3 (panel a) to 2 (panel f) when amplitude = 50 mV, period = 50 ms, switching potential = -500 mV, log k^0 = -3, and $D_{Ox} = D_{Red} = 5 \times 10^{-6}$.

Increment affects voltammograms corresponding to the CE_q and CE mechanisms. $\Delta\Psi^{+}_{p,f}$ and $\Delta\Psi^{+}_{p,r}$ values are lower for the CE_q mechanism than the CE. Furthermore, when $\log (k_f + k_b) > 2$, peak currents increase with increment for the CE_q case whereas they are invariant with increment for the CE case. Trends in peak ratio with increment are similar for the two mechanisms, but the magnitudes for the CE_q case is higher than for the CE mechanism. Generally, $E_{p,f}$ shifts negatively with increment for the CE_q case whereas $E_{p,f}$ either shifts positively or is invariant with increment depending on $k_f + k_b$ and K for the CE case. Similarly, $E_{p,r}$ commonly shifts positively with increment for the CE_q case while $E_{p,f}$ is either invariant or shifts positively with increment depending on $k_f + k_b$ and K for the CE case. Thus, increment may be used to discriminate between the CE_q and CE mechanisms when examining the magnitude and trend of peak ratios and peak potentials.

10.2.5 Effect of Switching Potential (E_λ)

The effect of switching potential on the CE_q mechanism is shown in Figure 10.17. The reverse peak is greatly affected by switching potential whereas the forward peak is not. $E_{p,f}$ and $\Delta\Psi^{+}_{p,f}$ are invariant with switching potential. $E_{p,r}$ shifts negatively as switching potential approaches E^0 (see Figure 10.17b). $\Delta\Psi^{+}_{p,r}$ decreases as switching potential approaches E^0 (see Figure 10.17c). As a result, peak ratio decreases as the switching potential nears E^0 (see Figure 10.17d).

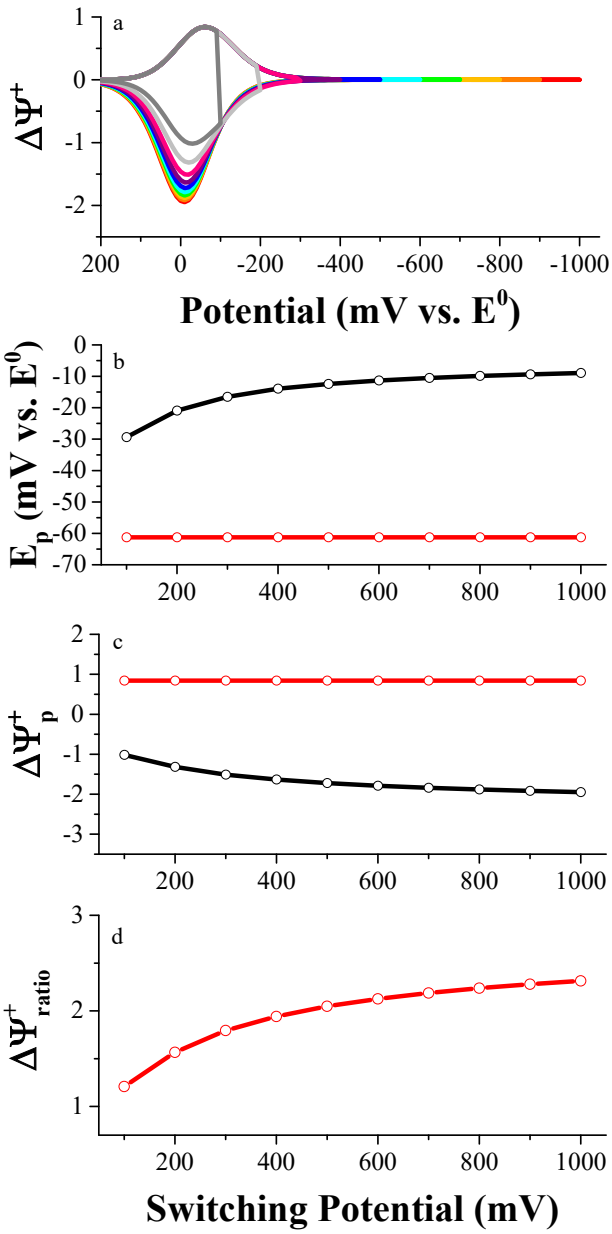

Figure 10.17. The impact of switching potential on the shape of the voltammogram when amplitude = 50 mV, increment = 10 mV, period = 50 ms, log K = -1, log ($k_f + k_b$) = 2, log k^0 = -3, and $D_{Ox} = D_{Red}$ = 5 x 10^{-6}. Panel a): Switching potential ranges from 1000 mV (red), 900 mV (orange), 800 mV (yellow), 700 mV (green), 600 mV (cyan), 500 mV (blue), 400 mV (purple), 300 mV (magenta), 200 mV (light gray), and 100 mV (dark gray). Panel b): $E_{p,f}$ (red) and $E_{p,r}$ (black). Panel c): $\Delta\Psi^+_{p,f}$ (red) and $\Delta\Psi^+_{p,r}$ (black). Panel d): Peak ratio (red).

Switching potential affects peak ratio as shown in Figure 10.18. For log K < 0, peak ratio decreases as the switching potential approaches E^0 though the magnitude of the decrease depends on K. For the scenario when log K ≥ 0, peak ratio is essentially unity and invariant with switching potential.

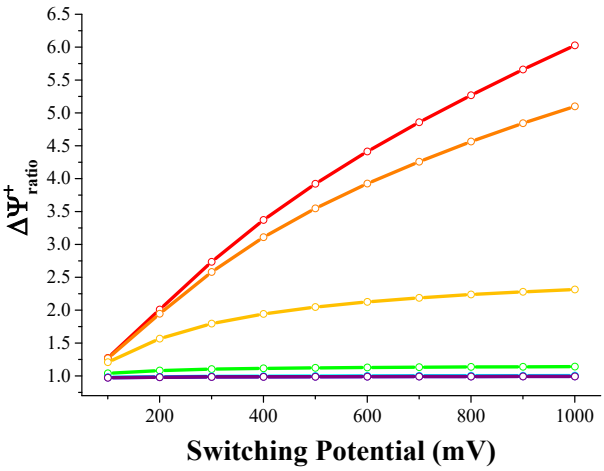

Figure 10.18. The impact of switching potential on the peak ratio as log K is varied from -3 (red) to 3 (purple) in steps of 1 when increment = 10 mV, period = 50 ms, switching potential = -500 mV, log ($k_f + k_b$) = 2 log k^0 = -3, and $D_{Ox} = D_{Red} = 5 \times 10^{-6}$.

Further investigation of the relationship between $k_f + k_b$, K, switching potential, and peak ratio is presented in Figure 10.19. When log K ≤ 0 and when log ($k_f + k_b$) < -1, peak ratio is essentially unity and invariant with switching potential. When log ($k_f + k_b$) > -1, peak ratio may decrease or remain constant depending on K and $k_f + k_b$. When log K > 0, peak ratio is nearly unity and invariant with switching potential.

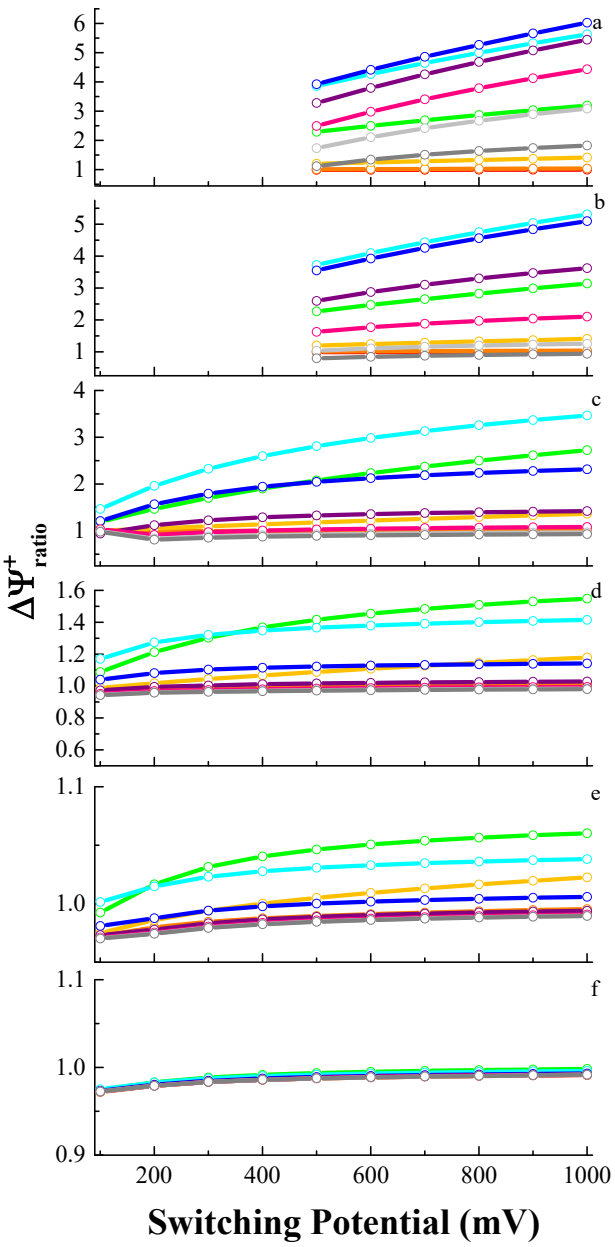

Figure 10.19. The impact of switching potential on peak ratio over the log ($k_f + k_b$) range -3 (red) to 6 (dark gray) for log K = -3 (panel a) to 2 (panel f) when increment = 10 mV, amplitude = 50 mV, period = 50 ms, log k^0 = -3, and $D_{Ox} = D_{Red} = 5 \times 10^{-6}$.

The effect of switching potential on $\Delta\Psi^+_{p,f}$ and $\Delta\Psi^+_{p,r}$ is shown in Figure 10.20.

$\Delta\Psi^+_{p,f}$ is independent of switching potential, but the magnitude of $\Delta\Psi^+_{p,f}$ is influenced by $k_f + k_b$. $\Delta\Psi^+_{p,r}$ is invariant with switching potential when log ($k_f + k_b$) $\leq$ -2 and decreases

as switching potential approaches E^0 when log ($k_f + k_b$) > -2. The magnitude of $\Delta\Psi^+_{p,r}$ also depends on $k_f + k_b$.

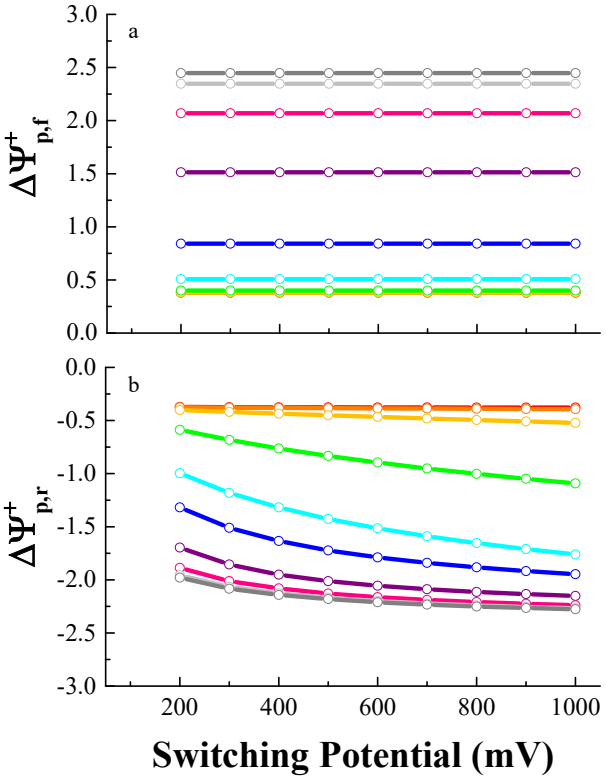

Figure 10.20. The impact of switching potential on $\Delta\Psi^+_{p,f}$ and $\Delta\Psi^+_{p,r}$ when amplitude = 50 mV, increment = 10 mV, period = 50 ms, switching potential = -500 mV, log K = -1, log k^0 = -3, $D_{Ox} = D_{Red} = 5 \times 10^{-6}$, and log ($k_f + k_b$) ranges from -3 (red) to 6 (dark gray).

The relationship between $k_f + k_b$, K, and peak potentials is shown in Figures 10.21 and 10.22. $E_{p,f}$ is invariant with switching potential unless the switching potential occurs before the current returns to baseline. The magnitude of $E_{p,f}$ is dependent on $k_f + k_b$ and K as displayed in Figure 10.21. $E_{p,r}$ shifts negatively with switching potential. The location of $E_{p,r}$ relative to E^0 and the magnitude of the shift is presented in Figure 10.22. Generally, the shift is ~10 mV which is within the error of the increment. However, in

some cases, i.e. log K = -1 and log ($k_f + k_b$) > 2, the shift is much greater and could be experimentally observed.

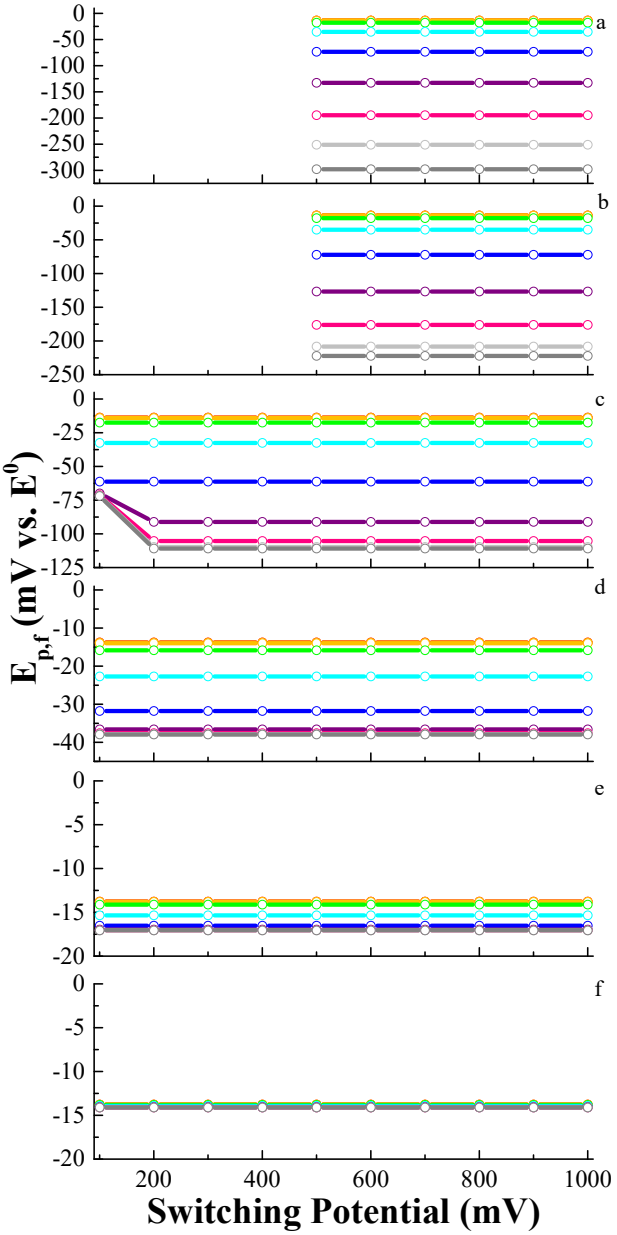

Figure 10.21. The impact of switching potential on $E_{p,f}$ over the log ($k_f + k_b$) range -3 (red) to 6 (dark gray) for log K = -3 (panel a) to 2 (panel f) when amplitude = 50 mV, increment = 10 mV, period = 50 ms, log k^0 = -3, and $D_{Ox} = D_{Red} = 5 \times 10^{-6}$.

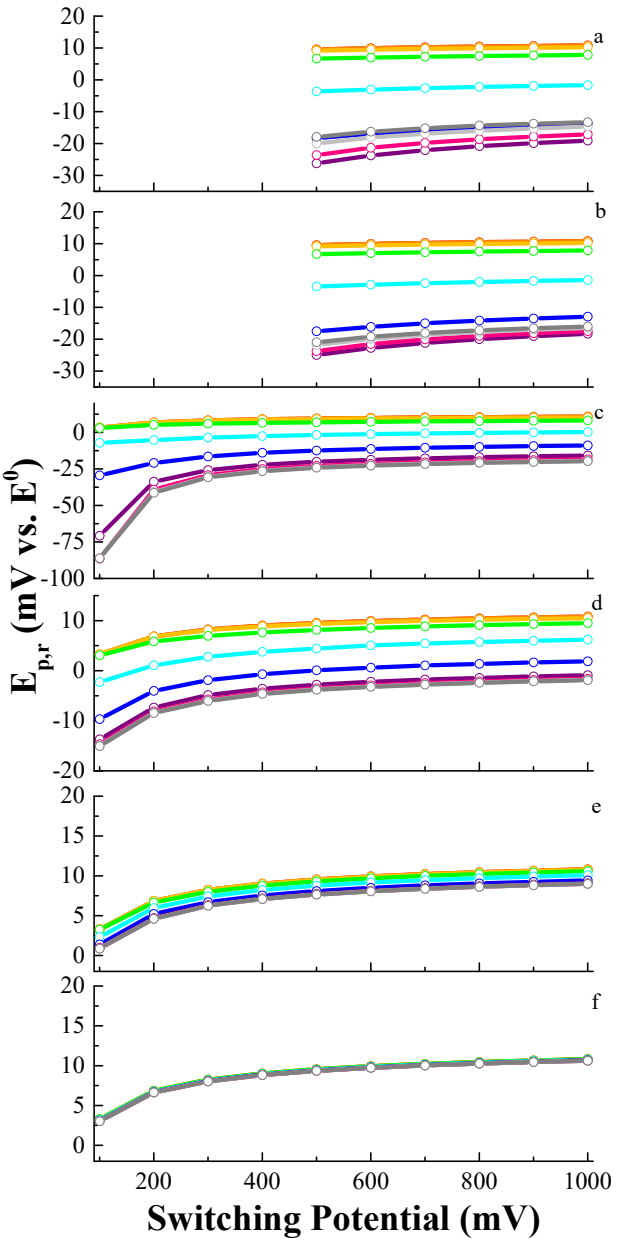

Figure 10.22. The impact of switching potential on $E_{p,r}$ over the log ($k_f + k_b$) range -3 (red) to 6 (dark gray) for log K = -3 (panel a) to 2 (panel f) when amplitude = 50 mV, increment = 10 mV, period = 50 ms, log k^0 = -3, and $D_{Ox} = D_{Red} = 5 \times 10^{-6}$.

Switching potential greatly affects chemically-coupled mechanisms. $\Delta\Psi^{+}_{p,f}$ is unaffected by switching potential for both the CE_q and CE mechanisms though the magnitude is generally lower for the CE_q case. Similarly, $\Delta\Psi^{+}_{p,r}$ is affected by switching

potential for both mechanisms as the switching potential approaches E^0; furthermore, the magnitude of $\Delta\Psi^+_{p,r}$ is generally lower for the CE_q case than the CE. Peak ratio trends with switching potential are similar for the two mechanisms and hard to distinguish. $E_{p,f}$ is unaffected by switching potential for both mechanisms but is determined by $k_f + k_b$ and K for each mechanism. $E_{p,r}$ shifts negatively when switching potential approaches E^0 for the CE_q case whereas it shifts positively for the CE case. In most cases, the shifts are within the error of the increment except for a few select values of $k_f + k_b$ for the CE_q mechanism. Thus, switching potential cannot be used to distinguish between the CE_q and the CE mechanisms though it is readily used to identify a chemically-coupled mechanism.

10.2.6 Effect of Amplitude (E_{SW})

The effect of amplitude on the voltammogram for the CE_q mechanism is shown in Figure 8. As with other empirical parameters, the reverse peak is more affected by amplitude than the forward peak. $E_{p,f}$ is nearly constant with amplitude while $E_{p,r}$ shifts negatively with amplitude (see Figure 10.23b). Both peak currents increase with amplitude though $\Delta\Psi^+_{p,r}$ increases more than $\Delta\Psi^+_{p,f}$ (see Figure 10.23c). Peak ratio decreases with amplitude (see Figure 10.23d).

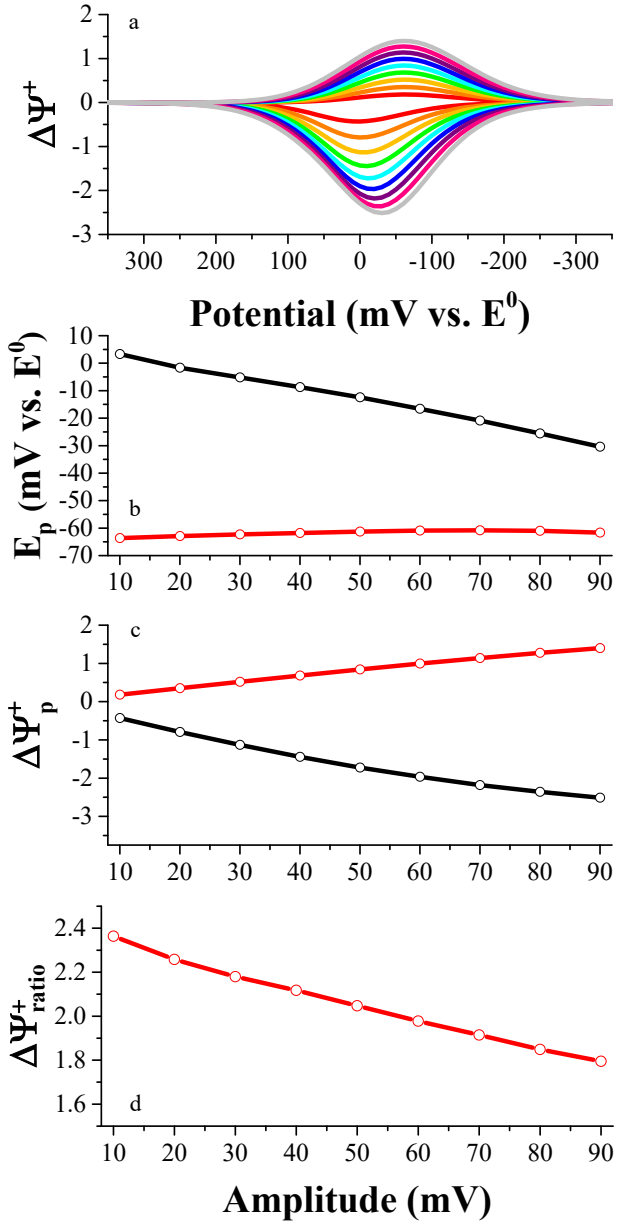

Figure 10.23. The impact of amplitude on the shape of the voltammogram when increment = 10 mV, period = 50 ms, switching potential = -500 mV, log K = -1, log ($k_f + k_b$) = 2, log k^0 = -3, and $D_{Ox} = D_{Red}$ = 5 x 10^{-6}. Panel a): Amplitude ranges from 10 mV (red), 20 mV (orange), 30 mV (yellow), 40 mV (green), 50 mV (cyan), 60 mV (blue), 70 mV (purple), 80 mV (magenta), and 90 mV (light gray). Panel b): $E_{p,f}$ (red) and $E_{p,r}$ (black). Panel c): $\Delta\Psi^+_{p,f}$ (red) and $\Delta\Psi^+_{p,r}$ (black). Panel d): Peak ratio (red).

Peak ratio and its relationship to amplitude is examined in Figure 10.24. When log K < 0, peak ratio decreases with amplitude; the magnitude of peak ratio depends on K. When log K ≥ 0, peak ratio is essentially unity and invariant with amplitude.

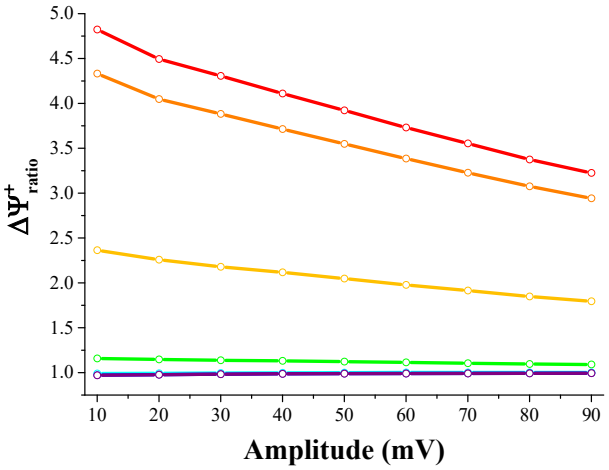

Figure 10.24. The impact of amplitude on the peak ratio as log K is varied from -3 (red) to 3 (purple) in steps of 1 when increment = 10 mV, period = 50 ms, switching potential = -500 mV, log ($k_f + k_b$) = 2, log k^0 = -3, and $D_{Ox} = D_{Red} = 5 \times 10^{-6}$.

Further investigation of peak ratio, $k_f + k_b$, K, and amplitude is presented in Figure 10.25. When log K ≤ 0, peak ratio may be at or greater than unity. Generally, if peak ratio is greater than unity, peak ratio decreases with amplitude. Some exceptions do exist, and the magnitude of the decrease and its maximum value depend on K and $k_f + k_b$. When log K > 0, peak ratio is essentially unity and invariant with amplitude. Figure 10.26 shows the effect of amplitude on $\Delta\Psi^{+}_{p,f}$ and $\Delta\Psi^{+}_{p,r}$. Both $\Delta\Psi^{+}_{p,f}$ and $\Delta\Psi^{+}_{p,r}$ increase with amplitude though the magnitude depends on $k_f + k_b$.

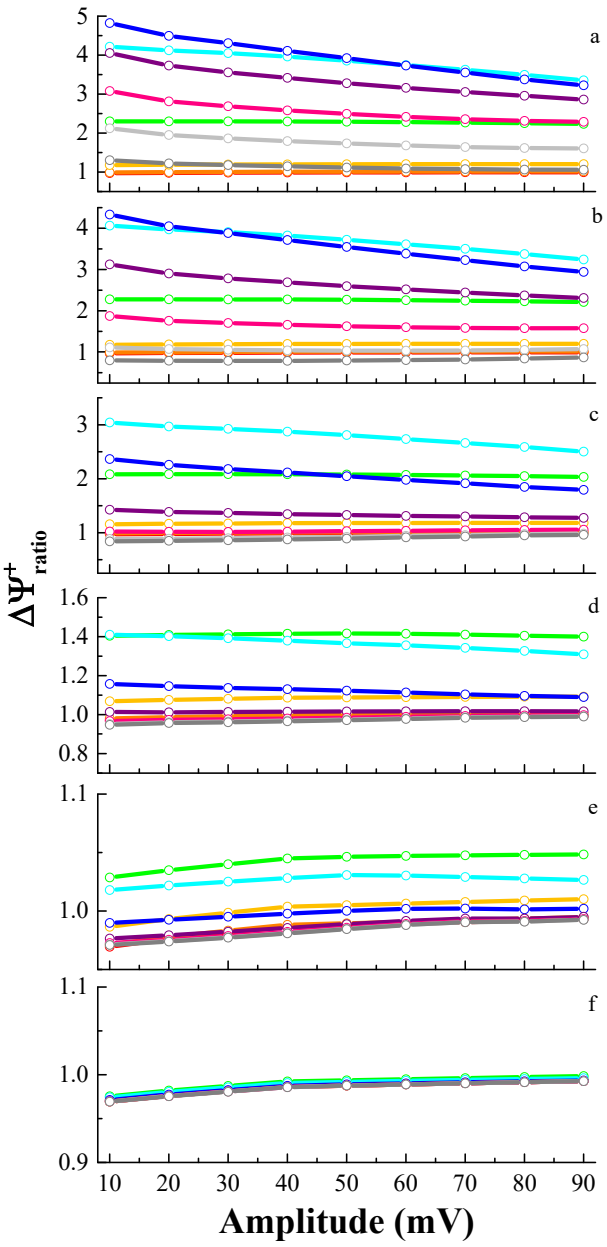

Figure 10.25. The impact of amplitude on peak ratio over the log ($k_f + k_b$) range -3 (red) to 6 (dark gray) for log K = -3 (panel a) to 2 (panel f) when increment = 10 mV, period = 50 ms, switching potential = -500 mV, log k^0 = -3, and $D_{Ox} = D_{Red} = 5 \times 10^{-6}$.

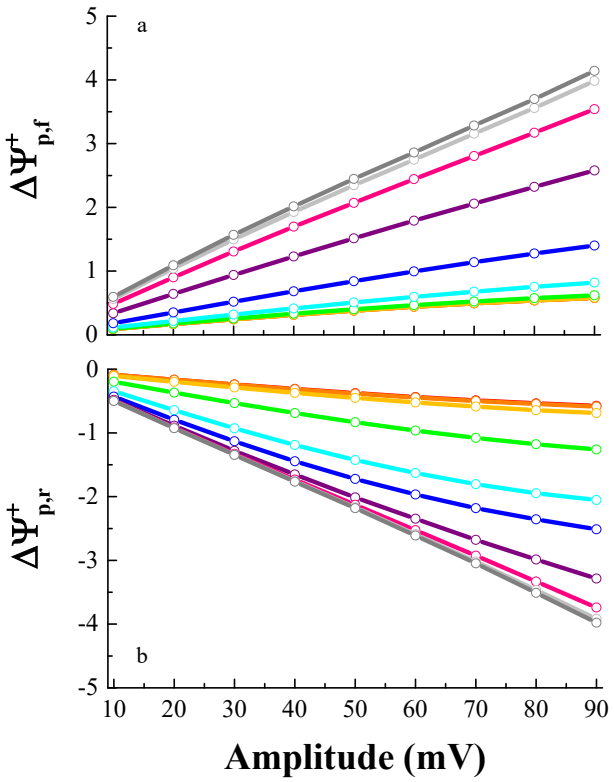

Figure 10.26. The impact of amplitude on $\Delta\Psi^{+}_{p,f}$ and $\Delta\Psi^{+}_{p,r}$ when increment = 10 mV, period = 50 ms, switching potential = -500 mV, log K = -1, log k^0 = -3, and $D_{Ox} = D_{Red} = 5 \times 10^{-6}$ and log ($k_f + k_b$) ranges from -3 (red) to 6 (dark gray).

The effect of amplitude on peak potentials $E_{p,f}$ and $E_{p,r}$ are shown in Figures 10.27 and 10.28, respectively. Generally, $E_{p,f}$ shifts positively with amplitude. The location of $E_{p,f}$ relative to E^0 and the magnitude of the shift depends on $k_f + k_b$ and K. $E_{p,r}$ tends to shift negatively with amplitude, but like $E_{p,f}$ the magnitude of the shift depends on $k_f + k_b$ and K. Most $E_{p,r}$ values begin near E^0 (within ~20 mV of E^0).

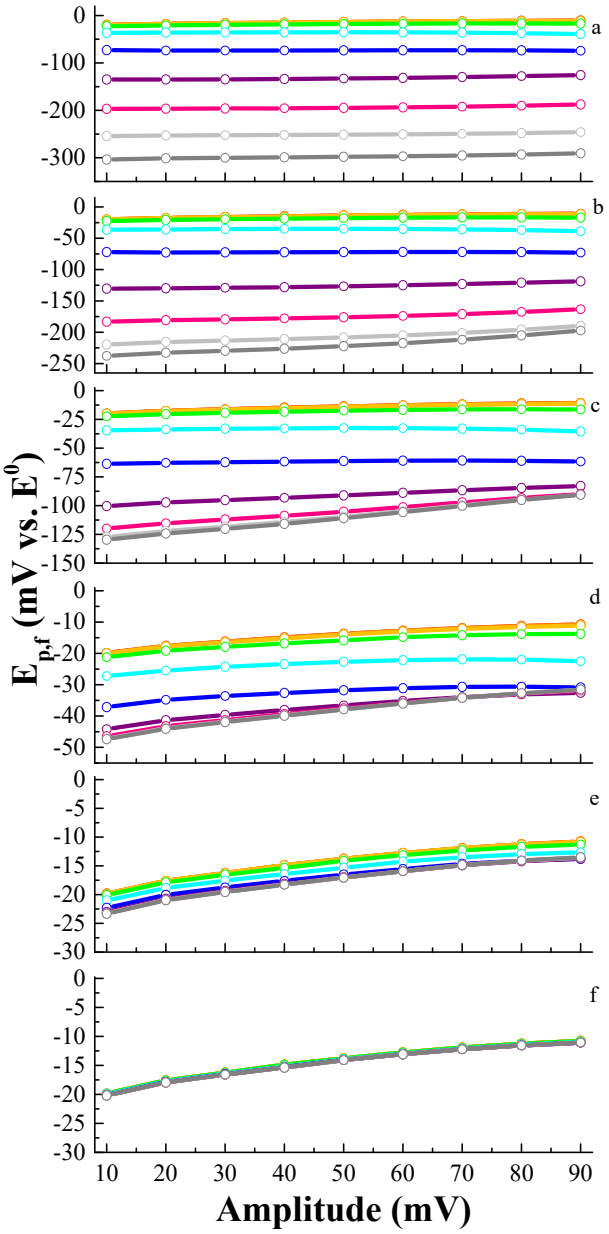

Figure 10.27. The impact of amplitude on $E_{p,f}$ over the log ($k_f + k_b$) range -3 (red) to 6 (dark gray) for log K = -3 (panel a) to 2 (panel f) when increment = 10 mV, period = 50 ms, switching potential = -500 mV, log k^0 = -3, and $D_{Ox} = D_{Red} = 5 \times 10^{-6}$.

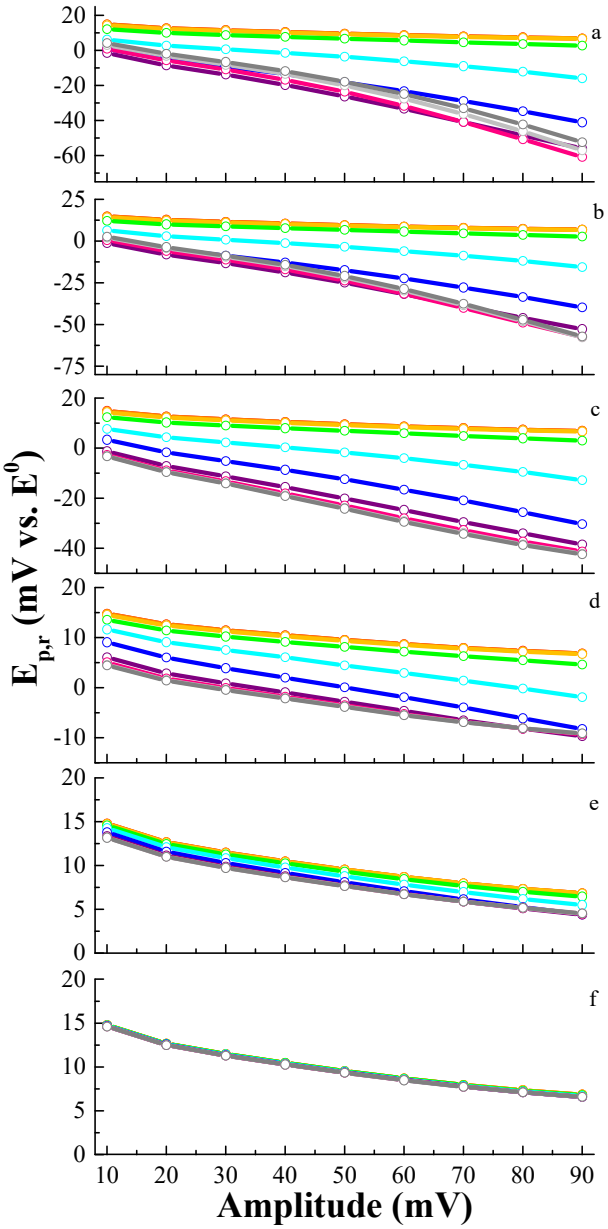

Figure 10.28. The impact of amplitude on $E_{p,r}$ over the log ($k_f + k_b$) range -3 (red) to 6 (dark gray) for log K = -3 (panel a) to 2 (panel f) when increment = 10 mV, period = 50 ms, switching potential = -500 mV, log k^0 = -3, and $D_{Ox} = D_{Red} = 5 \times 10^{-6}$.

Amplitude affects both the CE_q and CE mechanisms. $\Delta\Psi^+_{p,f}$ and $\Delta\Psi^+_{p,r}$ increase with amplitude for both mechanisms. However, the magnitude of the CE_q case is lower than that of the CE case and the trend is usually curvilinear for the CE case and linear for the

CE_q case. Peak ratio is affected by amplitude though the trends for the CE_q and CE mechanisms are nearly the same. $E_{p,f}$ may shift up to 40 mV positively with amplitude for the CE_q case whereas $E_{p,f}$ shifts negatively by no more than 15 mV for the CE case. If $E_{p,r}$ shifts for either mechanism, it shifts negatively with amplitude. The magnitude of the shift and the displacement from E^0 depend on K and $k_f + k_b$. Thus, amplitude may be used to aid in discerning between the CE_q and CE mechanisms.

10.2.7 Effect of k^0

The impact of heterogeneous kinetics on the shape of the voltammogram depends upon the magnitude of k^0 relative to period. The values of α, k^0, D_{ox} and D_{red} are quantities intrinsic to the analyte undergoing an electron transfer reaction at a particular electrode immersed in a specific electrolyte. Though the experimenter varies period and determines k^0 from changes in the shape of the voltammograms, systematically varying k^0 and evaluating the effect on the voltammogram is helpful to understand the effects on the voltammogram waveshape. Hence, in varying k^0 at a fixed value of period is, the responses for different analytes and/or different electrode/electrolyte combinations can be considered.

The effect of k^0 on the shape of the voltammogram for the CE_q mechanism is shown in Figure 10.29. At low values of k^0, peaks are asymmetrically displaced from E^0. One peak appears on the forward sweep, and two peaks are present on the reverse sweep. As k^0 increases, only one peak is present on the reverse sweep, and the peaks approach E^0.

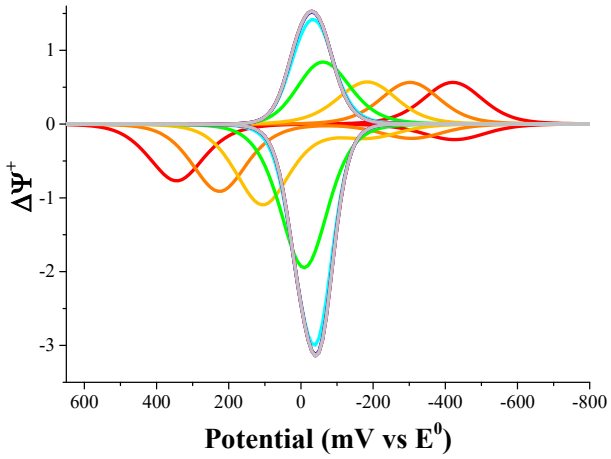

Figure 10.29. The effect of k^0 on the shape of the voltammogram for the CE_q mechanism when amplitude = 50 mV, increment = 10 mV, E_λ = -1000, log K = -1, log (k_f + k_b) = 2, $D_{Ox} = D_{Red} = 5 \times 10^{-6}$, and log k^0 = -6 (red), -5 (orange), -4 (yellow), -3 (green), -2 (cyan), -1 (blue), 0 (purple), 1 (magneta), and 2 (light gray).

The relationship between peak current, k^0, and period is presented in Figure 10.30. $\Delta\Psi^+_{p,f}$ is linearly related to period$^{-1/2}$ at short periods and curvilinearly related to period$^{-1/2}$ at long periods. The slope of the relationship decreases as k^0 decreases. Similarly, $\Delta\Psi^+_{p,r}$ is curvilinearly related to period$^{-1/2}$ for all k^0 investigated, and the slope of the relationship decreases with decreasing k^0. Peak ratio increases then decreases with increasing period as shown in Figure 10.31. Though all traces have the same shape, the maximum magnitude depends on k^0. Thus, the magnitude of maximum peak ratio depends on k^0.

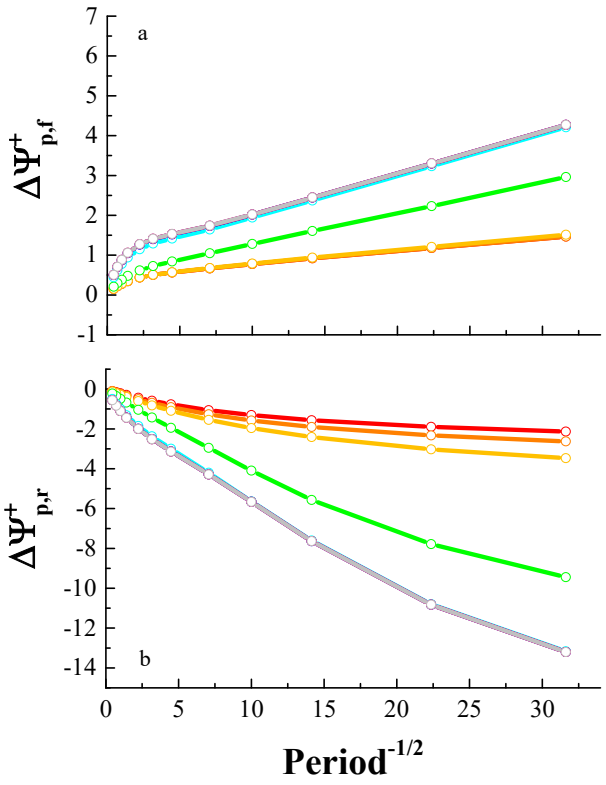

Figure 10.30. The effect of k^0 and period on peak current $\Delta\Psi^{+}_{p,f}$ (panel a) and $\Delta\Psi^{+}_{p,r}$ (panel b) when amplitude = 50 mV, increment = 10 mV, E_λ = -1000, log K = -1, log ($k_f + k_b$) = 2, $D_{Ox} = D_{Red} = 5 \times 10^{-6}$, and log k^0 = -6 (red), -5 (orange), -4 (yellow), -3 (green), -2 (cyan), -1 (blue), 0 (purple), 1 (magneta), and 2 (light gray).

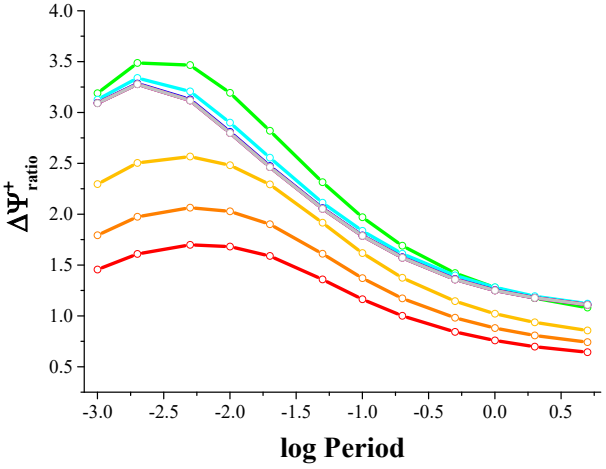

Figure 10.31. The effect of k^0 and period on peak ratio when amplitude = 50 mV, increment = 10 mV, E_λ = -1000, log K = -1, log ($k_f + k_b$) = 2, $D_{Ox} = D_{Red} = 5 \times 10^{-6}$, and log k^0 = -6 (red), -5 (orange), -4 (yellow), -3 (green), -2 (cyan), -1 (blue), 0 (purple), 1 (magneta), and 2 (light gray).

Peak potentials are also affected by k^0 as shown in Figure 10.32. $E_{p,f}$ shifts negatively with period for all values of k^0 though the magnitude and negative offset from E^0 depend on k^0. Trends in $E_{p,f}$ for log $k^0 > -3$ are indistinguishable.

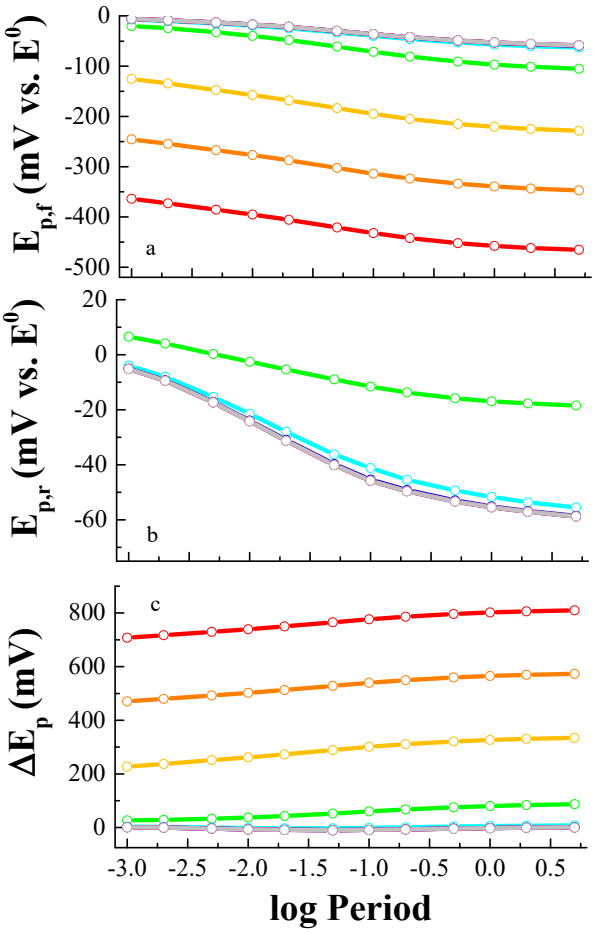

Figure 10.32. The effect of k^0 and period on peak potential: a) $E_{p,f}$, b) $E_{p,r}$, and c) ΔE_p when amplitude = 50 mV, increment = 10 mV, E_λ = -1000 mV, log K = -1, log ($k_f + k_b$) = 2, $D_{Ox} = D_{Red} = 5 \times 10^{-6}$, and log k^0 = -6 (red), -5 (orange), -4 (yellow), -3 (green), -2 (cyan), -1 (blue), 0 (purple), 1 (magneta), and 2 (light gray).

$E_{p,r}$ is constant and offset positively from E^0 for log $k^0 < -3$. When log $k^0 \geq -3$, $E_{p,r}$ shifts negatively with period though only the trend for log $k^0 = -3$ is discernable from faster electron transfer rates. As a result of these trends, ΔE_p increases with period for log $k^0 \leq$

-3, and ΔE_p is essentially invariant for log $k^0 > -3$. Thus, peak potentials are discernably affected by period and k^0 when the magnitude of k^0 approaches irreversibility.

Throughout this chapter, comparisons have been made between the CE_q and CE mechanisms. Next, comparisons must be made between the E_{quasi} mechanism and the CE_q mechanism so that the user can readily discern the two by using the variation of period. Peak currents are linearly or curvilinearly related to period$^{-1/2}$ for both mechanisms. However, the trends in peak ratio are quite different. Peak ratio increases towards unity with period for the E_{quasi} mechanism but increases then decreases towards unity for the CE_q mechanism as shown in Figure 10.33. Readers are reminded that peak ratio is generally greater than unity for the CE_q case and that peak ratio depends on k^0 for both mechanisms. A singular value of k^0 was chosen to emphasize the differences in trends for these mechanisms.

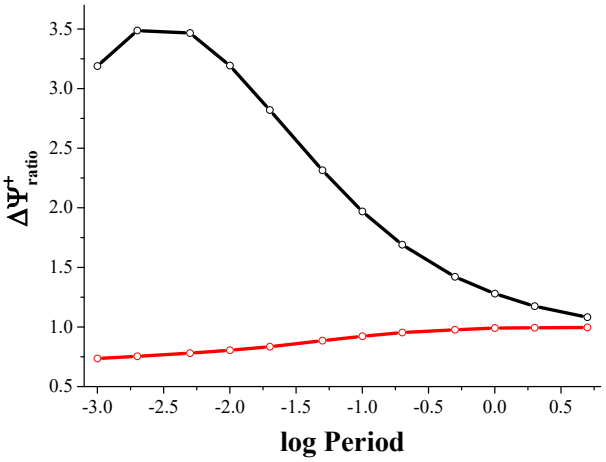

Figure 10.33. The effect of period on peak ratio for the E_{quasi} (red) and CE_q (black) mechanisms when amplitude = 50 mV, increment = 10 mV, E_λ = -1000 mV, $D_{Ox} = D_{Red} = 5 \times 10^{-6}$, and log $k^0 = -3$. For the CE_q case, Elog K = -1, log $(k_f + k_b) = 2$.

Trends in peak potentials differ drastically for the two mechanisms as presented in Figure 10.34. Peak potentials approach E^0 for the E_{quasi} case; $E_{p,r}$ shits negatively while $E_{p,f}$ shifts positively. In contrast, $E_{p,f}$ and $E_{p,r}$ both shift negatively for the CE_q case with the magnitude of the shift and the displacement from E^0 dependent on k^0. As a result of these trends in peak potentials, ΔE_p decreases for the E_{quasi} case whereas is either constant or increases for the CE_q case. It should be noted that the displacement of peak potentials and magnitude of peak separation depends on k^0 for both mechanisms. Thus, the variation of period can be used to distinguish between these mechanisms.

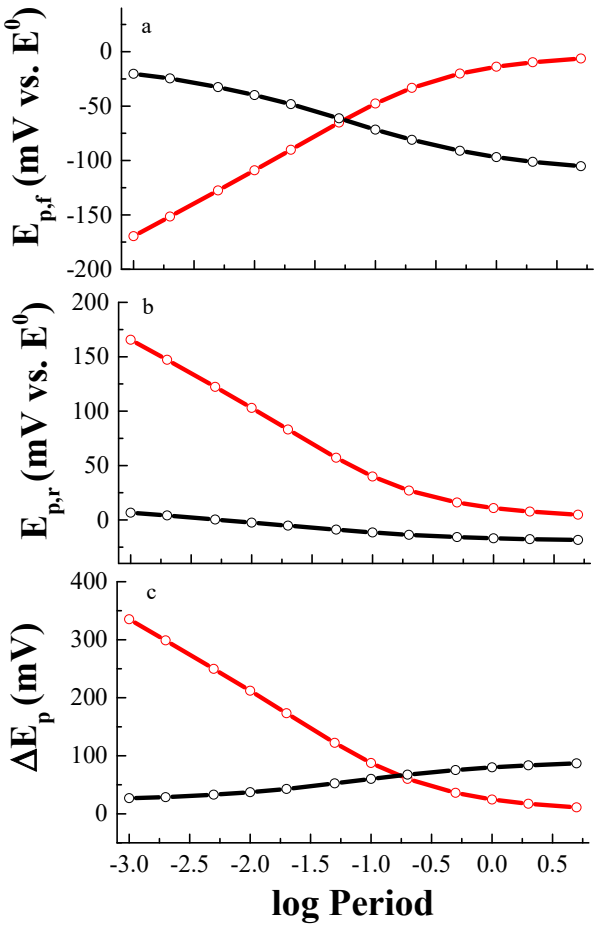

Figure 10.34. The effect of period on a) $E_{p,f}$, b) $E_{p,r}$, and c) ΔE_p for the E_{quasi} (red) and CE_q (black) mechanisms when amplitude = 50 mV, increment = 10 mV, E_λ = -1000 mV, $D_{Ox} = D_{Red} = 5 \times 10^{-6}$, and log k^0 = -3. For the CE_q case, Elog K = -1, log ($k_f + k_b$) = 2.

10.3 Conclusion

This work has shown the effect of empirical parameters on peak parameters for the CE_q mechanism. Furthermore, the effect of K and $k_f + k_b$ on the shape of the voltammogram for the CE_q mechanism has been presented. The diagnostic criteria for the CE_q mechanism have been elucidated as a result of the investigation of trends in of peak parameters as a function of empirical parameters as presented in Table 10.1. This table in combination with the figures presented in this work allows the experimenter to identify the CE_q reaction mechanism and determine kinetic parameters associated with the chemical reaction. Comparisons have been made throughout this work to highlight the differences in peak parameter trends for the CE and CE_q mechanisms.

Table 10.1. Diagnostic Plots and Protocol for Assessing a CE_q Electrode Reaction by CSWV

	Empirical variables							
Waveform parameters	***Period, τ***		***Increment, δE***		***Switching potential, E_λ***		***Amplitude, E_{SW}***	
	Plot	**Trace**	**Plot**	**Trend**	**Plot**	**Trend**	**Plot**	**Trend**
Peak currents	ΔI_p vs. $\tau^{-1/2}$	ΔI_p may be linear or curvilinear with period$^{-1/2}$ depending on K and $k_f + k_b$ (see Figures 10.5c and 10.8)	ΔI_p vs. δE	ΔI_p has a complex relationship with δE; the trend depends on K and $k_f + k_b$ (see Figures 10.11c and 10.14)	ΔI_p vs. E_λ	$\Delta I_{p,f}$ is invariant with E_λ whereas $\Delta I_{p,r}$ decreases as E_λ approaches E^0 (see Figures 10.17c and 10.20)	ΔI_p vs. E_{SW}	ΔI_p increases with amplitude (see Figures 10.23c and 10.26)
Peak ratio	Peak ratio vs. log τ	Peak ratio ≥ 1 but the trend depends on K and $k_f + k_b$ (see Figures 10.5d, 10.6, and 10.7)	Peak ratio vs. δE	Peak ratio ≥ 1 but the trend depends on K and $k_f + k_b$ (see Figures 10.11d, 10.12, and 10.13)	Peak ratio vs. E_λ	Peak ratio decreases as E_λ approaches E^0 for log K < 0 and is unity for log K ≥ 0; the decrease depends on K and $k_f + k_b$ (see Figures 10.17d, 10.18, and 10.19)	Peak ratio vs. E_{SW}	Peak ratio decreases or is invariant and is ≥ unity (see Figures 10.23d, 10.24, and 10.25)
Peak potentials	E_p vs. log τ	E_p values are either invariant or shifts negatively with period; the magnitude of the shift and displacement from E^0 depends on K and $k_f + k_b$ (see Figures 10.5b, 10.9, and 10.10)	E_p vs. δE	$E_{p,f}$ shifts negatively and $E_{p,r}$ shifts positively with δE though sometimes Ep is invariant with δE; the magnitude of the shift and displacement from E^0 depends on K and $k_f + k_b$ (see Figures 10.11b, 10.15, and 10.16)	E_p vs. E_λ	$E_{p,f}$ is invariant with E_λ; $E_{p,r}$ may or may not shift negatively with E_λ approaches E^0. The magnitude of each depends on K and $k_f + k_b$ (see Figures 10.17b, 10.21, and 10.22)	E_p vs. E_{SW}	$E_{p,f}$ shifts positively while $E_{p,r}$ shifts negatively; the magnitude of the shift and displacement from E^0 depends on $k_f + k_b$ and K (see Figures 10.23b, 10.27, and 10.28)
Peak separation	ΔE_p vs. log τ	Invariant when log K > -1; increases or invariant when log K ≤ -1 (see Figures 10.5b, 10.9, and 10.10)	ΔE_p vs. δE	Generally increases negatively with δE	ΔE_p vs. E_λ	Generally constant but may be decrease as E_λ approaches E^0	ΔE_p vs. E_{SW}	$\Delta E_p \geq 0$ for log K < 0 and $\Delta E_p = 0$ for log K ≥ 0
Peak widths	$W_{1/2}$ vs. log τ	Invariant when log K > -1; increases or invariant when log K ≤ -1	$W_{1/2}$ vs. δE	Generally increases with δE	$W_{1/2}$ vs. E_λ	$W_{1/2}$ is only affected if E_λ occurs before the current returns to baseline	$W_{1/2}$ vs. E_{SW}	$W_{1/2}$ increases with amplitude

10.4 References

1. Nicholson, R.S. and I. Shain. *Anal. Chem.*, **1964**. 36, 706-723.

2. O'Dea, J.J., J. Osteryoung, and R.A. Osteryoung. *Anal, Chem.*, **1981**. 53, 695-701.

3. Saveant, J.M. and F. Xu. *J. Electroanal. Chem. Interfacial Electrochem.*, **1986**. 208, 197-217.

4. Bilewicz, R., K. Wikiel, R. Osteryoung, and J. Osteryoung. *Anal. Chem.*, **1989**. 61, 965-972.

5. Horno, J., M.T. Garcia-Hernandez, and C.F. Gonzalez-Fernandez. *J. Electroanal. Chem.*, **1994**. 377, 53-60.

6. El-Hallag, I.S., M.M. Ghoneim, and E. Hammam. *Anal. Chim. Acta*, **2000**. 414, 173-180.

7. Moharram, Y.I. *J. Electroanal. Chem.*, **2004**. 563, 283-290.

8. Mirčeski, V., Š. Komorsky-Lovrić, and M. Lovrić, *Square Wave Voltammetry: Theory and Application*, *Monographs in Electrochemistry*. **2007**, Springer-Verlag: Berlin.

9. Molina, A. and I. Morales. *Int. J. Electrochem. Sci.*, **2007**. 2, 386-405.

10. Molina, A., F. Martinez-Ortiz, E. Laborda, and I. Morales. *J. Electroanal. Chem.*, **2009**. 633, 7-14.

11. Moulton, R.D., A.J. Bard, and S.W. Feldberg. *J. Electroanal. Chem. Interfacial Electrochem.*, **1988**. 256, 291-307.

12. Garay, F. and M. Lovrić. *Electroanalysis*, **2002**. 14, 1635-1643.

13. Garay, F. and M. Lovrić. *J. Electroanal. Chem.*, **2002**. 518, 91-102.

14. Erdey-Gruz, T., *Kinetics of Electrode Processes*. **1972**, Wiley-Interscience Division: New York.

15. Nicholson, R.S. and M.L. Olmstead, *Electrochemistry: Calculations, Simulation and Instrumentation,*. **1972**, Marcel Dekker: New York. Ch. 5

16. Mann, M.A., J.C. Helfrick, Jr., and L.A. Bottomley. *Anal. Chem.*, **2014**. 86, 8183-8191.

CHAPTER 11

COMPARISON OF DIAGNOSTIC CRITERIA TO DISCRIMINATE BETWEEN MECHANISMS

11.1 Introduction

One of the overarching goals of this thesis was to generate diagnostic criteria for electrode reaction mechanisms using CSWV. This was accomplished by evaluating the peak parameters as a function of the empirical parameters for every mechanism investigated herein. The aim of this chapter is to provide the experimentalist with the ability to rapidly and easily distinguish one mechanism from another using CSWV. To do so, plots of peak parameters versus empirical parameters were collected for several mechanisms. Specifically, mechanisms presented in this chapter include the reversible, quasireversible, surface-confined, and chemically coupled electron transfer reactions. The nomenclature used for the chemically coupled mechanisms assumes that electron transfers are either reversible or quasireversible (denoted by a q), and the chemical reaction is either irreversible (irrev) or reversible (rev). The following conditions were used for each mechanism: for the quasireversible mechanism, is $\log k^0 = -3$; for the surface-confined mechanism, $\log k^0 = -1$; for the EC_{irrev} mechanism, $\log K = 3$ and $\log k_f + k_b = 0$; for the E_qC_{irrev} mechanism, $\log K = 3$, $\log k_f + k_b = 0$, and $\log k^0 = -3$; for the EC_{rev} mechanism, $\log K = 0$ and $\log k_f + k_b = 0$; for the E_qC_{rev} mechanism, $\log K = 0$, $\log k_f + k_b = 0$, and $\log k^0 = -3$; for the $C_{irrev}E$ mechanism, $\log K = -1$ and $\log k_f + k_b = 2$; for the $C_{irrev}E_q$ mechanism, $\log K = -1$, $\log k_f + k_b = 2$, and $\log k^0 = -3$; for the $C_{rev}E$ mechanism, $\log K = 0$ and $\log k_f + k_b = 0$, and for the $C_{rev}E_q$ mechanism, $\log K = 0$, $\log k_f + k_b = 0$, and $\log k^0 = -3$. Comparisons to the Nicholson and Shain diagnostic criteria[1]

were made where possible. Additionally, comparisons to published SWV work were made to examine the similarities between SWV and CSWV and highlight the mechanistic information gained by using a technique comprised of two potential sweeps. This chapter concludes with a protocol for experimentalists to distinguish reaction mechanisms and the future work regarding CSWV as a mechanistic tool.

11.2 Effect of Period (τ)

Peak parameters are markedly dependent on period as shown in Chapters 3-10. The relationship between peak currents and period has been shown in Figures 3.15, 3.22, 4.22, 5.5c, 5.9, 6.5c, and 6.9. Here, the trends are compiled for comparison in Figure 11.1 so that the experimenter can visualize the differences between mechanisms. Peak currents are linearly related to period$^{-1/2}$ for all diffusional mechanisms shown except for $C_{irrev}E$ where $\Delta\Psi^{+}_{p,r}$ is curvilinearly related to period$^{-1/2}$ as shown in Figures 11.1a and 11.1b. Peak currents for the surface-confined case are linear to period^{-1} as displayed in Figures 11.1c and 11.1d. Experimenters can easily discriminate the between the surface-confined and diffusion controlled processes by plotting peak current versus period$^{-1/2}$ and peak current versus period^{-1}. Whichever trend is linear signifies a diffusional or surface-confined processes, respectively.

The differing slopes of the diffusion controlled processes warrant further examination. It is interesting to note that the slope of peak current versus period$^{-1/2}$ for the quasireversible, E_qC_{irrev}, E_qC_{rev}, $C_{irrev}E$, $C_{irrev}E_q$, $C_{rev}E_q$, $C_{rev}E$ mechanisms is less than the slope for the reversible, EC_{irrev}, and EC_{rev} mechanisms. The mechanisms with smaller slopes are all complicated by a process that inhibits the electron transfer – for the

quasireversible cases, sluggish electron kinetics, and for the CE cases, the amount of Ox available is limited by the conversion of Y to Ox.

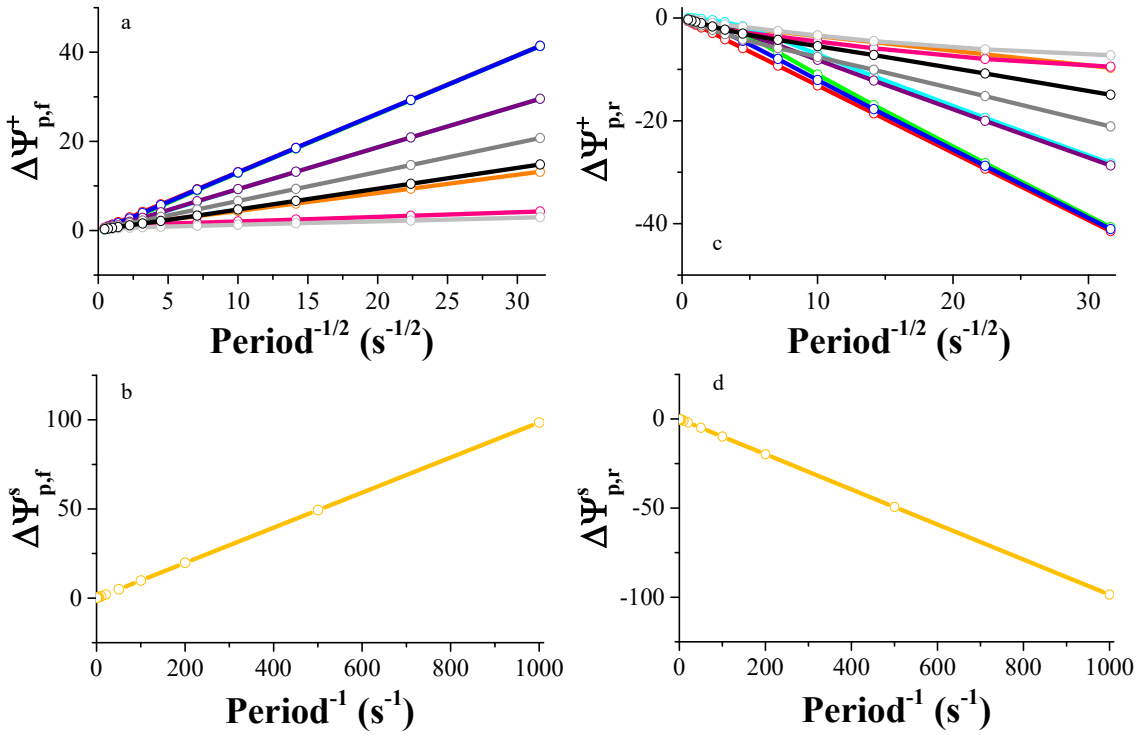

Figure 11.1. The effect of period on peak current $\Delta\Psi^{+}_{p,f}$ (panel a), $\Delta\Psi^{s}_{p,f}$ (panel b), $\Delta\Psi^{+}_{p,r}$ (panel c), and $\Delta\Psi^{s}_{p,r}$ (panel d) for the reversible (red), quasireversible (orange), surface-confined (yellow), EC_{irrev} (green), E_qC_{irrev} (cyan), EC_{rev} (blue), E_qC_{rev} (purple), $C_{irrev}E$ (magenta), $C_{irrev}E_q$ (light gray), $C_{rev}E$ (dark gray), and $C_{rev}E_q$ (black) mechanisms. For all simulations, amplitude = 50 mV, increment = 10 mV, and kinetic parameters match those listed in the introduction.

In comparison to the reversible case, the sluggish electron transfer cannot be completed within the time allowed nor can the complete conversion of Y to Ox and subsequently Red cannot be completed. As a result, the slope of current as a function of period is less than that of a reversible process. If an experimenter observes a decrease in peak current versus period$^{-1/2}$ after switching electrode type and/or electrolyte (assuming all other variables including electrode area are constant), then the analyte may be kinetically controlled in that set of experimental conditions. Alternatively, if an experimenter

observes a decrease in slope for the relationship between peak current and period$^{-1/2}$ after the addition of a substrate to the electrochemical cell, then this evidence supports a chemical reaction preceding or following the electron transfer. Thus, the trends in peak currents with the variation of period aid in enabling the user to discriminate between mechanisms.

Similar trends for several mechanisms have been previously published for current as a function of scan rate when using CV.[1] Moreover, Nicholson and Shain stated that the current-scan rate relationship for chemically coupled mechanisms has a differing magnitude and trend than that obtained for a reversible process. Readers are reminded that increasing period in CSWV corresponds to a decrease in sweep rate for CV and that the current function used by Nicholson and Shain is not the same as the one used within this thesis.

The trends in Figure 11.1 appear drastically different than those presented in SWV work by O'Dea and the Osteryoungs[2-4] as well as Mirceski and coworkers[5]. The plots of $\Delta\Psi_p^+$ and $\Delta\Psi_p^s$ versus period$^{-1/2}$ and period^{-1} are used exclusively in this thesis except for one similar appearance in Figure 2.8 of the book by Mirceski et al.[5] Otherwise, for a given mechanism investigated with SWV, $\Delta\Psi$ is plotted versus a dimensionless kinetic parameter that contains either period or frequency. As discussed in Chapter 1, the plotting convention used with SWV does not match experimental observations and is difficult to interpret by the experimentalist. If the trends obtained with SWV were treated as those presented here (i.e., using the normalized faradaic current and separation of the kinetic parameter from time), the forward sweep of CSWV would be identical to that obtained with SWV. $\Delta\Psi_{p,r}^+$ and $\Delta\Psi_{p,r}^s$ are not comparable to SWV trends as a reverse

sweep is not measured. However, reports of inverse scan SWV have been presented.[6, 7] The magnitudes of the current with inverse scan SWV would only be the same as those obtained with CSWV for a reversible process. Otherwise, to obtain comparable results, the initial potential would have to be held constant for the amount of time it would have taken for the forward scan to be completed with CSWV.

Broadly, the effects of kinetically controlled and chemically coupled reactions on peak current presented here parallels work by O'Dea, Osteryoung, and Osteryoung, and Mirceski et al. For instance, it has been shown with SWV that quasireversible mechanisms have a lower current than their reversible counterpart (see Figure 5 in O'Dea[3] and Figure 2.7 in Mirceski et al[5]; assume a fixed period or frequency to interpret the plots). This is in agreement with the results presented in Figures 3.14 and 11.1. Furthermore, both SWV and CSWV agree that chemically coupled reactions affect the magnitude of the current relative to that obtained the reversible mechanism. This is displayed in Figures 10 and 13 in O'Dea[3] and Figures 2.28 and 2.30 in Mirceski et al[5] for the CE and EC mechanisms, respectively. Their plots show the magnitude of the current is dependent on the dimensionless kinetic parameter and the equilibrium constant of the chemical reaction. This relationship is similarly represented Figures 5.2 and 6.2 for the EC and CE mechanisms in this thesis. The results in Figure 11.1 are in agreement with previously published work and are enhanced to show the expected experimentally observed trends as period is varied.

Since the magnitude of currents change with the variation of period, it is imperative to investigate trends in peak ratio. Figures demonstrating the relationships of peak ratio and period have been shown in Figures 3.15, 3.22, 4.22, 5.5d, 5.6, 5.7, 5.8, 6.5d, 6.6, 6.7, and

6.8. The collected plot of peak ratio versus log period is shown in Figure 11.2. For the reversible and surface-confined cases, peak ratio is invariant with period at unity. Kinetically-controlled or chemically coupled electrode reactions deviate from this trend. For the quasireversible mechanism, peak ratio increases with log period. As period lengthens, more time is allowed for the electron transfer to occur, and the peak ratio approaches that for a reversible reaction.

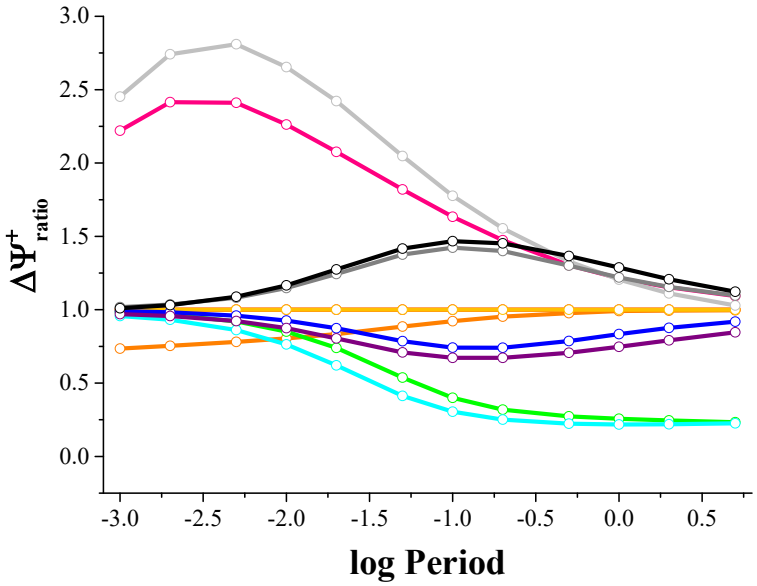

Figure 11.2. The effect of period on peak ratio for the reversible (red), quasireversible (orange), surface-confined (yellow), EC_{irrev} (green), E_qC_{irrev} (cyan), EC_{rev} (blue), E_qC_{rev} (purple), $C_{irrev}E$ (magenta), $C_{irrev}E_q$ (light gray), $C_{rev}E$ (dark gray), and $C_{rev}E_q$ (black) mechanisms. For all simulations, amplitude = 50 mV, increment = 10 mV, and kinetic parameters match those listed in the introduction.

For the mechanism in which a chemical reaction follows the electron transfer, peak ratio will always be less than or equal to unity. For all of the EC mechanisms investigated here, peak ratio begins at unity and then decreases with log period as more time is allowed for the chemical reaction to occur. The amount of Red available for conversion

back to Ox has decreased as more Red is converted to Z. Subsequently, peak ratio decreases. For the EC_{irrev} and E_qC_{irrev} mechanisms, peak ratio remains constant after the decrease. For the EC_{rev} and E_qC_{rev} mechanisms, peak ratio increases towards unity after the initial decrease. For the mechanism in which a chemical reaction precedes an electron transfer, the peak ratio will always be greater than or equal to unity. At longer periods, more time is allowed for the conversion of Y to Ox, which at potentials negative of E^0 is immediately converted to Red. As a result, Red accumulates and more is available to be converted to Ox on the reverse sweep. For the $C_{irrev}E$ and $C_{irrev}E_q$ cases, peak ratio > 2, increases slightly with log period, then decreases towards unity. For the $C_{rev}E$ and $C_{rev}E_q$ cases, peak ratio begins at unity, increase with log period, and then decreases towards unity. Thus, peak ratio can be used to rapidly discriminate between mechanisms.

The trends in peak ratio can only be compared to CV since a reverse peak (and subsequently peak ratio) do not exist in SWV. It is essential to note that peak ratio of the net peak currents in CSWV is not equal to ratio of individual currents in SWV. The relationships between peak ratio and period as presented in Figure 11.2 are in agreement for those presented for CV.[1] Both techniques show that peak ratio is greater than unity and decreases with period for the CE_{rev} case. Furthermore, peak ratio is less than unity for both EC cases presented though trends differ for the EC_{rev} case. Readers are reminded that slight differences between the two reports are the result of differing kinetic and equilibrium values as well as the magnitude of period and scan rate. Specific values of $k_f + k_b$ and K were chosen to create Figure 11.2 and as shown in Figures 5.7 and 5.8, the trend for peak ratio with period depends greatly on both $k_f + k_b$ and K. If different

values of $k_f + k_b$ and K had been chosen to describe the EC_{rev} case, the results would be identical to those obtained with CV. Thus, results in peak ratio for CSWV are in agreement with by those presented for CV.

Peak potentials have been examined throughout this thesis in Figures 3.20, 3.21, 4.1, 4.20a, 4.21, 5.5b, 5.10, 5.11, 6.5b, 6.10, and 6.11. The effect of period on $E_{p,f}$ is shown in Figure 11.3. The reversible, E_qC_{irrev}, EC_{rev}, E_qC_{rev}, and $C_{rev}E$ mechanisms remain at or near E^0 regardless of period. All other mechanisms exhibit a shift from E^0.

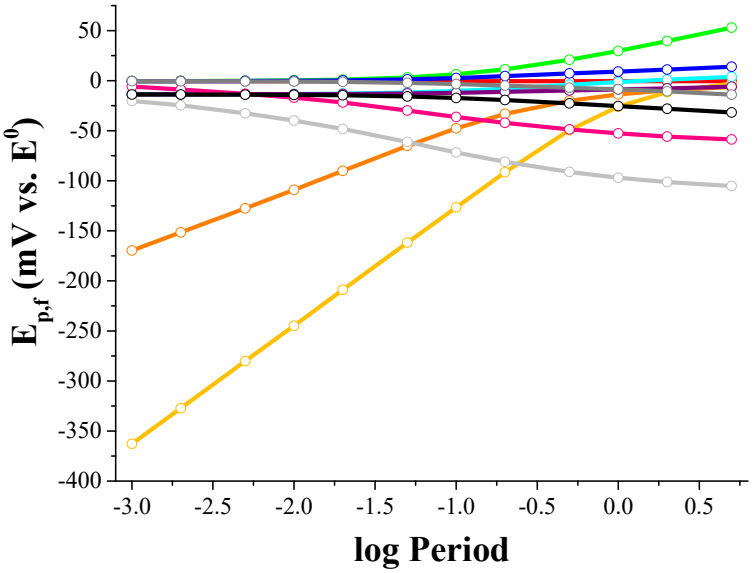

Figure 11.3. The effect of period on $E_{p,f}$ for the reversible (red), quasireversible (orange), surface-confined (yellow), EC_{irrev} (green), E_qC_{irrev} (cyan), EC_{rev} (blue), E_qC_{rev} (purple), $C_{irrev}E$ (magenta), $C_{irrev}E_q$ (light gray), $C_{rev}E$ (dark gray), and $C_{rev}E_q$ (black) mechanisms. For all simulations, amplitude = 50 mV, increment = 10 mV, and kinetic parameters match those listed in the introduction.

For both the quasireversible and surface-confined mechanisms, $E_{p,f}$ begins negative of E^0 and shifts positively with period. For the EC_{irrev} case, $E_{p,f}$ originates at E^0 then shifts positively with period. In contrast, for the $C_{irrev}E$ case, peak $E_{p,f}$ begins at E^0 then shifts negatively with period. $E_{p,f}$ begins slightly negative of E^0 then shifts more negatively

with period for the $C_{irrev}E_q$ and $C_{rev}E_q$ cases though the shift for the latter is smaller than the former.

The relationship between $E_{p,r}$ and period is presented in Figure 11.4. For the reversible, EC_{rev}, EqCrev, $C_{rev}E$, and $C_{rev}E_q$ mechanisms, $E_{p,r}$ remains at or near E^0 regardless of period. For the quasireversible and surface-confined mechanisms, $E_{p,r}$ begins positive of E^0 and shifts towards E^0 with period. $E_{p,r}$ begins at E^0 and shifts positively with period for the EC_{irrev} case whereas $E_{p,r}$ begins slightly positive of E^0 and shifts negatively with period for the E_qC_{irrev}. $E_{p,r}$ begins at E^0 and shifts negatively with period for the $C_{irrev}E$ and $C_{irrev}E_q$ cases though the magnitude of the shift for $C_{irrev}E$ is greater than that for $C_{irrev}E_q$.

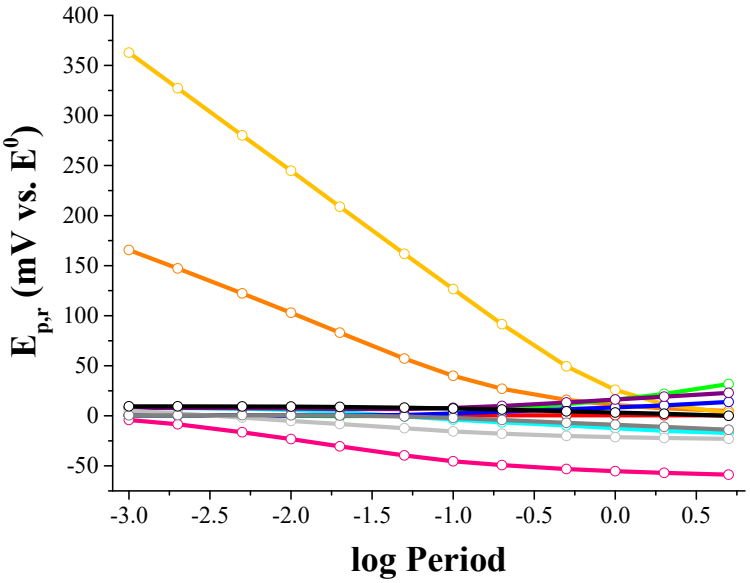

Figure 11.4. The effect of period on $E_{p,r}$ for the reversible (red), quasireversible (orange), surface-confined (yellow), EC_{irrev} (green), E_qC_{irrev} (cyan), EC_{rev} (blue), E_qC_{rev} (purple), $C_{irrev}E$ (magenta), $C_{irrev}E_q$ (light gray), $C_{rev}E$ (dark gray), and $C_{rev}E_q$ (black) mechanisms. For all simulations, amplitude = 50 mV, increment = 10 mV, and kinetic parameters match those listed in the introduction.

Subsequently, peak separation is affected by period as presented in Figure 11.5. The greatest effect of period on peak separation is for the quasireversible and surface-

confined cases as they both have drastic decreases from several hundred millivolts to zero as period increases. Peak separation for the reversible, EC_{rev}, $C_{irrev}E$, and $C_{rev}E$ essentially zero while period is varied. Peak separation increases negatively with period for the EC_{irrev} mechanism and positively for the $C_{irrev}E_q$ mechanism. Peak separation is constant for a value greater than zero for the E_qC_{rev} and $C_{rev}E_q$ mechanisms. Lastly, peak separation changes by a 40 mV and in sign for the E_qC_{irrev} mechanism. Thus, the effect of period on peak potentials can be used to discern between many mechanisms.

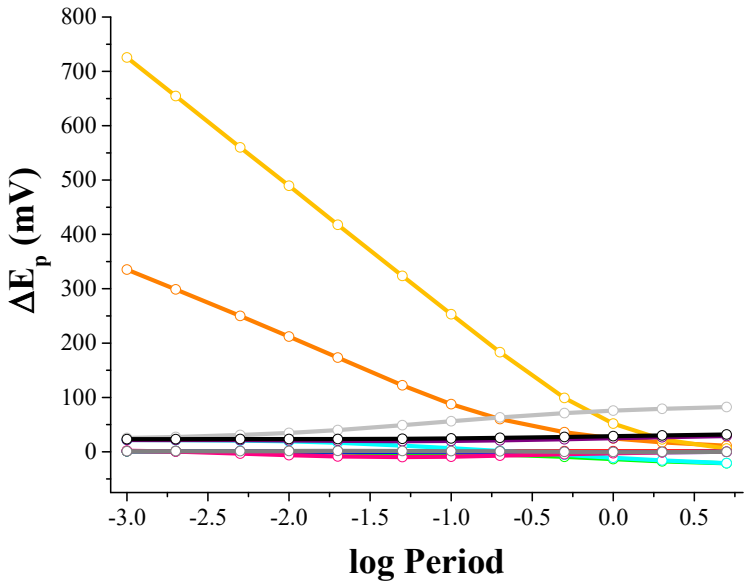

Figure 11.5. The effect of period on ΔE_p for the reversible (red), quasireversible (orange), surface-confined (yellow), EC_{irrev} (green), E_qC_{irrev} (cyan), EC_{rev} (blue), E_qC_{rev} (purple), $C_{irrev}E$ (magenta), $C_{irrev}E_q$ (light gray), $C_{rev}E$ (dark gray), and $C_{rev}E_q$ (black) mechanisms. For all simulations, amplitude = 50 mV, increment = 10 mV, and kinetic parameters match those listed in the introduction.

The magnitude of the change in half wave potential with scan rate has been reported for CV.[1] Peak potentials are invariant with scan rate for the reversible mechanism, shift negatively with period for the CE_{irrev}, CE_{rev}, and positively for the EC_{irrev} and EC_{rev} mechanisms for both CV and CSWV. The trends obtained for $E_{p,f}$ parallel the predicted

trends using SWV (see Figures 4, 9, and 12 in O'Dea[3] and be mindful of the x-axis as they differ between SWV and CSWV). However, $E_{p,r}$ and ΔE_p cannot be obtained with SWV and thus comparisons cannot be made between SWV and CSWV. If inverse SWV were used, the values of $E_{p,r}$ should be consistent between the two techniques though the magnitude of the peaks will differ.

11.3 Effect of Increment (δE)

Similar to period, the effect of increment on peak parameters can also be used to discern between mechanisms. The effect of increment on peak current is shown in Figure 11.6 as compiled from Figures 3.4, 4.3, 5.12c, 5.15, 6.12c and 6.15. $\Delta\Psi^{+}_{p,f}$ is invariant with increment for the reversible case whereas $\Delta\Psi^{+}_{p,f}$ and $\Delta\Psi^{s}_{p,f}$ increase for the quasireversible and surface-confined cases, respectively.

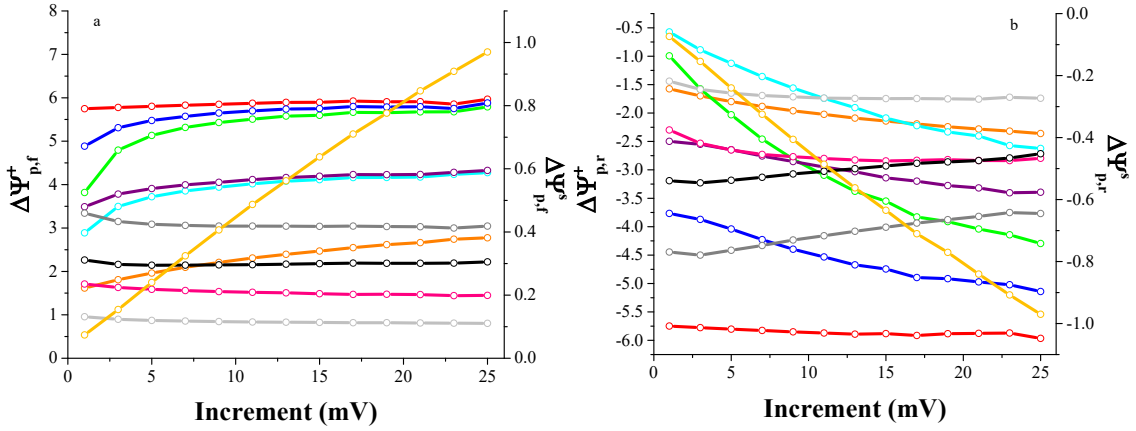

Figure 11.6. The effect of increment on peak current $\Delta\Psi^{+}_{p,f}$ and $\Delta\Psi^{s}_{p,f}$ (panel a) and $\Delta\Psi^{+}_{p,r}$ and $\Delta\Psi^{s}_{p,r}$ (panel b) for the reversible (red), quasireversible (orange), surface-confined (yellow), EC_{irrev} (green), E_qC_{irrev} (cyan), EC_{rev} (blue), E_qC_{rev} (purple), $C_{irrev}E$ (magenta), $C_{irrev}E_q$ (light gray), $C_{rev}E$ (dark gray), and $C_{rev}E_q$ (black) mechanisms. For all simulations, amplitude = 50 mV, period = 50 ms, and kinetic parameters match those listed in the introduction. Note: A secondary axis is used for $\Delta\Psi^{s}_{p,f}$ and $\Delta\Psi^{s}_{p,r}$.

Similarly, $\Delta\Psi^{+}_{p,f}$ increases slightly with increment for the EC_{irrev}, E_qC_{irrev}, EC_{rev}, and E_qC_{rev} cases whereas $\Delta\Psi^{+}_{p,f}$ decreases slightly for the $C_{irrev}E$, $C_{irrev}E_q$, $C_{rev}E$, and $C_{rev}E_q$ cases. $\Delta\Psi^{+}_{p,r}$ is also invariant with increment for the reversible case; $\Delta\Psi^{+}_{p,r}$ and $\Delta\Psi^{s}_{p,r}$ increase with increment for the quasireversible and surface-confined cases, respectively, as displayed in Figure 11.6b. Furthermore, $\Delta\Psi^{+}_{p,r}$ increases with increment for the EC_{irrev}, E_qC_{irrev}, EC_{rev}, and E_qC_{rev} cases though the magnitude differs for each. $\Delta\Psi^{+}_{p,r}$ is essentially invariant with increment for the $C_{irrev}E$ and CirrevEq cases though the magnitude differs from the reversible case. $\Delta\Psi^{+}_{p,r}$ decreases with increment for the $C_{rev}E$ and $C_{rev}E_q$ cases.

As a result of the trends in peak currents, peak ratio depends on increment (see Figure 11.7 as a compilation of Figures 3.4, 4.3, 5.12d, 5.13, 5.14, 6.12d, 6.13, and 6.14). Peak ratio is invariant at unity for the reversible and surface-confined cases whereas peak ratio is less than unity for the quasireversible, EC_{irrev}, E_qC_{irrev}, EC_{rev}, and E_qC_{rev} cases. Peak ratio decreases with increment for the quasireversible case and increases with increment for the EC_{irrev}, E_qC_{irrev}, EC_{rev}, and E_qC_{rev} cases though the magnitude of each depends on the mechanism. As expected for a CE mechanism, peak ratio is greater than unity for the $C_{irrev}E$, $C_{irrev}E_q$, $C_{rev}E$, and $C_{rev}E_q$ mechanisms though the magnitude and trend differ. Peak ratio increases with increment for the $C_{irrev}E$ and $C_{irrev}E_q$ cases and decreases slightly for the $C_{rev}E$ and $C_{rev}E_q$ cases. Thus, the trends in peak currents and peak ratio with the variation of increment can be used to identify electrode reaction mechanisms.

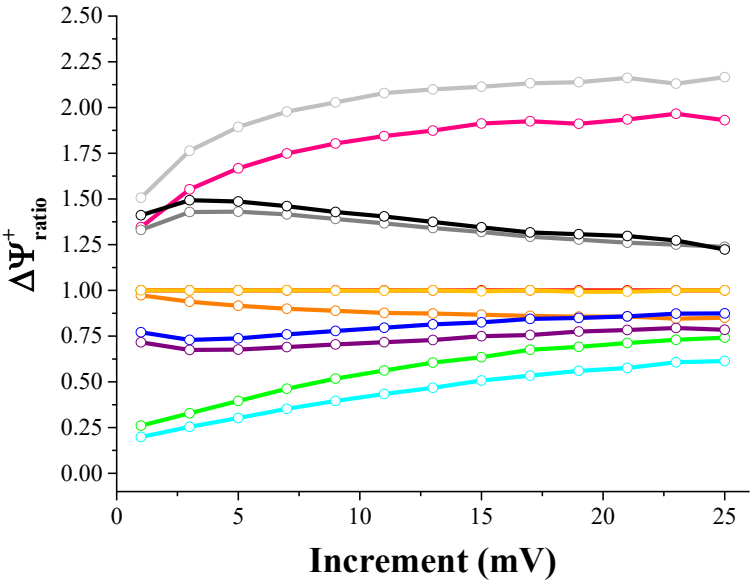

Figure 11.7. The effect of increment on peak ratio for the reversible (red), quasireversible (orange), surface-confined (yellow), EC_{irrev} (green), E_qC_{irrev} (cyan), EC_{rev} (blue), E_qC_{rev} (purple), $C_{irrev}E$ (magenta), $C_{irrev}E_q$ (light gray), $C_{rev}E$ (dark gray), and $C_{rev}E_q$ (black) mechanisms. For all simulations, amplitude = 50 mV, period = 50 ms, and kinetic parameters match those listed in the introduction.

Peak potentials can also be used to determine the electrode reaction pathway. The effect of increment on $E_{p,f}$ and $E_{p,r}$ is shown in Figures 11.8 and 11.9, respectively as originally presented in Figures 3.5, 4.4 5.12b, 5.16, 5.17, 6.12b, 6.16, and 6.17. $E_{p,f}$ is remains at E^0 for the reversible, EC_{rev}, and $C_{rev}E$ cases. $E_{p,f}$ shifts negatively with increment for the quasireversible and surface-confined cases and are located negative of E^0. $E_{p,f}$ shifts negatively at low increments for the EC_{irrev} case and rapidly approaches E^0. Similarly, $E_{p,f}$ shifts negatively for the E_qC_{irrev} and E_qC_{rev} cases though they begin positive of and at E^0, respectively. $E_{p,f}$ shifts positively with increment and is shifted negatively of E^0 for the $C_{irrev}E$ case. For the $C_{irrev}E_q$ and $C_{rev}E_q$ cases, $E_{p,f}$ begins negative of E^0 and shifts slightly more negative with increment though their displacement from E^0 differs for each mechanism.

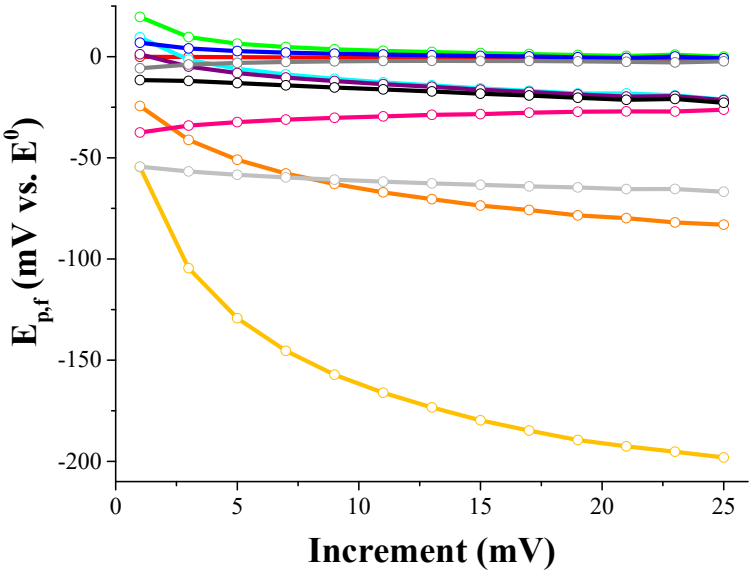

Figure 11.8. The effect of increment on $E_{p,f}$ for the reversible (red), quasireversible (orange), surface-confined (yellow), EC_{irrev} (green), E_qC_{irrev} (cyan), EC_{rev} (blue), E_qC_{rev} (purple), $C_{irrev}E$ (magenta), $C_{irrev}E_q$ (light gray), $C_{rev}E$ (dark gray), and $C_{rev}E_q$ (black) mechanisms. For all simulations, amplitude = 50 mV, period = 50 ms, and kinetic parameters match those listed in the introduction.

$E_{p,r}$ is invariant with increment at E^0 for the reversible, EC_{irrev}, E_qC_{irrev}, EC_{rev}, E_qC_{rev}, and $C_{rev}E$ mechanisms. $E_{p,r}$ shifts positively with increment for the quasireversible and surface-confined cases and are located positive of E^0. The slight positive shift in $E_{p,r}$ that originates at E^0 may be detectable for the $C_{rev}E_q$ case. $E_{p,r}$ shifts positively with increment for the $C_{irrev}E$ and $C_{irrev}E_q$ cases though it is negatively offset from E^0.

Subsequently, for this set of mechanisms, ΔE_p changes for the quasireversible, surface-confined, E_qC_{irrev}, E_qC_{rev}, $C_{irrev}E_q$, and $C_{rev}E_q$ mechanisms (see Figure 11.10). The magnitude of the increase differs for these mechanisms. All other mechanisms have essentially zero peak separation as increment is varied. Thus, the effect of increment on peak potentials can be used to identify reaction mechanisms.

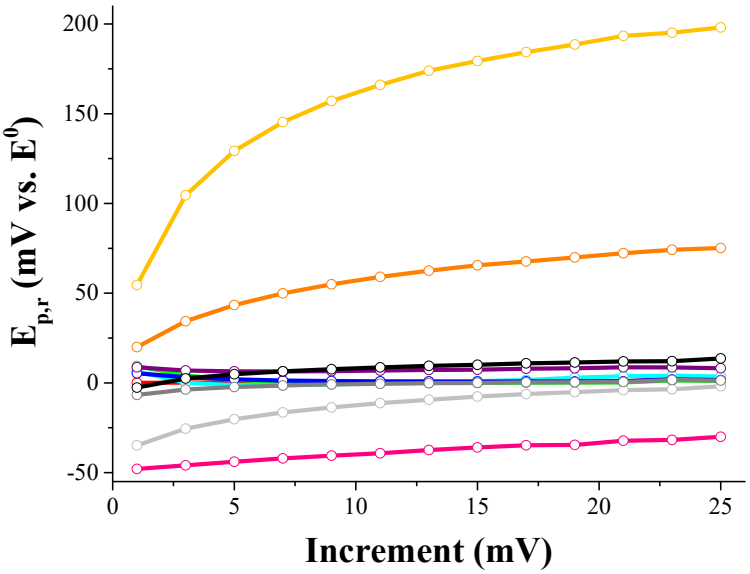

Figure 11.9. The effect of increment on $E_{p,r}$ for the reversible (red), quasireversible (orange), surface-confined (yellow), EC_{irrev} (green), E_qC_{irrev} (cyan), EC_{rev} (blue), E_qC_{rev} (purple), $C_{irrev}E$ (magenta), $C_{irrev}E_q$ (light gray), $C_{rev}E$ (dark gray), and $C_{rev}E_q$ (black) mechanisms. For all simulations, amplitude = 50 mV, period = 50 ms, and kinetic parameters match those listed in the introduction.

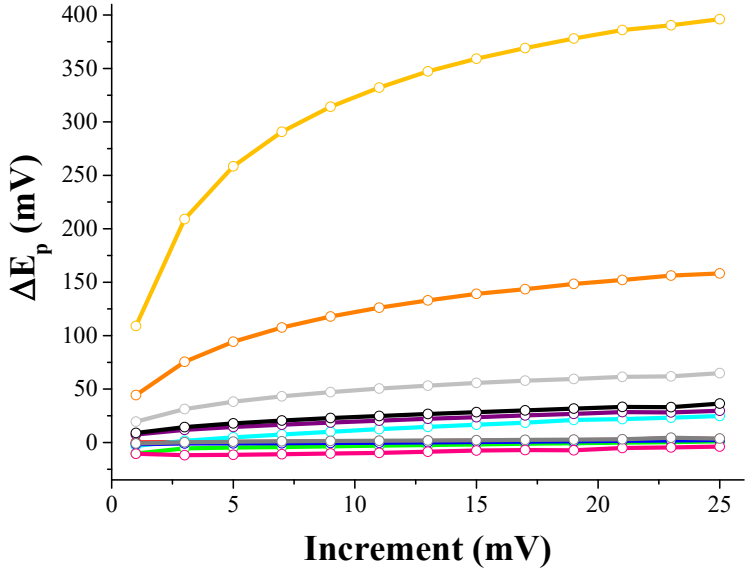

Figure 11.10. The effect of increment on ΔE_p for the reversible (red), quasireversible (orange), surface-confined (yellow), EC_{irrev} (green), E_qC_{irrev} (cyan), EC_{rev} (blue), E_qC_{rev} (purple), $C_{irrev}E$ (magenta), $C_{irrev}E_q$ (light gray), $C_{rev}E$ (dark gray), and $C_{rev}E_q$ (black) mechanisms. For all simulations, amplitude = 50 mV, period = 50 ms, and kinetic parameters match those listed in the introduction.

The diagnostic trends in peak parameters presented here are parallel to those reported for an increase in sweep rate for CV.[1] It should be noted that the change in effective sweep rate by changing increment is at most an order of magnitude whereas CV trends are reported over several orders of magnitude. Trends in increment have not previously been reported for SWV, so a comparison between the two techniques is not possible. However, if the reports for SWV were generated, they would be in agreement with the forward sweep trends presented here assuming dimensionless current is treated in the same way as for CSWV.

11.4 Effect of Switching Potential (E_λ)

The effect of switching potential on peak parameters can be used to identify electrode reaction mechanisms. $\Delta\Psi^+_{p,f}$ is unaffected by switching potential regardless of the mechanism; however, the magnitude of $\Delta\Psi^+_{p,f}$ depends on the mechanism (see Figure 11.11a). $\Delta\Psi^+_{p,r}$ is independent of switching potential for the reversible and surface-confined mechanisms (see Figure 11.11b). Figure 11.1 has been created from Figures 3.8, 4.7, 5.18c, 5.21, 6.18c and 6.21. $\Delta\Psi^+_{p,r}$ decreases slightly as E_λ approaches E^0 for the quasireversible mechanism and more so for the $C_{irrev}E$ and $C_{rev}E$ mechanisms. $\Delta\Psi^+_{p,r}$ increases slightly as E_λ approaches E^0 for the EC_{irrev}, E_qC_{irrev}, EC_{rev}, and E_qC_{rev} cases. For all mechanisms, the magnitude of $\Delta\Psi^+_{p,r}$ depends on the mechanism type.

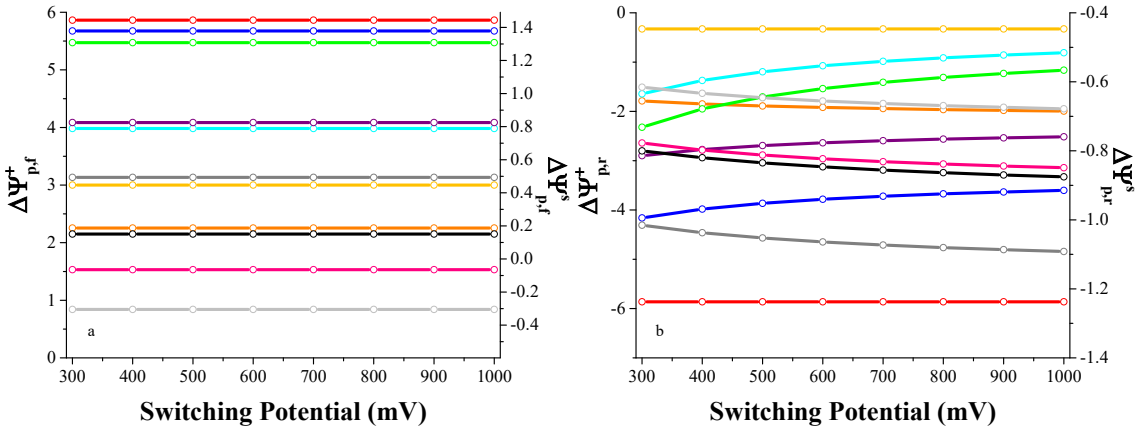

Figure 11.11. The effect of switching potential on peak current $\Delta\Psi^{+}_{p,f}$ and $\Delta\Psi^{s}_{p,f}$ (panel a) and $\Delta\Psi^{+}_{p,r}$ and $\Delta\Psi^{s}_{p,r}$ (panel b) for the reversible (red), quasireversible (orange), surface-confined (yellow), EC_{irrev} (green), E_qC_{irrev} (cyan), EC_{rev} (blue), E_qC_{rev} (purple), $C_{irrev}E$ (magenta), $C_{irrev}E_q$ (light gray), $C_{rev}E$ (dark gray), and $C_{rev}E_q$ (black) mechanisms. For all simulations, increment = 10 mV, amplitude = 50 mV, period = 50 ms, and kinetic parameters match those listed in the introduction. Note: A secondary axis is used for $\Delta\Psi^{s}_{p,f}$ and $\Delta\Psi^{s}_{p,r}$.

Because $\Delta\Psi^{+}_{p,r}$ is affected by E_λ, peak ratio is also affected as shown in Figure 11.12. These trends are assembled from Figures 3.8, 4.7, 5.18d, 5.19, 5.20, 6.18d, 6.19, and 6.20. Peak ratio is invariant at unity for the reversible and surface-confined mechanisms. Peak ratio is less than unity for the quasireversible, EC_{irrev}, E_qC_{irrev}, EC_{rev}, and E_qC_{rev} mechanisms. For the quasireversible mechanism, peak ratio decreases slightly as E_λ approaches E^0 for the as less time is allowed for the electron transfer to proceed. Peak ratio increases as E_λ approaches E^0 for the EC_{irrev}, E_qC_{irrev}, EC_{rev}, and E_qC_{rev} mechanisms as less time is allowed for the conversion of Red to Z, and as a result, more Red is available to be converted back to Ox. Peak ratio is greater than unity and decreases as E_λ approaches E^0 for the $C_{irrev}E$, $C_{irrev}E_q$, $C_{rev}E$, and $C_{rev}E_q$ cases there is less time for the conversion of Y to Ox. The magnitude of peak ratio for each of the chemically coupled

pairs differs. Thus, the effect of switching potential on reverse peak current and peak ratio can be used to identify electrode reaction mechanisms.

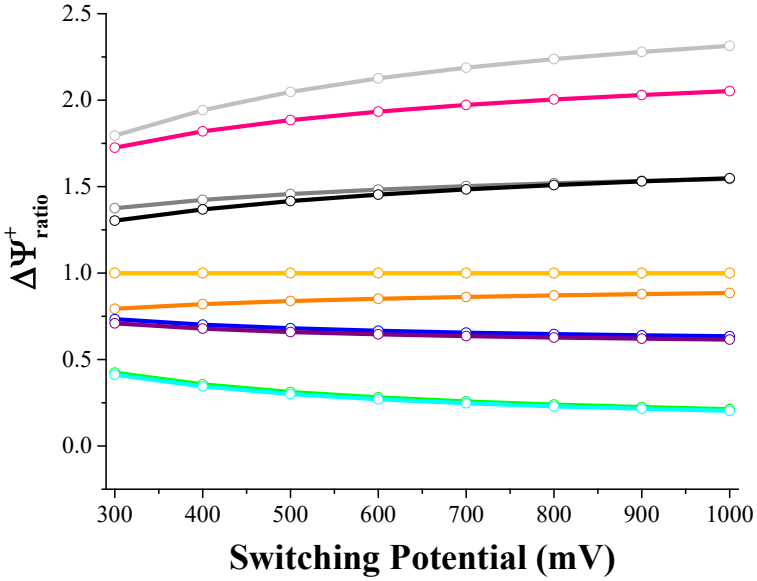

Figure 11.12. The effect of switching potential on peak ratio for the reversible (red), quasireversible (orange), surface-confined (yellow), EC_{irrev} (green), E_qC_{irrev} (cyan), EC_{rev} (blue), E_qC_{rev} (purple), $C_{irrev}E$ (magenta), $C_{irrev}E_q$ (light gray), $C_{rev}E$ (dark gray), and $C_{rev}E_q$ (black) mechanisms. For all simulations, increment = 10 mV, amplitude = 50 mV, period = 50 ms, and kinetic parameters match those listed in the introduction.

Peak potentials are generally unaffected by switching potential. $E_{p,f}$ and $E_{p,r}$ only shift with E_λ if E_λ occurs before the current returns to baseline (see Figures 11.13a and 11.13b, respectively).

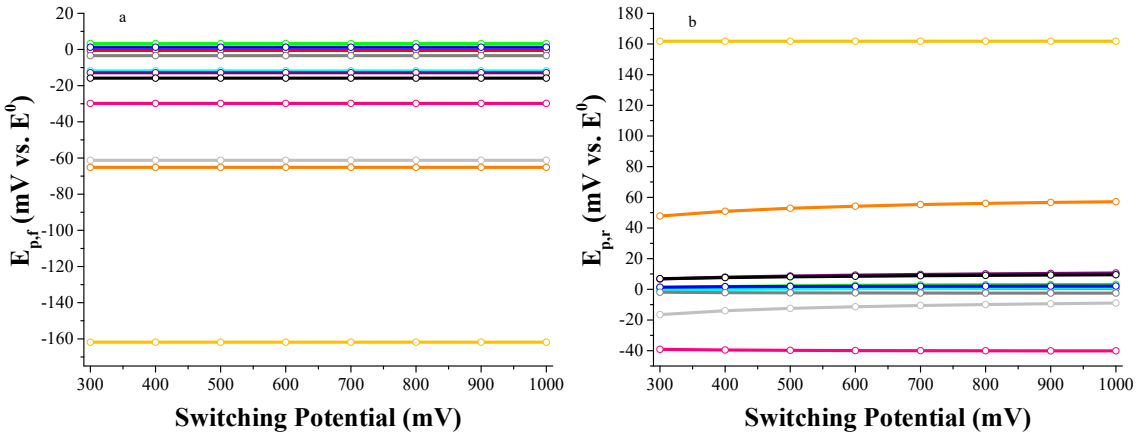

Figure 11.13. The effect of switching potential on $E_{p,f}$ (panel a) and $E_{p,r}$ (panel b) for the reversible (red), quasireversible (orange), surface-confined (yellow), EC_{irrev} (green), E_qC_{irrev} (cyan), EC_{rev} (blue), E_qC_{rev} (purple), $C_{irrev}E$ (magenta), $C_{irrev}E_q$ (light gray), $C_{rev}E$ (dark gray), and $C_{rev}E_q$ (black) mechanisms. For all simulations, increment = 10 mV, amplitude = 50 mV, period = 50 ms, and kinetic parameters match those listed in the introduction.

As a result, ΔE_p is invariant with E_λ (see Figure 11.14). However, the offset of $E_{p,f}$ and $E_{p,r}$ from E^0 and the magnitude of ΔE_p may be helpful in identifying the reaction mechanism. Figures 11.13 and 11.14 are based on Figures 4.8, 5.18b, 5.22, 5.23, 6.18b, 6.22, and 6.23. Thus, the effect of switching potential on peak potential is not practical for identifying a reaction mechanism.

Trends in switching potential are analogous to those obtained with CV. Forward peak currents and both peak potentials are essentially invariant with switching potential for both CV and CSWV. However, the reverse peak current and peak ratio are greatly affected by switching potential for both cyclic techniques. Comparisons cannot be made between SWV and CSWV for switching potential as this variable does not exist for SWV. Thus, variation of switching potential enables the user to distinguish between mechanisms in a manner that SWV is not capable of while providing additional information on the stability of the product of the electron transfer.

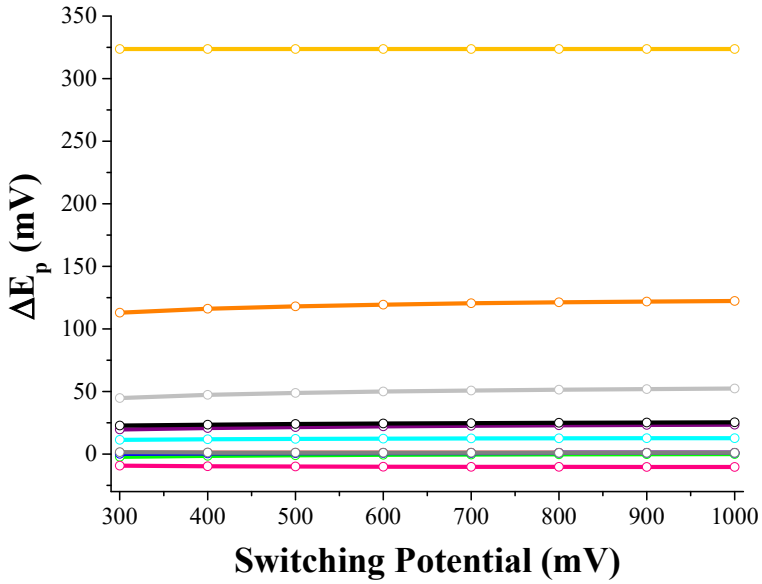

Figure 11.14. The effect of switching potential on ΔE_p for the reversible (red), quasireversible (orange), surface-confined (yellow), EC_{irrev} (green), E_qC_{irrev} (cyan), EC_{rev} (blue), E_qC_{rev} (purple), $C_{irrev}E$ (magenta), $C_{irrev}E_q$ (light gray), $C_{rev}E$ (dark gray), and $C_{rev}E_q$ (black) mechanisms. For all simulations, increment = 10 mV, amplitude = 50 mV, period = 50 ms, and kinetic parameters match those listed in the introduction.

11.5 Effect of Amplitude (Esw)

The effect of amplitude on peak parameters is also useful in identifying electrode reaction mechanisms. Both $\Delta\Psi^+_{p,f}$ and $\Delta\Psi^+_{p,r}$ increase with amplitude; the curvature of the trend and the magnitude of the increase depend on each mechanism (see Figures 11.15a and 11.15b, respectively). It is important to note that the extent of the increase may differ for $\Delta\Psi^+_{p,f}$ and $\Delta\Psi^+_{p,r}$. Figure 11.15 is based on the trends in Figures 3.11, 4.10, 4.11, 5.24c, 5.26, 6.24c and 6.27.

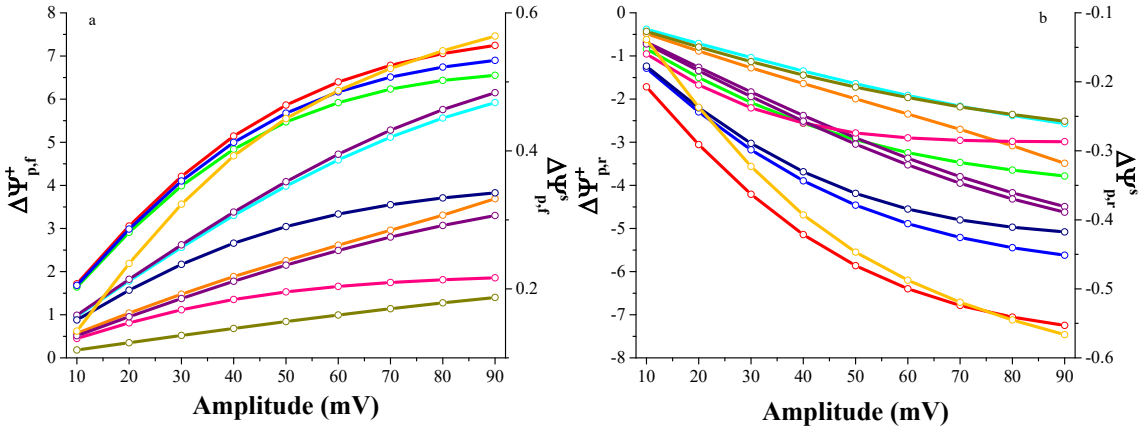

Figure 11.15. The effect of amplitude on peak current $\Delta\Psi^{+}_{p,f}$ and $\Delta\Psi^{s}_{p,f}$ (panel a) and $\Delta\Psi^{+}_{p,r}$ and $\Delta\Psi^{s}_{p,r}$ (panel b) for the reversible (red), quasireversible (orange), surface-confined (yellow), EC_{irrev} (green), E_qC_{irrev} (cyan), EC_{rev} (blue), E_qC_{rev} (purple), $C_{irrev}E$ (magenta), $C_{irrev}E_q$ (light gray), $C_{rev}E$ (dark gray), and $C_{rev}E_q$ (black) mechanisms. For all simulations, increment = 10 mV, period = 50 ms, and kinetic parameters match those listed in the introduction. Note: A secondary axis is used for $\Delta\Psi^{s}_{p,f}$ and $\Delta\Psi^{s}_{p,r}$.

Peak ratio is affected by amplitude as displayed in Figure 11.16 and originally presented in Figures 3.11, 4.11, 5.24d, 5.25, 6.24d and 6.26. Peak ratio is invariant at unity for the reversible and surface-confined cases. Peak ratio is less than unity and increases with amplitude for the quasireversible, EC_{irrev}, E_qC_{irrev}, EC_{rev}, and E_qC_{rev} mechanisms; the magnitude differs for all five cases. Peak ratio is greater than unity for the $C_{irrev}E$, $C_{irrev}E_q$, $C_{rev}E$, and $C_{rev}E_q$ mechanisms. Peak ratio decreases with amplitude for the $C_{irrev}E$ and $C_{irrev}E_q$ cases and is relatively constant for the $C_{rev}E$ and $C_{rev}E_q$ cases. Thus, peak ratios may be advantageous for identifying reaction mechanisms.

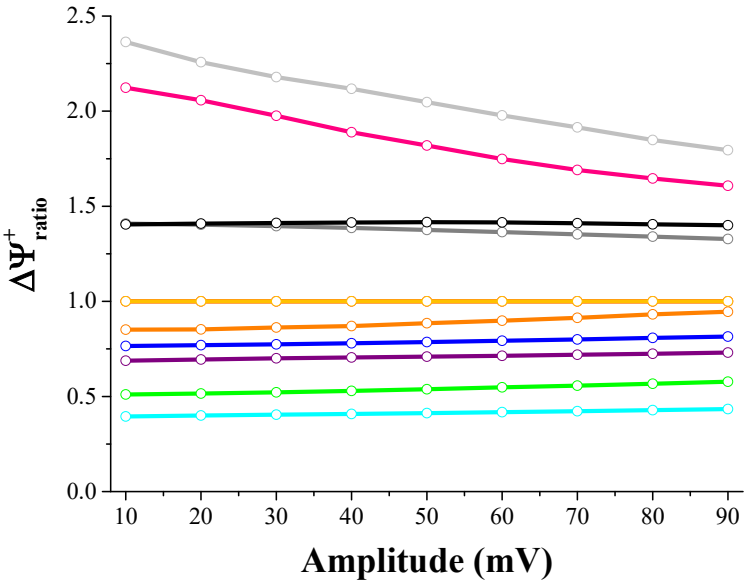

Figure 11.16. The effect of amplitude on peak ratio for the reversible (red), quasireversible (orange), surface-confined (yellow), EC_{irrev} (green), E_qC_{irrev} (cyan), EC_{rev} (blue), E_qC_{rev} (purple), $C_{irrev}E$ (magenta), $C_{irrev}E_q$ (light gray), $C_{rev}E$ (dark gray), and $C_{rev}E_q$ (black) mechanisms. For all simulations, increment = 10 mV, period = 50 ms, and kinetic parameters match those listed in the introduction.

The effect of amplitude on peak potentials is also beneficial when trying to discern between reaction mechanisms. The relationship between $E_{p,f}$ and $E_{p,r}$ and amplitude is shown in Figures 11.17a and 11.17b, respectively as previously presented in Figures 3.10, 4.12, 5.24b, 5.27, 5.28, 6.24b, 6.28, and 6.29. $E_{p,f}$ is invariant at E^0 for the reversible case and essentially invariant and at E^0 for the EC_{irrev}, EC_{rev}, and $C_{rev}E$ mechanisms; these mechanisms only deviate from E^0 at high amplitudes. $E_{p,f}$ for both the quasireversible and surface-confined mechanisms are located negative of E^0 and shift positively towards E^0 with amplitude. $E_{p,f}$ for the E_qC_{irrev}, E_qC_{rev}, and $C_{rev}E_q$ cases is located negative of E^0 and shifts slightly positive with amplitude. $E_{p,f}$ for the $C_{irrev}E$ case is located negative of E^0 and shifts slightly negative with increasing amplitude whereas $E_{p,f}$ is essentially constant negative of E^0 for the $C_{irrev}E_q$ case. Similarly, $E_{p,r}$ is at E^0 and

invariant with amplitude for the reversible, EC_{irrev}, E_qC_{irrev}, EC_{rev}, E_qC_{rev}, $C_{rev}E$, and $C_{rev}E_q$ cases. $E_{p,r}$ is positive of E^0 and shifts negative toward E^0 with amplitude for the quasireversible and surface-confined cases. $E_{p,r}$ is located negative of E^0 and shifts negatively with amplitude for the $C_{irrev}E$ case whereas $E_{p,r}$ begins at E^0 and shifts negatively with amplitude for the $C_{irrev}E_q$ case.

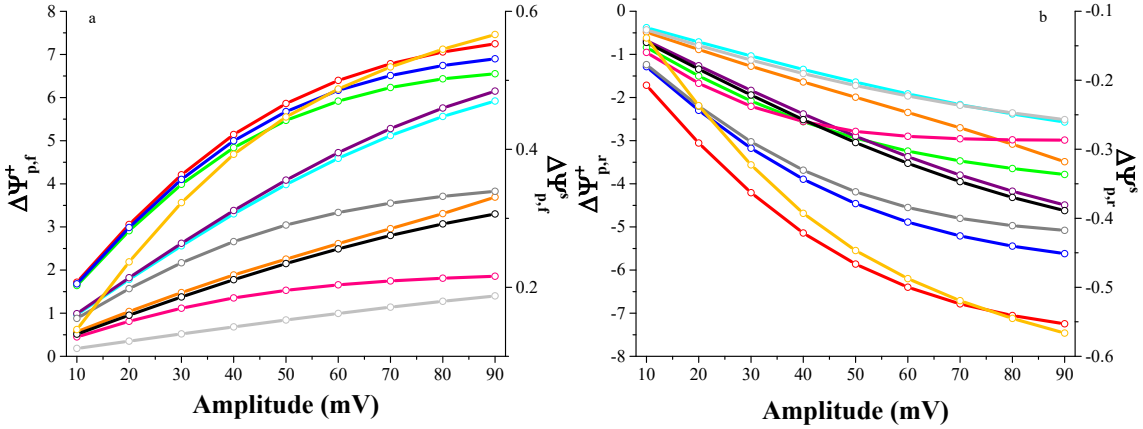

Figure 11.17. The effect of amplitude on $E_{p,f}$ (panel a) and $E_{p,r}$ (panel b) for the reversible (red), quasireversible (orange), surface-confined (yellow), EC_{irrev} (green), E_qC_{irrev} (cyan), EC_{rev} (blue), E_qC_{rev} (purple), $C_{irrev}E$ (magenta), $C_{irrev}E_q$ (light gray), $C_{rev}E$ (dark gray), and $C_{rev}E_q$ (black) mechanisms. For all simulations, increment = 10 mV, period = 50 ms, and kinetic parameters match those listed in the introduction.

As a result, peak separation may change for some mechanisms as displayed in Figure 11.18. ΔE_p is invariant and zero for the reversible, EC_{rev}, and $C_{rev}E$ cases. ΔE_p decreases with increasing amplitude for the quasireversible, surface-confined, E_qC_{irrev}, E_qC_{rev}, $C_{irrev}E_q$, and $C_{rev}E_q$ cases while ΔE_p increases negatively with amplitude for the EC_{irrev} and $C_{irrev}E$ cases. Hence, peak potentials may be beneficial in identifying reaction mechanisms.

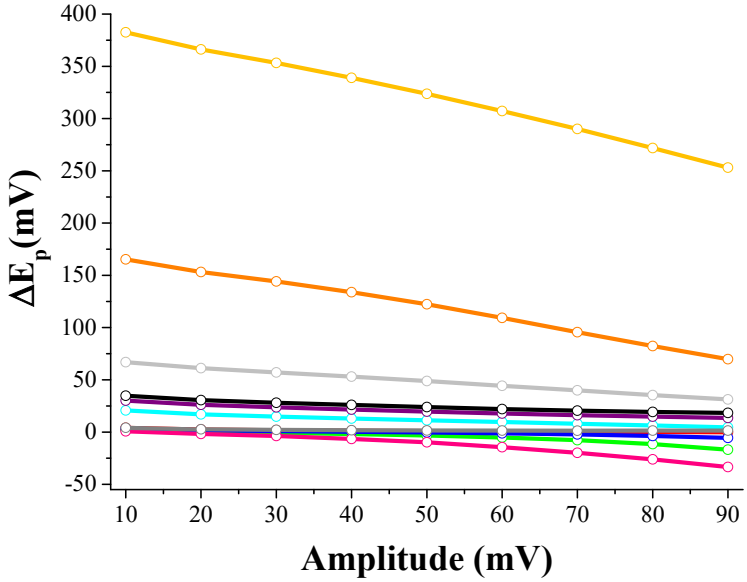

Figure 11.18. The effect of amplitude on ΔE_p for the reversible (red), quasireversible (orange), surface-confined (yellow), EC_{irrev} (green), E_qC_{irrev} (cyan), EC_{rev} (blue), E_qC_{rev} (purple), $C_{irrev}E$ (magenta), $C_{irrev}E_q$ (light gray), $C_{rev}E$ (dark gray), and $C_{rev}E_q$ (black) mechanisms. For all simulations, increment = 10 mV, period = 50 ms, and kinetic parameters match those listed in the introduction.

The trends in peak parameters with amplitude are not comparable to CV as this variable does not exist in the CV waveform. Few reports of the variation of amplitude have been presented for SWV for the quasireversible, surface-confined, and E_qC mechanisms.[5, 8] Previous SWV results only investigate the effect of amplitude on peak current. Peak currents increase with amplitude for all mechanisms investigated with SWV and CSWV. Furthermore, peak splitting occurs for the surface-confined mechanism with both techniques. If peak potentials had been previously evaluated with SWV, their trends would match those obtained on the forward sweep of CSWV.

11.6 Protocol to Assign Electrode Reaction Mechanism

An experimenter can assign an electrode reaction mechanism to the analyte of interest by acquiring data and creating plots which match those presented in the previous four sections of this chapter. Experimenters are reminded to use the same empirical parameters as those listed for each plot within this chapter as some mechanisms are highly subjective to variation empirical parameters as shown in the chapters throughout this thesis. If an experimental data set matches the trends in peak parameters shown for period for a given mechanism, the data should also match the trends for that mechanism for increment, switching potential, and amplitude. If the experimenter desires determination of rates of electron transfer or chemical reactions, then the experimental data sets should be compared to the plots presented in the specific chapter addressing that mechanism.

11.7 Conclusion

This chapter includes a series of plots examining the effect of empirical parameters on peak parameters for seven of the mechanisms investigated in this thesis. These plots enable the experimentalist to identify the mechanism corresponding to experimental data. In evaluating these plots, it is evident that every relationship between empirical parameter and parameters is vital for the proper assignment of electrode reaction mechanisms. This presentation of expected trends for a collection of electrode reaction mechanisms is the first of its kind in decades[1, 3, 4] and most certainly the first for using CSWV.

Not only do the many figures presented in this chapter provide a means for mechanistic identification, they confirm that CSWV is an excellent electrochemical

technique for mechanism assignment. These plots give merit to the need for both forward and reverse sweeps over one-direction SWV as tremendous, vital information is gained in the reverse sweep. The added information is reflected in peak ratio, reverse peak potential, and peak separation that can aid in assessing the stability of the electrochemical species. Additionally, these plots show that the separation of kinetic parameters and period and treatment of the normalized peak current is essential in relating the expected trends to those obtained experimentally.

In addition the work presented in this thesis, several topics could be studied in the future. Experimental verification of the diagnostic criteria for the EC, CE, ECE, E_qC, CE_q, and E_qC_{cat} mechanisms should be performed. This will further demonstrate the capability of CSWV as a mechanistic tool which enables experimentalists to identify reactions and determine associated rates. Also, there are a variety of electrode reaction mechanisms in the literature that have not been investigated with CSWV. Specifically, there is a need for the investigation of surface-confined mechanism complicated by interactions[9, 10] and chemically coupled reactions[11-14] with CSWV. Other mechanisms that need to be examined by CSWV include second order chemical reactions like dimerization and disproportionation[15-20], and the ECE mechanism complicated by quasireversible electron transfers. Finally, as indicated in Chapter 1, there is a great disconnect in the diagnostic criteria presented for CV and the trends obtained experimentally with current instrumentation. This is due to the transition from analog to digital equipment and the sampling point used within a potential pulse used to measure current.[21-28] The codes used for simulations within this thesis could simply be modified for a cyclic staircase waveform and to control the current sampling point. The variation

of empirical parameters and identification of diagnostic criteria as performed in this thesis would update previous diagnostic criteria to match current instrumentation.

11.8 References

1. Nicholson, R.S. and I. Shain. *Anal. Chem.*, **1964**. 36, 706-723.

2. O'Dea, J.J., *Ph.D. Dissertation*, in *Chemistry*. 1979, Colorado State University: Fort Collins, CO.

3. O'Dea, J.J., J. Osteryoung, and R.A. Osteryoung. *Anal. Chem.*, **1981**. 53, 695-701.

4. Osteryoung, J.G. and J.J. O'Dea, *Electroanal. Chem.* **1986**, Marcel Dekker: New York. 209-224

5. Mirčeski, V., Š. Komorsky-Lovrić, and M. Lovrić, *Square Wave Voltammetry: Theory and Application*, *Monographs in Electrochemistry*. **2007**, Springer-Verlag: Berlin.

6. Lovrić, M. and D. Jadreško. *Electrochim. Acta*, **2010**. 55, 948-951.

7. Lovrić, M. and Š. Komorsky-Lovrić. *Cent. Eur. J. Chem.*, **2010**. 8, 513-518.

8. Mirčeski, V., E. Laborda, D. Guziejewski, and R.G. Compton. *Anal. Chem.*, **2013**. 85, 5586-5594.

9. Laviron, E. *J. Electroanal. Chem. Interfacial Electrochem.*, **1974**. 52, 395-402.

10. Mirčeski, V., M. Lovrić, and R. Gulaboski. *J. Electroanal. Chem.*, **2001**. 515, 91-100.

11. Laviron, E. *J. Electroanal. Chem. Interfacial Electrochem.*, **1972**. 34, 463-473.

12. Mirčeski, V. and R. Gulaboski. *Electroanalysis*, **2001**. 13, 1326-1334.

13. Mirceski, V. and M. Lovric. *Croat. Chem. Acta*, **2000**. 73, 305-329.

14. Mirceski, V. and M. Lovric. *J. Electroanal. Chem.*, **2004**. 565, 191-202.

15. Mastragostino, M., L. Nadjo, and J.M. Savéant. *Electrochim. Acta*, **1968**. 13, 721–749.

16. Nadjo, L. and J.M. Savéant. *J. Electroanal. Chem. Interfacial Electrochem.*, **1973**. 48, 113-145.

17. Plichon, V. and E. Laviron. *J. Electroanal. Chem. Interfacial Electrochem.*, **1976**. 71, 143-156.

18. Amatore, C. and J.M. Savéant. *J. Electroanal. Chem. Interfacial Electrochem.*, **1977**. 85, 27-46.

19. Amatore, C. and J.M. Savéant. *J. Electroanal. Chem.*, **1979**. 102, 21-40.

20. Mozo, J.D., J. Carbajo, J.C. Sturm, L.J. Nunez-Vergara, R. Moscoso, and J.A. Squella. *Anal. Chim. Acta*, **2011**. 699, 33-43.

21. Zipper, J.J. and S.P. Perone. *Anal. Chem.*, **1973**. 45, 452-458.

22. Miaw, L.H.L., P.A. Boudreau, M.A. Pichler, and S.P. Perone. *Anal. Chem.*, **1978**. 50, 1988-1996.

23. Bilewicz, R., R.A. Osteryoung, and J. Osteryoung. *Anal. Chem.*, **1986**. 58, 2761-2765.

24. Seralathan, M., R. Osteryoung, and J. Osteryoung. *J. Electroanal. Chem. Interfacial Electrochem.*, **1986**. 214, 141-156.

25. Seralathan, M., R.A. Osteryoung, and J.G. Osteryoung. *J. Electroanal. Chem. Interfacial Electrochem.*, **1987**. 222, 69-100.

26. Bilewicz, R., K. Wikiel, R. Osteryoung, and J. Osteryoung. *Anal. Chem.*, **1989**. 61, 965-972.

27. Bott, A.W. *Curr. Sep.*, **1997**. 16, 23-26.

28. Batchelor-McAuley, C., M. Yang, E.M. Hall, and R.G. Compton. *J. Electroanal. Chem.*, **2015**. 758, 1-6.